# NANOMEDICINE IN CANCER TARGETING AND THERAPY

EDITED BY: João Paulo Longo, Marcelo Calderon, Luis Alexandre Muehlmann, Ricardo Bentes Azevedo and Christian Stockmann

PUBLISHED IN: Frontiers in Oncology

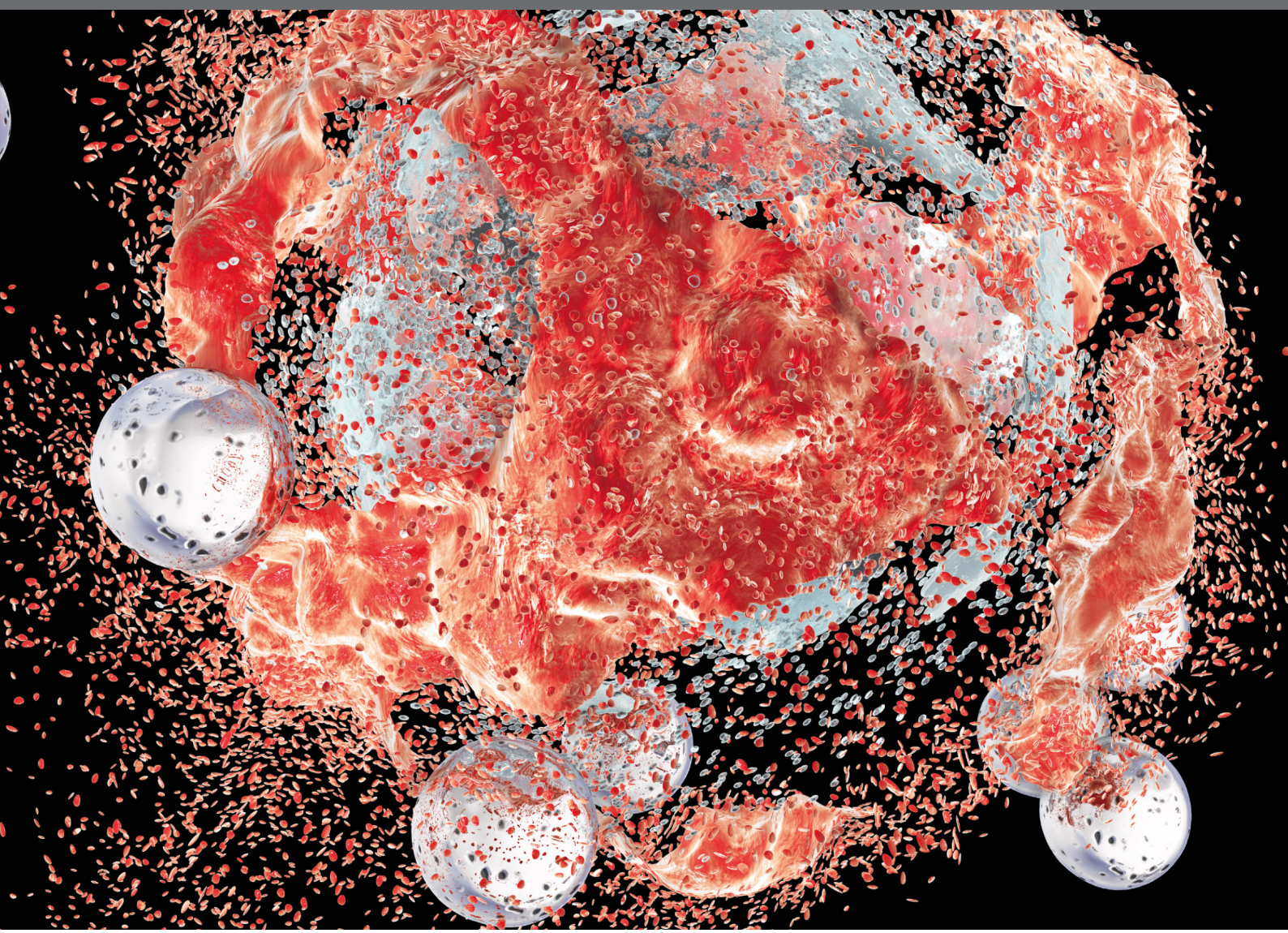

frontiers Research Topics

ISSN 1664-8714
ISBN 978-2-88974-071-0
DOI 10.3389/978-2-88974-071-0

## About Frontiers

Frontiers is more than just an open-access publisher of scholarly articles: it is a pioneering approach to the world of academia, radically improving the way scholarly research is managed. The grand vision of Frontiers is a world where all people have an equal opportunity to seek, share and generate knowledge. Frontiers provides immediate and permanent online open access to all its publications, but this alone is not enough to realize our grand goals.

## Frontiers Journal Series

The Frontiers Journal Series is a multi-tier and interdisciplinary set of open-access, online journals, promising a paradigm shift from the current review, selection and dissemination processes in academic publishing. All Frontiers journals are driven by researchers for researchers; therefore, they constitute a service to the scholarly community. At the same time, the Frontiers Journal Series operates on a revolutionary invention, the tiered publishing system, initially addressing specific communities of scholars, and gradually climbing up to broader public understanding, thus serving the interests of the lay society, too.

## Dedication to Quality

Each Frontiers article is a landmark of the highest quality, thanks to genuinely collaborative interactions between authors and review editors, who include some of the world's best academicians. Research must be certified by peers before entering a stream of knowledge that may eventually reach the public - and shape society; therefore, Frontiers only applies the most rigorous and unbiased reviews.
Frontiers revolutionizes research publishing by freely delivering the most outstanding research, evaluated with no bias from both the academic and social point of view. By applying the most advanced information technologies, Frontiers is catapulting scholarly publishing into a new generation.

## What are Frontiers Research Topics?

Frontiers Research Topics are very popular trademarks of the Frontiers Journals Series: they are collections of at least ten articles, all centered on a particular subject. With their unique mix of varied contributions from Original Research to Review Articles, Frontiers Research Topics unify the most influential researchers, the latest key findings and historical advances in a hot research area! Find out more on how to host your own Frontiers Research Topic or contribute to one as an author by contacting the Frontiers Editorial Office: frontiersin.org/about/contact

# NANOMEDICINE IN CANCER TARGETING AND THERAPY

Topic Editors:
**João Paulo Longo,** University of Brasilia, Brazil
**Marcelo Calderon,** Polymat, Spain
**Luis Alexandre Muehlmann,** University of Brasilia, Brazil
**Ricardo Bentes Azevedo,** University of Brasilia, Brazil
**Christian Stockmann,** University of Zurich, Switzerland

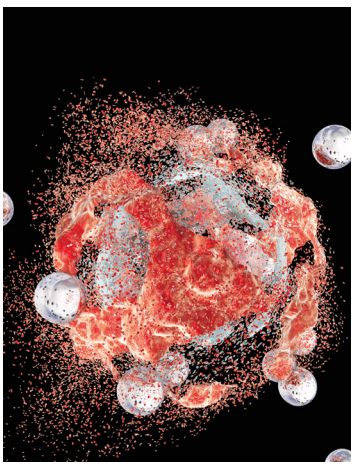

Image: Kateryna Kon/Shutterstock.com

**Citation:** Longo, J. P., Calderon, M., Muehlmann, L. A., Azevedo, R. B., Stockmann, C., eds. (2022). Nanomedicine in Cancer Targeting and Therapy. Lausanne: Frontiers Media SA. doi: 10.3389/978-2-88974-071-0

# Table of Contents


04 ***Editorial: Nanomedicine in Cancer Targeting and Therapy***
João Paulo Figueiró Longo, Luis Alexandre Muehlmann, Marcelo Calderón, Christian Stockmann and Ricardo Bentes Azevedo

07 ***Polymeric Nanoscale Drug Carriers Mediate the Delivery of Methotrexate for Developing Therapeutic Interventions Against Cancer and Rheumatoid Arthritis***
Wen-Jun Yu, Dong-Xu Huang, Shuang Liu, Ying-Li Sha, Feng-hui Gao and Hong Liu

20 ***Green Biosynthesized Silver Nanoparticles With Aqueous Extracts of* Ginkgo Biloba *Induce Apoptosis* via *Mitochondrial Pathway in Cervical Cancer Cells***
Zhen Xu, Qi Feng, Min Wang, Huange Zhao, Yingying Lin and Songlin Zhou

30 ***Dual-Target Peptide-Modified Erythrocyte Membrane-Enveloped PLGA Nanoparticles for the Treatment of Glioma***
Yuexin Cui, Jiejie Sun, Wenyan Hao, Mengyu Chen, Yingzi Wang, Fenghua Xu and Chunsheng Gao

45 ***Regulation of Hedgehog Signaling by miRNAs and Nanoformulations: A Possible Therapeutic Solution for Colorectal Cancer***
Zeeshan Javed, Muhammad Javed Iqbal, Amna Rasheed, Haleema Sadia, Shahid Raza, Asma Irshad, Wojciech Koch, Wirginia Kukula-Koch, Anna Głowniak-Lipa, William C. Cho and Javad Sharifi-Rad

61 ***Targeted Chinese Medicine Delivery by A New Family of Biodegradable Pseudo-Protein Nanoparticles for Treating Triple-Negative Breast Cancer:* In Vitro *and* In Vivo *Study***
Hiu Yee Kwan, Qinghua Xu, Ruihong Gong, Zhaoxiang Bian and Chih-Chang Chu

79 ***Extracellular Vesicles: An Emerging Nanoplatform for Cancer Therapy***
Yifan Ma, Shiyan Dong, Xuefeng Li, Betty Y. S. Kim, Zhaogang Yang and Wen Jiang

94 ***The Role of Exosomes in Pancreatic Cancer From Bench to Clinical Application: An Updated Review***
Kai Chen, Qi Wang, Marko Kornmann, Xiaodong Tian and Yinmo Yang

105 **In Vivo *Efficacy and Toxicity of Curcumin Nanoparticles in Breast Cancer Treatment: A Systematic Review***
Alicia S. Ombredane, Vitória R. P. Silva, Laise R. Andrade, Willie O. Pinheiro, Mayara Simonelly, Jaqueline V. Oliveira, Andréia C. Pinheiro, Gabriel F. Gonçalves, Gisela J. Felice, Mônica P. Garcia, Patrícia M. Campos, Glécia V. S. Luz and Graziella A. Joanitti

123 ***Triggered Drug Release From Liposomes: Exploiting the Outer and Inner Tumor Environment***
Marina Santiago Franco, Eliza Rocha Gomes, Marjorie Coimbra Roque and Mônica Cristina Oliveira

146 ***Can Nimesulide Nanoparticles Be a Therapeutic Strategy for the Inhibition of the KRAS/PTEN Signaling Pathway in Pancreatic Cancer?***
Roseane Guimarães Ferreira, Luis Eduardo Mosquera Narvaez, Kaio Murilo Monteiro Espíndola, Amanda Caroline R. S. Rosario, Wenddy Graziela N. Lima and Marta Chagas Monteiro

frontiers in Oncology

EDITORIAL
published: 25 October 2021
doi: 10.3389/fonc.2021.788210

# Editorial: Nanomedicine in Cancer Targeting and Therapy

*João Paulo Figueiró Longo[1]*, Luis Alexandre Muehlmann[2], Marcelo Calderón[3,4], Christian Stockmann[5] and Ricardo Bentes Azevedo[1]*

*[1] Department of Genetics and Morphology, Institute of Biological Sciences, University of Brasília, Brasilia, Brazil, [2] Faculty of Ceilândia, University of Brasilia, Brasilia, Brazil, [3] POLYMAT, Applied Chemistry Department, Faculty of Chemistry, University of the Basque Country, Universidad del País Vasco/ Euskal Herriko Unibertsitatea (UPV/EHU), Donostia-San Sebastián, Spain, [4] IKERBASQUE, Basque Foundation for Science, Bilbao, Spain, [5] Institute of Anatomy, University of Zurich, Zurich, Switzerland*

**Keywords: nanomedicine, nanotecehnology, immunology, oncology, innovation**

**Editorial on the Research Topic**

**Nanomedicine in Cancer Targeting and Therapy**

OPEN ACCESS

***Edited and reviewed by:***
*Giuseppe Giaccone, Cornell University, United States*

****Correspondence:***
*João Paulo Figueiró Longo*
*jplongo82@gmail.com*

***Specialty section:***
*This article was submitted to Cancer Molecular Targets and Therapeutics, a section of the journal Frontiers in Oncology*

***Received:*** *01 October 2021*
***Accepted:*** *05 October 2021*
***Published:*** *25 October 2021*

***Citation:***
*Longo JPF, Muehlmann LA, Calderón M, Stockmann C and Azevedo RB (2021) Editorial: Nanomedicine in Cancer Targeting and Therapy. Front. Oncol. 11:788210. doi: 10.3389/fonc.2021.788210*

Nanomedicine is a scientific field that uses nanotechnology in the development of diagnostic and therapeutic solutions for medical purposes. The field emerged in the literature during the 1980s, when the first papers involving nanomedical applications were published (1, 2). A second important milestone was the launch, in the 1990s, of the first two pharmaceutical nanomedical products, Doxil®, and Myocet®, liposomes carrying chemotherapeutical drugs. These oncological applications were important in reducing the toxicity and improving the effectiveness of chemotherapy, thus improving the quality of life of thousands of people (3).

In addition, the most relevant recent application of nanomedicine has been in the development of COVID mRNA vaccines, which involved the use of lipid nanoparticles (**Figure 1**). Due to the instability of the RNA sequences, the use of lipid nanoparticles was a crucial step to keep the integrity of the oligonucleotides. It would be impossible to use these vaccines without the protection and stability conferred by these lipid nanoparticles (4). Indeed, due to the importance of the pandemic, and as these vaccines were applied to billions of people, we can say that it was the most impactful use of nanomedicine to date. Furthermore, these technologies have the potential to be used as new therapeutic platforms for other medical conditions, such as cancer and autoimmune disease, because other possibilities for their use are continuously under investigation (5, 6).

Within this historical context, we proposed this Research Topic to Frontiers in Oncology, aiming to invite authors to publish the most recent scientific and technological advances in the field of nanomedicine. After almost two years, we had received 25 article submissions, and 10 of them were accepted and included in our special issue "Nanomedicine in Cancer Targeting and Therapy". Five tfmkoriginal articles, six review articles, and one systematic review article were chosen for publication.

Among the original articles, one describes polymeric nanoparticles used to encapsulate gambogic acid, a phytochemical compound commonly used in Chinese medicine. As the main results, Kwan et al. showed the effectiveness of this nanocarrier against triple-negative breast cancer cells, in both

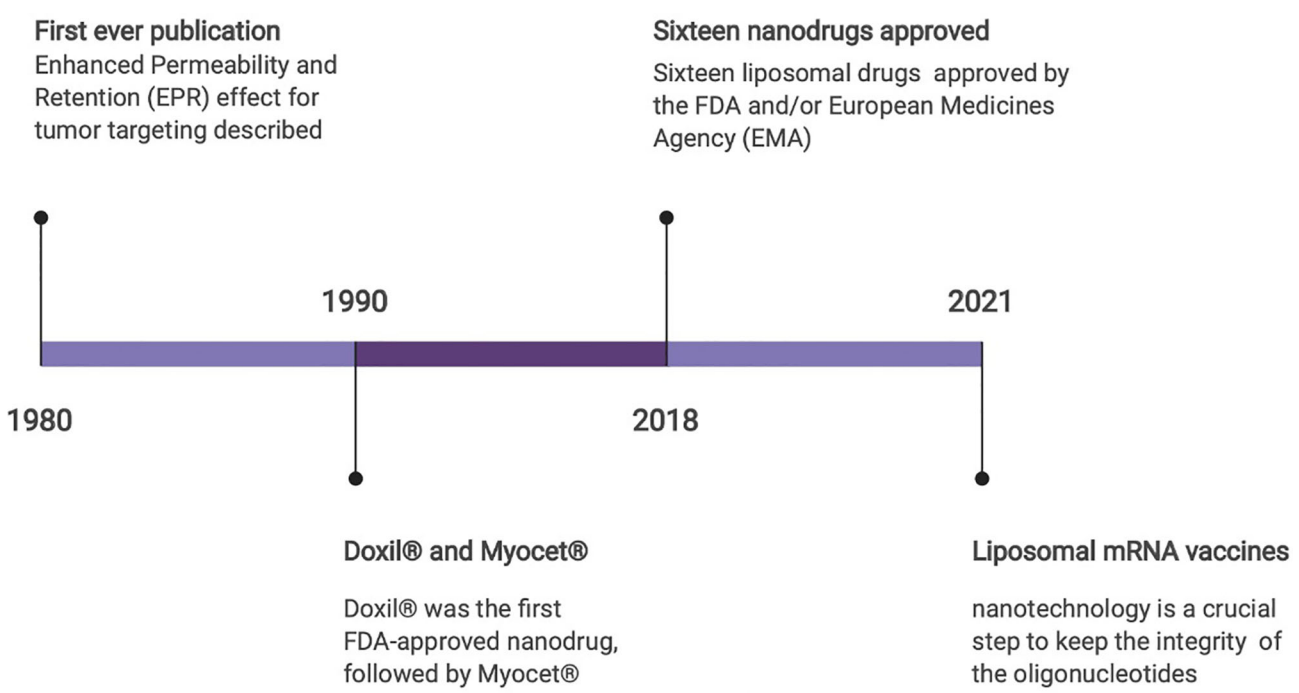


**FIGURE 1** | Nanomedicine milestones.

*in vitro* and *in vivo* models. Another original article describing a nanoformulation of natural products was published by Xu et al. The authors showed that *Ginkgo biloba* aqueous extract was a useful natural source to synthesize silver nanoparticles by a green method. The authors also showed that the prepared silver nanoparticles were able to induce apoptosis in cervical cancer cells. They suggested that these silver nanoparticles could be used as an alternative therapy for cervical cancer.

Still in the context of natural products, we received the submission of a systematic review published by Ombredane et al. In this article, the authors presented an important overview on the use of curcumin, a plant-derived molecule, in the treatment of breast cancer, and how nanoencapsulation could improve the effectiveness of this compound. This approach is interesting, because several plant-derived compounds have problems such as instability and/or solubility, issues that impair their use in biomedical applications.

Another important application of nanoparticles in medical applications is the ability to modulate the pharmacokinetics of small-molecule drugs. Two review articles discussed the ability of different types of nanocarriers to optimize the effect of two small-molecule drugs, methotrexate and nimesulide. Yu et al. presented some insights regarding the use of nanoparticles as drug delivery agents to target methotrexate for both cancer and rheumatoid arthritis. And Ferreira et al. discussed the use of nanotechnology to improve the efficacy of nimesulide as a repositioned drug for the treatment of pancreatic tumors, due to its anti-inflammatory properties.

The last original article presented here was published by Cui et al. In this report, the authors describe a novel PLGA nanoparticle coated with red blood cell membranes and decorated with two different peptides. The aim of this interesting surface modification was to improve the crossing of the blood-brain barrier, a property that was achieved as shown in mice models for glioma. The strategy of using biological membranes in nanomedicine was also the subject of two review articles available in this edition. These two reviews, published by Ma at al. and Chen et al., described the potential use of extracellular vesicles, or exosomes, as candidate nanosized drug carriers for cancer therapy. These natural vesicles were the inspiration for liposome development, and are basically composed of a phospholipid bilayer containing cholesterol and also proteins, an organization resembling that of cell membranes. As the main advantage in comparison to liposomes, these natural vesicles can overcome natural barriers and can circulate freely in the bloodstream. Moreover, the presence of specific proteins on the vesicle surface can address these exosomes to specific target tissues. Limiting issues regarding the industrial biotechnology production of these natural nanocarriers are also discussed in the two review articles.

Finally, we present two review articles discussing some innovative approaches in the nanomedical field. First, Franco et al. present some important issues related to the tumor environment that could be used to trigger the release of carried drugs in the tumor site. This is an interesting approach that has also been published by our research group. Finally, Javed et al. reviewed some important aspects of gene signaling by miRNA as

a potential therapy for colorectal cancer. The instability of nucleic acids requires the use of drug delivery systems, such as nanocarriers, that can protect and transport miRNA to target cells.

In conclusion, this special issue brings together a group of original and review articles addressing different aspects of nanomedicine. We believe that this published information can help to understand nanomedicine more deeply and to develop new therapeutic approaches for cancer. We are certain that all the high-quality information published in this issue is interesting both to researchers and to those interested in alternative cancer treatments using nanotechnological approaches.

## REFERENCES


1. Lammers T, Ferrari M. The Success of Nanomedicine. *Nano Today* (2020) 31:100853–4. doi: 10.1016/j.nantod.2020.100853
2. Figueiró Longo JP, Muehlmann LA. Nanomedicine Beyond Tumor Passive Targeting: What Next? *Nanomedicine* (2020) 15:19. doi: 10.2217/nnm-2020-0208
3. Metselaar JM, Lammers T. Challenges in Nanomedicine Clinical Translation. *Drug delivery Trans Res* (2020) 10:3. doi: 10.1007/s13346-020-00740-5
4. Figueiró Longo JP, Muehlmann LA. How has Nanomedical Innovation Contributed to the COVID-19 Vaccine Development? *Nanomedicine* (2021) 16:14. doi: 10.2217/nnm-2021-0035
5. Adams D, Gonzalez-Duarte A, O'Riordan WD, Yang CC, Ueda M, Kristen AV, et al. Patisiran, an RNAi Therapeutic, for Hereditary Transthyretin Amyloidosis. *N Engl J Med* (2018) 379:1. doi: 10.1056/NEJMoa1716153
6. Bordon Y. An RNA Vaccine for Advanced Melanoma. *Nat Rev Immunol* (2020) 20:9. doi: 10.1038/s41586-020-2537-9


## AUTHOR CONTRIBUTIONS

JL – discuss the editorial content and prepared the first version of the editorial. LM, MC, CS and RA - discuss the editorial content and revised the final editorial text. All authors contributed to the article and approved the submitted version.

## ACKNOWLEDGMENTS

We thank Msc Camila Magalhães Cardador for the editorial figure preparation, and Mr Gabriel Longo Ferreira for the cover art of this Research Topic Edition.

**Conflict of Interest:** The authors declare that the research was conducted in the absence of any commercial or financial relationships that could be construed as a potential conflict of interest.

frontiers in Oncology

REVIEW
published: 16 September 2020
doi: 10.3389/fonc.2020.01734

# Polymeric Nanoscale Drug Carriers Mediate the Delivery of Methotrexate for Developing Therapeutic Interventions Against Cancer and Rheumatoid Arthritis

*Wen-Jun Yu*[1]*, *Dong-Xu Huang*[1], *Shuang Liu*[2], *Ying-Li Sha*[3], *Feng-hui Gao*[4] and *Hong Liu*[5]

[1] The Eastern Division, Department of Hand and Foot Surgery, The First Hospital of Jilin University, Changchun, China, [2] The Eastern Division, Department of Nursing Management, The First Hospital of Jilin University, Changchun, China, [3] The Eastern Division, Department of Pediatrics, The First Hospital of Jilin University, Changchun, China, [4] The Eastern Division, Department of Orthopaedics, The First Hospital of Jilin University, Changchun, China, [5] The Eastern Division, Department of Otolaryngology, The First Hospital of Jilin University, Changchun, China

Methotrexate (MTX) is widely used as an anticancer and anti-inflammtory drug for treating various types of cancer and autoimmune diseases. The optimal dose of MTX is known to inhibit the dihydrofolatereductase that hinders the replication of purines. The nanobiomedicine has been extensively explored in the past decade to develop myriad functional nanostructures to facilitate the delivery of therapeutic agents for various medical applications. This review is focused on understanding the design and development of MTX-loaded nanoparticles alongside the inclusion of recent findings for the treatment of cancers. In this paper, we have made a coordinated effort to show the potential of novel drug delivery systems by achieving effective and target-specific delivery of methotrexate.

**Keywords: methotrexate, cancer, liposomes, LPHNPs, NLCs**

OPEN ACCESS

***Edited by:***
*Luis Alexandre Muehlmann, University of Brasilia, Brazil*

***Reviewed by:***
*Sandeep Mittal, University of Texas MD Anderson Cancer Center, United States*
*Fong-Yu Cheng, Chinese Culture University, Taiwan*

***Correspondence:**
*Wen-Jun Yu*
*wen567jy@aliyun.com*

***Specialty section:***
*This article was submitted to Cancer Molecular Targets and Therapeutics, a section of the journal Frontiers in Oncology*

***Received:*** *26 May 2020*
***Accepted:*** *03 August 2020*
***Published:*** *16 September 2020*

***Citation:***
*Yu W-J, Huang D-X, Liu S, Sha Y-L, Gao F-h and Liu H (2020) Polymeric Nanoscale Drug Carriers Mediate the Delivery of Methotrexate for Developing Therapeutic Interventions Against Cancer and Rheumatoid Arthritis. Front. Oncol. 10:1734. doi: 10.3389/fonc.2020.01734*

## INTRODUCTION

The aim of achieving the utmost therapeutic efficacy with the fewest drug hazards is always a priority for any pharmaceutical researcher. The available therapeutic options, such as chemotherapy and radiotherapy, need skilled personnel to lead to better results from the target-specificity of the drug(s) in question. The traditional drug delivery systems earned popularity due to their economic, simple, and user-friendly approach, but recently developed specific drug-delivery systems, such as lipid-polymer hybrid nanoparticles (1), have drawn attention due to their target-specificity, effectiveness, and fewer adverse effects.

Methotrexate (MTX) (also known as amethoptrein; MW: 454 g/mol) is a widely used drug for multiple medical conditions, such as psoriasis, rheumatoid arthritis (RA), and cancer (2). This drug is also approved for the treatment of Crohn's disease by the U.S. Foog and Drug Administration (3). MTX (2,4-diamino-N10-methyl propylglutamic acid) was first synthesized by Seeger et al. nearly 65 years ago (4). Its structure encompasses three parts: (1) a pteridine ring, (2) p-aminobenzoic acid, and (3) glutamic acid (4). It is a weak, pH-dependent bicarboxylic acid having pKa values of 3.8, 4.8, and 5.6 with low permeability ($\log p = 0.53$) (5). It is heat- and light-sensitive and degrades upon exposure, and its solubility in distilled water at 20°C is 0.01 mg/ml; suitable pH for MTX falls in the range of 6.6–8.2 (6).

Methotrexate blocks the activity of the dihydrofolatereductase (DHFR) enzyme and leads to the inhibition of DNA synthesis at higher dosages (2). MTX is not considered to be an antiproliferative agent in the inflammatory joints during RA pathology. However, lower dosages of MTX and its discontinuation show an anti-inflammatory effect of MTX (4). MTX-mediated inhibition of DHFR and other folate-dependent enzymes leads to the overproduction of adenosine, which drives immunosuppression (7). Despite initial obstacles to the use of novel drug-delivery systems (NDDS), the nanotechnology helps in achieving maximum drug therapeutics. Nanotechnology is seen as a promising strategy for the treatment of various medical conditions by active and passive targeting (8). The effectiveness of treatment is associated with the ability of a drug to target and affect the biological functions of ailing cells, leaving minimal damage to healthy tissues (8). Nanoparticles take advantage of unique characteristics, such as the enhanced permeation and retention (EPR) effect, a large surface-to-volume ratio, extended residence time in circulation, biodegradability, low toxicity, and small size in the range of 10–500 nm, thus conferring sustained and targeted drug delivery (9, 10). Efforts have been made to develop nanodrug delivery vehicles, including polymeric nanoparticles (PNPs) (11), lipid-polymer hybrid nanoparticles (LPHNPs) (12), nanostructured lipid carriers (NLCs) (13), solid lipid nanoparticles (SLNs) (14), and liposomes (15) for the controlled and targeted delivery of MTX. This paper reviews the development of surface-engineered, lipid-based nanocarriers (SLNs and LPHNPs), which are proposed to improve the delivery of drugs.

In the end, this review has been designed to explore the applications of MTX in different clinical settings with cancer. We discuss the role of NDDS to find out the solutions by improvising the treatment strategies. We believe this review is a compilation of our concerted efforts to cover all aspects and dimensions of drug delivery.

**Abbreviations:** MTX, Methotrexate; MW, Molecular weight; RA, Rheumatoid arthritis; DHFR, Dihydrofolatereductase; NDDS, Novel drug delivery systems; NPs, Polymeric nanoparticles; LPHNPs, Lipid polymer hybrid nanoparticles; NLCs, Nanostructured lipid carrier; SLNs, Solid lipid nanoparticles; HPLC, High performance liquid chromatography; FPI, Fluorescence polarization immunoassay; IV, Intravenous; SC, subcutaneous; IM, Intramuscular; CNS, Central nervous system; CSF, Cerebrospinal fluid; PLGA, Polylactic-co-glycolic acid; PLA, Poly lactic acid; PGA, Poly glumatic acid; PEG, Polyethylene glycol; EPR, Enhanced permeability and retention time; ATIC, 5-aminoimidazole-4-carboxamide ribonucleotide (AICAR) transformylase; PC, Phosphatidylcholine; AUC, Area under the curve; EE, Entrapment efficiency; GVHD, Graft versus host disease; aGVHD, acute graft versus host disease; cGVHD, Chronic graft versus host disease; ACE, Acelofenac; MTT, 3-(4,5-Dimethylthiazol-2-yl)-2,5-Diphenyltetrazolium Bromide; BC, Beta carotene; DMBA, 7,12-Dimethylbenzathracene; RF, Rheumatoid factor; ACAP, Anti-citrullinated peptide antibodies; AUR, American college of Rheumatology; EULAR, European League Against Rheumatism; csDMARD, Conventional synthetic diseases-modifying antirheumatic drugs; bDMARD, Biological DMARD; HA; Hyaluronic acid; FA, Folic acid; AIA, Adjuvant induced arthritis; siRNA, Small interfering RNA; APCs, Antigen presenting cells; LFA, Lymphocyte functional antigen; Th cells, T helper cells; PASI 75, Psoriasis area and severity index; SUV, Small unilamellar vesicles; LUV, Large unilamellar vesicles; MLV, Multilammellar vesicles; OA, Oleic acid; NIPAM, N-isopropylacrylamide; $PEG_2$, Prostaglandin E2; GFLG, Glycine-phenylalanine-leucine-glycine; GILGVP, Glycine-isoleucine-leucine-glycine-valine-proline; HCT, Hematopoietic cell transplantation; BSA, Body surface area; GM-CSF, Granulocyte-macrophage colony-stimulating factor; ABCC, ATP-binding cassette proteins.

## MECHANISM OF ACTION OF MTX AND CLINICAL PHARMACOLOGY

### Clinical Pharmacodynamic

MTX inhibits the DHFR enzyme, which is required to reduce dihydrofolates to tetrahydrofolates before they are utilized as carbon carriers during purine nucleotide synthesis. Therefore, MTX hinders the synthesis, repair, and cellular replication of DNA (16). In addition to the abovementioned action for the clinical efficacy of MTX, several other interlinked biochemical mechanisms are involved, substantiating its usefulness in the treatment of other diseases, such as neoplastic diseases, psoriasis, and adult RA (7). MTX is more sensitive to actively proliferating cells, such as malignant cells, fetal cells, bone marrow, buccal and intestinal mucosa, and urinary bladder cells (2). MTX impairs malignant growth without irreversible damage to the normal tissues during cellular proliferation in which malignant tissues outgrow the normal tissues. The wider range of applications and selective action of MTX proves it to be an efficacious therapeutic drug (3, 4), and therefore, its pharmacology is extensively studied (13).

### Clinical Pharmacokinetics

The pharmacokinetics of MTX were performed by various techniques (bacteriological assay followed by fluorometric assay). Currently, it is mainly measured in biological fluids by high-performance liquid chromatography or fluorescence polarization immunoassay (FPI) (2). Currently, FPI is in use for the measurement of plasma concentration when a high dose of MTX ($>$ 1 g/m$^2$) with the low limit quantitation (0.02 $\mu$M or 9 $\mu$g/l) is employed. The bioavailability of MTX delivered through different routes of administration is accounted and described below:

#### Oral Absorption

A high dose ($\leq$ 25 mg) of MTX is generally administered through the oral route in a week. This was found to be dose-dependent, incomplete, and highly variable (absolute bioavailability range: 13% $-$ 76%) (17). It has been observed that oral absorption is better at a dose of $<$40 mg/m$^2$ (median bioavailability: 42%), and for dosage more than 40 mg (median bioavailability: 18%), use of the intravenous (IV) route is generally recommended. Moreover, oral administration of MTX (7.5 mg) is not influenced by food in healthy volunteers (17).

#### Subcutaneous (SC) Absorption

This is an alternative to the oral route as the drug is completely absorbed (MTX; 40 mg/m$^2$) compared to that seen with the IV route when injecting in acute lymphoblastic leukemia children. $C_{max}$ was found to be 7.4 and 1.4 $\mu$M for subcutaneous and intravenous routes, respectively (18).

### Intramuscular (IM) Absorption

This is an alternative to the oral route for achieving low-dose administration. The bioavailability of MTX when delivered through the IM route is found to be 76%, which falls in the range between the SC and oral routes (17). Further, it is also used off-label in the treatment of tubal ectopic pregnancy. It is administered as a 1 mg/kg or 50 mg/m$^2$ formulation in a single- or multiple-dose regimen (19).

### Intrathecal Absorption

This is used in some local treatment of hematological disease via systemic diffusion of MTX after regional administration at very low doses (6–15 mg) (20).

### Distribution

Approximately 46% of MTX binds to human serum albumin. It is given as a prophylactic or curative treatment via the intrathecal route in combination with systemic treatment with a fixed dosage between 6 and 15 mg depending upon age (20). Generally, it is administered at higher IV dosage during primary or secondary CNS treatment. The penetration of the drug into the cerebrospinal fluid is less but clinically sufficient, and it does not depend on the administered dose (2 or 5 g/m$^2$) (21).

### Metabolism and Elimination

MTX is rapidly eliminated from the human body through the renal route (90% of an intravenously injected dose is excreted in 24 h and 95% in 30 h) after being metabolized into 7-hydroxy MTX. The aldehyde oxidase mediates the biotransformation, and the metabolite is found in blood, urine, and bile due to partial intestinal reabsorption; 1–2% of the drug is also found in stool samples of patients having an intravenously administered dose in the form of the parent drug and metabolites. It is known to have a terminal half-life of 8–15 h (22). The derivatives of MTX include 7-hydroxy MTX and 2,4-diamino-N10-methylpetroic acid, which have a similar half-life of 10.2 and 9 h, respectively. Once it enters the body, irrespective of the route, mean clearance is found to be 50–135 ml/min/m$^2$ (23). In a study of leukemic children receiving 1 g/m$^2$ MTX, a similar pattern of clearance was observed for 1–24 h (11 and 123 ml/min/m$^2$, respectively).

Recently, various molecular determinants of MTX (drug metabolizing enzymes, transporter) have been discovered, and they are involved in the pharmacokinetic process to prevent drug interactions and understand their disposition. The membrane transporters OATP1B1, OATP1B3, MRP2, MRP3, MRP4, BCRP, and RFC regulate hepatic clearance, whereas OAT1, OAT3, MRP2, MRP4, BCRP, and RFC are involved in renal elimination (2).

## RATIONALE OF USING MTX-LOADED DELIVERY SYSTEM

Despite being a widely used drug for the treatment of tumors and autoimmune disorders, the suboptimal pharmacological response of MTX limits its use (4).

## Adverse Effects of MTX

The commonly noticed adverse effects of MTX are vomiting, nausea, anemia, diarrhea, dermatitis, bruising, hepatitis, pulmonary fibrosis, and bone marrow depression (4). MTX produces dose- and duration-dependent teratogenicity (24). MTX is not recommended for pregnant and breast-feeding women as it causes severe fetal defects, mainly neural tube defects (25), because of its teratogenic nature. Also, it affects the process of spermatogenesis, altering male fertility and producing congenital defects at 6–8 week of gestation (26). MTX could be iatrogenic because four cases of medical malpractice were reported in China due to overdose of MTX, including 10 (two cases), 15 (one case), and 20 mg (one case) per day rather than the weekly recommended dosage, and they led to mucositis and death (27). High and low doses of MTX may cause severe complications: a high dose (>1 g/m$^2$) of MTX may result in kidney injury due to the crystallization of drugs or their derivatives inside the nephrons, prompting delays in renal elimination and rendering systemic toxicity (28). The delayed elimination has resulted in ≥grade 2 nephrotoxicity in 1.8 and 9.1% of osteosarcoma and lymphoma (elder) patients, respectively (2). There could be interindividual variability between 30 and 90% in peak levels, duration to achieve peak time, dose absorbance rate, and area under the serum concentration–time curve (29). MTX dose also plays a crucial role in the bioavailability of MTX as the higher dose is quickly eliminated by the kidneys, thus conferring its short half-life (5–8 h). Moreover, target specificity and drug efficacy are issues faced due to the administration of lower doses (4). The pharmacokinetics of MTX mainly depend on the route of administration when measuring the level of MTX in CSF and blood in rats. The low plasma levels in intranasally administered animals were comparable to those seen with the intravenous route, and greater MTX concentration was quantified in animals administered the drug through the intranasal route compared to the intravenous route (30). MTX was injected in a rodent animal model through transcutaneous puncture at the level of the cisterna magna, and it shows the cognitive and neurotoxic effects. In spite of the reduction seen in the folate levels in CSF and serum, a higher amount of homocystine was quantified, which supports the intrathecal delivery of MTX (31). Choudhary et al. administered MTX by the intraperitoneal route in mouse bone marrow with three different dosages (2, 10, and 20 mg/kg). It was found to be brutally effective in male mice compared to female mice. The intermediate dose of 10 mg/kg was found to be effective out of the concentrations tested (32). The use of implantable calcium phosphate systems in rabbits showed the extended release of MTX due to its adsorption on deficient apatite and favors enhanced antirheumatic activity (33).

## Targeted and Controlled Drug Delivery System

The difference in $t_{1/2}$ needs a continuous dose of MTX to achieve optimal bioactivity within its therapeutic range as its cytotoxicity directly depends upon the mean residence time in plasma (3). For the controlled release of the drug, an encapsulated lipid-based

delivery system was developed for cutaneous administration of MTX, and it enhanced plasma $t_{1/2}$ from 0.53–100 h (190 times), and lowered $C_{max}$ (120 times) with 130 times higher efficacy against L1210 leukemia cells (34) was estimated. Likewise, with intracavitary administration, $t_{1/2}$ was reached in 39.6 h (encapsulated MTX) from 0.5 (unencapsulated MTX), and another lipid-based formulation injected via the intracisternal route was increased up to 5.4 days (encapsulated) from 0.30 (unencapsulated) (3). In addition, chitosan microspheres (35) and water-in-oil microemulsion (36) delivered MTX within the therapeutic range, and the inhibition of tumor growth was observed by extending apoptosis.

Therefore, the route of MTX may be an alternative approach, but the patient specificity might not work for all patients. The cause of side effects still exists irrespective of the route of drug administration. The controlled and targeted delivery approaches may have overcome the repetitive administration of MTX, but none of them are target-specific. Recently, many studies have been carried out to overcome the limitations of different NDDS. These NDDS provide better results in terms of safety, efficacy, target-specificity, improved bioavailability, and sustained drug release with higher stability of the therapeutic effect against various biochemical mechanisms. We discuss various drug delivery systems employed in cancer, RA, and psoriasis for MTX therapeutics.

## Role of MTX in Cancer Therapeutics

### Pathophysiology of Cancer

Cancer is the second leading cause of death around the globe (37), and according to global cancer statistics in 2018 (GLOBOCAN), there are 18.1 million new cancer cases with a death toll of 9.6 million (excluding data on non-melanoma skin cancer). Lung cancer is the most commonly diagnosed type of cancer (11.6% of the total) and the leading cause of cancer death (18.4% of total deaths) followed by female breast cancer (11.6%) (by combining both genders) (38). Cancer occurs due to interruption in the routine signal transduction mechanism mediated by a normal cell, and more than 277 types of cancers are diagnosed (37). It is mainly afflicted due to the specific DNA damage mediating several mechanisms, such as activation of proto-oncogenes by translocation or by point mutation and inactivation of a gene resulting in tumor formation (39). Chemical compounds also play a role in gene mutation, including smoking and environmental chemical substances (directly/indirectly influence the cytoplasm and nucleus and leads to the gene defect/disorder/mutation) (37). There are other carcinogenic factors, such as bacteria, viruses, and radiation responsible for around 7% of total cancers (40). Cancer disturbs the cellular mechanism and, thus, leads to inappropriate function of a gene, affecting the cell cycle and abnormal proliferation. Proto-oncogenes responsible for cell growth and division are converted into oncogenes during the mutation, disrupting the entire process. The tumor suppressor genes mediate uncontrolled cell division (37). DNA methylation, histone modification, and nucleosome position are some of the epigenetic factors playing an important role during cancer (41). The detailed mechanism of cancer at the molecular level has been reviewed (37, 42).

### Underlying Mechanism of MTX Action in Cancer (Pharmacodynamic)

MTX is considered to be the "targeted" therapy in oncology since its development. Moreover, it was first used in acute lymphoblastic leukemia for its known character of the folate pathway–dependent antimetabolite drug aminoptrein (43). Ironically, it was starting to be used in clinical trials by 1953, but its intracellular targets and DHFR were discovered later (2). This is the first drug used as a single-agent therapy to cure cancer (44) and was used to treat types of cancer, such as leukemia, non-Hodgkin's lymphoma, breast cancer, head and neck cancer, stomach cancer, bladder cancer, bone cancer, and choriocarcinoma (a type of uterine cancer) (2). The oncologic mechanism plays a part in inhibition of purine synthesis, and it stops the cell cycle process in the S phase, subsequently leading to cell apoptosis (7). The mechanism of MTX as a folate antagonist has been considered as a main action in oncology. It acts as an antifolate agent, wherein folates are the building blocks that maintain cell growth (2). The cellular uptake of MTX mediated by the folate receptor group of proteins and their mechanism is described in the later section on RA. MTX mainly blocks the activity of enzyme 5-aminoimidazole-4-carboxamide *ribonu*cleotide (AICAR) transformylase (ATIC) and inhibits the activity of DHFR, an enzyme responsible for catalyzing dihydrofolate (DHF) to tetrahydroflate (THF). The end product of this reaction inhibits the synthesis of thymidylate synthetase (TYMS), which plays a vital role during the synthesis of thymidine residues (7). It has been observed that it reduces the level of both the purine and pyrimidine pool in human T cells together by increasing the level of UTP and decreasing the level of ATP and GTP. It restrains T cell proliferation and enhances apoptosis (7).

### Nanocarriers for the Effective Delivery of MTX in Cancer Therapeutics

The carrier is one of the most important entities essentially required for the successful transportation of loaded drug(s). The carrier systems are capable of doing so by either inherent or acquired (through structural modification) characteristics to interact selectively with biological targets, or they are engineered to release the drug in close proximity to the target cells *in vitro*, requiring optimal pharmacological action (therapeutic index) (45). Various potential drug delivery carriers and their structure are shown in **Figure 1** (46).

#### *Polymeric Nanocarriers (PNPs)*

Polymeric nanoparticles, polymeric micelles, and dendrimers are the commonly used nanocarriers for the delivery of bioactives (47). PNPs are a type of colloidal drug-delivery system in which the active drug is reduced to the nano-size range (10–1,000 nm), and biodegradable or non-biodegradable polymers are used for the sustained release of the drug (48). Nowadays, biodegradable polymers are used as they are compatible with the body, and no harmful products are formed upon their degradation.

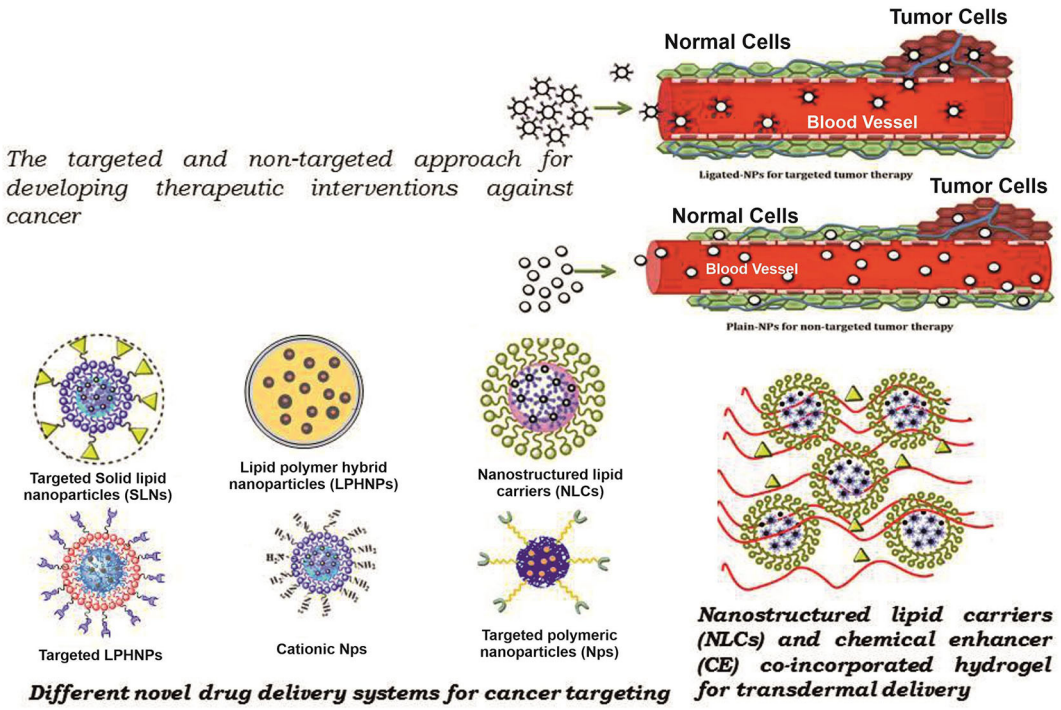


**FIGURE 1 |** Diagramatic illustration of various potential drug delivery carriers and their structures.

Synthetic [polylactic-co-glycolic acid (PLGA), poly(lactic acid) particles (PLA), poly glutamic acid (PGA)] and natural (collagen, chitosan, gelatin) polymers are used in the formulation of PNPs (49). Solvent evaporation, nano-precipitation, emulsification, dialysis, spray drying, salting out, freeze-drying, etc., are commonly used methods for the preparation of PNPs (50).

All polymeric nanoparticle–mediated delivery systems for methotrexate that show an improved drug efficacy for crossing the blood–brain barrier and therapeutic efficacy against brain cancer (11) (**Figure 2**). However, difficulty in scaling up and understudied toxicological studies limits their use and poses challenges to their use as potentially effective novel scale drug carriers (**Table 1**).

Polymeric micelles are an impressive drug delivery system for poorly water-soluble drugs consisting of hydrophilic polyethylene glycol (PEG) with the particle size range of 10–100 nm, exhibiting EPR and enhanced drug accumulation at the target site (51). Additionally, a computational approach helps in the tailored design of an improved micelles system for multiple drugs in cancer therapy (52). Chen et al. prepared the pluronic-based polymeric mixed micelle (F127/P105-MTX) and compared it with a conventional MTX-loaded polymeric micelle against the overly expressed folate receptor tumor cells *in vitro* (KBv cells) and *in vivo* (KBv tumor-bearing mice). F127/P105-MTX showed the higher (1.36-fold) cellular uptake compared to the conventional conjugate micelle in KBv cells and enhanced antitumor efficacy (53). This result indicates that it could be a possible safe and effective nano-drug delivery system for folate receptor–rich cancer therapy. The hydrophobic core, which is mostly a non-degradable polymer, such as polyacrylamide or polyacrylate, is a concern. Therefore, recently, a bioreducible cross-linked core polymer methoxypoly(ethyleneglycol)-*b*-poly(ε-caprolactone-*co*-α-azido-ε-caprolactone) (mPEG-*b*-poly(ε-CL-*co*-α$N_3$εCL)) has been used, and this MTX-loaded core cross-linked micelle was assessed in human breast cancer MCF-7 cells (54). The sustained drug release (76% present inside the cross-linked micelle after 96 h at 37°C in PBS as compared to 90% drug was seen released in the un-cross-linked one) localization at the targeted site (94% uptake without affecting its entry), no toxicity, and significant higher cell death occurred via apoptosis, which make the core cross-linked micelles an emerging and attractive drug delivery system. However, drug release under a reducing environment and further validation through *in vivo* experiments are required (54). Similarly, a novel micelle poly (2-hydroxyethyl methacrylate-Lactide-dimethylaminoethyl methacrylate quaternary ammonium alkyl halide) [P(HEMA-LA-MADQUAT)] was developed for the codelivery of two different anticancer drugs; MTX and chrysin, assessed in MCF-7. Based on cytotoxicity assays, enhanced anticancer activity and suitability as a nanocarrier delivery system showed its importance for use as an anticancer codelivery system for *in vivo* studies followed by clinical trials (55).

To enhance the cellular uptake at the tumor site together with sustained drug release, the novel approach of surface functionalization and changes in the shape of the nanoparticles is proposed as elongated nanoparticles are reported to achieve better drug-delivery efficacy compared to spherical ones (56).

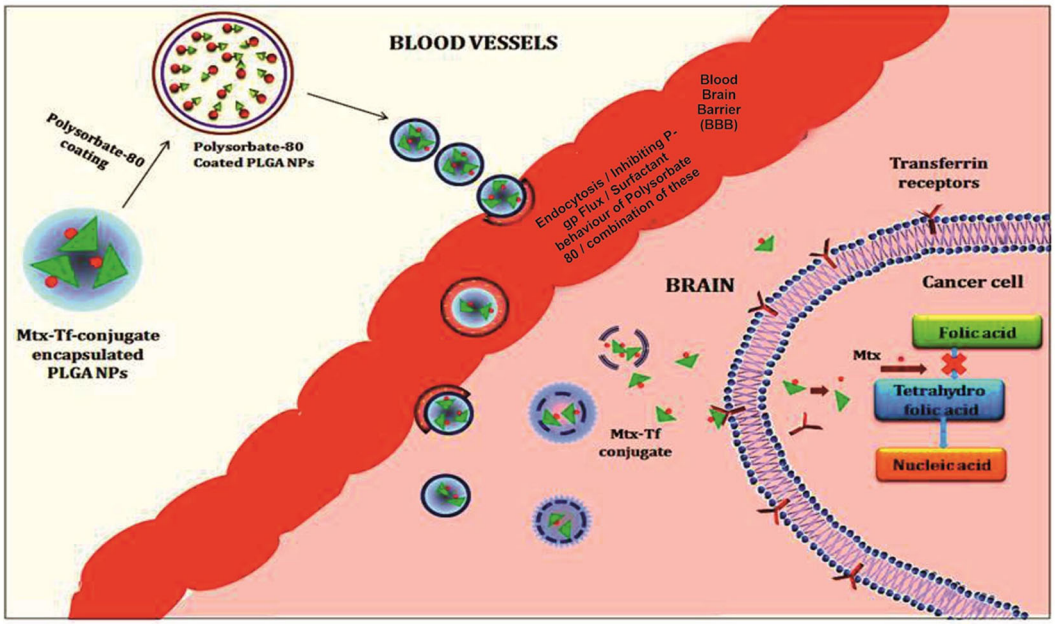


**FIGURE 2 |** Illustration of the polymeric nanoparticles mediated delivery of methotrexate showing an improved drug efficacy for crossing the blood brain barriers and therapeutic efficacy against brain cancer.

**TABLE 1 |** The advantages and limitations of various nano delivery systems.

| S. no. | Nano-delivery systems | Advantages | Limitation |
|---|---|---|---|
| 1. | Polymeric Nanocarriers | • Improved drug efficacy for crossing the blood–brain barrier<br>• Therapeutic efficacy against brain cancer | • Difficulty in scaling up<br>• Understudied toxicological studies only for lipophilic drugs<br>• Low drug-loading efficiency, Dependency on the concentration of micelle |
| 2. | Dendrimers | • Higher stability<br>• Sustained drug releases | • Poor carrier capacity<br>• Rendered cellular cytotoxicity<br>• Elimination and metabolism depending on the generation and materials and high cost of synthesis |
| 3. | Liposomes | • Surpass the limitation of site-specific oral chemotherapy with the reduced the side effects,<br>• Lower doses need *in vivo* validation | • Require a high production cost<br>• Leakage and fusion of encapsulated drugs<br>• May undergo oxidation and hydrolysis<br>• Shorter half-life and lower solubility |
| 4. | Solid lipid Nanoparticles | • Increase drug stability<br>• Sustained release of drugs<br>• Less toxicity due to the absence of organic solvents, biodegradable, feasible for both kind of drugs<br>• Easy at handling regulatory affairs | • Low drug-loading capacities<br>• Presence of alternative colloidal structures<br>• Complexity of the physical state of the lipid<br>• Possibility of super cooled melts which cause stability issues |
| 5. | Nanostructured Lipid carriers | • Physical stability<br>• Improved drug entrapment and loading efficiencies<br>• Bioavailability and drug release modulation | • Presence of organic solvent residue<br>• Uneven distribution<br>• Complex production process<br>• Poor stability |
| 6. | Lipid polymer hybrid nanoparticles | • Better drug entrapment<br>• Controlled and sustained drug release<br>• Great *in vitro* and *in vivo* stability | |

Lin et al. used their own previously synthesized PNPs to make functionalized MPEG-PLA-MTX-Cy5.5 nanobacillus by a self-assembly technique in addition to the extrusion-induced transition for local drug delivery at the tumor site (56). The *in vivo* ($H_{22}$ tumor bearing mice) result delineates that intratumorally injected MPEG-PLA-MTX-Cy5.5 showed better target-specific intracellular localization in addition to effective antitumor activity compared to the free MTX and other MPEG-PLA PNP core without drugs. These formulated NPs were employed for conducting *in vivo* fluorescence imaging (56).

This novel approach to a delivery system indicates its use for local and tumor-specific cancer therapy without harming the normal tissues, and therefore, it may become a promising delivery system for target-specific cancer treatment. The use of polymeric micelles only for lipophilic drugs, low drug-loading efficiency, and dependency on the concentration of micelle concentration of these carriers are a few obvious limitations. These limitations need to be addressed prior to licensing these carriers for effective delivery of drugs to strategize a treatment strategy against cancer or autoimmune diseases (**Table 1**).

Dendrimers, are small-sized denritic polymers, a well-organized 3-D structure having a symmetric core and an inner and outer shell, that maintains its structure, density, and function of the surface (57). They have been in use for drug delivery and gene therapy, including other biomedical and translational applications, to study various parameters related to pharmacokinetics and drug delivery systems (58) because they may be used for both hydrophilic and hydrophobic drugs delivered through different routes of administration (59). Kong et al. prepared MTX complexes of classic poly amidoamine (PAMAM) and PEGylated (PAMAM-PEG) dendrimer and administered the formulation in tumor-bearing mice through the intravenous route of administration. The plasma half-lives and mean retention times of MTX complexes were estimated to be higher than MTX with higher antitumor activity (60). Advancement of technologies allowed the deployment of different types of MTX-conjugated dendrimers prepared through various linkages to enhance the antitumor activity (4). Dongen et al. show the binding mechanism of generation 5 (G5) monomer (G5) & dimer (G5-G5) PAMAM-MTX dendrimers with folate-binding protein (61). To address the issue of drug retention, the approach of a dendrimer-conjugated drug with a linker was used by reducing the length of the linkers to make the MTX conjugates (200 Da PEG chain) compared with larger linker conjugates of (GFLG) 450 Da & (GILGVP) 650 Da (62). The smaller length of the linker resulted in less exposure of MTX present in the dendrimer core of PEG and increased bioavailability and transport. These results indicate the potential use of a subcutaneous route for targeted drug delivery specifically for lymphatic sites. Recently, novel dendrimers of MTX (MTX/PGD) were prepared with a co-dendrimer from PAMAM and oligoethylene glycol (OEG) dendrimers to assist in the antitumor efficacy *in vitro* (MCF-7 & 4T1 cells) and *in vivo* (4T1 breast tumor model of BALB/c mice) (63). Significant results in both conditions (cell cytotoxicty $IC_{50}$ after 48 h for MCF-7 and 4T1 was 7.5- and 8-fold higher in MTX/PGD compared to the free MTX) show the potential of MTX/PGD as a promising nanoparticle system with higher stability and sustained drug release due to its highly branched structure and effective biocompatibility (63). Recently, current status in the development of dendrimer-based nanomedicine has been reviewed (64). The poor carrier capacity of dendrimers, rendered cellular cytotoxicity, elimination and metabolism depending on the generation and materials, and high cost of synthesis are obvious limitations of dendrimers (**Table 1**).

### *Liposomes*

Liposomes are artificially prepared spherical vesicles that are composed of a phospholipid bilayer in which cholesterol is usually added to confer stability to the lipid bilayer for optimum drug release (65). Liposomes are composed of one or more lipid bilayers and categorized as small unilamellar vesicles (SUV), large unilamellar vesicles (LUV), and multilamellar vesicles (MLV) (66) based on their size and number. They are versatile as they may deliver both hydrophilic and lipophilic therapeutic agents (67, 68). Moreover, targeting can be achieved by anchoring ligands on the surface of the liposomes that are specific to a particular cell type. The choice of phospholipids used during the preparation of liposomes largely depends upon the desired rigidity and permeability (65, 69).

The poor water solubility of MTX and good lipophilic properties of liposomes establish their use for its effective delivery (3, 4). Despite the advantages of the liposomal drug delivery system, the foremost goal of NDDS is to improve the bioavailability of the therapeutic agents and reduce the side effects by enhancing the pharmacokinetic and pharmacodynamic properties (68).

The interest in local targeted drug delivery systems gained attention as muco-adhesive patches of MTX-loaded liposomes (MTX-L) were prepared by the thin film hydration method using phosphatidylcholines (PC) and cholesterol (70) for targeted delivery in oral cancer to circumvent side effects of conventional methods, including chemotherapy, radiation, and surgical excision. MTX-L was cast in muco-adhesive film by using different polymers, such as hydroxyethyl cellulose (HEC), PVA, PEG, and chitosan (CH), and assessed for their parameters, including thickness, weight, percentage swelling index, sustained drug release, and pattern (70). An *in vitro* cell viability assay confirmed the significant cell death measured by $IC_{50}$ was 180 μg/mL (free MTX) and 75 μg/mL (MTX-LP-F7, different mucoadhesive buccal films with different concentrations of polymer). In conclusion, the liposomes prepared for oral delivery by using different polymers may have the advantage for sustained drug release with increased bioavailability. The MTX patches can surpass the limitation of site-specific oral chemotherapy with the reduced side effects and lower doses needing *in vivo* validation. Of late, the role of surface functionalization and different targeting strategies for the liposomal drug delivery system in solid tumors have been extensively studied (71). Despite the abovementioned advantages, following are the limitations of liposomes as nanodrug delivery vehicles (**Table 1**):

a) Liposome-encapsulated drugs require a high production cost.
b) Liposomes may have leakage and fusion of encapsulated drugs.
c) The liposome phospholipid may undergo oxidation and hydrolysis.
d) Liposomes have a shorter half-life and lower solubility.

### *Solid Lipid Nanoparticles (SLNs)*

The different issues related to drug delivery, regulatory affairs, and the availability of cheaper liposomal formulation are some of the concerns related to the development of an

advanced nanoparticle, resulting in the formulation of first-generation nanoparticles. These nanoparticles prepared using solid phase lipids and surfactants are famously termed "solid lipid nanoparticles" (72). The solid lipid remains in its intact form at body and ambient temperatures, whereas surfactants are used as an emulsifier in the range of 0.5–5% to confer stability (72, 73). Among the methods used for the preparation of SLNs, commonly used methods are high-pressure homogenization; high-shear homogenization; and ultrasound, hot/cold homogenization, solvent evaporation, spray drying and emulsification (72, 74). The drug load in SLNs is dependent upon the solubility of the drug molecule in the lipid, the polymorphic state of the drug molecule, and the properties of the solid lipid matrix (73). SLNs may be administered by different routes, such as oral, parenteral, nasal, ocular, and transdermal. The release of the drug from SLNs is inversely related to the partition coefficient of the drug and its crystalline behavior (74). Based on the preparation method, SLNs are divided into three main types: (1) solid solution, (2) drug-enriched shell, and (3) drug-enriched core (74). These NPs have the advantages of drug stability, sustained release of drugs, less toxicity due to the absence of organic solvents, biodegradability, feasibility for both kind of drugs, and easy handling of regulatory affairs (72, 74, 75). Solid lipid nanoparticles have many potential applications in developing therapeutic interventional approaches against cancer chemotherapy, brain targeting, parasitic diseases, tuberculosis, gene delivery, and in dermatological preparations (72, 73, 75).

The overexpression of lectin receptors on cancerous cells was used as a target, and MTX-SLNs were prepared by the hot microemulsion method followed by fucose coating (MTX-SLN-F). The *in vitro* cell cytotoxicity (MCF-7 cells) was reported ($IC_{50}$) to be higher in MTX-SLN-F (∼2 μg/mL) compared to MTX-SLN (∼3 μg/mL) and free MTX (∼7 μg/mL) after 72 h with an increased cell uptake of ∼70% after 3 h in the case of MTX-SLN-F compared to ∼45 and ∼10% for MTX-SLN and free MTX, respectively (14). The *in vivo* antitumor effects of MTX-SLN-F and free intravenous MTX injection were observed in breast cancer–bearing female Wistar rats and the percentage of tumor burden was significantly high ($P < 0.001$): ∼ 30, 53.8, and 62% by MTX-SLN-F, MTX-SLN, and free MTX after 4 weeks of treatment, respectively. There was no mortality found after several rounds of injection in the case of MTX-SLN-F compared to 66.66 and 50% of mortality observed in free MTX and MTX-SLN formulation 10 weeks posttreatment (14). Results of the experiments favored the approach of preparing a ligand-anchored SLN-encapsulated drug for breast cancer therapy. Recently, Battaglia et al. prepared MTX-SLN by using the method called "coacervation" (76): a solvent-free method wherein fatty acid precipitation was seen due to the reduction of pH by acidification of micellar solutions in the presence of a polymeric stabilizer (77). They used the prepared SLNs against a glioblastoma multiforme (GBM) stage IV glioma. Didoceylmethotrexate (ddMTX), a lipophilic MTX ester, is used as MTX has issues with entrapment. The *in vitro* cytotoxicity against rat F98 cells was found to be encouraging (however, not significant) and provided some preliminary data for GBM (77). All above-given accounts suggest an advantage of SLNs over traditional drug-delivery systems for poorly water-soluble drugs. It is advised that SLNs be used as efficient delivery systems. However, there are some constraints in using these SLNs, and they include low drug-loading capacities, presence of alternative colloidal structures (micelles, liposomes, mixed micelles, drug nanocrystals), the complexity of the physical state of the lipid (transformation between different modifications), and the possibility of super-cooled melts, which cause stability issues (**Table 1**).

### *Nanostructured Lipid Carriers (NLCs)*

Second-generation solid lipid nanoparticles called "nanostructured lipid carriers" (NLCs) are formulated to address the existing limitations of SLNs (72, 74). NLCs are the most preferred nanodrug delivery system nowadays among NDDS due to their advantage over others with respect to physical stability, improved drug entrapment and loading efficiencies, bioavailability, and drug release modulation (78). NLCs are colloidal lipid nanoparticles prepared by mixing solid and liquid lipids together with surfactants (as an emulsifier). Most of the drugs are fairly soluble in liquid lipids compared to solid lipids; thus, the drug leaching observed with SLNs is overcome by the entrapment of the drug (72, 79). During the preparation and storage of NLCs, the formulation goes through lower temperatures during homogenization and crystallization. The cooling process decreases the solubility of the drug in the lipophilic phase, therefore, showing drug expulsion from the nanoparticles, especially with the use of higher concentration drug formulations (78–80). A drug can be encapsulated in the space between the solid lipid molecules in a crystalline structure that is created due to the imperfections in the organization of the crystal. Thus, the higher the disturbance in a crystalline structure, the more the drug is encapsulated (72, 74, 79, 80). For achieving maximum stability, the recrystallization of the lipid in the cooling process is reduced and retarded in the case of NLCs compared to the extent seen in SLNs because the crystal order is highly disturbed because of oil particles remaining in the liquid phase in NLCs (74, 79). The engineering of NLCs is aimed at increasing drug loading of therapeutic agents and preventing the leakage of drugs upon storage (79, 81, 82). High-pressure homogenization, hot/cold homogenization, solvent evaporation, emulsification, solvent diffusion, solvent emulsification-evaporation, phase inversion, solvent injection/displacement method, etc., are some of the commonly employed methods for the preparation of NLCs (74, 79, 81). Different types of liquid lipids—mainly soybean oil; medium chain triglycerides/caprylic- and capric-triglycerides; oleic acid; corn oil; and solid lipids, such as stearic acid, glyceryl monostearate, cetyl palmitate, glyceryl palmitostearate, glyceryl behenate, grades of witeposl® and softisan®–are used in the preparation of NLCs (81, 83). Surfactants (Tween 80, lecithin, poloxamer 188, Polyglyceryl-3-methylglucose distearat, sodium dodecyl sulfate, sodium deoxycholate, Tween 20, Myverol™ 18-04K, PVA, solutol® HS 15 and polyoxyl castor oil) are used during the preparation of NLCs to provide stability to the formulation. Drug-loaded NLCs are administered by oral, topical, parenteral, and ocular routes to address brain-related issues (72, 78, 80, 81, 83). In cancer therapy, two important

factors, namely real-time monitoring or diagnosis and treatment of affected tissues, play a central role. By focusing on these aspects, Kohler et al. formulated magnetic nanoparticles using a modified coprecipitation method (84). Magnetite, $Fe_3O_4$, nanoparticles were first surface-modified with (3-aminopropyl) trimethoxysilane (APS) to make the self-assembled monolayer followed by amidation between carboxylic acid end groups on MTX and an amide group present on the surface of the particle. Prepared MTX-NLCs were studied in MCF-7 and human cervical cancer cells (HeLa) for drug efficacy and drug release to determine the cell uptake (84). Cell viability after 120 h was found to be similar to free MTX. The cell uptake via MTX-NLCsbyMCF-7 (20 times) and HeLa (10 times) was found to be higher. TEM image analysis after the internalization of MTX-NLCs confirms the release of MTX within the lysosomal compartment (84).

The preparation strategies of NLCs, considering selection of solid and liquid lipids, type of surfactants and their formulation, play an instrumental role in biomedical applications in cancer therapy (85) and autoimmune systemic inflammatory diseases, such as psoriasis and RA (86). At present, research on NLCs is limited to preclinical studies with clinical applications remaining far from realization. There are some limitations, such as the presence of organic solvent residue, uneven distribution, complex production process, and poor stability (**Table 1**).

### *Lipid Polymer Hybrid Nanoparticles (LPHNPs)*

The low solubility, dose-related toxicity, non-specificity, rapid diffusion throughout the body, short half-life in the bloodstream, and development of drug-resistance of conventional lipid- and polymer-based nanoparticles by the target cell (87) are some of the glaring issues with the existing drug-delivery vehicles. The innovative NDDS lipid–polymer hybrid nanoparticles (LPHNPs) combine the attributes of polymeric and lipid nanoparticles (PNPs) (46, 87–89). Lipophilic and poorly water-soluble drugs can be incorporated in the hydrophobic core of the polymer. They are prepared by two methods: (1) two-step (conventional and non-conventional) and (2) one-step (by nano-precipitation and emulsification-solvent-evaporation) (89, 90). LPHNPs offer a versatile drug-delivery system with better drug entrapment, controlled and sustained drug release, great *in vitro* and *in vivo* stability (89). In addition, the lipid layer slows down the rate of polymer degradation of LPHNP products by limiting inward water diffusion and helps the sustained-release kinetics of loaded content (89). The properties of LPHNPs advocate for their utility and prove advantageous over existing delivery vehicles (87, 91). Thus, well-designed LPHNPs contain hydrophobic polymeric core functions, whereas the surrounding lipid coat is a biocompatible shield and a barrier preventing the fast leakage of water-soluble drugs (92, 93). Properties such as biocompatibility, biodegradability, sustained drug-release profiles, and greater loading capacity are attributed to a stable, high-payload, targeted drug-delivery system that might maximize chemotherapeutic efficacy against targeted cancer cells (90, 94). Recently, self-assembled polymer-lipid hybrid NPs were developed aiming at overcoming the limitations seen with conventional drug-delivery systems. The polymer-lipid hybrid NPs gained significant attention for drug and gene delivery (95, 96). LPHNPs were engineered with an intent to explore the characteristics of lipid and polymeric nanoparticles in one delivery system (89, 91) to achieve controlled and targeted drug delivery for the treatment of cancer and other inflammatory diseases (90, 97). Therefore, Tahir et al. used different concentrations of polymer (PLGA), lipid (Lipoid S100), and surfactant (Lutrol® F-68) for the preparation of MTX-LPHNPs by the single-step, self-assembly, modified nano-precipitation method to check the influence of variation on particle size, entrapment efficiency (EE), and drug release using a three-level box Behnken design (Design-Expert®software) (98). Particle size range was increased with polymer concentration, whereas EE was dependent on both the lipid and polymer concentrations. The antiproliferative activity against the PC3 and MDA-MB-231 cells by the ATP activity–based assay showed higher growth inhibition even at the highest concentration (200 μg/mL) when MTX was encapsulated in LPHNPs compared to free MTX (98).

The surface of NPs is conjugated with the targeting molecules, which are recognized by the receptors expressed by the ailing cells (99) to achieve better targeting efficiency and offer novel and much better cancer therapeutic approaches (100–103). Further, active targeting of LPHNPs increases the probability of drug availability at the target site, which eventually reduces the chances of exposure of healthy cells and reduces adverse effects (104). The overly expressed membrane receptors (lectin receptors/LRs) are exploited by the drug targets during tumor pathogenesis (105–108). The presence of lectin (carbohydrate) moieties on the surface of therapeutic NPs can efficiently enhance specificity and binding affinity, eventually leading to significantly higher cellular uptake through receptor-mediated endocytosis (105, 107–111). The lectin receptor-mediated targeting employs the interaction of endogenous ligands with different sugar moieties, such as galactose (G), mannose (M), fucose (F), fructose, and lactose (109–112). This nano-carrier system results in glycosylated carriers comprising carbohydrate as stratum ligands, which are known for quick internalization through lectin receptor-mediated endocytosis (105–108).

MTX-acelofenac (ACE)-loaded LPHNPs were prepared by a single-step, self-assembled, nano-precipitation method to achieve codelivery of MTX and ACE in fucose-anchored LPHNP (LPHNP-MTX+ACL-Fu) approaches against breast cancer cells (MCF-7 and MDA-MB-231) (88). The immediate localization (within 2 h of incubation), enhanced bioavailability (8–10 times higher than free drugs), and higher cell cytotoxicity (increased cell death of MTX during coencapsulation with ACL compare to free drugs) was observed in the MTT assays conducted *in vitro* (88). The *in vivo* experiments were carried out in DMBA-induced cancer BALB/c mice. The pharmacokinetics (mean residence time 5–6 times higher than free MTX and ACL), sustained drug release (measured up to 72 h when administered intravenously), and antitumor activity (residual tumor burden 19.54%, 33.73%, and 163.8% for LPHNP-MTX+ACl-Fu, LPHNP-MTX+ACl, and normal saline-untreated control for 5 weeks, respectively) (88) confirmed the synergistic effects as evaluated by the pharmacological parameters, conferred by the codelivery of drugs. Later on, fructose-tethered MTX and beta carotene (BC)-loaded LPHNPs (F-MTX+BC-LPHNPs) were engineered by the self-assembled

nano-precipitation method for the treatment of breast cancer to find out the role of BC on MTX-mediated cytotoxicity (113). F-MTX+BC-LPHNPs showed a high apoptosis index (0.89) in MCF-7 cells and sustained drug release in a biphasic manner up to 120 h for F-MTX+BC-LPHNPs and MTX+BC-LPHNPs, resulting in improved bioavailability with enhanced localization at the tumor site. Similarly, female Wistar rats bearing cancer induced by DMBA were injected with different formulation's repeated intravenous administration (once in 3 days) [114]. The tumor progression was measured 30 days posttreatment and found to be 32% in F-MTX+BC-LPHNPs compared to 43.2 and 63.1% with MTX+BC-LPHNPs and free MTX, respectively. Moreover, β-carotene helps in the refinement of renal and hepatic toxicity [114] when mixed in the formulations. Results uncover the potential use of bioactives in the future with LPHNPs for targeted and sustained drug delivery for various treatments of cancer, autoimmune diseases such as RA, and psoriasis.

We have, as have others (1, 90), recently reviewed the current status and future application of LPHNPs in details for cancer therapeutics (46).

## CONCLUDING REMARKS AND FUTURE DIRECTIONS

Various studies demonstrate MTX as a revolutionary medicine in the field of biomedical sciences as it shows significant therapeutic potential, selective targeting, robust biological response, and ensured safety. In addition, the residence time of MTX in NLCs is extended in blood circulation and, thus, permits MTX to accumulate at the desired sites. There is lots of research going on focusing on combinatorial cancer therapy and in inflammatory disorders, and it is likely to expand in the future. Moreover, the MTX platform may be utilized for multiple activities simultaneously with imaging and drug-delivery characteristics. They may have multiple applications in cancer chemotherapy and other clinical settings.

## AUTHOR CONTRIBUTIONS

W-JY conceived the idea and prepared, edited, and finalized the manuscript. D-XH and SL helped write the manuscript. Y-LS rendered all chemicals and helped write the manuscript. FG and HL provided reagents and helped prepare the manuscript. All authors contributed to the article and approved the submitted version.

## ACKNOWLEDGMENTS

We thank the First Hospital of Jilin University–The Eastern Division for rendering financial assistance to carry out this study. The central instrument facility of First Hospital of Jilin University, China is duly acknowledged.

## REFERENCES

1. Bose RJC, Ravikumar R, Karuppagounder V, Bennet D, Rangasamy S, Thandavarayan RA, et al. Lipid–polymer hybrid nanoparticle-mediated therapeutics delivery: advances and challenges. *Drug Discov Today*. (2017) 22:1258–65. doi: 10.1016/j.drudis.2017.05.015
2. Levêque D, Levêque D, Becker G, Toussaint E, Fornecker LM, Paillard C, et al. Clinical pharmacokinetics of methotrexate in oncology. *Int J Pharmacokinet.*(2017) 2:137–47. doi: 10.4155/ipk-2016-0022
3. Khan ZA, Tripathi R, Mishra B. Methotrexate: a detailed review on drug delivery and clinical aspects. *Expert Opin Drug Deliv*. (2012) 9:151–69. doi: 10.1517/17425247.2012.642362
4. Abolmaali SS, Tamaddon AM, Dinarvand R. A review of therapeutic challenges and achievements of methotrexate delivery systems for treatment of cancer and rheumatoid arthritis. *Cancer Chemother Pharmacol.* (2013) 71:1115–30. doi: 10.1007/s00280-012-2062-0
5. Rahman LK, Chhabra SR. The chemistry of methotrexate and its analogues. *Med Res Rev*. (1988) 8:95–155. doi: 10.1002/med.2610080106
6. Chatterji DC, Gallelli JF. Thermal and photolytic decomposition of methotrexate in aqueous solutions. *J Pharm Sci.* (1978) 67:526–531. doi: 10.1002/jps.2600670422
7. Friedman B, Cronstein B. Methotrexate mechanism in treatment of rheumatoid arthritis. *Joint Bone Spine.* (2019) 86:301–7. doi: 10.1016/j.jbspin.2018.07.004
8. Rizvi SA, Saleh AM. Applications of nanoparticle systems in drug delivery technology. *Saudi Pharmac J.* (2018) 26:64–70. doi: 10.1016/j.jsps.2017.10.012
9. Xu X, Ho W, Zhang X, Bertrand N, Farokhzad O. Cancer nanomedicine: from targeted delivery to combination therapy. *Trends Mol Med.* (2015) 21:223–32. doi: 10.1016/j.molmed.2015.01.001
10. Hoshyar N, Gray S, Han H, Bao G. The effect of nanoparticle size on *in vivo* pharmacokinetics and cellular interaction. *Nanomedicine.* (2016) 11:673–92. doi: 10.2217/nnm.16.5
11. Jain A, Jain A, Garg NK, Tyagi RK, Singh B, Katare O, et al. Surface engineered polymeric nanocarriers mediate the delivery of transferrin–methotrexate conjugates for an improved understanding of brain cancer. *Acta Biomater*. (2015) 24:140–51. doi: 10.1016/j.actbio.2015.06.027
12. Garg NK, Singh B, Kushwah V, Tyagi RK, Sharma R, Jain S, et al. The ligand (s) anchored lipobrid nanoconstruct mediated delivery of methotrexate: an effective approach in breast cancer therapeutics. *Nanomedicine.* (2016) 12:2043–60. doi: 10.1016/j.nano.2016.05.008
13. Garg NK, Tyagi RK, Singh B, Sharma G, Nirbhavane P. Nanostructured lipid carrier mediates effective delivery of methotrexate to induce apoptosis of rheumatoid arthritis via NF-κB and FOXO1. *Int J Pharm*. (2016) 499:301–320. doi: 10.1016/j.ijpharm.2015.12.061
14. Garg NK, Singh B, Jain A, Nirbhavane P, Sharma R, Tyagi RK, et al. Fucose decorated solid-lipid nanocarriers mediate efficient delivery of methotrexate in breast cancer therapeutics. *Colloids Surf B Biointerfaces.* (2016) 146:114–26. doi: 10.1016/j.colsurfb.2016.05.051
15. Kuznetsova N, Kandyba A, Vostrov I, Kadykov V, Gaenko G, Molotkovsky J, Vodovozova E, et al. Liposomes loaded with lipophilic prodrugs of methotrexate and melphalan as convenient drug delivery vehicles. *J Drug Deliv Sci Technol.* (2009) 19:51–9. doi: 10.1016/S1773-2247(09)50007-X
16. Brown PM, Pratt AG, Isaacs JD. Mechanism of action of methotrexate in rheumatoid arthritis, and the search for biomarkers. *Nat Rev Rheumatol.* (2016) 12:731–42. doi: 10.1038/nrrheum.2016.175
17. Teresi ME, Crom WR, Choi KE, Mirro J, Evans WE. Methotrexate bioavailability after oral and intramuscular administration in children. *J Pediatr.* (1987) 110:788–92. doi: 10.1016/S0022-3476(87)80025-2
18. Balis FM, Mirro J Jr., Reaman GH, Evans WE, McCully C, Doherty KM, et al. Pharmacokinetics of subcutaneous methotrexate. *J Clin Oncol.* (1988) 6:1882–6. doi: 10.1200/JCO.1988.6.12.1882
19. Mol F, Mol BW, Ankum WM, van der Veen F, Hajenius PJ. Current evidence on surgery, systemic methotrexate and expectant management in the treatment of tubal ectopic pregnancy: a systematic review and meta-analysis. *Hum Reprod Update.* (2008)14:309–19. doi: 10.1093/humupd/dmn012

20. Kwong YL, Yeung DY, Chan JC. Intrathecal chemotherapy for hematologic malignancies: drugs and toxicities. *Ann Hematol.* (2009) 88:193. doi: 10.1007/s00277-008-0645-y
21. Csordas K, Hegyi M, Eipel OT, Muller J, Erdelyi DJ, Kovacs GT, et al. Comparison of pharmacokinetics and toxicity after high-dose methotrexate treatments in children with acute lymphoblastic leukemia. *Anticancer Drugs.* (2013) 24:189–197. doi: 10.1097/CAD.0b013e32835b8662
22. Bleyer WA. The clinical pharmacology of methotrexate. *new applications of an old drug. Cancer.* (1978) 41:36–513. doi: 10.1002/1097-0142(197801)41:1<36::AID-CNCR2820410108>3.0.CO;2-I
23. Leveque D. Subcutaneous administration of anticancer agents. *Anticancer Res.* (2014) 34:1579–86.
24. Savion S, Shtelman E, Orenstein H, Torchinsky A, Fein A, Toder V, et al. Bax-associated mechanisms underlying the response of embryonic cells to methotrexate. *Toxicol Vitro.* (2009) 23:1062–8. doi: 10.1016/j.tiv.2009.06.004
25. Lloyd ME, Carr M, McElhatton P, Hall GM, Hughes RA. The effects of methotrexate on pregnancy, fertility and lactation. *QJM.* (1999) 92:551–63. doi: 10.1093/qjmed/92.10.551
26. Kalb RE, Strober B, Weinstein G, Lebwohl M. Methotrexate and psoriasis: 2009 *National psoriasis foundation consensus conference. J Am Acad Dermatol.* (2009) 60:824–37. doi: 10.1016/j.jaad.2008.11.906
27. Moisa A, Fritz P, Benz D, Wehner HD. Iatrogenically-related, fatal methotrexate intoxication: a series of four cases. *Forensic Sci Int.* (2006) 156:154–7. doi: 10.1016/j.forsciint.2004.12.031
28. Garneau AP, Riopel J, Isenring P. Acute methotrexate-induced crystal nephropathy. *N Engl J Med.* (2015) 373:2691–3. doi: 10.1056/NEJMc1507547
29. Grim J, Chládek J, Martínková J. Pharmacokinetics and pharmacodynamics of methotrexate in non-neoplastic diseases. *Clin Pharmacokinet.* (2003) 42:139–51. doi: 10.2165/00003088-200342020-00003
30. Wang F, Jiang X, Lu W. Profiles of methotrexate in blood and CSF following intranasal and intravenous administration to rats. *Int J Pharm.* (2003) 263:1–7. doi: 10.1016/S0378-5173(03)00341-7
31. Li Y, Vijayanathan V, Gulinello M, Cole PD. Intrathecal methotrexate induces focal cognitive deficits and increases cerebrospinal fluid homocysteine. *Pharmacol Biochem Behav.* (2010) 95:428–33. doi: 10.1016/j.pbb.2010.03.003
32. Choudhury RC, Ghosh SK, Palo AK. Cytogenetic toxicity of methotrexate in mouse bone marrow. *Environ Toxicol Pharmacol.* (2000) 8:191–6. doi: 10.1016/S1382-6689(00)00041-7
33. Lebugle A, Rodrigues A, Bonnevialle P, Voigt JJ, Canal P, Rodriguez F, et al. Study of implantable calcium phosphate systems for the slow release of methotrexate. *Biomaterials.* (2002) 23:3517–22. doi: 10.1016/S0142-9612(02)00082-0
34. Bonetti A, Chatelut E, Kim S. An extended-release formulation of methotrexate for subcutaneous administration. *Cancer Chemother Pharmacol.* (1994) 33:303–6. doi: 10.1007/BF00685904
35. Singh U, Udupa N. Methotrexate loaded chitosan and chitin microspheres—*in vitro* characterization and pharmacokinetics in mice bearing Ehrlich ascites carcinoma. *J Microencapsul.* (1998) 15:581–94. doi: 10.3109/02652049809008242
36. Karasulu HY, Karabulut B, Göker E, Güneri T, Gabor F. Controlled release of methotrexate from w/o microemulsion and its *in vitro* antitumor activity. *Drug Deliv.* (2007) 14:225–33. doi: 10.1080/10717540601067760
37. Hassanpour SH, Dehghani M. Review of cancer from perspective of molecular. *J Cancer Res Pract.* (2017) 4:127–9. doi: 10.1016/j.jcrpr.2017.07.001
38. Bray F, Ferlay J, Soerjomataram I, Siegel RL, Torre LA, Jemal A, et al. Global cancer statistics 2018: GLOBOCAN estimates of incidence and mortality worldwide for 36 cancers in 185 countries. *CA Cancer J Clin.* (2018) 68:394–424. doi: 10.3322/caac.21492
39. Koeffler HP, McCormick F, Denny C. Molecular mechanisms of cancer. *West J Med.* (1991) 155:505–14.
40. Parkin DM. The global health burden of infection-associated cancers in the year 2002. *Int J Cancer.* (2006) 118:3030–44. doi: 10.1002/ijc.21731
41. Portela A, Esteller M. Epigenetic modifications and human disease. *Nat Biotechnol.* (2010) 28:1057–68. doi: 10.1038/nbt.1685
42. Feitelson MA, Arzumanyan A, Kulathinal RJ, Blain SW, Holcombe RF, Mahajna J, et al. Sustained proliferation in cancer: mechanisms and novel therapeutic targets. In: *Seminars in Cancer Biology.* Baltimore, MD: Elsevier (2015). p. S25–54. doi: 10.1016/j.semcancer.2015.02.006
43. Farber S, Diamond LK. Temporary remissions in acute leukemia in children produced by folic acid antagonist, 4-aminopteroyl-glutamic acid (aminopterin). *N Engl J Med.* (1948) 238:787–93. doi: 10.1056/NEJM194806032382301
44. Bertino JR. Karnofsky memorial lecture. *Ode to methotrexate. J Clin Oncol.* (1993) 11:5–14. doi: 10.1200/JCO.1993.11.1.5
45. Shi J, Kantoff PW, Wooster R, Farokhzad OC. Cancer nanomedicine: progress, challenges and opportunities. *Nat Rev Cancer.* (2017) 17:20. doi: 10.1038/nrc.2016.108
46. Garg NK, Tandel N, Jadon RS, Tyagi RK, Katare OP. Lipid–polymer hybrid nanocarrier-mediated cancer therapeutics: current status and future directions. *Drug Discov Today.* (2018) 23:1610–21. doi: 10.1016/j.drudis.2018.05.033
47. Prabhu RH, Patravale VB, Joshi MD. Polymeric nanoparticles for targeted treatment in oncology: current insights. *Int J Nanomed.* (2015) 10:1001–18. doi: 10.2147/IJN.S56932
48. Naha A. A review on polymeric nanoparticles: a promising novel drug delivery system. *J Glob Pharm Technol.* (2018) 10:10–7.
49. Karlsson J, Vaughan HJ, Green JJ. Biodegradable polymeric nanoparticles for therapeutic cancer treatments. *Annu Rev Chem Biomol Eng.* (2018) 9:105–27. doi: 10.1146/annurev-chembioeng-060817-084055
50. Nasir A, Kausar A, Younus, A. A review on preparation, properties and applications of polymeric nanoparticle-based materials. *Polym Plast Technol Eng.* (2015) 54:325–41. doi: 10.1080/03602559.2014.958780
51. Zhang Y, Huang Y, Li S. Polymeric micelles: nanocarriers for cancer-targeted drug delivery. *AAPS PharmSciTech.* (2014) 15:862–71. doi: 10.1208/s12249-014-0113-z
52. Cho H, Lai TC, Tomoda K, Kwon GS. Polymeric micelles for multi-drug delivery in cancer. *AAPS PharmSciTech.* (2015) 16:10–20. doi: 10.1208/s12249-014-0251-3
53. Chen Y, Zhang W, Huang Y, Gao F, Sha X, Lou K, et al. The therapeutic effect of methotrexate-conjugated Pluronic-based polymeric micelles on the folate receptor-rich tumors treatment. *Int J Nanomed.* (2015) 10:4043–57. doi: 10.2147/IJN.S79045
54. Gulfam M, Matini T, Monteiro PF, Riva R, Collins H, Spriggs K, et al. Bioreducible cross-linked core polymer micelles enhance *in vitro* activity of methotrexate in breast cancer cells. *Biomater Sci.* (2017) 5:532–50. doi: 10.1039/C6BM00888G
55. Davaran S, Fazeli H, Ghamkhari A, Rahimi F, Molavi O, Anzabi M, et al. Synthesis and characterization of novel P (HEMA-LA-MADQUAT) micelles for co-delivery of methotrexate and chrysin in combination cancer chemotherapy. *J Biomater Sci Polym Edn.* (2018) 29:1265–86. doi: 10.1080/09205063.2018.1456026
56. Lin J, Li Y, Li Y, Cui F, Yu F, Wu H, et al. Self-targeted, bacillus-shaped, and controlled-release methotrexate prodrug polymeric nanoparticles for intratumoral administration with improved therapeutic efficacy in tumor-bearing mice. *J Mater Chem B.* (2015) 3:7707–17. doi: 10.1039/C5TB00724K
57. Abbasi E, Aval SF, Akbarzadeh A, Milani M, Nasrabadi HT. Dendrimers: synthesis, applications, and properties. *Nanoscale Res Lett.* (2014) 9:247. doi: 10.1186/1556-276X-9-247
58. Parajapati SK, Maurya SD, Das MK, Tilak VK, Verma K, Dhakar RC, et al. Potential application of dendrimers in drug delivery: a concise review and update. *J Drug Deliv Ther.* (2016) 6:71–88. doi: 10.22270/jddt.v6i2.1195
59. Sherje AP, Jadhav M, Dravyakar BR, Kadam D. Dendrimers: a versatile nanocarrier for drug delivery and targeting. *Int J Pharm.* (2018) 548:707–20. doi: 10.1016/j.ijpharm.2018.07.030
60. Kong SY, Tang GT, Pei YY, Jiang Z. Preparation and *in vitro* release of methotrexate complexation with PEGylated dendrimers. *Chinese Pharm J.* (2008) 43:1085.
61. van Dongen MA, Rattan R, Silpe J, Dougherty C, Michmerhuizen NL, Winkle MV, et al. Poly (amidoamine) dendrimer–methotrexate conjugates: the mechanism of interaction with folate binding protein. *Mol Pharm.* (2014) 11:4049–58. doi: 10.1021/mp500608s
62. Ryan GM, McLeod VM, Mehta D, Kelly BD, Stanislawski PC, Owen DJ, et al. Lymphatic transport and lymph node targeting of methotrexate-conjugated PEGylated dendrimers are enhanced by reducing the length of the drug

linker or masking interactions with the injection site. *Nanomedicine*. (2017) 13:2485–94. doi: 10.1016/j.nano.2017.08.003
63. Zhao Y, Guo Y, Li R, Wang T, Han M, Zhu C, et al. Methotrexate nanoparticles prepared with codendrimer from polyamidoamine (PAMAM) and oligoethylene glycols (OEG) dendrons: antitumor efficacy *in vitro* and *in vivo*. *Sci Rep*. (2016) 6:28983. doi: 10.1038/srep28983
64. Kim Y, Park EJ, Na DH. Recent progress in dendrimer-based nanomedicine development. *Arch Pharm Res*. (2018) 41:571–82. doi: 10.1007/s12272-018-1008-4
65. Bunker A, Magarkarab A, Viitalaa, T. Rational design of liposomal drug delivery systems, a review: combined experimental and computational studies of lipid membranes, liposomes and their PEGylation. *Biochim Biophys Acta*. (2016) 1858:2334–52. doi: 10.1016/j.bbamem.2016.02.025
66. Akbarzadeh A, Rezaei-Sadabady R, Davaran S, Joo SW, Zarghami N, Hanifehpour Y, et al. Liposome: classification, preparation, and applications. *Nanoscale Res Lett*. (2013) 8:102. doi: 10.1186/1556-276X-8-102
67. Bulbake U, Doppalapudi S, Kommineni N, Khan W. Liposomal formulations in clinical use: an updated review. *Pharmaceutics*. (2017) 9:12. doi: 10.3390/pharmaceutics9020012
68. Zylberberg C, Matosevic S. Pharmaceutical liposomal drug delivery: a review of new delivery systems and a look at the regulatory landscape. *Drug Deliv*. (2016) 23:3319–29. doi: 10.1080/10717544.2016.1177136
69. Pattni BS, Chupin VV, Torchilin VP. New developments in liposomal drug delivery. *Chem Rev*. (2015) 115:10938–66. doi: 10.1021/acs.chemrev.5b00046
70. Jin BZ, Dong XQ, Xu X, Zhang FH. Development and *in vitro* evaluation of mucoadhesive patches of methotrexate for targeted delivery in oral cancer. *Oncol Lett*. (2018) 15:2541–9. doi: 10.3892/ol.2017.7613
71. Riaz MK, Riaz MA, Zhang X, Lin C, Wong KH, Chen X, et al. Surface functionalization and targeting strategies of liposomes in solid tumor therapy: a review. *Int J Mol Sci*. (2018) 19:195. doi: 10.3390/ijms19010195
72. Naseri N, Valizadeh H, Zakeri-Milani P. Solid lipid nanoparticles and nanostructured lipid carriers: structure, preparation and application. *Adv Pharm Bull*. (2015) 5:305. doi: 10.15171/apb.2015.043
73. Mehnert W, Mäder K. Solid lipid nanoparticles: production, characterization and applications. *Adv Drug Deliv Rev*. (2012) 64:83–101. doi: 10.1016/j.addr.2012.09.021
74. Ganesan P, Narayanasamy D. Lipid nanoparticles: different preparation techniques, characterization, hurdles, and strategies for the production of solid lipid nanoparticles and nanostructured lipid carriers for oral drug delivery. *Sust Chem Pharm*. (2017) 6:37–56. doi: 10.1016/j.scp.2017.07.002
75. Mukherjee S, Ray S, Thakur RS. Solid lipid nanoparticles: a modern formulation approach in drug delivery system. *Indian J Pharm Sci*. (2009) 71:349. doi: 10.4103/0250-474X.57282
76. Battaglia L, Serpe L, Muntoni E, Zara G, Trotta M, Gallarate M, et al. Methotrexate-loaded SLNs prepared by coacervation technique: *in vitro* cytotoxicity and *in vivo* pharmacokinetics and biodistribution. *Nanomedicine*. (2011) 6:1561–73. doi: 10.2217/nnm.11.52
77. Battaglia L, Serpe L, Muntoni E, Zara G, Trotta M, Gallarate M, et al. Solid lipid nanoparticles by coacervation loaded with a methotrexate prodrug: preliminary study for glioma treatment. *Nanomedicine*. (2017) 12:639–56. doi: 10.2217/nnm-2016-0380
78. Beloqui A, Solinís MÁ, Rodríguez-Gascón A, Almeida AJ, Préat V. Nanostructured lipid carriers: promising drug delivery systems for future clinics. *Nanomedicine*. (2016) 12:143–61. doi: 10.1016/j.nano.2015.09.004
79. Li Q, Cai T, Huang Y, Xia X, Cole SPC, Cai Y, et al. A review of the structure, preparation, and application of NLCs, PNPs, and PLNs. *Nanomaterials*. (2017) 7:122. doi: 10.3390/nano7060122
80. Jaiswal P, Gidwani B, Vyas A. Nanostructured lipid carriers and their current application in targeted drug delivery. *Artif Cells Nanomed Biotechnol*. (2016) 44:27–40. doi: 10.3109/21691401.2014.909822
81. Khosa A, Reddi S, Saha RN. Nanostructured lipid carriers for site-specific drug delivery. *Biomed Pharmacother*. (2018) 103:598–613. doi: 10.1016/j.biopha.2018.04.055
82. Poonia N, Kharb R, Lather V, Pandita D. Nanostructured lipid carriers: versatile oral delivery vehicle. *Future Sci OA*. (2016) 2:FSO135. doi: 10.4155/fsoa-2016-0030
83. Tamjidi F, Nasirpour A, Varshosaz J, Shahedi, M. Nanostructured lipid carriers (NLC): a potential delivery system for bioactive food molecules. *Innov Food Sci Emerg Technol*. (2013) 19:29–43. doi: 10.1016/j.ifset.2013.03.002
84. Kohler N, Sun C, Wang J, Zhang M. Methotrexate-modified superparamagnetic nanoparticles and their intracellular uptake into human cancer cells. *Langmuir*. (2005) 21:8858–64. doi: 10.1021/la0503451
85. Rizwanullah M, Ahmad J, Amin S. Nanostructured lipid carriers: a novel platform for chemotherapeutics. *Curr Drug Deliv*. (2016) 13:4–26. doi: 10.2174/1567201812666150817124133
86. Chuang SY, Lin CH, Huang TH, Fang JY. Lipid-based nanoparticles as a potential delivery approach in the treatment of rheumatoid arthritis. *Nanomaterials*. (2018) 8:42. doi: 10.3390/nano8010042
87. Zhang L, Chan JM, Gu FX, Rhee JW, Wang AZ, Radovic-Moreno AF, et al. Self-assembled lipid– polymer hybrid nanoparticles: a robust drug delivery platform. *ACS Nano*. (2008) 2:1696–702. doi: 10.1021/nn800275r
88. Garg NK, Tyagi RK, Sharma G, Jain A, Singh B, Jain S, et al. Functionalized lipid–polymer hybrid nanoparticles mediated codelivery of methotrexate and aceclofenac: a synergistic effect in breast cancer with improved pharmacokinetics attributes. *Mol Pharm*. (2017) 14:1883–97. doi: 10.1021/acs.molpharmaceut.6b01148
89. Hadinoto K, Sundaresan A, Cheow WS. Lipid–polymer hybrid nanoparticles as a new generation therapeutic delivery platform: a review. *Eur J Pharm Biopharm*. (2013) 85:427–43. doi: 10.1016/j.ejpb.2013.07.002
90. Date T, Nimbalkar V, Kamat J, Mittal A, Mahato RI, Chitkara D, et al. Lipid-polymer hybrid nanocarriers for delivering cancer therapeutics. *J Control Release*. (2017) 271:60–73. doi: 10.1016/j.jconrel.2017.12.016
91. Garg NK, Singh B, Sharma G, Kushwah V, Tyagi RT, Jain S, et al. Development and characterization of single step self assembled lipid polymer hybrid nanoparticles for effective delivery of methotrexate. *RSC Adv*. (2015) 5:62989–99. doi: 10.1039/C5RA12459J
92. Fang RH, Aryal S, Hu CM, Zhang L. Quick synthesis of lipid-polymer hybrid nanoparticles with low polydispersity using a single-step sonication method. *Langmuir*. (2010) 26:16958–62. doi: 10.1021/la103576a
93. Cheow WS, Hadinoto K. Factors affecting drug encapsulation and stability of lipid–polymer hybrid nanoparticles. *Colloids Surf B Biointerfaces*. (2011) 85:214–20. doi: 10.1016/j.colsurfb.2011.02.033
94. Hu CM, Kaushal S, Tran Cao HS, Aryal S, Sartor M, Esener S, et al. Half-antibody functionalized lipid-polymer hybrid nanoparticles for targeted drug delivery to carcinoembryonic antigen presenting pancreatic cancer cells. *Mol Pharm*. (2010) 7:914–20. doi: 10.1021/mp900316a
95. Ling G, Zhang P, Zhang W, Sun J, Meng X, Qin Y, et al. Development of novel self-assembled DS-PLGA hybrid nanoparticles for improving oral bioavailability of vincristine sulfate by P-gp inhibition. *J Control Release*. (2010) 148:241–8. doi: 10.1016/j.jconrel.2010.08.010
96. Shi J, Xiao Z, Votruba AR, Vilos C, Farokhzad OC. Differentially charged hollow core/shell lipid-polymer-lipid hybrid nanoparticles for small interfering RNA delivery. *Angew Chem Int Ed Engl*. (2011) 50:7027–31. doi: 10.1002/anie.201101554
97. Chaudhary Z, Ahmed N, Rehman AU, Khan GM. Lipid polymer hybrid carrier systems for cancer targeting: a review. *Int J Polym Mater Polym Biomater*. (2018) 67:86–100. doi: 10.1080/00914037.2017.1300900
98. Tahir N, Madni A, Balasubramanian V, Rehman M, Correia A, Kashif AM, et al. Development and optimization of methotrexate-loaded lipid-polymer hybrid nanoparticles for controlled drug delivery applications. *Int J Pharm*. (2017) 533:156–68. doi: 10.1016/j.ijpharm.2017.09.061
99. Pan J, Feng SS. Targeted delivery of paclitaxel using folate-decorated poly(lactide)-vitamin E TPGS nanoparticles. *Biomaterials*. (2008) 29:2663–72. doi: 10.1016/j.biomaterials.2008.02.020
100. Farokhzad OC, Langer R. Nanomedicine: developing smarter therapeutic and diagnostic modalities. *Adv Drug Deliv Rev*. (2006) 58:1456–9. doi: 10.1016/j.addr.2006.09.011
101. Brannon-Peppas L, Blanchette JO. Nanoparticle and targeted systems for cancer therapy. *Adv Drug Deliv Rev*. (2004) 56:1649–59. doi: 10.1016/j.addr.2004.02.014
102. Bertrand N, Wu J, Xu X, Kamaly N, Farokhzad OC. Cancer nanotechnology: the impact of passive and active targeting in the era of modern cancer biology. *Adv Drug Deliv Rev*. (2014) 66:2–25. doi: 10.1016/j.addr.2013.11.009

103. Peer D, Karp JM, Hong S, Farokhzad OC, Margalit R, Langer R, et al. Nanocarriers as an emerging platform for cancer therapy. *Nat Nanotechnol.* (2007) 2:751–60. doi: 10.1038/nnano.2007.387
104. Koo OM, Rubinstein I, Onyuksel H. Role of nanotechnology in targeted drug delivery and imaging: a concise review. *Nanomedicine.* (2005) 1:193–212. doi: 10.1016/j.nano.2005.06.004
105. Bies C, Lehr CM, Woodley JF. Lectin-mediated drug targeting: history and applications. *Adv Drug Deliv Rev.* (2004) 56:425–35. doi: 10.1016/j.addr.2003.10.030
106. East L, Rushton S, Taylor ME, Isacke CM. Characterization of sugar binding by the mannose receptor family member, Endo180. *J Biol Chem.* (2002) 277:50469–75. doi: 10.1074/jbc.M208985200
107. Gabius HJ, Gabius S, Brinck U, Schauer A. Endogenous lectins with specificity to beta-galactosides and alpha- or beta-N-acetyl-galactosaminides in human breast cancer. Their glycohistochemical detection in tissue sections by synthetically different types of neoglycoproteins, their quantitation on cultured cells by neoglycoenzymes and their usefulness as targets in lectin-mediated phototherapy *in vitro*. *Pathol Res Pract.* (1990) 186:597–607. doi: 10.1016/S0344-0338(11)80223-2
108. Jain K, Kesharwani P, Gupta U, Jain NK. A review of glycosylated carriers for drug delivery. *Biomaterials.* (2012) 33:4166–86. doi: 10.1016/j.biomaterials.2012.02.033
109. Kesharwani P, Tekade RK, Gajbhiye V, Jain K, Jain NK. Cancer targeting potential of some ligand-anchored poly(propylene imine) dendrimers: a comparison. *Nanomedicine.* (2011) 7:295–304. doi: 10.1016/j.nano.2010.10.010
110. Jain A, Agarwal A, Majumder S, Lariya N, Khaya A, Agrawal H, et al. Mannosylated solid lipid nanoparticles as vectors for site-specific delivery of an anti-cancer drug. *J Control Release.* (2010) 148:359–67. doi: 10.1016/j.jconrel.2010.09.003
111. Jain A, Kesharwani P, Garg NK, Jain A, Jain SA, Jain AK, et al. Galactose engineered solid lipid nanoparticles for targeted delivery of doxorubicin. *Colloids Surf B Biointerfaces.* (2015) 134:47–58. doi: 10.1016/j.colsurfb.2015.06.027
112. Kesharwani P, Iyer AK. Recent advances in dendrimer-based nanovectors for tumor-targeted drug and gene delivery. *Drug Discov Today.* (2015) 20:536–47. doi: 10.1016/j.drudis.2014.12.012
113. Jain A, Kesharwani P, Garg NK, Jain A, Jain SA, Jain AK, et al. Methotrexate and beta-carotene loaded-lipid polymer hybrid nanoparticles: a preclinical study for breast cancer. *Nanomedicine.* (2017) 12:1851–72. doi: 10.2217/nnm-2017-0011


**Conflict of Interest:** The authors declare that the research was conducted in the absence of any commercial or financial relationships that could be construed as a potential conflict of interest.

frontiers in Oncology

ORIGINAL RESEARCH
published: 20 October 2020
doi: 10.3389/fonc.2020.575415

# Green Biosynthesized Silver Nanoparticles With Aqueous Extracts of *Ginkgo Biloba* Induce Apoptosis *via* Mitochondrial Pathway in Cervical Cancer Cells

*Zhen Xu*[1†], *Qi Feng*[2†], *Min Wang*[3†], *Huange Zhao*[1], *Yingying Lin*[1] *and Songlin Zhou*[1*]

[1] *Key Laboratory of Tropical Translational Medicine of the Ministry of Education and Hainan Provincial Key Laboratory of Tropical Medicine, Hainan Medical University, Haikou, China,* [2] *Jiangsu Provincial Key Laboratory of Veterinary Bio-pharmaceutical High-tech Research, Jiangsu Agri-Animal Husbandry Vocational College, Taizhou, China,* [3] *Health and Family Planning Commission of Wanzai County of Jiangxi Province, Yichun, China*

OPEN ACCESS

**Edited by:**
*Christian Stockmann, Institut National de la Santé et de la Recherche Médicale (INSERM), France*

**Reviewed by:**
*Fong-Yu Cheng, Chinese Culture University, Taiwan*
*Liwen Li, Indiana University, United States*

***Correspondence:**
*Songlin Zhou*
*zhousonglin106@163.com*

[†]*These authors have contributed equally to this work*

**Specialty section:**
*This article was submitted to Cancer Molecular Targets and Therapeutics, a section of the journal Frontiers in Oncology*

**Received:** *23 June 2020*
**Accepted:** *28 September 2020*
**Published:** *20 October 2020*

**Citation:**
*Xu Z, Feng Q, Wang M, Zhao H, Lin Y and Zhou S (2020) Green Biosynthesized Silver Nanoparticles With Aqueous Extracts of Ginkgo Biloba Induce Apoptosis via Mitochondrial Pathway in Cervical Cancer Cells. Front. Oncol. 10:575415. doi: 10.3389/fonc.2020.575415*

Biosynthetic silver nanoparticles (AgNPs), specifically formed using medicinal plant extracts, have recently exhibited a remarkable therapeutic effect due to their anticancer potential. Here, we synthesized AgNPs using an aqueous extract of *Ginkgo biloba* leaves and evaluated its activity against cervical cancer (CCa) and the related molecular mechanisms. The physiochemical properties of the AgNPs were measured by ultraviolet-visible spectrophotometry, nanometre particle size analyzer and transmission electron microscopy. The AgNPs effects on cell proliferation and apoptosis were investigated through MTT, MTS, and colony formation assay; Hoechst 33258 staining; and flow cytometry. The intracellular ROS and oxidative stress levels were assessed using the appropriate commercial kits. Apoptosis-related protein levels were determined by western blotting. We prepared a series of different sized ginkgo extract synthesized AgNPs (GB-AgNPs), and the smallest mean particle size was 40.2 ± 1.2 nm with low polydispersity (0.091 ± 0.011), zeta potential values showed -34.56 mV. Compared to the controls, the GB-AgNP treatment inhibited the cell proliferation and induced the apoptosis of HeLa and SiHa cells. In addition, GB-AgNP treatment led to markedly increased levels of intracellular ROS, the release of cytochrome c (Cyt C) from mitochondria into the cytosol and the cleavage of caspase -9 and -3 in both CCa cell lines. Moreover, NAC, an ROS scavenger, eliminated the effect of GB-AgNPs on the HeLa and SiHa cells. This study reveals that GB-AgNPs suppresses cancer cell proliferation and induces apoptosis by upregulating intracellular ROS generation and inducing the activation of the caspase-dependent mitochondrial apoptotic pathway in CCa cells. Thus, GB-AgNPs may be a potential alternative drug for CCa therapy.

**Keywords: silver nanoparticles, *Ginkgo biloba*, apoptosis, mitochondrial signaling pathway, cervical cancer**

## INTRODUCTION

In the past several decades, cancer has ranked as the second leading cause of death in worldwide (1). For females, cervical cancer (CCa) is becoming more prevalent, in terms of both incidence and mortality, which are ranked fourth, globally (2). Despite new chemotherapeutic agents, human papillomavirus vaccination and other therapeutic approaches, which seem to offer effective control or prevention of cervical cancer, metastatic CCa is an incurable tumour for which new anticancer agents and therapeutic strategies are urgently needed (3, 4).

Nanoparticles (NPs) are new materials with dimension between approximately 1 and 100 nm in at least one dimension and in as many as three dimensions (5). Due to their physiochemical properties and characteristics, NPs exhibit therapeutic potential for numerous diseases (6). Silver nanoparticles (AgNPs) constitute a new type of nanometal particle that has been widely used in biological, medical, and engineering science (6). In particular, synthetic biologically active AgNPs have exhibited extensive therapeutic potential with broad spectrum antibacterial, antifungal, anticancer, anti-inflammatory, wound healing, antioxidative, and anti-diabetic activity (7–9).

In this study, our group applied an aqueous *Ginkgo biloba* leaf extract (GB-extract) as a reducing agent during AgNPs synthesis. *G. biloba*, commonly known as gingko or ginkgo, is classified in the Ginkgoaceae family and Ginkgo genus (10). Gingko leaf extracts have obvious effects as treatments for coronary heart disease, angina pectoris and hyperlipidaemia, and they exhibit anticancer, anti-inflammatory, antioxidant, anti-allergic, anti-ulcerogenic, and antibacterial activities because they are enriched in active metabolites, such as vitamin C, vitamin E, octacosanol, β-sitosterol, stigmasterol, alkaloids, and a variety of flavonoids (11, 12). In our study, we found that gingko leaf extract-based synthesis of silver nanoparticles (GB-AgNPs) exhibited good inhibitory effects on cell proliferation and induced the apoptosis of CCa cells. However, the molecular mechanism by which GB-AgNPs affect on CCa cells remains unknown.

Several studies have shown correlations between the activation of apoptosis and various synthetic AgNPs based on different medicinal plants. Recent evidence indicates that different mechanisms are involved in AgNP-induced apoptosis; such as ER stress mediation, altered ubiquitination, changed intracellular calcium ($Ca^{2+}$) concentration, and induced reactive oxygen species (ROS) production (13–16). In this study, we analyzed the characteristics of GB-AgNPs and the inhibition of cervical cancer cell proliferation to investigate the underlying mechanism of GB-AgNP-induced apoptosis in cervical cancer cell lines.

## MATERIALS AND METHODS

### Chemicals, Solvents, and Antibodies

For cell cultures, DMEM, FBS, penicillin, streptomycin, and trypsin-EDTA were purchased from GE Life (HyClone, USA). DMSO, MTT, MTS, and Hoechst 33258 were purchased from Sigma (Santa Clara, USA). An annexin V-FITC/PI apoptosis detection Kit, reactive oxygen species (ROS) assay kit, malondialdehyde (MDA) assay kit, glutathione peroxidase (GSH-Px) assay kit and superoxide dismutase (SOD) assay kit were purchased from KeyGen Biotech (Beijing, CN).The primary antibodies against β-actin, Bax, Bcl-2, Caspase-9, Caspase-3, Cyt C, and Vadc 1 were purchased from Cell Signaling (Massachusetts, USA). Horseradish peroxidase-conjugated goat anti-rabbit antibody was also purchased from Cell Signaling and was used as the secondary antibody. All the other fine chemicals and solvents used for this study were of analytical grade.

### The Extract of *Ginkgo Biloba* Leaves

*G. biloba* grown in the Taizhou region and ginkgo leaves were purchased from in the local public market (Taizhou, CN). The ginkgo leaves were washed three times with deionized water, freeze-dried, and pulverized through a 40-mesh sieve, and stored in a darkened room at 4 °C. The resulting gingko leaf powder (1.0 g) was dissolved in ultrapure water (60 ml), placed in an ultrasonic bath at 80 °C for 30 min, and cooled. After centrifugation at 10,000 g for 20 min, the supernatant was obtained to generate aqueous extracts of the *G. Biloba* leaves (GB-extracts).

### Synthesis and Characterization of the GB-AgNPs

Different concentrations of GB-extracts and $AgNO_3$ were combined to synthesize GB-AgNPs at different temperatures and time. Detailed synthetic conditions are shown in **Supplementary Materials Table 1**. The size of the AgNPs was determined using a nanoparticle size analyser, and the synthesis conditions were determined, with conditions for synthesizing the smallest mean particles found to be the best. The synthesized silver nanoparticle gel solution was freeze-dried to obtain GB-AgNP powder.

The physiochemical properties and characteristics of the GB-AgNPs were analyzed by ultraviolet-visible spectroscopy with absorbance between 200 and 800 nm (Shimadzu, Japan), and the particle size and shape were measured by a NanoBrook Omni nanometre particle size analyser (Brookhaven, USA) and an HT-7700 transmission electron microscope (Hitachi, Japan).

### Cell Lines and Culture

Human cervical epithelial cells (HcerEpic cell), HeLa, and SiHa human CCa cell lines were purchased from ATCC (Manassas, USA). The cells were cultured in DMEM supplemented with FBS (10%, v/v), penicillin (100 U/ml), and streptomycin (100 μg/ml) at 37 °C in a humidified incubator with 5% $CO_2$. The cells were passaged when the confluence reached 80%. The cells in the logarithmic growth phase were used for assays.

### Cell Viability and Proliferation Assay

Cell viability and proliferation were determined using MTT, MTS, and colony formation assays were performed as described in our previous reports (17). Briefly, for MTT assay, cells were incubated in 96-well plates and exposed to the indicated concentration of 40, 60, 90 nm GB-AgNPs or GB-extracts or

$AgNO_3$ or no-treatment control for 24 h. 10 μl MTT (5 mg/ml) was added to each well and incubated for 4 h. The medium was replaced with 150 μl of DMSO to dissolve the crystal formazan dye and absorbance was detected at 540 nm using an ELX808IU Microplate Reader (BioTek, USA). For MTS assay, cells were plated in 96-well plates and exposed to the indicated concentrations of 40 nm GB-AgNPs or no-treatment control for 12, 24, and 36 h. 20 μl of MTS was added to each well and incubated for 1 h, after which the absorbance of the MTS signal was calculated after absorbance detection at 490 nm. For colony formation assay, cells were treated with the indicated amount of 40 nm GB-AgNPs or no-treatment control for 24 h and cultured at a density of 500 cells/well in 6-well plates. Then the medium was changed every 3 d, and after two weeks cell colonies were stained with Giemsa stain solution (Solarbio, CN). Visible colonies were photographed and counted using a Gel DocTMXR$^+$ Molecular Imager system (BioRad, USA).

## Hoechst 33258 Staining

Hoechst 33258 staining was performed as described in our previous report (17). Briefly, cells were seeded in 6-well plates and added to indicated concentrations of 40 nm GB-AgNPs or a no-treatment control for 24 h, and then were stained using a Hoechst 33258 Staining Kit according to the manufacturer's instructions. The morphology of the apoptotic cells was observed, and the number of cells was counted under an IX73-AF12/PH fluorescence microscope (Olympus, Japan).

## Flow Cytometry

Cells were seeded in 6-well plates and added to different concentrations of 40 nm GB-AgNPs or a control for 24 h. The apoptosis rate was measured by an Annexin-V FITC/PI staining kit according to the manufacturer's protocol. These data were analyzed using FlowJo software (BD Biosciences, USA).

## ROS and Oxidative Stress Measurements

The intracellular ROS level and oxidative stressindexes were measured by a ROS assay kit, MDA assay kit, GSH-Px assay kit, and SOD assay kit according to the manufacturers' instructions.

## Western Blotting

Western blotting was performed as described in our previous reports (17). Briefly, cells were homogenized in RIPA lysis buffer. Total protein extracts and concentrations were measured using the BCA protein assay kit (Pierce, 23225). Proteins were separated on 12% SDS-PAGE and transferred to PVDF (Bio-Rad, USA) membranes. After blocking, the membranes were incubated with primary antibodies at 4°C overnight, and were subsequently incubated with secondary antibodies at room temperature for 1 h. Target proteins were detected and quantified using Enhanced Chemiluminescence reagents (Millipore, WBKLS0100).

## Statistical Analysis

Statistical analyses were performed with Prism 7 software. Differences were analyzed by one-way ANOVA or two-sample equal variance Student's *t* test. Data are expressed as the means ± SD. A value of $P < 0.05$ was considered significant.

# RESULTS

## Characterization of the Synthesized GB-AgNPs

During GB-AgNPs synthesis, the colour of the reaction solution changed significantly, and eventually, the colourless solution gradually became brown-orange, suggesting the surface plasmon resonance excitation of the synthesized AgNPs (**Figure 1A**). As shown in **Figure 1B**, the UV-Vis spectra were recorded for the GB-extracts and synthetic GB-AgNPs, with the optical characteristic peak of nanoparticles at approximately 400–450 nm. The absorption spectrum of the GB-AgNPs spanned a wide range, from 320 to 600 nm, with a prominent peak at 448 nm, while the GB-extract shown no similar peak between 400 and 600 nm.

To assess the size, the distribution of the synthesized AgNPs with the GB-extract, the dynamic lights scattering (DLS) method was used. In the series of silver nanoparticles we synthesized (**Supplementary Table 1** and **Figure 1**), the smallest average particle size was 40.2 ± 1.2 nm with low polydispersity (0.091 ± 0.011), and the zeta potential values was measured -34.56 mV with low mobility (-2.95), meantime no particle agglomeration was observed (**Figures 1C, D**). Moreover, to analyze the size and physical characteristics of the GB-AgNPs, transmission electron microscopy was performed. As shown in **Figure 1E**, the shape of the GB-AgNPs seemed spherical or oval with diameters between 90 and 20 nm on average. These results supported and statistically correlated with the DLS images of the GB-AgNPs. In addition, the UV absorption spectrum and particle size of synthesized GB-AgNPs (40 nm) were monitored in two weeks, and there was no significant change to be observed, which shows that our synthesized GB-AgNPs have good stability (**Supplementary Figures 2 and 3**). These results suggest that we could use aqueous extracts of the *G. Biloba* leaves as a reducing agent to prepare a series of stabilized AgNPs.

## Cytotoxic Effects of the GB-AgNPs on CCa Cells

To assess the cytotoxic effects of green-synthesized GB-AgNPs, the cell growth and proliferation of two CCa lines, HaLa and SiHa, were determined. First, these two cell lines were exposed to different concentrations and sizes of GB-AgNPs or different concentrations of GB-Extract and $AgNO_3$ for the indicated durations, followed by analysis of whether the GB-AgNPs affected cell viability by MTT assay. The results of the MTT assays suggested that the viability of both the HaLa and SiHa cells was not only dose-dependent but also size-dependent with the viability suppression by GB-AgNPs greater than that by the controls (**Figures 2A, B**). In addition, the various sizes of the GB-AgNPs not only failed to inhibit cell growth but also promoted cell growth at low concentrations: cell growth was inhibited only when the concentration was greater than 1.5 mg/ml. At the same

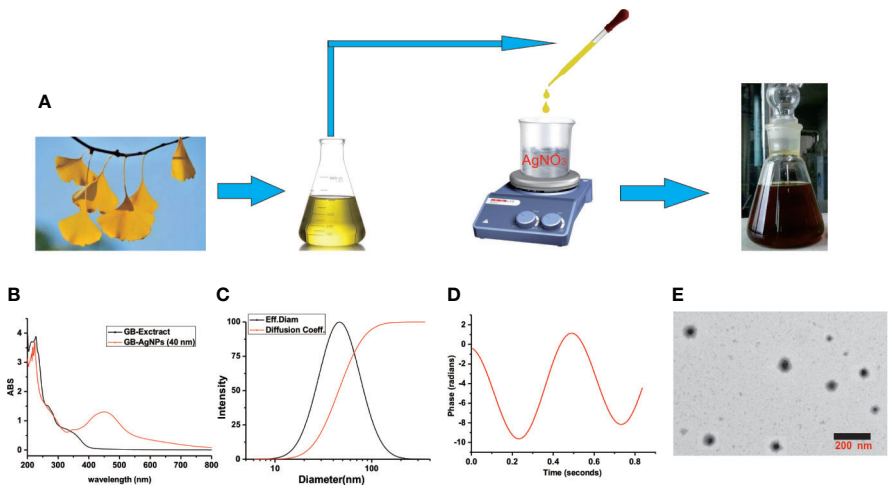


**FIGURE 1** | Schematic representation of silver nanoparticle synthesis with aqueous extracts of *G.biloba* leaves. **(A)** Step silver nanoparticle (AgNP) synthesis; **(B)** UVspectrum; **(C)** dynamic lights scattering (DLS) images; **(D)** Zeta-potential images; and **(E)** TEM images.

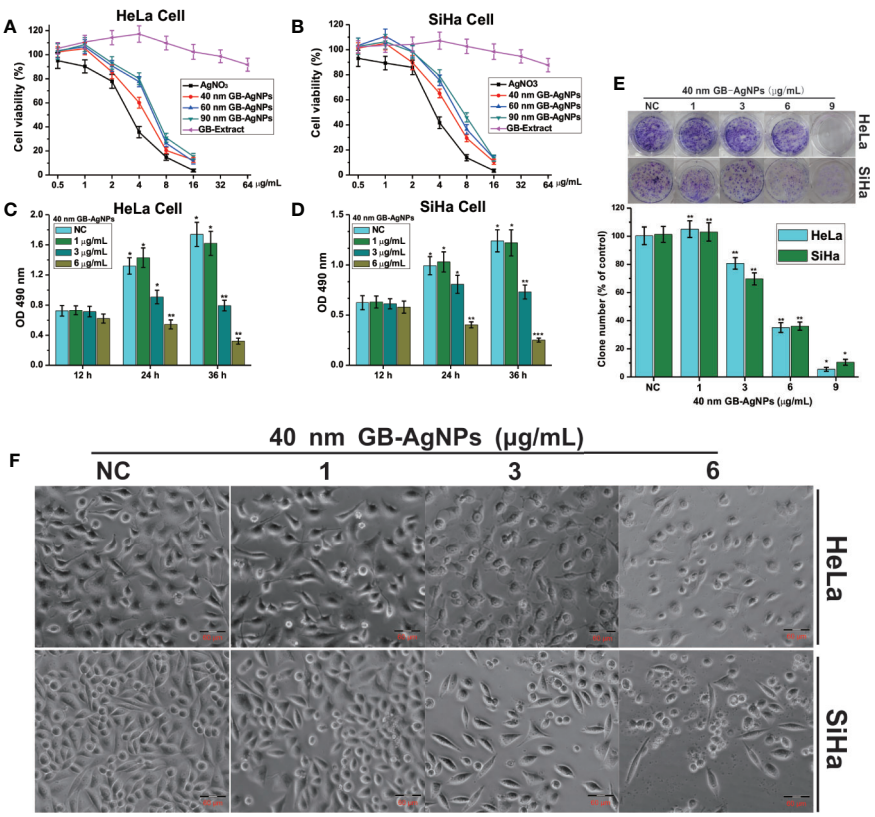


**FIGURE 2** | Ginkgo extract synthesized silver nanoparticles (GB-AgNPs) inhibit the proliferation of cervical cancer cells. **(A, B)** HeLa and SiHa cells were treated with different sizes of GB-AgNPs or $AgNO_3$ or GB-Extract for 24 h, and cell viability was measured with an MTT assay; **(C, D)** HeLa and SiHa Cells were treated with indicated concentrations of 40 nm GB-AgNPs for 12, 24, and 36 h, and MTS-incorporating live cells were detected with an MTS proliferation assay; **(E)** Cells were treated with indicated concentrations of 40 nm GB-AgNPs for 14 days, and live cells were detected with a colony formation assay; **(F)** cells were treated with indicated concentrations of 40 nm GB-AgNPs for 24 h, cell morphology was observed under an inverted phase-contrast microscope and images were obtained. Data are expressed as the means ± SD; $^{*}P < 0.05$, $^{**}P < 0.01$, $^{***}P < 0.001$.

time, the cytotoxicity of $AgNO_3$ was greater than that of all GB-AgNPs at the same concentration, while the GB extract was relatively less cytotoxic at high concentrations (**Figures 2A, B**).

We also assessed whether PAC is toxic to normal human gastric mucosal cells (GES-1), and the results showed that PAC at <1.6 μM was not cytotoxic to normal gastric cells; the dose that produced obvious cytotoxicity was ∼3.2 μM, more than eightfold the dose used in our assays.

Subsequently, to examine whether the 40 nm GB-AgNPs affected cell proliferation, MTS and colony formation assays were performed. The MTS assays showed that cytotoxic effects of the 40 nm GB-AgNPs on both the HaLa and SiHa cells not only increased with exposure time but also with increasing doses (**Figures 2C, D**). Similarly, the colony formation assays indicated that 40 nm GB-AgNPs treatment markedly inhibited that proliferation of these two CCa cell lines compared to the controls (**Figure 1E**). Moreover, microscopy images showed that, compared with the controls, both the HaLa and SiHa cells had noticeably increased cellular atrophy and decreased cellular attachment after 24 h of exposure to the 40 nm GB-AgNPs (**Figure 2F**). Additionally, the toxicity of 40 nm GB-AgNPs to normal human cervical epithelial cells (HcerEpic) was assessed and the results show that the dose of 40 nm GB-AgNPs (>8.0 μg/ml) has obvious cytotoxicity to normal cervical epithelial cells (**Supplementary Figure 4**). All the results indicate that GB-AgNPs could specifically suppress the proliferation and viability of the cervical cells. As shown in **Figures 2A, B**, the $IC_{50}$ value of 40 nm GB-AgNPs was approximately 3 μg/ml for both HeLa and SiHa cells.

Furthermore, colony formation assays suggested that PAC treatment markedly suppressed proliferation in MGC-803 and SGC-7901 cells compared to controls (**Figure 1E**). We also assessed whether PAC is toxic to normal human gastric mucosal cells (GES-1), and the results showed that PAC at <1.6 μM was not cytotoxic to normal gastric cells; the dose that produced obvious cytotoxicity was ∼3.2 μM, more than eightfold the dose used in our assays (**Supplementary Figure 1**).

## GB-AgNPs Induced the Apoptosis of the CCa Cells

Next, we examined whether the suppression of cell proliferation after GB-AgNP treatment was accompanied by apoptosis. HaLa and SiHa cells were exposed to different amounts of 40 nm GB-AgNPs for 24 h, followed by Hoechst 33258 staining to examine whether apoptosis occurs. Hoechst 33258 staining showed changes in nuclear morphology, including cell nucleus shrinkage and chromatin condensation, which are typical apoptotic morphological features, after the 40 nm GB-AgNPs (6 μg/ml) were added to these two CCa cell lines (**Figure 3A**). Furthermore, to verify the apoptotic effects of the GB-AgNPs on HaLa and SiHa cells, we carried out flow cytometry on Annexin V-FITC/PI stained cells and discovered that GB-AgNPs induced both early

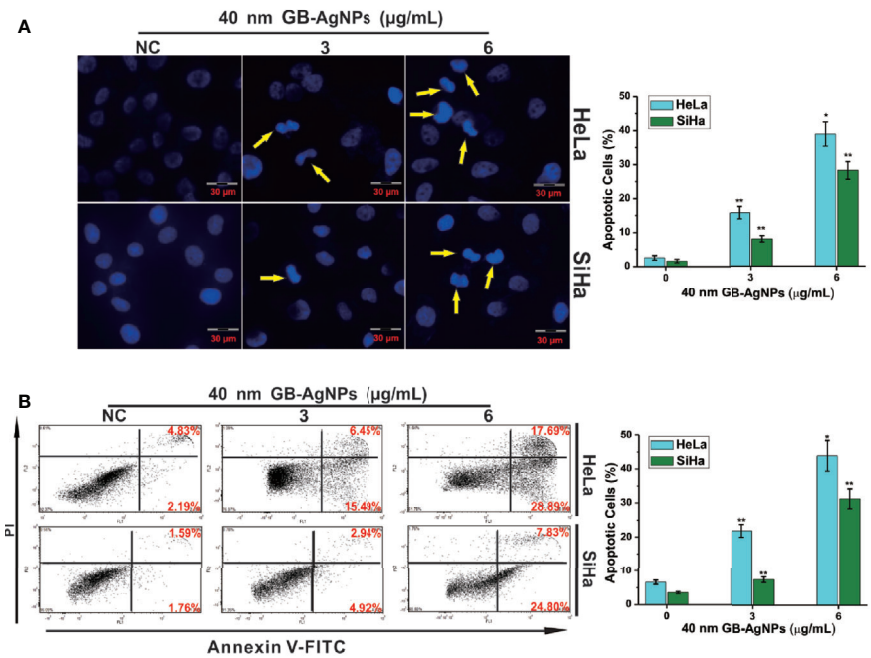


**FIGURE 3** | Ginkgo extract synthesized silver nanoparticles (GB-AgNPs) induce apoptosis in cervical cancer cells. **(A)** HeLa and SiHa cells were treated with the indicated concentrations of 40 nm GB-AgNPs for 24 h and stained with Hoechst 33258. Typical apoptotic morphology was observed in treated cells compared to untreated cells; **(B)** Cells were treated as in **(A)** for 24 h, apoptotic cells were stained by PI/annexin-V, and flow cytometry was performed. Data are expressed as the means ± SD; $^{*}P < 0.05$, $^{**}P < 0.01$.

and late apoptosis in a dose-dependent manner. **Figure 3B** clearly shows that the percent of apoptotic HeLa cells was 6.57 ± 0.62% for the control group and was increased to 21.78 ± 1.91%, and 43.92 ± 4.53% for the treatment groups; for the SiHa cells, the percent of apoptotic cells was 3.51 ± 3.51% for the control group and was 7.57 ± 0.85% and 31.23 ± 2.93% for the treatment groups. These findings confirmed that GB-AgNPs can induce the apoptosis of CCa cells in a dose-dependent manner.

## GB-AgNP Induced Oxidative Stress and ROS Generation

AgNPs can effectively block the respiratory chain of bacteria and thus have antibacterial effects (18). The production of intracellular ROS plays a critical role in oxidative stress and apoptosiss (19). Therefore, we assessed the oxidative stress and ROS levels, which play important role in the apoptosis induced by various anticancer agents, in both CCa cell lines after GB-AgNPs treatment. As shown in **Figure 4**, upon 40 nm GB-AgNPs treatment, the levels of intracellular ROS and malondialdehyde (MDA), an endproduct of lipid oxidation, were sharply increased compared with those of the control group (**Figures 4A, B**), whereas the levels of antioxidant enzymes such as GSH-Px and SOD were remarkably decreased (**Figures 4C, D**). Additionally, when the 40 nm GB-AgNPs (6 μg/ml) with 20 μM N-acetyl-L-cysteine (NAC, an ROS scavenger) were added, the levels of ROS and MDA, which had sharply increased, were significantly reduced, and the originally low content levels of SOD and GSH-Px were obviously increased. These results showed that GB-AgNPs can induce oxidative stress by generating intracellular ROS.

## GB-AgNPs Induced Apoptosis *Via* the Mitochondrial Pathway

The overproduction of ROS may cause mitochondrial dysfunction or damage, which may affect the expression of some antiapoptotic and proapoptotic genes in the mitochondria (19). We then analyzed the expression levels of antiapoptotic Bcl-2 protein and proapoptotic Bax protein by western blotting. As shown in **Figure 5**, upon 40 nm GB-AgNP treatment, the expression levels of Bcl-2 were decreased in the HeLa and SiHa cells, while the expression levels of Bax were obviously increased in both CCa cell lines. Considering that Bax activation would change the permeabilization of the outer mitochondrial membrane and cause about the release of some proapoptotic mitochondrial proteins into cytosol, the release of cytochrome c (Cyt C) was analyzed (20). Compared with the control group, the content level of Cyt C in the mitochondria was sharply decreased in a dose-dependent manner in these two CCa cell lines after 24 h of exposure to GB-AgNPs; in contrast, the expression of Cyt C in the cytosol was markedly increased by GB-AgNPs treatment of the HeLa and SiHa cells (**Figure 5**). Cyt C released into the cytoplasm can induce apoptosis by activating downstream caspase-dependent apoptotic proteins; therefore, the expression of caspase-9 and caspase-3 was measured. As shown in **Figure 5**, the expressions levels of cleaved caspase-9 and caspase-3 were obviously increased in a dose-dependent manner in the HeLa and SiHa cells treated with GB-AgNPs; whereas the expression levels of pro-caspase 9 and pro-caspase 3 were noticeably decreased in both CCa cell lines. These results clearly indicate that GB-AgNPs induced the apoptosis of cervical cancer cells by generating excess ROS that permeabilized of the outer mitochondrial membrane

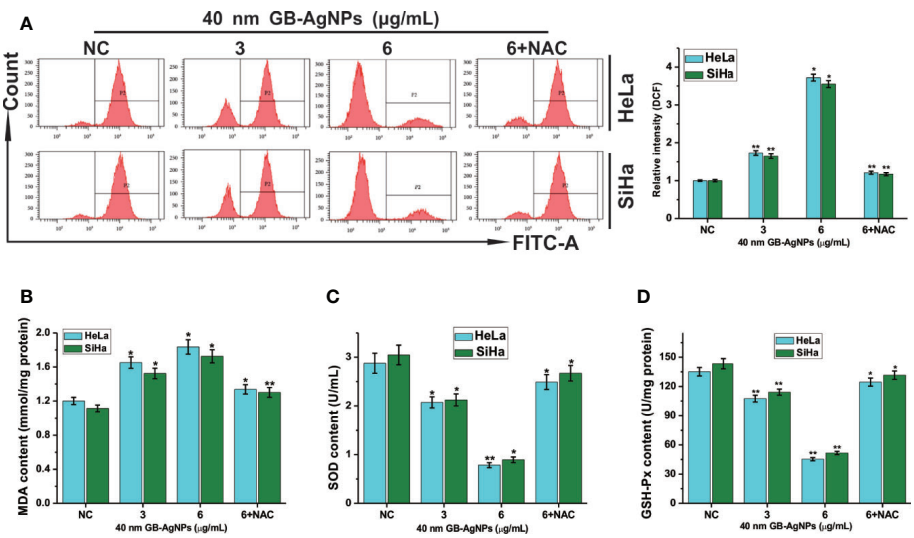


**FIGURE 4** | Ginkgo extract synthesized silver nanoparticle (GB-AgNP)-induced oxidative stress in cervical cancer cells. **(A)** HeLa and SiHa cells were treated with various doses of 40 nm GB-AgNPs for 24 h, and then intracellular ROS were measured by flow cytometry; **(B)** the content of lipid peroxidation MDA in cells was measured; **(C)** the level of SOD was measured in the cells; and **(D)** the level of GSH-Px was measured in the cells. Data are expressed as the means ± SD; *P < 0.05, **P < 0.01.

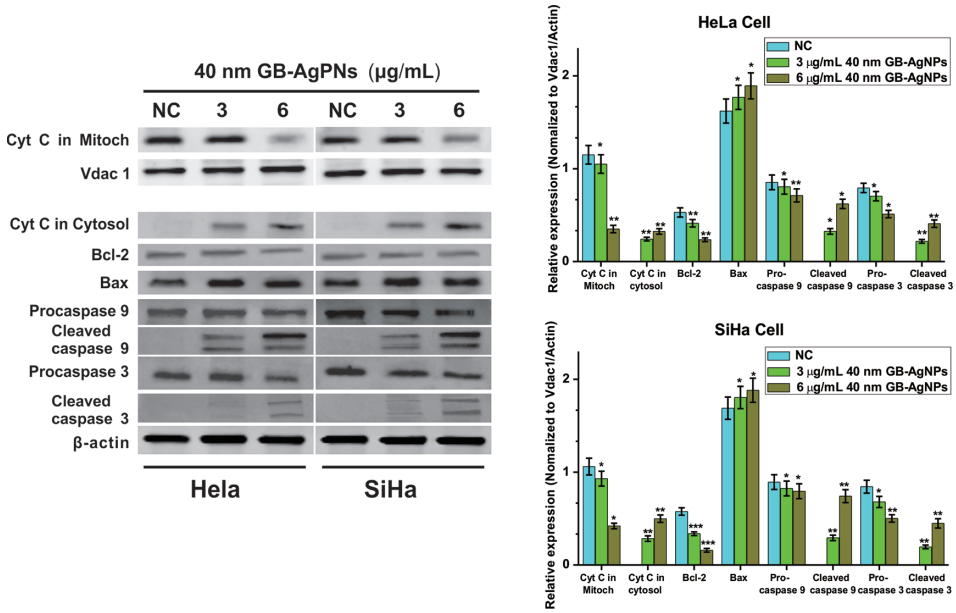


**FIGURE 5** | Ginkgo extract synthesized silver nanoparticles (GB-AgNPs) induce apoptosis through caspase-dependent mitochondrial signalling pathways. Expression levels of apoptosis-related proteins were detected by western blot analysis after HeLa and SiHa cervical cancer cells were treated with the indicated concentrations of 40 nm GB-AgNPs. Data are expressed as the means ± SD; *P < 0.05, **P < 0.01.

and increase the amount of Cyt C released from the mitochondria into the cytosol.

Furthermore, to confirm that GB-AgNPs induced apoptosis through the ROS/Cyt C signaling pathway, we employed the ROS scavenger NAC to measure the effects of Cyt C in the cytosol and caspase-9 and caspase-3 on the apoptosis induced by GB-AgNPs. As shown in **Figure 6**, the effects of the GB-AgNPs on Cyt C release in the cytosol and the cleavage of caspase-9 and caspase-3 were diminished by 20 μM NAC treatment. This finding indicated that NAC blocked the apoptosis induced by the GB-AgNPs, which corroborates the ROS assay results describe above.

## DISCUSSION

In recent decades, AgNPs, particularly green-biosynthesized AgNPs, have exhibited promising potency for biomedical applications due to their powerful antimicrobial properties, effective inhibition of tumour cell proliferation, potent anti-inflammatory and wound healing effects, and substantial chemical stability and biocompatibility (9, 21, 22). On the one hand, green biosynthesis of AgNPs can be undertaken using different natural resources, such as microorganisms, fruit extracts, and medicinal plants, to minimize the amount of stabilizing agents, which adsorb different biologically active

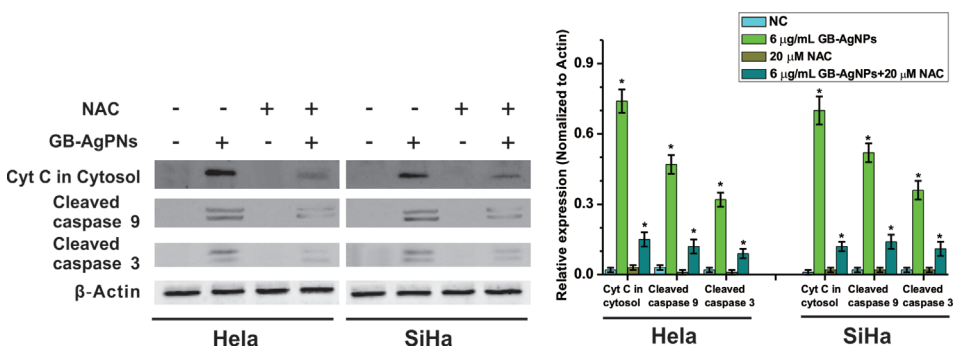


**FIGURE 6** | Ginkgo extract synthesized silver nanoparticles (GB-AgNPs) induce apoptosis through mediated intracellular ROS generation. HeLa and SiHa cells were treated with or without NAC (20 μM) for 4 h and then cells were incubated with GB-AgNPs (6 μg/ml) for 24 h, and the expression levels of apoptosis-related proteins were measured by western blot analysis. Data are expressed as the means ± SD; *P < 0.05.

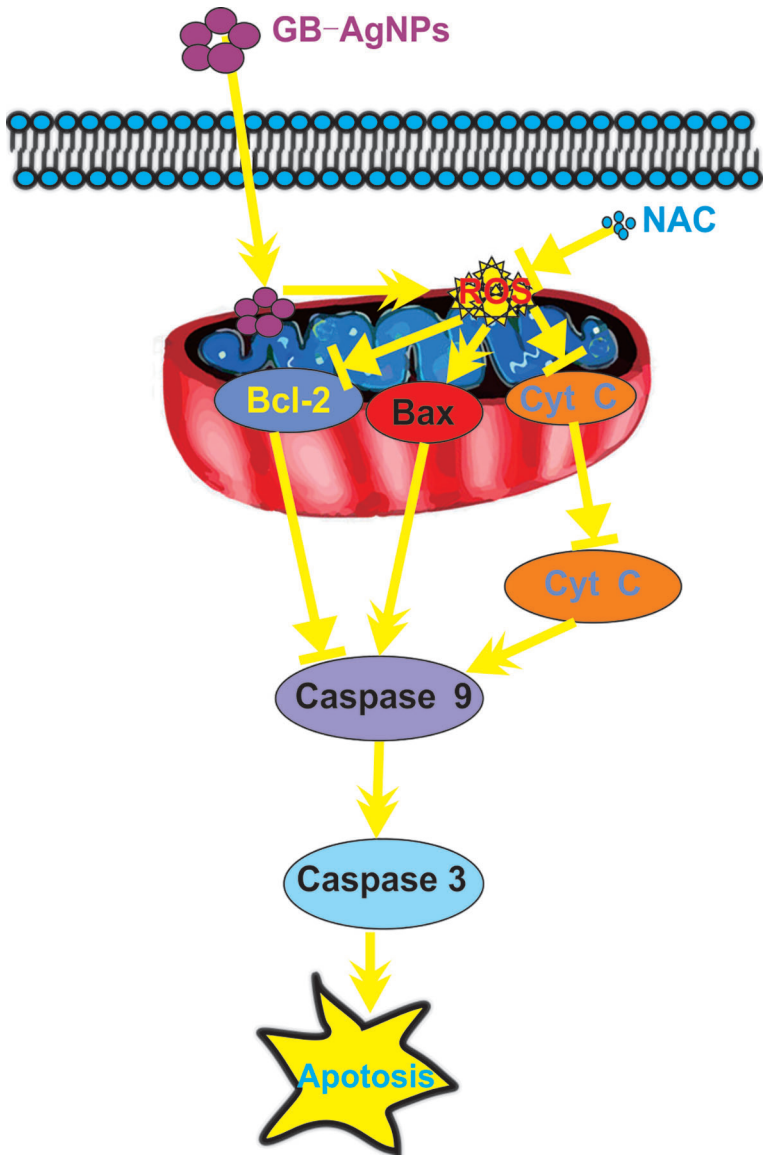


**FIGURE 7** | Schematic mechanisms of Ginkgo extract synthesized silver nanoparticle (GB-AgNP)-induced apoptosis by caspase-dependent mitochondrial signalling pathways in cervical cancer cells.

substances during synthesis, endowing AgNPs with different biological activities (23). On the other hand, green-synthesized AgNPs are generally less toxic to mammalian cells and more environmental friendly than AgNPs synthesized by other methods (24). Biosynthetic AgNPs are larger than the chemosynthetic and physic synthetic AgNPs (9). Interestingly, we know that smaller AgNPs induces greater cytotoxicity, and we verified this phenomenon by MTT assay. Herein, a series of GB-AgNPs were prepared using different concentrations of gingko aqueous extracts, and nanoparticles smaller than 100 nm had narrow distribution and a good coefficient of dispersion, which means that the GB-AgNPs can easily pass through the vascular gap in capillary tumour tissue (25).

The commonly known notable hallmark of cancer is uncontrolled proliferation, which may indicate dysfunctional apoptotic machinery in the cell (4). We first tested whether the GB-AgNPs are capable of inhibiting the proliferation of two CCa cell lines. The results of the MTT, MTS and colony formation assays showed that the GB-AgNPs obviously inhibited the growth and proliferation of HeLa and SiHa cells in a dose-, size-, and time-dependent manner. Second, we discovered that GB-AgNPs induced apoptosis by generating ROS and increasing oxidative stress, which is usually involved in cell apoptosis and mitochondrial dysfunction (26). As expected, the levels of intracellular ROS and lipid oxidation end-product MDA were significantly increased after treatment with GB-AgNPs, compared to those of the controls, which affected the

mitochondrial respiratory chain complex and key enzyme activity in mitochondria *in vitro* (26). Then, the antioxidant enzymes SOD and GSH-Px were found to be consumed at high levels to abrogate the increased ROS levels. Subsequently, we assessed several relative mitochondrial antiapoptotic and proapoptotic proteins by western blot assays. The Cyt C level in the mitochondria was sharply decreased upon GB-AgNP treatment compared to that of the controls, while the Cyt C level in the cytosol was dramatically increased after treatment with GB-AgNPs compared to the level in the controls, and this increase induced the caspase-dependent apoptosis pathway. Additionally, two CCa cells were treated with GB-AgNPs and the antioxidant NAC, and the increased levels of ROS and Cyt C in the cytosol and the extent of caspase-9 and caspase-3 cleavage were diminished. Our study findings strongly indicate that GB-AgNPs generate excess of ROS and induce apoptosis.

ROS play important roles in the progression of cancers (26). Compared to normal cells, cancer cells usually have higher levels of ROS and oxidative stress (27). However, the effect of ROS on the development of cancer is complex. Several studies have shown that ROS can induce DNA mutation and prooncogenic expression, thus promoting cancer formation (26, 27). ROS can also influence cell survival or proliferation by cellular processes (27, 28). Hence, a powerful strategy to fight cancer may be realized by destroying the balanced of intracellular ROS to induce their accumulation. Many studies have shown that many agents could induce cell apoptosis by generating ROS in a verity of cancer cells (29–31). Interestingly, in different studies, AgNPs were found to be antioxidants or prooxidants promoters (7, 8). These contradictory actions may be due to the synthesis of AgNPs using various medicinal plants, not the size of AgNPs nor the dose or duration of the treatment (8). In this study, high ROS levels were observed in both CCa cell lines treated with the GB-AgNPs, which implies that mitochondrial injury is probably involved in the apoptosis induced by GB-AgNPs. Mitochondria are the main production sites of ROS, and high levels of ROS induces mitochondrial membrane permeability, which lead to the release of several mitochondrial proteins into the cytosol (29). Cyt C is known as a proapoptotic protein and activates downstream caspase-dependent apoptosis when it is released from mitochondria into the cytosol (19). Bcl-2 is an antiapoptotic protein that can maintain the integrity of the mitochondrial membrane and prevent the release of Cyt C into the cytosol (32).

In summary, novel green biosynthetic AgNPs were prepared with aqueous extracts of *G. biloba* leaves, and the molecular mechanism of the effect of GB-AgNPs on human CCa (HeLa and SiHa) cell cytotoxicity and apoptosis was explored. Exposure to GB-AgNPs for 24 h induced an increase in ROS generation and mitochondrial membrane permeability, Cyt C release into the cytosol, and the cleavage of caspase-9 and caspase-3. All assays results indicated that GB-AgNPs contributed to the cell apoptosis of HeLa and SiHa cells (**Figure 7**). Herein, the results of this study offer further evidence of the cytotoxicity and the anticancer efficacy caused by increased ROS levels that induce the caspase-dependent mitochondrial apoptotic signaling pathways, which justifies further exploration of GB-AgNP potential for cancer therapeutics and preventive CCa treatments.

## DATA AVAILABILITY STATEMENT

All datasets generated for this study are included in the article/ **Supplementary Material**.

## AUTHOR CONTRIBUTIONS

ZX and MW: Data analysis and interpretation. QF: Data analysis writing. HZ: Data collection and analysis. YL: Data collection. SZ: Conception and design, data analysis and interpretation, and writing. All authors contributed to the article and approved the submitted version.

## FUNDING

This work was supported by the Key Research and Development Project of Hainan Province (Grant No.ZDYF2019177), the Open Fund Project of Hainan Provincial Key Laboratory of Basic Medicine (Grant No.JCKF2020010), and the National Natural Science Foundation of China (Grant No. 81560484).

## SUPPLEMENTARY MATERIAL

The Supplementary Material for this article can be found online at: https://www.frontiersin.org/articles/10.3389/fonc.2020.575415/full#supplementary-material

## REFERENCES

1. Siegel RL, Miller KD, Jemal A. Cancer statistics, 2020. *CA Cancer J Clin* (2020) 70(1):7–30. doi: 10.3322/caac.21590
2. Canfell K, Kim JJ, Brisson M, Keane A, Simms KT, Caruana M, et al. Mortality impact of achieving WHO cervical cancer elimination targets: a comparative modelling analysis in 78 low-income and lower-middle-income countries. *Lancet* (2020) 395(10224):591–603. doi: 10.1016/S0140-6736(20)30157-4
3. Brisson M, Kim JJ, Canfell K, Drolet M, Gingras G, Burger EA, et al. Impact of HPV vaccination and cervical screening on cervical cancer elimination: a comparative modelling analysis in 78 low-income and lower-middle-income countries. *Lancet* (2020) 395(10224):575–90. doi: 10.1016/S0140-6736(20)30068-4
4. Cohen AC, Roane BM, Leath CA,3. Novel Therapeutics for Recurrent Cervical Cancer: Moving Towards Personalized Therapy. *Drugs* (2020) 80 (3):217–27. doi: 10.1007/s40265-019-01249-z
5. Merz SN, Farrell ZJ, Dunn CJ, Swanson RJ, Egorov SA, Green DL. Theoretical and Experimental Investigation of Microphase Separation in Mixed Thiol Monolayers on Silver Nanoparticles. *ACS Nano* (2016) 10(11):9871–8. doi: 10.1021/acsnano.6b02091
6. Krasniewska K, Galus S, Gniewosz M. Biopolymers-Based Materials Containing Silver Nanoparticles as Active Packaging for Food Applications-A Review. *Int J Mol Sci* (2020) 21(3):698. doi: 10.3390/ijms 21030698
7. Docea AO, Calina D, Buga AM, Zlatian O, Paoliello MMB, Mogosanu GD, et al. The Effect of Silver Nanoparticles on Antioxidant/Pro-Oxidant Balance

in a Murine Model. *Int J Mol Sci* (2020) 21(4):1233. doi: 10.3390/ijms21041233
8. Chinnasamy G, Chandrasekharan S, Bhatnagar S. Biosynthesis of Silver Nanoparticles from Melia azedarach: Enhancement of Antibacterial, Wound Healing, Antidiabetic and Antioxidant Activities. *Int J Nanomed* (2019) 14:9823–36. doi: 10.2147/IJN.S231340
9. Guilger-Casagrande M, de Lima R. Synthesis of Silver Nanoparticles Mediated by Fungi: A Review. *Front Bioeng Biotechnol* (2019) 7:287. doi: 10.3389/fbioe.2019.00287
10. Bader BM, Jugelt K, Schultz L, Schroeder OH, Ginkgo biloba L. (Ginkgoaceae) Leaf Extract Medications From Different Providers Exhibit Differential Functional Effects on Mouse Frontal Cortex Neuronal Networks. *Front Pharmacol* (2018) 9:848. doi: 10.3389/fphar.2018.00848
11. Ude C, Schubert-Zsilavecz M, Wurglics M. Ginkgo biloba extracts: a review of the pharmacokinetics of the active ingredients. *Clin Pharmacokinet* (2013) 52 (9):727–49. doi: 10.1007/s40262-013-0074-5
12. Omidkhoda SF, Razavi BM, Hosseinzadeh H. Protective effects of Ginkgo biloba L. against natural toxins, chemical toxicities, and radiation: A comprehensive review. *Phytother Res* (2019) 33(11):2821–40. doi: 10.1002/ptr.6469
13. Zhang K, Liu X, Samuel Ravi SOA, Ramachandran A, Aziz Ibrahim IA, Nassir AM, et al. Synthesis of silver nanoparticles (AgNPs) from leaf extract of Salvia miltiorrhiza and its anticancer potential in human prostate cancer LNCaP cell lines. *Artif Cells Nanomed Biotechnol* (2019) 47(1):2846–54. doi: 10.1080/21691401.2019.1638792
14. Prateeksha, BR S, VK G, Deeba F, Bajpai R, Pandey V, et al. Non-Toxic and Ultra-Small Biosilver Nanoclusters Trigger Apoptotic Cell Death in Fluconazole-Resistant Candida albicans via Ras Signaling. *Biomolecules* (2019) 9(2):47. doi: 10.3390/biom9020047
15. Li L, Li L, Zhou X, Yu Y, Li Z, Zuo D, et al. Silver nanoparticles induce protective autophagy via Ca(2+)/CaMKKbeta/AMPK/mTOR pathway in SH-SY5Y cells and rat brains. *Nanotoxicology* (2019) 13(3):369–91. doi: 10.1080/17435390.2018.1550226
16. Kanipandian N, Li D, Kannan S. Induction of intrinsic apoptotic signaling pathway in A549 lung cancer cells using silver nanoparticles from Gossypium hirsutum and evaluation of in vivo toxicity. *Biotechnol Rep (Amst)* (2019) 23: e00339. doi: 10.1016/j.btre.2019.e00339
17. Wang M, Zhao H, Hu J, Xu Z, Lin Y, Zhou S, et al. A New Azaphilone, Induces Apoptosis in Gastric Cancer by Blocking the Notch Signaling Pathway. *Front Oncol* (2020) 10:116. doi: 10.3389/fonc.2020.00116
18. Sanyasi S, Majhi RK, Kumar S, Mishra M, Ghosh A, Suar M, et al. Polysaccharide-capped silver Nanoparticles inhibit biofilm formation and eliminate multi-drug-resistant bacteria by disrupting bacterial cytoskeleton with reduced cytotoxicity towards mammalian cells. *Sci Rep* (2016) 6:24929. doi: 10.1038/srep24929
19. You L, Yang C, Du Y, Liu Y, Chen G, Sai N, et al. Matrine Exerts Hepatotoxic Effects via the ROS-Dependent Mitochondrial Apoptosis Pathway and Inhibition of Nrf2-Mediated Antioxidant Response. *Oxid Med Cell Longev* (2019) 2019:1045345. doi: 10.1155/2019/1045345
20. Yao W, Lin Z, Wang G, Li S, Chen B, Sui Y, et al. Delicaflavone induces apoptosis via mitochondrial pathway accompanying G2/M cycle arrest and inhibition of MAPK signaling cascades in cervical cancer HeLa cells. *Phytomedicine* (2019) 62:152973. doi: 10.1016/j.phymed.2019.152973
21. Gnanakani PE, Santhanam P, Premkumar K, Eswar Kumar K, Dhanaraju MD. Nannochloropsis Extract-Mediated Synthesis of Biogenic Silver Nanoparticles, Characterization and In Vitro Assessment of Antimicrobial, Antioxidant and Cytotoxic Activities. *Asian Pac J Cancer Prev* (2019) 20 (8):2353–64. doi: 10.31557/APJCP.2019.20.8.2353
22. Villeret B, Dieu A, Straube M, Solhonne B, Miklavc P, Hamadi S, et al. Silver Nanoparticles Impair Retinoic Acid-Inducible Gene I-Mediated Mitochondrial Antiviral Immunity by Blocking the Autophagic Flux in Lung Epithelial Cells. *ACS Nano* (2018) 12(2):1188–202. doi: 10.1021/acsnano.7b06934
23. Sathiyaseelan A, Saravanakumar K, Mariadoss AVA, Wang MH. Biocompatible fungal chitosan encapsulated phytogenic silver nanoparticles enhanced antidiabetic, antioxidant and antibacterial activity. *Int J Biol Macromol* (2020) 153:63–71. doi: 10.1016/j.ijbiomac.2020.02.291
24. Pedziwiatr-Werbicka E, Horodecka K, Shcharbin D, Bryszewska M. Nanoparticles in combating cancer: Opportunities and limitations. A brief review. *Curr Med Chem* (2020) 27. doi: 10.2174/0929867327666200130101605
25. Erdogan O, Abbak M, Demirbolat GM, Birtekocak F, Aksel M, Pasa S, et al. Green synthesis of silver nanoparticles via Cynara scolymus leaf extracts: The characterization, anticancer potential with photodynamic therapy in MCF7 cells. *PLoS One* (2019) 14(6):e0216496. doi: 10.1371/journal.pone.0216496
26. Shadel GS, Horvath TL. Mitochondrial ROS signaling in organismal homeostasis. *Cell* (2015) 163(3):560–9. doi: 10.1016/j.cell.2015.10.001
27. Yamada M, Han X, Benfey PN. RGF1 controls root meristem size through ROS signalling. *Nature* (2020) 577(7788):85–8. doi: 10.1038/s41586-019-1819-6
28. Lee CH, Ying TH, Chiou HL, Hsieh SC, Wen SH, Chou RH, et al. Alpha-mangostin induces apoptosis through activation of reactive oxygen species and ASK1/p38 signaling pathway in cervical cancer cells. *Oncotarget* (2017) 8 (29):47425–39. doi: 10.18632/oncotarget.17659
29. Yee C, Yang W, Hekimi S. The intrinsic apoptosis pathway mediates the pro-longevity response to mitochondrial ROS in C. elegans. *Cell* (2014) 157 (4):897–909. doi: 10.1016/j.cell.2014.02.055
30. Anupama N, Preetha Rani MR, Shyni GL, Raghu KG. Glucotoxicity results in apoptosis in H9c2 cells via alteration in redox homeostasis linked mitochondrial dynamics and polyol pathway and possible reversal with cinnamic acid. *Toxicol In Vitro* (2018) 53:178–92. doi: 10.1016/j.tiv.2018.08.010
31. Fu SC, Liu JM, Lee KI, Tang FC, Fang KM, Yang CY, et al. Cr(VI) induces ROS-mediated mitochondrial-dependent apoptosis in neuronal cells via the activation of Akt/ERK/AMPK signaling pathway. *Toxicol In Vitro* (2020) 65:104795. doi: 10.1016/j.tiv.2020.104795
32. Lv J, Guan W, You Q, Deng L, Zhu Y, Guo K, et al. RIPC provides neuroprotection against ischemic stroke by suppressing apoptosis via the mitochondrial pathway. *Sci Rep* (2020) 10(1):5361. doi: 10.1038/s41598-020-62336-w

**Conflict of Interest:** The authors declare that the research was conducted in the absence of any commercial or financial relationships that could be construed as a potential conflict of interest.

frontiers in Oncology

ORIGINAL RESEARCH
published: 21 October 2020
doi: 10.3389/fonc.2020.563938

# Dual-Target Peptide-Modified Erythrocyte Membrane-Enveloped PLGA Nanoparticles for the Treatment of Glioma

*Yuexin Cui[1,2], Jiejie Sun[2], Wenyan Hao[2], Mengyu Chen[1,2], Yingzi Wang[1]*, Fenghua Xu[3]* and Chunsheng Gao[2]**

[1] School of Chinese Materia Medica, Beijing University of Chinese Medicine, Beijing, China, [2] State Key Laboratory of Toxicology and Medical Countermeasures, Beijing Institute of Pharmacology and Toxicology, Beijing, China, [3] Department of Pharmacy, People's Liberation Army of China (PLA) General Hospital, Beijing, China

OPEN ACCESS

**Edited by:**
João Paulo Longo,
University of Brasilia, Brazil

**Reviewed by:**
Shanmugarajan Krishnan,
Massachusetts General Hospital, United States
Pablo Lorenzano Menna,
National University of Quilmes, Argentina

***Correspondence:**
Yingzi Wang
wangyzi@sina.com
Fenghua Xu
xufh@301hospital.com.cn
Chunsheng Gao
largedna@163.com

**Specialty section:**
This article was submitted to Cancer Molecular Targets and Therapeutics, a section of the journal Frontiers in Oncology

**Received:** 20 May 2020
**Accepted:** 30 September 2020
**Published:** 21 October 2020

**Citation:**
Cui Y, Sun J, Hao W, Chen M, Wang Y, Xu F and Gao C (2020) Dual-Target Peptide-Modified Erythrocyte Membrane-Enveloped PLGA Nanoparticles for the Treatment of Glioma. Front. Oncol. 10:563938. doi: 10.3389/fonc.2020.563938

Penetration of the blood–brain barrier (BBB) and the blood–brain tumor barrier (BBTB) remains a significant challenge for the delivery of drugs in the treatment of glioma. Therefore, the development of targeted preparations with the ability to penetrate the BBB and BBTB, and target gliomas, is an important approach if we are to improve the efficacy of glioma treatment. In the current study, an active targeting preparation based on PLGA nanoparticles coated with erythrocyte membranes (RBCNPs) and dual-modified with $^{D}$WSW and NGR peptide ligands ($^{D}$WSW/NGR-RBCNPs). Euphorbia factor L1 (EFL1) extracted from euphorbiae semen was used as the model drug. The final nanoparticles were characterized by *in vivo* and *in vitro* tests. *In vitro* results showed that EFL1-loaded $^{D}$WSW/NGR-RBCNPs were taken up by cells and had the ability to penetrate the BBB and BBTB and produce cytotoxic effects. Furthermore, *in vivo* studies in mice showed that when injected intravenously, these specialized NPs could enter the brain, target tumor tissue, and significantly extend life span. The results showed that dual-targeting EFL1-loaded $^{D}$WSW/NGR-RBCNPs have significant potential as a nanotherapeutic tool for the treatment of brain glioma.

**Keywords: dual-targeting, biomimetic nanoparticles, NGR, $^{D}$WSW, blood–brain barrier, blood–brain tumor barrier, euphorbia factor L1, glioma**

## INTRODUCTION

Biomimetics has been recognized as an important mission in science and engineering for a long time. Currently developed drug delivery carrier materials are usually synthetic polymer compounds. The carrier materials or the carrier surface are modified according to the different purposes of use (1–4). However, such modification often fails to fully recognize complex endogenous substances in the body. And sometimes it is even regarded as exogenous poisons excreted from the body, failing to reach the lesion site and achieve the desired effect as designed. Cell membrane biomimetic nanoparticles are realized by using natural cell membrane as the shell to encapsulate the synthesized nanoparticles. Through this strategy, the structure and function of the cell

membrane, especially the specific functional proteins on the cell membrane surface, are preserved (2, 5, 6). This means it can also reduce the elimination of nanoparticles.

Glioma is a fatal disease that has high incidence, recurrence, and mortality rates. Clinical data demonstrates that the cure rates for this disease are low (7). The current methods that are commonly used for the treatment of glioma are surgery, radiotherapy, and chemotherapy. However, the clinical efficacy of the drugs used to treat glioma is not satisfactory. Many drugs cannot be used in patients with glioma because of their poor physicochemical properties, lack of targeting capability, and their inability to penetrate the blood–brain barrier (BBB) and blood –brain tumor barrier (BBTB) (8–10). Therefore, there is significant interest in developing new ways to deliver therapeutic drugs to the site of gliomas.

Dual-targeting nanocarriers have already demonstrated their ability to circumvent the BBB and BBTB and deliver specific drugs to glioma sites (11). Over the past few decades, a range of nanocarriers have emerged; many of these exploit different materials to alter their properties. However, these synthetic materials are generally associated with poor efficacy and commonly cause toxicity (12, 13). Research has shown that many nanoparticles are eliminated by the immune system, thus resulting in a reduction in therapeutic effect (14–17). Over recent years, the membranes of erythrocytes have attracted significant attention within the nanotechnology sector, largely because of they are easily obtained and their low levels of immunogenicity. Encapsulating erythrocyte/red blood cell membranes on poly(lactic-co-glycolic acid) (PLGA) nanoparticles (RBCNPs) with targeting modifications has already been shown to achieve unexpected therapeutic effects (1, 2, 18–20).

Typically, the surface of the erythrocyte membrane is modified with a peptide by lipid-insertion. Quorum sensing (QS) signaling molecules are one of them. Coordinated changes in a growing microbial population that are achieved through signaling molecules is referred to as quorum sensing (QS). Some peptides can selectively penetrate the BBB. For example, the $^{D}$WSW ($^{D}$W$^{D}$S$^{D}$W$^{D}$G$^{D}$P$^{D}$Y$^{D}$S) peptide originates from Clostridium acetobutylicum and could be used to target the brain (21, 22). In addition, specific drugs can be designed in such a way that they can target highly expressed targets in glioma cells. CD13 is one such target and can be targeted by NGR (Asn-Gly-Arg), a peptide that exhibits high affinity for CD13. The CD13 receptor also plays a crucial role in promoting angiogenesis in receptor-mediated anti-angiogenic therapy. Over recent years, $^{D}$WSW- and NGR-modified nanocarriers have been developed (23–26).

Euphorbia factor L1 (EFL1) is a lathyrane-type diterpenoid active component that is extracted and separated from Euphorbiae Semen (seeds of *Euphorbia lathyris* L.), a traditional form of Chinese medicine. Existing research shows that EFL1 has significant antitumor effects and has been demonstrated to exert cytotoxic effects in HeLa, A549, C6, MCF-7, and HL-60 cells; it can also reverse activity against P-glycoprotein-mediated multidrug resistance in cells (27–31). However, the clinical application of EFL1 is limited by its poor water solubility and low bioavailability. The solubility of EFL1 can be increased by encapsulation in PLGA nanoparticles (32, 33).

Based on these previous findings, we designed dual-targeting RBCNPs that were modified with $^{D}$WSW and NGR by lipid insertion. These nanocarriers were able to penetrate the BBB and the BBTB synergistically and target glioma cells. The efficacy of these dual-modified RBCNPs ($^{D}$WSW/NGR-RBCNPs) following EFL1 encapsulation with respect to glioma treatment was evaluated using both *in vitro* and *in vivo* approaches (**Figure 1**). The current study aimed to develop a safe and effective treatment for glioma.

# MATERIALS AND METHODS

## Materials

PLGA, with a lactic/glycolic acid ratio of 75/25 (5600 Da), was obtained from Jinan Daigang Biomaterial Co., Ltd (Shandong, China). 1,2-distearoyl-sn-glycero-3-phosphoethanolamine -N-[maleimide(polyethylene glycol)-2000] (DSPE-PEG$_{2000}$-Mal), $^{D}$WSW, and NGR peptides were purchased from Xi`an ruixi Biological Technology Co., Ltd (Shanxi, China). Euphorbia factor L1 (EFL1) was obtained from Chendu Dsiter Co., Ltd (Sichuan, China). Anti-CD47 antibodies were purchased from Abcam (Cambridge, UK). All chemical reagents were of analytical grade and were purchased from Macklin Biochemical Co., Ltd (Shanghai, China).

## Cells and Experimental Animals

Glioma cells (C6), mouse brain endothelial cells (bEnd.3), and human umbilical vascular endothelial cells (HUVECs), were supplied by the Cell Resource Centre of IBMS (Beijing, China) and cultured in Dulbecco's modified Eagle's medium (DMEM) containing 10% FBS (Gibco) and 100 IU penicillin.

Female and male ICR mice (initially weighing 18–22 g) were purchased from SPF Biotechnology Co., Ltd (Permit number: SCXK (Jing) 2019-0010, Beijing, China). All animal experiments complied with the National Laboratory Animal Management Regulations, and the Beijing Municipal Laboratory Animal Management Regulations. All procedures and experiments involving the care and handling of animals were carried out with the approval of the Animal Care and Use Ethics Committee of Beijing Institute of Pharmacology and Toxicology (Beijing, China).

## Preparation of Peptide-Modified RBCNPs

### Synthesis and Characterization of Materials

DSPE-PEG$_{2000}$-$^{D}$WSW and DSPE-PEG$_{2000}$-NGR were synthesized using the sulfhydryl-maleimide coupling method between thiolated peptides and DSPE-PEG$_{2000}$-Mal. In brief, DSPE-PEG$_{2000}$-Mal in PBS (pH 7.4) was slowly added to a $^{D}$WSW or NGR (1:1 molar ratio) solution (PBS, pH 7.4) at room temperature for 24 h while stirring. Unreacted compounds were then removed by washing with distilled water (MWCO 3.0

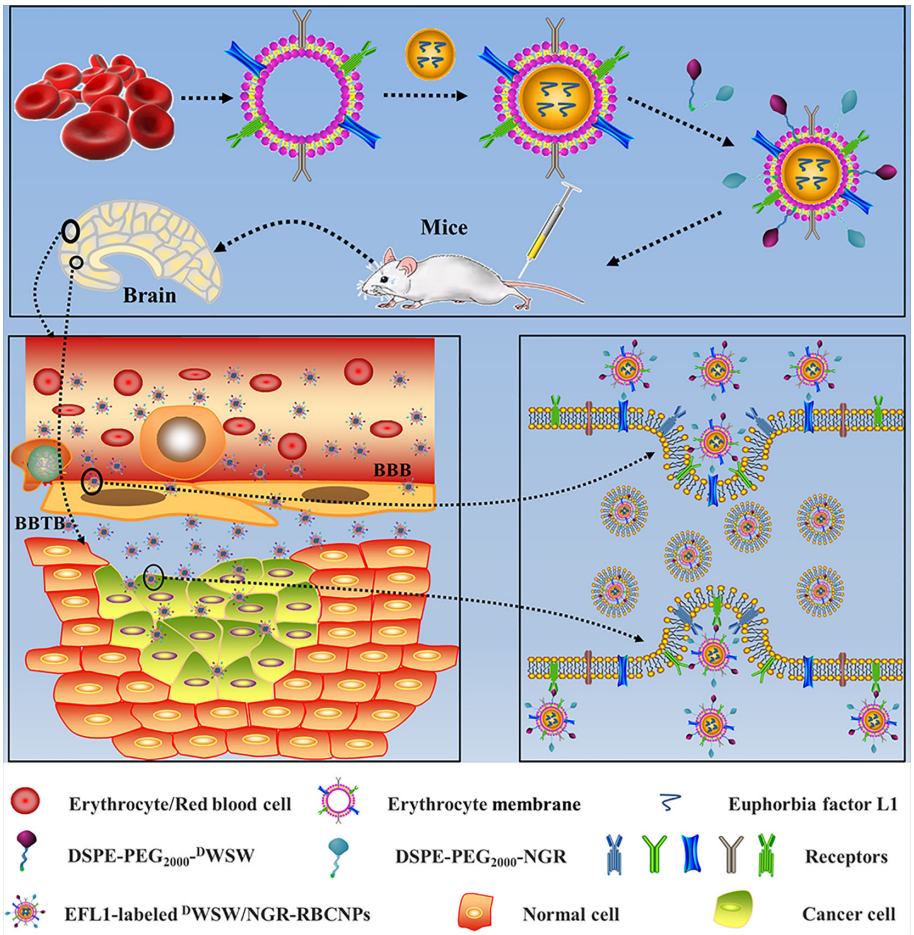


**FIGURE 1** | Graphical abstract of this study. Schematic illustration of dual-target peptides modified using erythrocyte membrane-enveloped PLGA nanoparticles for the treatment of glioma. The nanoparticles were designed to penetrate the BBB and BBTB and then to aggregate at tumor sites. $^{D}$WSW peptide was used to penetrate BBB and NGR was used to target tumor. $^{D}$WSW/NGR-RBCNPs were observed to selectively accumulate in tumor tissue and exert a therapeutic effect.

kDa). The final solution was freeze-dried to await further use. Prior to application, the compounds were assessed by MALDI-TOF mass spectrometry (MALDI-TOF MS).

## Collection of Erythrocyte Membranes

Erythrocyte membranes were collected as previously reported (34, 35). In brief, cells were collected from mice and transferred into tubes coated with an anticoagulant. Plasma and leukocytes were removed by centrifugation (3,000 rpm for 10 min at 4°C). PBS (pH = 7.4) was then added into the tubes and centrifuged at 3,000 rpm for 10 min at 4°C; this procedure was repeated three times. The red blood cells (RBCs) were suspended in 0.25 × PBS (pH = 7.4), stored at 4°C for 0.5 h, and then centrifuged (8000 rpm for 10 min at 4°C); this procedure was repeated three times. Finally, the erythrocyte membranes were suspended in PBS (pH = 7.4) and stored at 4°C to await further use.

## Preparation of PLGA Nanoparticles

PLGA nanoparticles (NPs) were prepared by a nano-precipitation method, as described previously (36–38). A total of 40 mg of PLGA, and 4 mg of EFL1 or Cy5.5 (hydrophobic probe, 100 μL), was added to 4 mL of acetone. Once completely dissolved, the mixture was poured into 10 mL of water slowly. Then, the mixture was then stirred in open air for 24 h to eliminate the organic solvent; the resultant products were EFL1-loaded NPs or Cy5.5-labelled NPs.

## Preparation of RBCNPs Modified With Peptides

Erythrocyte membranes were sonicated for 3 min in a bath sonicator (KQ3200, Kunshan, China) at a frequency of 37 kHz and a power of 250 W. Using a mini-extruder (Avanti Polar Lipids, AL, USA), we isolated erythrocyte membrane vesicles by extruding the membranes repeatedly through 400 nm and 200 nm polycarbonate porous membranes.

To prepare nonmodified-RBCNPs (N-RBCNPs), EFL1-labelled NPs or Cy5.5-loaded NPs were mixed with erythrocyte membrane vesicles (at a ratio of 3:1) and then extruded through a 200 nm polycarbonate membrane at least 10 times; this procedure created EFL1-loaded RBCNPs or Cy5.5-labelled RBCNPs. The $^{D}$WSW-modified RBCNPs ($^{D}$WSW-RBCNPs),

NGR-modified RBCNPs (NGR-RBCNPs), and $^{D}$WSW/NGR modified RBCNPs ($^{D}$WSW/NGR-RBCNPs), were prepared using a lipid-insertion technique. DSPE-$PEG_{2000}$-$^{D}$WSW (4%, weight ratio of DSPE-$PEG_{2000}$-$^{D}$WSW to NPs), or DSPE-$PEG_{2000}$-NGR (3%, weight ratio), was added to RBCNPs in PBS (pH 7.4) at 37°C with stirring for approximately 0.5 h. In order to prepare $^{D}$WSW/NGR-RBCNPs, both DSPE-$PEG_{2000}$-$^{D}$WSW and DSPE-$PEG_{2000}$-NGR were added to the solution.

## Physicochemical Characterization of Dual-Modified RBCNPs

### Binding Efficiency of Peptides Onto RBCNPs

We created a DSPE-$PEG_{2000}$-peptide-fluorescent probe by reacting the carboxyl group in a fluorescent probe with the primary amine group in the DSPE-$PEG_{2000}$-peptide. Specifically, DSPE-$PEG_{2000}$-NGR was labelled with 5-(and 6)-carboxyfluoresceindiacetate (CFDA) using the following protocol. First, CFDA was dissolved in dimethyl sulfoxide; we then added N, N'-dicyclohexyl carbodiimide and N-hydroxysuccinimide (4:2:1). This solution was stirred in the dark for 24 h at room temperature and then centrifuged (4,000 r/min, 15 min) to obtain a supernatant. Next, 1.2% of DSPE-$PEG_{2000}$-NGR, and one drop of triethylamine, were added and allowed to react for 24 h in the dark. Then, the products were dialyzed (MWCO 3.5 kDa) in purified water for 24 h in a light-proof environment. The purified solid product (DSPE-$PEG_{2000}$-NGR-CFDA) was obtained by freeze-drying. Using the same methodology, we labelled DSPE-$PEG_{2000}$-$^{D}$WSW with 5-carboxy-X-rhodamine (5-ROX). The purified solid product (DSPE-$PEG_{2000}$-$^{D}$WSW-5-ROX) was also obtained by freeze-drying. The preparation of fluorescent probe-labelled dual-modified RBCNPs ($^{D}$WSW-5-ROX/CFDA-NGR-RBCNPs) involved DSPE-$PEG_{2000}$-$^{D}$WSW-5-ROX and DSPE-$PEG_{2000}$-NGR-CFDA; the methodology was the same as that used to prepare the $^{D}$WSW/NGR-RBCNPs.

The DSPE-$PEG_{2000}$-NGR-CFDA, DSPE-$PEG_{2000}$-$^{D}$WSW-5-ROX, or N-RBCNPs, were dispersed in PBS (pH 7.4). Next, the maximum absorption wavelengths of DSPE-$PEG_{2000}$-NGR-CFDA and DSPE-$PEG_{2000}$-$^{D}$WSW-5-ROX were determined using a UV-visible spectrophotometer (scanned at 200-800 nm). The absorbance (A) of CFDA was measured at 493 nm while that of 5-ROX was measured at 578 nm (standard solution, 0.5 to 3.50 μg/mL); this allowed us to perform linear regression analysis.

$^{D}$WSW-5-ROX/NGR-CFDA-RBCNPs were diluted with PBS to measure the total absorbance ($A_{Total}$). Then, the absorbance of the free targeting-peptide ($A_{Free}$) was determined by ultrafiltration centrifugation (MWCO 300 kDa, 12000 r/min). The formula used to determine the connection efficiency of $^{D}$WSW-5-ROX/NGR-CFDA-RBCNPs is given in Equation (1).

$$\text{Connection efficiency} = (A_{Total} - A_{Free})/A_{Total} \times 100\,\% \quad (1)$$

### Characterization of Dual-Modified RBCNPs

Biomimetic nanoparticle particle size distribution and zeta potential were measured by dynamic light scattering (Litesizer™ 500, Anton-Paar, Austria). Transmission electron microscopy (TEM) (HITACHI, H-7650, Japan) was used to characterize the morphology of EFL1-loaded $^{D}$WSW/NGR-RBCNPs. Protein analysis was performed by sodium dodecyl sulfate-polyacrylamide gel electrophoresis (SDS-PAGE) (39). Protein concentration was determined using a BCA assay kit (Pierce, China) and western blotting was used to analyze the expression levels of the glycoprotein CD47 (40). Turbiscan Lab® Expert (Formulaction, L'Union, France) was used to evaluate the 72-hour stability of EFL1-loaded $^{D}$WSW/NGR-RBCNPs in FBS (37°C); we also used this instrument's software to apply a variety of back-scattering (ΔBS) profiles to investigate stability.

Equation (2) and (3) was used to calculate the EFL1 encapsulation efficiency (EE) and drug loading capacity (DL) for various particles.

$$\text{EE}\,\% = (W_{total\ drug} - W_{free\ drug})/W_{total\ drug} \times 100\,\% \quad (2)$$

$$\text{DL}\,\% = (W_{total\ drug} - W_{free\ drug})/W_{total\ drug\ and\ carriers} \times 100\,\% \quad (3)$$

$W_{total\ drug}$ represents the total drug in the NPs, $W_{free\ drug}$ represents the amount of free drug removed by ultrafiltration while $W_{total\ drug\ and\ carriers}$ represents the weight of total drug and carriers. The amount of EFL1 was determined by HPLC analysis.

## *In Vitro* Evaluation of Dual-Modified RBCNPs

### *In Vitro* Release

The release of EFL1 from different nano-preparations was determined using dialysis buffer (pH 7.4). Approximately 1 mL of the various nanoparticle solutions was added to a dialysis bag (MWCO 12 kDa). A release study was then performed in 100 mL of medium at 37°C; 1 mL of medium was removed for analysis at 0, 0.5, 1, 2, 4, 6, 8, 10, 12, 24, 36, and 48 h and was replaced with the same volume of fresh medium. HPLC was then used to determine the concentration of EFL1 released at different times.

### *In Vitro* Cell Uptake

In order to investigate the uptake of various RBCNPs, we incubated a variety of different cells (C6, bEnd.3, and HUVECs) in 200 μL of DiI-labeled mono- or dual-modified RBCNPs at 37°C for 2 h. Controls were also included in these experiments; these involved nanoparticles that were devoid of ligands. After the experiment, cells were washed and centrifuged three times with cold PBS. We then analyzed the cells qualitatively using confocal laser scanning microscopy (LSM 880, Zeiss, Germany); quantitative analysis was performed by flow cytometry (FCM).

### *In Vitro* Cytotoxicity Assays

The MTT assay was used to evaluate the cytotoxicity of different nanoparticles in C6 cells. Cells were first seeded in 96-well plates (approximately 5,000 cells per well). Then, cells were exposed to various concentrations of the RBCNP formulations. After 48 h, we added 20 μL of MTT solution (5 mg/mL in PBS) to each well. After a 4 h period of incubation, we determined cell viability at 490 nm using a plate reader (Tecan Spark, Austria).

### *In Vitro* Transport Across the BBB and BBTB

An *in vitro* BBB model was established as reported previously by Ying Man et al. (41). To summarize, bEnd.3 cells were inoculated at a density of $1.0 \times 10^5$ cells per well (Corning, NY, USA). Successful creation of the BBB was confirmed by measuring transendothelial electrical resistance; the BBB transport assay was performed when resistance reached 200 $\Omega.cm^2$ (42). Different Cy5.5-labeled RBCNPs (50 μM) were then added to DMEM containing 10% FBS for further culture. After 4 h, the solution was collected from the basal chamber and the fluorescence intensity was monitored using a fluorescence spectrophotometer (Agilent Cary Eclipse, USA). HUVECs were seeded in the upper inserts of the transwell and C6 cells were seeded in the lower chamber (at a ratio of 5:1) to create the final *in vitro* BBTB model (43). Different Cy5.5-labeled RBCNPs were then added to the culture medium in each upper chamber. After 4 h, the solution was collected from the lower chamber and the fluorescence intensity was determined by fluorescence spectrophotometry.

### *In Vitro* Targeting Ability

The *in vitro* BBB model was created by bEnd.3 and C6 cells, as previously reported (43). To summarize, the upper side of a transwell insert was seeded with approximately $1.0 \times 10^5$ bEnd.3 cells. The basolateral compartment was then seeded with 2000 C6 cells per compartment. The experiment was performed after 5 d of incubation. Free EFL1, and various EFL1-loaded nanoparticles, were added to the apical compartment. The final concentration of EFL1 in each compartment was 50 μg/mL. Then, 48 h later, the survival rate of the C6 cells was determined with a sulforhodamine-B staining assay (44).

## *In Vivo* Evaluation of Dual-Modified RBCNPs

### *In Vivo* Glioma Targeting Ability

A glioma-bearing mouse model was established by inoculating C6 cells into the brain, as described previously (45). After 7 d, the brain glioma was evaluated by magnetic resonance imaging (MRI) (PharmaScan 70T/16, Bruke, US). We then selected glioma-bearing mice with similar tumor volumes and measured their basal levels of fluorescence levels prior to treatment. Different RBCNPs were then labeled with DiR for *in vivo* imaging studies. Next, the animals were administered with DiR-loaded N-RBCNPs, DiR-loaded $^{D}$WSW-RBCNPs, DiR-loaded NGR-RBCNPs, and DiR-loaded $^{D}$WSW/NGR-RBCNPs, *via* tail vein injection. *In vivo* imaging was carried out 12 h later using a small animal imaging system (IVIS® Spectrum, PerkinElmer, USA) and Living Image® software (Caliper, Alameda, CA) used to quantify bioluminescence and fluorescence signals. Following *in vivo* imaging, we isolated the main organs of each mouse and determined the tissue distribution of each type of nanoparticle. DiI-labeled RBCNPs were then used for brain distribution studies. After 4 h, mice were sacrificed and the brain tissues were harvested. These tissues were then frozen in O.C.T. (Sakura, Torrance, CA, USA), cut into 5 mm frozen sections, stained with DAPI, and analyzed by CLSM.

### Antitumor Effect in Mice

Glioma-bearing mice were randomly divided into six groups (10 mice per group): a normal saline group, a free EFL1 group, an EFL1-loaded N-RBCNP group, an EFL1-loaded $^{D}$WSW-RBCNP group, an EFL1-loaded NGR-RBCNP group, and an EFL1-loaded $^{D}$WSW/NGR-RBCNP group. Seven days after the injection of C6 cells, each mouse received a drug at a dose of 100 μg/kg (based on EFL1 in the formulations); the dose was administered once each day. In each mouse, we then recorded the length of time between tumor cell inoculation and death. Survival times were used to plot Kaplan-Meier survival curves for each group.

### Histopathological Examination of Brain Tumors

Mice were sacrificed at the end of drug treatment, and their brains were isolated. Each brain was fixed in 10% formalin buffer for 24 h, embedded in paraffin, cut into 5 μm sections, and stained with hematoxylin and eosin. Histopathological examinations were then carried out with a light microscope (Olympus, Japan) with a view to identify tumor tissue and acquire representative digital images.

## Acute Toxicity Evaluation

Mice were randomly divided into three groups (6 mice per group) as follows: a normal saline group, a free EFL1 group, and an EFL1-loaded $^{D}$WSW/NGR-RBCNP group. Mice were administered with 0.1 mL of drug (equivalent to 100 μg/kg of EFL1) and saline by intravenous injection. After 15 d, we extracted blood from the eyeball to perform routine blood tests and to investigate liver and kidney function. We also removed the main organs for histopathological examination (46, 47).

## Statistical Analysis

Quantitative data are expressed as mean ± standard deviation (SD) unless otherwise indicated. One-way analysis of variance (ANOVA) was used to determine significant differences between different groups, and $p<0.05$ was considered to indicate statistical significance.

# RESULTS

## Physicochemical Characterization of Dual-Modified RBCNPs

### Preparation and Characterization of Dual-Modified RBCNPs

The method used to prepare $^{D}$WSW/NGR RBCNPs is shown in **Figure 2A**. We synthesized DSPE-$PEG_{2000}$-$^{D}$WSW and DSPE-$PEG_{2000}$-NGR and then prepared double-modified biomimetic PLGA nanoparticles using a lipid-insertion method. **Figure 2B** shows the process used to synthesize the two functional targeting materials. We then coupled the thiol sulfhydryl (-SH) in the $^{D}$WSW and NGR targeting peptides with DSPE-$PEG_{2000}$-Mal using a sulfhydryl-maleimide reaction. The successful formation of DSPE-$PEG_{2000}$-$^{D}$WSW and DSPE-$PEG_{2000}$-NGR was confirmed by MALDI-TOF MS, with observed mass-charge

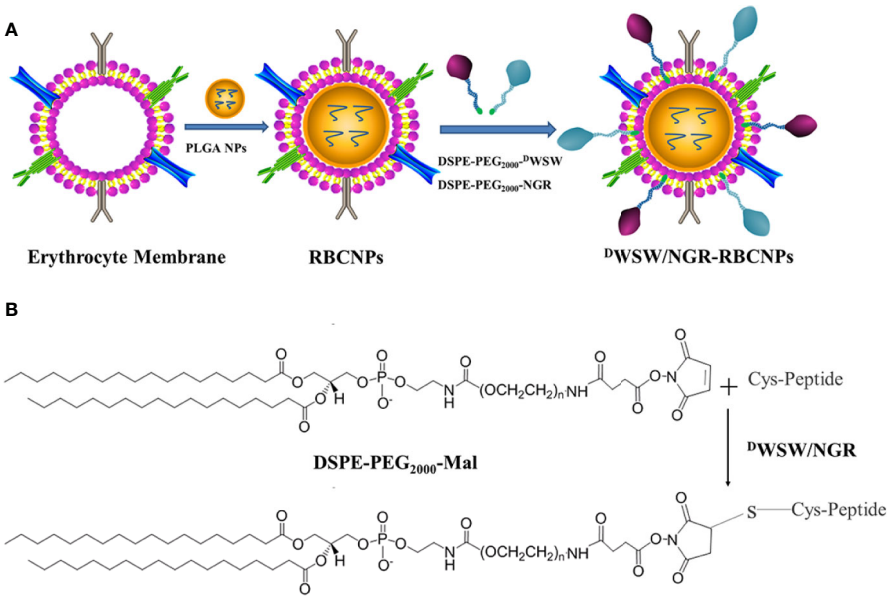


**FIGURE 2** | Preparation of $^{D}$WSW/NGR-RBCNPs. First, the drug was loaded into PLGA, coated with erythrocyte membrane, and finally target-modified **(A)**. The targeting ligand was then synthesized by conjugating DSPE-$PEG_{2000}$-Mal to the cysteine residue on both $^{D}$WSW and NGR **(B)**. The Michael addition reaction was used in chemical synthesis.

ratios of approximately 3913 (**Supplementary Figure S1A**) and 3713 (**Supplementary Figure S1B**), respectively; these data confirmed the that the targeted molecular conjugates had been synthesized correctly. The DSPE-$PEG_{2000}$-$^{D}$WSW and DSPE-$PEG_{2000}$-NGR were then used for the target modification of RBCNPs.

After preparation, we used TEM to characterize the morphology of the EFL1-loaded $^{D}$WSW/NGR-RBCNPs. The typical core-shell structure of EFL1-loaded $^{D}$WSW/NGR-RBCNPs is shown in **Figure 3A** while **Table 1** summarizes the four distinct RBCNP formulations. The EFL1 encapsulation efficiency (EE) of the erythrocyte membrane-encapsulated nanoparticles was greater than 70%, and the final drug amount was not affected by the targeted peptide modification. The size of nanoparticles is known to be an important determinant of their potential applications *in vivo* and *in vitro*. As shown in **Table 1**, the nanoparticles have a low polydispersity index (DPI) and exhibited a narrow size distribution. It is important that nanoparticles exhibit a uniform size when applied used *in vivo*; physical size is known to influence the therapeutic efficacy of nanoparticles after they have successfully reached the target site (48). In addition, the nanoparticle sizes determined by TEM images (**Figure 3A**) were similar to those determined by a laser particle analyzer (**Supplementary Figure S2B**). Following the encapsulation of erythrocyte membranes, we found that the size of the nanoparticles increased (**Supplementary Figures S2A, B**) while the zeta potential decreased (**Supplementary Figures S2C, D**). The zeta potential of the formulations was important as this ensured that the nanoparticles remained stable in solution.

Analysis of the protein content of the $^{D}$WSW/NGR-RBCNPs was carried out to confirm successful functionalization of the nanoparticles with erythrocyte membrane antigens. The proteins in erythrocyte membrane-encapsulated nanoparticles and erythrocyte membranes were assayed in parallel through BCA assay kit. The protein concentration of erythrocyte membrane was 309.0 ± 2.52 μg/mL, and that of double-targeted modified nanoparticles was 244.6 ± 8.22 μg/mL. Considering the dilution of the erythrocyte membrane, the process of erythrocyte membrane-encapsulated nanoparticle formation and targeted modification did not lead to erythrocyte membrane protein loss. The proteins in erythrocyte membrane-encapsulated nanoparticles, and erythrocyte membranes, were assayed in parallel by SDS-PAGE. Neither the formation of erythrocyte membrane-encapsulated nanoparticles, or targeted modification, led to the significant loss of erythrocyte membrane proteins (**Figure 3B**). It was evident that the erythrocyte membrane-encapsulated nanoparticles retained the properties of erythrocyte membranes.

The *in vivo* application of EFL1-loaded $^{D}$WSW/NGR-RBCNPs requires that they are stable under physiological conditions. Therefore, we used fetal calf serum (FBS) to test the stability of the nanoparticles in blood. We used the Turbiscan Lab® Expert system to evaluate the *in vitro* stability of the EFL1-loaded $^{D}$WSW/NGR RBCNPs in serum at 37°C for 72 h. This methodology has been reported previously (49), and in the present study indicated that EFL1-loaded $^{D}$WSW/NGR RBCNPs showed no significant aggregation or sedimentation (transmission or back-scattering profiles of less than 2.0%) in FBS (**Figure 3C**). Increasing evidence has shown that the combined action of multiple membrane components on the

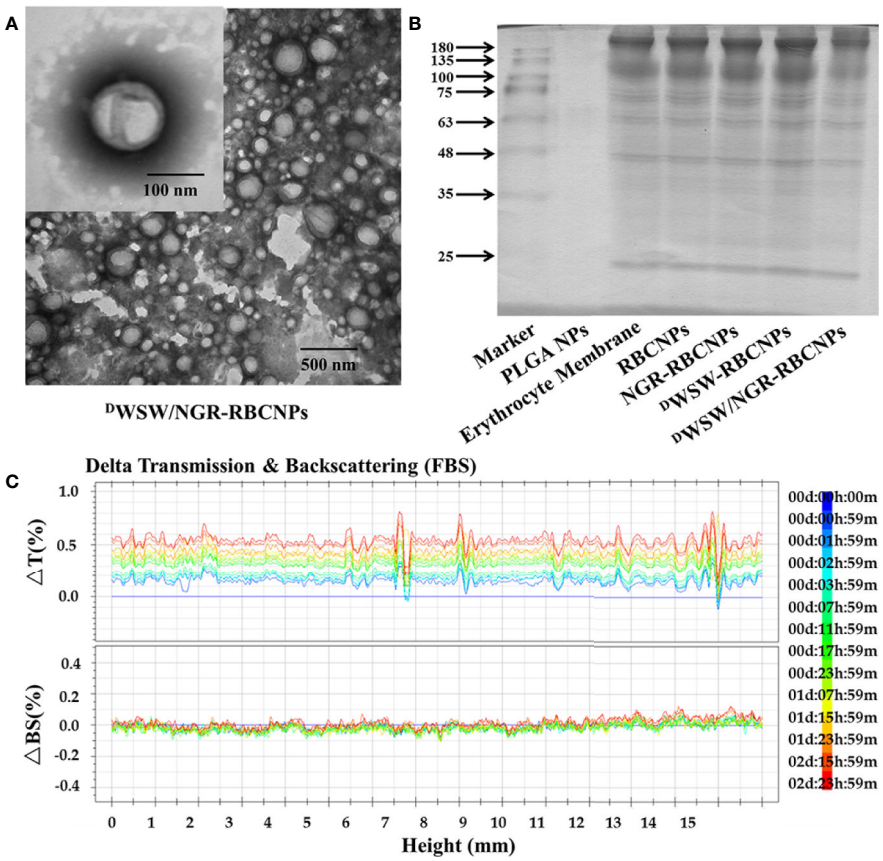


**FIGURE 3** | Characterization of nanoparticles. Transmission electron microscopy (TEM) photos of $^{D}$WSW/NGR-RBCNPs. **(A)** Nanoparticles showing the core-shell structure. **(B)** Erythrocyte membrane proteins in different nanoparticles, showing the protein had not been lost. Similar bands of protein appear in the same location. **(C)** Stability of EFL1-loaded $^{D}$WSW/NGR-RBCNPs in the presence of FBS; stability fluctuated within a range of 2%. No serious aggregation or sedimentation of the nanoparticles during the measurement period.

**TABLE 1** | Characterization of different nanoparticles.

| Sample | Diameter (nm) | PDI | EE (%) | DL (%) |
|---|---|---|---|---|
| PLGA NPs | 129.84 ± 0.48 | 0.067 ± 0.004 | 82.95 ± 1.03 | 2.3 ± 0.4 |
| RBCNPs-EFL1 | 144.37 ± 1.57 | 0.106 ± 0.011 | 77.36 ± 1.12 | 2.1 ± 0.2 |
| $^{D}$WSW-RBCNPs-EFL1 | 146.85 ± 1.45 | 0.116 ± 0.017 | 74.87 ± 1.45 | 2.0 ± 0.1 |
| NGR-RBCNPs-EFL1 | 145.67 ± 1.88 | 0.119 ± 0.011 | 76.36 ± 1.17 | 2.0 ± 0.3 |
| $^{D}$WSW/NGR-RBCNPs-EFL1 | 148.48 ± 1.20 | 0.082 ± 0.014 | 73.65 ± 1.07 | 1.9 ± 0.1 |

*Data are represented as mean ± SD, n = 3.*

cell surface ensures that RBCs are not engulfed by macrophages. In particular, CD47, a protein marker of the erythrocyte membrane, has been shown to inhibit macrophage phagocytosis by interacting with SIRP-α receptors (50). In order to confirm the presence of CD47 on the $^{D}$WSW/NGR-RBCNPs, we carried out western blotting analysis on a series of distinct samples (NPs, RBC lysate, erythrocyte membranes, and $^{D}$WSW/NGR-RBCNPs). As shown in **Supplementary Figure S3A**, the results showed that after the process of nanoparticle synthesis and modification had been completed, CD47 was still present on the surface of the RBCNPs. This suggests that nanoparticles coated with erythrocyte membranes can circulate for longer durations in the body and are subject to reduced levels of phagocytosis.

Next, we carried out *in vitro* release studies to investigate the release characteristics of EFL1 in the RBCNPs. There was no significant difference in the EFL1 release behavior of the biomimetic nanocarriers in buffer solution (PH=7.4, **Supplementary Figure S3B**). This finding indicated that targeted modification did not affect drug release.

### The Efficiency of Connection Between Targeting Peptides and RBCNPs

We used a simple method to investigate the connection efficiency between $^{D}$WSW and NGR peptides and RBCNPs. First, the two targeting conjugates were reacted with CFDA and 5-ROX to obtain DSPE-PEG$_{2000}$-NGR-CFDA and DSPE-PEG$_{2000}$-$^{D}$WSW-5-ROX, respectively. The maximum UV absorption of DSPE-PEG$_{2000}$-NGR-CFDA was 493 nm while that of DSPE-PEG$_{2000}$-$^{D}$WSW-5-ROX was 578 nm. A mixture of the two peptides could be measured at different wavelengths. Unmodified RBCNPs did not interfere with such measurements (**Supplementary Figure S3C**). Using this method, we were able to ascertain that the connection efficiencies of DSPE-PEG$_{2000}$-NGR and DSPE-PEG$_{2000}$-$^{D}$WSW in the double-modified RBCNPs were 71.27% and 73.45%, respectively.

## *In Vitro* Evaluation

### Cellular Uptake

Cellular uptake experiments were performed to investigate the affinity of the different types of modified RBCNPs to specific cells. To do this, we incubated bEnd.3, HUVECs, and C6 cells, with different types of DiI-labeled RBCNPs for 2 h at 37°C. A previous study used bEnd.3 cells as a model of the BBB in order to study the penetrating ability of $^{D}$WSW (51). HUVECs have also been used previously as a model cell for tumor angiogenesis and thus confirm the ability of NGR to target the neovasculature (52).

As shown in **Figure 4A**, the intracellular fluorescence intensity of the NGR-RBCNPs was similar to that of the N-RBCNPs, thus indicating that the NGR-RBCNPs cannot be recognized effectively, and they could therefore evade uptake by bEnd.3 cells. This implies that NGR cannot penetrate the BBB effectively. However, both $^{D}$WSW-RBCNPs and $^{D}$WSW/NGR-RBCNPs underwent significant uptake by bEnd.3 cells, indicating that $^{D}$WSW-modified nanoparticles possess good brain-targeting properties. As shown in **Figure 4B**, untargeted modified nanoparticles were not taken up effectively by cells. We also found that free $^{D}$WSW (1 mg/mL) significantly inhibited the cellular uptake of $^{D}$WSW-RBCNPs and $^{D}$WSW/NGR-RBCNPs (by a factor of 4.5), thus indicating that the $^{D}$WSW peptide specifically targeted the QS receptor of bEnd.3 cells (21, 53).

Furthermore, to verify the ability of the nanoparticles to target tumor tissues, we measured the cell uptake of NGR-RBCNPs and

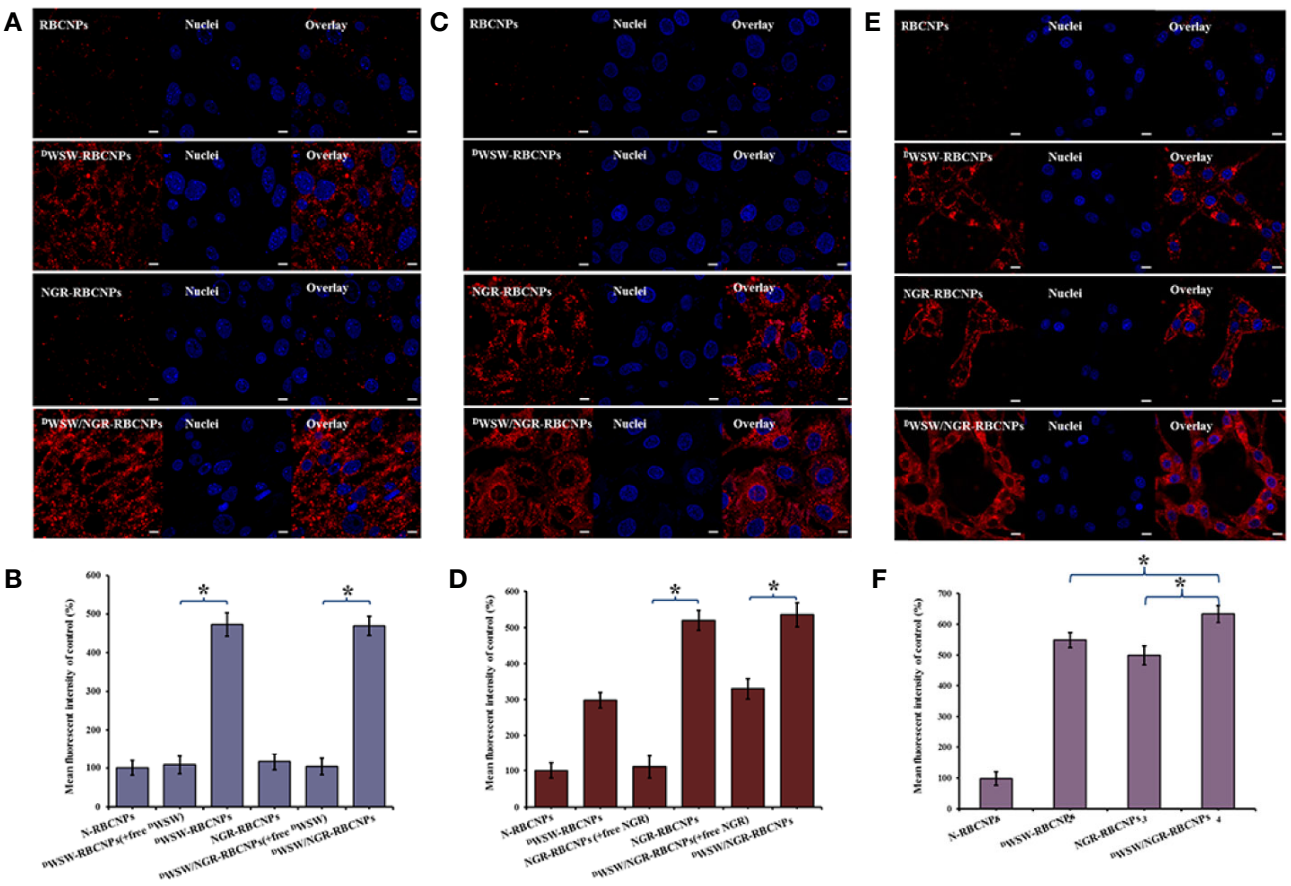


**FIGURE 4** | Targeting ability test with different cells. Cellular uptake of different DiI-labelled RBCNPs by bEND.3 cells **(A, B)**. $^{D}$WSW exhibited the ability to cross the BBB and the free peptide was able to compete for the target. NGR exhibited the ability to cross the BBTB and the free peptide was able to compete for the receptor in HUVECs cells **(C, D)**. $^{D}$WSW- and NGR-modified nanoparticles showed good tumor-targeting in C6 cells **(E, F)**. DiI-positive cells were counted by FCM and intracellular fluorescence was captured by CLSM. Nanoparticles show different targeting capabilities. Scale bars, 10 μm. * indicates $P < 0.05$.

$^{D}$WSW/NGR-RBCNPs by using CD13-positive HUVECs. As shown in **Figure 4C**, NGR-RBCNPs and $^{D}$WSW/NGR-RBCNPs showed stronger intracellular fluorescence than RBCNPs and $^{D}$WSW-RBCNPs in HUVECs, thus indicating that NGR peptide-modified nanoparticles have good tumor-targeting ability. **Figure 4D** also illustrates the effect of NGR; competition from free NGR (1 mg/mL) for the CD13 receptor led to a reduction in the uptake of NGR-modified nanoparticles (by a factor of 1.5). The rate of uptake for NGR-modified nanoparticles was approximately 1.5 times lower than that of the unmodified nanoparticles. These results indicated that NGR-modified nanoparticles require high expression levels of the CD13 receptor on the target cell in order to function in an appropriate manner. On the other hand, the nanoparticles modified by $^{D}$WSW peptides showed certain targeting ability, which was consistent with the literature reports (22).

Finally, we investigated the glioma-targeting and uptake ability of the nanoparticles in C6 cells. Compared with unmodified RBCNPs, NGR-RBCNPs, $^{D}$WSW-RBCNPs, and $^{D}$WSW/NGR-RBCNPs, were taken up by C6 cells; of these, $^{D}$WSW/NGR-RBCNPs demonstrated the highest levels of cellular uptake (**Figures 4E, F**). The results showed that $^{D}$WSW and NGR peptide-functionalized RBCNPs have significant tumor-targeting abilities. Overall, these cellular uptake results strongly supported the hypothesis that $^{D}$WSW and NGR could play a key role in the enhancement of cell recognition and uptake, and the reduction of nonspecific cellular uptake. The data also indicate that $^{D}$WSW/NGR-RBCNPs would be able to target tumors *in vitro* with reduced levels of non-specific cell uptake. Moreover, as shown in **Figure 4**, preincubation with serum did not impair the cellular uptake of $^{D}$WSW/NGR-RBCNPs in bEnd.3 cells, HUVECs, and C6 cells, thus indicating that all of the peptide-modified nanoparticles retained their targeting properties in plasma. These results provide a key foundation for further *in vivo* experiments.

## *In Vitro* Cytotoxicity

We incubated a range of EFL1-loaded nanoparticles, containing different concentrations of EFL1, with C6 cells *in vitro*, and then determined cell survival rate using the MTT assay. As shown in **Supplementary Figure S3D**, increased concentrations of EFL1 were associated with a significant increase in the anti-proliferative activities of free-EFL1 in C6 cells, thus indicating that EFL1 has anti-cancer effects in this type of brain tumor. In addition, all of the formulations containing EFL1 showed cytotoxicity; the largest effect was observed in the free EFL1 group. These results could be explained by the fact that free drugs can rapidly enter cells by passive diffusion under *in vitro* conditions, and with a high concentration gradient. However, nanoparticle-loaded drugs must be released slowly in order to exert their therapeutic effects successfully (**Supplementary Figure S3B**). Accordingly, we found that when compared with free-EFL1, EFL1-loaded biomimetic nanoparticles exhibited a weaker inhibitory effect on the proliferation of C6 cells. These biomimetic nanoparticles can exert important therapeutic effects through targeted modification to enhance the drug concentration delivered to tumor sites. The minor differences in cytotoxicity that were evident between different types of nanoparticles may be related to their uptake by C6 cells and similar patterns of drug release. Further investigation is now needed to investigate these differences further.

## Transcytosis Efficiency: *In Vitro* BBB and BBTB Models

In order to exert their therapeutic effects for brain disease, it is necessary for drugs to first cross the BBB and then reach a therapeutically relevant concentration. We constructed an *in vitro* BBB model with which to evaluate the penetration effect of nanoparticles with different target modifications. As shown in **Supplementary Figure S4A**, the penetration efficiencies of Cy5.5-labeled $^{D}$WSW/NGR-RBCNPs (3.22 ± 0.28%) and Cy5.5-labeled $^{D}$WSW-RBCNPs (3.18 ± 0.32%) were significantly higher than that of Cy5.5-labelled NRG-RBCNPs following a 4 h period of incubation. This showed that the $^{D}$WSW peptide-modified nanoparticles were highly capable of penetrating the BBB. In addition, to verify the ability of the target-modified nanoparticles to localize to brain tumors, we constructed an *in vitro* BBTB model. Using previously described methods, we successfully established an *in vitro* BBTB model by co-culturing HUVECs/C6 cells and then incubating these co-cultures with various types of RBCNPs (41, 43). As shown in **Supplementary Figure S4B**, the percentage penetration of Cy5.5-labeled $^{D}$WSW/NGR-RBCNPs (4.09 ± 0.20%), and Cy5.5-labeled NGR-RBCNPs (4.08 ± 0.18%), was significantly higher than that of Cy5.5-labelled $^{D}$WSW-RBCNPs (1.09 ± 0.23%) after a 4 h period of incubation. This indicated that the NGR peptide-modified nanoparticles exhibited good BBTB penetration. However, NGR-modified nanoparticles must cross the BBB in order to reach the tumor site. These results indicate that the dual-target modified $^{D}$WSW/NGR-RBCNPs possess the ability to penetrate the BBB and BBTB. These data also confirmed the cellular uptake results (**Figure 4**).

## Targeting Ability of Biomimetic Nanoparticles in a BBB/C6 Tumor Co-Culture Model

We established a BBB/C6 tumor coculture model to investigate the anti-tumor effect of the target- modified nanoparticles *in vitro*. Once the co-culture model had been established, we used the upper transwell chamber to culture different EFL1-loaded formulations. At the end of the experiment, a sulforhodamine-B staining assay was used to determine the survival rate of C6 cells in the basal chamber. The cell survival rate of C6 cells exposed to free EFL1, EFL1-loaded N-RBCNPs, EFL1-loaded NGR-RBCNPs, EFL1-loaded $^{D}$WSW-RBCNPs, and EFL1-loaded $^{D}$WSW/NGR-RBCNPs, was 98.87 ± 13.04%, 97.02 ± 12.36%, 96.88 ± 12.45%, 50.28 ± 5.12%, and 47.02 ± 2.92%, respectively. Results showed that the $^{D}$WSW peptide-modified nanoparticles could cross the BBB in the *in vitro* model and that the EFL1 drug could be delivered to C6 glioma cells. However, free EFL1, and nanoparticles without $^{D}$WSW peptide modification, could not pass into the bEnd.3 cells. In contrast with the *in vitro* cytotoxicity testing (**Supplementary Figure S3D**), we found that a single drug could not enter the lesion site in order to provide therapeutic effects, and that drugs require a targeting carrier; in this context, the $^{D}$WSW peptide is an ideal targeting molecule. The results also

showed that the NGR peptide plays a key role when $^{D}$WSW peptide-modified nanoparticles enter the brain. After passing through the BBB, NGR peptide-modified nanoparticles showed better targeting ability to tumor cells than any of the other preparations. This shows that a dual-target modification strategy was more effective than a single-target modification strategy.

## *In Vitro* Evaluation

### *In Vivo* Distribution of Biomimetic Nanoparticles

Although various anti-tumor drugs are currently available, it is highly evident that the BBB and BBTB create a significant hurdle for drug entry. These important structured makes the clinical treatment of gliomas very challenging. Moreover, because most therapeutic drugs are distributed systemically, they are commonly associated with significant side effects. Therefore, the use of carriers to enable targeted drug delivery to tumor tissue not only increases therapeutic efficacy, but also reduces levels of drug toxicity. To evaluate the brain targeting ability of $^{D}$WSW/NGR-RBCNPs, we measured whole-body fluorescence signals from intracranial C6 glioma mice. We also investigated the biodistribution of different RBCNPs labeled with DiR within brain tissue. As shown in **Figure 5A**, $^{D}$WSW-functionalized RBCNPs ($^{D}$WSW-RBCNPs and $^{D}$WSW/NGR-RBCNPs) were showed good distribution in the brains of experimental mice; the other RBCNP formulations (N-RBCNPs and NGR-RBCNPs) exhibited only minimal brain-targeting ability when compared with controls (basal fluorescence levels). As shown in **Figure 5B**, the distribution of DiR-labelled $^{D}$WSW/NGR-RBCNPs in brain tissue was more intense than that of DiR-labelled $^{D}$WSW-RBCNPs, thus suggesting the importance of dual modification. We also investigated the distribution of nanoparticles in other key organs that were harvested at the time of sacrifice. When comparing these other organs, we found that the liver showed the highest nanoparticle content, thus suggesting that the nanoparticles were mainly eliminated by this organ (**Figure 5C**). These results suggest that the $^{D}$WSW/NGR-RBCNPs could mitigate the toxicity of EFL1.

To determine the targeting capability of the $^{D}$WSW/NGR-RBCNPs to gliomas *in vivo*, we used DiI-labeled RBCNPs to

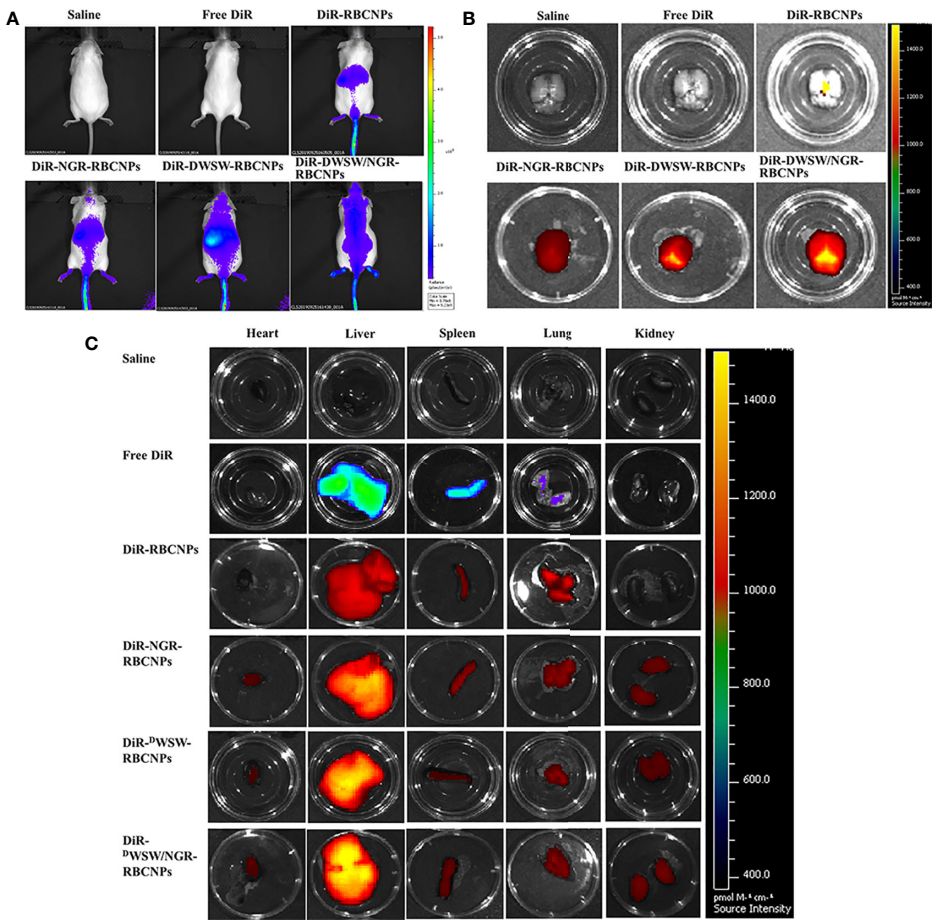


**FIGURE 5** | *In vivo* targeting ability test. *In vivo* real-time imaging of different DiR-encapsulated nanoparticles in the brain showing the biodistribution of nanocarriers in animals **(A)**, brain tissue **(B)** and distribution of different DiR-encapsulated nanoparticles in different organs **(C)**. The enhancement of targeted modification leads to increased brain fluorescence. As the liver plays a predominant role in the elimination of these nanoparticles, it was no surprise that the liver showed the highest levels of accumulation when compared to other organs. These data show that these nanoparticles can target drugs to the brain tissue in an effective manner.

perform immunofluorescence studies on mouse gliomas. As shown in **Figure 6**, unmodified DiI-labeled RBCNPs did not produce fluorescence at the tumor site, thus indicating that the RBCNPs were unable to reach the brain. Only a small number of DiI-labelled NGR-RBCNPs were seen to enter the brain tumor tissue, thus indicating that these nanoparticles were not able to penetrate the BBB effectively. In contrast, we found that DiI-labeled $^{D}$WSW-RBCNPs were distributed throughout the brain, thus implying that these nanoparticles possessed good levels of ability to penetrate the BBB. DiI-labeled $^{D}$WSW/NGR-RBCNPs showed stronger levels of fluorescence intensity than DiI-labeled $^{D}$WSW-RBCNPs in the brain and were also able to enter tumor tissues. This suggests that dual-targeted modified nanoparticles successfully reach tumor tissues after crossing the BBB and BBTB. These results revealed the necessity for dual target modification involving $^{D}$WSW and NGR.

## Anti-Glioma Effect *In Vivo*

Using survival time as the main indicator, we performed *in vivo* pharmacodynamic tests on different types of nanoparticles, and used the survival time of each group of mice to plot Kaplan-Meier survival curves. **Figure 7A** shows that treatment with EFL1-loaded $^{D}$WSW/NGR-RBCNPs achieved the best anti-glioma effect by prolonging the median survival time (36 d); this was 1.8-, 1.6-, 1.5-, 1.3-, and 1.2-fold, longer than that of normal saline, free EFL1, EFL1-loaded N-RBCNPs, EFL1-loaded NGR-RBCNPs, and EFL1-loaded $^{D}$WSW-RBCNPs, respectively. Because of their inability to penetrate the BBB, the median survival time of the free EFL1 and EFL1-loaded RBCNP groups was similar to that of the normal saline group. Similarly, EFL1-loaded NGR-RBCNPs did not significantly extend the median survival time in the experimental mice. We found that NGR peptide-modified nanocarriers could not transport drugs into the brain tissue. In contrast, $^{D}$WSW peptide-modified nanocarriers prolonged the survival time of experimental mice. When compared with other groups on day 16, tumor diameter was smallest in the group of mice treated with EFL1-loaded $^{D}$WSW/NGR-RBCNPs, as determined by MRI (**Figure 7B**). According to previous reports (22), $^{D}$WSW

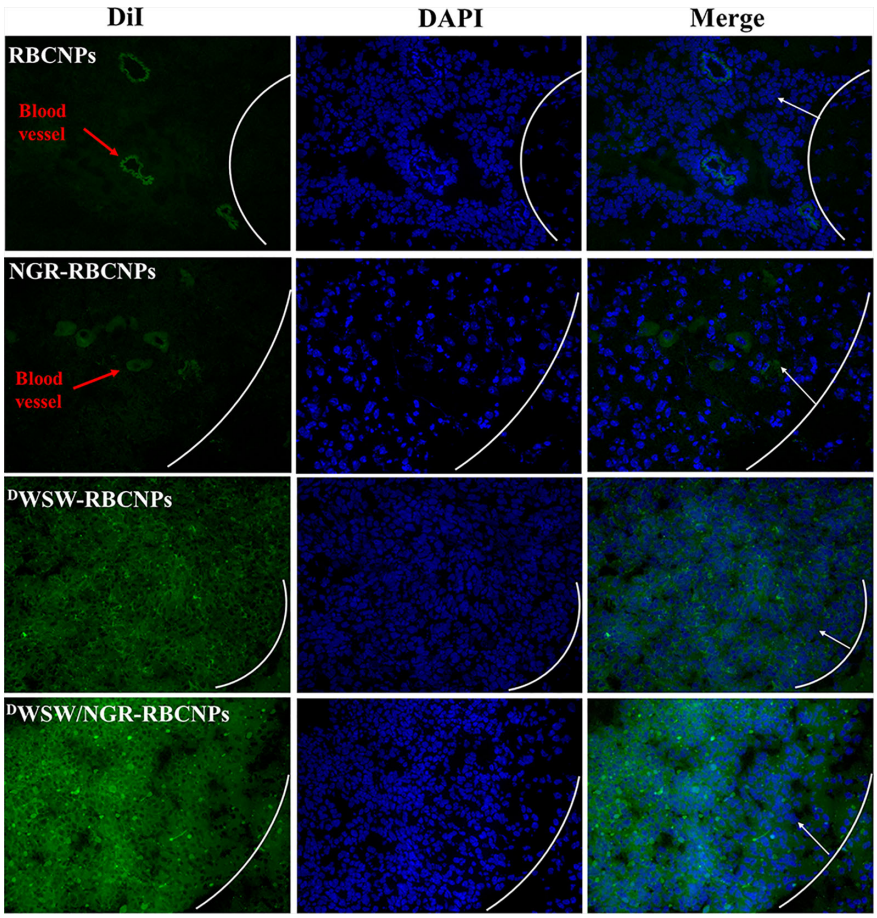


**FIGURE 6** | Targeted distribution of nanoparticles in brain tissue. Distribution of DiI-encapsulated nanoparticles in the brain of mice bearing intracranial C6 gliomas, as determined by confocal laser microscopy. The white line shows the margin of the intracranial glioma while the arrows indicate glioma cells. The green color represents DiI-encapsulated nanoparticles, while nuclei are shown in blue (DAPI). 784 DWSW/NGR-RBCNPs showed the strongest targeting ability. Scale bar, 20 μm.

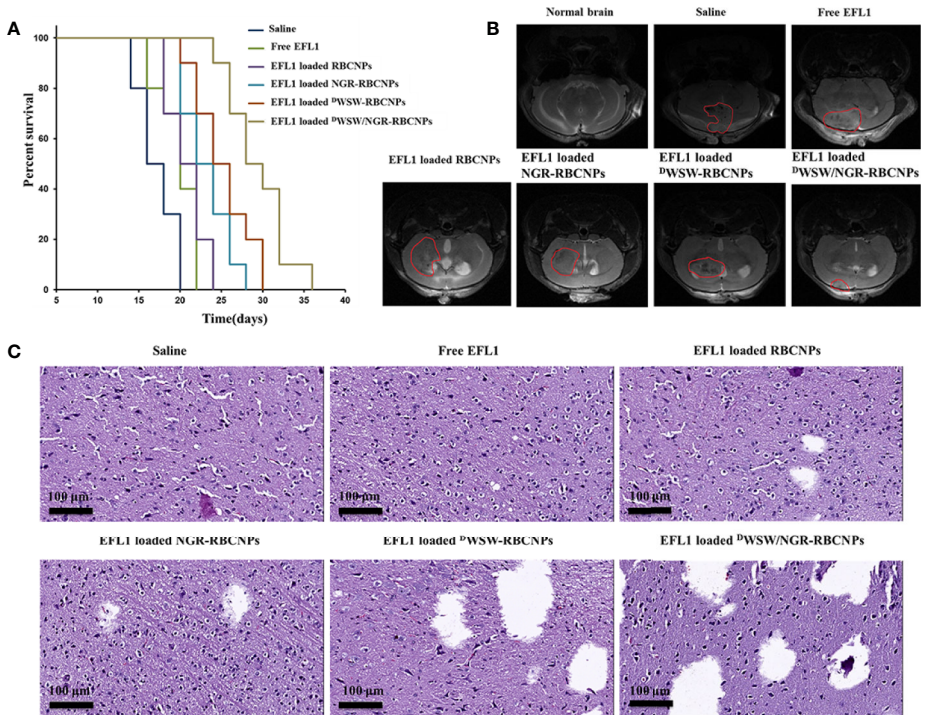


**FIGURE 7** | Antitumor effects of nanoparticles *in vivo*. Kaplan-Meier survival curves of nude mice **(A)**, brain MRI images **(B)**, and histological changes in gliomas **(C)** following treatment with different nanoparticles. The strongest therapeutic effect was achieved by the dual-targeted modified nanoparticles.

has the ability to improve the brain-targeting of nanodrug delivery systems. The current results indicate that EFL1-loaded RBCNPs with dual ligand functionalization could significantly improve the treatment efficacy for glioma.

At the end of treatment, we used harvested brain tissue to perform histopathological examinations. Compared with other treatments, the mice treated with EFL1-loaded $^{D}$WSW/NGR-RBCNPs showed the highest levels of apoptosis (**Figure 7C**). The normal saline group, free EFL1 group, and the EFL1-loaded RBCNP group, showed dense cellular tissues. The data showed that EFL1-loaded $^{D}$WSW/NGR-RBCNPs were the most effective preparation for the treatment of gliomas.

## Safety Evaluation

Nanoparticles can penetrate into membrane cells and spread along nerve cell synapses, blood and lymphatic vessels. The strong permeability of nanoparticles not only provides effectiveness for the use of drugs, but also poses a potential threat to biological health. In this research, the acute toxicity test in mice was used for safety evaluation. The diet of the experimental mice was maintained at a normal level, and no abnormality in body weight and behavior was observed. The analysis detected no obvious pathological damage in the organs of mice from the saline, free EFL1, and EFL1-loaded $^{D}$WSW/NGR-RBCNP groups, as shown in **Supplementary Figure S5A**. Furthermore, the three different groups of mice all showed data within the normal range for the following parameters: red blood cell (RBC) count, white blood cell (WBC) count, mean red cell volume (MCV), hemoglobin (HGB), platelet count (PLT), and mean platelet volume (MPV) (**Supplementary Figure S5B**). Further analysis also showed that the following parameters were also within the normal range: alanine aminotransferase (ALT), aspartate aminotransferase (AST), uric acid (UA), triglyceride (TG), high density lipoprotein (HDL), and low-density lipoprotein (LDL) (**Supplementary Figure S5C**). These results indicate that at the experimental doses used herein, the mice showed no obvious abnormalities and no symptoms relating to acute or severe toxicity.

# DISCUSSION

In recent years, biomimetic nano drug delivery system represented by erythrocyte membrane has promoted the development of nanoparticles in the field of nanomedicine and pharmacy (54). Drug molecules can be coupled or complexed with host molecule, adsorbed on the surface, buried under the matrix, or enclosed in the cavity of carriers (55). Commonly used organic nanocarriers include liposomes, solid lipid nanoparticles, nanocapsules, nanospheres, micelles, etc., and inorganic nanocarriers include silica, $Fe_3O_4$, gold nanoparticles, etc. The physicochemical properties of the nanocarrier (size, shape, surface chemical properties, porosity, elasticity, etc.) will affect its biological properties. For example, the size can significantly affect the blood circulation and biological distribution, less than 6 nm is easy to be cleared by the liver, and more than 200 nm is easy to be captured by the liver and spleen. And

30-200 nm nanoparticles can aggregate in tumor site through EPR (enhanced permeability and retention effect) effect. In addition, the shape mainly affects cell phagocytosis, and the surface chemical properties will change the interaction with the physiological environment. Erythrocyte membrane coated nanoparticles have potential applications in many fields (56). First of all, anti-tumor therapy is the most widely studied, including chemotherapy and immunotherapy for glioma, breast cancer, lung cancer and so on. Secondly, inorganic nano carriers were encapsulated for tumor diagnosis and imaging, and the efficiency of photodynamic therapy medium was enhanced to improve its anti-tumor effect. Moreover, nanoparticles prepared by erythrocyte membrane can also be used to treat infectious diseases and autoimmune anemia (57, 58). Erythrocyte membrane is an ideal nanocarrier, and targeted modification enhances its precise treatment of diseases. In the future, it may be widely used in drug delivery, immune regulation, poison adsorption and other fields.

The use of chemotherapeutic approaches for glioma is very challenging. In this study, we developed functional targeted EFL1 nanoparticles in order to deliver drugs to tumor tissue. Historically, the most problematical aspect of delivering drugs into the brain is that most anticancer drugs are unable to penetrate the BBB and BBTB. As a consequence, functional targeted drug nanoparticles are becoming an increasingly attractive option for the treatment of brain cancer. Targeting ligand-modified drug-loaded nanoparticles can improve drug transport through the BBB by recognizing specific receptors that are overexpressed and thus triggering the process of receptor-mediated endocytosis. Of these receptors, the QS receptor is an effective targeting ligand for transporting drugs across the BBB while CD13 can be used as a tumor marker, or tumor cell surface antigen, to transport drugs through the BBTB. In this study, we synthesized DSPE-$PEG_{2000}$-$^{D}$WSW and DSPE-$PEG_{2000}$-NGR conjugates. These were integrated into drug-loaded nanoparticles to transport drugs across the BBB and then target tumor cells. The observed cytotoxicity reflected the levels of apoptosis induced in cancer cells by functional targeted nanoparticles. Transport capacity across the BBB was confirmed by the use of a co-culture model. The analysis of mice with intracranial gliomas clearly demonstrated the accumulation of functional targeted DiR nanoparticles in the brain. The *in vivo* experiments, using mice with intercranial gliomas, confirmed that the targeted DiR nanoparticles exhibited strong antitumor and curative effects, but with minimal levels of toxicity to the experimental animals. As a new drug delivery system, RBCNPs could be used to "disguise" nanoparticles as endogenous substances, thus reducing the risk of recognition by the immune system and uptake by the reticuloendothelial system.

## CONCLUSIONS

In the current study, we constructed dual-modified erythrocyte membrane-enveloped PLGA nanoparticles. By modification with $^{D}$WSW and NGR peptides, the newly developed nanoparticles could be used to deliver drugs to gliomas *via* systemic administration. This drug carrier has two outstanding characteristics: a biomimetic structure and dual targeting capability. $^{D}$WSW/NGR-RBCNPs were first able to penetrate the BBB and the BBTB, and then target glioma cells. EFL1-loaded $^{D}$WSW/NGR-RBCNPs significantly improved the efficacy of anti-glioma treatment both *in vitro* and *in vivo*. This research provides a new targeting strategy for the treatment of gliomas. Preliminary validation results showed that NGR and $^{D}$WSW represent effective ligands for the modification of nano-drug delivery systems. Collectively, the data indicate that $^{D}$WSW/NGR-RBCNPs have significant potential as a targeted drug delivery system for the treatment of glioma.

## DATA AVAILABILITY STATEMENT

The raw data supporting the conclusions of this article will be made available by the authors, without undue reservation.

## ETHICS STATEMENT

The animal study was reviewed and approved by Animal Care and Use Ethics Committee of Beijing Institute of Pharmacology and Toxicology.

## AUTHOR CONTRIBUTIONS

YC wrote the manuscript and performed the experiments. JS, WH, and MC revised the manuscript. YW, FX, and CG proposed the outline of the article and revised the draft before submission. All authors contributed to the article and approved the submitted version.

## FUNDING

This research was funded by the Beijing Municipal Natural Science Foundation (grant numbers: 7182097 and 7172162), National Natural Science Foundation of China (grant numbers: 81673597 and 81874305), National Key Research and Development Program of China (grant numbers: 2018YFE0197900 and 2018YFC0115604).

## ACKNOWLEDGMENTS

We thank Yang Yang for his support.

## SUPPLEMENTARY MATERIAL

The Supplementary Material for this article can be found online at: https://www.frontiersin.org/articles/10.3389/fonc.2020.563938/full#supplementary-material

## REFERENCES


1. Fang RH, Jiang Y, Fang JC, Zhang L. Cell membrane-derived nanomaterials for biomedical applications. *Biomaterials* (2017) 128:69–83. doi: 10.1016/j.biomaterials.2017.02.041
2. Li R, He Y, Zhang S, Qin J, Wang J. Cell membrane-based nanoparticles: a new biomimetic platform for tumor diagnosis and treatment. *Acta Pharm Sin B* (2018) 8(1):14–22. doi: 10.1016/j.apsb.2017.11.009
3. Sharma G, Sharma AR, Lee SS, Bhattacharya M, Nam JS, Chakraborty C. Advances in nanocarriers enabled brain targeted drug delivery across blood brain barrier. *Int J Pharm* (2019) 559:360–72. doi: 10.1016/j.ijpharm.2019.01.056
4. Vijayan V, Mohapatra A, Uthaman S, Park I-K. Recent Advances in Nanovaccines Using Biomimetic Immunomodulatory Materials. *Pharmaceutics* (2019) 11(10):534. doi: 10.3390/pharmaceutics11100534
5. Fang RH, Kroll AV, Gao W, Zhang L. Cell Membrane Coating Nanotechnology. *Adv Mater* (2018) 30(23):e1706759. doi: 10.1002/adma.201706759
6. Jin J, Bhujwalla ZM. Biomimetic Nanoparticles Camouflaged in Cancer Cell Membranes and Their Applications in Cancer Theranostics. *Front Oncol* (2020) 9:1560. doi: 10.3389/fonc.2019.01560
7. d'Angelo M, Castelli V, Benedetti E, Antonosante A, Catanesi M, Dominguez-Benot R, et al. Theranostic Nanomedicine for Malignant Gliomas. *Front Bioeng Biotechnol* (2019) 7:325. doi: 10.3389/fbioe.2019.00325
8. Siegelin MD, Schneider E, Westhoff MA, Wirtz CR, Karpel-Massler G. Current state and future perspective of drug repurposing in malignant glioma. *Semin Cancer Biol* (2019). doi: 10.1016/j.semcancer.2019.10.018
9. Zhan C, Lu W. The blood-brain/tumor barriers: challenges and chances for malignant gliomas targeted drug delivery. *Curr Pharm Biotechnol* (2012) 13(12):2380–7. doi: 10.2174/138920112803341798
10. Raucher D, Dragojevic S, Ryu J. Macromolecular Drug Carriers for Targeted Glioblastoma Therapy: Preclinical Studies, Challenges, and Future Perspectives. *Front Oncol* (2018) 8. doi: 10.3389/fonc.2018.00624
11. Gao H. Perspectives on Dual Targeting Delivery Systems for Brain Tumors. *J Neuroimmune Pharmacol* (2017) 12(1):6–16. doi: 10.1007/s11481-016-9687-4
12. Guerrero-Cázares H, Tzeng SY, Young NP, Abutaleb AO, Quiñones-Hinojosa A, Green JJ. Biodegradable polymeric nanoparticles show high efficacy and specificity at DNA delivery to human glioblastoma in vitro and in vivo. *ACS Nano* (2014) 8(5):5141–53. doi: 10.1021/nn501197v
13. Nativo P, Prior IA, Brust M. Uptake and intracellular fate of surface-modified gold nanoparticles. *ACS Nano* (2008) 2(8):1639–44. doi: 10.1021/nn800330a
14. Chen Z, Zhai M, Xie X, Zhang Y, Ma S, Li Z, et al. Apoferritin Nanocage for Brain Targeted Doxorubicin Delivery. *Mol Pharm* (2017) 14(9):3087–97. doi: 10.1021/acs.molpharmaceut.7b00341
15. Gao Y, Liu XL, Li XR. Research progress on siRNA delivery with nonviral carriers. *Int J Nanomed* (2011) 6:1017–25. doi: 10.2147/IJN.S17040
16. Moghimi SM, Symonds P, Murray JC, Hunter AC, Debska G, Szewczyk A. A two-stage poly(ethylenimine)-mediated cytotoxicity: implications for gene transfer/therapy. *Mol Ther* (2005) 11(6):990–5. doi: 10.1016/j.ymthe.2005.02.010
17. Symonds P, Murray JC, Hunter AC, Debska G, Szewczyk A, Moghimi SM. Low and high molecular weight poly(L-lysine)s/poly(L-lysine)-DNA complexes initiate mitochondrial-mediated apoptosis differently. *FEBS Lett* (2005) 579(27):6191–8. doi: 10.1016/j.febslet.2005.09.092
18. Luk BT, Zhang L. Cell membrane-camouflaged nanoparticles for drug delivery. *J Control Release* (2015) 220(Pt B):600–7. doi: 10.1016/j.jconrel.2015.07.019
19. Bose RJ, Paulmurugan R, Moon J, Lee SH, Park H. Cell membrane-coated nanocarriers: the emerging targeted delivery system for cancer theranostics. *Drug Discov Today* (2018) 23(4):891–9. doi: 10.1016/j.drudis.2018.02.001
20. Chai Z, Hu X, Wei X, Zhan C, Lu L, Jiang K, et al. A facile approach to functionalizing cell membrane-coated nanoparticles with neurotoxin-derived peptide for brain-targeted drug delivery. *J Control Release* (2017) 264:102–11. doi: 10.1016/j.jconrel.2017.08.027
21. Wynendaele E, Verbeke F, Stalmans S, Gevaert B, Janssens Y, Van De Wiele C, et al. Quorum Sensing Peptides Selectively Penetrate the Blood-Brain Barrier. *PLoS One* (2015) 10(11):e0142071. doi: 10.1371/journal.pone.0142071
22. Ran D, Mao J, Zhan C, Xie C, Ruan H, Ying M, et al. d-Retroenantiomer of Quorum-Sensing Peptide-Modified Polymeric Micelles for Brain Tumor-Targeted Drug Delivery. *ACS Appl Mater Interfaces* (2017) 9(31):25672–82. doi: 10.1021/acsami.7b03518
23. Fu S, Liang M, Wang Y, Cui L, Gao C, Chu X, et al. Dual-Modified Novel Biomimetic Nanocarriers Improve Targeting and Therapeutic Efficacy in Glioma. *ACS Appl Mater Interfaces* (2019) 11(2):1841–54. doi: 10.1021/acsami.8b18664
24. Shi NQ, Li Y, Zhang Y, Li ZQ, Qi XR. Deepened cellular/subcellular interface penetration and enhanced antitumor efficacy of cyclic peptidic ligand-decorated accelerating active targeted nanomedicines. *Int J Nanomed* (2018) 13:5537–59. doi: 10.2147/IJN.S172556
25. Zheng YB, Gong JH, Liu XJ, Li Y, Zhen YS. A CD13-targeting peptide integrated protein inhibits human liver cancer growth by killing cancer stem cells and suppressing angiogenesis. *Mol Carcinog* (2017) 56(5):1395–404. doi: 10.1002/mc.22600
26. Taylor RE, Zahid M. Cell Penetrating Peptides, Novel Vectors for Gene Therapy. *Pharmaceutics* (2020) 12(3). doi: 10.3390/pharmaceutics12030225
27. Wang Y-Z, Zhang X-T, Li S-J, Zhang Y, Li F-Y, Zhang C-N, et al. Expression of AQP2, AQP4 and AQP 8 in mouse intestine induced by unprocessed and processed Euphorbia lathyris. *Pakistan J Pharm Sci* (2018) 31(4):1229–35.
28. Zhang JY, Lin MT, Yi T, Tang YN, Fan LL, He XC, et al. Apoptosis sensitization by Euphorbia factor L1 in ABCB1-mediated multidrug resistant K562/ADR cells. *Molecules* (2013) 18(10):12793–808. doi: 10.3390/molecules181012793
29. Choi JS, Kang NS, Min YK, Kim SH. Euphorbiasteroid reverses P-glycoprotein-mediated multi-drug resistance in human sarcoma cell line MES-SA/Dx5. *Phytother Res* (2010) 24(7):1042–6. doi: 10.1002/ptr.3073
30. Park SJ, Park JH, Han A, Davaatseren M, Kim HJ, Kim MS, et al. Euphorbiasteroid, a component of Euphorbia lathyris L., inhibits adipogenesis of 3T3-L1 cells via activation of AMP-activated protein kinase. *Cell Biochem Funct* (2015) 33(4):220–5. doi: 10.1002/cbf.3107
31. Lu J, Li G, Huang J, Zhang C, Zhang L, Zhang K, et al. Lathyrane-type diterpenoids from the seeds of Euphorbia lathyris. *Phytochemistry* (2014) 104:79–88. doi: 10.1016/j.phytochem.2014.04.020
32. Arafa MG, Girgis GNS, El-Dahan MS. Chitosan-Coated PLGA Nanoparticles for Enhanced Ocular Anti-Inflammatory Efficacy of Atorvastatin Calcium. *Int J Nanomed* (2020) 15:1335–47. doi: 10.2147/IJN.S237314
33. Rigon L, Salvalaio M, Pederzoli F, Legnini E, Duskey JT, D'Avanzo F, et al. Targeting Brain Disease in MPSII: Preclinical Evaluation of IDS-Loaded PLGA Nanoparticles. *Int J Mol Sci* (2019) 20(8):2014. doi: 10.3390/ijms20082014
34. Que X, Su J, Guo P, Kamal Z, Xu E, Liu S, et al. Study on preparation, characterization and multidrug resistance reversal of red blood cell membrane-camouflaged tetrandrine-loaded PLGA nanoparticles. *Drug Deliv* (2019) 26(1):199–207. doi: 10.1080/10717544.2019.1573861
35. Dodge JT, Mitchell C, Hanahan DJ. The preparation and chemical characteristics of hemoglobin-free ghosts of human erythrocytes. *Arch Biochem Biophysics* (1963) 100(1):119–30. doi: 10.1016/0003-9861(63)90042-0
36. Huang W, Zhang C. Tuning the Size of Poly(lactic-co-glycolic Acid) (PLGA) Nanoparticles Fabricated by Nanoprecipitation. *Biotechnol J* (2018) 13(1). doi: 10.1002/biot.201700203
37. Madani F, Esnaashari SS, Mujokoro B, Dorkoosh F, Khosravani M, Adabi M. Investigation of Effective Parameters on Size of Paclitaxel Loaded PLGA Nanoparticles. *Adv Pharm Bull* (2018) 8(1):77–84. doi: 10.15171/apb.2018.010
38. Katara R, Sachdeva S, Majumdar DK. Enhancement of ocular efficacy of aceclofenac using biodegradable PLGA nanoparticles: formulation and characterization. *Drug Deliv Transl Res* (2017) 7(5):632–41. doi: 10.1007/s13346-017-0416-1
39. Rao L, Bu LL, Xu JH, Cai B, Yu GT, Yu X, et al. Red Blood Cell Membrane as a Biomimetic Nanocoating for Prolonged Circulation Time and Reduced Accelerated Blood Clearance. *Small* (2015) 11(46):6225–36. doi: 10.1002/smll.201502388
40. Fang RH, Hu CM, Luk BT, Gao W, Copp JA, Tai Y, et al. Cancer cell membrane-coated nanoparticles for anticancer vaccination and drug delivery. *Nano Lett* (2014) 14(4):2181–8. doi: 10.1021/nl500618u

41. Ying M, Zhan C, Wang S, Yao B, Hu X, Song X, et al. Liposome-Based Systemic Glioma-Targeted Drug Delivery Enabled by All-d Peptides. *ACS Appl Mater Interfaces* (2016) 8(44):29977–85. doi: 10.1021/acsami.6b10146
42. Raymond A, Diaz P, Chevelon S, Agudelo M, Yndart-Arias A, Ding H, et al. Microglia-derived HIV Nef+ exosome impairment of the blood–brain barrier is treatable by nanomedicine-based delivery of Nef peptides. *J Neurovirol* (2016) 22(2):129–39. doi: 10.1007/s13365-015-0397-0
43. Khodarev NN, Yu J, Labay E, Darga T, Brown CK, Mauceri HJ, et al. Tumour-endothelium interactions in co-culture: coordinated changes of gene expression profiles and phenotypic properties of endothelial cells. *J Cell Sci* (2003) 116(6):1013–22. doi: 10.1242/jcs.00281
44. Li XY, Zhao Y, Sun MG, Shi JF, Ju RJ, Zhang CX, et al. Multifunctional liposomes loaded with paclitaxel and artemether for treatment of invasive brain glioma. *Biomaterials* (2014) 35(21):5591–604. doi: 10.1016/j.biomaterials.2014.03.049
45. Zhai M, Wang Y, Zhang L, Liang M, Fu S, Cui L, et al. Glioma targeting peptide modified apoferritin nanocage. *Drug Deliv* (2018) 25(1):1013–24. doi: 10.1080/10717544.2018.1464082
46. Vakili T, Iranshahi M, Arab H, Riahi B, Roshan NM, Karimi G. Safety evaluation of auraptene in rats in acute and subacute toxicity studies. *Regul Toxicol Pharmacol* (2017) 91:159–64. doi: 10.1016/j.yrtph.2017.10.025
47. Alnajar ZA, Abdulla MA, Ali HM, Alshawsh MA, Hadi AH. Acute toxicity evaluation, antibacterial, antioxidant and immunomodulatory effects of Melastoma malabathricum. *Molecules* (2012) 17(3):3547–59. doi: 10.3390/molecules17033547
48. Zhao ZX, Gao SY, Wang JC, Chen CJ, Zhao EY, Hou WJ, et al. Self-assembly nanomicelles based on cationic mPEG-PLA-b-Polyarginine(R15) triblock copolymer for siRNA delivery. *Biomaterials* (2012) 33(28):6793–807. doi: 10.1016/j.biomaterials.2012.05.067
49. Celia C, Trapasso E, Cosco D, Paolino D, Fresta M. Turbiscan lab expert analysis of the stability of ethosomes and ultradeformable liposomes containing a bilayer fluidizing agent. *Colloids Surf B Biointerfaces* (2009) 72(1):155–60. doi: 10.1016/j.colsurfb.2009.03.007
50. Anniss AM, Sparrow RL. Expression of CD47 (integrin-associated protein) decreases on red blood cells during storage. *Transfusion Apheresis Sci* (2002) 27(3):233–8. doi: 10.1016/S1473-0502(02)00070-8
51. Hu K, Li J, Shen Y, Lu W, Gao X, Zhang Q, et al. Lactoferrin-conjugated PEG-PLA nanoparticles with improved brain delivery: in vitro and in vivo evaluations. *J Control Release* (2009) 134(1):55–61. doi: 10.1016/j.jconrel.2008.10.016
52. Zhu S, Qian L, Hong M, Zhang L, Pei Y, Jiang Y. RGD-modified PEG-PAMAM-DOX conjugate: in vitro and in vivo targeting to both tumor neovascular endothelial cells and tumor cells. *Adv Mater* (2011) 23(12):H84–9. doi: 10.1002/adma.201003944
53. Janssens Y, Wynendaele E, Verbeke F, Debunne N, Gevaert B, Audenaert K, et al. Screening of quorum sensing peptides for biological effects in neuronal cells. *Peptides* (2018) 101:150–6. doi: 10.1016/j.peptides.2018.01.013
54. Rossi L, Fraternale A, Bianchi M, Magnani M. Red Blood Cell Membrane Processing for Biomedical Applications. *Front Physiol* (2019) 10:1070. doi: 10.3389/fphys.2019.01070
55. Wang N, Cheng X, Li N, Wang H, Chen H. Nanocarriers and Their Loading Strategies. *Adv Healthc Mater* (2019) 8(6):e1801002. doi: 10.1002/adhm.201801002
56. Zhao Z, Ukidve A, Krishnan V, Mitragotri S. Effect of physicochemical and surface properties on in vivo fate of drug nanocarriers. *Adv Drug Deliv Rev* (2019) 143:3–21. doi: 10.1016/j.addr.2019.01.002
57. Hu CM, Fang RH, Copp J, Luk BT, Zhang L. A biomimetic nanosponge that absorbs pore-forming toxins. *Nat Nanotechnol* (2013) 8(5):336–40. doi: 10.1038/nnano.2013.54
58. Copp JA, Fang RH, Luk BT, Hu CM, Gao W, Zhang K, et al. Clearance of pathological antibodies using biomimetic nanoparticles. *Proc Natl Acad Sci U S A* (2014) 111(37):13481–6. doi: 10.1073/pnas.1412420111

**Conflict of Interest:** The authors declare that the research was conducted in the absence of any commercial or financial relationships that could be construed as a potential conflict of interest.

frontiers in Oncology

REVIEW
published: 07 January 2021
doi: 10.3389/fonc.2020.607607

# Regulation of Hedgehog Signaling by miRNAs and Nanoformulations: A Possible Therapeutic Solution for Colorectal Cancer

*Zeeshan Javed[1], Muhammad Javed Iqbal[2], Amna Rasheed[3], Haleema Sadia[4], Shahid Raza[1], Asma Irshad[5], Wojciech Koch[6]*, Wirginia Kukula-Koch[7], Anna Głowniak-Lipa[8], William C. Cho[9]* and Javad Sharifi-Rad[10,11]**

[1] Office for Research Innovation and Commercialization, Lahore Garrison University, Lahore, Pakistan, [2] Department of Biotechnology, Faculty of Sciences, University of Sialkot, Sialkot, Pakistan, [3] School of Basic Medical Sciences, Lanzhou University, Lanzhou, China, [4] Department of Biotechnology, Balochistan University of Information Technology, Engineering and Management Sciences, Quetta, Pakistan, [5] Department of Life Sciences, University of Management and Technology, Lahore, Pakistan, [6] Chair and Department of Food and Nutrition, Medical University of Lublin, Lublin, Poland, [7] Department of Pharmacognosy, Medical University of Lublin, Lublin, Poland, [8] Department of Cosmetology, University of Information Technology and Management in Rzeszów, Rzeszów, Poland, [9] Department of Clinical Oncology, Queen Elizabeth Hospital, Kowloon, Hong Kong, [10] Phytochemistry Research Center, Shahid Beheshti University of Medical Sciences, Tehran, Iran, [11] Facultad de Medicina, Universidad del Azuay, Cuenca, Ecuador

Hedgehog (Hh) signaling aberrations trigger differentiation and proliferation in colorectal cancer (CRC). However, the current approaches which inhibit this vital cellular pathway provoke some side effects. Therefore, it is necessary to look for new therapeutic options. MicroRNAs are small molecules that modulate expression of the target genes and can be utilized as a potential therapeutic option for CRC. On the other hand, nanoformulations have been implemented in the treatment of plethora of diseases. Owing to their excessive bioavailability, limited cytotoxicity and high specificity, nanoparticles may be considered as an alternative drug delivery platform for the Hh signaling mediated CRC. This article reviews the Hh signaling and its involvement in CRC with focus on miRNAs, nanoformulations as potential diagnostic/prognostic and therapeutics for CRC.

**Keywords: Hedgehog signaling, miRNAs, nanoformulations, nanoparticle, therapeutics, colorectal cancer**

OPEN ACCESS

***Edited by:***
*Marcelo Calderon, Polymat, Spain*

***Reviewed by:***
*Paul B. Fisher, Virginia Commonwealth University, United States*
*Magnolia Laam Pak, University of Massachusetts Medical School, United States*

****Correspondence:***
*Wojciech Koch*
*kochw@interia.pl*
*William C. Cho*
*chocs@ha.org.hk*
*Javad Sharifi-Rad*
*javad.sharifirad@gmail.com*

***Specialty section:***
*This article was submitted to Cancer Molecular Targets and Therapeutics, a section of the journal Frontiers in Oncology*

***Received:*** *17 September 2020*
***Accepted:*** *10 November 2020*
***Published:*** *07 January 2021*

***Citation:***
*Javed Z, Javed Iqbal M, Rasheed A, Sadia H, Raza S, Irshad A, Koch W, Kukula-Koch W, Głowniak-Lipa A, Cho WC and Sharifi-Rad J (2021) Regulation of Hedgehog Signaling by miRNAs and Nanoformulations: A Possible Therapeutic Solution for Colorectal Cancer. Front. Oncol. 10:607607. doi: 10.3389/fonc.2020.607607*

## INTRODUCTION

Colorectal cancer (CRC) is one of the leading causes of death globally with incidence rate around two million (1). A number of factors such as the dietary habits, family history, inflammatory bowel disease, elevated body mass index, socioeconomic status, environmental and genetic factors affect the likelihood of developing CRC (2). Despite advancements in the preclinical and clinical researches, devising a suitable cure for CRC still remains bleak. Thus, researchers keep pursuing on personalized and targeted therapeutic approaches, development of efficient diagnosis/prognosis biomarkers and clinical management which could inhibit CRC development. The molecular landscape of CRC is multifarious and governed by various signaling pathways such as the hedgehog (Hh) signaling and Wnt signaling pathways which orchestrate growth and

development of tumor cells (3). Hh signaling play a crucial role in regeneration of adult tissues by regulating the stem cell behavior. It also interacts with other vital signaling molecular cascades to control cellular proliferation, polarity and differentiation (4). Aberrant expression of Hh signaling is reported to be the culprit of dysregulation in cellular behavior and contribute in the onset of many human malignancies (5). Hh signaling and aberrant expression of targeted molecules promote tumor microenvironment and induce stemness of cancer cells (6, 7). Aberrant expression of Hh signaling cascade has been reported to contribute in the cancer progression and metastasis including medulloblastoma, basal cell carcinoma, breast cancer, liver cancer, pediatric soft tissue cancer, prostate, stomach, pancreas, and colon cancer (8). Invertebrates and vertebrates share common signaling molecules and mechanism in general, involving Hh ligands, patched1/2 receptor, transcriptional factors GLI-1/2/3, smoothened (SMO) as a critical signal transducer and variety of regulatory molecules (8). In mammals three Hh genes have been identified namely, sonic hedgehog (SHH), Indian hedgehog (IHH), and Desert hedgehog (DHH) which play a vital role in the embryonic development and regeneration of different organs (9). Hh signaling pathway can modulate the self-renewal of cancer stem cells (CSCs) most commonly in hematological malignancies, breast cancer, and CRC (10). There has been significant progress regarding the development of small molecule inhibitors to block Hh signaling. Several of these molecules have been included in the clinical testing stage. Yet finding a sustainable small molecule inhibitor is still a challenge. On the other hand, microRNAs (miRNAs) are small molecules that effectively regulate and modulate the expression of target genes (11). Exploring miRNAs as diagnostic tool can aid in better clinical management of CRC. Nanoformulations have been investigated in many diseases for their efficient sustainability, limited cytotoxicity, increased bioavailability and few side effects. These features have urged scientists to explore these as a therapeutic option for different cancers. In this review, we delineate Hh signaling pathway as a vital therapeutic target for CRC and shed light on the role of miRNAs that may be used as potential diagnostic marker and therapeutic target for CRC. Furthermore, the role of nanoformulations as contenders for targeted delivery of Hh signaling inhibitors for the treatment of CRC is discussed.

## HEDGEHOG SIGNALING IN CANCER

Molecular link of Hh signaling with cancer was reported in basal cell carcinoma when mutation in human PTCH1 gene was observed (12, 13). It was confirmed that mutation in PTCH1 is responsible for SMO activation to trigger aberrant Hh cascade activation to induce carcinogenesis (**Figure 1**) (14, 15). Similarly, increased expression of Hh targeted gene was reported in different carcinomas including meningiomas, medulloblastoma (16), small cell lung carcinoma (SSLC), gastro-intestinal cancer (17), and colon cancer. Experimental work on genetically engineered mice models exhibits that in knock-out PTCH gene mice model organism, increased expression of SMO was observed with increased tumor size. The same experimental study designed to knock out SMO in mice models revealed reduction in tumor size and metastasis (6). However due to the complex behavior of cancer onset and variation in contributing factors, no significant molecular evidence was reported in KRAS associated onset of pancreas and prostate cancer (18). Hh signaling has been associated with cellular proliferation, tissue polarity, stem cell transformation and carcinogenesis. The first molecular association of Hh signaling with cancer was established in 1996 during experimental studies on Gorlin syndrome. Hh signaling was considered as a novel therapeutic target of cancer by clinical use of Hh inhibitors (erivedge/vismodegib) and was approved in 2012 by the FDA to treat basal cell carcinoma (BCC). In this article, Hh signal in carcinogenesis and recent molecular strategies to tackle cancer cell progression using Hh inhibitors (19) were discussed.

Cancer is a complex heterogenetic disorder that transform cellular microenvironment and involves multiple and complicated crosstalk of signaling pathways. In $PTCH^{+/-}$ mice models, inhibition of Hh signaling is an approach to limit cancer cell proliferation (20). It is also observed that STAT-3 knock-out significantly reduce the Hh-mediated delivery of BCC (21). It is widely accepted that Hh signaling has close association with the growth factor mediated pathways as Hh signaling is reported to regulate the platelet derived growth factor $\alpha$ (PDGFR-$\alpha$). Furthermore, molecular crosstalk of Hh is reported to interplay with many other pathways including NOTCH, mTOR, Wnt, Muc5, EGF, IGF, TGF-$\beta$, RACK1, and PKC in different types of cancers (22–25). It has been observed that TGF-$\beta$ regulates tumor microenvironment, while PDGFR-$\alpha$ and Notch play key role in triggering CSC (22, 25). Recent studies highlighted that inhibition of Hh signaling in cancer cells could be the iron gate for cancer therapy in many cancer types (21).

Aberrant Hh signaling is a distinguished feature of various human cancers (26). Gli1 and Gli2 are the two Hh pathway target genes that are overexpressed in the CRC (27). A gene expression microarray study conducted on 382 patients showed that Gli-1 was overexpressed in CRC patients. The expression of this target gene was responsible for the tumor recurrence and poor survival outcome in patients. In addition to this treatment of cell lines such as the HCT-116, SW480 and SW620 with SMO inhibitor GDC-0449 decreased the expression Gli target genes such as the PTCH1, HIP1, and MUC5AC. Furthermore, treatment of cell lines with GDC-0449 upregulated the expression of growth arrest gene p21 and downregulated the expression of cyclin D1 (28). The genetic silencing of SMO with 5E1, a specific antibody, prevented cell migration and invasion along with reduction in the expression of Hh target genes Gli-1 and Gli-2 (28). These findings suggest that Hh signaling affects cell plasticity, proliferation, invasion, and migration in CRC.

CSC functionality and polarity are dependent on the Hh signaling pathway (29). It has also been reported that Hh signaling induces chemotherapy and radiotherapy resistance in cancer cells (30, 31). However, Hh inhibitors are reported to

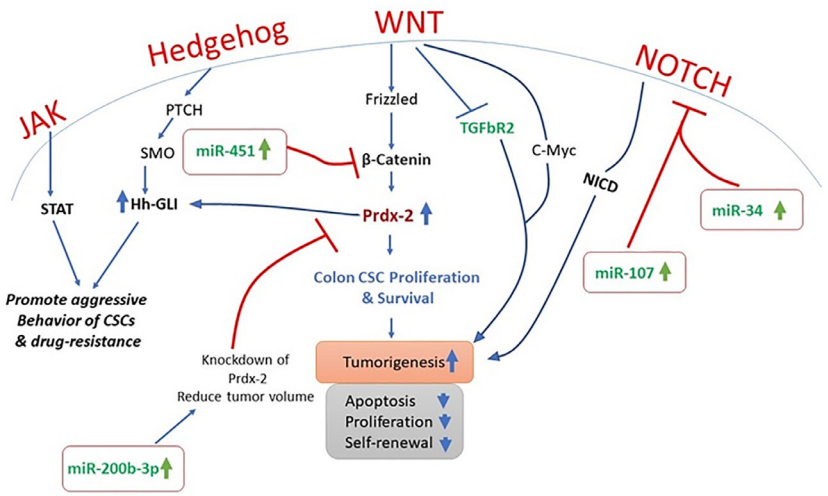


**FIGURE 1** | Therapeutic potential of miRNA inhibitors by targeting aberrant signaling cascades.

promote delivery of chemo-therapeutic agent including IPI-926 (31).

Hh signaling pathway has its prime role in embryogenesis, *i.e.* cell differentiation and growth. It does not always active in all adults cells. However, in cells where stem cell development and growth is required, Hh signaling triggers on (32). Genes involved in the cellular differentiation *i.e.* proto-oncogenes and growth factors are targeted by Hh pathway, but if these pathways get activated by any mutation or if its regulation gets disturbed, then it may lead to tumor development (33). It has been observed that abnormal activation of the Hh pathway can lead to CRC. Molecular evidence realized that in CRC tissues, SHh ligand gets higher in number and increase the expression of all its downstream components, particularly SMO upregulates dramatically and difference in expression of GLI1 protein is observed. From different studies, it was revealed that SHh is a paracrine factor that works like aberrant p53 to inhibit anti-oncogenes (34). SMO activation in an abnormal way causes progression in colon cancer, and its expression was sharply upregulated in colon cancer tissues as compared to the non-cancerous colon tissues. It was observed that SMO expression is directly proportional to the stages of cancer so its level of expression can be used as an independent biomarker for liver postoperative metastasis to liver (35). Similarly, a different expression level of GLI1 was noted in normal tissue and cancerous tissue. Increased expressions of GLI1 cause activation of Hh signaling, which induce anti-apoptotic and anti-inflammatory effects on cancer cells. These alterations are potential driving forces for therapeutics to target GLI by molecular inhibitors to induce the cellular deaths of colon cancer cells. In one study it was reported that GLI1 regulation is exceptional in colon tissues and it is also related to lymph node metastasis (36). Recently, tumor suppressor gene RUNX3 is reported to play a decisive molecular role to limit endothelial proliferation in CRC. It has been observed that RUNX3 expression has inverse correlation with GLI-1 protein and it promotes GLI-1 ubiquitination in CRC. Molecular interplay of RUNX-3 gene to limit metastasis and stemness by targeting hedgehog signaling cascade could be a new contributing therapeutic agent to conquer the unbeatable fort of carcinogenesis (37). Inhibitors of hedgehog pathway are recognized in the scientific community as a therapeutic strategy for cancer treatment. Hh inhibitors hold promise for the development of a potential treatment option in CRC as its results have been proved to be very promising, suggesting that the targeting treatment of signaling pathway is a hopeful way for antitumor treatment. Therefore, the members of hedgehog signaling pathway are considered as significant therapeutic targets for the clinical treatment of colon cancer (38). The Hh signaling pathway has been seen to act as an antagonist to Wnt pathway, which is directly involved in the rapid increase of CRC cells. 90% of CRC have an active mutation in the Wnt pathway; particularly APC gene mutations are responsible agent, but Hh pathway mutations were not found as a molecular culprit in majority of CRC cells (39). There is mounting evidence that over-expression of SHh and SMO participates in the onset of multiple cancers, also recognized as SHh related carcinomas (40). Both these pathways have a significant relation between them in the occurrence and development of CRC and have numerous avenues for molecular crosstalk between the two pathways (41). The colon's mucosa has a film of epithelial cells which gets replaced every week. It replaces large number of progenitor cells and generates plenty of new cells every day at the bottom of crypts *i.e.* small mucosal invaginations. Maintenance of the balance of cell is regulated by extrinsic signals. Morphogens, soluble proteins that make a long range of concentration gradients, produce cellular responses to target cells from a distance in a dose dependent way. It has been proved that morphogens are the main regulator in adult colon and support the notion that both Wnt and Hh pathways have significant roles in CRC (42). The metastatic transition of human

colon carcinomas, which mainly occurs in the $CD133^+$ epithelial tumor stem cell population, includes deregulation of the Wnt–TCF pathway and upregulation of the HH–GLI pathway (43). During this phase of metastatic transition all ligand-driven signaling pathways of Wnt are inhibited. In both $CD133^+$ and $CD133^-$ cells of colon carcinoma signatures of expression of gene in various stages show that activity of Wnt–TCF *i.e.* non-metastatic stops at early stages in colon carcinomas and to become metastatic, the HH–GLI works actively in stem cells. The molecular linkage was established in the deregulation and upregulation of early adenoma-like Wnt–TCF and HH–GLI1 respectively. It was experimentally proved that upregulation of HH–GLI causes downregulation of TCF and thus results in low Wnt–TCF and high HH–GLI expression in metastatic colon carcinomas. It was also observed that silencing of TCF induces the HH–GLI signaling. The high regulation of Wnt–TCF causes transcription repressor GLI3 and high regulation of HH–GLI causes repression of Wnt–TCF and GLI3 (44).

Drug resistance, tumorigenesis, tumor progression, metastasis, and tumor recurrence are the key functions that are regulated by the CSC (45). These are subpopulations of cancer cells with the ability of self-renewal. The Hh signaling pathway has been reported to be involved in the activation of CSCs in various neoplastic tumors such as the glioblastoma, leukemia, and myeloma (46). The activated stem cells have been demonstrated to play a pivotal role in the progression, metastasis, and recurrence of tumors in colon, breast, liver, and pancreatic tissues (47). In addition to its involvement in regulating the CSCs, the Hh signaling along with the SMO and Gli signaling pathways promotes cell migration, growth, and self-sustenance of CSCs (48). The non-canonical Hh-signaling has been reported as a crucial mediator for the survival of CSCs (49). Both the canonical signaling and non-canonical signaling are pivotal in regulating the expression of key genes involved in growth and proliferation of cells (45). Accumulating lines of evidence have reported the fact the aberrant non-canonical hedgehog signaling can trigger uninterrupted cellular growth in CRC. Zhang et al. demonstrated that both SMO and Gli proteins were overexpressed in colon cancer cells and colonic adenoma tissues (38). The SMO expression has been related to prognosis and tumor status in CRC patients. The CSCs are pivotal in stemness and growth of CRC. New studies have begun to shed light on the fact that non-canonical Hh signaling and Wnt signaling are the two key molecular cascades that are disrupted in CRC stem cells. Both canonical and non-canonical Hh-signaling positively and negatively regulates the expression of Wnt in CRC stem cells. Regan et al. demonstrated that non-canonical Hh signaling had a positive role in maintaining growth and differentiation of CRC stem cells. Moreover, continuous overexpression of non-canonical Hh signaling promoted resistance in CRC stem cells and increased their survival in a PTCH1-dependant, Gli-independent manner. In addition to this, SMO dysregulation has been affiliated with CSC growth and differentiation targeting; the dysregulated SMO can be a potential target for the treatment of CRC (50). A specifically designed Hh signaling antagonist GDC-0449 (Vismodegib) has been reported to suppress growth and trigger apoptosis in colon cancer cells *via* downregulating the expression of Bcl-2 (51). Another study confirmed that GDC-0449 has the ability to initiate apoptosis, decrease cellular plasticity and invasiveness of CRC (28). Altogether these findings indicate that non-canonical Hh-signaling has a regulatory role in progression and spread of CRC *via* CSCs modulation. Cancer is a multifactorial disease. There are number of factors such as the age, genetic predisposition, alteration in the genetic framework, diet and habits that can trigger tumorigenesis (52). Studies over the past decades have evidenced the involvement of various mutations in the signaling machinery that contribute towards development of cancer (53). Development of CRC like several other tumors involves mutations in the signaling machinery. Mutations in KRAS, MYB, and BRAF are the most critical mutations that trigger tumorigenesis and can be targeted for therapeutic purposes (54–57). The role of Hh signaling in CRC is still questionable. The exact mechanism by which Hh signaling triggers growth and proliferation, invasiveness and metastasis in CRC still requires aggressive research. The scientific community seems divided on the role of Hh signaling in CRC. Accumulating lines of evidence have suggested that Hh signaling has the following implications in CRC: 1) Hh signaling is expressed variably in CRC, and CRCs as different components of the Hh signaling machinery are expressed differently. 2) Hh pathway can trigger mutations in CRC. 3) Hh signaling plays a role during the transformation of the cells from adenoma-to-adenocarcinoma. 4) The SMO has the most crucial role in the regulation of carcinogenesis of CRC (58, 59). Taken together, it can be evidenced here that the Hh role in CRC still requires plenty of research.

## ROLE OF MIRNAS IN COLORECTAL CANCERS

MiRNAs are short non-coding single-stranded nucleotide sequences (60), which affect almost all physiological processes in cells such as development (61, 62), proliferation (63), differentiation (64), apoptosis (65), signal transduction (66) and many more. The altered expression patterns of miRNAs are tightly linked with a wide range of anomalies including various cancers; thus miRNAs screening could serve a very good therapeutic and diagnostic tool in molecular biology (67). Till date, more than 25,000 miRNA sequences have been identified, and this number is growing fast amid current research interests in miRNAs all over the world. According to an estimation, 3–4% of human genome comprises of miRNAs (68). These miRNAs interfere with numerous key regulators of cellular processes by binding with post-transcriptional products. For this reason, miRNAs are considered as important biomarkers for many cancers including CRC (42). In this section, we shall focus on miRNAs which interact with Hh signaling and may affect CRC. There is a long list of miRNAs which affect CRC progression. More than 500 miRNAs have been found to be linked with CRC. Among these miRNAs few

miRNAs such as miR-21 (69), miR-143, and miR-145 are reported most frequently and are summarized in (70). These miRNAs interact through various signaling pathways. For example miR-143 significantly inhibits KRAS which ultimately suppresses CRC (71). However, another study has shown the opposite phenomenon where reduced levels of miR-143 expression were detected in CRC tissues. Interestingly transfection of cells with transient miR-143 turns the cells to mimic SW480 cells, a CRC cell line, resulting in increased levels of cell proliferation and apoptosis (72). Thus, we may say that the role of particular miRNAs may also vary depending upon the cell type. On the other hand, the role of miR-145 remains much consistent as CRC suppressor in many studies. There has been a reverse interaction between erythroblast transformation-specific (ETS)-related gene (ERG) and miR-145 in CRC. Increased ERG results in decreased miR-145 levels and promotes CRC. The overexpression of miR-145 suppresses CRC by decreasing expression of ERG (73). A similar relation between P21-activated kinases 4 (PAK4), and miR-145 was also observed where miR-145 appeared to downregulate phosphorylation level of LIMK1 and cofilin in SW1116 cells through PAK4 (74). miR-224 activates the Wnt/$\beta$-catenin signaling by deregulation of GSK3$\beta$ and SFRP2 to translocate $\beta$-catenin in CRC (75). Similarly, miR-361 is also downregulated in CSC (65). miR-150 is negatively correlated with circular RNA named Circ-ZNF609 and important transcription factor of hedgehog signaling *i.e.* Gli1 in HCT-116 cells (76). Another study stated that overexpression of miR-150 positively affect the EMT and subsequent downregulation of Gli1, further confirming the role of miR-150 in CRC through hedgehog signaling (77). Similarly, miR-142-3p appeared to promote cell invasion in CRC by upregulation of RAC1 (78). There are miRNAs also targeting other key regulators of hedgehog signaling. One such miRNA-378 inhibits SUFU and promotes cell survival and tumor growth (79). Another molecule, miR-146a, activates the Wnt pathway and stabilizes $\beta$-catenin, thereby promoting CRC by regulating the symmetrical cell division by a feedback loop of Snail-miRNA-146a-$\beta$-catenin (80). All variants of hedgehog pathways work upstream of epithelial-mesenchymal transition (EMT) (81). A number of miRNAs regulate EMT in CRC such as miR-29c which has been shown to be remarkably downregulated and also associated with metastasis and significantly shorter patient survival and this effect was reverted by transient expression of miR-29c (82).

MiRNAs are crucial molecular factors to regulate post-transcriptional processing, and more than 60% protein coding genes are expected to regulate miRNAs, and their dysregulation is often reported to trigger different human disorders including cancer. In recent years, many reports highlighted the significance of miR-34a as tumor suppressive molecular entity. It has been figured out that miR-34a has inverse relation with the cancer progression, and the expression of miR-34a declines with the increased progression of cancer and *vice versa* (83).

*Scutellaria barbata* (SB) is a natural compound and has been used for years as a potential compound among traditional Chinese medicines against multiple cancers. *In vitro* and *in vivo* clinical trials have proved that its ethanol extract of SB is an effective agent to induce apoptosis and limit cancer cell proliferation (84). Ethanol extract of SB has been found effective against human CRC HCT-8 cells and regulates miR-34a expression. Molecular assay confirmed that SB extract upregulates the miR-34a expression and negatively regulates the Bcl-2, Notch and Jagged-1 gene expression. miR-34a mediated down-stream targeted gene regulation plays a decisive role in apoptosis and limits cancer cell proliferation. In one of the studies, exogenous inactivation of miR-34a by using anti-miR-34a oligonucleotide triggers Bcl-2, Notch1/2, and Jagged-1 genes and promotes cancer growth (84, 85). Activation of miR-34a has been associated with regulation of various cellular processes including apoptosis, proliferation, and invasion (85). Molecular evidence also established a link of miR-34a with downregulation of Notch1/2 in colorectal CRCs (86).

miR-449a has been documented as tumor suppressor gene and has been closely associated with SATB2 in different cancer types including CRC cells. SATB2 could be used as diagnostic marker for CRC and has comparative negative association with miR-449a. It has been noted that in CRC xenograft mouse models, increased expression of miR-449a promotes apoptosis by negatively regulating the expression of SATB2 (87). Similarly, molecular link has been established to understand the transcriptional deregulation of SMO by miR-326, and it was observed that upregulation of miR-326 negatively regulates SMO protein to induce apoptosis and limit cellular proliferation (88, 89).

Aberrant expression of GLI-1 (Glioma associated oncogene homolog 1) is a key culprit in the metastasis, invasion, and proliferation of various cancer cells. Ample lines of evidence have shown that expression of miR-150 declines with the pathogenesis of CRC. NCM-460 and SW-620 CRC cell lines were examined by using dual luciferase assay to decipher the molecular relation of miR-150 with GLI-1, and it has been noted that miR-150 inhibits the expression of GLI-1 protein in Hh signaling (77). Molecular evidence has proved that Hh is a cellular event responsible for structural development, cellular regeneration, and stemness. In multiple myeloma cancer (MMC), inverse relation of miR-324-5p and hedgehog signaling has been observed. Increased expression of miR-324-5p has significant inhibitory effect on SMO and GLi-1 and limits cancer stemness of cells (90). Pro-oncogenic effect of miR-212 is identified, and molecular relation was established that miR-212 induces pancreatic ductal adenocarcinoma (PDAC) by targeting PTCH-1 (91). miR-361-3P has been reported to have profound impact on different cancers including prostate cancer, breast cancer, lung cancer, and cervical cancer. To decipher the molecular interplay of miR-361-3p in retinoblastoma (RB) tissue and RB cell lines, Weri-Rb-1, and Y79, real-time PCR analysis was performed, and it is concluded that miR-361-3p expression is downregulated with cancer progression. Forced expression of miR-361-3p is reported to limit cancer cell proliferation by targeting GLI-1/3 and sonic hedgehog signaling (92). Multiple miRNA expressions have been associated with the onset of breast cancer including miR-454-3p, miR-130b-3p, miR-421, and miR-301a-3p. These miRNAs are

noted to target PIEZO-2 gene. Downregulation of PIEZO-2 gene in breast cancer has been molecularly linked with estrogen and progesterone receptors which are responsible agents for Hh signaling cascade in breast cancer (93).

Extensive research work on miRNAs has been done in recent years to unfold the molecular complexity of carcinoma and to bridge the gap towards new and effective therapeutic approaches. miR-338-3p interaction with hedgehog pathway by using recombinant lentiviral vectors PLV-THM-miR-338-3p and PLV-THM-miR-338-3p inhibitor has been reported and successful transfection in SW-620 CRC cells was achieved. Increased expression of miR-338-3p was observed, it significantly suppresses SMO protein and inhibits proliferation ability. Molecular interplay of miR-338-3p is also confirmed by using PLV-THM-miR-338-3p inhibitor, and it was concluded that it upregulates the SMO protein expression to initiate hedgehog signaling pathway and induces CRC onset. miR-338-3p could be a therapeutic agent to suppress CRC growth by targeting SMO, (**Figures 2** and **3**) (94). Now, withstanding the fact that SMO is a possible target of miR-338-3p. 40 CRC tissue samples and 2 CRC cell lines, SW620 and SW480 were investigated to understand the corresponding protein expression of SMO and miR-338-3p by using semi-quantitative RT-PCR, western and northern blotting assays. It was established that miR-338-3p plays a significant role in metastasis and progression of CRC carcinoma (95).

Accumulation of genetic and epigenetic errors can trigger the aberrant signaling cascades. miRNAs are the critical key players to

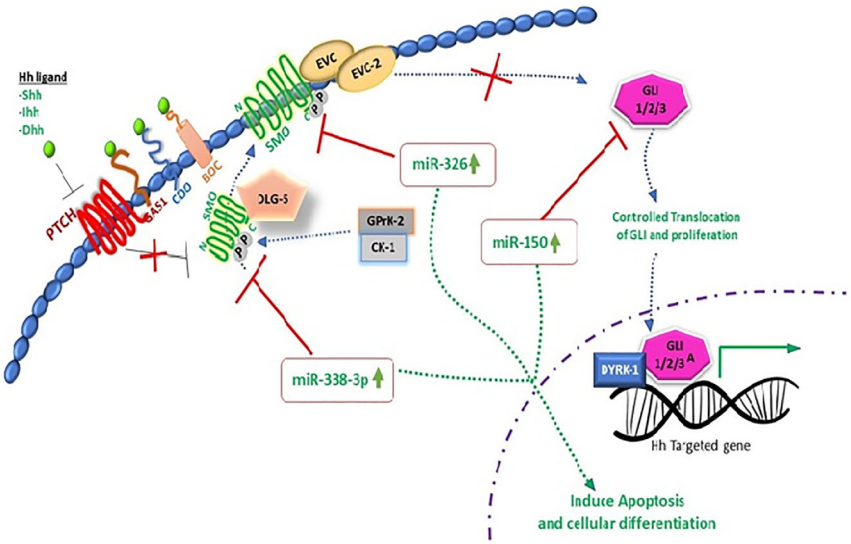


**FIGURE 2** | miRNAs targeting SMO oncogenic hedgehog pathway to induce apoptosis in CRC.

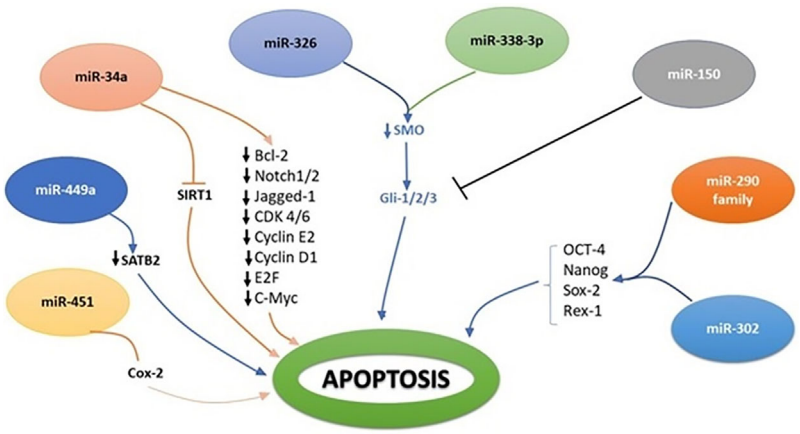


**FIGURE 3** | Molecular interplay between several miRNAs and their downstream target genes to induce apoptosis.

fine-tune genetic expression upon exogenous factors including DNA hypermethylation, hypomethylation, histone modification, and deacetylation. Thus epigenetic-miRNA regulatory molecular cascades are the contributing agents for onset of different types cancers (96). Tumorigenic activation of SMO by over-expression of Shh ligand is reported as responsible agent in 40% cases of human hepatocarcinogenesis (97). Molecular balance between cellular proliferation, differentiation, and renewal is modulated by epigenetic regulatory network and miRNAs. miRNAs are the functional short RNAs that control stemness of cancer cells and promote stem cell self-renewal (97). CSCs are believed to be the critical source for tumor initiation. It has been reported that SHH signaling has reprograming potential for epigenetic memory power within CSCs to modulate cancer hallmarks. miR-302-367 clusters regulate cellular plasticity molecular cascade by engaging cyclin-D1, CDK-4, OCT-4 and SOX-2 genes (98).

## MICRORNAS AS MASTER REGULATOR OF STEMNESS AND METASTASIS

Cancer stem cells are the cells with self-renewal potential within the tumor and are the key responsible agent for radio- and chemo-resistance behavior of cancer cells. Increasing evidence strongly suggests that CSCs are the responsible factor for the onset of carcinogenesis in many human cancer types as cancer cells have self-renewable stem cell like characteristics. Several microRNAs expression have been associated to regulate cancer stemness pathways and its downstream targeting genes (115). Tumor cells were believed to derived from normal stem cells or progenitor cells that undergo genetic or epigenetic modification and transform themselves into CSCs by attaining unlimited self-renewable and differentiation potential (116, 117). Recent findings provide striking evidence that dysregulation of miRNAs regulates CSC characteristics and induces tumorigenesis, and multi drug resistance behavior of cancer cells. The four basic stemness transcriptional factors, OCT4, Nanog, Sox2, and Rex1 are responsible entities for cellular pluripotency and differentiation (118, 119). Recent molecular evidence supports the notion that members of the miR-290 family provide protective defense again differentiation defects in ESCs and play a key role for OCT-4 stability (120). miR-302 family is reported to limit the self-renewal ability and cellular differentiation by regulating the expression of key genes in stem cells. miR-34 family members contribute effectively in P53 dependent reprograming of human ESCs, and it has been noted that loss of functional ability of miR-34 is associated with the upregulation of pluripotency genes including N-Myc, SOX2, and NANOG (115). miR-34a is also reported to modulate neural differentiation by targeting SIRT1. It has been widely accepted that miRNAs are the potential contributors to regulate stem cell properties and stemness of cancer cells (115).

To understand the molecular underpinning of cancer stemness, CSCs were isolated from SW-1116 colon cancer cell lines with both $CD133^{+}/CD44^{+}$ and $CD133^{-}/CD44^{-}$ surface phenotype antigen for comparative analysis. Researcher found 62 differentially expressed miRNAs in cancerous and non-cancerous stem cells and noted 31 miRNAs overexpressed including miR-29a and miR-29b, as well as 31 miRNAs under-expressed including miR-449a, miR-4524, and miR-451 (117). Exogenous expression of miR-451 declines the self-renewable capacity of stem cells and decreases multi drug resistant potential of cancer cells. Induced expression of miR-451 negatively regulates COX-2 gene that plays a decisive role in Wnt cascade activation and is believed to act as complementary factor for CSC activation. Wnt pathway has a key association with intestinal stem cell regulation and reported to linked with colon cancer onset (117, 121). Inhibition of Wnt pathway leads to the degradation of $\beta$-catenin in the cytoplasm and is unable to initiate epithelial renewal. Increased expression of miR-21 is noted to induce stemness by regulating Wnt activity and thus initiates carcinogenesis by inhibiting the tumor suppressor gene, TGF-βR2, that is a key regulatory gene for cellular differentiation (122). One of the fundamentals signaling pathway to regulate colon stemness is Notch. Notch cascade activation is believed to induce cellular proliferation of progenitor cells. miR-34a is shown to downregulate Notch signaling activity and regulate cellular differentiation of targeted cells and colon stem cells (123) (**Table 1**).

### Putative Markers for CRC

LGR5 is a member of G-protein coupled receptor that can interact and trigger activation of Wnt signaling *via* binding to furin-like repeat FU2 domain of R-spondin (133). LGR5 has been reported to be a putative marker for CRC stem cells. It has come to light less lately that LGR5 triggers the activation of both Wnt and TGF-$\beta$ signaling in cancer stem cells. Overexpression of LGR5 increases drug resistance and cancer stemness in both brain tumors and CRC. LGR5 has been reported to have high expression in most of the CRC cell lines and adenomas but this overexpression has nothing to do with progression of tumor as presence of LGR5 increases cell-cell adhesion which in turn promotes stemness and hampers invasiveness and migration (134). Experimentation conducted on the triple positive cells having LGR5-positive subpopulations demonstrated peculiar characteristics of self-renewal, differentiation, colony formation, tumorigenicity, and stemness (135). These findings suggest that LGR5 is a putative marker of CRC stem cells. A transgenic mice experiment confirmed the status of LGR5 as CRC stem cell marker. Addition of suicide gene to a transgenic mice genome that was activated in the presence of overexpressed LGR5 and tamoxifen resulted in the death of LGR5 rich colorectal stem cells. The absence of tamoxifen resulted in differentiation of LGR5 CSCs (136). From these findings it can be concluded that LGR5 is a putative CSC marker that should be considered as potential target for advanced grade CRC and such CSCs must be eradicated before the start of any combinational therapies for CRC. CD44 is a surface protein responsible for interaction between cells and also plays vital role in the adhesion and migration of the cells (137). The CD44 has a specific binding site for hyaluronic acid which facilitates interaction with selectin, osteopontin, fibronectin, laminin, and collagen in the extracellular matrix (138). The binding of hyaluronic acid with CD44 results in the activation of epidermal growth factor receptor family kinases such as the

**TABLE 1** | MicroRNA mediated control of CRC stemness and progression.

| MicroRNA | Expression pattern | Target | Function | Reference |
|---|---|---|---|---|
| miR-150 | Upregulated | Gli-1, 2 & 3 | Downregulation of the expression of Gli-1/2/3 in CRC thus prevents apoptosis | (77) |
| miR-34a | Upregulated | Bcl-2, Notch1/2, Jagged 1,2 CDK, Cyclin-D, E2F, c-Myc and Cyclin-E2 SIRT1 | Downregulates the expression of Bcl-2, Notch1 and 2, Jagged 1,2, and CDK, Cyclin-D, E2F trigger apoptosis in CRC | (124) |
| miR-338-p | Upregulated | SMO, DLG5, GPrK-2 and CK1 | Downregulates/inhibits the expression of SMO, DLG5, GPrK-2, and CK1 trigger apoptosis CRC | (94) |
| miR-150 | Upregulated | Gli-1/2/3 | Downregulates/inhibits the expression of Gli-1/2/3 thus preventing proliferation in CRC | (77) |
| miR-326 | Upregulated | SMO, EVC-1/EVC-2 | Downregulates/inhibits the expression of SMO and EVC-1/EVC-2 in CRC | (88) |
| miR-290/miR-302 | Upregulated | OCT-4, Nanog, Sox-2, and REX-1 | Upregulates the expression of OCT-4, Nanog, Sox-2, and REX-1 and triggers apoptosis in CRC | (125) |
| miR-21 | Upregulated | PTEN, AkT | Increases stemness and invasiveness in CRC *via* upregulation of Akt pathway | (69) |
| miR-148a | Downregulated | Wnt/$\beta$-catenin | Reduces cancer stemness in CRC cell lines | (126) |
| miR-137 | Downregulated | Doublecortin-like kinase 1 (DCLK1) | Downregulates the DCLK1 and suppresses tumor growth in CRC | (127) |
| miR-372/373 | Upregulated | Nanog/SMO | Downregulates MAPK/ERK and VDR signaling thus increases cancer stemness in CRC | (128) |
| miR-196b-5p | Upregulated | STAT3 | Upregulates the expression of Nanog, SOX2 and OCT4 increases the stemness profile of CRC stem cells and triggers drug resistance. | (129) |
| miR-195-5p | Downregulated | SOX2, CD133 | Suppresses the stemness and chemo-resistance in CRC CSCs *via* modulation of key signaling pathways proteins such as Notch2 and RBPJ. | (130) |
| miR-199a/b | Downregulated | Glycogen synthase kinase 3 β (GSK3 β) | Increases chemo-resistance in CRC *via* modulation of Wnt/$\beta$-catenin and ABCG2 signaling pathway | (131) |
| miR-31 | Upregulated | EphB2/EphA2 signaling | Increases cancer stemness *via* modulation of the EphB2/EphA2 signaling in CRC CSc. | (132) |

MAPK and PI3/AkT that in turn promotes growth and proliferation in various cancers (138). Majority of CSCs population have CD44 surface markers along with other cell surface markers that increase invasiveness and stemness (139). Considering its abundance in CRC tumorous stem cells it has been reported as putative marker for the detection of invasiveness and metastasis. Cluster differentiation 24 is an emerging biomarker for CRC (140). Overexpression of CD24 is affiliated with tumor differentiation, invasion metastasis (141). In addition, CD24 overexpression also promotes poor survival rates in the patients with CRC. These findings suggest that CD24 involvement increases stemness in CRC stem cells and may be used as a prognostic marker for patients with CRC.

## NANOTHERAPEUTICS AS AN APPROACH FOR THE TREATMENT OF CRC

Hh pathway can be targeted by the specific inhibitors at various sites. Therefore, inhibitors of Hh pathway are useful anti-cancer agents. Till now, several small molecules inhibitors have been developed tested for their inhibitory effects on Hh signaling pathway. A natural alkaloid cyclopamine obtained from the corn lily V. californicum is the first Hh inhibitor reported. Cyclopamine impedes the functioning of smoothened *via* inhibiting its attachment to the heptahelical bundle (142). However, cyclopamine has several drawbacks such as the limited bioavailability, chemical instability, and shorter half-life. Therefore, it cannot be considered as potential therapeutic target. Several small molecule antagonists such as the SANT1, SANT2, SANT3, SANT4, CUR-61414, and GDC-0449 have been synthesized and evaluated in pre-clinical models for their anti-cancer activity in various solid tumors (143). The Hh small molecule inhibitors were first evaluated in basal cell carcinomas. Vismodegib a small molecule inhibitor of SMO is the first reported drug used for the treatment of basal cell carcinoma (144). In comparison to the cyclopamine, vismedegib was efficient to culminate cancer growth in both advanced and metastatic basal cell carcinomas. Over the years new therapeutic interventions in the development of SMO for Hh signaling antagonists such as LDE225 also known as the sonidegib has increased the drug efficacy *via* increasing tissue absorption and better penetration in the blood brain barrier for skin cancer and brain tumor respectively (144). There are several SMO antagonists designed to inhibit Hh pathway are in clinical trials that specifically target medulloblastoma, ovarian cancer, pancreatic cancer, and colon cancer (145). Yet the clinical success of these antagonists is still limited. In order to understand the effects of these SMOs on hedgehog dependent inhibition of CRC further investigation is required for finding suitable and effective drug. In recent years huge development in the field of nanotechnology has enabled us to devise efficient therapeutics for various diseases (146). In addition to this, nano-carriers have greater efficiency in delivering drug to target site with limited cytotoxicity. These observations have urged scientists to seek more efficient nano-drug delivery systems that can hamper cancer progression and increase apoptosis. There have been some serious drawbacks of utilizing SMO as inhibitors of Hh signaling (147). The SMO antagonists have poor bioavailability,

drug resistance and non-specific activation of Gli (148). Nanoformulations can address these drawbacks by increasing bioavailability, reducing drug resistance and specific activation of Gli. Based on current data there are two types of nano-based Hh signaling inhibitors: Natural Inhibitors and synthetic inhibitors. Cyclopamine comes under the list of natural inhibitor that has faced severe criticism because of its limited bioavailability, poor solubility, and several side effects. However, nanoformulations of cyclopamine have reduced these obstacles. It has been reported that cycolopamine loaded lipid nanoparticles (NPs) efficiently reduced the growth of radiation therapy treated breast and pancreatic cells (149, 150). In another study, polymeric nanoparticles designed to carry both cyclopamine and doxorubicin reduced the growth in orthotropic breast cancer model (151). The polymeric nanoformulations of cyclopamine and paclitaxel successfully cured prostate cancer (152) and pancreatic cancer (153) in combination with chemotherapy in mice. A biomimetic nanoparticle delivery system having cyclopamine encapsulated in erythrocyte membrane camouflaged PLGA resulted in super enhanced bioavailability of cyclopamine. Moreover, a combination of biomimetic NPs with paclitaxel NPs increased the delivery of paclitaxel to the tumor tissue increased tumor profusion and inhibited tumor growth *in vivo* (154). Vismodegib an FDA approved natural inhibitor for Hh signaling pathway has limited solubility and bioavailability. The polymeric nanoformulations for vismodegib have resolved these issues. The encapsulation of vismodegib in SN38 pro-drug polymer which is an active metabolite of irinotecan to treat pancreatic ductal carcinoma resulted in decreased tumor growth and reduced fibrosis. In addition to this SN38 NPs facilitate the inhibition of Hh signaling which is crucial for the communication between tumor and stromal cells. SN38 NPs provided better diffusion for vismodegib thus prevented the drug resistance. SN38 NP encapsulation of vismodgib suppressed Gil1 expression in the tumor microenvironment of xenograft model suggesting the fact that SN38 NPs could aid in restoring normal drug resistance of the tumor cells (155). In another study, pH-responsive polymeric NPs containing vismodegib and gemcitabine inhibited growth of pancreatic cancer cells (156). From these findings, NP mediated drug delivery of Hh signaling inhibitors can be used a potential tactic to trigger chemotherapy. Apart from cyclopamine and vismodegib, several other natural Hh signaling inhibitors have been reported to be delivered by the nanofomulations. Anthothecol carrying PLGA nanoparticles have been reported to suppress proliferation and colony formation of pancreatic cancer stem cells through modulating the activity of the Gli-DNA binding (68). Another study confirmed that $\alpha$-mangostin carrying PLGA nanoformulation disrupted the Gli-DNA binding activity in pancreatic cancer cells. This resulted in decreased growth, development, and metastasis of pancreatic cancer stem cells (157). Nanoformulation of glabrescione B has been reported to show tremendous anti-cancer activity in a Hh dependent manner (158). Nano-carriers have been employed in the delivery of the synthetic inhibitors of Hh signaling pathway. Quinacrine a synthetic inhibitor of Hh signaling when loaded into NP formulation triggered the recruitment of GSK-3$\beta$ and PTEN which induced the apoptosis in cancer stem cells. In addition to this qunacrine loaded NPs also reduced the expression of Gli vital for the self-renewal of CSCs (159, 160). PLGA NPs encapsulating the HPI-1 a specific inhibitor of Gli1 prevented growth and metastasis of hepatocellular carcinoma mice model. Moreover, HPl-1 delivery reduced the expression of $CD133^+$ cells a type of CSCs in hepatocellular carcinoma (161). A combination of the NPs and gemcitabine reduced cellular growth in xenograft model of pancreatic cancer in a ligand dependent paracrine activation of Hh signaling pathway (162). GANT61 a specific Gli1 inhibitor when encapsulated in PLGA NPs prevented the translocation of Gli-1 to the nucleus and reduced the growth of CSCs (163). Although there has been slight progress towards the utilization of nano-carriers as a module to treat Hh mediated CRC, these observations are in favor that nanoformulations could be used as small molecules Hh inhibitors to cancer. It has come to light less lately that nanoformulations can be used as a carrier for the targeted delivery of the miRNAs. There are different types of nanoparticle based formulations that are being used for this purpose. Lipid nanoparticles, extracellular vesicles, minicells (genetically developed from bacteria), dendrimers, polyamidoamine (PAMAM), and inorganic materials such as the silica, gold, and silver nanoparticles have been extensively synthesized for delivering specific miRNAs to targeted tumors. Oshima et al. have developed an *in-vivo* delivery system to target liver and CRC. They specifically designed nano-scale coordination polymers for the effective delivery of oligometastatic miR-655-3p. Their findings revealed that co-delivery of miR-655-3p along with oxaliplatin reduced tumor growth (164). Yang et al. successfully formulated polyethyleneimine/hyalouronic acid mesoporous silica nanoparticle loaded with oxaliplatin and miR-204-5p. This nanoformulation enhanced the apoptosis and therapeutic efficacy in HT-29 cell lines (165). Altogether these findings suggest that nanoformulations are a suitable platform for the delivery of miRNAs and can increase the therapeutic efficacy in CRC (**Table 2**).

## Oral Nanotherapeutics

Nanotherapeutics is one of the promising strategies that offer dynamic surface functionalized modifications to improve targeted drug delivery and to limit the adverse effects. Nano-platform for drug designing offers potent routes to enhance drug profile. Nanotherapeutics are generally comprise of three core elements including nano-vehicle as carrier agent, target ligand and therapeutic drug molecule (**Figures 3** and **4**) (166). Different nanotherapeutics including lipid nanoparticles, organic and inorganic nanoparticles, polymeric nanoparticles, nanocrystals and plant derived nanomaterials have been used clinically including Taxel®, Lipo-Dox®, Abraxene®, Abraxene®, Marqib®, Onivyde® *etc.*, and there is large number of nanotherapeutics in pre-clinical and clinical trials that can be fabricated to target Hh signaling cascade to reduce cancer cell proliferation (166, 167).

Oral chemotherapeutics are reported to have multiple limitations that demand novel alternative therapeutics for cancer treatment. Recently, the concept of oral nanotherapeutics paved

**TABLE 2** | CRC inhibitors and nanoformulations.

| Nanoformulation | Ligand | Target | Cell line(s) | Reference |
|---|---|---|---|---|
| Nanosized maghemite particle | Antibody | CEA | HCT-116 | (99) |
| Dextran- and PEG-coated superparamagnetic iron oxide nanoparticles (abf-SPION) | scFv | CEA | LS174T | (100) |
| Conatumumab (AMG 655)-coated nanoparticles | Antibody | DR5 | HCT-116 | (101) |
| Photosensitizer meso-Tetra(N-methyl-4-pyridyl) porphine tetra tosylate chitosan/alginate nanoparticles | Antibody | DR5 | HCT-116 | (102) |
| Gold and iron oxide HNPs | scFv | A33 antigen | SW1222 & HT-29 | (103) |
| Poly(lactide- coglycolide) nanoparticle loaded with camptothecin | Antibody | Fas receptor (CD95/Apo-1) | HCT-116 | (104) |
| Chitosan nanoparticles loaded with 5-ALA | Folic acid | FR | HT29 and Caco-2 colorectal cancer cell lines overexpressing folate receptor | (105) |
| FA-CS conjugates nanoparticles | Folic acid | FR | HT-29 | (106) |
| HPMA-copolymer-doxorubicin conjugates | Peptide GE11 | EGFR | HT-29, SW480 and A431 | (107) |
| T22-empowered protein-only nanoparticles | 18-mer peptide T22 (T22-GFP-H6) | CXCR4 | HeLa | (108) |
| Chitosan nanoparticles encapsulating oxaliplatin (L-OHP) | HA | HA receptor | HT-29 in C57BL mice | (109) |
| MSN | Coated with poly-(L-lysine) and HA | CD44 receptor | HCT-116 | (110) |
| rHDL nanoparticles loaded with siRNA | Apo A-I | SR-B1 | Model colorectal cancer metastasis in mice (HCT-116) | (111) |
| HA-lipid shell nanoparticles | Gene therapy, core shell | P21-saRNA-322 | HT-29 | (112) |
| Survivin siRNA | Cationic LCLs, Gene therapy | Lipolex | LoVo | (113) |
| Exosomes | Gene therapy | miR-128-3p | HCT-116oxR | (114) |

*Apo A-1, Apolipoprotien A-1; CEA, Carcinoembryonic antigen; CXCR4, CXC chemokine receptor 4; DR5, Death receptor 5; FR, Folate receptor; HA, Hyaluronic acid; HNP, Hybrid nanoparticle; EGFR, Epidermal growth factor receptor; DR5, Death receptor 5; HA, Hyaluronic acid; Scavenger receptor type B1.*

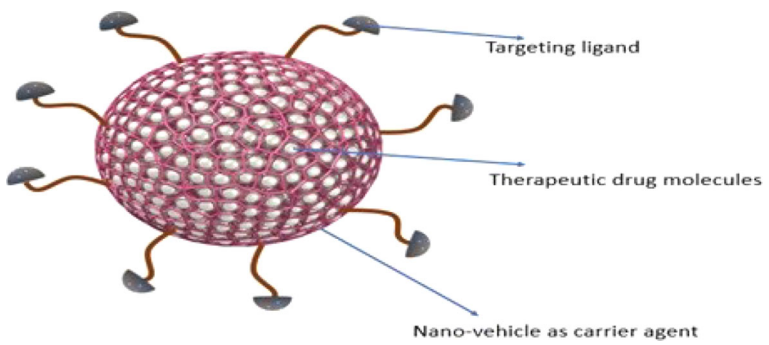


**FIGURE 4** | Schematic illustration of nanotherapeutic components.

the avenue in pharmaceutics towards more stable and high tumor targeted therapy with minimize adverse effects. A successful pre-clinical attempt has been performed by synthesizing redox nanoparticles (RNPs) for colon cancer treatment. This novel RNP contains nitroxide radicals for antioxidant activity and to scavenge ROS (reactive oxidative species) in cellular microenvironment. RNPs are specialized to accumulate in colonic mucosa and targeted cancer cells predominantly. These specialized oral-nanotherapeutics are also reported to limit cellular toxicity issues upon prolong exposure and is significant agent to inhibit tumor growth (**Figure 5**). It has been noticed that synergistic effect of RNP and conventional therapeutics can suppress adverse effects in gastro-intestinal tract and is an ideal candidate for future with significant potential in the existing pool for cancer treatment (168).

Various attempts have been made for successful oral delivery of targeted nanotherapeutics to treat cancer including bowel inflammatory cancer and colon cancers. Engineered chitosan based amphiphilic muco-adhesive drug-delivery strategies have been examined in *in-vivo* therapeutic studies. In one of the recent studies, SN38 (7-ethyl-10-hydroxycamptothecin) nanoparticles and water insoluble curcumin are proved to be a significant candidate to limit carcinogenesis and shrink tumor diameter >4 mm. Thus, bio-adhesive chitosan based stable colloidal nanotherapeutics is a novel and reliable approach to improve the outcome of colon cancer treatment (169).

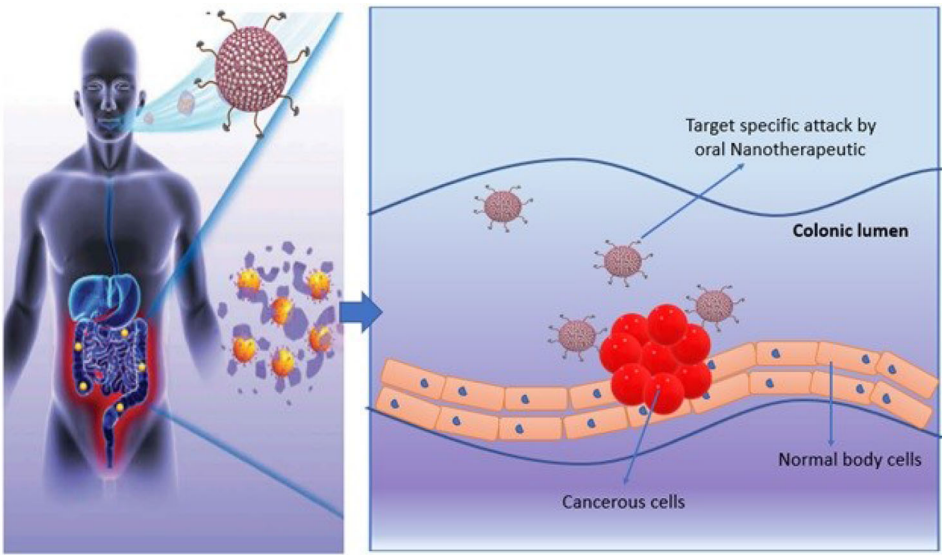


**FIGURE 5** | Schematical representation the passage of oral nanotherapeutics to treat colon cancer.

There are a number of inhibitors related to Hh signaling namely sonidegib, saridegib, itraconazole, BMS-833923, LEQ-506, Taladegib, Glasdegib, TAK-441, Vismodegib, and several others (**Table 3**). But a very limited data is available regarding the use of these inhibitors for CRC. In addition to this majority of work done so far is on Wnt/$\beta$-catenin and mutations in this pathway. Therefore a lot of potential works need to be done against the implementation of such inhibitors in the clinical trials (**Table 3**).

## FUTURE PERSPECTIVE

The Hh pathway is activated during regeneration and tissue repair in adults. Compelling pieces of evidence have indicated that inhibition of Hh pathway can prevent tumor progression and increased apoptosis. However, the clinical outcomes of such inhibition are unsatisfactory. The tumor heterogeneity and complex signaling crosstalk are the two major stumbling blocks that challenge the specificity of a specific Hh inhibitor. A tumor cell can trigger multiple signaling pathways simultaneously that can hamper the anti-proliferative abilities of a single inhibitor.

**TABLE 3** | Representation Hh signaling inhibitor under clinical trials.

| Therapeutic Agent | Development Phase | Type of Cancer | Trial Identity |
|---|---|---|---|
| **Vismodegib** | Phase I | Myelomas | NCT01330173 |
| | Phase II | Medulloblastoma | NCT01878617 |
| | Phase IV | Basal cell Carcinoma | NCT02436408 |
| | Phase II | Colorectal Cancer | NCT00636610 |

Therefore, an outlook for new inhibitors of Hh signaling pathway that can hamper the activity of interconnected pathways is necessary. miRNAs have been reported to regulate the expression of vital genes involved in the proliferation and spread of CRC. They have been extensively examined for their putative role as diagnosis and prognosis markers for stratification of risk groups. Exploring the interplay between miRNAs and Hh signaling can aid in the development of therapeutics for Hh mediated CRCs. In addition to this miRNAs can regulate the cancer stem cells proliferation and metastasis (170). Therefore, they can be utilized as a probe to investigate cancer stemness and drug resistance in CRC stem cells. miRNAs modulating the expression of the proliferative genes is a hallmark in CRCs. A suitable drug delivery system can transfer miRNA modulating moieties to the target cell can impede the proliferative capabilities. Development of such delivery system will revolutionize therapeutics. Considering such scenario, nanoformulations can be a suitable platform for the treatment of various malignancies including cancer. Nanoformulations are advantageous because of their specificity, low toxicity, limited side effects, and enhanced bioavailability of the cargo such as various natural compounds *i.e.*, berberine, paclitaxel curcumin, and SMOs. Hh signaling can be targeted with nanoparticles, but there are several drawbacks affiliated. Drug resistance is the major hurdle with the devising of NPs for Hh signaling. The complex interaction of Hh pathway makes it difficult to be targeted with nanoformulations of SMO. It has been reported that SMO nanoparticles were unable to hamper tumor growth when Gli was activated *via* non-canonical Hh signaling. In addition to this the interaction of Hh signaling with other molecular cascades such as the Wnt and Notch also affect the targeting capacity of small molecular inhibitors of Hh signaling. The nanoformulations have to overcome cellular resistance which is an effective barrier for suitable nano-drug delivery which can be overcome by the combination of nanoformulations such as

pegylated liposomes and formulations that prevent quick release of cargo (Chitosan). Compelling research has dictated the fact that only 0.7% of the total nanoformulation reaches the solid tumor (171). This can lead to the development of side toxicity which is a major concern for most of the nanoformulations. However, recent advances in nano-drug delivery have culminated the side toxicity by implementing the use of biphosphonates. In addition, combining NP formulation can modulate the tumor microenvironment to enhance the drug delivery. A combination of cycolopamine and paclitaxel nanoformulation designed to impede the Hh signaling disrupted the extracellular matrix of the tumor cells and increased drug profusion. In addition choice of nanoformulation, size of the NPs and their diffusion in the cell, cost of production, clinical translation, and cancer cell resistance are the limiting barriers that need to be addressed for designing specific Hh inhibitors. Overcoming these challenges can improve treatment methods for cancer patients. Altogether miRNAs and natural compounds mediated regulation of Hh signaling might help us devising new diagnostic/prognosis and therapeutics for CRC.

## AUTHOR CONTRIBUTIONS

ZJ, MJ, and AR drafted the manuscript. HS, SR, AI, and WC revised the draft. HS, WK, WK-K, AG-L, JS-R, and WC conceptualized the study and reviewed it critically. All authors contributed to the article and approved the submitted version.

## REFERENCES


1. Javed Z, Khan K, Sadia H, Raza S, Salehi B, Sharifi-Rad J, et al. LncRNA & Wnt signaling in colorectal cancer. *Cancer Cell Int* (2020) 20(1):1–10. doi: 10.1186/s12935-020-01412-7
2. Johnson CM, Wei C, Ensor JE, Smolenski DJ, Amos CI, Levin B, et al. Meta-analyses of colorectal cancer risk factors. *Cancer Causes Control* (2013) 24 (6):1207–22. doi: 10.1007/s10552-013-0201-5
3. Salaritabar A, Berindan-Neagoe I, Darvish B, Hadjiakhoondi F, Manayi A, Devi KP, et al. Targeting Hedgehog signaling pathway: paving the road for cancer therapy. *Pharmacol Res* (2019) 141:466–80. doi: 10.1016/j.phrs.2019.01.014
4. Tickle C, Towers M. Sonic hedgehog signaling in limb development. *Front Cell Dev Biol* (2017) 5:14. doi: 10.3389/fcell.2017.00014
5. Niewiadomski P, Niedziółka SM, Markiewicz Ł, Uśpieński T, Baran B, Chojnowska K. Gli proteins: Regulation in development and cancer. *Cells* (2019) 8(2):147. doi: 10.3390/cells8020147
6. Park K-S, Martelotto LG, Peifer M, Sos ML, Karnezis AN, Mahjoub MR, et al. A crucial requirement for Hedgehog signaling in small cell lung cancer. *Nat Med* (2011) 17(11):1504. doi: 10.1038/nm.2473
7. Bailey JM, Swanson BJ, Hamada T, Eggers JP, Singh PK, Caffery T, et al. Sonic hedgehog promotes desmoplasia in pancreatic cancer. *Clin Cancer Res* (2008) 14(19):5995–6004. doi: 10.1158/1078-0432.CCR-08-0291
8. Ingham PW, Placzek M. Orchestrating ontogenesis: variations on a theme by sonic hedgehog. *Nat Rev Genet* (2006) 7(11):841–50. doi: 10.1038/nrg1969
9. Skoda AM, Simovic D, Karin V, Kardum V, Vranic S, Serman L. The role of the Hedgehog signaling pathway in cancer: A comprehensive review. *Bosnian J Basic Med Sci* (2018) 18(1):8. doi: 10.17305/bjbms.2018.2756
10. Takebe N, Harris PJ, Warren RQ, Ivy SP. Targeting cancer stem cells by inhibiting Wnt, Notch, and Hedgehog pathways. *Nat Rev Clin Oncol* (2011) 8(2):97–106. doi: 10.1038/nrclinonc.2010.196
11. Wen D, Danquah M, Chaudhary AK, Mahato RI. Small molecules targeting microRNA for cancer therapy: Promises and obstacles. *J Controlled Release* (2015) 219:237–47. doi: 10.1016/j.jconrel.2015.08.011
12. Hahn H, Wicking C, Zaphiropoulos PG, Gailani MR, Shanley S, Chidambaram A, et al. Mutations of the human homolog of Drosophila patched in the nevoid basal cell carcinoma syndrome. *Cell* (1996) 85(6):841–51. doi: 10.1016/S0092-8674(00)81268-4
13. Johnson RL, Rothman AL, Xie J, Goodrich LV, Bare JW, Bonifas JM, et al. Human homolog of patched, a candidate gene for the basal cell nevus syndrome. *Science* (1996) 272(5268):1668–71. doi: 10.1126/science.272.5268.1668
14. Couvé-Privat S, Bouadjar B, Avril MF, Sarasin A, Daya-Grosjean L. Significantly high levels of ultraviolet-specific mutations in the smoothened gene in basal cell carcinomas from DNA repair-deficient xeroderma pigmentosum patients. *Cancer Res* (2002) 62(24):7186–9.
15. Xie J, Murone M, Luoh S-M, Ryan A, Gu Q, Zhang C, et al. Activating Smoothened mutations in sporadic basal-cell carcinoma. *Nature* (1998) 391 (6662):90–2. doi: 10.1038/34201
16. Clark VE, Erson-Omay EZ, Serin A, Yin J, Cotney J, Özduman K, et al. Genomic analysis of non-NF2 meningiomas reveals mutations in TRAF7, KLF4, AKT1, and SMO. *Science* (2013) 339(6123):1077–80. doi: 10.1126/science.1233009
17. Pelczar P, Zibat A, van Dop WA, Heijmans J, Bleckmann A, Gruber W, et al. Inactivation of Patched1 in mice leads to development of gastrointestinal stromal-like tumors that express Pdgfrα but not kit. *Gastroenterology* (2013) 144(1):134–44. e6. doi: 10.1053/j.gastro.2012.09.061
18. Mao J, Ligon KL, Rakhlin EY, Thayer SP, Bronson RT, Rowitch D, et al. A novel somatic mouse model to survey tumorigenic potential applied to the Hedgehog pathway. *Cancer Res* (2006) 66(20):10171–8. doi: 10.1158/0008-5472.CAN-06-0657
19. Xie J, Bartels CM, Barton SW, Gu D. Targeting hedgehog signaling in cancer: research and clinical developments. *Onco Targ Ther* (2013) 6:1425. doi: 10.2147/OTT.S34678
20. Kim J, Aftab BT, Tang JY, Kim D, Lee AH, Rezaee M, et al. Itraconazole and arsenic trioxide inhibit Hedgehog pathway activation and tumor growth associated with acquired resistance to smoothened antagonists. *Cancer Cell* (2013) 23(1):23–34. doi: 10.1016/j.ccr.2012.11.017
21. Gu D, Fan Q, Zhang X, Xie J. A role for transcription factor STAT3 signaling in oncogene smoothened-driven carcinogenesis. *J Biol Chem* (2012) 287 (45):38356–66. doi: 10.1074/jbc.M112.377382
22. Xie J, Aszterbaum M, Zhang X, Bonifas JM, Zachary C, Epstein E, et al. A role of PDGFRα in basal cell carcinoma proliferation. *Proc Natl Acad Sci* (2001) 98(16):9255–9. doi: 10.1073/pnas.151173398
23. Wang Y, Ding Q, Yen C-J, Xia W, Izzo JG, Lang J-Y, et al. The crosstalk of mTOR/S6K1 and Hedgehog pathways. *Cancer Cell* (2012) 21(3):374–87. doi: 10.1016/j.ccr.2011.12.028
24. Johnson RW, Nguyen MP, Padalecki SS, Grubbs BG, Merkel AR, Oyajobi BO, et al. TGF-β promotion of Gli2-induced expression of parathyroid hormone-related protein, an important osteolytic factor in bone metastasis, is independent of canonical Hedgehog signaling. *Cancer Res* (2011) 71 (3):822–31. doi: 10.1158/0008-5472.CAN-10-2993
25. Hsieh A, Ellsworth R, Hsieh D. Hedgehog/GLI1 regulates IGF dependent malignant behaviors in glioma stem cells. *J Cell Physiol* (2011) 226(4):1118–27. doi: 10.1002/jcp.22433
26. Niyaz M, Khan MS, Mudassar S. Hedgehog signaling: an Achilles' heel in cancer. *Trans Oncol* (2019) 12(10):1334–44. doi: 10.1016/j.tranon.2019.07.004
27. Wu C, Zhu X, Liu W, Ruan T, Tao K. Hedgehog signaling pathway in colorectal cancer: function, mechanism, and therapy. *OncoTarg Ther* (2017) 10:3249. doi: 10.2147/OTT.S139639
28. Magistri P, Battistelli C, Strippoli R, Petrucciani N, Pellinen T, Rossi L, et al. SMO inhibition modulates cellular plasticity and invasiveness in colorectal cancer. *Front Pharmacol* (2018) 8:956. doi: 10.3389/fphar.2017.00956
29. Dierks C, Beigi R, Guo G-R, Zirlik K, Stegert MR, Manley P, et al. Expansion of Bcr-Abl-positive leukemic stem cells is dependent on Hedgehog pathway activation. *Cancer Cell* (2008) 14(3):238–49. doi: 10.1016/j.ccr.2008.08.003
30. Yoshikawa R, Nakano Y, Tao L, Koishi K, Matsumoto T, Sasako M, et al. Hedgehog signal activation in oesophageal cancer patients undergoing

neoadjuvant chemoradiotherapy. *Br J Cancer* (2008) 98(10):1670–4. doi: 10.1038/sj.bjc.6604361
31. Reya T, Morrison SJ, Clarke MF, Weissman IL. Stem cells, cancer, and cancer stem cells. *nature* (2001) 414(6859):105–11. doi: 10.1038/35102167
32. di Magliano MP, Hebrok M. Hedgehog signalling in cancer formation and maintenance. *Nat Rev Cancer* (2003) 3(12):903–11. doi: 10.1038/nrc1229
33. Scarpa M, Scarpa M. Hedgehog signaling in colorectal cancer: A spiny issue gets smoothened. *Transl Cancer Res* (2016) 5:1051S–S4. doi: 10.21037/tcr.2016.11.52
34. Curtin JC, Lorenzi MV. Drug discovery approaches to target Wnt signaling in cancer stem cells. *Oncotarget* (2010) 1(7):563. doi: 10.18632/oncotarget.191
35. Yoshimoto AN, Bernardazzi C, Carneiro AJV, Elia CC, Martinusso CA, Ventura GM, et al. Hedgehog pathway signaling regulates human colon carcinoma HT-29 epithelial cell line apoptosis and cytokine secretion. *PloS One* (2012) 7(9):e45332. doi: 10.1371/journal.pone.0045332
36. Ding Y-L, Zhou Y, Xiang L, Ji Z-P, Luo Z-H. Expression of glioma-associated oncogene homolog 1 is associated with invasion and postoperative liver metastasis in colon cancer. *Int J Med Sci* (2012) 9 (5):334. doi: 10.7150/ijms.4553
37. Song I-S, Jeong YJ, Kim J, Seo K-H, Baek N-I, Kim Y, et al. Pharmacological inhibition of androgen receptor expression inducescell death in prostate cancer cells. *Cell Mol Life Sci* (2020) 77:4663–73. doi: 10.1007/s00018-019-03429-2
38. Zhang X, Zhang S-S, Wei G-J, Deng Z-M, Hu Y. Dysregulation of hedgehog signaling pathway related components in the evolution of colonic carcinogenesis. *Int J Clin Exp Med* (2015) 8(11):21379.
39. Miyaki M, Konishi M, Kikuchi-Yanoshita R, Enomoto M, Igari T, Tanaka K, et al. Characteristics of somatic mutation of the adenomatous polyposis coli gene in colorectal tumors. *Cancer Res* (1994) 54(11):3011–20.
40. Yoshikawa K, Shimada M, Miyamoto H, Higashijima J, Miyatani T, Nishioka M, et al. Sonic hedgehog relates to colorectal carcinogenesis. *J Gastroenterol* (2009) 44(11):1113. doi: 10.1007/s00535-009-0110-2
41. Song L, Li Z-Y, Liu W-P, Zhao M-R. Crosstalk between Wnt/β-catenin and Hedgehog/Gli signaling pathways in colon cancer and implications for therapy. *Cancer Biol Ther* (2015) 16(1):1–7. doi: 10.4161/15384047.2014.972215
42. To KK, Tong CW, Wu M, Cho WC. MicroRNAs in the prognosis and therapy of colorectal cancer: From bench to bedside. *World J Gastroenterol* (2018) 24(27):2949. doi: 10.3748/wjg.v24.i27.2949
43. Yochum GS, McWeeney S, Rajaraman V, Cleland R, Peters S, Goodman RH. Serial analysis of chromatin occupancy identifies β-catenin target genes in colorectal carcinoma cells. *Proc Natl Acad Sci* (2007) 104(9):3324–9. doi: 10.1073/pnas.0611576104
44. Varnat F, Siegl-Cachedenier I, Malerba M, Gervaz P, Ruiz i Altaba A. Loss of WNT-TCF addiction and enhancement of HH-GLI1 signalling define the metastatic transition of human colon carcinomas. *EMBO Mol med* (2010) 2 (11):440–57. doi: 10.1002/emmm.201000098
45. Phi LTH, Sari IN, Yang Y-G, Lee S-H, Jun N, Kim KS, et al. Cancer stem cells (CSCs) in drug resistance and their therapeutic implications in cancer treatment. *Stem Cells Int* (2018) 2018. doi: 10.1155/2018/5416923
46. Sari IN, Phi LTH, Jun N, Wijaya YT, Lee S, Kwon HY. Hedgehog signaling in cancer: a prospective therapeutic target for eradicating cancer stem cells. *Cells* (2018) 7(11):208. doi: 10.3390/cells7110208
47. Yang L, Shi P, Zhao G, Xu J, Peng W, Zhang J, et al. Targeting cancer stem cell pathways for cancer therapy. *Signal Transduct Targeted Ther* (2020) 5 (1):1–35. doi: 10.1038/s41392-020-0110-5
48. Jeng K-S, Sheen I, Leu C-M, Tseng P-H, Chang C-F. The Role of Smoothened in Cancer. *Int J Mol Sci* (2020) 21(18):6863. doi: 10.3390/ijms21186863
49. Pietrobono S, Gagliardi S, Stecca B. Non-canonical hedgehog signaling pathway in cancer: activation of GLI transcription factors beyond smoothened. *Front Genet* (2019) 10:556. doi: 10.3389/fgene.2019.00556
50. Regan JL, Schumacher D, Staudte S, Steffen A, Haybaeck J, Keilholz U, et al. Non-canonical hedgehog signaling is a positive regulator of the WNT pathway and is required for the survival of colon cancer stem cells. *Cell Rep* (2017) 21(10):2813–28. doi: 10.1016/j.celrep.2017.11.025
51. Wu C, Hu S, Cheng J, Wang G, Tao K. Smoothened antagonist GDC–0449 (Vismodegib) inhibits proliferation and triggers apoptosis in colon cancer cell lines. *Exp Ther Med* (2017) 13(5):2529–36. doi: 10.3892/etm.2017.4282
52. Rahman MS, Suresh S, Waly MI. Risk Factors for Cancer: Genetic and Environment. *Bioactive Components Diet Med Treat Cancer Prevent: Springer* (2018) 1–23. doi: 10.1007/978-3-319-75693-6_1
53. Williams JB, Li S, Higgs EF, Cabanov A, Wang X, Huang H, et al. Tumor heterogeneity and clonal cooperation influence the immune selection of IFN-γ-signaling mutant cancer cells. *Nat Commun* (2020) 11(1):1–14. doi: 10.1038/s41467-020-14290-4
54. Jeong WJ, Ro EJ, Choi KY. Interaction between Wnt/β-catenin and RAS-ERK pathways and an anti-cancer strategy via degradations of β-catenin and RAS by targeting the Wnt/β-catenin pathway. *NPJ Precis Oncol* (2018) 2 (1):5. doi: 10.1038/s41698-018-0049-y
55. Wu WK, Wang XJ, Cheng AS, Luo MX, Ng SS, To KF, et al. Dysregulation and crosstalk of cellular signaling pathways in colon carcinogenesis. *Crit Rev Oncol Hematol* (2013) 86(3):251–77. doi: 10.1016/j.critrevonc.2012.11.009
56. Li D, Masiero M, Banham AH, Harris AL. The notch ligand JAGGED1 as a target for anti-tumor therapy. *Front Oncol* (2014) 4:254. doi: 10.3389/fonc.2014.00254
57. Liao W, Li G, You Y, Wan H, Wu Q, Wang C, et al. Antitumor activity of Notch–1 inhibition in human colorectal carcinoma cells. *Oncol Rep* (2018) 39(3):1063–71. doi: 10.3892/or.2017.6176
58. Katoh Y, Katoh M. WNT antagonist, SFRP1, is Hedgehog signaling target. *Int J Mol Med* (2006) 17(1):171–5. doi: 10.3892/ijmm.17.1.171
59. Wang H, Ke F, Zheng J. Hedgehog-glioma-associated oncogene homolog-1 signaling in colon cancer cells and its role in the celecoxib-mediated anti-cancer effect. *Oncol Lett* (2014) 8(5):2203–8. doi: 10.3892/ol.2014.2439
60. Finotti A, Fabbri E, Lampronti I, Gasparello J, Borgatti M, Gambari R. MicroRNAs and Long Non-coding RNAs in Genetic Diseases. *Mol Diagn Ther* (2019) 23(2):155–71. doi: 10.1007/s40291-018-0380-6
61. Cho KHT, Xu B, Blenkiron C, Fraser M. Emerging Roles of miRNAs in Brain Development and Perinatal BrainInjury. *Front Physiol* (2019) 10(227):200–27. doi: 10.3389/fphys.2019.00227
62. Wienholds E, Plasterk RHA. MicroRNA function in animal development. *FEBS Lett* (2005) 579(26):5911–22. doi: 10.1016/j.febslet.2005.07.070
63. Zhuang M, Qiu X, Cheng D, Zhu C, Chen L. MicroRNA-524 promotes cell proliferation by down-regulating PTEN expression in osteosarcoma. *Cancer Cell Int* (2018) 18(1):114. doi: 10.1186/s12935-018-0612-1
64. Li L, Miu K-K, Gu S, Cheung H-H, Chan W-Y. Comparison of multi-lineage differentiation of hiPSCs reveals novel miRNAs that regulate lineage specification. *Sci Rep* (2018) 8(1):9630. doi: 10.1038/s41598-018-27719-0
65. Slattery ML, Mullany LE, Sakoda LC, Wolff RK, Samowitz WS, Herrick JS. Dysregulated genes and miRNAs in the apoptosis pathway in colorectal cancer patients. *Apoptosis* (2018) 23(3-4):237–50. doi: 10.1007/s10495-018-1451-1
66. Barbu MG, Condrat CE, Thompson DC, Bugnar OL, Cretoiu D, Toader OD, et al. MicroRNA Involvement in Signaling Pathways During ViralInfection. *Front Cell Dev Biol* (2020) 8(143):1–22. doi: 10.3389/fcell.2020.00143
67. Dwivedi S, Purohit P, Sharma P. MicroRNAs and Diseases: Promising Biomarkers for Diagnosis and Therapeutics. *Indian J Clin Biochem* (2019) 34(3):243–5. doi: 10.1007/s12291-019-00844-x
68. Valinezhad Orang A, Safaralizadeh R, Kazemzadeh-Bavili M. Mechanisms of miRNA-Mediated Gene Regulation from Common Downregulation to mRNA-Specific Upregulation. *Int J Genomics* (2014) 2014:970607. doi: 10.1155/2014/970607
69. Zhao J, Zhang Y, Zhao G. Emerging role of microRNA-21 in colorectal cancer. *Cancer Biomarkers* (2015) 15(3):219–26. doi: 10.3233/CBM-150468
70. Cekaite L, Eide PW, Lind GE, Skotheim RI, Lothe RA. MicroRNAs as growth regulators, their function and biomarker status in colorectal cancer. *Oncotarget* (2016) 7(6):6476–505. doi: 10.18632/oncotarget.6390
71. Chen X, Guo X, Zhang H, Xiang Y, Chen J, Yin Y, et al. Role of miR-143 targeting KRAS in colorectal tumorigenesis. *Oncogene* (2009) 28(10):1385–92. doi: 10.1038/onc.2008.474
72. Yang F, Xie Y-Q, Tang S-Q, Wu X-B, Zhu H-Y. miR-143 regulates proliferation and apoptosis of colorectal cancer cells and exhibits altered expression in colorectal cancer tissue. *Int J Clin Exp Med* (2015) 8(9):15308–12.
73. Li S, Wu X, Xu Y, Wu S, Li Z, Chen R, et al. miR-145 suppresses colorectal cancer cell migration and invasion bytargeting an ETS-related gene. *Oncol Rep* (2016) 36(4):1917–26. doi: 10.3892/or.2016.5042
74. Sheng N, Tan G, You W, Chen H, Gong J, Chen D, et al. MiR-145 inhibits human colorectal cancer cell migration and invasionvia PAK4-dependent pathway. *Cancer Med* (2017) 6(6):1331–40. doi: 10.1002/cam4.1029

75. Segditsas S, Tomlinson I. Colorectal cancer and genetic alterations in the Wntpathway. *Oncogene* (2006) 25(57):7531–7. doi: 10.1038/sj.onc.1210059
76. Wu L, Yang J, Shi Y, Xia H, Xiang X, Yu X, et al. Circ-ZNF609 promotes migration of colorectal cancer by inhibiting Gli1 expression via microRNA-150. *J BUON* (2018) 23(5):1343–9.
77. Fan H, Liu X, Zheng W, Zhuang Z, Wang C. MiR-150 alleviates EMT and cell invasion of colorectal cancer through targeting Gli1. *Eur Rev Med Pharmacol Sci* (2017) 21(21):4853–9.
78. Gao X, Xu W, Lu T, Zhou J, Ge X, Hua D. MicroRNA-142-3p Promotes Cellular Invasion of Colorectal CancerCells by Activation of RAC1. *Technol Cancer Res Treat* (2018) 17:1533033818790508. doi: 10.1177/1533033818790508
79. Lee DY, Deng C-H, Wang BB, Yang BB. MicroRNA-378 promotes cell survival, tumor growth, and angiogenesisby targeting SuFu and Fus-1 expression. *Proc Natl Acad Sci* (2007) 104(51):20350–5. doi: 10.1073/pnas.0706901104
80. Hwang W-L, Jiang J-K, Yang S-H, Huang T-S, Lan H-Y, Teng H-W, et al. MicroRNA-146a directs the symmetric division of Snail-dominant colorectal cancer stem cells. *Nat Cell Biol* (2014) 16(3):268–80. doi: 10.1038/ncb2910
81. Riaz SK, Ke Y, Wang F, Kayani MA, Malik MFA. Influence of SHH/GLI1 axis on EMT mediated migration and invasion of breast cancer cells. *Sci Rep* (2019) 9(1):6620. doi: 10.1038/s41598-019-43093-x
82. Zhang JX, Mai SJ, Huang XX, Wang FW, Liao YJ, Lin MC, et al. MiR-29c mediates epithelial-to-mesenchymal transition in humancolorectal carcinoma metastasis via PTP4A and GNA13 regulation of β-cateninsignaling. *Ann Oncol* (2014) 25(11):2196–204. doi: 10.1093/annonc/mdu439
83. Slabáková E, Culig Z, Remšík J, Souček K. Alternative mechanisms of miR-34a regulation in cancer. *Cell Death Dis* (2017) 8(10):e3100–e. doi: 10.1038/cddis.2017.495
84. Lin J, Chen Y, Cai Q, Wei L, Zhan Y, Shen A, et al. Scutellaria barbata D Don inhibits colorectal cancer growth via suppression of multiple signaling pathways. *Integr Cancer Ther* (2014) 13(3):240–8. doi: 10.1177/1534735413508811
85. Wei L-H, Lin J-M, Chu J-F, Chen H-W, Li Q-Y, Peng J. Scutellaria barbata D. Don inhibits colorectal cancer growth via suppression of Wnt/β-catenin signaling pathway. *Chin J Integr med* (2017) 23(11):858–63. doi: 10.1007/s11655-017-2775-3
86. Bu P, Chen K-Y, Chen JH, Wang L, Walters J, Shin YJ, et al. A microRNA miR-34a-regulated bimodal switch targets Notch in colon cancer stem cells. *Cell Stem Cell* (2013) 12(5):602–15. doi: 10.1016/j.stem.2013.03.002
87. Sun X, Liu S, Chen P, Fu D, Hou Y, Hu J, et al. miR-449a inhibits colorectal cancer progression by targeting SATB2. *Oncotarget* (2017) 8(60):100975. doi: 10.18632/oncotarget.10900
88. Babashah S, Sadeghizadeh M, Hajifathali A, Tavirani MR, Zomorod MS, Ghadiani M, et al. Targeting of the signal transducer Smo links microRNA-326 to the oncogenic Hedgehog pathway in CD34+ CML stem/progenitor cells. *Int J Cancer* (2013) 133(3):579–89. doi: 10.1002/ijc.28043
89. Sheybani Z, Rahgozar S, Ghodousi ES. The Hedgehog signal transducer Smoothened and microRNA-326: pathogenesis and regulation of drug resistance in pediatric B-cell acute lymphoblastic leukemia. *Cancer Manage Res* (2019) 11:7621. doi: 10.2147/CMAR.S214405
90. Tang B, Xu A, Xu J, Huang H, Chen L, Su Y, et al. MicroRNA-324-5p regulates stemness, pathogenesis and sensitivity to bortezomib in multiple myeloma cells by targeting hedgehog signaling. *Int J Cancer* (2018) 142 (1):109–20. doi: 10.1002/ijc.31041
91. Ma C, Nong K, Wu B, Dong B, Bai Y, Zhu H, et al. miR-212 promotes pancreatic cancer cell growth and invasion by targeting the hedgehog signaling pathway receptor patched-1. *J Exp Clin Cancer Res* (2014) 33 (1):54. doi: 10.1186/1756-9966-33-54
92. Zhao D, Cui Z. MicroRNA−361−3p regulates retinoblastoma cell proliferation and stemness by targeting hedgehog signaling. *Exp Ther Med* (2019) 17(2):1154–62. doi: 10.3892/etm.2018.7062
93. Lou W, Liu J, Ding B, Jin L, Xu L, Li X, et al. Five miRNAs-mediated PIEZO2 downregulation, accompanied with activation of Hedgehog signaling pathway, predicts poor prognosis of breast cancer. *Aging (Albany NY)* (2019) 11(9):2628. doi: 10.18632/aging.101934
94. Sun K, Deng H-J, Lei S-T, Dong J-Q, Li G-X. miRNA-338-3p suppresses cell growth of human colorectal carcinoma by targeting smoothened. *World J Gastroenterol: WJG* (2013) 19(14):2197. doi: 10.3748/wjg.v19.i14.2197
95. Sun K, Su G, Deng H, Dong J, Lei S, Li G. Relationship between miRNA-338-3p expression and progression andprognosis of human colorectal carcinoma. *Chin Med J* (2014) 127(10):1884–90. doi: 10a.3748/wjg.v19.i14.2197
96. Yu Z, Sze-Lok Cheng A. Epigenetic deregulation of microRNAs: new opportunities to target oncogenic signaling pathways in hepatocellular carcinoma. *Curr Pharm Design* (2013) 19(7):1192–200. doi: 10.2174/138161213804805757
97. Sicklick JK, Li Y-X, Jayaraman A, Kannangai R, Qi Y, Vivekanandan P, et al. Dysregulation of the Hedgehog pathway in human hepatocarcinogenesis. *Carcinogenesis* (2006) 27(4):748–57. doi: 10.1093/carcin/bgi292
98. Tandon I, Waghmode A, Sharma NK. Cancer stem cells equipped with powerful hedgehog signaling and better epigenetic memory: Avenues to look for cancer therapeutics. *Curr Cancer Drug Targ* (2019) 19(11):877–84. doi: 10.2174/1568009619666190808155432
99. da Paz MC, Santos Mde F, Santos CM, da Silva SW, de Souza LB, Lima EC, et al. Anti-CEA loaded maghemite nanoparticles as a theragnostic device for colorectal cancer. *Int J Nanomed* (2012) 7:5271–82. doi: 10.2147/IJN.S32139
100. Vigor KL, Kyrtatos PG, Minogue S, Al-Jamal KT, Kogelberg H, Tolner B, et al. Nanoparticles functionalized with recombinant single chain Fv antibody fragments (scFv) for the magnetic resonance imaging of cancer cells. *Biomaterials* (2010) 31(6):1307–15. doi: 10.1016/j.biomaterials.2009.10.036
101. Fay F, McLaughlin KM, Small DM, Fennell DA, Johnston PG, Longley DB, et al. Conatumumab (AMG 655) coated nanoparticles for targeted pro-apoptotic drug delivery. *Biomaterials* (2011) 32(33):8645–53. doi: 10.1016/j.biomaterials.2011.07.065
102. Abdelghany SM, Schmid D, Deacon J, Jaworski J, Fay F, McLaughlin KM, et al. Enhanced antitumor activity of the photosensitizer meso-Tetra(N-methyl-4-pyridyl) porphine tetra tosylate through encapsulation in antibody-targeted chitosan/alginate nanoparticles. *Biomacromolecules* (2013) 14(2):302–10. doi: 10.1021/bm301858a
103. Kirui DK, Rey DA, Batt CA. Gold hybrid nanoparticles for targeted phototherapy and cancer imaging. *Nanotechnology* (2010) 21(10):105105. doi: 10.1088/0957-4484/21/10/105105
104. McCarron PA, Marouf WM, Quinn DJ, Fay F, Burden RE, Olwill SA, et al. Antibody targeting of camptothecin-loaded PLGA nanoparticles to tumor cells. *Bioconjugate Chem* (2008) 19(8):1561–9. doi: 10.1021/bc800057g
105. Yang SJ, Lin FH, Tsai KC, Wei MF, Tsai HM, Wong JM, et al. Folic acid-conjugated chitosan nanoparticles enhanced protoporphyrin IX accumulation in colorectal cancer cells. *Bioconjugate Chem* (2010) 21 (4):679–89. doi: 10.1021/bc9004798
106. Li P, Wang Y, Zeng F, Chen L, Peng Z, Kong LX. Synthesis and characterization of folate conjugated chitosan and cellular uptake of its nanoparticles in HT-29 cells. *Carbohydr Res* (2011) 346(6):801–6. doi: 10.1016/j.carres.2011.01.027
107. Kopansky E, Shamay Y, David A. Peptide-directed HPMA copolymer-doxorubicin conjugates as targeted therapeutics for colorectal cancer. *J Drug Targeting* (2011) 19(10):933–43. doi: 10.3109/1061186X.2011.632011
108. Unzueta U, Céspedes MV, Ferrer-Miralles N, Casanova I, Cedano J, Corchero JL, et al. Intracellular CXCR4+ cell targeting with T22-empowered protein-only nanoparticles. *Int J Nanomed* (2012) 7:4533. doi: 10.2147/IJN.S34450
109. Jain A, Jain SK, Ganesh N, Barve J, Beg AM. Design and development of ligand-appended polysaccharidic nanoparticles for the delivery of oxaliplatin in colorectal cancer. *Nanomedicine* (2010) 6(1):179–90. doi: 10.1016/j.nano.2009.03.002
110. Gary-Bobo M, Brevet D, Benkirane-Jessel N, Raehm L, Maillard P, Garcia M, et al. Hyaluronic acid-functionalized mesoporous silica nanoparticles for efficient photodynamic therapy of cancer cells. *Photodiagn Photodynamic Ther* (2012) 9(3):256–60. doi: 10.1016/j.pdpdt.2011.12.010
111. Shahzad MM, Mangala LS, Han HD, Lu C, Bottsford-Miller J, Nishimura M, et al. Targeted delivery of small interfering RNA using reconstituted high-density lipoprotein nanoparticles. *Neoplasia (N Y NY)* (2011) 13(4):309–19. doi: 10.1593/neo.101372
112. Xu J, Tam M, Samaei S, Lerouge S, Barralet J, Stevenson MM, et al. Mucoadhesive chitosan hydrogels as rectal drug delivery vessels to treat ulcerative colitis. *Acta Biomater* (2017) 48:247–57. doi: 10.1016/j.actbio.2016.10.026

113. Wang T, Liu Z, Zhang Z, Tang S, Yue M, Feng S, et al. Evaluation of antitumor activity of survivin short interfering RNA delivered by lipid nanoparticles in colon cancer in vitro and in vivo. *Oncol Lett* (2017) 14 (2):2001–8. doi: 10.3892/ol.2017.6404
114. Liu T, Zhang X, Du L, Wang Y, Liu X, Tian H, et al. Exosome-transmitted miR-128-3p increase chemosensitivity of oxaliplatin-resistant colorectal cancer. *Mol Cancer* (2019) 18(1):43. doi: 10.1186/s12943-019-0981-7
115. Choi YJ, Lin C-P, Ho JJ, He X, Okada N, Bu P, et al. miR-34 miRNAs provide a barrier for somatic cell reprogramming. *Nat Cell Biol* (2011) 13(11):1353–60. doi: 10.1038/ncb2366
116. Sell S. Stem cell origin of cancer and differentiation therapy. *Crit Rev Oncol* (2004) 51(1):1–28. doi: 10.1016/j.critrevonc.2004.04.007
117. Li Q, Yao Y, Eades G, Liu Z, Zhang Y, Zhou Q. Downregulation of miR-140 promotes cancer stem cell formation in basal-like early stage breast cancer. *Oncogene* (2014) 33(20):2589–600. doi: 10.1038/onc.2013.226
118. Boyer LA, Lee TI, Cole MF, Johnstone SE, Levine SS, Zucker JP, et al. Core transcriptional regulatory circuitry in human embryonic stem cells. *Cell* (2005) 122(6):947–56. doi: 10.1016/j.cell.2005.08.020
119. Loh Y-H, Wu Q, Chew J-L, Vega VB, Zhang W, Chen X, et al. The Oct4 and Nanog transcription network regulates pluripotency inmouse embryonic stem cells. *Nat Genet* (2006) 38(4):431–40. doi: 10.1038/ng1760
120. Sinkkonen L, Hugenschmidt T, Berninger P, Gaidatzis D, Mohn F, Artus-Revel CG, et al. MicroRNAs control de novo DNA methylation through regulation of transcriptional repressors in mouse embryonic stem cells. *Nat Struct Mol Biol* (2008) 15(3):259. doi: 10.1038/nsmb.1391
121. Vermeulen L, Felipe De Sousa EM, Van Der Heijden M, Cameron K, De Jong JH, Borovski T, et al. Wnt activity defines colon cancer stem cells and is regulated by the microenvironment. *Nat Cell Biol* (2010) 12(5):468–76. doi: 10.1038/ncb2048
122. Yu Y, Kanwar SS, Patel BB, Oh P-S, Nautiyal J, Sarkar FH, et al. MicroRNA-21 induces stemness by downregulating transforming growth factor beta receptor 2 (TGFβR2) in colon cancer cells. *Carcinogenesis* (2012) 33(1):68–76. doi: 10.1093/carcin/bgr246
123. Fre S, Huyghe M, Mourikis P, Robine S, Louvard D, Artavanis-Tsakonas S. Notch signals control the fate of immature progenitor cells in the intestine. *Nature* (2005) 435(7044):964–8. doi: 10.1038/nature03589
124. Zhang X, Ai F, Li X, Tian L, Wang X, Shen S, et al. MicroRNA-34a suppresses colorectal cancer metastasis by regulating Notch signaling. *Oncol Lett* (2017) 14(2):2325–33. doi: 10.3892/ol.2017.6444
125. Chakraborty S, Ghosh Z. MicroRNAs shaping cellular reprogramming. In: *AGO-Driven Non-Coding RNAs*. Elsevier (2019). p. 75–97. doi: 10.1016/B978-0-12-815669-8.00004-X
126. Shi L, Xi J, Xu X, Peng B, Zhang B. MiR-148a suppressed cell invasion and migration via targeting WNT10b and modulating β-catenin signaling in cisplatin-resistant colorectal cancer cells. *Biomed Pharmacother* (2019) 109:902–9. doi: 10.1016/j.biopha.2018.10.080
127. Razi S, Sadeghi A, Asadi-Lari Z, Tam KJ, Kalantari E, Madjd Z. DCLK1, a promising colorectal cancer stem cell marker, regulates tumor progression and invasion through miR-137 and miR-15a dependent manner. *Clin Exp Med* (2020) 1–9. doi: 10.1007/s10238-020-00665-w
128. Wang LQ, Yu P, Li B, Guo YH, Liang ZR, Zheng LL, et al. miR-372 and miR-373 enhance the stemness of colorectal cancer cellsby repressing differentiation signaling pathways. *Mol Oncol* (2018) 12(11):1–9. doi: 10.1002/1878-0261.12376
129. Ren D, Lin B, Zhang X, Peng Y, Ye Z, Ma Y, et al. Maintenance of cancer stemness by miR-196b-5p contributes to chemoresistance of colorectal cancer cells via activating STAT3 signaling pathway. *Oncotarget* (2017) 8 (30):49807. doi: 10.18632/oncotarget.17971
130. Jin Y, Wang M, Hu H, Huang Q, Chen Y, Wang G. Overcoming stemness and chemoresistance in colorectal cancer through miR-195-5p-modulated inhibition of notch signaling. *Int J Biol Macromol* (2018) 117:445–53. doi: 10.1016/j.ijbiomac.2018.05.151
131. Zhu QD, Zhou QQ, Dong L, Huang Z, Wu F, Deng X. MiR-199a-5p Inhibits the Growth and Metastasis of Colorectal Cancer Cells by Targeting ROCK1. *Technol Cancer Res Treat* (2018) 17:1533034618775509–. doi: 10.1177/1533034618775509
132. De Robertis M, Mazza T, Fusilli C, Loiacono L, Poeta ML, Sanchez M, et al. EphB2 stem-related and EphA2 progression-related miRNA-based networks in progressive stages of CRC evolution: clinical significance and potential miRNA drivers. *Mol Cancer* (2018) 17(1):169. doi: 10.1186/s12943-018-0912-z
133. de Lau W, Peng WC, Gros P, Clevers H. The R-spondin/Lgr5/Rnf43 module: regulator of Wnt signal strength. *Genes Dev* (2014) 28(4):305–16. doi: 10.1101/gad.235473.113
134. Takahashi H, Ishii H, Nishida N, Takemasa I, Mizushima T, Ikeda M, et al. Significance of Lgr5+ ve cancer stem cells in the colon and rectum. *Ann Surg Oncol* (2011) 18(4):1166–74. doi: 10.1245/s10434-010-1373-9
135. Leng Z, Xia Q, Chen J, Li Y, Xu J, Zhao E, et al. Lgr5+ CD44+ EpCAM+ strictly defines cancer stem cells in human colorectal cancer. *Cell Physiol Biochem* (2018) 46(2):860–72. doi: 10.1159/000488743
136. Fumagalli A, Oost KC, Kester L, Morgner J, Bornes L, Bruens L, et al. Plasticity of Lgr5-negative cancer cells drives metastasis incolorectal cancer. *Cell* (2020) 26:569–78. doi: 10.1016/j.stem.2020.02.008
137. Chen L, Fu C, Zhang Q, He C, Zhang F, Wei Q. The role of CD44 in pathological angiogenesis. *FASEB J* (2020) 34(10):13125–39. doi: 10.1096/fj.202000380RR
138. Rios de la Rosa JM, Tirella A, Tirelli N. Receptor-Targeted Drug Delivery and the (Many) Problems We Know of: The Case of CD44 and Hyaluronic Acid. *Advanced Biosyst* (2018) 2(6):1800049. doi: 10.1002/adbi.201800049
139. Yan X, Han D, Chen Z, Han C, Dong W, Han L, et al. RUNX2 interacts with BRG1 to target CD44 for promoting invasion and migration of colorectal cancer cells. *Cancer Cell Int* (2020) 20(1):1–13. doi: 10.1186/s12935-020-01544-w
140. Chen Y-C, Lee T-H, Tzeng S-L. Reduced DAXX Expression Is Associated with Reduced CD24 Expression in Colorectal Cancer. *Cells* (2019) 8 (10):1242. doi: 10.3390/cells8101242
141. Wang J-L, Guo C-R, Su W-Y, Chen Y-X, Xu J, Fang J-Y. CD24 Overexpression Related to Lymph Node Invasion and PoorPrognosis of Colorectal Cancer. *Clinicallaboratory* (2018) 64(4):497–505. doi: 10.7754/Clin.Lab.2017.171012
142. Ecke I, Rosenberger A, Obenauer S, Dullin C, Aberger F, Kimmina S, et al. Cyclopamine treatment of full-blown Hh/Ptch-associated RMS partially inhibits Hh/Ptch signaling, but not tumor growth. *Mol Carcinogen: Published Cooperation Univ Texas MD Anderson Cancer Center* (2008) 47 (5):361–72. doi: 10.1002/mc.20394
143. Stanton BZ, Peng LF. Small-molecule modulators of the Sonic Hedgehog signaling pathway. *Mol BioSyst* (2010) 6(1):44–54. doi: 10.1039/B910196A
144. Jain S, Song R, Xie J. Sonidegib: mechanism of action, pharmacology, and clinical utility for advanced basal cell carcinomas. *OncoTarg Ther* (2017) 10:1645. doi: 10.2147/OTT.S130910
145. Rimkus TK, Carpenter RL, Qasem S, Chan M, Lo H-W. Targeting the sonic hedgehog signaling pathway: review of smoothened and GLI inhibitors. *Cancers* (2016) 8(2):22. doi: 10.3390/cancers8020022
146. Verma G, Shetake NG, Pandrekar S, Pandey B, Hassan P, Priyadarsini K. Development of surface functionalized hydroxyapatite nanoparticles for enhanced specificity towards tumor cells. *Eur J Pharm Sci* (2020) 144:105206. doi: 10.1016/j.ejps.2019.105206
147. Xin M, Ji X, De La Cruz LK, Thareja S, Wang B. Strategies to target the Hedgehog signaling pathway for cancer therapy. *Med Res Rev* (2018) 38 (3):870–913. doi: 10.1002/med.21482
148. Hong I-S, Jang G-B, Lee H-Y, Nam J-S. Targeting cancer stem cells by using the nanoparticles. *Int J Nanomed* (2015) 10(Spec Iss):251. doi: 10.2147/IJN.S88310
149. Taipale J, Chen JK, Cooper MK, Wang B, Mann RK, Milenkovic L, et al. Effects of oncogenic mutations in Smoothened and Patched can be reversed by cyclopamine. *Nature* (2000) 406(6799):1005–9. doi: 10.1038/35023008
150. You J, Zhao J, Wen X, Wu C, Huang Q, Guan F, et al. Chemoradiation therapy using cyclopamine-loaded liquid–lipid nanoparticles and lutetium-177-labeled core-crosslinked polymeric micelles. *J Controlled Release* (2015) 202:40–8. doi: 10.1016/j.jconrel.2015.01.031
151. Hu K, Zhou H, Liu Y, Liu Z, Liu J, Tang J, et al. Hyaluronic acid functional amphipathic and redox-responsive polymer particles for the co-delivery of doxorubicin and cyclopamine to eradicate breast cancer cells and cancer stem cells. *Nanoscale* (2015) 7(18):8607–18. doi: 10.1039/C5NR01084E
152. Yang R, Mondal G, Wen D, Mahato RI. Combination therapy of paclitaxel and cyclopamine polymer-drug conjugates to treat advanced prostate cancer.

*Nanomed: Nanotechnol Biol Med* (2017) 13(2):391–401. doi: 10.1016/j.nano.2016.07.017

153. Zhao J, Wang H, Hsiao C-H, Chow DS-L, Koay EJ, Kang Y, et al. Simultaneous inhibition of hedgehog signaling and tumor proliferation remodels stroma and enhances pancreatic cancer therapy. *Biomaterials* (2018) 159:215–28. doi: 10.1016/j.biomaterials.2018.01.014
154. Jiang T, Zhang B, Zhang L, Wu X, Li H, Shen S, et al. Biomimetic nanoparticles delivered hedgehog pathway inhibitor to modify tumour microenvironment and improved chemotherapy for pancreatic carcinoma. *Artif Cells Nanomed Biotechnol* (2018) 46(sup1):1088–101. doi: 10.1080/21691401.2018.1445093
155. Wang L, Liu X, Zhou Q, Sui M, Lu Z, Zhou Z, et al. Terminating the criminal collaboration in pancreatic cancer: nanoparticle-based synergistic therapy for overcoming fibroblast-induced drug resistance. *Biomaterials* (2017) 144:105–18. doi: 10.1016/j.biomaterials.2017.08.002
156. Ray P, Confeld M, Borowicz P, Wang T, Mallik S, Quadir M. PEG-b-poly (carbonate)-derived nanocarrier platform with pH-responsive properties for pancreatic cancer combination therapy. *Colloids Surfaces B: Biointerf* (2019) 174:126–35. doi: 10.1016/j.colsurfb.2018.10.069
157. Verma RK, Yu W, Shrivastava A, Shankar S, Srivastava RK. α-Mangostin-encapsulated PLGA nanoparticles inhibit pancreatic carcinogenesis by targeting cancer stem cells in human, and transgenic (KrasG12D, and KrasG12D/tp53R270H) mice. *Sci Rep* (2016) 6(1):32743. doi: 10.1038/srep32743
158. Ingallina C, Costa PM, Ghirga F, Klippstein R, Wang JT, Berardozzi S, et al. Polymeric glabrescione B nanocapsules for passive targeting of Hedgehog-dependent tumor therapy in vitro. *Nanomedicine* (2017) 12(7):711–28. doi: 10.2217/nnm-2016-0388
159. Nayak A, Satapathy SR, Das D, Siddharth S, Tripathi N, Bharatam PV, et al. Nanoquinacrine induced apoptosis in cervical cancer stem cells through the inhibition of hedgehog-GLI1 cascade: Role of GLI-1. *Sci Rep* (2016) 6 (1):20600. doi: 10.1038/srep20600
160. Nayak A, Siddharth S, Das S, Nayak D, Sethy C, Kundu CN. Nanoquinacrine caused apoptosis in oral cancer stem cells by disrupting the interaction between GLI1 and β catenin through activation of GSK3β. *Toxicol Appl Pharmacol* (2017) 330:53–64. doi: 10.1016/j.taap.2017.07.008
161. Xu Y, Chenna V, Hu C, Sun H-X, Khan M, Bai H, et al. Polymeric nanoparticle-encapsulated hedgehog pathway inhibitor HPI-1 (NanoHHI) inhibits systemic metastases in an orthotopic model of human hepatocellular carcinoma. *Clin Cancer Res* (2012) 18(5):1291–302. doi: 10.1158/1078-0432.CCR-11-0950
162. Chenna V, Hu C, Pramanik D, Aftab BT, Karikari C, Campbell NR, et al. A polymeric nanoparticle encapsulated small-molecule inhibitor of Hedgehog signaling (NanoHHI) bypasses secondary mutational resistance to Smoothened antagonists. *Mol Cancer Ther* (2012) 11(1):165–73. doi: 10.1158/1535-7163.MCT-11-0341
163. Nicolini C. Poly-lactic-co-glycolic acid nanoformulation of small moleculeantagonist GANT61 for cancer annihilation by modulating hedgehog pathway. *NanoWorld J* (2017) 1(2):1–10. doi: 10.17756/nwj.2017-038
164. Oshima G, Guo N, He C, Stack ME, Poon C, Uppal A, et al. In Vivo Delivery and Therapeutic Effects of a MicroRNA on Colorectal Liver Metastases. *Mol Ther J Am Soc Gene Ther* (2017) 25(7):1588–95. doi: 10.1016/j.ymthe.2017.04.005
165. Yang H, Liu Y, Qiu Y, Ding M, Zhang Y. MiRNA-204-5p and oxaliplatin-loaded silica nanoparticles for enhanced tumor suppression effect in CD44-overexpressed colon adenocarcinoma. *Int J Pharmaceut* (2019) 566:585–93. doi: 10.1016/j.ijpharm.2019.06.020
166. Zhang X, Song H, Canup BS, Xiao B. Orally delivered targeted nanotherapeutics for the treatment of colorectal cancer. *Expert Opin Drug Deliv* (2020) 1–10. doi: 10.1080/17425247.2020.1748005
167. Tyagi P, Subramony JA. Nanotherapeutics in oral and parenteral drug delivery: Key learningsand future outlooks as we think small. *J Controlled Release* (2018) 17(6):1–10. doi: 10.1016/j.jconrel.2018.01.009
168. Vong LB, Yoshitomi T, Matsui H, Nagasaki Y. Development of an oral nanotherapeutics using redox nanoparticles for treatment of colitis-associated colon cancer. *Biomaterials* (2015) 55:54–63. doi: 10.1016/j.biomaterials.2015.03.037
169. Han W, Xie B, Li Y, Shi L, Wan J, Chen X, et al. Orally deliverable nanotherapeutics for the synergistic treatment of colitis-associated colorectal cancer. *Theranostics* (2019) 9(24):7458. doi: 10.7150/thno.38081
170. Liu X, Fu Q, Du Y, Yang Y, C Cho W. MicroRNA as regulators of cancer stem cells and chemoresistance in colorectal cancer. *Curr Cancer Drug Targets* (2016) 16(9):738–54. doi: 10.2174/1568009616666151118114759
171. van de Ven AL, Tangutoori S, Baldwin P, Qiao J, Gharagouzloo C, Seitzer N, et al. Nanoformulation of Olaparib amplifies PARP inhibition and sensitizes PTEN/TP53-deficient prostate cancer to radiation. *Mol Cancer Ther* (2017) 16(7):1279–89. doi: 10.1158/1535-7163.MCT-16-0740

**Conflict of Interest:** The authors declare that the research was conducted in the absence of any commercial or financial relationships that could be construed as a potential conflict of interest.

frontiers in Oncology

ORIGINAL RESEARCH
published: 20 January 2021
doi: 10.3389/fonc.2020.600298

# Targeted Chinese Medicine Delivery by A New Family of Biodegradable Pseudo-Protein Nanoparticles for Treating Triple-Negative Breast Cancer: *In Vitro* and *In Vivo* Study

*Hiu Yee Kwan[1], Qinghua Xu[2], Ruihong Gong[1], Zhaoxiang Bian[1]* and Chih-Chang Chu[2]**

[1] School of Chinese Medicine, Hong Kong Baptist University, Hong Kong, China, [2] Biomedical Engineering Field, and Fiber Science Program, Department of Fiber Science and Apparel Design, Cornell University, Ithaca, NY, United States

OPEN ACCESS

**Edited by:**
*Luis Alexandre Muehlmann, University of Brasilia, Brazil*

**Reviewed by:**
*Fong-Yu Cheng, Chinese Culture University, Taiwan*
*Min Hee Kang, Texas Tech University Health Sciences Center, United States*

***Correspondence:**
*Chih-Chang Chu*
*cc62@cornell.edu*
*Zhaoxiang Bian*
*bzxiang@hkbu.edu.hk*

**Specialty section:**
*This article was submitted to Cancer Molecular Targets and Therapeutics, a section of the journal Frontiers in Oncology*

**Received:** *29 August 2020*
**Accepted:** *08 December 2020*
**Published:** *20 January 2021*

**Citation:**
*Kwan HY, Xu Q, Gong R, Bian Z and Chu C-C (2021) Targeted Chinese Medicine Delivery by A New Family of Biodegradable Pseudo-Protein Nanoparticles for Treating Triple-Negative Breast Cancer: In Vitro and In Vivo Study. Front. Oncol. 10:600298. doi: 10.3389/fonc.2020.600298*

Triple negative breast cancer (TNBC) has the worst overall survival among all breast cancer subtypes; 80% of TNBC harbors TP53 mutation. Gambogic acid (GA) is an herbal compound isolated from the dry brownish gamboge resin of *Garcinia hanburyi*. A new family of biodegradable polymer, the folate (FA)-conjugated arginine-based poly(ester urea urethane)s nanoparticles (FA-Arg-PEUU NP), was developed as nano-carrier for GA. Its anti-TNBC effects and the underlying mechanism of action were examined. The average diameters of FA-Arg-PEUU NP and GA-loaded FA-Arg-PEUU NP (NP-GA) in water are around 165 and 220nm, respectively. Rhodamine-tagged FA-Arg-PEUU NP shows that the conjugation of FA onto Arg-PEUU NPs facilitates the internalization of FA-Arg-PEUU-NP into TNBC. Compared to free-GA at the same GA concentrations, NP-GA exhibits higher cytotoxicity in both TP53-mutated and non-TP53 expressed TNBC cells by increasing intrinsic and extrinsic apoptosis. In HCC1806-bearing xenograft mouse model, the targeted delivery of GA by the FA-Arg-PEUU-NP nano-carriers to the tumor sites results in a more potent anti-TNBC effect and lower toxicity towards normal tissues and organs when compared to free GA. Furthermore, NP-GA also reduces the tumor-associated macrophage (TAM) M1/M2 ratio, suggesting that the use of Arg-based nanoparticles as carriers for GA not only makes the surface of the nanoparticles positively charged, but also confers on to the nanoparticles an ability to modulate TAM polarization. Our data clearly demonstrate that NP-GA exhibits potent anti-TNBC effects with reduced off-target toxicity, which represents novel alternative targeted therapeutics for TNBC treatment.

**Keywords: triple-negative breast cancer, gambogic acid, nanoparticle, poly(ester amide)s, apoptosis, tumor-associated macrophage**

## INTRODUCTION

Triple negative breast cancer (TNBC) is negative for estrogen receptor, progesterone receptor, and human epidermal growth factor receptor, which accounts for 10-17% of all breast cancer cases (1). TNBC has a distinct metastatic pattern. It is a high-grade invasive ductal carcinoma (2) and often spreads to the brain and lungs (3). TNBC is characterized by its poor prognosis and aggressive biological behavior. In a cohort of 1601 women with breast cancer, women with TNBC had an increased likelihood of death (hazard ratio 3.2; 95% CI, 2.3-4.5; $p<0.001$) within 5 years of diagnosis compared with other breast cancer subtypes. Indeed, TNBC is associated with the worst breast cancer specific and overall survival rates (hazard ratio for BCSS 2.99, 95% CI 2.59-3.45, $p<0.001$; hazard ratio for OS 2.72, 95% CI 2.39-3.10; $p< 0.0001$) among all breast cancer subtypes (3, 4).

TNBC patients have limited therapeutics options because they do not benefit from traditional anti-hormonal or anti-HER2-based therapies. The treatment approaches to TNBC include surgery, radiation therapy, and chemotherapy. Several targeted therapies are still under clinical trials. For example, neoadjuvant chemotherapy is used for TNBC patients with locally advanced disease, and this approach shows a high disease-free survival rate in TNBC patients (5) with 20% of the patients presenting a pathologic complete response (pCR) after neoadjuvant chemotherapy (6). However, TNBC patients who do not achieve pCR are very likely to suffer from early recurrence and die from metastatic diseases. Immunotherapy for TNBC is still under clinical trials (2, 7).

The Cancer Genome Atlas (TCGA) project has characterized the molecular profile of TNBC, including the mutations of the gene TP53. Up to 80% of TNBC harbors TP53 mutation (8). Protein p53 is one of the proteins that respond to DNA damage. Wild-type p53 protein induces the expressions of BCL-2 proteins, such as BIM, PUMA, and NOXA, that mediate the p53-dependent apoptosis; p53 mutant, however, cannot induce apoptosis in response to DNA damage in TNBC. Nevertheless, clinical data suggest that TNBC is sensitive to DNA-damaging agents such as the platinum-based drugs in chemotherapy (9), indicating that the induction of p53-independent apoptosis in TNBC is a promising therapeutic approach.

Gambogic acid (GA) is a xanthone structure isolated from the dry, brownish gamboge resin of *Garcinia hanburyi*. GA is a potent apoptosis inducer, as revealed by its structure-activity relationship (10). Studies show that GA triggers DNA damage signaling in liver cancer and non-small cell lung cancer (11). It also triggers the intrinsic caspase-dependent signaling pathway in neuroblastoma cells (12). In non-TNBC breast cancer, GA induces apoptosis by increasing reactive oxygen species (13); it also increases the sensitivity of breast cancer to TRAIL (TNF-related apoptosis-inducing ligand)-induced apoptosis by promoting the crosstalk between extrinsic and intrinsic apoptotic signaling pathways (14). Recently, a study also showed that GA increases sensitivity to paclitaxel in drug −resistant TNBC *via* the sonic hedgehog signaling pathway (15). He et al. also shows that GA-loaded biodegradable amino acid-based pseudo-protein nanoparticles exhibitspotent anticancer effects over free GA in several *in vitro* models, such as cervical cancer cells (Hela) and colorectal cancer cells (HCT116) (16).

Since GA is a potent anti-cancer agent, a phase IIa clinical trial has been conducted to test the efficacy of GA in treating non-small cell lung cancer (NSCLC), stomach cancer, colon cancer, breast cancer (non-TNBC type), liver cancer, and kidney cancer. Among these, GA enhanced the partial response (PR) in NSCLC, colon cancer, and renal cell cancer patients; GA also has a favorable safety profile at a dosage of 45mg $m^{-2}$ (17). A follow-up clinical trial in phase IIb investigated the therapeutic effects of GA in NSCLC, renal cell cancer, and colon cancer; a phase III trial also investigated the effects in NSCLC and renal cell cancer. However, both trials showed that GA did not have an apparent advantage over chemotherapy in treating these cancers (Study report 138997640-2008ZX09101024/01 by Zhangleilei Jiangsu Kanion Pharmaceutical Company and Zhaoyiwu Jiangsu Kanion Pharmaceutical Company). Besides, GA has poor water solubility (<1μg $ml^{-1}$) and it has a rapid clearance in plasma, which hinders its clinical applications. Therefore, a strategy to enhance the therapeutic effect of GA is needed.

Amino acid-based poly(ester amide)s (AA-PEAs) and their distant relative, poly(ester urea urethane) (AA-PEUU), are two relatively new families of biodegradable and biologically active polymers which have wide applications in the biomedical field (18–28). AA-PEAs are synthesized from three building blocks (amino acids, diols, and diacids), and AA-PEUU are prepared from four building blocks: amino acid, diols, diisocyanacide, and glycerol monoallyl ether. Amino acids such as arginine, lysine, and phenylalanine have been used to prepare AA-PEAs and AA-PEUUs with specific bioactivity. A series of AA-PEAs and AA-PEUUs with different structures have been developed in recent years to meet specific needs, ranging from wound dressings for burn treatments, drug eluting stent coatings for drug eluting stents and sutures, tissue engineering scaffolds, synthetic vaccines, and as drug and gene delivery carriers (23–28).

In a previously published *in vitro* study, He et al. designed a linear and branched Arg-based poly(ester urea urethane)s (Arg-PEUUs), folate (FA)-conjugated Arg PEUUs (FA-Arg-PEUUs), to deliver GA to different cancer cells like HeLa, A549, and HCT116 (16). The branched FA-Arg-PEUU NP design could improve the GA loading content and FA concentration on the surface of the nanoparticle compared to the linear FA-Arg-PEUU NP. When compared with free GA, the GA carried by the branched FA-Arg-PEUU NP exhibits higher cytotoxicity and induces more apoptosis and mitochondrial membrane potential disruption in the folate receptor-expressed cervical cancer cells and colorectal cancer cells (16).

In this study, we aimed to investigate the anti-TNBC effects of GA with a targeted delivery system utilizing folate (FA)-conjugated branched Arg-based PEUU biomaterial nano-carrier. FA and folate receptor alpha (FRα) are critical in regulating cell growth, DNA biosynthesis, repair, and methylation (29). FRα is expressed in 86% of the TNBC

patients (30), which serves as an ideal marker for targeted delivery. The efficacy of the GA-loaded FA-Arg-PEUU NPs in TNBC was systematically examined by both *in vitro* and *in vivo* studies, and the underlining mechanism of action was elucidated to explain its potent anti-TNBC effects and the reduced off-target toxicity in comparison to free GA.

# METHODS

## Materials

L-Arginine hydrochloride was purchased from Chem-Impex INT'L INC, hexamethylene diisocyanate (HDI) from Millipore Corporation, poly(ethylene glycol) (PEG, MCO 3400) from Aldrich, HHS-Rhodamine from Thermo Scientific, and gambogic acid (GA) was from Broadpharm. The dialysis bag with a MWCO of 10kg/mol was purchased from SnakeSkin™. PEG3400-$NH_2$ and Folate N-hydroxysuccinimidyl ester (FA-NHS) were synthesized and purified according to the published procedure (16).

## Synthesis of Folate Modified Arg-PEUU (FA-Arg-PEUU)

To prepare branched arginine-based poly(ester urea urethane) (Arg-PEUU), pentathriol (0.0102g) and stannous 2-ethyl-hexanoate catalyst (9μL) were dissolved in the mixture of 20mL DMSO and 4mL DMF. The solution was stirred at 4°C and HDI was added. After reacting in a nitrogen atmosphere at 4°C for 30min, the prepolymer solution was moved to an oil bath at 45°C. Glycerol a-monoallyl ether (GAE, 0.02g) and Arg-4-Cl diester (1.27g) were dissolved in 10mL DMSO and added to the prepolymer solution under stirring for the polymerization reaction. After reacting for 8h, PEG3400-$NH_2$ was added to cap the end of the PEUU chains and reacted for another 12h. The crude product of Arg-PEUU was obtained by precipitation in excess THF and dried under vacuum. The product was dissolved in DMSO and dialyzed in DI water for three days. The water was changed three times each day and the purified Arg-PEUU-PEG (6-Arg-4-PEUU-PEG) was collected by lyophilization (yield: 55%). Folate (FA) was tagged to the end of PEG to prepare the FA-Arg-PEUU. 6-Arg-4-PEUU-PEG (0.9g) was dissolved in 10mL DMSO and triethylamine (TEA, 12μL) was added to the solution. FA-NHS (0.145g) dissolved in 10mL DMSO was added to the 6-Arg-4-PEUU-PEG solution under stirring. After reacting in the dark at room temperature for 48h, the reaction solution was dialyzed in $NaHCO_3$ (pH 8) twice and DI water for two days. The yellowish product of FA-Arg-PEUU was obtained by lyophilization.

## Preparation of Rhodamine-Labelled FA-Arg-PEUU Nanoparticle

FA-Arg-PEUU (0.5g) was dissolved in 10mL DMSO and bubbled with nitrogen for 10min. Cystamine (0.03mg) was added to the solution and the mixture was stirred in an oil bath at 70°C under nitrogen atmosphere for 24h. Cystamine was conjugated to the side chain of the polymer *via* the thiolene reaction and FA-Arg-PEUU was modified with amine group. The reaction solution was dialyzed in DI water for two days and lyophilized. The product (0.2g) was dissolved in 5mL DMSO and NHS-Rhodamine (0.002g) was added under stirring. After reacting under dark conditions for 48h, the product was purified through dialysis. The rhodamine-tagged FA-Arg-PEUU was collected by lyophilization with a yield of 80%. The rhodamine-tagged Arg-PEUU was synthesized using the same method. To prepare the rhodamine-labelled FA-Arg-PEUU nanoparticle (NP), the rhodamine-tagged FA-Arg-PEUU (0.05g) was dissolved in 5mL DMSO and added into 20mL DI water dropwise under vigorous stirring. The mixture solution was stirred for 2h and then dialyzed in DI water for 24h. The rhodamine-tagged FA-Arg-PEUU NP was lyophilized and kept at 4°C.

## Preparation of GA-Loaded FA-Arg-PEUU NP

The GA-loaded FA-Arg PEUU NP was prepared using a dialysis method. FA-Arg-PEUU was dissolved in DMSO with the concentration of 5mg/mL and GA was added into the FA-Arg-PEUU solution with a feeding ratio of 15% w/w. After stirring for 1h, the solution was transferred to a dialysis bag and dialyzed against DI water for 48h. The water was changed every 6h. The FA-Arg-PEUU nanoparticle (NP) suspension formed in the dialysis bag. The FA-Arg-PEUU NP was lyophilized and stored at 4°C. The GA-loaded Arg-PEUU NP was prepared in the same way. The size and surface potential of the GA-loaded FA-Arg PEUU NP was measured by using a Malvern Zetasizer Nano. The morphology of the nanoparticle was observed by Transition Electron Microscope (TEM, FEI T12 Spirit TEM STEM). The GA loading content (LC%) was measured by using a UV–Vis spectrophotometer (PerkinElmer Lambada 35, Madison). The GA-loaded nanoparticle (1mg) was suspended in 5mL ethanol and stirred at 45°C for 2h and GA was extracted into the solvent. The solution was filtered, and the ethanol was evaporated. The residue was dissolved in 1mL DMSO and GA content was determined by the absorption at 360nm. The LC was calculated through the following equation:

$$LC = mass\ of\ loaded\ GA / total\ mass\ of\ GA\ loaded\ nanoparticle \times 100\,\%$$

## Cell Culture

Human triple negative breast cell lines HCC1806, HCC1143, and HCC1395 (ATCC) were maintained in RPMI-1640 medium and supplemented with 10% fetal bovine serum and 1% penicillin-streptomycin at 37°C incubator with 5% $CO_2$ and 95% humidity.

## *In Vitro* Uptake of FA-Arg-PEUU NP

Uptake of FA-Arg-PEUU NP and Arg-PEUU NP by HCC1806 cells was observed by a Zeiss 710 confocal microscope and measured by flow cytometry (BD FACSAria Fusion). HCC1806 cells ($1.0\times10^5$/well) were incubated with rhodamine-tagged FA-Arg-PEUU NP or Arg-PEUU NP at a final concentration of

0.1mg/mL for 1h or 6h. The cells were washed with PBS and fixed with buffered formaldehyde (1.5mL, 4%, w/v) for 10 min; cell nuclei were stained with DAPI for 3 min. Cell images were taken by Zeiss 710 confocal microscope. In a flow cytometry study, cells were treated with the same protocol; the treatment period was 1h, 3h, or 14h. Fluorescence intensities of intracellular nanoparticles were analyzed by flow cytometer.

## MTT Assay

HCC1806, HCC1143, and HCC1395 cells (5000 cells/well) were incubated with free-GA or GA-loaded FA-Arg-PEUU NP (NP-GA) for 3h at 37°C before MTT assay was performed. Signal was read by spectrometer at 574nm. $IC_{50}$ values (the GA concentration for the apoptosis study) were calculated using Graph Pad.

## Annexin V/PI Dye Staining

HCC1806, HCC1143, and HCC1395 ($5\times10^5$ cells/well) were treated by free-GA or NP-GA with the dosages of GA fixed at $IC_{50}$ values (30.27μM, 14.51μM, and 15.76μM for HCC1143, HCC1806, and HCC1395 cells, respectively). After 3h-treatment, apoptotic cells were assessed using Annexin V-FITC apoptosis detection kit (BD bioscience).

## Western Blot Analysis

HCC1806, HCC1143, and HCC1395 ($5\times10^5$ cells/well) was treated by free-GA or NP-GA for 3h. Whole cell lysates were obtained by suspending the cells in lysis buffer followed by centrifugation; tumors were dispersed in lysis buffer by sonication before centrifugation, and supernatants were collected. Total protein concentrations in these samples were measured by Pierce BCA protein Assay. Proteins were separated on 10% SDS-PAGE and transferred onto polyvinylidene difluoride membranes. After blocking with 5% milk in TBST for 1h, the membrane was incubated with the respective primary antibody (cleaved caspase-3, -6, -7, -8, -12, and cleaved PARP) overnight at 4°C before incubating with the secondary antibody for 1h. Chemiluminescence signals were detected by enhancing ECL (Bio-Rad).

## Mitochondrial Membrane Potential

HCC1143, HCC1806, and HCC1395 cells were treated by free GA or NP-GA at its $IC_{50}$ for 3h (30.27μM for HCC1143; 14.51μM for HCC1806, 15.76μM for HCC1395). Cells cultured in media served as controls. Changes in mitochondrial membrane potential were measured by cationic lipophilic dye JC-10 (Abcam) and the data were presented as the ratio of green fluorescent signal (520nm) to red fluorescent signal (590nm).

## HCC1806-Bearing Xenograft Mouse Model

All the animal studies obtained ethical approval from the Research Ethics Committee of the Hong Kong Baptist University. Female nude mice of 4-week old were obtained from The Chinese University of Hong Kong. Mice were kept in an animal room with 12h light/dark cycle and temperature control. Food and water were available *ad libitum*. HCC1806 ($1\times10^6$ cells/100μL) were suspended in PBS and inoculated into the left armpit of the mice. Tumors were formed 1 week after inoculation.

## Nanoparticle Carrier Tissue Distribution in HCC1806-Bearing Xenograft Mouse Model

Rhodamine-tagged Arg-PEUU NP or rhodamine-tagged FA-Arg-PEUU-NP at 72.7mg/kg was given to the TNBC-bearing xenograft mouse model by an intravenous route *via* the tail vein. Mice were killed at 30min, 1h, 2h, 4h, and 6h after injection. Tumors and major organs were collected. Images were acquired in IVIS Lumina XR imaging system with an exposure time of 1.5s (PerkinElmer).

## Anti-Tumor Activity of Free-GA or NP-GA

Mice were randomly divided into groups when tumors were grown to $100mm^3$. Free-GA or NP-GA at a dosage of 4mg $kg^{-1}$ or 8mg $kg^{-1}$ were given to mice *via* intravenous injection every two days for 17 days. Control groups were given vehicle or non-GA-loaded FA-Arg-PEUU NP. Body weight and tumor size were monitored every day. Tumor size was calculated by the formula $a^2\times b\times0.4$, where $a$ is the smallest diameter and b is the diameter perpendicular to $a$.

## Tissue and Organ Toxicity Analyzed by H&E Staining

After mice were sacrificed, tumors, hearts, lungs, livers, kidneys, and spleens were dissected and fixed in 10% neutral buffered paraformaldehyde at 4°C for 24h. Tissue sections were stained by hematoxylin and eosin (H&E). Image pictures were taken by microscope (NIKON Eclipse) and analyzed by a pathologist.

## Immunohistochemistry

Paraffin sections of tumors were deparaffinized and rehydrated. Endogenous peroxidase was quenched by incubating with 3% $H_2O_2$ before blocking by serum. The sections were incubated with anti-cleaved caspase 3 or cleaved PARP at 4°C overnight before incubating with biotinylated secondary antibody for 30 min, peroxidase substrate for 10 min, and then being deionized in water for 5 min and counterstained with hematoxylin.

## Tumor Associated Macrophage (TAM) Isolation

Mice were anesthetized by isoflurane. Tumors were dissected and kept in a serum-free medium. Liberase DL solution (Roche), Liberase TL solution (Roche), and DNase I were added to the samples, mixed, and incubated for 45 min at 37°C under continuous shaking. PBS was used to terminate the enzymatic digestion. Tumor cells were filtered using a 100μm cell strainer, centrifuged, and suspended in 1% w/v BSA containing PBS. TAM was isolated from tumors using Anti-F4/80 Microbeads Ultrapure Kit (Miltenyi Biotec). TAM was incubated with anti-CD80 or CD206 antibody for 30 min before analysis with flow cytometry (BD Calibur). FlowJo software was used to analyze the data.

## Bio-Distribution of GA-Loaded FA-Arg-PEUU NP

Free-GA and NP-GA (4mg $kg^{-1}$ or 8mg $kg^{-1}$) were given to the TNBC-bearing xenograft mouse models by an intravenous route *via* the tail vein. Mice were killed 15min, 30min, 1h, 2h, and 4h after injection. Tumors, serum, and major organs were collected. Serum samples and homogenized tumors were extracted with 1mol/L HCl and ethyl acetate and reconstituted in mobile phase for LC/MS analysis which was performed by Agilent 6460 Triple-Quad Mass Spectrometer. Gradient chromatographic separation was performed on a Luna C18 column (Phenomenex) with a security C18 guard column (Phenomenex). Mobile phase was delivered at 1 ml/min; column temperature was maintained at 40°C.

## Statistical Analysis

All statistical analyses were performed using GraphPad Prism software (Version 5.00). The quantitative data were presented as mean ± standard error of mean (SEM).

# RESULTS

## FA Conjugation Enhances the Internalization of Arg-PEUU NP Into TNBC Cells

FA-Arg-PEUU and GA-loaded FA-Arg-PEUU NP (NP-GA) were first prepared. The structure of the FA-Arg-PEUU is shown in **Figure 1A**. The branched polymer self-assembled into nanoparticles in aqueous solution. The average diameters of FA-Arg-PEUU NP and GA-loaded FA-Arg-PEUU NP (NP-GA) in water were around 165 and 220nm, respectively (**Figure 1B**). The surfaces of FA-Arg-PEUU NP and GA-loaded FA-Arg-PEUU NP were positively charged (25.3 and 26.8mV, respectively) due to the presence of the Arg component. The GA-loaded FA-Arg-PEUU NP had a spherical nano-micellar structure (**Figure 1C**). The GA loading content inside FA-Arg-PEUU NP was ~11%, which was 123.6μg GA per mg of FA-Arg-PEUU NP. In our previous *in vitro* release study (16), 40% GA was cumulatively released from the GA-loaded FA-Arg-PEUU NP at 18 hours, and 90% at 60 hours. We also examined the stability of the FA-Arg-PEUU NP. FA-Arg-PEUU-NP solution was stored at 4°C and the NP size was tested after 1 and 3 days. The Z-average diameter of the FA-Arg-PEUU NP was about 165 nm after 1 day and 156 nm after 3 days, indicating that the GA-loaded NP is relatively stable in aqueous solution.

Confocal imaging and flow cytometer techniques were used to examine whether the FA conjugation onto Arg-PEUU-NP enhances the internalization of the NPs into the TNBC cells (HCC1806) which express folate receptors (30). In rhodamine-labeled Arg-PEUU-NP (Rh-NP) and FA-Arg-PEUU-NP (Rh-FA-NP), the NPs are modified with rhodamine by a chemical bond in which rhodamine is a part of the polymer structure. Data show that both rhodamine-labeled Rh-NP and Rh-FA-NP could be taken up by HCC1806 cells as early as 1h (**Figure 1D**). More nanoparticles entered the cells as the incubation time increased from 1h to 6h. The much faster rate and higher level of endocytosis of the Rh-FA-NP compared to non-FA-tagged Rh-NP indicated the targeting effect of FA-modified nanoparticles toward HCC1806 cells.

The targeting effect of FA-tagged NP toward TNBC is further suggested by the subsequent *in vivo* tumor localization study with the HCC1806-bearing xenograft mouse model (**Figures 1E–J**). Thirty minutes after the injection, Rh-FA-NP started to accumulate at the tumor sites and its concentration kept increasing until 2h post-injection. In contrast, the non-FA tagged Rh-NP started to accumulate at tumor sites 1h post-injection. The non-FA tagged Rh-NP was totally cleared from the tumor site 4h after the injection, but it took 6h for the FA-tagged Rh-FA-NP to clear. Furthermore, the signals of Rh-FA-NP at tumor sites were significantly higher than Rh-NP in all the measurements (**Figures 1F–J**). Taken together, both the *in vitro* and *in vivo* data suggest that FA conjugation onto the Arg-PEUU NPs facilitates the internalization of FA-Arg-PEUU-NP into TNBC.

## NP-GA Exhibits Higher Cytotoxic Effect Than Free GA in TNBC Cells

Three TNBC cell lines (HCC1143, HCC1806, and HCC1395) expressing folate receptors (30) were used for cell viability study. HCC1143 and HCC1395 harbor TP53 mutation, while HCC1806 has no p53 expression (31). It is worth noting that TP53 gene mutations are the dominant mutations in TNBC (32). **Figure 2** showed that GA delivered by FA-Arg-PEUU-NP carriers (NP-GA) had significantly higher cytotoxicity in all three TNBC cell lines when compared to free GA (after 3h-incubation). The $IC_{50}$ for the NP-GA was 30.27μM for HCC1143 cells, 14.51μM for HCC1806 cells, and 15.76μM for HCC1395 cells, while the $IC_{50}$ for free GA was over 100μM in all these cell lines. The viability of HCC1143 cells was 90.94% after free GA treatment, and was 24.64% after the NP-GA treatment at the same GA dosage of 100μM (**Figure 2A**). Similar cell viability trends were observed in the two other cell lines: HCC1806 cells were 67.40% and 11.08% after free GA and NP-GA treatments at the GA dosage of 100μM, respectively (**Figure 2B**). HCC1395 cells were 61.50% and 23.18% after free GA and NP-GA treatments at the GA dosage of 100μM, respectively (**Figure 2C**). However, the cytotoxicity of the free GA and NP-GA in the HCC1806 and HCC1143 cells were not significantly different after 24-h treatment (**Supplementary Figure S1**), which may due to the GA levels in the free-GA-treated cells and NP-GA-treated cells becoming similar after a long incubation period of 24h.

Annexin V-FITC/PI staining was used to assess the percentage of the apoptotic cells after treatments. All three TNBC cell lines were treated with free GA or NP-GA for 3h and the dosages of GA were fixed at the $IC_{50}$ values of NP-GA (30.27μM, 14.51μM, and 15.76μM for HCC1143, HCC1806, and HCC1395 cells, respectively). The NP-GA treatment significantly induced more apoptosis in these cell lines than the free GA treatment (**Figures 3A–C** and **Supplementary Figure S2**). The percentages of HCC1143 apoptotic cells were 7.04% and 10.90% after free GA and NP-GA treatments, respectively (**Figure 3A**).

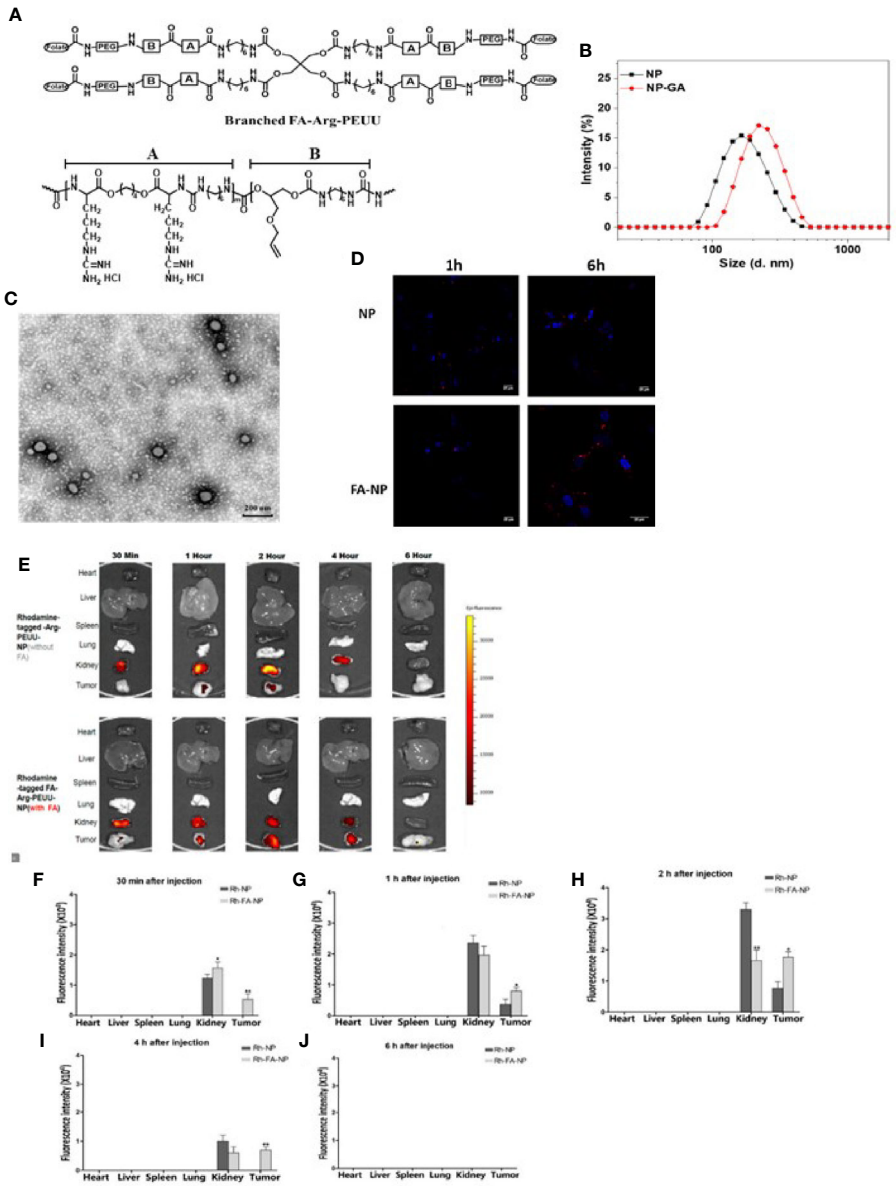


**FIGURE 1** | Uptake of the rhodamine-labelled FA-Arg-PEUU and Arg-PEUU nanoparticles by TNBC cells, and the tumor and major organs in the HCC1806-bearing xenograft mouse models. **(A)** The structure of branched FA-Arg-PEUU (6-Arg-4-PEUU), **(B)** size distribution of FA-Arg-PEUU NP and GA-loaded FA-Arg-PEUU NP (NP-GA), **(C)** transmission electron microscopy (TEM) image of NP-GA. **(D)** Confocal laser scanning microscopy images of HCC1806 cells after being incubated with rhodamine-labeled Arg-PEUU NP (Rh-NP) and FA-Arg-PEUU NP (Rh-FA-NP) for 1h and 6h. Red dots are rhodamine-labeled NPs. **(E)** The biodistribution and **(F–J)** fluorescent intensities of the rhodamine-tagged Arg-PEUU (Rh-NP) and rhodamine-labelled FA-Arg-PEUU nanoparticles (Rh-FA-NP) in the heart, liver, spleen, lung, kidney, and tumor of the HCC1806-bearing xenograft mouse model at the indicated time points after the injection of Rh-NP or Rh-FA-NP. The data are shown as the means ± SEM, n = 3 mice in each group, *$p < 0.05$, **$p < 0.01$.

Similar apoptosis data were observed in the two other TNBC cell lines: the percentages of HCC1806 apoptotic cells were 7.48% and 11.44% after free GA and NP-GA treatments, respectively (**Figure 3B**). The percentage of HCC1395 apoptotic cells were 7.13% and 14.08% after free GA and NP-GA treatments, respectively (**Figure 3C**). However, NP-GA did not significantly affect the percentages of the necrotic cells in these cell lines (**Figures 3A–C**).

The *in vitro* apoptosis data in **Figures 3A–C** was further examined in terms of the apoptotic pathways. As shown in **Figures 3D–F**, NP-GA enhanced both intrinsic and extrinsic apoptotic pathways as indicated by the elevated levels of cleaved caspases 8 & 12, which led to the increased cleavage of caspases 3, 6, 7, and poly(ADP-ribose) polymerase (PARP). The data suggest that NP-GA exerts a higher apoptotic effect than free GA in TNBC cells regardless of the TP53 mutation status, which

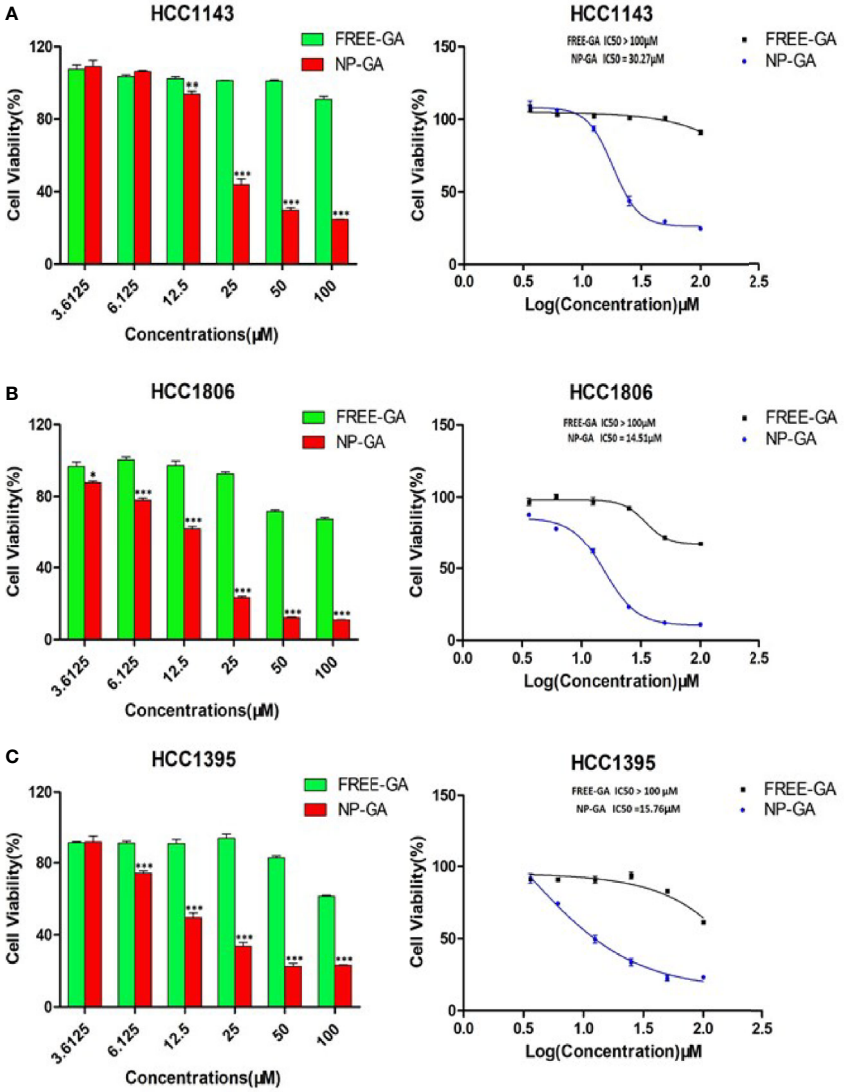


**FIGURE 2** | The *in vitro* cell viability of TNBC as a function of the GA drug and the NP carrier concentrations. **(A)** HCC1143, **(B)** HCC1806, and **(C)** HCC1395 after free-GA or GA-loaded FA-Arg-PEUU-NP (NP-GA) treatments for 3h at the indicated concentrations. X-axis on the left panel shows the concentrations of free-GA and NP-GA in μM; x-axis on the right panel shows the curves of the corresponding log concentration values of the free-GA and NP-GA. The data are shown as the means ± SEM, n = 3, *p < 0.05, **p < 0.01, ***p < 0.001 compared to free GA.

underlie the enhanced cytotoxicity of the NP-GA toward the TNBC cells.

Since collapse of mitochondrial membrane potential will initiate the apoptotic program, changes in the mitochondrial membrane potential ($\Delta\Psi m$) of the TNBC cells were examined. $\Delta\Psi m$ was measured by cationic lipophilic dye JC-10 which forms reversible red-fluorescent aggregates in the mitochondria with a polarized mitochondrial membrane. When mitochondrial membrane potential collapses, the cells fail to retain JC-10 in the mitochondria and the dye returns to its monomeric green fluorescent form. Therefore, increase in the ratio of green fluorescent signal (520nm) to red fluorescent signal (590nm) indicates the collapse of mitochondrial membrane potential. Compared to control, both free-GA and NP-GA disrupted the mitochondrial membrane potential as indicated by the elevated 520/590nm ratio (**Figures 3G–I**). Free GA increased the 520/590nm ratio by 21.02%, 5.63%, and 9.55% in HCC1806, HCC1143, and HCC1395 cells, respectively. NP-GA increased the 520/590nm ratio by 36.94%, 7.55%, and 14.22% in HCC1806, HCC1143, and HCC1395 cells, respectively. A significant difference of the 520/590nm ratio between free GA and NP-GA treatments was observed in HCC1806 cells, in which NP-GA significantly increased the ratio by 15.92% (**Figure 3G**).

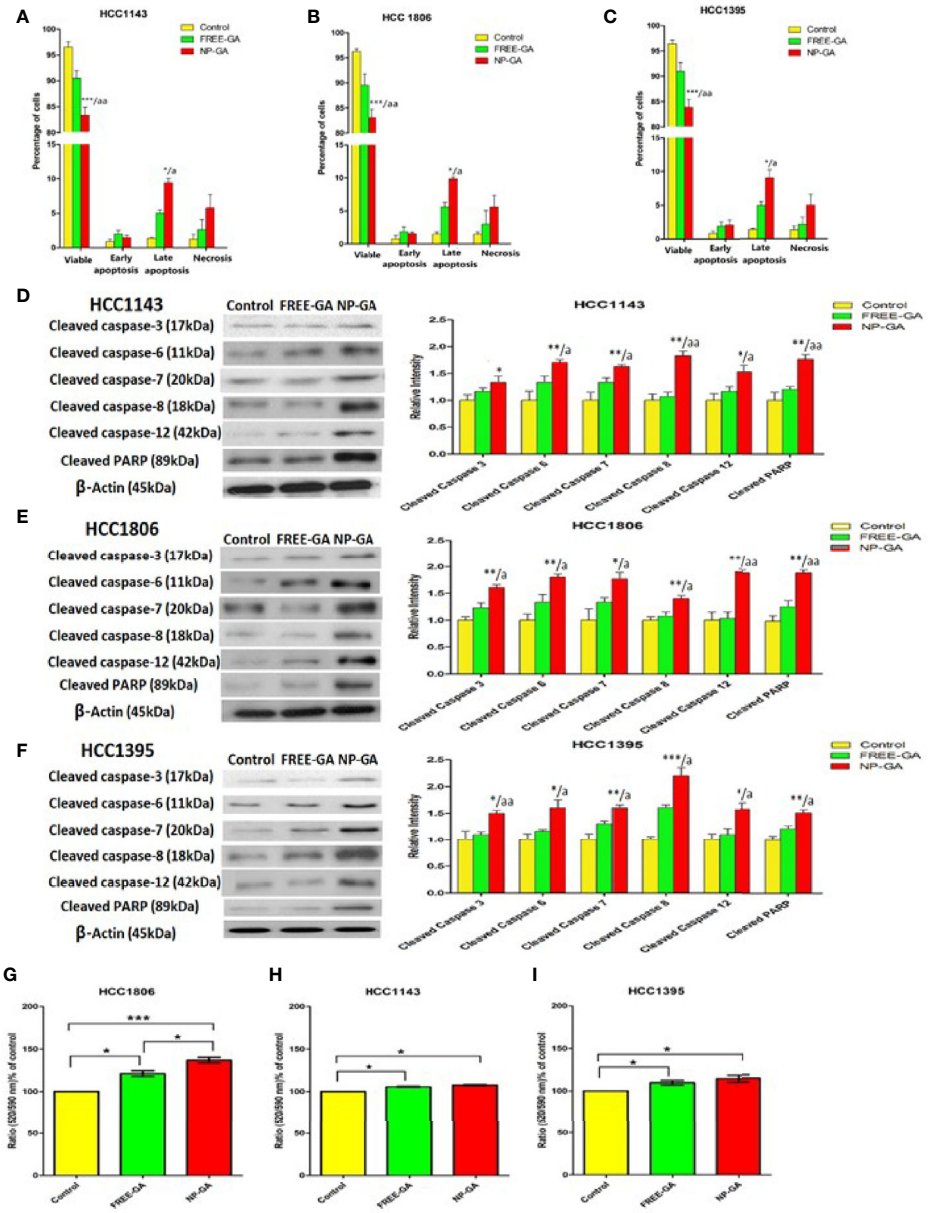


**FIGURE 3** | The percentages of the viable, early apoptotic, late apoptotic, and necrotic TNBC cells after free-GA and NP-GA treatments for 3 hours. Apoptosis and necrosis in **(A)** HCC1143, **(B)** HCC1806, and **(C)** HCC1395 cells after free-GA or GA-loaded FA-Arg-PEUU-NP (NP-GA) treatment for 3h. Cleaved caspase protein expressions in **(D)** HCC1143, **(E)** HCC1806, and **(F)** HCC1395 cells after free-GA or GA-loaded FA-Arg-PEUU-NP (NP-GA) treatment for 3h. Left panel: Western blot showing the protein expressions of cleaved caspase-3, cleaved caspase-6, cleaved caspase-7, cleaved caspase-8, cleaved caspase-12, and cleaved PARP. Right panel: the quantitative analysis of the corresponding protein expressions. The data are shown as the means ± SEM, n = 3, *p < 0.05, **p < 0.01, ***p < 0.001 compared to control group; a < 0.05, aa < 0.01 compared to free GA group. Changes in mitochondrial membrane potential (MMP) in **(G)** HCC1806, **(H)** HCC1143, and **(I)** HCC1395 cells after free-GA or GA-NP treatment for 3h. The y-axis is the ratio of green fluorescent signal (520nm) to red fluorescent signal (590nm). An increase in 520/590nm ratio indicates the collapse of MMP. The data are shown as the means ± SEM, n = 3, *p < 0.05, **p < 0.01, ***p < 0.001 as indicated.

However, there has no significant difference in HCC1143 and HCC1395 cells (**Figures 3H, I**).

Our data on apoptosis study suggest that NP-GA exerts a higher apoptotic effect than free GA in all three TNBC cell lines, which is not due to $\Delta\Psi m$ but instead to the caspase activation independent of the mitochondrial depolarization.

## NP-GA Has a More Significant Anti-TNBC Effect Than Free GA in HCC1806-Bearing Xenograft Mouse Model

The anti-TNBC effects were also examined in HCC1806-bearing xenograft mouse model. Mice were treated with free GA or NP-GA at 4 or 8mg $kg^{-1}$ GA equivalents by intravenous injection

when the tumors were grown to 100mm$^3$. Saline and blank FA-Arg-PEUU-NP (NP) were used as controls. NP alone did not significantly affect the tumor size and tumor weight when compared to the saline control group (**Figures 4A–C**), suggesting NP *per se* does not affect the growth of TNBC in these mice. However, NP-GA was more potent in reducing the tumor size and tumor weight when compared to free GA at the same GA dosage (**Figures 4A–C**). After 17 days of treatment, the average tumor weights for the NP-GA groups were statistically less than the free GA groups at both 4 and 8mg kg$^{-1}$ GA dosages (**Figure 4C**). The average tumor weight was 825mg for the saline group, 843mg for the NP group, 710mg and 640mg for the 4mg-free-GA group and 4mg-NP-GA group, respectively, and 500mg and 338mg for the 8mg-free-GA group and 8mg-NP-GA group, respectively.

The study of apoptotic markers in the tumor tissues suggest that NP-GA at both GA dosages induces more apoptosis in the tumors when compared to free GA, as shown by the elevated expression levels of cleaved caspases 12, 8, 3, 6, 7, and PARP in the tumor tissues (**Figures 5A, B**). These *in vivo* data were in parallel with the *in vitro* data (**Figures 3D–F**), which further suggest NP-GA induces more intrinsic and extrinsic apoptosis than free GA in TNBC. Immunohistochemistry study also suggests that the expressions of cleaved caspase 3 and PARP in the tumor tissues are higher in the NP-GA group than the free GA group (**Figure 5C**). The enhanced apoptosis in the tumors may underlie the potent anti-TNBC effects of the NP-GA treatments.

## The FA-Arg-PEUU-NP Carriers Increase Delivery of GA to TNBC In Vivo

**Figure 6** shows the LC-MS analysis of the GA levels in various organs and the tumors in the TNBC-bearing xenograft mouse models over a period of 4h after free GA or NP-GA treatments at the GA dosage of either 4 or 8mg kg$^{-1}$. At the 8mg kg$^{-1}$dosage, at 30 min post-administration, GA started to accumulate in the tumors of the free-GA and NP-GA groups (**Figure 6B**); the free GA group had 0.02μg mL$^{-1}$ while the NP-GA group had 0.06μg mL$^{-1}$ of GA in the tumors, i.e., 3 times more than the free GA group. A similar trend was also observed at 1h and 2h post-administration. At 1h post-administration, the free GA group had 0.06μg mL$^{-1}$ while the NP-GA group had 0.20μg mL$^{-1}$ of GA in the tumors (**Figure 6C**); at 2h post-administration, the free GA group had 0.07μg mL$^{-1}$ while the NP-GA group has 0.23μg mL$^{-1}$ in the tumors (**Figure 6D**). At the 4mg kg$^{-1}$ dosage, the NP-GA treatment barely registered a GA level in the tumor. At 30-minute post-administration, no GA could be detected in the tumor from the free GA group. At 1h post-administration, the free GA group had 0.01μg mL$^{-1}$ and NP-GA group had 0.06μg mL$^{-1}$ of GA in the tumors (**Figure 6C**); at 2h post-administration, the free GA group had 0.02μg mL$^{-1}$ and NP-GA group had 0.13μg mL$^{-1}$ of GA in the tumors (**Figure 6D**).

Since NP-GA was administrated by an intravenous route *via* the tail vein, the NP-GA was detected in the blood circulation 15 minutes post-administration (**Figure 6A**). Interestingly, our data showed that at 2h post-injection (**Figure 6D**), the concentration

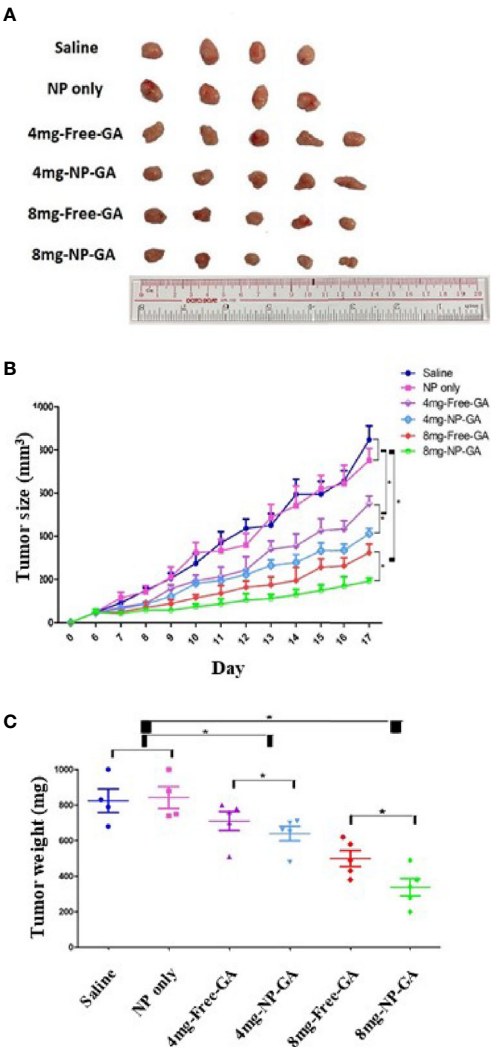


**FIGURE 4** | The tumor size and tumor weight of the HCC1806-bearing xenograft mouse models after saline, FA-Arg-PEUU-NP (NP), free GA, or GA-loaded FA-Arg-PEUU-NP (NP-GA) treatments. **(A)** Images, **(B)** volume, and **(C)** weight of the tumors dissected from the HCC1806-bearing xenograft mouse model after the saline, FA-Arg-PEUU-NP (NP), free GA, or GA-loaded FA-Arg-PEUU-NP (NP-GA) treatments. Day 0 indicated the day on which the tumor cells were inoculated into the nude mice. The data are shown as the means ± SEM, n = 4-5 mice in each group. *p < 0.05 as indicated.

of GA in the plasma was higher in the NP-GA groups than that in the free-GA groups, which were 0.03μg mL$^{-1}$ GA in the free-GA group and 0.07μg mL$^{-1}$ in the NP-GA group at 4mg kg$^{-1}$ dosage. At the 8mg kg$^{-1}$ dosage, it was 0.06μg mL$^{-1}$ GA in the free-GA group and 0.16μg mL$^{-1}$ in the NP-GA group. These data imply that GA carried by the NP carriers may have an increased circulating half-life.

GA was also detected in the liver because the liver functions to filter the blood. The concentrations of GA in the liver are lower in the NP-GA group when compared to free GA at all the time points. At 1h post-administration, at the 4mg kg$^{-1}$ dosage, mice

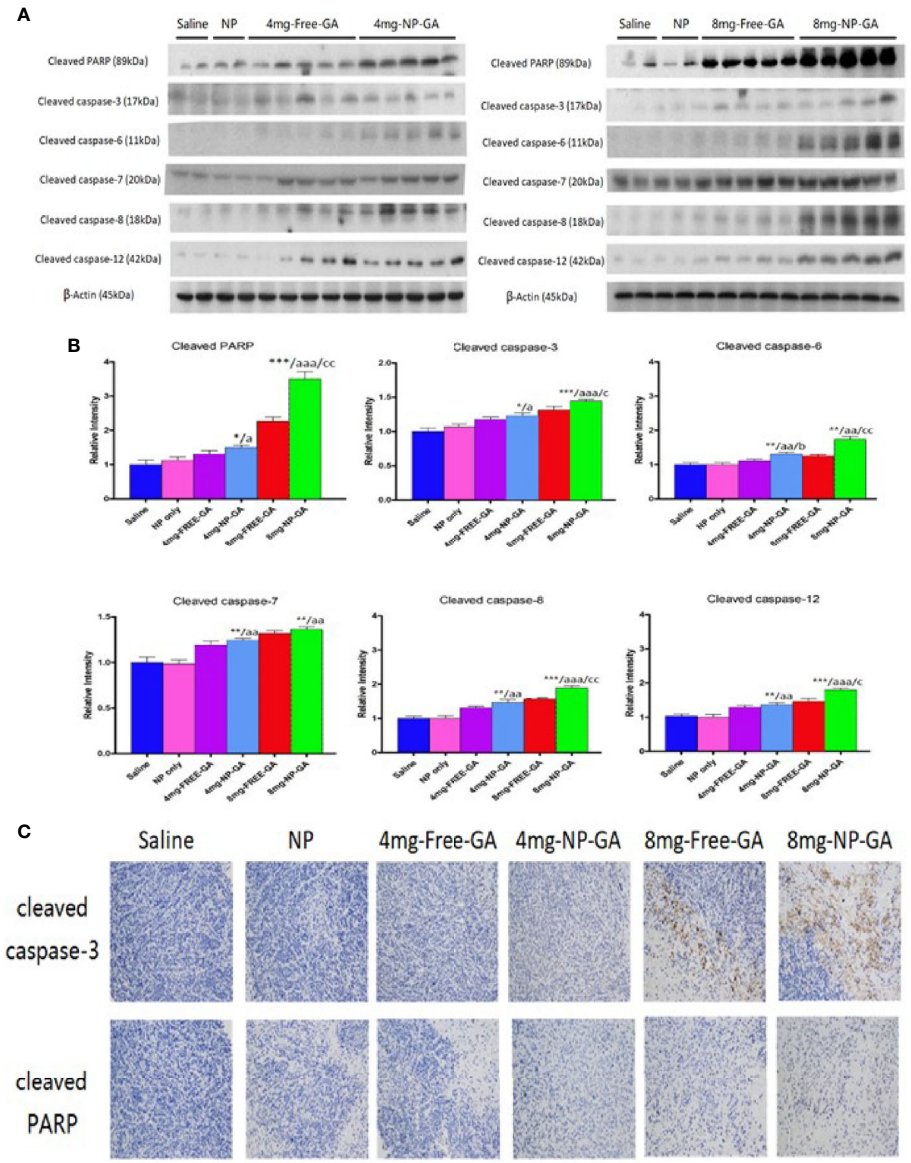


**FIGURE 5** | *In vivo* apoptotic protein expressions in the xenograft tissues of the HCC1806-bearing xenograft mouse models after saline, FA-Arg-PEUU-NP (NP), free GA, or GA-loaded FA-Arg-PEUU-NP (NP-GA) treatments. **(A)** Western blot showing the protein expressions of cleaved caspase-3, cleaved caspase-6, cleaved caspase-7, cleaved caspase-8, cleaved caspase-12, and cleaved PARP in the xenograft tissues and **(B)** quantitative analysis of the corresponding protein expressions. The data are shown as the means ± SEM, n = 4-5 mice in each group. *p < 0.05, **p < 0.01, ***p < 0.001 compared to saline group; a < 0.05, aa < 0.01, aaa < 0.001 compared to NP group; b < 0.05 compared to 4mg-free-GA group; c < 0.05, cc < 0.01 compared to 8mg-free-GA group. **(C)** Representative pictures showing the immunohistochemistry (IHC) staining of the cleaved capase-3 and cleaved PARP in the xenograft tissues in these mice.

treated by free GA had 0.45μg $mL^{-1}$ of GA in their livers, and those treated by NP-GA had only 0.25μg $mL^{-1}$ of GA in their livers. At the 8mg $kg^{-1}$ dosage, the free GA group had 0.63μg $mL^{-1}$ and NP-GA group had 0.33μg $mL^{-1}$ in their livers (**Figure 6C**). A similar trend was also observed at both 2h and 4h post-administration (**Figures 6D, E**).

NP-GA treatment also resulted in a lower GA concentration in the kidneys when compared to free GA at 30 minutes post-administration. At the 4mg $kg^{-1}$ dosage, the free GA group had 0.12μg $mL^{-1}$ and NP-GA group had only 0.07μg $mL^{-1}$ of GA in the kidneys; at the 8mg $kg^{-1}$ dosage, the free GA group had 0.22μg $mL^{-1}$ and NP-GA group had only 0.10μg $mL^{-1}$ in the kidneys (**Figure 6B**). At 1h post-administration, at 4 mg $kg^{-1}$ dosage, the free GA group had 0.21μg $mL^{-1}$ and NP-GA group had only 0.11μg $mL^{-1}$ of GA in the kidneys; at 8 mg $kg^{-1}$ dosage, the free GA group had 0.32μg $mL^{-1}$ and NP-GA group had only 0.19μg $mL^{-1}$ in the kidneys (**Figure 6C**). A similar trend was also observed at 2h post-administration (**Figure 6D**).

These results clearly demonstrated that mice treated by NP-GA had significantly higher GA levels in the tumors than

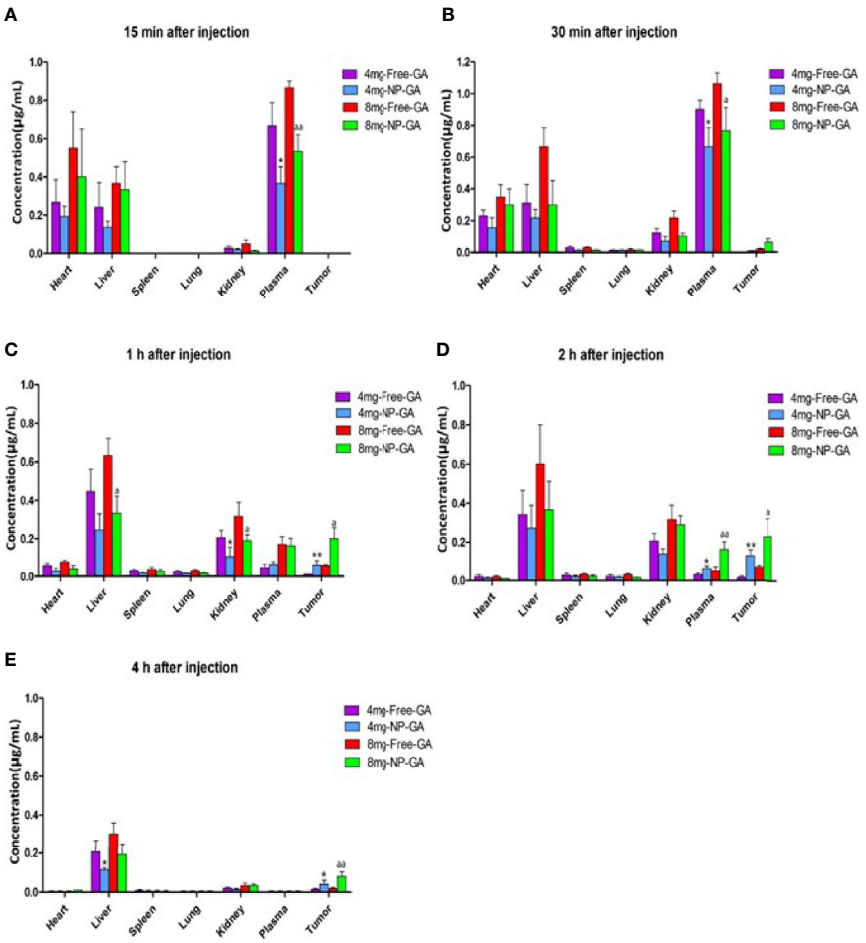


**FIGURE 6** | Biodistribution of GA as a function of time in a variety of tissues in the HCC1806-bearing xenograft mouse models after free GA or GA-loaded FA-Arg-PEUU-NP (NP-GA) treatments. **(A)** 15 min, **(B)** 30 min, **(C)** 1h, **(D)** 2h, and **(E)** 4h after intravenous injection of free GA or GA-loaded FA-Arg-PEUU-NP (NP-GA) at the indicated dosage. The data are shown as the means ± SEM, n = 3 mice in each group. *p < 0.05, **p < 0.01 compared to 4mg-free-GA group; a < 0.05, aa < 0.01 compared to 8mg-free-GA group.

those that received free-GA treatments, whereas the GA concentrations in the major organs were reduced, suggesting that NP-GA has fewer off-target side effects.

## NP-GA Has Lower Off-Target Side Effect Compared to Free GA

H&E staining of the major organs was done to further suggest NP-GA does less damage to the off-target major organs in mice when compared to free GA. **Figures 7A, B** showed that NP-GA had less damage to the heart, liver, and lung than the free GA. These off-target H&E image data, (**Figure 7A**) along with their quantified scores (**Figure 7B**), are consistent with the lower levels of GA in these organs after NP-GA treatments (**Figure 6**). Neither NP-GA nor free GA caused significant damage to kidney and spleen (**Figures 7A, B**), although GA was detected in these organs (**Figures 6B–D**). Both the qualitative H&E stained image data and their quantified scores clearly illustrate the benefits of treating TNBC with NP-GA, that is, achieving higher anti-TNBC effects but with fewer off-target side effects to the major organs, particularly at the 8mg $kg^{-1}$ GA dosage. Body weight variation is one of the parameters in toxicity testing.[34] **Supplementary Figure S3A** showed the body weight of the mice in different groups during the course of the treatments, which had no apparent difference between groups. Percentages of the changes in body weight were also calculated, that is the % difference of the body weight of each mouse between day 6 and day 17. The results showed that NP-GA at both dosages did not create significant differences in the % changes in body weight when compared with saline and NP-alone groups; however, the 8mg-Free-GA group had body weight reduced and the % changes in body weight was significantly different from those in the saline and NP-alone groups (**Supplementary Figure S3B**). These data suggest that free GA treatment at a high concentration has toxicity to the mice, whereas the toxicity is not observed in the NP-GA treatment group.

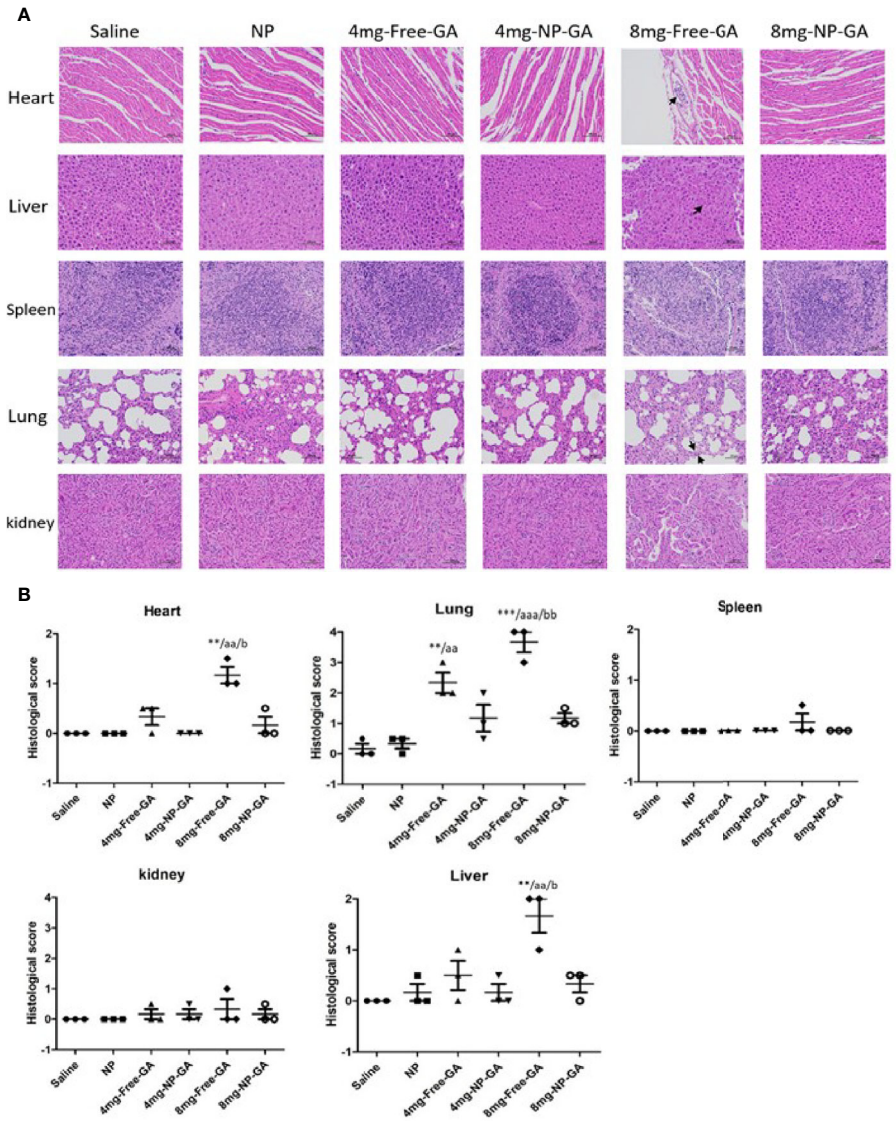


**FIGURE 7** | *In vivo* tissues and organ toxicity after free GA or GA-loaded FA-Arg-PEUU-NP (NP-GA) treatments. **(A)** H&E staining images and **(B)** quantification analysis of the heart, liver, spleen, lung, and kidney of the HCC1806-bearing xenograft mouse models after saline, FA-Arg-PEUU-NP (NP), free GA, or GA-loaded FA-Arg-PEUU-NP (NP-GA) treatments. The data are shown as the means ± SEM, n = 3 mice in each group. **p < 0.01, ***p < 0.001 compared to saline group; aa < 0.01, aaa < 0.01 compared to NP group; b < 0.05, bb < 0.01 compared to 8mg-NP-GA group.

## The FA-Arg-PEUU-NP Carriers Affect the Polarization of Tumor-Associated Macrophages (TAM)

Since Arg is present in the FA-Arg-PEUU NP carriers, it is interesting to examine whether the carrier *per se* or the GA-loaded NP will affect the polarization of TAM. Macrophages uptake Arg and process it *via* 2 different pathways: iNOS and arginase. The iNOS pathway produces M1 macrophage phenotype, while the arginase route produces M2 macrophage phenotype (33).

**Figures 8A–C** showed that the FA-Arg-PEUU-NP *per se* neither affected M1 nor M2 population. The percentage of M1 after FA-Arg-PEUU-NP treatment was 15.61%, and was 15.10% in the saline group (**Figure 8B**), and the percentage of M2 after FA-Arg-PEUU-NP treatment was 9.95%, and was 8.45% in the saline group (**Figure 8C**).

When comparing between the NP-GA and saline, the NP-GA at both dosages had significantly higher M2 populations than the saline control (**Figure 8C**). The percentage of M2 in the saline group was 8.45% while it was 9.94% in the 4mg-NP-GA group and 10.17% in the 8mg-NP-GA group. When comparing between the NP-GA and free GA, NP-GA treatment resulted in a slightly higher average M2 population than free GA at the 4 mg $kg^{-1}$ GA dosage level (**Figure 8C**). The M2 population of the

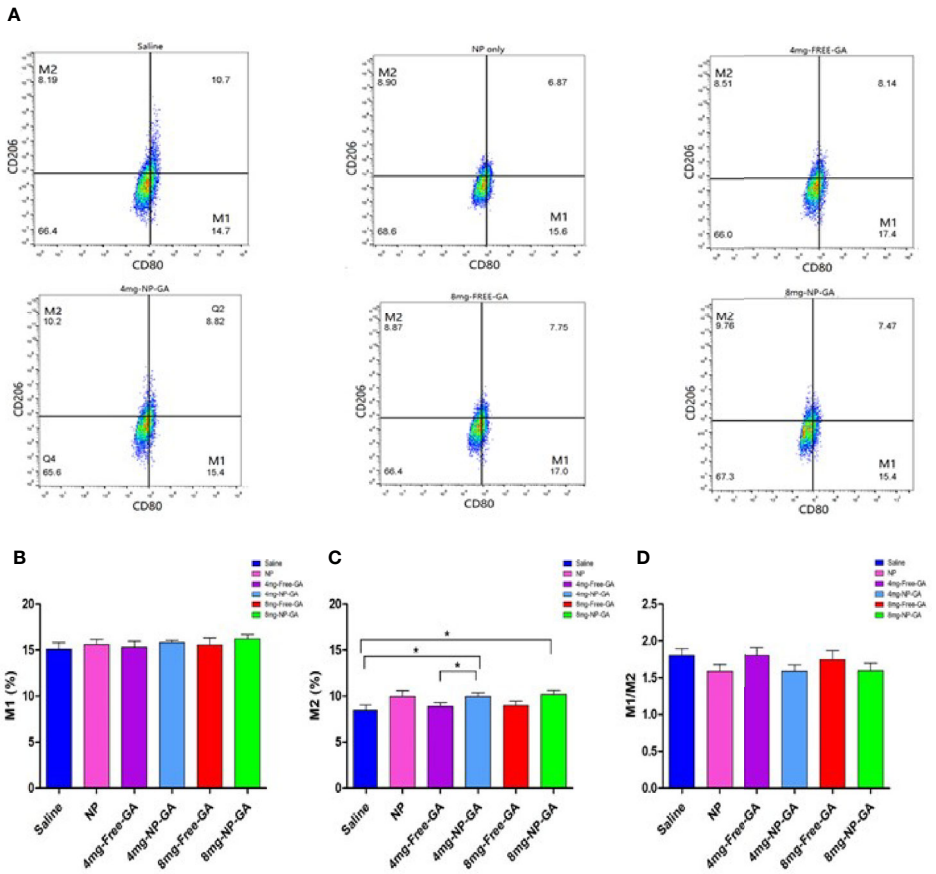


**FIGURE 8** | Polarization of tumor-associated macrophage (TAM) of the HCC1806-bearing xenograft mouse models after saline, FA-Arg-PEUU-NP (NP), free GA, or GA-loaded FA-Arg-PEUU-NP (NP-GA) treatments. **(A)** The polarization of the tumor-associated macrophages (TAM) of the HCC1806-bearing xenograft mouse models after the saline, FA-Arg-PEUU-NP (NP), free GA, or GA-loaded FA-Arg-PEUU-NP (NP-GA) treatments. The percentages of the **(B)** M1 phenotype, **(C)** M2 phenotype, and **(D)** M1/M2 ratio of the TAM. The data are shown as the means ± SEM, n = 5 mice in each group. *$p < 0.05$ as indicated.

free GA group was 8.89% and was 9.94% in the NP-GA group; the difference was statistically significance at $p<0.05$. However, NP-GA did not significantly affect the M2 population at the 8mg $kg^{-1}$GA dosage level or the M1 population at both dosage levels (**Figures 8A–C**).

Although there was no statistical difference of TAM M1/M2 ratios in all treatments, it appears that the average TAM M1/M2 values of the NP-GA treatment at both GA dosage levels were lower than the corresponding free GA treatment (**Figure 8D**). Similarly, the blank FA-Arg-PEUU NP treatment also showed a lower average M1/M2 ratio than the saline control (**Figure 8D**).

## DISCUSSION

Both *in vitro* and *in vivo* data in this study clearly show that the newly designed FA-Arg-PEUU-NP nano-carriers significantly increase the uptake of GA into TNBC, induce more apoptosis by activating both intrinsic and extrinsic apoptotic pathways, and exhibit more potent anti-TNBC effects with reduced off-target side effects. Our data strongly suggest that this new family of drug-loaded FA-Arg-PEUU-NP strategy can provide enhanced anti-TNBC effects regardless of the TP53 gene mutation status of the cancer. More importantly, the targeted delivery of GA to TNBC also significantly reduces off-target damage to the major organs, including the heart, liver, and lung, as demonstrated in the xenograft mouse models.

The efficacy and safety of GA for cancer treatment have been tested in clinical trials in China. In 2013, a phase IIa clinical study was conducted in China, which aimed to evaluate the safety and efficacy of GA treatment in patients with lung, gastrointestinal, breast, and liver cancer. Twenty-one patients received 45mg $m^{-2}$ GA intravenously from days 1 to 5 for a 2-week cycle. The clinical outcomes showed that the objective response rate which indicates the proportion of patients with reduction in tumor burden was 14.3%, and disease control rate, which is a composite of overall response rate and stable disease, was 76.2%. The observed toxicity was mostly mild or moderate adverse events (AE) (Grades I and II), but not severe or life-threatening AE (Grade III and IV) based on a standard criterion (NCI-CTCAE 3.0) of anticancer drug toxicity evaluation. The symptoms of the AE were abdominal pain, injection site reactions, phlebitis, and

nausea. The phase IIa clinical trial suggests that GA has a favorable safety profile and is effective in treating malignant cancers (17). However, a phase IIb clinical trial with 210 cases of non-small cell lung cancer (NSCLC), renal cell cancer, and colon cancer, and phase III clinical trial with 600 cases of advanced renal cell cancer and 300 cases of NSCLC documented that GA did not have an apparent advantage over chemotherapy, although no Grade III and IV adverse events were reported (Study report 138997640-2008ZX09101024/01 by Zhangleilei Jiangsu Kanion Pharmaceutical Company and Zhaoyiwu Jiangsu Kanion Pharmaceutical Company). The unsatisfactory clinical outcome of the free GA treatments in the malignant cancers led us to design FA-Arg-PEUU NP as a target nano-carrier for GA for the TNBC treatment, which can enhance therapeutic efficacy and also reduce off-target side effects as the data from this study showed. In the above clinical studies, the dosage of GA is at 45mg/$m^2$, which corresponds to 1.215mg $kg^{-1}$ assuming the reference body weight is 60kg and body surface area is 1.62$m^2$. The equivalent mouse dose to that clinical GA dosage is 14.985mg $kg^{-1}$, which is much higher than the dosages 4 or 8mg $kg^{-1}$ of GA or GA-loaded FA-Arg-PEUU NP used in our current animal study. As shown in **Figure 4**, NP-GA and free GA treatments at these low GA dosage levels show significantly reduced tumor growth when compared to saline control, suggesting a dosage lower than the reported clinical trial dosage can be used to treat TNBC. Furthermore, at this low GA dosage, the treatment with the NP-GA strategy shows an even more significant reduction in tumor growth than the free GA treatment.

The targeted delivery of GA to TNBC is far less studied. The reported studies mainly use NP carriers to deliver GA to non-TNBC breast cancer (34–36). For example, a study used MDA-MB-231 cells, MCF-7 breast cancer cell lines, and 4T1 cell-bearing mice as models to study the anti-cancer effect of the co-delivery of GA and TNF-related apoptosis-inducing ligand (TRAIL) plasmid by hyaluronic acid grafted PEI-PLGA nanoparticles (GA/pTRAIL-HA/PPNPs) (37). It is known that TRAIL *per se* induces apoptosis by binding to the TRAIL death receptors, which leads to the recruitment of Fas-associated death receptor and triggers the consequent apoptotic signaling cascade. The combined delivery of GA/pTRAIL-HA/PPNPs shows an enhanced anti-cancer effect over GA-HA/PPNPS and pTRIAL-NA/PPNPs as demonstrated in 4T1 cell-bearing mice. The tumor suppression rate of GA-HA/PPNPs, TRAIL-HA/PPNPs, and GA/pTRAIL-HA/PPNPs are 46.4%, 62.0%, and 84.1%, respectively. The enhanced anti-cancer effect of GA/pTRAIL-HA/PPNPs is due to the increased apoptosis level in the breast cancer cells. Co-delivery of TRAIL with GA demonstrates a pragmatic strategy which may be beneficial to modify our current FA-targeted Arg-PEUU-NP delivery system to further enhance the apoptosis level in the tumor sites. However, this study did not use free GA as reference group and hence the anti-cancer effects between free GA and GA/pTRAIL-HA/PPNPs cannot be assessed. However, our current study design permits such an assessment to determine whether GA delivered by the FA-Arg-PEUU-NP treatment would be better than free GA treatment.

The current data also show that NP-GA does significantly less damage to the heart, lung, and liver in the TNBC-bearing mouse model when compared to free GA (**Figure 7**). Therefore, the data in this study provide strong evidence to suggest a relatively low dosage of NP-GA can be used to treat TNBC with fewer off-target side effects. The reason behind this observed lower off-target side effect in the NP-GA treatment is attributed to the targeted delivery of GA to TNBC that highly expresses folate receptors (FRα) (30). FRα have a highly restricted expression in the luminal membrane of secretory ductal cells in normal breast [40]. FRα are also not expressed or have little expressions in the peritoneum, colon, small intestine, kidney, and ovary (38, 39). The specific expression of FRα in tumor has led to the development of FRα-targeted therapies which are in clinical trials for the treatment of TNBC. A multi-epitope FRα peptide vaccine is undergoing a randomized phase II trial studies with TNBC patients in the Academic and Community Cancer Research United in the US (ClinicalTrials.gov Identifier: NCT03012100).

The current target therapies for TNBC, such as epidermal growth factor receptor-targeted approach with cetuximab, only demonstrates a modest anti-cancer activity in the metastatic TNBC (40); bevacizumab, which targets vascular endothelial growth factor, does not show a pronounced benefit of overall survival (41). Concerning these unsatisfactory therapeutic outcomes, our proposed FRα-targeted NP-GA therapeutic strategy appears to be a better alternative to the TNBC treatment.

In this study, our data also show interesting and useful information about TNBC that harbor TP53 mutations. The NP-GA treatments induce apoptosis in TNBC in a p53-independenet manner. The TP53 gene is mutated in approximately 80% of TNBC cases (42, 43). Mutations in TP53 in TNBC are predominantly missense mutations, producing mutant p53 proteins that promote tumorigenesis (42). Our data demonstrate that NP-GA exerts a potent therapeutic effect in TNBC which either harbor TP53 mutations or has no TP53 expression. The enhanced apoptosis level after NP-GA treatment is, at least in part, due to the enhanced intrinsic and extrinsic apoptosis *via* the activation of caspases, but not the collapse of mitochondrial membrane potential. In general, the caspase activation is preceded by opening of the mitochondrial permeability transition pore (MPT), followed by dissipation of Δψm and release of cytochrome c. A possible explanation of our results is that mitochondria can also transiently maintain a membrane potential after the release of the apoptosis-inducing factors (44). Alternatively, NP-GA may induce a different regulation on the apoptotic machinery in TNBC, in which MPT may not be required for mitochondrial outer membrane permeabilization or cytochrome c release, and MPT may not participate in the apoptosis (45). Indeed, induction of caspase-3 activity and apoptosis in human blood granulocytes occurs without prior mitochondrial changes, such as the loss of mitochondrial membrane potential and release of cytochrome c (46). Further study is needed to examine the role of Δψm in GA-induced apoptosis in TNBC.

In addition to a conventional mechanistic study to reveal the mechanism of action underlying the enhanced therapeutic effects

of NP-GA, TAM level was also assessed to determine whether the newly designed FA-Arg-PEUU-NP drug nano-carrier would have any effect on TAM. In the tumors of the TNBC patients, TAM has the highest abundance and accounts for 25% of the total cell population (47). The increased recruitment of TAM to TNBC may be due to the reduced expression of Raf kinase inhibitory protein and reduced secretion of chemokines CCL5 in TNBC (48). The large infiltrate of TAM is associated with a high risk of distant metastasis, low disease-free survival, and low overall survival in the TNBC patient (49).

In this study, only a pure Arg was used as the amino acid building block in the FA-tagged Arg-PEUU-NP for the delivery of GA for TNBC treatment. Our *in vivo* TAM data show that the blank FA-Arg-PEUU-NP and the GA-loaded FA-Arg-PEUU-NP do not affect the M1 population (**Figure 8B**), but slightly increase (statistically significant at $p<0.05$) the M2 population in the TNBC tumors (**Figure 8C**), and hence cause a decrease in the M1/M2 ratio (**Figure 8D**). The incorporation of GA in the FA-Arg-PEUU-NP neither changes the M2 population nor the M1/M2 ratio against the blank FA-Arg-PEUU-NP, suggesting GA *per se* does not affect the polarization of the macrophages. Although M2 macrophages are known to promote cancer progression, the TNBC tumor size and tumor weight data (**Figure 4**) show that blank FA-Arg-PEUU-NP *per se* does not affect tumor growth *in vivo* when compared to the saline control, suggesting that the slight increase in the M2-polarized macrophage population in the tumor induced by the Arg-based nanoparticle carrier (Arg-PEUU-NP) does not promote the TNBC tumor growth. Our data suggest the extreme complexity of the role of TAM, and the role of Arg in TAM polarization and its effect on tumor growth. Therefore, additional in-depth study of the role of TAM under our GA-loaded FA-Arg-PEUU-NP strategy is needed to clarify the impact of the Arg-based NP delivery vehicle on TAM polarization. It is important to consider all the factors involved in assessing the collective effect of a new strategy on cancer therapy.

Since TAM changes the tumor microenvironment that promotes cancer development and progression, targeting TAM may be a potential therapeutic strategy to treat cancers. For example, the mannose receptors that are overexpressed in TAM can be used as a target for the design of nanoparticles for drug delivery. Previously, poly(lactic-co-glycolic)acid (PLGA) nanoparticles that are PEGylated with acid sensitive sheddable polyethylene glycol (PEG) and surface-modified with mannose (i.e. AS-M-PLGA-NPs) have been designed to actively target the nanoparticles to TAMs *via* mannose-mannose receptor recognition after acid-sensitive "shedding" of the PEG in the relatively low pH tumor microenvironment (50). The use of these nanoparticles to carry doxorubicin, i.e., TAM-targeting DOX-AS-M-PLGA-NPs, demonstrates a more potent effect than DOX alone or DOX-AS-PLGA-NPs in controlling the tumor growth of the orthotopic MMTV-M-Wnt-1 mammary tumor-bearing mouse model (50). A similar design can be incorporated into our GA-loaded FA-Arg-PEUU-NP to further enhance its therapeutic effects in TNBC treatment.

Another possible strategy to treat TNBC is to modulate the macrophage polarization. Arg is a common substrate for nitric oxide synthase and arginase pathways after macrophage uptake Arg. Depending on the type of Arg metabolic pathway, very different macrophage phenotypes can be produced. The M1 macrophage will convert Arg to citrulline and nitric oxide (NO), which is inflammatory and cytotoxic; the M2 macrophages hydrolyzes Arg to urea and ornithine, which is important for cellular proliferation and tissue repair (51, 52). Previously, the Chu lab has shown that the amino acid-based poly(ester amide) or poly(ester urea urethane) biomaterials synthesized from Arg have a tunable immune-modulating property (16, 24, 27, 28). For example, He et al. recently demonstrated that by incorporating an Arg derivative (L-nitroarginine, NOArg) into a pure Arg as the amino acid building block, a new family of NOArg-Arg PEA copolymers is synthesized that possesses the ability to polarize M1 to M2 and exhibits a wound healing property, as demonstrated in a diabetic 3$^{rd}$ degree burn wound mouse model (28). The significantly faster and better wound healing quality in the burn wound diabetic model is achieved with an optimal balance of M1/M2 mixture population more toward M2. Such a preferred M1 to M2 mixture population can only be achieved with a proper NOArg to pure Arg ratio in the NOArg-Arg PEA copolymers. More importantly, neither a pure NOArg nor pure Arg-based PEA can achieve such a preferred M1 to M2 mixture population for the desirable and more efficient wound healing quality. For the treatment of TNBC, a combination of NP-GA and Th1 cytokine interferon-γ (IFN-γ) can be administrated to enhance M1 polarization in the TNBC in our future study. IFN-γ is a useful adjuvant immunotherapy for many cancers (53). It also inhibits angiogenesis in the tumor (53).

In addition, the use of Arg-based nanoparticles as the carriers for anticancer drugs like GA for TNBC treatment may have the advantage of making the surface of the nanoparticles positively charged. It is reported that the dominant mechanism for the uptake of nanoparticles is an active process instead of a passive diffusion (54). Such an active uptake of cationic NPs like Arg-PEUU-NP (+10mV charge) (16) by cancer cells is further enhanced by the general anionic surface membrane of cells, particularly cancer cells, that express excessive anionic-charged sialic acid (55–60). Holmberg et al. (55) and Gakhar et al. (61) reported that the growth of tumor cells, including PC3 prostate cancer cells, is inhibited by the cationic polymers, such as dextran derivatives and vinyl-based Poly(AETA) synthesized from the [2-(acryloxy)ethyl]trimethylammonium chloride] monomer (AETA). Their data suggest that certain cationic polymers may represent an alternative strategy to target and inhibit the growth of malignant cancers.

Therefore, as shown in our current TNBC study, the design of cationic folate-targeted Arg-based pseudo-protein nanoparticles as anticancer herbal compound carriers offer many beneficial effects like overcoming the anionic cell membrane barrier, promoting internalization, and facilitating tumor-targeting for a more efficient delivery of the drug. Therefore, the design

achieves better therapeutic efficacy with reduced off-target side effects when compared to free drug delivery.

## CONCLUSION

In this study, a new targeted therapy for TNBC with a Chinese medicinal compound gambogic acid (GA) delivered by a newly designed folate (FA)-tagged biodegradable amino acid-based poly(ester urea urethane) nanoparticles, the GA-loaded FA-Arg-PEUUs (NP-GA), is reported. The conjugation of FA in the Arg-PEUU nano-carriers increases the cellular uptake of the nano-carriers into the TNBC both *in vitro* and *in vivo*. Compared to free GA, the NP-GA treatments exert higher cytotoxicity with increased intrinsic and extrinsic apoptosis in TNBC cells that either harbor TP53 mutations or without p53 protein expression. In the TNBC-bearing xenograft mouse model, the NP-GA treatments also demonstrate better therapeutic efficacy with increased apoptosis in the tumors and reduced off-target damages, as there is more efficient targeted delivery of GA to the tumor sites instead of non-discriminated delivery to other organs. Further investigations may develop this NP-GA system as alternative therapeutics for TNBC treatment.

## DATA AVAILABILITY STATEMENT

The raw data supporting the conclusions of this article will be made available by the authors, without undue reservation.

## ETHICS STATEMENT

The animal study was reviewed and approved by Hong Kong Baptist University.

## AUTHOR CONTRIBUTIONS

Conceptualization: C-CC, ZB, HK, and QX. Data curation and formal analysis: QX and RG. Funding acquisition: C-CC and ZB. Writing: HK and QX. Review and editing: C-CC and ZB. All authors contributed to the article and approved the submitted version.

## FUNDING

This study is supported by The Vincent and Lily Woo Foundation to both Chu at Cornell University in the USA and Bian in Hong Kong Baptist University in Hong Kong. The supported project title is "East Meet West: A revolutionized nanotechnology approach to modernize the delivery of Chinese medicine for vast improved cancer therapeutic efficacy".

## SUPPLEMENTARY MATERIAL

The Supplementary Material for this article can be found online at: https://www.frontiersin.org/articles/10.3389/fonc.2020.600298/full#supplementary-material

**SUPPLEMENTARY FIGURE 1 |** The viability of **(A)** HCC1143 and **(B)** HCC1806 cells after free GA or GA-loaded FA-Arg-PEUU-NP (NP-GA) treatments for 24 hours at the indicated concentrations. The data are shown as the means ± SEM, n = 3.

**SUPPLEMENTARY FIGURE 2 |** The apoptotic TNBC cell distribution after free-GA or GA-loaded FA-Arg-PEUU-NP (NP-GA) treatments for 3 hours.

**SUPPLEMENTARY FIGURE 3 | (A)** Body weight and **(B)** percentage changes in body weight of the HCC1806-bearing xenograft mouse models during the treatment period. The data are shown as the means ± SEM, n = 4-5 mice in each group. *p<0.05 compared to saline group; a<0.05 compared to NP group.

## REFERENCES

1. Reis-Filho JS, Tutt AN. Triple negative tumors: a critical review. *Histopathology* (2008) 52:108–18. doi: 10.1111/j.1365-2559.2007.02889
2. Chaudhary LN, Wilkinson KH, Kong A. Triple-negative breast cancer: who should receive neoadjuvant chemotherapy? *Surg Oncol Clin N Am* (2008) 27:141–53. doi: 10.1016/j.soc.2017.08.004
3. Lin NU, Vanderplas A, Hughes ME, Theriault RL, Edge SB, Wong YN, et al. Clinicopathologic features, patterns of recurrence, and survival among women with triple-negative breast cancer in the National Comprehensive Cancer Network. *Cancer* (2012) 118:5463–72. doi: 10.1002/cncr.27581
4. Dent R, Trudeau M, Pritchard KI, Hanna WM, Kahn HK, Sawka CA, et al. Triple-negative breast cancer: clinical features and patterns of recurrence. *Clin Cancer Res* (2007) 13:4429–34. doi: 10.1158/1078-0432.CCR-06-3045
5. von Minckwitz G, Untch M, Blohmer JU, Costa SD, Eidtmann H, Fasching PA, et al. Definition and impact of pathologic complete response on prognosis after neoadjuvant chemotherapy in various intrinsic breast cancer subtypes. *J Clin Oncol* (2012) 30:1796–804. doi: 10.1200/JCO.2011.38.8595
6. Liedtke C, Mazouni C, Hess KR, André F, Tordai A, Mejia JA, et al. Response to neoadjuvant therapy and long-term survival in patients with triple-negative breast cancer. *J Clin Oncol* (2008) 26:1275–81. doi: 10.1200/JCO.2007.14.4147
7. Schmid P, Rugo HS, Adams S, Schneeweiss A, Barrios CH, Iwata H, et al. Impassion 130 Investigators Atezolizumab plus nab-paclitaxel as first-line treatment for unresectable, locally advanced or metastatic triple-negative breast cancer (IMpassion130): updated efficacy results from a randomised, double-blind, placebo-controlled, phase 3 trial. *Lancet Oncol* (2020) 21:44–59. doi: 10.1016/S1470-2045(19)30689-8
8. Santarpia L, Qi Y, Stemke-Hale K, Wang B, Young EJ, Booser DJ, et al. Mutation profiling identifies numerous rare drug targets and distinct mutation patterns in different clinical subtypes of breast cancers. *Breast Cancer Res Treat* (2012) 13:333–43. doi: 10.1007/s10549-012-2035-3
9. Hurley J, Reis IM, Rodgers SE, Gomez-Fernandez C, Wright J, Leone JP, et al. The use of neoadjuvant platinum-based chemotherapy in locally advanced breast cancer that is triple negative: retrospective analysis of 144 patients. *Pegram Breast Cancer Res Treat* (2013) 138:783–94. doi: 10.1007/s10549-013-2497-y
10. Zhang HZ, Kasibhatla S, Wang Y, Herich J, Guastella J, Tseng B, et al. Discovery, characterization and SAR of gambogic acid as a potent apoptosis inducer by a HTS assay. *Bioorg Med Chem* (2004) 12:309–17. doi: 10.1016/j.bmc.2003.11.013
11. Rong JJ, Hu R, Song XM, Ha J, Lu N, Qi Q, et al. Gambogic acid triggers DNA damage signaling that induces p53/p21(Waf1/CIP1) activation through the ATR-Chk1 pathway. *Cancer Lett* (2010) 296:55–64. doi: 10.1016/j.canlet.2010.03.016
12. Rahman MA, Kim NH, Huh SO. Cytotoxic effect of gambogic acid on SH-SY5Y neuroblastoma cells is mediated by intrinsic caspase-dependent signaling pathway. *Mol Cell Biochem* (2013) 377:187–96. doi: 10.1007/s11010-013-1584-z
13. Zhen YZ, Lin YJ, Li KJ, Yang XS, Zhao YF, Wei J, et al. Gambogic acid lysinate induces apoptosis in breast cancer mcf-7 cells by increasing reactive oxygen

species. Evid. Based Complement. *Alternat Med* (2015) 2015:842091. doi: 10.1155/2015/842091
14. Wang S, Xu Y, Li C, Tao H, Wang A, Sun C, et al. Gambogic acid sensitizes breast cancer cells to TRAIL-induced apoptosis by promoting the crosstalk of extrinsic and intrinsic apoptotic signaling. *Food Chem Toxicol* (2018) 119:334–41. doi: 10.1016/j.fct.2018.02.037
15. Wang Y, Sui Y, Tao Y. Gambogic acid increases the sensitivity to paclitaxel in drug–resistant triple–negative breast cancer via the SHH signaling pathway. *Mol Med Rep* (2019) 20:4515–22. doi: 10.3892/mmr.2019.10697
16. He M, Ro L, Liu J, Chu CC. Folate-decorated arginine-based poly(ester urea urethane) nanoparticles as carriers for gambogic acid and effect on cancer cells. *J Biomed Mater Res Part A* (2017) 105A:475–90. doi: 10.1002/jbm.a.35924
17. Chi Y, Zhan XZ, Yu H, Xie GR, Wang ZZ, Xiao W, et al. An open-labeled, randomized, multicenter phase IIa study of gambogic acid injection for advanced malignant tumors. *Chin Med J (Engl)* (2013) 126:1642–46. doi: 10.3760/cma.j.issn.0366-6999.20122582
18. Guo K, Chu CC J. Synthesis and characterization of novel biodegradable unsaturated poly(ester amide)/poly(ethylene glycol) diacrylate hydrogels. *Polym Sci Pol Chem* (2005) 43:3932–44. doi: 10.1002/pola.20781
19. Ji Y, Shan S, Chu CC. A novel pseudo-protein-based biodegradable nanomicellar platform for the delivery of anticancer drugs. *Small* (2017) 13:1601491. doi: 10.1002/smll.201601491
20. Liu J, Liu XL, Xi TF, Chu CC. A novel pseudo-protein-based biodegradable coating for magnesium substrates: in vitro corrosion phenomena and cytocompatibility. *J Mat Chem B* (2015) 3:878–93. doi: 10.1039/c4tb01527d
21. Wu J, Wu D, Mutschler MA, Chu CC. Cationic hybrid hydrogels from amino-acid-based poly (ester amide): Fabrication, characterization, and biological properties. *Adv Funct Mater* (2012) 22:3815–23. doi: 10.1002/adfm.201103147
22. Zhu J, Han H, Li F, Wang X, Yu J, Chu CC, et al. Self-assembly of amino acid-based random copolymers for antibacterial application and infection treatment as nanocarriers. *J Colloid Interface Sci* (2019) 540:634–46. doi: 10.1016/j.jcis.2018.12.091
23. Chu CC. An Overview of A Novel Family of Nature-Inspired Design of Biodegradable Functional Amino Acid-based Poly(ester amide) Biomaterials: New Development, Property and Biomedical Applications. In: CC Chu, editor. *Biodegradable Polymers*, vol. 2 . New York: Nova Science Publisher (2015). p. Chapter 3.
24. Chu CC. Novel Synthetic Biodegradable Arginine-Rich Implantable Biomaterials And Devices For Human Body Repair And Reconstruction. In: BL Soto, editor. *L-Arginine: Structure, Dietary Sources and Beneficial Effects*, vol. Chapter 4. New York: Nova Science Publisher (2016). p. 89–126.
25. Katsarava R, Beridze V, Arabuli N, Kharadze D, Chu CC, Won CY. Amino acid based bioanalogous polymers: Synthesis and study of regular poly(ester amide)s based on bis(amino acid) alkylene diesters and aliphatic dicarboxylic acid. *J Polym Sci Pol Chem* (1999) 37:391–407. doi: 10.1002/(SICI)1099-0518(19990215)37:4<391::AID-POLA3>3.0.CO;2-E
26. Pang X, Chu CC. Synthesis, characterization and biodegradation of functionalized amino acid-based poly (ester amide)s. *Biomaterials* (2010) 31:3745–54. doi: 10.1016/j.biomaterials.2010.01.027
27. You X, Gu Z, Huang J, Kang Y, Chu CC, Wu J. Arginine-based poly(ester amide) nanoparticle platform: From structure-property relationship to nucleic acid delivery. *Acta Biomater* (2018) 74:180–91. doi: 10.1016/j.actbio.2018.05.040
28. He M, Sun L, Fu X, McDonough SP, Chu C. Biodegradable amino acid-based poly(ester amine) with tunable immunomodulating properties and their in vitro and in vivo wound healing studies in diabetic rats' wounds. *Acta Biomater* (2019) 84:114–32. doi: 10.1016/j.actbio.2018.11.053
29. Locasale JW. Serine, glycine and one-carbon units: cancer metabolism in full circle. *Nat Rev Cancer* (2013) 13:572–83. doi: 10.1038/nrc3557
30. Necela BM, Crozier JA, Andorfer CA, Lewis-Tuffin L, Kachergus JM, Geiger XJ, et al. Folate receptor-α (FOLR1) expression and function in triple negative tumors. *PloS One* (2015) 10:e0122209. doi: 10.1371/journal.pone.0122209
31. Shtraizent N, Matsui H, Poloskaia A, Bargonetti J. Hot spot mutation in TP53 (R248Q) causes oncogenic gain-of-function phenotypes in a breast cancer cell line derived from an African American patient. *Int J Environ Res Public Health* (2016) 13:22. doi: 10.3390/ijerph13010022
32. Shi M, Shtraizent N, Polotskaia A, Bargonetti J, Matsui H. Impedimetric detection of mutant p53 biomarker-driven metastatic breast cancers under hyposmotic pressure. *PloS One* (2014) 9:e99351. doi: 10.1371/journal.pone.0099351
33. Shapouri-Moghaddam A, Mohammadian S, Vazini H, Taghadosi M, Esmaeili SA, Mardani F, et al. Macrophage plasticity, polarization, and function in health and disease. *J Cell Physiol* (2018) 233(9):6425–40 doi: 10.1002/jcp.26429
34. Sang MM, Liu FL, Wang Y, Luo RJ, Huan XX, Han LF, et al. A novel redox/pH dual-responsive and hyaluronic acid-decorated multifunctional magnetic complex micelle for targeted gambogic acid delivery for the treatment of triple negative breast cancer. *Drug Deliv* (2018) 25:1846–57. doi: 10.1080/10717544.2018.1486472
35. Xu Y, Wang C, Ding Y, Wang Y, Liu K, Tian Y, et al. Nanoparticles with optimal ratiometric co-delivery of docetaxel with gambogic acid for treatment of multidrug-resistant breast cancer. *J Biomed Nanotechnol* (2016) 12:1774–81. doi: 10.1166/jbn.2016.2282
36. Wang C, Kar S, Lai X, Cai W, Arfuso F, Sethi G, et al. Triple negative breast cancer in Asia: An insider's view. *Cancer Treat Rev* (2017) 62:29–38. doi: 10.1016/j.ctrv.2017.10.014
37. Wang S, Shao M, Zhong Z, Wang A, Cao J, Lu Y, et al. Co-delivery of gambogic acid and TRAIL plasmid by hyaluronic acid grafted PEI-PLGA nanoparticles for the treatment of triple negative breast cancer. *Drug Deliv* (2017) 24:1791–800. doi: 10.1080/10717544.2017.1406558
38. Azaïs H, Schmitt C, Tardivel M, Kerdraon O, Stallivieri A, Frochot C, et al. Assessment of the specificity of a new folate-targeted photosensitizer for peritoneal metastasis of epithelial ovarian cancer to enable intraperitoneal photodynamic therapy. A preclinical study. *Photodiagnosis Phogodyn Ther* (2016) 13:130–8. doi: 10.1016/j.pdpdt.2015.07.005
39. O'Shannessy DJ, Somers EB, Wang LC, Wang H, Hsu R. Expression of folate receptors alpha and beta in normal and cancerous gynecologic tissues: correlation of expression of the beta isoform with macrophage markers. *J Ovarian Res* (2015) 8:29. doi: 10.1186/s13048-015-0156-0
40. Baselga J, Gómez P, Greil R, Braga S, Climent MA, Wardley AM, et al. Randomized phase II study of the anti-epidermal growth factor receptor monoclonal antibody cetuximab with cisplatin versus cisplatin alone in patients with metastatic triple-negative breast cancer. *J Clin Oncol* (2013) 31:5286–92. doi: 10.1200/JCO.2012.46.2408
41. Miles DW, Diéras V, Cortés J, Duenne AA, Yi J, O'Shaughnessy J. First-line bevacizumab in combination with chemotherapy for HER2-negative metastatic breast cancer: pooled and subgroup analyses of data from 2447 patients. *Ann Oncol* (2013) 2:2773–80. doi: 10.1093/annonc/mdt276
42. Cancer Genome Atlas Network. Comprehensive molecular portraits of human breast tumors. *Nature* (2012) 490:61–70. doi: 10.1038/nature11412
43. Park A, Heo SH, Kim YA, Gong G, Lee HJ. Association between p53 expression and amount of tumor-infiltrating lymphocytes in triple-negative breast cancer. *J Pathol Transl Med* (2019) 53:180–7. doi: 10.4132/jptm.2019.02.08
44. Düßmann H, Rehm M, Kögel, Prehn JHM. Outer mitochondrial membrane permeabilization during apoptosis triggers caspase-independent mitochondrial and caspase-dependent plasma membrane potential depolarization: a single-cell analysis. *J Cell Sci* (2003) 116:525. doi: 10.1242/jcs.00236
45. Ricci JE, Munoz-Pinedo C, Fitzgerald P, Bailly-Maitre B, Perkins GA, Yadava N, et al. Disruption of Mitochondrial Function during Apoptosis Is Mediated by Caspase Cleavage of the p75 Subunit of Complex I of the Electron Transport Chain. *Cell* (2004) 117(6):773–86. doi: 10.1016/j.cell.2004.05.008
46. Nopp A, Lundahl J, STridh H. Caspase activation in the absence of mitochondrial changes in granulocyte apoptosis. *Clin Exp Immunol* (2002) 128(2):267–74. doi: 10.1046/j.1365-2249.2002.01824.x
47. Keren L, Bosse M, Marquez D, Angoshtari R, Jain S, Varma S, et al. A structured tumor-immune microenvironment in triple negative breast cancer revealed by multiplexed ion beam imaging. *Cell* (2018) 174:1373–87. doi: 10.1016/j.cell.2018.08.039
48. Frankenberger C, Rabe D, Bainer R, Sankarasharma D, Chada K, Krausz T, et al. Metastasis suppressors regulate the tumor microenvironment by

blocking recruitment of prometastatic tumor-associated macrophages. *Cancer Res* (2015) 75:4063–73. doi: 10.1158/0008-5472.CAN-14-3394
49. Yuan ZY, Luo RZ, Peng RJ, Wang XX, Xue C. High infiltration of tumor-associated macrophages in triple-negative breast cancer is associated with a higher risk of distant metastasis. *Onco Targets Ther* (2014) 7:1475–80. doi: 10.2147/OTT.S61838
50. Niu M, Valdes S, Naquib YW, Hursting SD, Chi Z. Tumor-Associated macrophage-mediated targeted therapy of triple-negative breast cancer. *Mol Pharm* (2016) 13:1833–42. doi: 10.1021/acs.molpharmaceut.5b00987
51. Rath M, Müller I, Kropf P, Closs EI, Munder M. Metabolism via arginase or nitric oxide synthase: two competing arginine pathways in macrophages. *Front Immunol* (2014) 5:532. doi: 10.3389/fimmu.2014.00532
52. MacMicking J, Xie QW, Nathan C. Nathan, Nitric oxide and macrophage function. *Annu Rev Immunol* (1997) 15:323–50. doi: 10.1146/annurev.immunol.15.1.323
53. Jorgovanovic D, Song M, Wang L, Zhang Y. Roles of IFN-γ in tumor progression and regression: a review. *Biomarker Res* (2020) 8:49. doi: 10.1186/s40364-020-00228-x
54. Panariti G, Miserocch R, Rivolta I. The effect of nanoparticle uptake on cellular behavior: disrupting or enabling functions? *Nanotechnol Sci Appl* (2012) 5:87. doi: 10.2147/NSA.S25515
55. Holmberg R, Wilchek M, Marquez M, Westlin JE, Du J, Nilsson S. Ion exchange tumor targeting: A new approach. *Clin Cancer Res* (1999) 5:3056s–8s.
56. Kawai T, Kato A, Higashi H, Kato S, Naiki M. Quantitative determination of N-glycolylneuraminic acid expression in human cancerous tissues and avian lymphoma cell lines as a tumor associated sialic acid by gas chromatography-mass spectrometry. *Cancer Res* (1991) 51:1242–46.
57. Kokoglu E, Sonmez H, Uslu E, Uslu I. Sialic acid levels in various types of cancer. *Cancer Biochem Biophys* (1992) 13:57–64.
58. Lin S, Kemmner W, Grigull S, Schlag PM. Cell surface alpha 2,6 sialylation affects adhesion of breast carcinoma cells. *Exp Cell Res* (2002) 276:101–10. doi: 10.1006/excr.2002.5521
59. Kim B, Han G, Toley BJ, Kim CK, Rotello M, Forbes NS. Tuning payload delivery in tumour cylindroids using gold nanoparticles. *Nat Nanotechnol* (2010) 5:465–72. doi: 10.1038/nnano.2010.58
60. Yue ZG, Wei W, Yue H, Wang LY, Su LG, Ma GH. Surface charge affects cellular uptake and intracellular trafficking of chitosan-based nanoparticles. *Biomacromolecules* (2011) 12:2440–6. doi: 10.1021/bm101482r
61. Gakhar G, Liu H, Shen R, Scherr D, Wu DQ, Nanus D, et al. Anti-tumor effect of novel cationic biomaterials in prostate cancer. *Anticancer Res* (2014) 34:3981–90.

**Conflict of Interest:** The authors declare that the research was conducted in the absence of any commercial or financial relationships that could be construed as a potential conflict of interest.

frontiers in Oncology

REVIEW
published: 08 February 2021
doi: 10.3389/fonc.2020.606906

# Extracellular Vesicles: An Emerging Nanoplatform for Cancer Therapy

*Yifan Ma[1], Shiyan Dong[2,3], Xuefeng Li[4], Betty Y. S. Kim[5], Zhaogang Yang[2]* and Wen Jiang[2]**

[1] Department of Chemical and Biomolecular Engineering, The Ohio State University, Columbus, OH, United States, [2] Department of Radiation Oncology, University of Texas Southwestern Medical Center, Dallas, TX, United States, [3] School of Life Sciences, Jilin University, Changchun, Jilin, China, [4] Shenzhen Luohu People's Hospital, The Third Affiliated Hospital of Shenzhen University, Shenzhen, China, [5] Department of Neurosurgery, The University of Texas MD Anderson Cancer Center, Houston, TX, United States*

Extracellular vesicles (EVs) are cell-derived membrane particles that represent an endogenous mechanism for cell-to-cell communication. Since discovering that EVs have multiple advantages over currently available delivery platforms, such as their ability to overcome natural barriers, intrinsic cell targeting properties, and circulation stability, the potential use of EVs as therapeutic nanoplatforms for cancer studies has attracted considerable interest. To fully elucidate EVs' therapeutic function for treating cancer, all current knowledge about cellular uptake and trafficking of EVs will be initially reviewed. In order to further improve EVs as anticancer therapeutics, engineering strategies for cancer therapy have been widely explored in the last decade, along with other cancer therapies. However, therapeutic applications of EVs as drug delivery systems have been limited because of immunological concerns, lack of methods to scale EV production, and efficient drug loading. We will review and discuss recent progress and remaining challenges in developing EVs as a delivery nanoplatform for cancer therapy.

**Keywords: extracellular vesicle, exosome, therapeutic nanoplatform, cancer therapy, drug delivery**

OPEN ACCESS

***Edited by:***
*Luis Alexandre Muehlmann, University of Brasilia, Brazil*

***Reviewed by:***
*Gaoxing Su, Nantong University, China*
*Luca Tamagnone, Institute for Cancer Research and Treatment (IRCC), Italy*

****Correspondence:***
*Zhaogang Yang*
*zhaogang.yang@utsouthwestern.edu*
*Wen Jiang*
*wen.jiang@utsouthwestern.edu*

***Specialty section:***
*This article was submitted to Cancer Molecular Targets and Therapeutics, a section of the journal Frontiers in Oncology*

***Received:*** *16 September 2020*
***Accepted:*** *18 December 2020*
***Published:*** *08 February 2021*

***Citation:***
*Ma Y, Dong S, Li X, Kim BYS, Yang Z and Jiang W (2021) Extracellular Vesicles: An Emerging Nanoplatform for Cancer Therapy. Front. Oncol. 10:606906. doi: 10.3389/fonc.2020.606906*

## INTRODUCTION

Cell-secreted extracellular vesicles (EVs) have attracted considerable attention over the last decades. These micro- or nano-sized membrane vesicles derived from various cell types are enriched in biological fluids, such as blood plasma, serum, saliva, and urine (1–4). According to disparate biogenesis, EVs can be primarily characterized into three groups: microvesicles (MVs), exosomes, and apoptotic bodies (5). MVs, with a diameter of 100–1,000 nm, are released by outward budding and fission of the plasma membrane. Growing evidence has shown that MVs can package bioactive molecules, nucleic acids (microRNAs (miRNAs) or mRNAs), and proteins that are reflective of the original cell type (6, 7). Similarly, exosomes also contain massive and complex cargos of contents derived from parent cells. Compared with MVs, exosomes are in nanoscale sizes ranging from 30 to 150 nm and mainly originate from intracellular multivesicular bodies; then they are released into the extracellular environment by fusing multivesicular bodies with the cell membrane (8–10). Such distinction suggests that exosomes are more tightly associated with neighbor cell-to-cell communication, whereas MVs may cover distant transportation, thus enabling packaged bioactive effectors to distal sites. Other than MVs and exosomes, apoptotic bodies, with larger diameters of 500 nm to 5 μm, are shed by cells throughout the execution

phase of the apoptotic process; their function and related mechanisms are not clearly understood (11). Altogether, EVs that contain diverse cargos (proteins, RNA, DNA, and lipids) trafficked from host cells can be applied not only as mere probes for mechanistic physiology research but also as therapeutic and diagnostic agents for many diseases (12).

EVs have been identified as critical mediators of intercellular communication in both normal and pathological physiological processes, such as cell maintenance and differentiation, tissue regeneration, immune modulation, and tumor development (13–16). EVs are known to be involved in a wide range of processes that underlie tumor development, including tumor microenvironment modulation, angiogenesis, lymphogenesis and tumor invasion, progression, and metastasis (17). EVs that originated from tumor cells have been acknowledged to play a crucial role in driving tumor microenvironment cells toward exacerbating tumor development. These EVs also include specific tumor antigens that can activate a series of immunogenic responses for cancer immunotherapy. Moreover, EVs released from immune cells are known to carry specific proteins and endosome-associated peptides and can induce antigen-specific immune responses for tumor suppression, while EVs derived from mesenchymal stem cells (MSCs) are believed to be paracrine mediators for regulating immune-modulating capacity and tend to accumulate at the tumor site (18, 19). Because of their endogenous functionalities, EVs have been implicated in many aspects of cancer development and, thus, are promising biomarkers and therapeutic candidates for cancer treatment (16, 20–24). Despite multiple advantages, the application of EVs has been limited because of insufficient production and relatively low loading of the desired bioagents. Based on these inadequacies, many approaches have been explored to boost yield and incorporate biomolecules and nucleic acids into EVs for cancer therapy (25–28). Among them, physicochemical technologies, including electroporation, sonication, extrusion, freeze-thaw cycles, membrane permeabilization, and surface functionalization, have been developed to stimulate cells to secrete sufficient amount of EVs, and extracellularly or intracellularly load cargos. Another example of a technology is modification for generating engineered EVs. Besides these exogenous approaches, endogenous methods that highly rely on biological approaches at the cellular level are also known to lead to mass production of EVs and effectively enable bioagent packaging. All these methods make EVs as more attractive delivery vehicles in cancer therapy. When combined with conventional cancer therapy such as chemotherapy and immunotherapy, EVs-based antitumor treatment can be a promising candidate for future clinical application.

## EXTRACELLULAR VESICLES' ROLE IN CANCER DEVELOPMENT AND ITS THERAPEUTIC IMPLICATIONS

Readily found in different body fluids, the number of circulating EVs is significantly higher in cancer patients, as reported in previous studies (7, 29, 30). Because of its transmission capacity in the tumor microenvironment or specific distant sites, these EVs have increasingly become recognized as key players in the cellular processes related to cancer pathogenesis, including tumorigenesis, angiogenesis, tumor invasion, progression, and metastasis (**Figure 1**). When it comes to the source of circulating EVs, tumor cells are the first to dominate cancer development and affect other cells for tumor progression. As the initial step in cancer development, tumor formation involves the accumulation of genetic alterations. Tumor-derived EVs (TEVs) have been shown to directly contribute to the spread of phenotypic transformation by transferring their oncogenic traits, and therefore enroll normal cells into the tumorigenic process, enhancing tumorigenesis (32). As a major component of the tumor stroma, fibroblasts can be activated to a cancer-associated phenotype (cancer-associated fibroblasts (CAFs)) in the tumor microenvironment (33). With an abundance of TEVs and increased TGF-β, fibroblasts were shown to undergo transformation from a normal to a CAF-like phenotype when prostate cancer developed; therefore, TEVs appear to facilitate tumorigenesis (34). Another study suggested that apoptotic bodies derived from cancer cells can transfer tumor DNA from H-Ras$^{V12}$-and human c-myc-transfected rat embryonic fibroblasts (REF) to wild-type mouse embryonic fibroblasts (MEF), activating normal fibroblasts and developing the tumorigenic potential of other wild-type cells (35). Additionally, TEVs can support cancer cells to evade apoptosis and promote malignancy in recipient tumor cells. Activating PI3K/AKT and MAP/ERK pathways mediated by TEVs is a common route and has been verified in multiple cancers (36–38). Besides, a protein known as chloride intracellular channel-1 (CLIC1), found to be enriched in some TEVs, can be transferred *via* EVs into other recipient tumor cells and, thus, enhance tumor growth (39).

Tumor growth beyond microscopic size highly relies on increased angiogenesis, a process defined as the new formation of blood vessels for adequate nutrient and oxygen supply throughout tumor development. The communication promoted between tumor cells and endothelial cells and, in particular, with TEVs can facilitate endothelial angiogenic responses for further tumor progression. In most cases, angiogenesis is enhanced by upregulating endogenous vascular endothelial growth factor (VEGF) and other angiogenic signaling pathways in endothelial cells, which are ascribed to the pro-angiogenic effects of tumor-derived EVs. Many studies have reported that a series of proangiogenic cytokines are enriched in tumor-derived EVs, such as VEGF, fibroblast growth factor (FGF), interleukin (IL)-6, IL-1α, and tumor necrosis factor alpha (TNF-α), which directly contribute to tumor angiogenesis (40, 41). Moreover, TEVs have also been shown to promote angiogenesis by transferring genetic information, including messenger RNAs (mRNAs) (e.g., hypoxia inducible factor 1 (HIF-1) and VEGF), long noncoding RNA (lncRNA) (e.g., H19 lncRNA, lncRNA POU3F3 and lncRNA CCAT2), microRNAs (miRNAs) (e.g., miR-9, miR-21, miR-105, miRNA-141-3p, miR-142-3p and miR-210), and chemokine

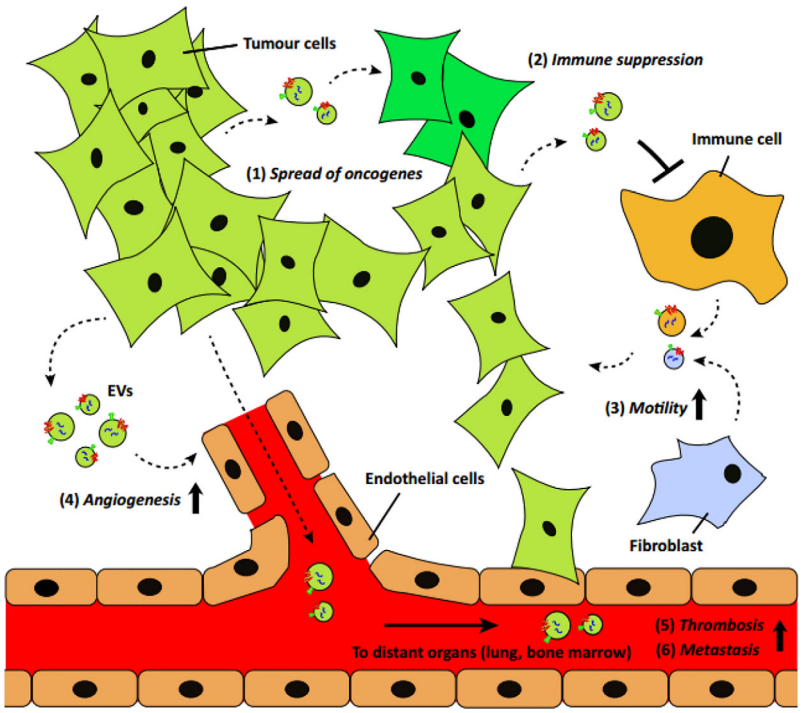


**FIGURE 1** | A schematic of EV's role in cancer development and progression (31) (with reproduction permission).

receptors (e.g., EGFR and CXCR4) (42–46). Notably, hypoxic conditions, which are often associated with tumor aggressiveness, can not only merely produce TEVs but also exert a more pronounced effect of these TEVs on ECs than the TEVs released by normoxic tumor cells. According to a glioblastoma multiforme (GBM) model in a previous study, exosomes derived from hypoxic GBM cells can program endothelial cells to secrete potent cytokines, stimulate PI3K/AKT signaling in pericytes, and, thus, facilitate tumor vascularization and pericyte vessel coverage (47). Moreover, hypoxia also results in tumor microenvironment acidification, which could further bolster tumor EVs trafficking within relevant cells and support tumor progression (48).

During tumor progression, several categories of EVs are actively involved in exerting immunostimulatory and immunosuppressive effects on the host's immune system and counteract antitumor activities. EVs, especially TEVs involved in tumor progression, are known to be closely associated with inflammatory responses and are actively engaged in deregulating the activity of various types of neighboring immune cells. Macrophages are present in all stages of tumor progression; many studies have shown that EVs released by tumor cells can transfer their cargo to macrophages and induce inflammatory responses and promote cancer progression. For example, EVs released by ovarian cancer cells could transfer oncogenic miR-1246 to M2-type tumor-associated macrophages (TAMs) and induce the secretion of tumor-supportive factors, including IL-10 and metalloproteinases (MMPs), while miR-25-3p and miR-921-3p present in EVs secreted by liposarcoma cells could stimulate the secretion of the pro-inflammatory cytokine IL-6 from macrophages, thus triggering tumor progression (49–51). Apart from macrophages, lymphocytes can be significantly modulated by TEVs for tumor progression. Recently, tumor immune evasion regulated through the inhibition of T cell function was found as a result of the binding of programmed death ligand-1 (PD-L1) to programmed cell death protein-1 (PD1). Growing evidence has also showed that PD-L1 highly expressed in TEVs from different cancer types could inhibit T cell functions and contribute to tumor progression (52–54). Furthermore, miRNAs such as miR-24-3p were found to be incorporated within TEVs, triggering T-cell dysfunction and leading to lower patient survival. Admittedly, TEVs play a crucial immunosuppressive role, which can affect the behavior of most immune cells and thus accelerate tumor progression. Notably, EVs sourced from various cancers were also shown to express specific tumor antigens that could be taken up by immune cells to induce profound tumor-specific immunological enhancement responses. From this viewpoint, TEVs that are generally considered as promoters of tumor progression can also work as therapeutic agents or cancer diagnosis and treatment signals. For instance, EVs shed by melanoma cell lines were reported to effectively activate macrophages and improve the maturation of dendritic cells (DCs) and T-cell proliferation, which subsequently promoted antitumor effects (55). In other studies, DCs primed with EVs originated from mesothelioma cells and glioblastoma cells could induce potent antitumor

responses and significantly increase survival rate (56, 57). These evidence implicated that EVs involved in cancer development could be a promising therapeutic nanoplatforms for cancer treatment.

## ENGINEERED EXTRACELLULAR VESICLES FOR CANCER THERAPY

EVs have emerged as novel and promising therapeutic agents because they can be used for a wide range of tumor-related processes and deliver therapeutic cargos, including nucleic acids and proteins, into tumor sites. Despite multiple advantages, the application of EVs for anticancer therapy has been limited because of insufficient production and relatively low loading of the desired bioagents. As such, many approaches have been explored for mass production and for incorporating a substantial amount of nucleic acids and small biomolecules into EVs. These engineering approaches can be primarily categorized into two groups: direct extracellular modification and indirect engineering of donor cells. These engineering strategies involved in current EVs-based cancer therapy will be summarized and discussed (**Figure 2**).

### Direct Extracellular Modification of Extracellular Vesicles for Cancer Therapy

Extracellular modification of EVs often refers to the direct load of cargos such as genetic elements and biomolecules or drugs and surface modification after EV isolation and purification.

### Post-Load of Cargos into Extracellular Vesicles for Cancer Therapy

Direct encapsulation of cargos into EVs often relies on a series of physical procedures or technologies including incubation, freeze-thaw cycles, electroporation, sonication, extrusion, and membrane permeabilization. Among them, incubation and freeze-thaw cycles are two of the easiest methods for engineering EVs. As for incubation, highly concentrated cargos tend to interact with the vesicle's lipid biolayers and be passively diffused into the EV cavity (58). Because of its maneuverability, researchers have widely used incubation to modify EVs for treating multiple diseases (59–61). When it comes to cancer treatment, small nucleic acids and chemotherapeutic agents (paclitaxel (PTX) and doxorubicin (DOX)) are common cargos co-incubated with endogenous EVs. In a study by Saari et al., PTX was incubated with extracted exosomes derived from prostate cancer cells at 22 °C, and the resulting loaded vesicles could enhance PTX's cytotoxic effect when treating autologous prostate cancer (62). However, the low loading capacity as well as the limited selectivity of encapsulated cargos are considered main challenges for applying this method. Alternatively, the freeze-thaw cycle is also a straightforward method where the desired cargos are incubated with EVs combined with RT, and then the mixture is processed with repeated cycles from freezing in −80 °C or liquid nitrogen to RT re-thawing to encapsulate cargos. Following this method, Goh et al. developed DOX-loaded EVs (derived from monocytes) to preferentially target cancer cells and induce apoptosis (63). Like the incubation method, the freeze-thaw cycles method for EVs engineering also suffers

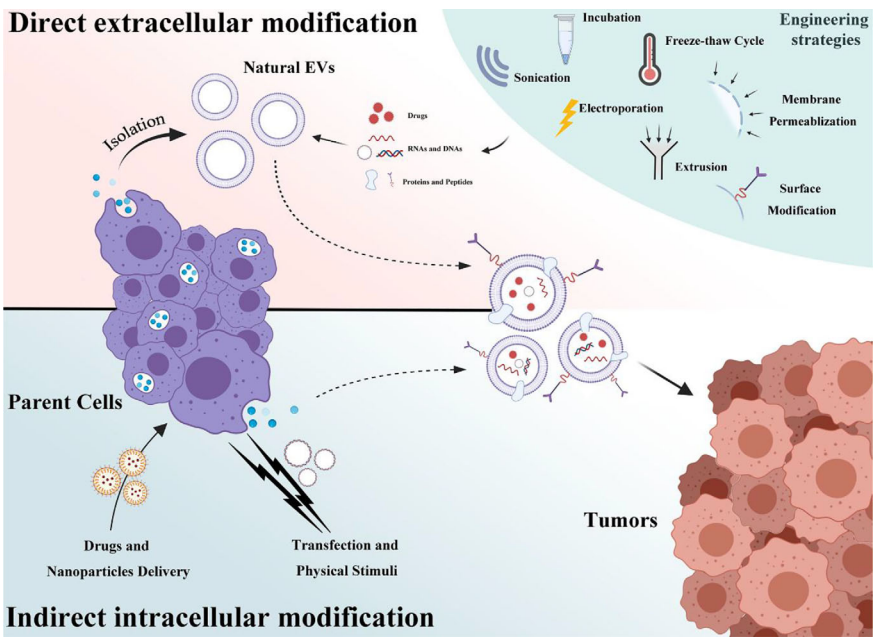


**FIGURE 2** | A schematic of EVs engineering strategies that is categorized into two groups: direct extracellular modification and indirect intracellular modification.

from inefficient cargos loading, which can be ascribed to passive diffusion as well as severe aggregation during the cycles.

For efficient cargo loading, many physical strategies have been introduced to optimize EV engineering in cancer therapy. As an established non-viral technique for traditional extracellular delivery, electroporation has been extensively used for direct engineering of EVs (64). Similarly to cell structure, EVs are composed of a bilayer lipid membrane, which allows genetic elements, small molecules, or drugs to be incorporated into their structure through pores induced by the electric field. Generally, the loading efficiency can be affected by voltage, pulse times, pulse interval, and protection buffer, and highly depends on the category of loading cargos. Cargo encapsulation into EVs *via* conventional electroporation is generally low because the lipid membrane structure of the EVs can be damaged under electric fields. Therefore, many electroporation protocols have been developed to optimize this procedure and efficiently engineer EVs. Zhang et al. introduced an miRNA loading strategy in virtue of calcium chloride-mediated electroporation into EVs for *in vitro* and *in vivo* delivery. Their results showed that specific miRNAs in exosomes could be efficiently manipulated *via* modified transfection with buffer protection (65). Nonetheless, such transfection may be associated with contaminating transfection reagents (buffer or residue cargos) in the resulting engineered EVs products, possibly impairing subsequent applications. As shown in **Figure 3A**, Pamotto et al. screened different electroporation parameters including voltages and pulses, and found that setting with 750 V and 10 pulses allowed significant miRNA enrichment. Two kinds of engineered EVs that incorporated antitumor miRNAs (miR-31 and miR-451a) showed they could silence target genes involved in anti-apoptotic pathways and, thus, promote apoptosis of the HepG2 hepatocellular carcinoma cell lines (66). In another study associated with engineered EVs for treating pancreatic cancer, Kamerkar et al. also used electroporation to enrich specific siRNA or shRNA in EVs for targeting $KRAS^{G12D}$, a common mutation in the GTPase KRAS involved in pancreatic ductal adenocarcinoma (PDAC). With a specific electroporation buffer and Gene Pulser Xcell Electroporation System (parameters: 400 V, 125 μF and ∞ ohms), $KRAS^{G12D}$ siRNA and shRNA plasmid could be efficiently encapsulated into isolated and purified exosomes. These $KRAS^{G12D}$-related engineered exosomes (also termed as iExosomes), together with the modification of CD47 peptides on the surface of iExosomes for

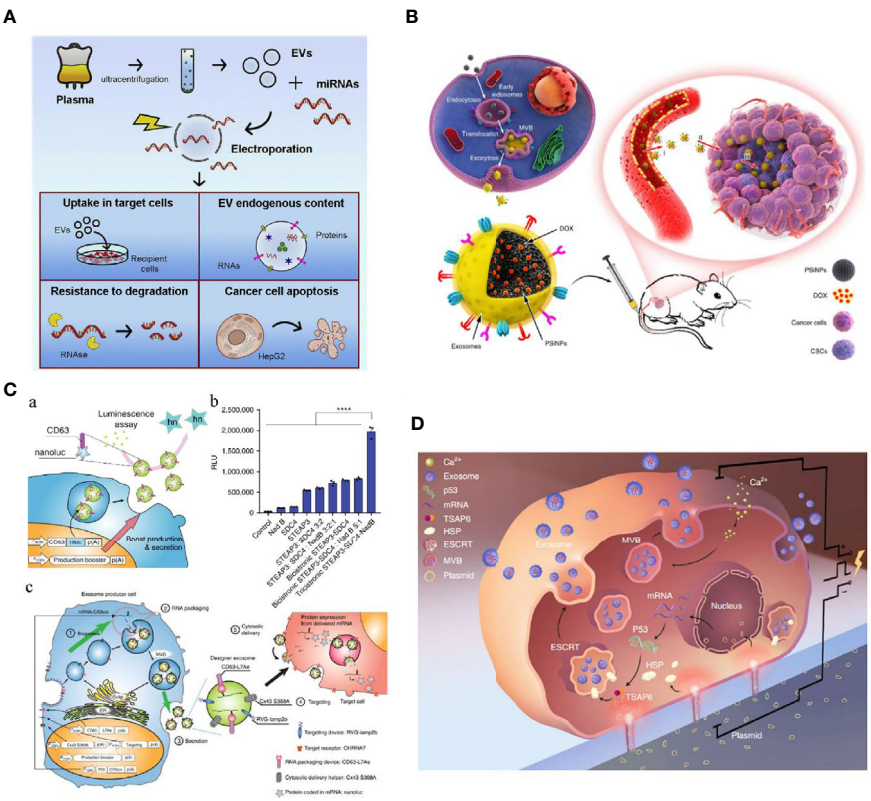


**FIGURE 3** | **(A)** Optimized electroporation parameters for direct EVs loading were screened including voltages and pulses. When the desired cargos were miRNAs, 750 V and 10 pulses showed the most significant miRNA enrichment (66). **(B)** A novel tumor-cell-exocytosed exosome-biomimetic porous silicon nanoparticles (PSiNPs) was developed through the incubation of the synthetic nanoparticles with parent cells. Such engineered exosomes significantly increased DOX loading and improved antitumor efficacy (67). **(C)** An exosomal transfer into cells (EXOtic) device enables exosome mass production and efficient exosomal mRNA delivery (68). **(D)** A cellular nanoporation (CNP) technology trigger a 50-fold increase of exosomes yield and thousand-fold increase of mRNA transcripts in the released exosomes from CNP-transfected cells release (69) (with reproduction permission).

escaping phagocytosis, can significantly suppress tumor growth in multiple mouse models of pancreatic cancer and support increased survival (70). On the basis of these promising preclinical results, a clinical trial using iExosomes to target metastatic pancreatic cancer was recently registered (NCT03608631). Together with other specific RNAs enriched in EVs for treating multiple diseases (i.e., miR-124 enriched MSCs' EVs for acute ischemic stroke, NCT03384433), these clinical trials will hopefully give us further insight into the potential of EVs as drug delivery vehicles for RNA species.

Other than electroporation, alternative approaches such as sonication, extrusion, and membrane permeabilization have also been used to engineer EVs with therapeutic agents for cancer therapy. Sonication has emerged as a potential strategy for generating engineered EVs. When compared to electroporation, EVs engineering through sonication can prevent charged cargo aggregation and also distribute cargos for cancer treatment in the EVs. Lamichhane et al. reported the efficient application of sonication for actively delivering oncogenic siRNAs into EVs. In their study, EVs could be loaded with small RNAs with no aggregation; these therapeutic EVs were taken up by HEK293T and MCF-7 and could target HER2 knockdown, thus resulting in tumor growth inhibition (71). In addition to the nucleic acids, small molecular drugs such as chemotherapeutic agents have also been applied to engineered EVs for cancer therapy. After isolating and purifying exosomes from macrophages, Kim et al. applied mild sonication to encapsulate PTX for treating multiple drug resistance cancer. According to the results, sonication delivery of PTX showed significantly better loading efficiency than routine RT incubation and electroporation. With the high payload of PTX in the engineered EVs, a potent anticancer effect was further confirmed in a tumor-bearing model (72). Extrusion is another direct extracellular approach to modify EVs. During extrusion with specific porous membrane, the EV lipid membrane tends to be disrupted, following cargzo loading into EVs. Using the extrusion method, Fuhrmann et al. showed that porphyrins could readily be loaded into exosomes collected from diverse stem cells. The authors showed that artificial exosomes produced by the extrusion method had a better anticancer effect than the exosomes prepared *via* traditional passive methods (incubation and freeze-thaw cycles). As a method based on membrane permeabilization, saponin-assisted modification has also been extensively applied to engineering EVs for cancer therapy. Unlike the strategies discussed earlier, saponin-associated approaches are based on surfactant molecules that can generate pores in the EV membrane by interacting with cholesterol during co-incubation.

The engineering methods mentioned earlier allow EVs to be more attractive delivery vehicles for cancer treatment. Physical technology-assisted approaches are definitely more potent and promising than conventional incubation or freeze-thaw cycles, where encapsulation efficiency and loading capacity are often low. Among them, electroporation was shown to be effective for post-loading cargos, while sonication, extrusion, and membrane permeabilization are rarely used. These direct engineering strategies face similar challenges associated with low EV recovery and limited cargo loading efficiency, which impair subsequent application in cancer therapy. With the physical technology applied, membrane disruption cannot be avoided and can only be partially recovered. Moreover, loading capacity and efficiency highly depend on the physicochemical properties of cargos categories and operating loading techniques. As a result, advanced strategies for improving direct EVs modification need to be developed for efficient delivery of therapeutic agents in cancer treatment.

## Surface Functionalization of Extracellular Vesicles for Tumor Targeting

EV surface is known to include membrane proteins that can contribute to their biodistribution and targeting capabilities. For cancer therapy, interest has grown in surface membrane protein modification to improve EVs' targeting efficiency to tumor sites for therapeutic functions. Multiple studies have developed extracellular strategies where isolated and purified EVs were post-handled to modify the EV surface. Multivalent electrostatic interactions and receptor-ligand binding are frequently leveraged for surface engineering of EVs. Nakase et al. exploited electrostatic interactions to bind cationic lipids to the surface of exosomes to enhance intracellular release efficiency of encapsulated cargos in the isolated exosomes. Such interactions produced exosomes with a pH-sensitive fusogenic peptide that could promote binding and uptake by targeted HeLa cells, subsequently inducing efficient cytotoxicity (73). In another study by Qi et al., receptor-ligand binding was developed to generate a dual-functional blood exosome-based superparamagnetic vehicle for cancer therapy. By conjugating transferrin-superparamagnetic nanoparticles with blood derived exosomes, enhanced tumor targeting could be observed under an external magnetic field, followed by significantly inhibiting tumor growth (74).

Many covalent approaches were also used to provide more stable surface engineering of EVs. Among multiple covalent strategies, moderate and specific cross-linking reactions are preferred because the reaction conditions for EV surface modification are in place to prevent EVs from potential disruption or aggregation due to additional buffer solution, osmotic stress, and reaction temperature. As a highly specific click reaction, azide-alkyne cycloaddition can work in aqueous media and low temperatures, rendering it ideal for EVs surface modification. Wang et al. developed a combination of metabolic labeling of newly synthesized proteins or glycan/glycoproteins of parent cells with chemically active azide groups and bioorthogonal click conjugation to engineer exosomes (75). After metabolically engineering parent cells, azide-integrated exosomes were generated, and a variety of small molecules and proteins attached on dibenzocyclooctyne-amine were specifically conjugated. These engineered exosomes have showed promise in the biomedical field because they can efficiently deliver to target sites. In a similar study, Smyth et al. developed engineered exosomes with active terminal alkyne groups (76). According to these methods, the amine groups of the exosomal proteins were first cross-linked with the carboxyl group of 4-pentynoic acid using carbodiimide activation. Then, alkyne-functionalized

EVs were conjugated with azide-fluorescence groups through a specific click reaction. These covalent approaches for direct EV surface modification seem to have more advantages than the non-covalent ones because click chemistry is considered a non-invasive strategy that allows exogenous molecules to be incorporated onto the EV surface, with no negative effects on EVs' physicochemical characteristics. However, only a few reports on engineered EVs used for cancer therapy are available. As such, more systematic studies are needed to support their use in cancer treatment, especially targeting efficiency and safety.

## Indirect Intracellular Modification for Engineering Extracellular Vesicles

Indirect intracellular modification is another promising strategy for massively producing artificial EVs. With this approach, parental cells are initially manipulated through physical or genetic approaches, so they can release the engineered EVs. Many cancer researchers have used this concept to endogenously package specific substances into EVs by simply incubating donor cells with the desired cargos, particularly chemotherapeutic agents. In a study conducted by Pascucci et al., PTX was initially co-incubated with bone marrow stromal cells for 24 h. PTX-loaded-exosomes primed with high dose of PTX were then recovered. The results showed that such PTX-engineered exosomes could significantly inhibit the proliferation of CFPAC-1 human pancreatic cells (77). Moreover, studies found that anticancer drugs could stimulate donor cells to secret more EVs with enriched therapeutic agents being packaged, thereby contributing to tumor suppression. According to Lv et al., co-incubating PTX and hepatocellular carcinoma cells (HepG2) *in vitro* could simultaneously increase exosome secretion and exosomal heat shock proteins (HSPs) loading. Notably, these engineered exosomes led to immunogenic responses and, thus, to increased NK cell cytotoxicity toward cancer cells (78). Considering the low efficiency of drug encapsulation, another study (**Figure 3B**) led by Yang et al. developed tumor-cell-exocytosed exosome-biomimetic porous silicon nanoparticles (PSiNPs) as drug carriers, greatly increasing drug loading. The authors claimed that engineered exosomes could be exocytosed from tumor cells after incubating with DOX@PSiNPs. These exosomes effectively augmented *in vivo* DOX enrichment in total tumor cells and significantly improved anticancer efficacy (67). Other than routine chemotherapeutic drugs, other therapeutic substances were also applied for indirect intracellular modification. In a study by Behzadi et al., an HSP70-enriched cell lysate was introduced into J774 cells to obtain the desired exosomes. After incubation, HSP70-loaded exosomes could be recovered from conditioned medium and were found to play an immunoadjuvant role in cancer immunotherapy and significantly delay the occurrence of fibrosarcoma tumors (79). Certainly, not all substances can readily enter parent cells and be encapsulated into EVs by simple incubation because hydrophobic/hydrophilic and charging properties of the substances will greatly influence this process and ultimate loading efficiency. That is, other external assistance and physical or genetic technologies need to be introduced to optimize indirect EV engineering for cancer therapy.

External stresses, such as starvation, hypoxia, and heat treatment through which cells can be activated to produce functional EVs have been gaining interest. For example, previous studies have observed that umbilical-derived MSCs and human leukemia cell line (K562) under hypoxia profoundly elevated EV secretion; these EVs promoted angiogenesis more effectively than EVs from normoxic cells. Further scrutiny revealed that hypoxic exosomes contained abundant amounts of miRNAs (e.g. miRNA-150 and miRNA-210) which could target angiogenesis signaling pathways (80–82). Similar results were reported when cells are under other cellular stresses. Despite the useful strategies used to produce EVs by incorporating a few genetic messages, only moderate EVs can be released and limited cargos can be encapsulated for cancer treatment. To improve modification efficiency, parent cell transfection is the most widely used and efficient method. Ding et al. delivered exogenous miRNA into exosomes produced by human umbilical cord mesenchymal stromal cells (hucMSCs) through lipofectamine transfection. After hucMSCs transfection, miR-145−5p accumulation was detected in hucMSC-derived exosomes, which were shown to effectively inhibit PDAC cells proliferation and invasion *in vitro*, and significantly reduce the growth of xenograft PDAC tumors *in vivo* (83). With the assistance of vector transfection, Ohno et al. also showed that the Let-7a-loaded exosomes could effectively target recipient tumor cells after engineering their surface with targeting peptides (GE11 and EGF). They also showed that intravenously-injected engineered exosomes could accumulate in the tumor site and effectively suppress tumor growth (84). Many studies have recently focused on approaches that cannot merely enrich EVs' contents but increase EVs' production. In a recent study by Ibrahim et al., skin fibroblasts engineered by canonical Wnt signaling (overexpress β-catenin and the transcription factor Gata4) were turned to a exosome factory that promoted exosome secretion with specific therapeutic functions (85). Moreover, Ryosuke et al. (**Figure 3C**) developed a novel exosomal transfer into cells (EXOtic) device that enables exosome mass production and efficient exosomal mRNA delivery. By transfecting CD63 plasmids in parent cells with encoding candidates, including STEAP3, syndecan-4 (SDC4), and a fragment of L-aspartate oxidase (NadB), the exosomes yield could be boosted by over 40-fold. Also, a specific packaging device, archaeal ribosomal protein L7Ae, and a cytosolic delivery helper, connexin 43 (Cx43), were used to deliver mRNA into the cytosol of target cells and, thus, produce mRNA-engineered exosomes. By combining these two synthetic bioinspired devices, many exosomes with enriched cargos could be delivered to the desired sites for therapeutic functions (68). Because of the exciting results found for treating other diseases, these promising biological endogenous EVs engineering methods can provide a new horizon of engineered EVs for cancer therapy. In addition to endogenous loading *via* lipid transfection and biological approaches, physical transfection is another promising strategy for therapeutic cargo encapsulation during EV biogenesis. As shown in **Figure 3D**, Yang et al. developed a cellular nanoporation (CNP) technology

through which functional mRNAs can be encapsulated into exosomes *via* physical nanoelectroporation. Interestingly, a 50-fold increase of exosomes yield and thousand-fold increase of mRNA transcripts could be observed when compared with traditional bulk electroporation. These PTEN-engineered exosomes were simultaneously functionalized with targeting peptide-modified CD47 and were shown to successfully cross the brain blood barrier for targeting restored tumor suppressor function, enhance inhibition of tumor growth, and increase survival (69). Although these indirect intracellular modification methods can be mass produced and widely enrich EV function, the major challenges are that the amount of active substances encapsulated in EVs cannot be quantified precisely, and the extraction yield and purity of the cargo-loaded EVs obtained by this method are relatively low. Hence, more systematic studies and appropriate analytic tools associated with EVs engineering, and also advanced purification technologies are needed to be developed for applying these therapeutic EVs' in cancer therapy.

## EXTRACELLULAR VESICLES' ROLE IN DIFFERENT CANCER THERAPIES

Three subsections of EVs-based anticancer treatment are included: cancer chemotherapy, immunotherapy and phototherapy (67, 86–89). Because of their low toxicity and ability to get through biological barriers to reach remote tissues, EV-based platforms have been designed for shuttling chemotherapeutics to the desired tumor tissue. Besides, endogenous functionalities ascribed to self-carrying specific proteins, trans-membrane markers, and tumor antigens make EVs promising immunotherapeutic platforms.

### Extracellular Vesicles Involved in Cancer Chemotherapy

Chemotherapy is one of the gold standards in cancer treatment. In addition to cytotoxic side effects, pro-metastatic effects of chemotherapy are important and should be addressed. Keklikoglou et al. reported pro-metastatic effects triggered by chemotherapy in a breast cancer model (90). Two broadly used cytotoxic drugs, taxanes and anthracyclines, were found to enhance the pro-metastatic ability of tumor-derived EVs, which were enriched with annexin A6 (ANXA6), a protein that promotes the activation of NF-κB-dependent endothelial cells (**Figure 4A**). Moreover, ANXA6 was also abundant in EVs of breast cancer patients who received neoadjuvant chemotherapy. The expression of cytokines (e.g., C-C motif chemokine ligand 2 (CCL2)) that facilitate mammary tumor metastasis was also examined using tumor-free and 4T1-mCh tumor-bearing *Rag1*$^{-/-}$ mice. CCL2 was upregulated in mice treated with PTX. In addition, Ly6C$^{+}$CCR2$^{+}$ monocytes that trigger metastasis of mammary tumors were also found to be higher, which is inconsistent with the expression of CCL2, which is known to enhance the establishment of Ly6C$^{+}$CCR2$^{+}$ monocyte-assisted lung metastasis (93, 94). Also, Andrade et al. found that more EVs were secreted by melanoma cells after temozolomide and cisplatin treatment; these EVs facilitated re-growth of melanoma *in vivo* (95).

Growing evidence indicates that chemotherapy-induced EVs and the cargos they carry caused chemoresistance in addition to altering tumor behavior and promoting inflammation in the tumor microenvironment. Kreger et al. found that EVs secreted from breast cancer MDA-MB231 cells treated with paclitaxel contained abundant surviving cargo molecules associated with therapy resistance (96). In another study, apoptotic glioblastoma multiforme cells after chemotherapeutic treatment could generate more apoptotic EVs enriched with spliceosomes (e.g., RBM111, a representative splicing factor), which would also promote proliferation and therapy resistance *via* altering RNA splicing in recipient cells (97). The same effect was found not only in solid tumors but also in blood cancers. A study conducted using bone marrow stromal cell-derived exosomes also proved to induce drug resistance to bortezomib in myeloma cells (98). Kim et al. investigated chemodrug resistance in multidrug resistance tumor cells using PTX-loaded exosomes (72). According to the results, cytotoxicity was found to increase more than 50 times in drug-resistant tPgp protein-overexpressing Madin-Darby canine kidney $MDCK_{MDR1}$ cells. Moreover, potent antitumor effects were observed when these PTX-loaded exosomes were used in a Lewis Lung Carcinoma (LLC) model through airway delivery. Notably, 97.9 ± 2.0% of exosomes were found to be co-localized with lung metastases, revealing an effective targeting of the exosomes. Similarly, autologous prostate cancer-derived EVs were proved to be effective drug carriers to deliver PTX to cells they originated from and increased cytotoxicity was observed because drugs were delivered through an endocytic pathway (62). In PC-3 cells, the cytotoxic effects could reach the most significant when doses of PTX was over 50 nM, while the cytotoxic effects of PTX at 10 nM and below was significantly weaker. The maximum decrease of PC-3 cells' viability was around 60% after 48 h, while in LNCaP cells, the maximum decrease of cell viability was up to 80% regardless of the dose. Even though improved cytotoxicity was found when using cancer-cell derived EVs, cancer cell viability was enhanced when non-drug loaded EVs were involved. Therefore, several clinical trials (i.e., NCT01854866) using tumor-derived EVs plus with chemotherapeutic drugs was initiated to further evaluate their performance.

MSC-derived exosomes are good candidates for drug delivery in tumor therapy because of their reduced intrinsic immunogenicity. Melzer et al. incubated MSCs with taxol for 24 h and showed the efficiency of taxol-loaded MSC-derived exosomes in targeting primary tumors and metastases (99). In vitro studies showed that equivalent cytotoxic effects were achieved between exosomes and taxol substances, although a 7.6-fold reduced taxol concentration in exosomes was applied. Also, a 60% reduction of primary tumors and 50% reduction of distant organ metastases were observed in breast tumor mouse models using MSC taxol exosomes and taxol. In contrast, the concentration of taxol in exosomes was 1,000-fold lower than with taxol substances to obtain similar results. Other than stems cells, Tian et al. showed that exosomes derived from mouse immature dendritic cells (imDCs) and encapsulated with doxorubicin (Dox) *via* electroporation with up to 20% efficiency facilitated *in vitro*

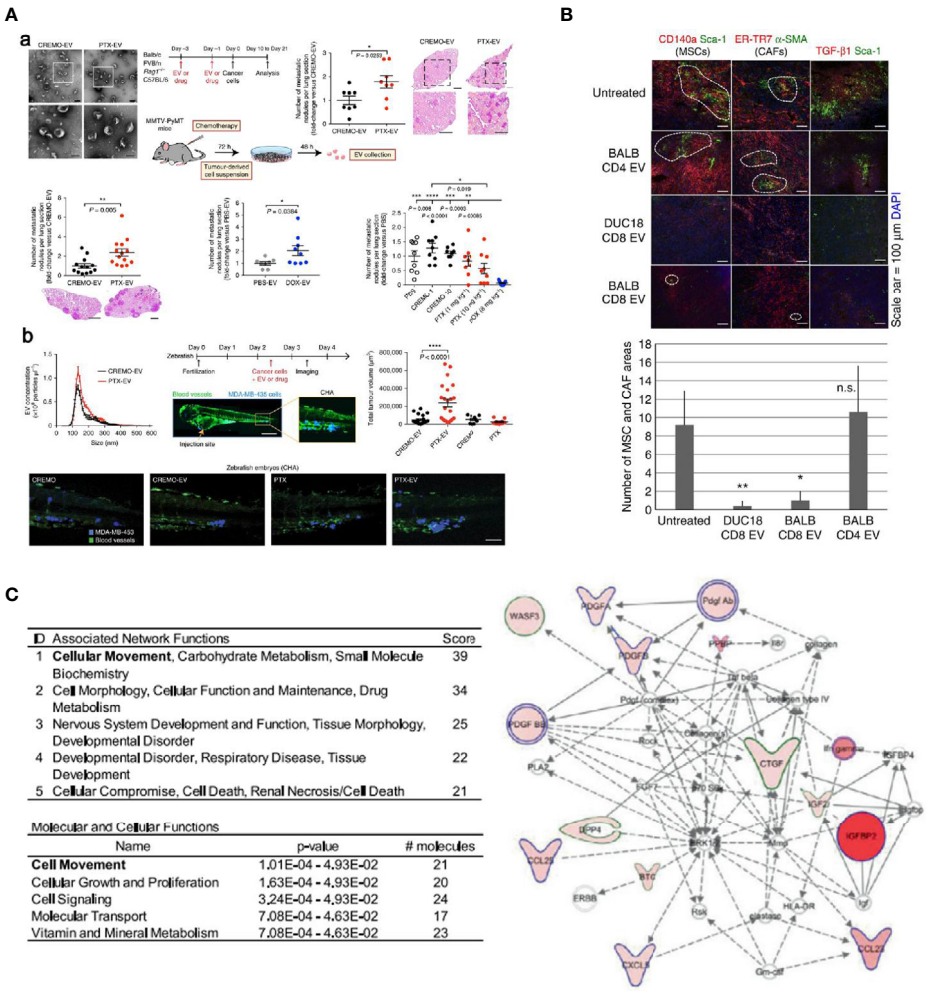


| ID | Associated Network Functions | Score |
|---|---|---|
| 1 | **Cellular Movement**, Carbohydrate Metabolism, Small Molecule Biochemistry | 39 |
| 2 | Cell Morphology, Cellular Function and Maintenance, Drug Metabolism | 34 |
| 3 | Nervous System Development and Function, Tissue Morphology, Developmental Disorder | 25 |
| 4 | Developmental Disorder, Respiratory Disease, Tissue Development | 22 |
| 5 | Cellular Compromise, Cell Death, Renal Necrosis/Cell Death | 21 |

Molecular and Cellular Functions

| Name | p-value | # molecules |
|---|---|---|
| **Cell Movement** | 1,01E-04 - 4,93E-02 | 21 |
| Cellular Growth and Proliferation | 1,63E-04 - 4,93E-02 | 20 |
| Cell Signaling | 3,24E-04 - 4,93E-02 | 24 |
| Molecular Transport | 7,08E-04 - 4,63E-02 | 17 |
| Vitamin and Mineral Metabolism | 7,08E-04 - 4,63E-02 | 23 |

**FIGURE 4** | **(A)** EVs elicited from two cytotoxic drugs, taxanes and anthracyclines, were found to enhance the pro-metastatic ability in mouse **(a)** and zebrafish **(b)** tumor models (90). **(B)** EVs collected from activated CD8+ T cells were found to be actively involved in interrupting fibroblastic stroma-mediated tumor progression by depleting tumor mesenchymal cells (91). **(C)** Molecular profile of radiation-derived exosomes demonstrated that radiation increased the exosomal proteins related to tumor migration and progression (92) (with reproduction permission).

and *in vivo* anti-tumor effects (87). Briefly, imDCs were engineered to express a well-characterized exosomal membrane protein (Lamp2b) fused to an αv integrin-specific iRGD peptide. Consequently, iRGD exosomes could target αv integrin-positive breast cancer cells. Overall, high targeting efficiency and the ability to inhibit tumor growth without overt toxicity were achieved using this proposed platform. Exosome-biomimetic nanoparticles also exerted satisfactory effects for targeted chemotherapy as drug carriers. As aforementioned (**Figure 3C**), a novel tumor-cell-exocytosed exosome-biomimetic PSiNPs that contained with exosome-sheathed DOX loading was developed for cancer chemotherapy (67). PSiNPs were produced using the electrochemical etching method (100) by stirring the DOX solution with PSiNPs to obtain DOX@E-PSiNPs. Subsequently, cells were treated with either PSiNPs or DOX@PSiNPs to form DOX@E-PSiNPs. This technology resulted in anticancer activity and cancer stem cell reduction in various tumor models with high cellular uptake and cytotoxicity effects.

## Extracellular Vesicle-Based Cancer Immunotherapy

EVs are known to play integral roles in tumor development and progression. According to multiple studies, EVs derived from immune cells are primed with specific proteins and endosome-associated peptides, while EVs secreted by tumor cells contain specific tumor antigens. Because of their endogenous functionalities, EVs have been identified as promising immunotherapeutic nanoplatforms for cancer treatment. In terms of excreting cells, EV-based cancer immunotherapy can be mainly categorized into two groups: TEVs and immune cells-derived EVs (ICEVs).

TEVs are more productive than other kinds of EVs because tumor cells tend to be more aggressive under specific tumor

microenvironments and stimuli during development, including pH and hypoxic conditions. As mentioned earlier, these TEVs have been known to play a crucial role in promoting tumor progression by transferring their specific cargos between tumor cells and related cells. Otherwise, these secretions were also found to express specific tumor antigens that could be taken up by immune cells to induce profound tumor-specific CTL responses. Many studies have exploited this TEV function to develop specific immunogenic responses for cancer immunotherapy. In studies by Mahaweni et al. and Liu et al., DCs primed with exosomes that were isolated from mesothelioma cells and glioblastoma cells could induce significant antitumor responses and resulted in increased survival rates (56, 57). Menay et al. found that exosomes isolated from ascites of murine T cell lymphoma could markedly induce specific Th1 responses and increase CD4+ and CD8 + T cells by secreting IFN-γ, thus prolonging survival (101). Moreover, the efficacy of immunogenic activation induced by TEVs can be improved by incorporating stimulating drugs and TEV modification. For instance, Xiao et al. investigated antitumor efficacy after co-delivering DCs/pancreatic cancer cell-derived exosomes and cytotoxic drugs for treating pancreatic cancer. The authors found that including sunitinib and gemcitabine with DCs/Exo could significantly induce higher cytotoxic T-cell activity and more prolonged survival times than each treatment alone (102). As for TEV modification, Koyama et al. introduced a *Mycobacterium tuberculosis* antigen, early secretory antigenic target-6 (ESAT-6), into exosomes sourced from B16 melanoma cells through transfection and found that the engineered exosomes could remarkably suppress tumor growth in syngeneic B16 tumor-bearing mice. Dai et al. modified colorectal tumor-derived exosomes by incorporating IL-18 and indicated that these modified exosomes induced better DC maturation and T cell activation than unmodified exosomes. Similar results obtained by Yang et al. showed that engineered exosomes derived from IL-2-modifed ovalbumin (OVA)-expressing EL-4 lymphoma cells (Exo/IL-2) effectively inhibited tumor growth (103). These TEVs could trigger potent immune responses that may be beneficial in cancer immunotherapy. Notably, some TEVs also showed negative immunosuppressive properties and contributed to inhibiting immune activation and, thus, to evading immune surveillance. Multiple studies have recently focused on immune checkpoint receptor ligand PD-L1 that highly expressed TEVs and substantially contributed to immunosuppressive phenotypes in different cancer types (52–54). In this respect, the specific effects and functions of TEVs in immunity remain unclear, thus, more detailed studies associated with the therapeutic functions of TEVs are needed in cancer immunotherapy.

ICEVs, especially DCs-derived EVs, have been widely explored as the other primary source of EVs for cancer immunotherapy. Reports have suggested that these EVs carried MHC complexes and T cell co-stimulatory molecules that could activate T cells and present their antigens, thereby stimulating antigen-specific CD8+ and CD4+ immune responses for tumor suppression (86, 104). Moreover, DC-derived EVs have also been reported to activate natural killer (NK) cells and lead to the proliferation of NK cells for tumor suppression. According to multiple studies, trans-presentation of TNF, BAT3, NKG2D, IL-15Rα, and rhIL-15 in DCs-derived EVs were found to be the mechanism involved in NK cells' ability to inhibit tumor growth (105–107). In clinical studies of EVs, DCs-derived EVs were firstly used to validate EVs' safety and anti-tumor responses in cancer treatment. In 2005, DCs-derived exosomes pulsed with tumor antigenic peptides were found to be safe in patients with metastatic melanoma and non-small cell lung cancer in two phase I clinical trials (108, 109). Despite feasibility and safety of EV administration, the beneficial effects of the therapy seemed to be minor or negligible. In other phase II trials conducted in non-small cell carcinoma patients, exosomes derived from IFN-γ over-expressed DCs were reported to highly improve the function of NK cells; about 32% of patients experienced stabilization without tumor progression for over 4 months after chemotherapy. Although these clinical trials associated with DCs-derived EVs presented undesirable efficacy, the ICEVs' therapy was found to be safe and feasible, paving the way for the ensuing clinical trials using EVs from other source or engineered EVs. Also, EVs that originated from T cells, NK cells, and macrophages can also be used as potent agents for inducing immunogenic functions in cancer immunotherapy. Growing evidence has indicated that regulatory T cell-derived EVs can work as suppressors against pathogenic Th1 responses through miRNAs (91). More specifically, Seo et al. reported that EVs collected from activated CD8+ T cells could be actively involved in interrupting fibroblastic stroma-mediated tumor progression by depleting tumor mesenchymal cells (**Figure 4B**). A similar activity was also observed in NK cell-derived EVs. Zhu et al. found that NK cell-derived EVs showed a significant cytolytic effect against multiple cells from glioblastoma, breast cancer, and thyroid cancer; the involvement of IL-15 could effectively increase the immunotherapeutic effects of NK cells-derived EVs (110). In addition to T cells and NK cells, EVs derived macrophages have also been considered a promising immunotherapeutic nanoplatform in combination with chemotherapy for treating cancer. Various chemotherapeutic drugs, such as PTX and DOX, have been encapsulated within macrophages-derived EVs. All these studies confirmed the therapeutic benefit of EVs, which significantly increased antitumor effects when combined with chemotherapeutic drugs (34, 72, 111, 112).

## Extracellular Vesicles Involved in Cancer Radiotherapy

Radiotherapy has been widely used to clinically treat localized cancer because of minimal invasiveness, low adverse effects, and outstanding selectivity and reproducibility. Rising evidence presented that EVs play a critical role in the cancer radiotherapy and greatly affect the tumor progression and therapeutic responses. As a primary light source, radiation has been well known as a powerful strategy to induce distinct tumor cell death process. During the apoptotic process, a series of pro-inflammatory cytokines including tumor-associated antigens (TAAs) and damage-associated molecular pattern (DAMPs) tend to be overexpressed, which can further trigger antitumor immunity. Based on this mechanism, several research found that radiation can also enrich EVs with a variety of TAAs and DAMPs and

contribute to the antitumor immunity. In a study conducted by Lin et al., EVs derived from irradiated tumor cells were demonstrated to trigger antitumor immunity against tumor growth and metastasis by enhancing CD8+ and CD4+ T cells infiltration (113). Notably, a novel TAAs, CUB domain-containing protein 1 (CDCP1) was found in radiation-induced EVs and this antigen could be hopefully developed as a peptide vaccine for potent antitumor immune responses. In another study, Farias et al. showed that exosomes derived from MSCs, combined with radiotherapy, could lead to a significant enhancement of radiation-induced tumor apoptosis and metastatic tumor foci in a melanoma mouse model, suggesting that exosome-derived factors could be therapeutic after treatment of the tumors with radiation plus MSCs (114). These studies clearly presented a positive appearance of EVs induced by radiation against tumor; however, more reports indicated that radiation-derived EVs could exert negative effects on the cancer treatment. Growing evidence suggests that radiation-induced EVs are crucial driver in promoting tumor cell motility and assisting in the pre-metastatic niche formation in glioblastoma (GBM), lung cancer and head and neck squamous cell carcinoma (HNSCC). Arscott et al. reported that radiation-derived exosomes could significantly enhance the migration of receiving cells when compared to the exosomes derived from nonirradiated cells (92). These aggressively released EVs derived from cells after radiation exposure were altered in composition and became more oncogenic than normal EVs. According to the profiling results, radiation increased the exosomal connective tissue growth factor (CTGF) and insulin like growth factor binding protein 2 (IGFBP2) proteins, both of which were ascribed to favor tumor migration and progression (**Figure 4C**). Similarly, Zheng et al. recently found that tumor angiogenesis effect could be enhanced by exosomes when lung cancer cells were exposed to radiation. In this process, miR23 was enriched in these radiation-induced exosomes, subsequently mediating PTEN downregulation and facilitating tumor progression (115). Moreover, EVs has been widely identified as one of the crucial factors of in the development of radioresistance. Multiple studies found exosomes could increase radioresistance in GBM), lung cancer and HNSCC through exosomal miRNAs (e.g., miR-208a and miR-889), non-coding RNAs (e.g., circATP8B4 and AHIF), mRNA (e.g. CCND1, WWC1 and DNM2), and pathways crosstalk (e.g., AKT/mTOR and STAT1/NOTCH3) (116–120). Based on the aforementioned studies, EVs' roles involved in phototherapy for cancer treatment are controversial and complicated, and could be affected by many factors such as various tumor types, tumor microenvironment and combinations with other therapies. As such, further preclinical and clinical studies are warranted for a more explicit version of EVs-based cancer phototherapy.

## CONCLUSION AND FUTURE PERSPECTIVES

Over the last decade, awareness in EVs in cancer development and progression has increased, and using EVs-based nanoplatforms for cancer treatment has advanced. We have discussed multiple kinds of EVs derived from different parent cells that are actively involved in tumorigenesis and progression, as well as their roles, functions, and potential in cancer diagnostics and therapeutics. Because of the specific roles of EVs in cancer development and promising potential application as therapeutic agents for cancer therapy, studies have focused on resolving limited production and inadequate content loading within EVs. Current engineering strategies, including both direct extracellular modification and indirect engineering of donor cells, make EVs as more attractive delivery vehicles in cancer therapy. In combination of conventional cancer therapies, such as chemotherapy and immunotherapy, the clinical use of EVs-based therapy will hopefully become feasible. Despite numerous exciting results in preclinical studies, many challenges remain and, thus, more systematic studies are needed to improve clinical translation. The main challenge EVs-based applications are facing is whether their use from allogenic sources will initiate immune responses or other negative responses. In other words, safety after uptake is a major challenge. As mentioned in earlier, EVs may function differently because they are delivery nanoplatforms derived from different parent cells sources. Some TEVs were found to have specific immunogenic responses for tumor suppression, while others may have immunosuppressive properties and contribute to inhibiting immune activation. Also, safety concerns exist. Therefore, more fundamental studies related to the specific roles of EVs from different sources in tumor development and their therapeutic functions are needed in EVs-based cancer therapy. Challenges in using engineered EVs and, especially, direct engineering strategies, include low EV recovery and limited cargos loading efficiency, which impair their application in cancer therapy to some extent. Several indirect intracellular manipulations that modified EVs through engineering parent cells have emerged, simultaneously increasing EV mass production and enriching cargos encapsulation. However, low isolation yield and inadequate purification of EVs after donor cell modification are current limitations along with potential safety issues. Moreover, because precisely quantifying active substances encapsulated in EVs is a concern, appropriate analytic platforms are required. Despite these challenges, EV-based cancer therapy is highly promising and may lead to advancing future cancer treatment.

## AUTHOR CONTRIBUTIONS

All the authors contributed to the writing of the manuscript. All authors contributed to the article and approved the submitted version.

## FUNDING

This work was partially supported by the Innovation Program of Shenzhen (Grant No. JCYJ20180508165208399) (XL) and China Postdoctoral Science Foundation (2018M640834 and 2019T120756) (XL).

## ACKNOWLEDGMENTS

We thank Dr. Damiana Chiavolini for scientific editing.

## REFERENCES


1. Witwer KW, Buzás EII, Bemis LT, Bora A, Lässer C, Lötvall J, et al. Standardization of sample collection, isolation and analysis methods in extracellular vesicle research. *J Extracell Vesicles* (2013) 2(1):20360. doi: 10.3402/jev.v2i0.20360
2. Zhang Y, Liu Y, Liu H, Tang WH. Exosomes: biogenesis, biologic function and clinical potential. *Cell Biosci* (2019) 9(1):19. doi: 10.1186/s13578-019-0282-2
3. Lee LJ, Yang Z, Rahman M, Ma J, Kwak KJ, Mcelroy J, et al. Extracellular mRNA Detected by Tethered Lipoplex Nanoparticle Biochip for Lung Adenocarcinoma Detection. *Am J Respir Crit Care Med* (2016) 193 (12):1431–3. doi: 10.1164/rccm.201511-2129LE
4. Wang X, Kwak KJ, Yang Z, Zhang A, Zhang X, Sullivan R, et al. Extracellular mRNA detected by molecular beacons in tethered lipoplex nanoparticles for diagnosis of human hepatocellular carcinoma. *PloS One* (2018) 13(6): e0198552. doi: 10.1371/journal.pone.0198552
5. Zaborowski MP, Balaj L, Breakefield XO, Lai CP. Extracellular Vesicles: Composition, Biological Relevance, and Methods of Study. *BioScience* (2015) 65(8):783–97. doi: 10.1093/biosci/biv084
6. Samanta S, Rajasingh S, Drosos N, Zhou Z, Dawn B, Rajasingh J. Exosomes: new molecular targets of diseases. *Acta Pharmacol Sin* (2018) 39(4):501–13. doi: 10.1038/aps.2017.162
7. Ma C, Jiang F, Ma Y, Wang J, Li H, Zhang J. Isolation and Detection Technologies of Extracellular Vesicles and Application on Cancer Diagnostic. *Dose-Response* (2019) 17(4):1559325819891004. doi: 10.1177/1559325819891004 1559325819891004.
8. Doyle LM, Wang MZ. Overview of Extracellular Vesicles, Their Origin, Composition, Purpose, and Methods for Exosome Isolation and Analysis. *Cells* (2019) 8(7):727. doi: 10.3390/cells8070727
9. Hessvik NP, Llorente A. Current knowledge on exosome biogenesis and release. *Cell Mol Life Sci* (2018) 75(2):193–208. doi: 10.1007/s00018-017-2595-9
10. Liu Y, Ma Y, Zhang J, Yuan Y, Wang J. Exosomes: A Novel Therapeutic Agent for Cartilage and Bone Tissue Regeneration. *Dose-Response* (2019) 17 (4):1559325819892702. doi: 10.1177/1559325819892702 1559325819892702.
11. Battistelli M, Falcieri E. Apoptotic Bodies: Particular Extracellular Vesicles Involved in Intercellular Communication. *Biology* (2020) 9(1):21. doi: 10.3390/biology9010021
12. Lee Y, El Andaloussi S, Wood MJA. Exosomes and microvesicles: extracellular vesicles for genetic information transfer and gene therapy. *Hum Mol Genet* (2012) 21(R1):R125–34. doi: 10.1093/hmg/dds317
13. Yáñez-Mó M, Siljander PRM, Andreu Z, Bedina Zavec A, Borràs FE, Buzas EII, et al. Biological properties of extracellular vesicles and their physiological functions. *J Extracell Vesicles* (2015) 4(1):27066. doi: 10.3402/jev.v4.27066
14. Simeone P, Bologna G, Lanuti P, Pierdomenico L, Guagnano MT, Pieragostino D, et al. Extracellular Vesicles as Signaling Mediators and Disease Biomarkers across Biological Barriers. *Int J Mol Sci* (2020) 21 (7):2514. doi: 10.3390/ijms21072514
15. Becker A, Thakur BK, Weiss JM, Kim HS, Peinado H, Lyden D. Extracellular Vesicles in Cancer: Cell-to-Cell Mediators of Metastasis. *Cancer Cell* (2016) 30(6):836–48. doi: 10.1016/j.ccell.2016.10.009
16. Kalluri R. The biology and function of exosomes in cancer. *J Clin Invest* (2016) 126(4):1208–15. doi: 10.1172/JCI81135
17. Xu R, Rai A, Chen M, Suwakulsiri W, Greening DW, Simpson RJ. Extracellular vesicles in cancer — implications for future improvements in cancer care. *Nat Rev Clin Oncol* (2018) 15(10):617–38. doi: 10.1038/s41571-018-0036-9
18. Abreu SC, Weiss DJ, Rocco PRM. Extracellular vesicles derived from mesenchymal stromal cells: a therapeutic option in respiratory diseases? *Stem Cell Res Ther* (2016) 7(1):53. doi: 10.1186/s13287-016-0317-0
19. Lai P, Weng J, Guo L, Chen X, Du X. Novel insights into MSC-EVs therapy for immune diseases. *Biomarker Res* (2019) 7(1):6. doi: 10.1186/s40364-019-0156-0
20. Skog J, Würdinger T, Van Rijn S, Meijer DH, Gainche L, Curry WT, et al. Glioblastoma microvesicles transport RNA and proteins that promote tumour growth and provide diagnostic biomarkers. *Nat Cell Biol* (2008) 10(12):1470–6. doi: 10.1038/ncb1800
21. Melo SA, Luecke LB, Kahlert C, Fernandez AF, Gammon ST, Kaye J, et al. Glypican-1 identifies cancer exosomes and detects early pancreatic cancer. *Nature* (2015) 523(7559):177–82. doi: 10.1038/nature14581
22. Costa-Silva B, Aiello NM, Ocean AJ, Singh S, Zhang H, Thakur Basant K, et al. Pancreatic cancer exosomes initiate pre-metastatic niche formation in the liver. *Nat Cell Biol* (2015) 17(6):816–26. doi: 10.1038/ncb3169
23. Kahlert C, Kalluri R. Exosomes in tumor microenvironment influence cancer progression and metastasis. *J Mol Med* (2013) 91(4):431–7. doi: 10.1007/s00109-013-1020-6
24. Sun J, Yang Z, Teng L. Nanotechnology and Microtechnology in Drug Delivery Systems. *Dose Response* (2020) 18(2):1559325820907810. doi: 10.1177/1559325820907810 1559325820907810.
25. El Andaloussi S, Mäger I, Breakefield XO, Wood MJA. Extracellular vesicles: biology and emerging therapeutic opportunities. *Nat Rev Drug Discovery* (2013) 12(5):347–57. doi: 10.1038/nrd3978
26. Yeo RWY, Lai RC, Zhang B, Tan SS, Yin Y, Teh BJ, et al. Mesenchymal stem cell: An efficient mass producer of exosomes for drug delivery. *Adv Drug Deliv Rev* (2013) 65(3):336–41. doi: 10.1016/j.addr.2012.07.001
27. Kao C-Y, Papoutsakis ET. Extracellular vesicles: exosomes, microparticles, their parts, and their targets to enable their biomanufacturing and clinical applications. *Curr Opin Biotechnol* (2019) 60:89–98. doi: 10.1016/j.copbio.2019.01.005
28. Yang Z, Xie J, Zhu J, Kang C, Chiang C, Wang X, et al. Functional exosome-mimic for delivery of siRNA to cancer: in vitro and in vivo evaluation. *J Control Release* (2016) 243:160–71. doi: 10.1016/j.jconrel.2016.10.008
29. Boukouris S, Mathivanan S. Exosomes in bodily fluids are a highly stable resource of disease biomarkers. *Proteomics – Clin Appl* (2015) 9(3-4):358–67. doi: 10.1002/prca.201400114
30. Minciacchi VR, Zijlstra A, Rubin MA, Di Vizio D. Extracellular vesicles for liquid biopsy in prostate cancer: where are we and where are we headed? *Prostate Cancer Prostatic Dis* (2017) 20(3):251–8. doi: 10.1038/pcan.2017.7
31. Vader P, Breakefield XO, Wood MJA. Extracellular vesicles: emerging targets for cancer therapy. *Trends Mol Med* (2014) 20(7):385–93. doi: 10.1016/j.molmed.2014.03.002
32. Jabalee J, Towle R, Garnis C. The Role of Extracellular Vesicles in Cancer: Cargo, Function, and Therapeutic Implications. *Cells* (2018) 7(8):93. doi: 10.3390/cells7080093
33. Liu T, Han C, Wang S, Fang P, Ma Z, Xu L, et al. Cancer-associated fibroblasts: an emerging target of anti-cancer immunotherapy. *J Hematol Oncol* (2019) 12(1):86. doi: 10.1186/s13045-019-0770-1
34. Chulpanova DS, Kitaeva KV, James V, Rizvanov AA, Solovyeva VV. Therapeutic Prospects of Extracellular Vesicles in Cancer Treatment. *Front Immunol* (2018) 9:1534. doi: 10.3389/fimmu.2018.01534
35. Bergsmedh A, Szeles A, Henriksson M, Bratt A, Folkman MJ, Spetz A-L, et al. Horizontal transfer of oncogenes by uptake of apoptotic bodies. *Proc Natl Acad Sci* (2001) 98(11):6407. doi: 10.1073/pnas.101129998
36. Vella LJ, Behren A, Coleman B, Greening DW, Hill AF, Cebon J. Intercellular Resistance to BRAF Inhibition Can Be Mediated by Extracellular Vesicle–Associated PDGFRβ. *Neoplasia* (2017) 19(11):932–40. doi: 10.1016/j.neo.2017.07.002
37. Yang L, Wu X-H, Wang D, Luo C-L, Chen L-X. Bladder cancer cell-derived exosomes inhibit tumor cell apoptosis and induce cell proliferation in vitro. *Mol Med Rep* (2013) 8(4):1272–8. doi: 10.3892/mmr.2013.1634
38. Qu JL, Qu XJ, Zhao MF, Teng YE, Zhang Y, Hou KZ, et al. Gastric cancer exosomes promote tumour cell proliferation through PI3K/Akt and MAPK/ERK activation. *Dig Liver Dis* (2009) 41(12):875–80. doi: 10.1016/j.dld.2009.04.006
39. Setti M, Osti D, Richichi C, Ortensi B, Bene MD, Fornasari L, et al. Extracellular vesicle-mediated transfer of CLIC1 protein is a novel mechanism for the regulation of glioblastoma growth. *Oncotarget* (2015) 6 (31):31413–27. doi: 10.18632/oncotarget.5105
40. Fahey E, Doyle SL. IL-1 Family Cytokine Regulation of Vascular Permeability and Angiogenesis. *Front Immunol* (2019) 10:1426. doi: 10.3389/fimmu.2019.01426
41. Ucuzian AA, Gassman AA, East AT, Greisler HP. Molecular Mediators of Angiogenesis. *J Burn Care Res* (2010) 31(1):158–75. doi: 10.1097/BCR.0b013e3181c7ed82
42. Hernández-Romero IA, Guerra-Calderas L, Salgado-Albarrán M, Maldonado-Huerta T, Soto-Reyes E. The Regulatory Roles of Non-coding RNAs in Angiogenesis and Neovascularization From an Epigenetic Perspective. *Front Oncol* (2019) 9:1091. doi: 10.3389/fonc.2019.01091

43. Kohlhapp FJ, Mitra AK, Lengyel E, Peter ME. MicroRNAs as mediators and communicators between cancer cells and the tumor microenvironment. *Oncogene* (2015) 34(48):5857–68. doi: 10.1038/onc.2015.89
44. Lang H-L, Hu G, Chen Y, Liu Y, Tu W, Lu Y, et al. Glioma cells promote angiogenesis through the release of exosomes containing long non-coding RNA POU3F3. *Eur Rev Med Pharmacol Sci* (2017) 21(5):959–72.
45. Zhao J, Li L, Han Z-Y, Wang Z-X, Qin L-X. Long noncoding RNAs, emerging and versatile regulators of tumor-induced angiogenesis. *Am J Cancer Res* (2019) 9(7):1367–81.
46. Sheng S-R, Wu J-S, Tang Y-L, Liang X-H. Long noncoding RNAs: emerging regulators of tumor angiogenesis. *Future Oncol* (2017) 13(17):1551–62. doi: 10.2217/fon-2017-0149
47. Kucharzewska P, Christianson HC, Welch JE, Svensson KJ, Fredlund E, Ringnér M, et al. Exosomes reflect the hypoxic status of glioma cells and mediate hypoxia-dependent activation of vascular cells during tumor development. *Proc Natl Acad Sci* (2013) 110(18):7312. doi: 10.1073/pnas.1220998110
48. Parolini I, Federici C, Raggi C, Lugini L, Palleschi S, De Milito A, et al. Microenvironmental pH Is a Key Factor for Exosome Traffic in Tumor Cells. *J Biol Chem* (2009) 284(49):34211–22. doi: 10.1074/jbc.M109.041152
49. Kanlikilicer P, Bayraktar R, Denizli M, Rashed MH, Ivan C, Aslan B, et al. Exosomal miRNA confers chemo resistance via targeting Cav1/p-gp/M2-type macrophage axis in ovarian cancer. *EBioMedicine* (2018) 38:100–12. doi: 10.1016/j.ebiom.2018.11.004
50. Cooks T, Pateras IS, Jenkins LM, Patel KM, Robles AII, Morris J, et al. Mutant p53 cancers reprogram macrophages to tumor supporting macrophages via exosomal miR-1246. *Nat Commun* (2018) 9(1):771. doi: 10.1038/s41467-018-03224-w
51. Casadei L, Calore F, Creighton CJ, Guescini M, Batte K, Iwenofu OH, et al. Exosome-Derived miR-25-3p and miR-92a-3p Stimulate Liposarcoma Progression. *Cancer Res* (2017) 77(14):3846. doi: 10.1158/0008-5472.CAN-16-2984
52. Chen G, Huang AC, Zhang W, Zhang G, Wu M, Xu W, et al. Exosomal PD-L1 contributes to immunosuppression and is associated with anti-PD-1 response. *Nature* (2018) 560(7718):382–6. doi: 10.1038/s41586-018-0392-8
53. Sheehan C, Souza-Schorey C. Tumor-derived extracellular vesicles: molecular parcels that enable regulation of the immune response in cancer. *J Cell Sci* (2019) 132(20):jcs235085. doi: 10.1242/jcs.235085
54. Ricklefs FL, Alayo Q, Krenzlin H, Mahmoud AB, Speranza MC, Nakashima H, et al. Immune evasion mediated by PD-L1 on glioblastoma-derived extracellular vesicles. *Sci Adv* (2018) 4(3):eaar2766. doi: 10.1126/sciadv.aar2766
55. Maus RLG, Jakub JW, Nevala WK, Christensen TA, Noble-Orcutt K, Sachs Z, et al. Human Melanoma-Derived Extracellular Vesicles Regulate Dendritic Cell Maturation. *Front Immunol* (2017) 8:358. doi: 10.3389/fimmu.2017.00358
56. Liu H, Chen L, Liu J, Meng H, Zhang R, Ma L, et al. Co-delivery of tumor-derived exosomes with alpha-galactosylceramide on dendritic cell-based immunotherapy for glioblastoma. *Cancer Lett* (2017) 411:182–90. doi: 10.1016/j.canlet.2017.09.022
57. Mahaweni NM, Kaijen-Lambers MEH, Dekkers J, Aerts JGJV, Hegmans JPJJ. Tumour-derived exosomes as antigen delivery carriers in dendritic cell-based immunotherapy for malignant mesothelioma. *J Extracell Vesicles* (2013) 2(1):22492. doi: 10.3402/jev.v2i0.22492
58. Antimisiaris SG, Mourtas S, Marazioti A. Exosomes and Exosome-Inspired Vesicles for Targeted Drug Delivery. *Pharmaceutics* (2018) 10(4):218. doi: 10.3390/pharmaceutics10040218
59. Didiot M-C, Hall LM, Coles AH, Haraszti RA, Godinho BMDC, Chase K, et al. Exosome-mediated Delivery of Hydrophobically Modified siRNA for Huntingtin mRNA Silencing. *Mol Ther* (2016) 24(10):1836–47. doi: 10.1038/mt.2016.126
60. Luan X, Sansanaphongpricha K, Myers I, Chen HW, Yuan HB, Sun DX. Engineering exosomes as refined biological nanoplatforms for drug delivery. *Acta Pharmacol Sin* (2017) 38(6):754–63. doi: 10.1038/aps.2017.12
61. Zhuang X, Xiang X, Grizzle W, Sun D, Zhang S, Axtell RC, et al. Treatment of Brain Inflammatory Diseases by Delivering Exosome Encapsulated Anti-inflammatory Drugs From the Nasal Region to the Brain. *Mol Ther* (2011) 19(10):1769–79. doi: 10.1038/mt.2011.164
62. Saari H, Lázaro-Ibáñez E, Viitala T, Vuorimaa-Laukkanen E, Siljander P, Yliperttula M. Microvesicle- and exosome-mediated drug delivery enhances the cytotoxicity of Paclitaxel in autologous prostate cancer cells. *J Controlled Release* (2015) 220:727–37. doi: 10.1016/j.jconrel.2015.09.031
63. Sun J, Jiang L, Lin Y, Gerhard EM, Jiang X, Li L, et al. Enhanced anticancer efficacy of paclitaxel through multistage tumor-targeting liposomes modified with RGD and KLA peptides. *Int J Nanomed* (2017) 12:1517–37. doi: 10.2147/IJN.S122859
64. Shi JF, Ma YF, Zhu J, Chen YX, Sun YT, Yao YC, et al. A Review on Electroporation-Based Intracellular Delivery. *Molecules* (2018) 23(11):3044. doi: 10.3390/molecules23113044
65. Zhang D, Lee H, Zhu Z, Minhas JK, Jin Y. Enrichment of selective miRNAs in exosomes and delivery of exosomal miRNAs in vitro and in vivo. *Am J Physiol-Lung Cell Mol Physiol* (2016) 312(1):L110–21. doi: 10.1152/ajplung.00423.2016
66. Pomatto MAC, Bussolati B, D'antico S, Ghiotto S, Tetta C, Brizzi MF, et al. Improved Loading of Plasma-Derived Extracellular Vesicles to Encapsulate Antitumor miRNAs. *Mol Ther - Methods Clin Dev* (2019) 13:133–44. doi: 10.1016/j.omtm.2019.01.001
67. Yong T, Zhang X, Bie N, Zhang H, Zhang X, Li F, et al. Tumor exosome-based nanoparticles are efficient drug carriers for chemotherapy. *Nat Commun* (2019) 10(1):3838. doi: 10.1038/s41467-019-11718-4
68. Kojima R, Bojar D, Rizzi G, Hamri GC-E, El-Baba MD, Saxena P, et al. Designer exosomes produced by implanted cells intracerebrally deliver therapeutic cargo for Parkinson's disease treatment. *Nat Commun* (2018) 9(1):1305. doi: 10.1038/s41467-018-03733-8
69. Yang Z, Shi J, Xie J, Wang Y, Sun J, Liu T, et al. Large-scale generation of functional mRNA-encapsulating exosomes via cellular nanoporation. *Nat Biomed Eng* (2020) 4(1):69–83. doi: 10.1038/s41551-019-0485-1
70. Kamerkar S, Lebleu VS, Sugimoto H, Yang S, Ruivo CF, Melo SA, et al. Exosomes facilitate therapeutic targeting of oncogenic KRAS in pancreatic cancer. *Nature* (2017) 546(7659):498–503. doi: 10.1038/nature22341
71. Lamichhane TN, Jeyaram A, Patel DB, Parajuli B, Livingston NK, Arumugasaamy N, et al. Oncogene Knockdown via Active Loading of Small RNAs into Extracellular Vesicles by Sonication. *Cell Mol Bioeng* (2016) 9(3):315–24. doi: 10.1007/s12195-016-0457-4
72. Kim MS, Haney MJ, Zhao Y, Mahajan V, Deygen I, Klyachko NL, et al. Development of exosome-encapsulated paclitaxel to overcome MDR in cancer cells. *Nanomed: Nanotechnol Biol Med* (2016) 12(3):655–64. doi: 10.1016/j.nano.2015.10.012
73. Nakase I, Futaki S. Combined treatment with a pH-sensitive fusogenic peptide and cationic lipids achieves enhanced cytosolic delivery of exosomes. *Sci Rep* (2015) 5(1):10112. doi: 10.1038/srep10112
74. Qi H, Liu C, Long L, Ren Y, Zhang S, Chang X, et al. Blood Exosomes Endowed with Magnetic and Targeting Properties for Cancer Therapy. *ACS Nano* (2016) 10(3):3323–33. doi: 10.1021/acsnano.5b06939
75. Wang M, Altinoglu S, Takeda YS, Xu Q. Integrating Protein Engineering and Bioorthogonal Click Conjugation for Extracellular Vesicle Modulation and Intracellular Delivery. *PloS One* (2015) 10(11):e0141860. doi: 10.1371/journal.pone.0141860
76. Smyth T, Petrova K, Payton NM, Persaud I, Redzic JS, Graner MW, et al. Surface Functionalization of Exosomes Using Click Chemistry. *Bioconjugate Chem* (2014) 25(10):1777–84. doi: 10.1021/bc500291r
77. Pascucci L, Coccè V, Bonomi A, Ami D, Ceccarelli P, Ciusani E, et al. Paclitaxel is incorporated by mesenchymal stromal cells and released in exosomes that inhibit in vitro tumor growth: A new approach for drug delivery. *J Controlled Release* (2014) 192:262–70. doi: 10.1016/j.jconrel.2014.07.042
78. Lv L-H, Wan Y-L, Lin Y, Zhang W, Yang M, Li G-L, et al. Anticancer Drugs Cause Release of Exosomes with Heat Shock Proteins from Human Hepatocellular Carcinoma Cells That Elicit Effective Natural Killer Cell Antitumor Responses in Vitro. *J Biol Chem* (2012) 287(19):15874–85. doi: 10.1074/jbc.M112.340588
79. Behzadi E, Hosseini HM, Halabian R, Fooladi AAII. Macrophage cell-derived exosomes/staphylococcal enterotoxin B against fibrosarcoma tumor. *Microb Pathogenesis* (2017) 111:132–8. doi: 10.1016/j.micpath.2017.08.027

80. Zhang Y, Liu D, Chen X, Li J, Li L, Bian Z, et al. Secreted Monocytic miR-150 Enhances Targeted Endothelial Cell Migration. *Mol Cell* (2010) 39(1):133–44. doi: 10.1016/j.molcel.2010.06.010
81. Salomon C, Ryan J, Sobrevia L, Kobayashi M, Ashman K, Mitchell M, et al. Exosomal Signaling during Hypoxia Mediates Microvascular Endothelial Cell Migration and Vasculogenesis. *PloS One* (2013) 8(7):e68451. doi: 10.1371/journal.pone.0068451
82. Tadokoro H, Umezu T, Ohyashiki K, Hirano T, Ohyashiki JH. Exosomes Derived from Hypoxic Leukemia Cells Enhance Tube Formation in Endothelial Cells. *J Biol Chem* (2013) 288(48):34343–51. doi: 10.1074/jbc.M113.480822
83. Ding Y, Cao F, Sun H, Wang Y, Liu S, Wu Y, et al. Exosomes derived from human umbilical cord mesenchymal stromal cells deliver exogenous miR-145-5p to inhibit pancreatic ductal adenocarcinoma progression. *Cancer Lett* (2019) 442:351–61. doi: 10.1016/j.canlet.2018.10.039
84. Ohno S-I, Takanashi M, Sudo K, Ueda S, Ishikawa A, Matsuyama N, et al. Systemically Injected Exosomes Targeted to EGFR Deliver Antitumor MicroRNA to Breast Cancer Cells. *Mol Ther* (2013) 21(1):185–91. doi: 10.1038/mt.2012.180
85. Ibrahim AGE, Li C, Rogers R, Fournier M, Li L, Vaturi SD, et al. Augmenting canonical Wnt signalling in therapeutically inert cells converts them into therapeutically potent exosome factories. *Nat Biomed Eng* (2019) 3(9):695–705. doi: 10.1038/s41551-019-0448-6
86. Yang Z, Ma Y, Zhao H, Yuan Y, Kim BYS. Nanotechnology platforms for cancer immunotherapy. *WIREs Nanomed Nanobiotechnol* (2020) 12(2): e1590. doi: 10.1002/wnan.1590
87. Tian Y, Li S, Song J, Ji T, Zhu M, Anderson GJ, et al. A doxorubicin delivery platform using engineered natural membrane vesicle exosomes for targeted tumor therapy. *Biomaterials* (2014) 35(7):2383–90. doi: 10.1016/j.biomaterials.2013.11.083
88. Sancho-Albero M, Encabo-Berzosa MDM, Beltrán-Visiedo M, Fernández-Messina L, Sebastián V, Sánchez-Madrid F, et al. Efficient encapsulation of theranostic nanoparticles in cell-derived exosomes: leveraging the exosomal biogenesis pathway to obtain hollow gold nanoparticle-hybrids. *Nanoscale* (2019) 11(40):18825–36. doi: 10.1039/C9NR06183E
89. Okoye IS, Coomes SM, Pelly VS, Czieso S, Papayannopoulos V, Tolmachova T, et al. MicroRNA-Containing T-Regulatory-Cell-Derived Exosomes Suppress Pathogenic T Helper 1 Cells. *Immunity* (2014) 41(1):89–103. doi: 10.1016/j.immuni.2014.05.019
90. Keklikoglou I, Cianciaruso C, Güç E, Squadrito ML, Spring LM, Tazzyman S, et al. Chemotherapy elicits pro-metastatic extracellular vesicles in breast cancer models. *Nat Cell Biol* (2019) 21(2):190–202. doi: 10.1038/s41556-018-0256-3
91. Seo N, Shirakura Y, Tahara Y, Momose F, Harada N, Ikeda H, et al. Activated CD8+ T cell extracellular vesicles prevent tumour progression by targeting of lesional mesenchymal cells. *Nat Commun* (2018) 9(1):435. doi: 10.1038/s41467-018-02865-1
92. Arscott WT, Tandle AT, Zhao S, Shabason JE, Gordon IK, Schlaff CD, et al. Ionizing Radiation and Glioblastoma Exosomes: Implications in Tumor Biology and Cell Migration. *Trans Oncol* (2013) 6(6):638–IN6. doi: 10.1593/tlo.13640
93. Qian B-Z, Li J, Zhang H, Kitamura T, Zhang J, Campion LR, et al. CCL2 recruits inflammatory monocytes to facilitate breast-tumour metastasis. *Nature* (2011) 475(7355):222–5. doi: 10.1038/nature10138
94. Bonapace L, Coissieux M-M, Wyckoff J, Mertz KD, Varga Z, Junt T, et al. Cessation of CCL2 inhibition accelerates breast cancer metastasis by promoting angiogenesis. *Nature* (2014) 515(7525):130–3. doi: 10.1038/nature13862
95. Andrade LNDS, Otake AH, Cardim SGB, Da Silva FII, Ikoma Sakamoto MM, Furuya TK, et al. Extracellular Vesicles Shedding Promotes Melanoma Growth in Response to Chemotherapy. *Sci Rep* (2019) 9(1):14482. doi: 10.1038/s41598-019-50848-z
96. Kreger BT, Johansen ER, Cerione RA, Antonyak MA. The Enrichment of Survivin in Exosomes from Breast Cancer Cells Treated with Paclitaxel Promotes Cell Survival and Chemoresistance. *Cancers* (2016) 8(12):111. doi: 10.3390/cancers8120111
97. Pavlyukov MS, Yu H, Bastola S, Minata M, Shender VO, Lee Y, et al. Apoptotic Cell-Derived Extracellular Vesicles Promote Malignancy of Glioblastoma Via Intercellular Transfer of Splicing Factors. *Cancer Cell* (2018) 34(1):119–135 e10. doi: 10.1016/j.ccell.2018.05.012
98. Zaky SH, Lee KW, Gao J, Jensen A, Close J, Wang YD, et al. Poly(Glycerol Sebacate) Elastomer: A Novel Material for Mechanically Loaded Bone Regeneration. *Tissue Eng Part A* (2014) 20(1-2):45–53. doi: 10.1089/ten.tea.2013.0172
99. Melzer C, Rehn V, Yang Y, Bähre H, Von Der Ohe J, Hass R. Taxol-Loaded MSC-Derived Exosomes Provide a Therapeutic Vehicle to Target Metastatic Breast Cancer and Other Carcinoma Cells. *Cancers (Basel)* (2019) 11(6):798. doi: 10.3390/cancers11060798
100. Park J-H, Gu L, Von Maltzahn G, Ruoslahti E, Bhatia SN, Sailor MJ. Biodegradable luminescent porous silicon nanoparticles for in vivo applications. *Nat Mater* (2009) 8(4):331–6. doi: 10.1038/nmat2398
101. Menay F, Herschlik L, De Toro J, Cocozza F, Tsacalian R, Gravisaco MJ, et al. Exosomes Isolated from Ascites of T-cell Lymphoma-Bearing Mice Expressing Surface CD24 and HSP-90 Induce a Tumor-Specific Immune Response. *Front In Immunol* (2017) 8:286. doi: 10.3389/fimmu.2017.00286
102. Xiao L, Erb U, Zhao K, Hackert T, Zöller M. Efficacy of vaccination with tumor-exosome loaded dendritic cells combined with cytotoxic drug treatment in pancreatic cancer. *OncoImmunology* (2017) 6(6):e1319044. doi: 10.1080/2162402X.2017.1319044
103. Eurosurveillance Editorial Team, C. Note from the editors: The 2012 impact factors. *Eurosurveillance* (2013) 18(26):20515. doi: 10.2807/ese.18.26.20515-en
104. Liu Y, Gu Y, Cao X. The exosomes in tumor immunity. *Oncoimmunology* (2015) 4(9):e1027472. doi: 10.1080/2162402X.2015.1027472
105. Munich S, Sobo-Vujanovic A, Buchser WJ, Beer-Stolz D, Vujanovic NL. Dendritic cell exosomes directly kill tumor cells and activate natural killer cells via TNF superfamily ligands. *Oncoimmunology* (2012) 1(7):1074–83. doi: 10.4161/onci.20897
106. Simhadri VR, Reiners KS, Hansen HP, Topolar D, Simhadri VL, Nohroudi K, et al. Dendritic Cells Release HLA-B-Associated Transcript-3 Positive Exosomes to Regulate Natural Killer Function. *PloS One* (2008) 3(10):e3377. doi: 10.1371/journal.pone.0003377
107. Viaud S, Terme M, Flament C, Taieb J, André F, Novault S, et al. Dendritic Cell-Derived Exosomes Promote Natural Killer Cell Activation and Proliferation: A Role for NKG2D Ligands and IL-15Rα. *PloS One* (2009) 4 (3):e4942. doi: 10.1371/journal.pone.0004942
108. Escudier B, Dorval T, Chaput N, André F, Caby M-P, Novault S, et al. Vaccination of metastatic melanoma patients with autologous dendritic cell (DC) derived-exosomes: results of thefirst phase I clinical trial. *J Trans Med* (2005) 3(1):10. doi: 10.1186/1479-5876-3-10
109. Morse MA, Garst J, Osada T, Khan S, Hobeika A, Clay TM, et al. A phase I study of dexosome immunotherapy in patients with advanced non-small cell lung cancer. *J Trans Med* (2005) 3(1):9. doi: 10.1186/1479-5876-3-9
110. Zhu L, Kalimuthu S, Oh JM, Gangadaran P, Baek SH, Jeong SY, et al. Enhancement of antitumor potency of extracellular vesicles derived from natural killer cells by IL-15 priming. *Biomaterials* (2019) 190:38–50. doi: 10.1016/j.biomaterials.2018.10.034
111. Kim MS, Haney MJ, Zhao Y, Yuan D, Deygen I, Klyachko NL, et al. Engineering macrophage-derived exosomes for targeted paclitaxel delivery to pulmonary metastases: in vitro and in vivo evaluations. *Nanomed: Nanotechnol Biol Med* (2018) 14(1):195–204. doi: 10.1016/j.nano.2017.09.011
112. Jang SC, Kim Oy Fau - Yoon CM, Yoon Cm Fau - Choi D-S, Choi Ds Fau - Roh T-Y, Roh Ty Fau - Park J, Park J Fau - Nilsson J, et al. Bioinspired exosome-mimetic nanovesicles for targeted delivery of chemotherapeutics to malignant tumors(1936-086X (Electronic)). *ACS Nano* (2013) 7(9):7698–710. doi: 10.1021/nn402232g
113. Lin W, Xu Y, Chen X, Liu J, Weng Y, Zhuang Q, et al. Radiation-induced small extracellular vesicles as "carriages"promote tumor antigen release and trigger antitumor immunity. *Theranostics* (2020) 10(11):4871–84. doi: 10.7150/thno.43539
114. De Araujo Farias V, O'valle F, Serrano-Saenz S, Anderson P, Andrés E, López-Peñalver J, et al. Exosomes derived from mesenchymal stem cells enhance radiotherapy-induced cell death in tumor and metastatic tumor foci. *Mol Cancer* (2018) 17(1):122. doi: 10.1186/s12943-018-0867-0
115. Zheng Y, Liu L, Chen C, Ming P, Huang Q, Li C, et al. The extracellular vesicles secreted by lung cancer cells in radiation therapy promote endothelial cell angiogenesis by transferring miR-23a. *PeerJ* (2017) 5: e3627. doi: 10.7717/peerj.3627

116. Mrowczynski OD, Madhankumar AB, Sundstrom JM, Zhao Y, Imamura Kawasawa Y, Slagle-Webb B, et al. Exosomes impact survival to radiation exposure in cell line models of nervous system cancer. *Oncotarget* (2018) 9 (90):36083–101. doi: 10.18632/oncotarget.26300
117. Boelens MC, Wu TJ, Nabet BY, Xu B, Qiu Y, Yoon T, et al. Exosome Transfer from Stromal to Breast Cancer Cells Regulates Therapy Resistance Pathways. *Cell* (2014) 159(3):499–513. doi: 10.1016/j.cell.2014.09.051
118. Tang Y, Cui Y, Li Z, Jiao Z, Zhang Y, He Y, et al. Radiation-induced miR-208a increases the proliferation and radioresistance by targeting p21 in human lung cancer cells. *J Exp Clin Cancer Res* (2016) 35(1):7. doi: 10.1186/s13046-016-0285-3
119. Zhao M, Xu J, Zhong S, Liu Y, Xiao H, Geng L, et al. Expression profiles and potential functions of circular RNAs in extracellular vesicles isolated from radioresistant glioma cells. *Oncol Rep* (2019) 41(3):1893–900. doi: 10.3892/or.2019.6972
120. Dai X, Liao K, Zhuang Z, Chen B, Zhou Z, Zhou S, et al. AHIF promotes glioblastoma progression and radioresistance via exosomes. *Int J Oncol* (2019) 54(1):261–70. doi: 10.3892/ijo.2018.4621

**Conflict of Interest:** The authors declare that the research was conducted in the absence of any commercial or financial relationships that could be construed as a potential conflict of interest.

frontiers in Oncology

REVIEW
published: 26 February 2021
doi: 10.3389/fonc.2021.644358

# The Role of Exosomes in Pancreatic Cancer From Bench to Clinical Application: An Updated Review

*Kai Chen*[1], *Qi Wang*[1], *Marko Kornmann*[2], *Xiaodong Tian*[1]* *and Yinmo Yang*[1]*

[1] Department of General Surgery, Peking University First Hospital, Beijing, China, [2] Clinic of General, Visceral and Transplantation Surgery, University of Ulm, Ulm, Germany

Pancreatic ductal adenocarcinoma (PDAC) remains one of the most dismal gastrointestinal malignancies with an overall 5-year survival rate of 8%–9%. The intra-tumor heterogeneity and special tumor microenvironment in PDAC make it challenging to develop effective treatment strategies. Exosomes are extracellular vesicles that originate from the endosomes and have a diameter of 40–160 nm. A growing body of evidence has shown that exosomes play vital roles in tumor initiation and development. Recently, extensive application of exosomes as biomarkers and drug carriers has rendered them attractive in the field of PDAC. This review summarizes the latest progress in the methodologies for isolation, modification, and tracking of exosomes, exosome-mediated cell-to-cell communication, clinical applications of exosome as minimally invasive liquid biopsy and drugs carriers, as well as their involvement in the angiogenic regulation in PDAC. In spite of these advancements, some obstacles are still required to be overcome to use the exosome-based technologies for early diagnosis or improvement of prognosis of patients with PDAC.

**Keywords: pancreatic cancer, exosome, cell-to-cell communication, biomarker, therapeutic vehicle**

OPEN ACCESS

***Edited by:***
*João Paulo Longo, University of Brasilia, Brazil*

***Reviewed by:***
*Jafar Rezaie, Urmia University of Medical Sciences, Iran*
*Sonia A. Melo, University of Porto, Portugal*

***Correspondence:**
*Yinmo Yang*
*yangyinmo@263.net*
*Xiaodong Tian*
*tianxiaodong@pkufh.cn*

***Specialty section:***
*This article was submitted to Cancer Molecular Targets and Therapeutics, a section of the journal Frontiers in Oncology*

***Received:*** *21 December 2020*
***Accepted:*** *12 January 2021*
***Published:*** *26 February 2021*

***Citation:***
*Chen K, Wang Q, Kornmann M, Tian X and Yang Y (2021) The Role of Exosomes in Pancreatic Cancer From Bench to Clinical Application: An Updated Review. Front. Oncol. 11:644358. doi: 10.3389/fonc.2021.644358*

## INTRODUCTION

Pancreatic ductal adenocarcinoma (PDAC) remains one of the most dismal gastrointestinal malignancies with an overall 5-year survival rate of 8%–9%, which brings great challenges for developing effective therapeutic strategies (1). Although radical excision is the only potentially curative therapy for PDAC, only 15%–20% of PDAC patients are eligible for radical excision at the time of diagnosis due to either major vascular invasion or distant metastasis (2, 3). Even after curative resection, the majority of patients still encounter local recurrence or systematic metastasis within just 12 months, with a 5-year survival rate after surgery of 20%–30% (4). Nowadays, the paradigm shift from the traditional "surgery first" approach to the modern "multi-disciplinary team (MDT)" treatment significantly improved the short-term prognosis of patients with PDAC; however this MDT approach is not sufficient enough to markedly increase long-term survival of the majority of patients with PDAC (5). Thus, it is imperative to develop new diagnostic and treatment strategies for PDAC.

Exosomes are members of the extracellular vesicle (EV) family and have an endosomal origin. Exosomes have a diameter of 40–160 nm (average, 100 nm). Under physiological or pathological

conditions, all the cells inside the human body secrete exosomes into the body fluid – plasma, urine, saliva, ascites, and bile (6, 7). Similar to their parental cells, exosomes contain cell-derived biological molecules such as DNA, miRNA, mRNA, lncRNA, proteins, lipids, and metabolites (**Figure 1**). The constituents of exosomes vary a lot under different circumstances due to diverse original cell types and status. Because of the features of wide distribution and cell specificity, identification of cancer-specific exosomes *via* minimally invasive liquid biopsy might be critical for the early diagnosis, prognosis prediction and development of therapeutic strategies related to malignancies (7). Meanwhile, a growing body of evidence has revealed that the cell-to-cell communication *via* exosomes in different types of cells plays a vital role in the physiological and pathological processes such as immune response, tissue fibrosis, reproduction, tumorigenesis, and metastasis (8–11). Recently, exosomes have become a popular research area of PDAC. Studies have highlighted the clinical value of exosomes as biomarkers and drug carriers in PDAC patients (12–14). In this review, we describe the recent progress in the basic research of exosomes and discuss its clinical applications in PDAC.

## NEW METHODOLOGIES IN EXOSOME RESEARCH

### Isolation of High-Quality Exosomes

Isolation of high-quality exosomes is a prerequisite of all the exosome-related studies. The International Society for Extracellular Vesicles (ISEV) classified the exosomes isolation strategies into four categories according to the recovery rate and specificity. Further, the society declared there is no gold standard for the isolation of exosomes at present (15). Although ISEV did not provide clear guidelines on the use of specific exosome

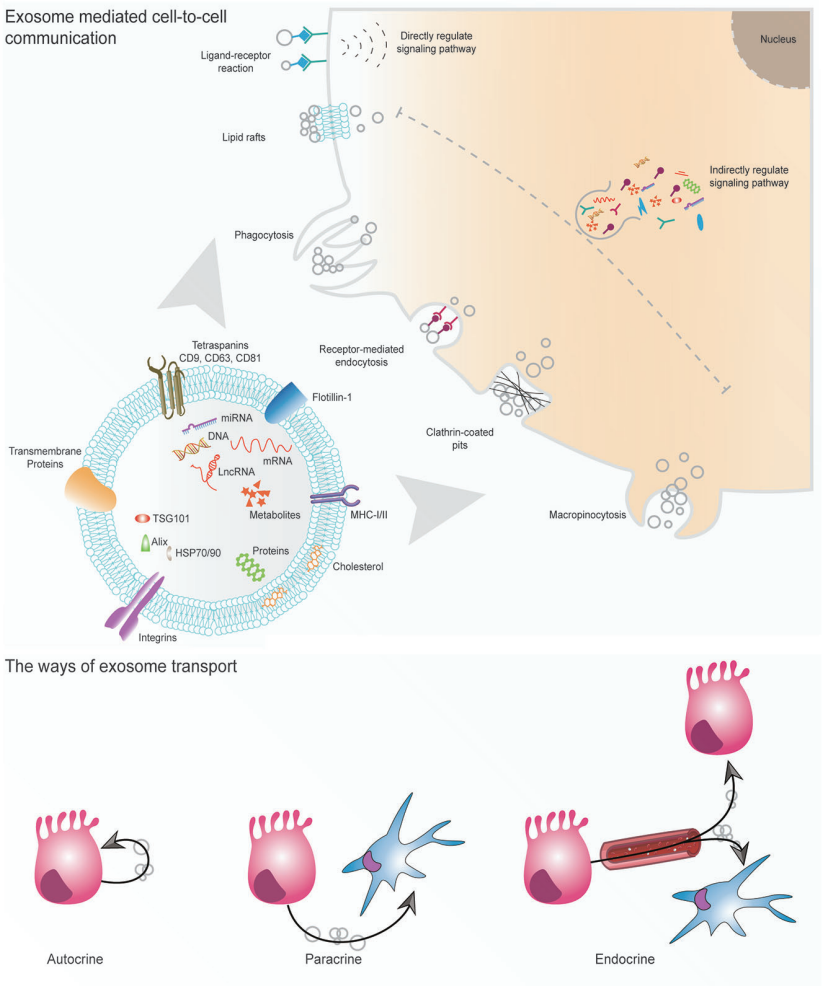


**FIGURE 1** | Exosomes involve intercellular communication. Exosomes derived from the parental cells affect the biological function of the recipient cells through ligand-receptor interactions and uptake of exosomal cargo. Exosome transport ways can be autocrine, paracrine, or endocrine.

isolation methods, it suggested that the investigators should give the detailed protocol in the ensuing scientific publications to guarantee the reliability and reproducibility of results. The most popular technology for purifying exosomes is ultracentrifugation (UC). UC is extensively used in almost all exosome-related studies. For isolating the high-quality exosomes from complicated body fluids such as plasma or urine, researchers also prefer a combination of isolation methods, including UC or polymer precipitation plus size exclusion chromatography (SEC). Unfortunately, the collection of pure exosomes is impossible because of the unavoidable contamination with soluble proteins and larger vesicles. Each isolation method has its specific advantages and disadvantages and results in heterogeneity in terms of size, surface markers, and contaminants in the isolated exosomes (**Figure 2**) (16, 17). Besides the traditional isolation methods such as UC, SEC, polymer precipitation, and immunocapture, some novel isolation technologies also yield high-quality exosomes (18, 19). Zhang and colleagues (20) developed the Asymmetric Flow Field-Flow Fractionation (AF4) technique, which can identify three diverse exosome subsets, including large exosome vesicles (Exo-L, 90–120 nm), small exosome vesicles (Exo-S, 60–80 nm), and non-membranous nanoparticles (exomeres, 35 nm). The proteomic profiling revealed that the biological function carried out by each subset of exosomes varies considerably. Thus, the AF4 can separate the specific subsets of vesicles for understanding the heterogeneity of exosomal populations. Niu et al. (21) introduced a new exosome isolation platform involving integrated microfluidic chip with a combination of the traditional immunomagnetic bead-based technology and the latest microfluidic method. This platform is automatic and more efficient, which is helpful in obtaining highly pure and intact exosomes. Moreover, this platform can also isolate a certain subset of exosomes with a specific protein marker (CD63). In addition, Lee and colleagues (22) developed an acoustic nano filter system that can separate nanoscale vesicles (<200 nm) in a continuous and contact-free way. The differential acoustic force was created on the basis of the size and density of the nanoparticles by ultrasound standing waves. This system can isolate exosomes with high separation yield and resolution. In recent years, novel purification methods to achieve high-quality isolation of exosomes have progressed rapidly. With the innovation in technology, efficient isolation of exosomes with high purity and quality should be the fundamental benchmark for exosome-related research.

## Engineering Exosomes

Exosomes modification through genetic or nongenetic methods can change exosomal components and improve the targeting capability of therapeutic agents. The techniques of engineering exosomes include modifications of nucleic acid, protein, and glycoprotein, which provide a new targeted strategy for tumor precision medicine. Because genetic manipulation is relatively easier to implement at a cellular level, the complicated exosome engineering mainly focusses on the genetic modification of the parental cells at present.

The small RNAs (siRNAs or miRNAs) can be directly inserted into the exosomes through temporary permeation of the exosomal membrane using either physical or chemical methods, thereby modifying the exosomal nucleic acids. The most common methodology of delivering the target siRNAs or miRNAs into exosomes is electroporation (23, 24). The nucleic

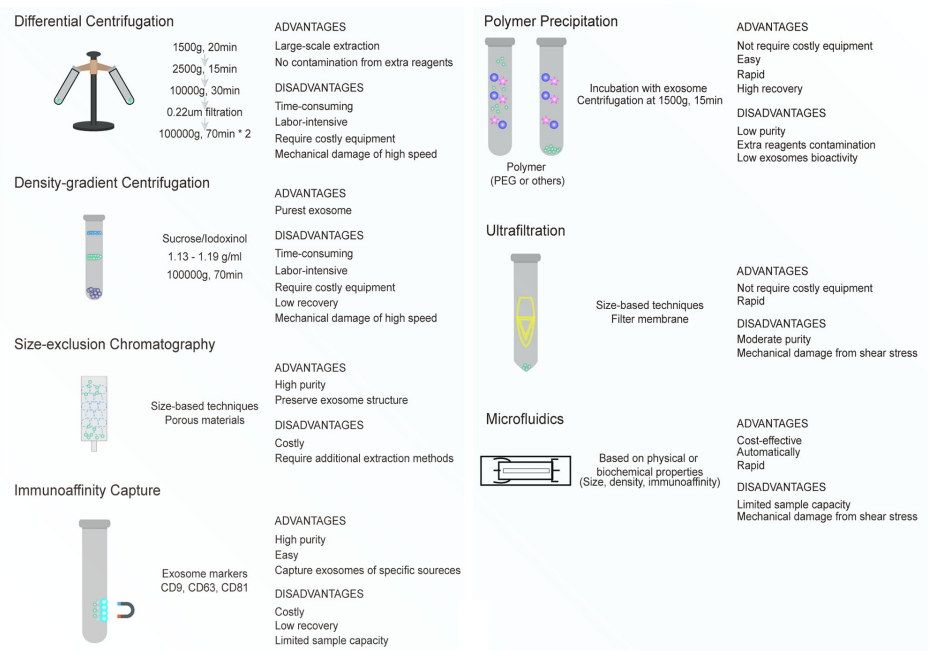


**FIGURE 2** | Different isolation methods of exosomes. Each method has their own advantages and disadvantages based on recovery, purity, operation, and cost.

acid-modified exosomes can serve as drug carriers because they interfere with the expression of target genes *in vitro* or *in vivo*. However, the current technique of exosomal nucleic acid modification still needs further optimization, since it often causes RNA aggregation, which limits the transfection efficiency. Meanwhile, the surface proteins of the parental cells can also be modified using gene editing methods, and the exosomes would then express these modified membrane proteins. These exosomes can be used to target specific cells or tissues and exert the required therapeutic effects with reduced off-target effects. Alvarez-Erviti et al. (23) engineered dendritic cells to express Lamp2b, an exosomal membrane protein that was fused with the neuron-specific RVG peptide to produce brain-specific exosomes. They loaded the purified brain-specific exosomes with exogenous siRNAs against BACE1 using electroporation, and successfully knocked down the specific gene in the brain of a murine Alzheimer's disease model. Except for the membrane proteins, the ubiquitinated proteins can be sorted into the endosomal sorting complexes required for transport, and entrapped in the exosomes. Based on this sorting mechanism, Sterzenbach and colleagues (25) designed a fusion protein of Cre recombinase and WW tag that recognized the L-domain containing protein Ndfip1 and resulted in ubiquitination of the target protein (Cre). The fusion protein was successfully loaded into the exosomes, demonstrating a potential strategy to load specific proteins into exosomes.

Besides the modification of nucleic acids and proteins, changing the structure of glycoproteins present on the surface of exosomes may also significantly influence the exosomal physicochemical properties and biological functions. Royo et al. (26) reported that a modification of glycosylate complexes through the degradation of terminal sialic acid residues present on the surface of mouse liver-derived EVs resulted in the accumulation of EVs in the lungs. Moreover, Lee et al. (27) developed a targeting strategy to engineer EVs. The investigators observed that, when 3-(diethylamino) propylamine (DEAP) was anchored to EVs, the structure of EVs was maintained in physiological conditions (pH = 7.4); however, this structure collapsed in the acidic environment (pH < 7.0), and the contents inside the EVs were released. Using this strategy, they developed a pH-responsive drug vehicle using nano-sized vesicles. These modified vehicles remained stable in the blood circulation. The encapsulated drugs were released after the vesicles reached the acidic tumor microenvironment and were engulfed by the tumor cells. The results from the xenograft model have demonstrated that DEAP-EVs could significantly increase the concentration of doxorubicin inside the tumors and inhibit tumor growth effectively (27). These novel modification strategies may act as breakthroughs for exosome-mediated targeting of tumors.

## Exosome Tracking

Exosome tracking is a visualization technique to label exosomes with specific materials and investigates their bio-distribution at cellular or animal levels using optical, magnetic resonance, or radionuclide imaging. This technique opens up the possibility to measure the metabolic kinetics parameters of exosomes inside the body. The exosome tracking technique consists of three features – labeling, imaging, and data processing.

The labeling of exosomes is classified into two categories – indirect labeling and direct labeling. The indirect labeling method refers to the genetic manipulation, and the modification of metabolites and membranes of the parental cells. The direct labeling method includes click-chemistry-based lipophilic staining and membrane modification for purified exosomes. Investigators have constructed a fusion protein using eGFP, luciferase, and tetraspanins (CD9, CD63, and CD81– anchored on the surface of exosomes), which was then expressed inside the parental cells to mark the exosomes and enable their tracing *via* an imaging system (28–30). Recently, Tung and colleagues (31) reported a facile exosome labeling strategy. They added tetra-acetylated N-azidoacetyl-D-mannosamine (Ac4ManNAz) to the culture medium. Ac4ManNAz was spontaneously incorporated into the process of glycometabolism and loaded into the exosomes. These azido-containing exosomes were then conjugated with fluorescent dyes *via* click reaction, so the distribution of the labeled exosomes can be observed *in vivo*. Busato et al. (32) developed an innovative exosome labeling approach based on magnetic resonance imaging (MRI). The adipose stem cells (ASCs) were incubated with ultrasmall superparamagnetic iron oxide nanoparticles (USPIO, 4–6 nm) for 72 h. Then the ASCs-derived exosomes labeled with these nanoparticles were visualized *via* MRI. Further, their morphological and physiological features were also preserved. These indirect exosome labeling methods by modifying parental cells have little effect on exosomal properties. However, the efficiency is usually lower, and the procedure is more complex and time-consuming as compared with the direct labeling method using purified exosomes. The most common method of labeling purified exosomes is directly incubating the exosomes with lipophilic fluorescent dyes such as PKH67 and Dio to uniformly stain the exosomal membrane. However, most of these lipophilic dyes tend to aggregate into a mass, thus reducing the imaging quality. So, the aggregation effect must be treated carefully. Furthermore, a recent study showed that gold-carbon quantum dots (GCDs), a novel fluorescent nanomaterial, can serve as a labeling dye for tracing exosomes. GCDs could conjugate with antibodies and label the exosomes *via* the antigen-antibody reaction. Using this exosome-specific nanoprobe, investigators successfully analyzed the tracks of labeled exosomes after the exosomes were engulfed by live cells (33).

The dynamic visualization of the distribution and biological process of exosomes in high resolution *in vitro* and *in vivo* is vital. Real-time imaging for nano-sized vesicles poses a challenge for the spatial and temporal resolution of imaging systems. MRI has a great advantage in spatial resolution as compared with traditional optical imaging. In addition, the latest exosome-tracking method based on radionuclide imaging holds a great promise for dynamic detection of the bio-distribution of exosomes. Hwang et al. (34) used SPECT/CT to continuously observe the distribution of macrophage-derived exosomes labeled with (99m) Tc-HMPAO under physiological conditions. The investigators observed the redistribution of labeled exosomes from liver to brain.

Most of the current imaging techniques for exosome tracking are adapted from the mature cell tracking or medical imaging protocols and lack the specific imaging platform. The multimodal exosome imaging systems are being developed to integrate the advantages of optical, magnetic resonance, and radionuclide imaging (34). These systems can improve the quality of image reconstruction, broaden the scope of their applications, and hence, would play a significant role in the field of exosome research.

## Role of Exosomes on Tumor Microenvironment – Cell Messengers

Many studies have indicated that exosomes participate in the process of tumorigenesis and tumor progression. Nowadays, researchers are trying to explore the *in vivo* biodistribution, content heterogeneity, and biological function of these nano-sized vesicles. The exosomes originating from different cells inside a tumor have built up a unique tumor nano environment (TNE) and act as significant cell-to-cell communication mediators. The living cells shed a large number of exosomes, not only to communicate with themselves and adjacent cells through autocrine and paracrine mechanisms, but also to communicate with distant tissues or organs, playing a regulatory role, through endocrine signaling (**Figure 1**). *Via* shedding exosomes, cancer cells promote their own proliferation and migration (7). The low-grade malignant chemosensitive tumor cells may develop a malignant and chemoresistant phenotype after endocytosing exosomes from the high-grade malignant chemoresistant cells (35, 36). Moreover, tumor metastasis model experiments indicated that the exosomes from primary tumor location traveled to the target organs such as the liver and brain by the circulatory system and induced pre-metastasis niche formation, resulting in increasing the possibility of tumor metastasis (37, 38). The exosomes mediate cell-to-cell communication primarily in two ways: (A) The specific proteins on the surface of exosomes directly regulate the signaling pathway inside the recipient cell *via* receptor-ligand interaction; (B) The recipient cells engulf the exosomes loaded with miRNAs, proteins or metabolites through receptor-mediated endocytosis, clathrin-coated pits, lipid rafts, phagocytosis, or macropinocytosis, then these payloads involve intracellular signaling regulation (**Figure 1**) (39).

The physiological significance of cells shedding the exosomes remains largely unclear. Early studies hypothesized that similar to garbage bags, exosomes help in the removal of excess waste products from the cell to maintain cellular homeostasis (40). It is hard to discern if the package of exosomal constituents is accurately controlled by the specific sorting system or random assortment. However, nowadays researchers have confirmed that exosome contents play a vital role in cell-to-cell interaction, among which miRNAs are the most widely studied components (41). MiRNAs are small and endogenous non-coding RNA molecules containing about 19-24 nucleotides, which completely or partially bind the 3' UTR within mRNA *via* base-pairing principle, resulting in target gene silencing or degradation in the post-transcriptional level (42). Recently, a growing body of studies has revealed that the cell-to-cell communication networks mediated by exosomal miRNAs act as cell messengers in PDAC, highlighting the complex tumor microenvironment of PDAC (**Table 1**). Wang et al. (43) reported that the exosomes derived from hypoxic pancreatic cancer cells (PCCs) could be engulfed by macrophages and release miR-301a to induce M2 polarization *via* activation of PTEN/PI3K signaling pathway. The macrophages with the M2 phenotype promoted malignant behaviors in pancreatic cancer cells (PCCs) by secreting TGFβ, IL10, and arginase in return. Natural killer (NK) cells can regulate the expression level of IL-26 in PCCs by shedding exosomes loaded with miR-3607-3p and inhibiting pancreatic cancer progression *in vitro* and *in vivo* (44). Exosomes loaded with miR-210 mediate the horizontal transfer of a drug-resistant phenotype from gemcitabine-resistant PCCs to chemosensitive PCCs (36). Cancer-associated fibroblast (CAF) derived exosomal miR-106b enhanced the proliferation and gemcitabine resistance of PCCs by directly targeting TP53INP1 (45). Activated pancreatic stellate cells (PSCs) continuously released exosomes containing high levels of miR-21. PCCs internalize these exosomes, resulting in the upregulation of miR-21. PSC-derived exosomal miR-21 was able to promote epithelial-to-mesenchymal transition (EMT), migration, and enhanced Ras/ERK signaling pathway activity in PCCs (46). Exosomal miR-194-5p shed from the dying tumor cells under radiotherapy was found to induce G1/S arrest and promote DNA damage repair of residual tumor repopulating cells (TRCs) to potentiate pancreatic cancer repopulation (47).

**TABLE 1** | Exosome miRNA-mediated cell-to-cell communication network in pancreatic ductal adenocarcinoma (PDAC) microenvironment.

| Parental cell | Recipient cell | Cargo | Isolation method | Culture conditions | Biological function | Reference |
|---|---|---|---|---|---|---|
| PCCs | Macrophages | miR-301a | Ultracentrifugation | Hypoxia | Induce M2 polarization | (43) |
| NKs | PCCs | miR-3607 | Ultracentrifugation | Normoxia | Inhibit progression | (44) |
| Gemcitabine-resistant PCCs | Chemosensitive PCCs | miR-210 | ExoQuick-TC | Normoxia | Transfer of drug-resistant phenotype | (36) |
| CAFs | PCCs | miR-106b | ExoQuick-TC | Normoxia | Promote proliferation and Gemcitabine resistance | (45) |
| PSCs | PCCs | miR-21 | Ultracentrifugation | Normoxia | Induce EMT | (46) |
| Dying tumor cells | TRCs | miR-194-5p | Ultracentrifugation | Normoxia | Promote G1/S arrest and DNA damage repair | (47) |

*PCCs, Pancreatic cancer cells; NKs, Natural killer cells; CAFs, Cancer-associated fibroblasts; PSCs, Pancreatic stellate cells; EMT, Epithelial-to-mesenchymal transition; TRCs, Tumor repopulating cells.*

In summary, exosomal miRNA mediates complicated cell-to-cell communication network inside the PDAC microenvironment involving PCCs, NK cells, macrophages, and CAFs. However, the interaction mechanisms involving other components such as endothelial cells (ECs) in PDAC are currently unknown. Further research is needed to study the bi-directional communication among these components in PDAC, which even forms a positive feedback loop for promoting the tumor progression. Besides miRNAs, LncRNAs and proteins in exosomes, although with low abundance, also play a pivotal role in PDAC microenvironment.

# CLINICAL APPLICATIONS OF EXOSOMES

## Exosomes as Biomarkers for Early and Non-Invasive Diagnosis of PDAC

The blur clinical signs and symptoms of PDAC result in a very low diagnosis rate during the early stages. Moreover, the current diagnostic techniques are insufficient to screen out early asymptomatic patients, and the serum tumor markers of PDAC, such as carbohydrate antigen 19-9 (CA19-9) and carcinoembryonic antigen (CEA), have limited specificity and sensitivity. Thus, the development of new and reliable biomarkers of PDAC is critical to improve the early detection and radical resection rates. Recently, the new liquid biopsy strategy mediated by exosomal markers has showed potential value as a non-invasive diagnostic method (**Figure 3**). Under the protection of endogenous membrane of the exosomes, the diagnostic markers can remain stable inside the blood circulation, which makes the diagnosis more reliable. Therefore, this strategy may become crucial for the non-invasive diagnosis of PDAC in the near future.

Exosomes loaded with multiple diagnostic molecules can be isolated from different types of body fluids, making the exosomal markers-based liquid biopsy more attractive for early tumor detection, tumor progression monitoring, and prognosis assessment. Many studies have highlighted the possibility of clinical translation of exosomal biomarkers in PDAC (**Table 2**). Plasma exosomal miR-21 could be used to differentiate patients with PDAC, intraductal papillary mucinous neoplasm (IPMN) and healthy participants (HP) (48, 49). Goto et al. (50) reported that exosomal miR-21 isolated from pancreatic juice using ultracentrifugation could also differentiate PDAC and chronic pancreatitis (CP). The patients with PDAC had a higher level of exosomal miR-451 than the HP, and the expression level of miR-451 wassignificantly correlated with recurrence and survival time (48, 51). Plasma exosomal miR-196a and miR-1246 also showed diagnostic value for localized pancreatic cancer (52). Moreover, the combination of multiple exosomal biomarkers to create a predictive model significantly improved the accuracy of diagnosis and prognosis (53, 55). In a clinical study with large cohorts, Melo et al. (54) found that Glypican-1 (GPC1), a cell surface proteoglycan, was specifically enriched in tumor cell-derived exosomes, and GPC1+ exosomes in the serum served as a non-invasive diagnostic and screening biomarker with absolute sensitivity and specificity (AUC = 1.0). GPC1+ exosomes could also distinguish patients with early and late PDAC from HP and patients with benign pancreatic disease (BPD) (56–58).

In summary, the exosome-mediated non-invasive diagnosis strategy may overcome the shortages of traditional serum tumor markers for early detection of PDAC. However, a single exosomal marker used for diagnosis is usually associated with high specificity and low sensitivity (59). Thus, comprehensive diagnostic strategies combining exosomal miRNAs, proteins and traditional serum tumor markers are urgently needed to improve the specificity and sensitivity of PDAC diagnosis.

## Exosomes as a Therapeutic Vehicle of PDAC

In recent years, researchers have made great progress in the development of exosomes as drug carriers (60, 61). As compared with liposomes and other nanoparticles, exosomes possess better biocompatibility as drug carriers (62). Injected exosomes shed from endogenous cells of the body are tolerated with minimal immune reaction and toxicity (63, 64). The cargos can be efficiently delivered into the tumor microenvironment using exosomes since these vesicles have the ability to penetrate the blood-tissue barrier. For instance, Alvarez-Erviti et al. (23) demonstrated that the self-derived exosomes were able to deliver siRNA to the brain through the blood-brain barrier. The therapeutic exosomes were found to be taken up by the target tissues in mice with low immune clearance rate *via* intravenous injection (55, 63). Mesenchymal cells- or epithelial cells- derived exosomes did not cause toxic side effects even after being repeatedly injected in mice (14). Kordelas et al. (65) isolated exosomes from the mesenchymal stem cells (MSCs) to treat graft-versus-host disease (GvHD) and found that the exosomes were well tolerated.

Since exosomal miRNAs have the potential capability to suppress the expression of target genes in recipient cells, investigators have tried to engineer the exosomes by loading target specific miRNA or siRNA to block the abnormal signaling pathways in PDAC cells in recent years. With the protection of the bilayer lipid membrane, exosomal RNAs can be safely transported to the lesion sites without any degradation by natural ribonucleases in the blood (66). The first clinical-grade MSCs-derived exosomes loaded with siRNA against $Kras^{G12D}$ was reported in 2017, which served as a promising therapeutic strategy in PDAC animal models (13). By targeting $Kras^{G12D}$ mutation of PDAC cells *in vivo*, these engineered exosomes showed a significantly increased overall survival without any toxicity. Moreover, this strategy has found its way to a Phase-I clinical trial in PDAC patients with $Kras^{G12D}$ mutation (NCT03608631).

In order to develop exosomes with a better target ability, we can conduct the modification of exosomes by direct or indirect methods, as discussed previously. For example, mouse immature dendritic cell-derived exosomes loaded with doxorubicin showed targeted αv integrin positive cancer cells with high efficacy, though engineering exosomes to express a fusion protein of Lamp2b and αv integrin-specific RGD (67). Thus, to achieve high targeting of PDAC tumor cells, a new therapeutic strategy

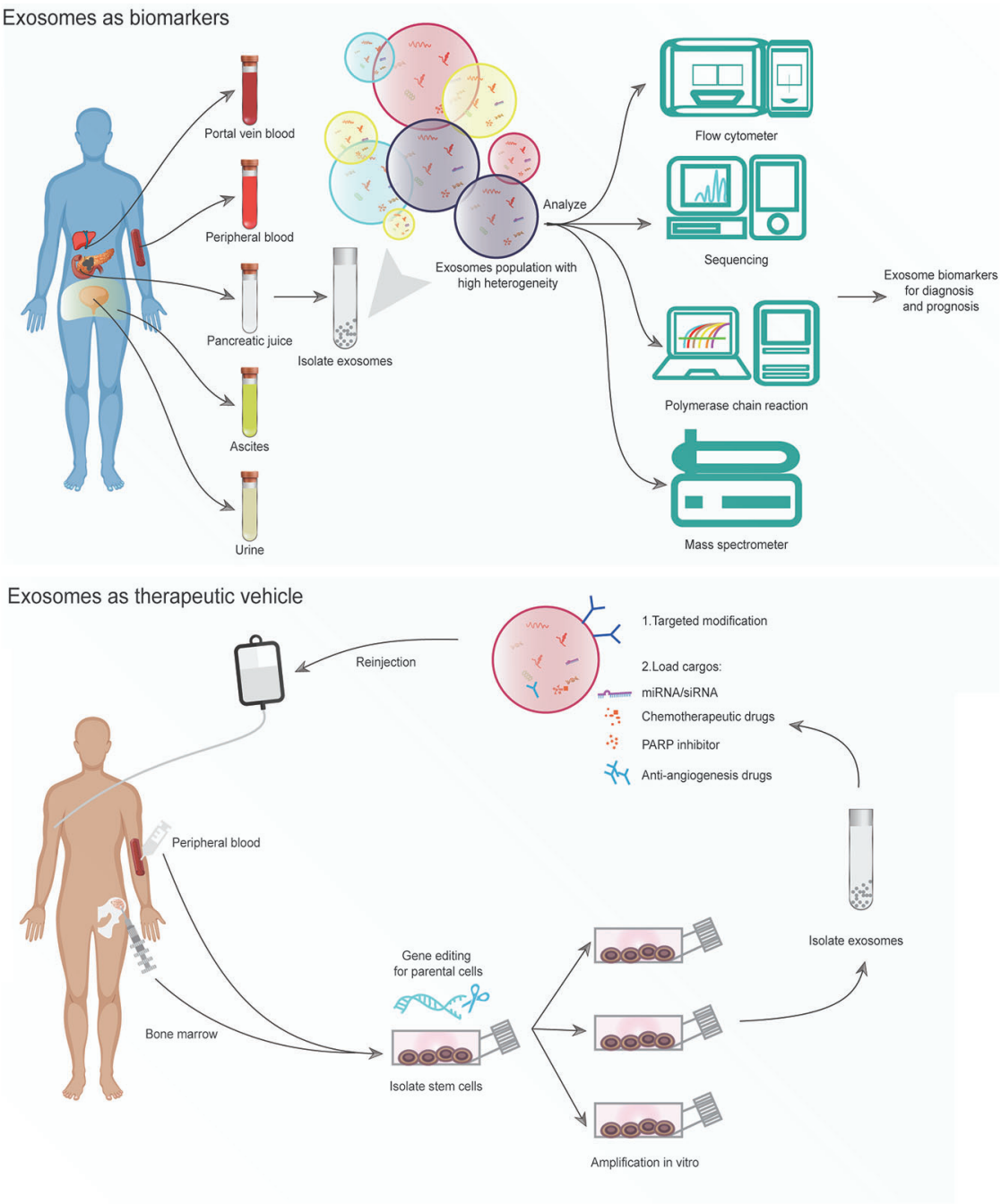


**FIGURE 3** | The clinical application of exosomes in pancreatic cancer. Exosomes are isolated from complex body fluids, including portal vein blood, peripheral blood, pancreatic juice, ascites, and urine. Exosomal miRNAs or proteins are identified as biomarkers for early diagnosis and the evaluation of prognosis. It is feasible to collect clinical-grade exosomes on a large scale to culture stem cells. The strategy of using exosomes as drug carriers holds significant therapeutic value when combined with exosome modification techniques.

can be developed by engineering exosomes and loading specific payloads such as siRNAs, inhibitors, or chemotherapy drugs followed by verifying the safety and efficacy of the exosomes in organoid and patient-derived tumor xenograft models.

## Exosomes and Tumor-Associated Neovasculature in PDAC

Tumor-associated neovasculature helps tumor cells in acquiring nutrients and oxygen and clearing metabolic wastes efficiently

**TABLE 2 |** Exosomes as biomarkers for diagnosis and prognosis of pancreatic ductal adenocarcinoma (PDAC).

| Exosomal cargo | Body fluid | Isolation method | Sample size | Clinical application | Reference |
|---|---|---|---|---|---|
| miR-21 | PVB and PB | Ultracentrifugation | 55 PDAC | Evaluation of recurrence and prognosis | (48) |
| | PB | ExoQuick-TC | 32 PDAC, 29 IPMN, and 22 HP | Early diagnosis | (49) |
| | Pancreatic juice | Ultracentrifugation | 27 PDAC and 8 CP | Early diagnosis | (50) |
| miR-451a | PVB and PB | Ultracentrifugation | 55 PDAC | Evaluation of recurrence and prognosis | (48) |
| | PB | Ultracentrifugation | 56 PDAC and 3 HP | Evaluation of recurrence and prognosis | (51) |
| miR-196a, miR-1246 | PB | ExoQuick-TC | 15 PDAC and 15 HP | Screen localized PDAC | (52) |
| Panel: CD44v6, Tspan8, EpCAM, MET, CD104 and miR-1246, miR-4644, miR-3976, miR-4306 | PB | Sucrose-gradient centrifugation | 131 PDAC, 25CP, 22 BPD and 42 HP | Early diagnosis | (53) |
| Glypican-1 | PB | Sucrose-gradient centrifugation | 246 PDAC, 24 CP, 5 IPMN, 8 BPD, and 20 HP | Early screening tool and evaluation of tumor burden and prognosis | (54) |

*PVB, Portal vein blood; PB, Peripheral blood; PDAC, Pancreatic adenocarcinoma; IPMN, Intraductal papillary mucinous neoplasm; HP, Healthy participants; CP, Chronic pancreatitis; BPD, Benign pancreatic disease.*

(68, 69). In the process of tumor development, angiogenesis-related signaling pathways are highly activated to support the continued growth of tumor lesions, which pave the way for local invasion and distant metastasis of tumor cells. However, PDAC is characterized by a lower microvascular density (MVD) with a high desmoplastic stromal reaction as compared with other tumors. The desmoplastic reaction results in a high pressure and collapse of the vascular structure inside PDAC. Thus, the limited vascular bed causes severe hypoxia stress in the tumor cells (70, 71). In order to adapt to the hypoxic environment, the endothelial cells (ECs) in PDAC develop hairy-like base microvilli to extend the vascular surface area, enhancing the glucose uptake rate. In addition, the basement membranes of blood vessels usually lose their integrity and develop various abnormal features such as variable diameters, excessive branching, and destroyed inter-endothelial junctions (69). All these features increase the possibility of early tumor metastasis. Thus, anti-angiogenesis therapy may bring hope for patients with PDAC. Unfortunately, the underlying mechanism of how the PDAC cells regulate angiogenesis is still not fully understood. Some clinical trials have demonstrated that anti-angiogenesis therapies failed to improve the prognosis of patients with PDAC (72–75). The complex tumor microenvironment and cell-to-cell communication among different components may contribute to the angiogenic regulation network in PDAC. Serving as a cell messenger, exosomes may play an essential role in cell-to-cell communication between ECs and other cells.

Accumulating evidences have suggested that angiogenesis inside tumors is regulated by cell-to-cell communication between ECs and other components of the tumors, including tumor cells, CAFs, and tumor-infiltrating lymphocytes (TILs), through soluble cytokines, gap junctions, and physical contact (68). Stromal cells and TILs were found to promote tumor growth *via* secreting VEGF (76). Masamune et al. (77) found that PSCs in the hypoxic environment release multiple angiogenic factors such as VEGF, MMP9, IL-8, and FGF-2 to induce ECs proliferation, migration, and angiogenesis *in vitro* and *in vivo*. In recent years, exosome-mediated cell-to-cell communications between ECs and other components inside tumors have attracted considerable attention (78). Hsu and colleagues (79) found that lung cancer derived exosomal miR-23a under hypoxic condition could inhibit the expression of PHD and ZO-1, resulting in an increase in angiogenesis and vascular permeability. Umezu et al. (80) demonstrated that exosomal miR-135b shed from hypoxic multiple myeloma cells enhanced angiogenesis *via* targeting HIF-1α. In addition, hypoxic glioblastoma derived exosomes were found to contain multiple angiogenic factors such as VEGFA, to promote the proliferation of ECs and increase the permeability of the blood-brain barrier (81, 82). However, in the field of PDAC, exosome-mediated interactions between ECs and other cells have not been elucidated. Fully understanding of these interactions under hypoxia is critical for the investigation of the special angiogenic regulation in PDAC, which will also help develop new anti-angiogenesis therapeutic strategies.

## CONCLUSIONS

PDAC is still one of the most lethal human cancers. The development of novel biomarkers and therapeutic targets is essential to improve the prognosis of patients with PDAC. Exosomes are becoming a promising tool for the early detection, prognosis assessment, and even therapeutic modality of PDAC. The studies on exosomes have progressed very rapidly in recent years. In this review, we have summarized the latest progress in the methodologies for isolation, modification, and tracking of exosomes, exosome-mediated cell-to-cell communication, clinical applications of exosome as minimally invasive liquid biopsy and drugs carrier, and their contribution to the angiogenic regulation in PDAC. Despite a lot of advancements, enormous challenges also exist. Firstly, there is still no gold standard for the isolation and identification of exosomes. The reported methods for purifying exosomes in reported studies vary a lot, making the results less reproducible or convincing. Secondly, the development of ideal exosome

isolation strategies with high purity and efficiency is currently unachievable and hence clinical-grade exosomes are difficult to acquire on a large scale. Most of the exosome engineering applications for the treatment of PDAC are only limited to cell or animal experiments. Thirdly, biogenesis and sorting mechanisms for exosomes have to be further explored to efficiently engineer exosomes with specific nucleic acids, proteins, and even exogenous drugs. Finally, most of the recent exosome-related mechanistic studies were conducted in normoxic conditions that only involved cancer cells. These situations do not represent the actual hypoxic microenvironment and the complicated components of PDAC. Considering the fact that exosome-mediated cell-to-cell communications among the different entities in PDAC may form a feedback loop instead of unidirectional signaling transmission, *in vitro* experimental results should be verified using animal models, or in patients with PDAC. In conclusion, there are still a few obstacles to be overcome before exosome-based technologies can be used for early diagnosis or improving the prognosis of patients with PDAC.

## AUTHOR CONTRIBUTIONS

KC designed this review and drafted the manuscript. KC and QW searched the related literature. KC prepared the tables and figures. MK, XT, and YY revised and polished the manuscript, and approved to submit manuscript. All authors contributed to the article and approved the submitted version.

## FUNDING

This study was supported by The Natural Science Foundation of China (NO. 81672353 and 81871954) and the Interdisciplinary Clinical Research Project of Peking University First Hospital.

## REFERENCES

1. Siegel RL, Miller KD, Jemal A. Cancer statistics, 2020. *CA Cancer J Clin* (2020) 70:7–30. doi: 10.3322/caac.21590
2. Ryan DP, Hong TS, Bardeesy N. Pancreatic adenocarcinoma. *N Engl J Med* (2014) 371:1039–49. doi: 10.1056/NEJMra1404198
3. Vincent A, Herman J, Schulick R, Hruban RH, Goggins M. Pancreatic cancer. *Lancet* (2011) 378:607–20. doi: 10.1016/S0140-6736(10)62307-0
4. Garrido-Laguna I, Hidalgo M. Pancreatic cancer: from state-of-the-art treatments to promising novel therapies. *Nat Rev Clin Oncol* (2015) 12:319–34. doi: 10.1038/nrclinonc.2015.53
5. Yang Y. Current status and future prospect of surgical treatment for pancreatic cancer. *Hepatobiliary Surg Nutr* (2020) 9:89–91. doi: 10.21037/hbsn.2019.12.04
6. Wunsch BH, Smith JT, Gifford SM, Wang C, Brink M, Bruce RL, et al. Nanoscale lateral displacement arrays for the separation of exosomes and colloids down to 20 nm. *Nat Nanotechnol* (2016) 11:936–40. doi: 10.1038/nnano.2016.134
7. Li Z, Tao Y, Wang X, Jiang P, Li J, Peng M, et al. Tumor-Secreted Exosomal miR-222 Promotes Tumor Progression via Regulating P27 Expression and Re-Localization in Pancreatic Cancer. *Cell Physiol Biochem* (2018) 51:610–29. doi: 10.1159/000495281
8. Sullivan R, Saez F, Girouard J, Frenette G. Role of exosomes in sperm maturation during the transit along the male reproductive tract. *Blood Cells Mol Dis* (2005) 35:1–10. doi: 10.1016/j.bcmd.2005.03.005
9. Gehrmann U, Naslund TI, Hiltbrunner S, Larssen P, Gabrielsson S. Harnessing the exosome-induced immune response for cancer immunotherapy. *Semin Cancer Biol* (2014) 28:58–67. doi: 10.1016/j.semcancer.2014.05.003
10. Melo SA, Sugimoto H, O'Connell JT, Kato N, Villanueva A, Vidal A, et al. Cancer exosomes perform cell-independent microRNA biogenesis and promote tumorigenesis. *Cancer Cell* (2014) 26:707–21. doi: 10.1016/j.ccell.2014.09.005
11. Fukushima K, Satoh T, Sugihara F, Sato Y, Okamoto T, Mitsui Y, et al. Dysregulated Expression of the Nuclear Exosome Targeting Complex Component Rbm7 in Nonhematopoietic Cells Licenses the Development of Fibrosis. *Immunity* (2020) 52:542–56.e13. doi: 10.1016/j.immuni.2020.02.007
12. Kahlert C, Melo SA, Protopopov A, Tang J, Seth S, Koch M, et al. Identification of double-stranded genomic DNA spanning all chromosomes with mutated KRAS and p53 DNA in the serum exosomes of patients with pancreatic cancer. *J Biol Chem* (2014) 289:3869–75. doi: 10.1074/jbc.C113.532267
13. Kamerkar S, LeBleu VS, Sugimoto H, Yang S, Ruivo CF, Melo SA, et al. Exosomes facilitate therapeutic targeting of oncogenic KRAS in pancreatic cancer. *Nature* (2017) 546:498–503. doi: 10.1038/nature22341
14. Mendt M, Kamerkar S, Sugimoto H, McAndrews KM, Wu CC, Gagea M, et al. Generation and testing of clinical-grade exosomes for pancreatic cancer. *JCI Insight* (2018) 3:e99263. doi: 10.1172/jci.insight.99263
15. Li Z, Jiang P, Li J, Peng M, Zhao X, Zhang X, et al. Tumor-derived exosomal lnc-Sox2ot promotes EMT and stemness by acting as a ceRNA in pancreatic ductal adenocarcinoma. *Oncogene* (2018) 37:3822–38. doi: 10.1038/s41388-018-0237-9
16. Lobb RJ, Becker M, Wen SW, Wong CS, Wiegmans AP, Leimgruber A, et al. Optimized exosome isolation protocol for cell culture supernatant and human plasma. *J Extracell Vesicles* (2015) 4:27031. doi: 10.3402/jev.v4.27031
17. Stranska R, Gysbrechts L, Wouters J, Vermeersch P, Bloch K, Dierickx D, et al. Comparison of membrane affinity-based method with size-exclusion chromatography for isolation of exosome-like vesicles from human plasma. *J Transl Med* (2018) 16:1. doi: 10.1186/s12967-017-1374-6
18. Gurunathan S, Kang MH, Jeyaraj M, Qasim M, Kim JH. Review of the Isolation, Characterization, Biological Function, and Multifarious Therapeutic Approaches of Exosomes. *Cells* (2019) 8:307. doi: 10.3390/cells8040307
19. Yang D, Zhang W, Zhang H, Zhang F, Chen L, Ma L, et al. Progress, opportunity, and perspective on exosome isolation - efforts for efficient exosome-based theranostics. *Theranostics* (2020) 10:3684–707. doi: 10.7150/thno.41580
20. Zhang H, Freitas D, Kim HS, Fabijanic K, Li Z, Chen H, et al. Identification of distinct nanoparticles and subsets of extracellular vesicles by asymmetric flow field-flow fractionation. *Nat Cell Biol* (2018) 20:332–43. doi: 10.1038/s41556-018-0040-4
21. Niu F, Chen X, Niu X, Cai Y, Zhang Q, Chen T, et al. Integrated Immunomagnetic Bead-Based Microfluidic Chip for Exosomes Isolation. *Micromachines (Basel)* (2020) 11:503. doi: 10.3390/mi11050503
22. Lee K, Shao H, Weissleder R, Lee H. Acoustic purification of extracellular microvesicles. *ACS Nano* (2015) 9:2321–7. doi: 10.1021/nn506538f
23. Alvarez-Erviti L, Seow Y, Yin H, Betts C, Lakhal S, Wood MJ. Delivery of siRNA to the mouse brain by systemic injection of targeted exosomes. *Nat Biotechnol* (2011) 29:341–45. doi: 10.1038/nbt.1807
24. Ohno S, Takanashi M, Sudo K, Ueda S, Ishikawa A, Matsuyama N, et al. Systemically injected exosomes targeted to EGFR deliver antitumor microRNA to breast cancer cells. *Mol Ther* (2013) 21:185–91. doi: 10.1038/mt.2012.180
25. Sterzenbach U, Putz U, Low LH, Silke J, Tan SS, Howitt J. Engineered Exosomes as Vehicles for Biologically Active Proteins. *Mol Ther* (2017) 25:1269–78. doi: 10.1016/j.ymthe.2017.03.030

26. Royo F, Cossio U, Ruiz de Angulo A, Llop J, Falcon-Perez JM. Modification of the glycosylation of extracellular vesicles alters their biodistribution in mice. *Nanoscale* (2019) 11:1531–37. doi: 10.1039/c8nr03900c
27. Lee H, Park H, Noh GJ, Lee ES. pH-responsive hyaluronate-anchored extracellular vesicles to promote tumor-targeted drug delivery. *Carbohydr Polym* (2018) 202:323–33. doi: 10.1016/j.carbpol.2018.08.141
28. Hikita T, Miyata M, Watanabe R, Oneyama C. Sensitive and rapid quantification of exosomes by fusing luciferase to exosome marker proteins. *Sci Rep* (2018) 8:14035. doi: 10.1038/s41598-018-32535-7
29. Suetsugu A, Honma K, Saji S, Moriwaki H, Ochiya T, Hoffman RM. Imaging exosome transfer from breast cancer cells to stroma at metastatic sites in orthotopic nude-mouse models. *Adv Drug Deliv Rev* (2013) 65:383–90. doi: 10.1016/j.addr.2012.08.007
30. Takahashi Y, Nishikawa M, Shinotsuka H, Matsui Y, Ohara S, Imai T, et al. Visualization and in vivo tracking of the exosomes of murine melanoma B16-BL6 cells in mice after intravenous injection. *J Biotechnol* (2013) 165:77–84. doi: 10.1016/j.jbiotec.2013.03.013
31. Lee TS, Kim Y, Zhang W, Song IH, Tung CH. Facile metabolic glycan labeling strategy for exosome tracking. *Biochim Biophys Acta Gen Subj* (2018) 1862:1091–100. doi: 10.1016/j.bbagen.2018.02.001
32. Busato A, Bonafede R, Bontempi P, Scambi I, Schiaffino L, Benati D, et al. Magnetic resonance imaging of ultrasmall superparamagnetic iron oxide-labeled exosomes from stem cells: a new method to obtain labeled exosomes. *Int J Nanomed* (2016) 11:2481–90. doi: 10.2147/IJN.S104152
33. Jiang X, Zong S, Chen C, Zhang Y, Wang Z, Cui Y. Gold-carbon dots for the intracellular imaging of cancer-derived exosomes. *Nanotechnology* (2018) 29:175701. doi: 10.1088/1361-6528/aaaf14
34. Hwang DW, Choi H, Jang SC, Yoo MY, Park JY, Choi NE, et al. Noninvasive imaging of radiolabeled exosome-mimetic nanovesicle using (99m)Tc-HMPAO. *Sci Rep* (2015) 5:15636. doi: 10.1038/srep15636
35. Fan J, Wei Q, Koay EJ, Liu Y, Ning B, Bernard PW, et al. Chemoresistance Transmission via Exosome-Mediated EphA2 Transfer in Pancreatic Cancer. *Theranostics* (2018) 8:5986–94. doi: 10.7150/thno.26650
36. Yang Z, Zhao N, Cui J, Wu H, Xiong J, Peng T. Exosomes derived from cancer stem cells of gemcitabine-resistant pancreatic cancer cells enhance drug resistance by delivering miR-210. *Cell Oncol (Dordr)* (2020) 43:123–36. doi: 10.1007/s13402-019-00476-6
37. Gao X, Wan Z, Wei M, Dong Y, Zhao Y, Chen X, et al. Chronic myelogenous leukemia cells remodel the bone marrow niche via exosome-mediated transfer of miR-320. *Theranostics* (2019) 9:5642–56. doi: 10.7150/thno.34813
38. Costa-Silva B, Aiello NM, Ocean AJ, Singh S, Zhang H, Thakur BK, et al. Pancreatic cancer exosomes initiate pre-metastatic niche formation in the liver. *Nat Cell Biol* (2015) 17:816–26. doi: 10.1038/ncb3169
39. Kalluri R. The biology and function of fibroblasts in cancer. *Nat Rev Cancer* (2016) 16:582–98. doi: 10.1038/nrc.2016.73
40. Mashouri L, Yousefi H, Aref AR, Ahadi AM, Molaei F, Alahari SK. Exosomes: composition, biogenesis, and mechanisms in cancer metastasis and drug resistance. *Mol Cancer* (2019) 18:75. doi: 10.1186/s12943-019-0991-5
41. Valadi H, Ekstrom K, Bossios A, Sjostrand M, Lee JJ, Lotvall JO. Exosome-mediated transfer of mRNAs and microRNAs is a novel mechanism of genetic exchange between cells. *Nat Cell Biol* (2007) 9:654–U72. doi: 10.1038/ncb1596
42. Rachagani S, Macha MA, Heimann N, Seshacharyulu P, Haridas D, Chugh S, et al. Clinical implications of miRNAs in the pathogenesis, diagnosis and therapy of pancreatic cancer. *Adv Drug Deliv Rev* (2015) 81:16–33. doi: 10.1016/j.addr.2014.10.020
43. Wang X, Luo G, Zhang K, Cao J, Huang C, Jiang T, et al. Hypoxic Tumor-Derived Exosomal miR-301a Mediates M2 Macrophage Polarization via PTEN/PI3Kgamma to Promote Pancreatic Cancer Metastasis. *Cancer Res* (2018) 78:4586–98. doi: 10.1158/0008-5472.CAN-17-3841
44. Sun H, Shi K, Qi K, Kong H, Zhang J, Dai S, et al. Natural Killer Cell-Derived Exosomal miR-3607-3p Inhibits Pancreatic Cancer Progression by Targeting IL-26. *Front Immunol* (2019) 10:2819. doi: 10.3389/fimmu.2019.02819
45. Fang Y, Zhou W, Rong Y, Kuang T, Xu X, Wu W, et al. Exosomal miRNA-106b from cancer-associated fibroblast promotes gemcitabine resistance in pancreatic cancer. *Exp Cell Res* (2019) 383:111543. doi: 10.1016/j.yexcr.2019.111543
46. Ma Q, Wu H, Xiao Y, Liang Z, Liu T. Upregulation of exosomal microRNA21 in pancreatic stellate cells promotes pancreatic cancer cell migration and enhances Ras/ERK pathway activity. *Int J Oncol* (2020) 56:1025–33. doi: 10.3892/ijo.2020.4986
47. Jiang MJ, Chen YY, Dai JJ, Gu DN, Mei Z, Liu FR, et al. Dying tumor cell-derived exosomal miR-194-5p potentiates survival and repopulation of tumor repopulating cells upon radiotherapy in pancreatic cancer. *Mol Cancer* (2020) 19:68. doi: 10.1186/s12943-020-01178-6
48. Kawamura S, Iinuma H, Wada K, Takahashi K, Minezaki S, Kainuma M, et al. Exosome-encapsulated microRNA-4525, microRNA-451a and microRNA-21 in portal vein blood is a high-sensitive liquid biomarker for the selection of high-risk pancreatic ductal adenocarcinoma patients. *J Hepatobiliary Pancreat Sci* (2019) 26:63–72. doi: 10.1002/jhbp.601
49. Goto T, Fujiya M, Konishi H, Sasajima J, Fujibayashi S, Hayashi A, et al. An elevated expression of serum exosomal microRNA-191, - 21, -451a of pancreatic neoplasm is considered to be efficient diagnostic marker. *BMC Cancer* (2018) 18:116. doi: 10.1186/s12885-018-4006-5
50. Nakamura S, Sadakari Y, Ohtsuka T, Okayama T, Nakashima Y, Gotoh Y, et al. Pancreatic Juice Exosomal MicroRNAs as Biomarkers for Detection of Pancreatic Ductal Adenocarcinoma. *Ann Surg Oncol* (2019) 26:2104–11. doi: 10.1245/s10434-019-07269-z
51. Takahasi K, Iinuma H, Wada K, Minezaki S, Kawamura S, Kainuma M, et al. Usefulness of exosome-encapsulated microRNA-451a as a minimally invasive biomarker for prediction of recurrence and prognosis in pancreatic ductal adenocarcinoma. *J Hepatobiliary Pancreat Sci* (2018) 25:155–61. doi: 10.1002/jhbp.524
52. Xu YF, Hannafon BN, Zhao YD, Postier RG, Ding WQ. Plasma exosome miR-196a and miR-1246 are potential indicators of localized pancreatic cancer. *Oncotarget* (2017) 8:77028–40. doi: 10.18632/oncotarget.20332
53. Madhavan B, Yue S, Galli U, Rana S, Gross W, Muller M, et al. Combined evaluation of a panel of protein and miRNA serum-exosome biomarkers for pancreatic cancer diagnosis increases sensitivity and specificity. *Int J Cancer* (2015) 136:2616–27. doi: 10.1002/ijc.29324
54. Melo SA, Luecke LB, Kahlert C, Fernandez AF, Gammon ST, Kaye J, et al. Glypican-1 identifies cancer exosomes and detects early pancreatic cancer. *Nature* (2015) 523:177–82. doi: 10.1038/nature14581
55. Ferguson SW, Nguyen J. Exosomes as therapeutics: The implications of molecular composition and exosomal heterogeneity. *J Control Release* (2016) 228:179–90. doi: 10.1016/j.jconrel.2016.02.037
56. Frampton AE, Prado MM, Lopez-Jimenez E, Fajardo-Puerta AB, Jawad ZAR, Lawton P, et al. Glypican-1 is enriched in circulating-exosomes in pancreatic cancer and correlates with tumor burden. *Oncotarget* (2018) 9:19006–13. doi: 10.18632/oncotarget.24873
57. Buscail E, Chauvet A, Quincy P, Degrandi O, Buscail C, Lamrissi I, et al. CD63-GPC1-Positive Exosomes Coupled with CA19-9 Offer Good Diagnostic Potential for Resectable Pancreatic Ductal Adenocarcinoma. *Transl Oncol* (2019) 12:1395–403. doi: 10.1016/j.tranon.2019.07.009
58. Xiao D, Dong Z, Zhen L, Xia G, Huang X, Wang T, et al. Combined Exosomal GPC1, CD82, and Serum CA19-9 as Multiplex Targets: A Specific, Sensitive, and Reproducible Detection Panel for the Diagnosis of Pancreatic Cancer. *Mol Cancer Res* (2020) 18:300–10. doi: 10.1158/1541-7786.MCR-19-0588
59. Ye H, Wang H, Wang P, Song CH, Wang KJ, Dai LP, et al. Systematic review: exosomal microRNAs associated with pancreatic cancer for early detection and prognosis. *Eur Rev Med Pharmacol Sci* (2019) 23:9351–61. doi: 10.26355/eurrev_201911_19428
60. Jabbari N, Akbariazar E, Feqhhi M, Rahbarghazi R, Rezaie J. Breast cancer-derived exosomes: Tumor progression and therapeutic agents. *J Cell Physiol* (2020) 235:6345–56. doi: 10.1002/jcp.29668
61. Jabbari N, Karimipour M, Khaksar M, Akbariazar E, Heidarzadeh M, Mojarad B, et al. Tumor-derived extracellular vesicles: insights into bystander effects of exosomes after irradiation. *Lasers Med Sci* (2020) 35:531–45. doi: 10.1007/s10103-019-02880-8
62. Akbari A, Jabbari N, Sharifi R, Ahmadi M, Vahhabi A, Seyedzadeh SJ, et al. Free and hydrogel encapsulated exosome-based therapies in regenerative medicine. *Life Sci* (2020) 249:117447. doi: 10.1016/j.lfs.2020.117447
63. Fitts CA, Ji N, Li Y, Tan C. Exploiting Exosomes in Cancer Liquid Biopsies and Drug Delivery. *Adv Healthc Mater* (2019) 8:e1801268. doi: 10.1002/adhm.201801268
64. Zhu X, Badawi M, Pomeroy S, Sutaria DS, Xie Z, Baek A, et al. Comprehensive toxicity and immunogenicity studies reveal minimal effects in mice following

sustained dosing of extracellular vesicles derived from HEK293T cells. *J Extracell Vesicles* (2017) 6:1324730. doi: 10.1080/20013078.2017.1324730
65. Kordelas L, Rebmann V, Ludwig AK, Radtke S, Ruesing J, Doeppner TR, et al. MSC-derived exosomes: a novel tool to treat therapy-refractory graft-versus-host disease. *Leukemia* (2014) 28:970–3. doi: 10.1038/leu.2014.41
66. Cheng L, Sharples RA, Scicluna BJ, Hill AF. Exosomes provide a protective and enriched source of miRNA for biomarker profiling compared to intracellular and cell-free blood. *J Extracell Vesicles* (2014) 3. doi: 10.3402/jev.v3.23743
67. Tian Y, Li S, Song J, Ji T, Zhu M, Anderson GJ, et al. A doxorubicin delivery platform using engineered natural membrane vesicle exosomes for targeted tumor therapy. *Biomaterials* (2014) 35:2383–90. doi: 10.1016/j.biomaterials.2013.11.083
68. Lopes-Bastos BM, Jiang WG, Cai J. Tumour-Endothelial Cell Communications: Important and Indispensable Mediators of Tumour Angiogenesis. *Anticancer Res* (2016) 36:1119–26.
69. Zhang Z, Ji S, Zhang B, Liu J, Qin Y, Xu J, et al. Role of angiogenesis in pancreatic cancer biology and therapy. *BioMed Pharmacother* (2018) 108:1135–40. doi: 10.1016/j.biopha.2018.09.136
70. Provenzano PP, Cuevas C, Chang AE, Goel VK, Von Hoff DD, Hingorani SR. Enzymatic targeting of the stroma ablates physical barriers to treatment of pancreatic ductal adenocarcinoma. *Cancer Cell* (2012) 21:418–29. doi: 10.1016/j.ccr.2012.01.007
71. Longo V, Brunetti O, Gnoni A, Cascinu S, Gasparini G, Lorusso V, et al. Angiogenesis in pancreatic ductal adenocarcinoma: A controversial issue. *Oncotarget* (2016) 7:58649–58. doi: 10.18632/oncotarget.10765
72. Kindler HL, Niedzwiecki D, Hollis D, Sutherland S, Schrag D, Hurwitz H, et al. Gemcitabine plus bevacizumab compared with gemcitabine plus placebo in patients with advanced pancreatic cancer: phase III trial of the Cancer and Leukemia Group B (CALGB 80303). *J Clin Oncol* (2010) 28:3617–22. doi: 10.1200/JCO.2010.28.1386
73. Goncalves A, Gilabert M, Francois E, Dahan L, Perrier H, Lamy R, et al. BAYPAN study: a double-blind phase III randomized trial comparing gemcitabine plus sorafenib and gemcitabine plus placebo in patients with advanced pancreatic cancer. *Ann Oncol* (2012) 23:2799–05. doi: 10.1093/annonc/mds135
74. Bergmann L, Maute L, Heil G, Russel J, Weidmann E, Koberle D, et al. A prospective randomised phase-II trial with gemcitabine versus gemcitabine plus sunitinib in advanced pancreatic cancer: a study of the CESAR Central European Society for Anticancer Drug Research-EWIV. *Eur J Cancer* (2015) 51:27–36. doi: 10.1016/j.ejca.2014.10.010
75. El-Khoueiry AB, Ramanathan RK, Yang DY, Zhang W, Shibata S, Wright JJ, et al. A randomized phase II of gemcitabine and sorafenib versus sorafenib alone in patients with metastatic pancreatic cancer. *Invest N Drugs* (2012) 30:1175–83. doi: 10.1007/s10637-011-9658-9
76. Fukumura D, Xavier R, Sugiura T, Chen Y, Park EC, Lu N, et al. Tumor induction of VEGF promoter activity in stromal cells. *Cell* (1998) 94:715–25. doi: 10.1016/s0092-8674(00)81731-6
77. Masamune A, Kikuta K, Watanabe T, Satoh K, Hirota M, Shimosegawa T. Hypoxia stimulates pancreatic stellate cells to induce fibrosis and angiogenesis in pancreatic cancer. *Am J Physiol Gastrointest Liver Physiol* (2008) 295:G709–17. doi: 10.1152/ajpgi.90356.2008
78. Ahmadi M, Rezaie J. Tumor cells derived-exosomes as angiogenenic agents: possible therapeutic implications. *J Transl Med* (2020) 18:249. doi: 10.1186/s12967-020-02426-5
79. Hsu YL, Hung JY, Chang WA, Lin YS, Pan YC, Tsai PH, et al. Hypoxic lung cancer-secreted exosomal miR-23a increased angiogenesis and vascular permeability by targeting prolyl hydroxylase and tight junction protein ZO-1. *Oncogene* (2017) 36:4929–42. doi: 10.1038/onc.2017.105
80. Umezu T, Tadokoro H, Azuma K, Yoshizawa S, Ohyashiki K, Ohyashiki JH. Exosomal miR-135b shed from hypoxic multiple myeloma cells enhances angiogenesis by targeting factor-inhibiting HIF-1. *Blood* (2014) 124:3748–57. doi: 10.1182/blood-2014-05-576116
81. Zhao C, Wang H, Xiong C, Liu Y. Hypoxic glioblastoma release exosomal VEGF-A induce the permeability of blood-brain barrier. *Biochem Biophys Res Commun* (2018) 502:324–31. doi: 10.1016/j.bbrc.2018.05.140
82. Skog J, Wurdinger T, van Rijn S, Meijer DH, Gainche L, Sena-Esteves M, et al. Glioblastoma microvesicles transport RNA and proteins that promote tumour growth and provide diagnostic biomarkers. *Nat Cell Biol* (2008) 10:1470–6. doi: 10.1038/ncb1800

**Conflict of Interest:** The authors declare that the research was conducted in the absence of any commercial or financial relationships that could be construed as a potential conflict of interest.

frontiers in Oncology

SYSTEMATIC REVIEW
published: 09 March 2021
doi: 10.3389/fonc.2021.612903

# *In Vivo* Efficacy and Toxicity of Curcumin Nanoparticles in Breast Cancer Treatment: A Systematic Review

*Alicia S. Ombredane[1,2], Vitória R. P. Silva[1], Laise R. Andrade[3], Willie O. Pinheiro[4], Mayara Simonelly[3], Jaqueline V. Oliveira[5], Andréia C. Pinheiro[1,2], Gabriel F. Gonçalves[1], Gisela J. Felice[1], Mônica P. Garcia[2,3], Patrícia M. Campos[6], Glécia V. S. Luz[7,8] and Graziella A. Joanitti[1,2,3]**

[1] Laboratory of Bioactive Compounds and Nanobiotechnology (LBCNano), University of Brasilia, Brasilia, Brazil, [2] Post-Graduation Program in Nanoscience and Nanobiotechnology, Institute of Biological Sciences, University of Brasilia, Brasilia, Brazil, [3] Department of Genetics & Morphology, Institute of Biological Sciences, University of Brasilia, Brasilia, Brazil, [4] Post-Graduation Program in Sciences and Technologies in Health, Faculty of Ceilandia, University of Brasilia, Brasilia, Brazil, [5] Department of Immunology, Institute of Biomedical Sciences, University of Sao Paulo, Sao Paulo, Brazil, [6] Pharmaceutical Sciences Department, State University of Ponta Grossa, Parana, Brazil, [7] Post-Graduate Program in Biomedical Engineering-PPGEB, Faculty of Gama-FGA, University of Brasilia, Brasilia, Brazil, [8] Health Technology Assessment Center-NATS/UnB, University of Brasília, Brasilia, Brazil

OPEN ACCESS

**Edited by:**
*Marcelo Calderon, Polymat, Spain*

**Reviewed by:**
*Biana Godin, Houston Methodist Research Institute, United States*
*Michele Caraglia, University of Campania Luigi Vanvitelli, Italy*

***Correspondence:**
*Graziella A. Joanitti*
*bygra1@gmail.com*

**Specialty section:**
*This article was submitted to Cancer Molecular Targets and Therapeutics, a section of the journal Frontiers in Oncology*

**Received:** *01 October 2020*
**Accepted:** *20 January 2021*
**Published:** *09 March 2021*

**Citation:**
*Ombredane AS, Silva VRP, Andrade LR, Pinheiro WO, Simonelly M, Oliveira JV, Pinheiro AC, Gonçalves GF, Felice GJ, Garcia MP, Campos PM, Luz GVS and Joanitti GA (2021) In Vivo Efficacy and Toxicity of Curcumin Nanoparticles in Breast Cancer Treatment: A Systematic Review. Front. Oncol. 11:612903. doi: 10.3389/fonc.2021.612903*

Breast cancer is one of the most prevalent types of malignant tumors in the world, resulting in a high incidence of death. The development of new molecules and technologies aiming to apply more effective and safer therapy strategies has been intensively explored to overcome this situation. The association of nanoparticles with known antitumor compounds (including plant-derived molecules such as curcumin) has been considered an effective approach to enhance tumor growth suppression and reduce adverse effects. Therefore, the objective of this systematic review was to summarize published data regarding evaluations about efficacy and toxicity of curcumin nanoparticles (Cur-NPs) in *in vivo* models of breast cancer. The search was carried out in the databases: CINAHL, Cochrane, LILACS, Embase, FSTA, MEDLINE, ProQuest, BSV regional portal, PubMed, ScienceDirect, Scopus, and Web of Science. Studies that evaluated tumor growth in *in vivo* models of breast cancer and showed outcomes related to Cur-NP treatment (without association with other antitumor molecules) were included. Of the 528 initially gathered studies, 26 met the inclusion criteria. These studies showed that a wide variety of NP platforms have been used to deliver curcumin (*e.g.*, micelles, polymeric, lipid-based, metallic). Attachment of poly(ethylene glycol) chains (PEG) and active targeting moieties were also evaluated. Cur-NPs significantly reduced tumor volume/weight, inhibited cancer cell proliferation, and increased tumor apoptosis and necrosis. Decreases in cancer stem cell population and angiogenesis were also reported. All the studies that evaluated toxicity considered Cur-NP treatment to be safe regarding hematological/biochemical markers, damage to major organs, and/or weight loss. These effects were observed in different *in vivo* models of breast cancer (*e.g.*, estrogen

receptor-positive, triple-negative, chemically induced) showing better outcomes when compared to treatments with free curcumin or negative controls. This systematic review supports the proposal that Cur-NP is an effective and safe therapeutic approach in *in vivo* models of breast cancer, reinforcing the currently available evidence that it should be further analyzed in clinical trials for breast cancer treatments.

**Keywords: breast cancer, nanoparticle, curcumin, apoptosis, antitumor, toxicity, *in vivo*, systematic review**

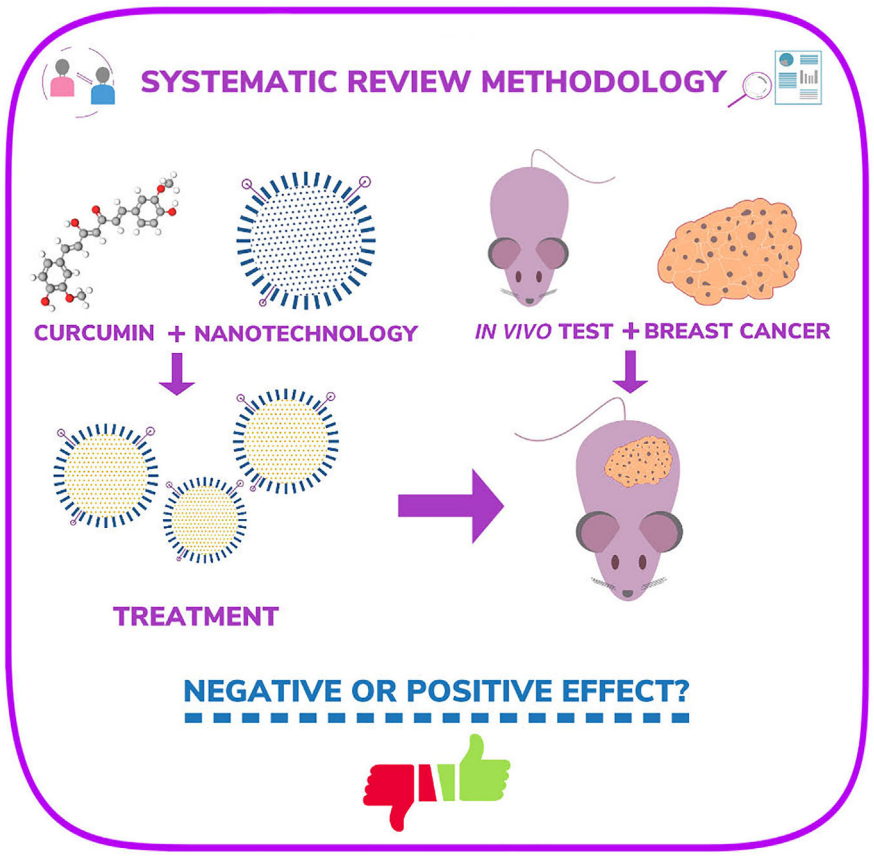


**GRAPHICAL ABSTRACT** |

## INTRODUCTION

Among women, breast cancer is the most prevalent cancer worldwide, with 2.1 million cases reported in 2018 (with an annual increase of 3.1%) and more than 620,000 deaths per year (1, 2). Breast cancer is divided into five major intrinsic molecular subtypes: luminal A-like (60–70%), luminal B-like human epidermal growth factor receptor-type 2 negative (HER2–) (10–20%), HER2-enriched (non-luminal) and luminal B-like HER2+ (13–15%), and triple-negative (10–15%) (1). Early diagnosis of breast cancer raises the chances of total recuperation of patients, and the treatment concept is decided based on several criteria such as subtype and grade (3). Chemotherapy and endocrine therapy are typical systemic therapies in non-metastatic breast cancer. They can be associated with local therapy like surgery and radiation (3). In most cases, metastatic breast cancer remains incurable and therapy aims to prolong life and alleviate symptoms (3). However, these conventional treatments present some limitations, like resistance to chemotherapy or endocrine therapy, and some adverse effects (4). Thus, alternative treatments must be investigated to improve the recovery of breast cancer patients, reduce adverse effects, and circumvent therapy resistance.

Natural products are considered as promising alternatives for the development of new antitumor drugs (5, 6). Curcumin, or diferuloylmethane, is a yellow pigment extracted from the rhizomes of *Curcuma longa* Linn, also known as turmeric. It is the most abundant polyphenol and curcuminoid present in the

root of this plant (7). Usually used in culinary and traditional medicine, curcumin also interests conventional medicine by demonstrating antioxidant and anti-inflammatory activities (7). Its anti-cancer effect was reported for the first time in 1985, by Kuttan and co-workers, in cells and animal models of lymphoma (8). In breast cancer, curcumin inhibits cell proliferation, induces apoptosis (5) and acts as a potent antiangiogenic, anti-invasive, and anti-metastatic agent *in vitro* and *in vivo* (9). Curcumin also demonstrated the capacity to reverse chemotherapeutic resistance in doxorubicin-resistant breast cancer cells (MCF-7/DOX and MDA-MB-231/DOX) (10). Moreover, curcumin led to the downregulation of aldehyde dehydrogenase-1, and p-glycoprotein-mediated multidrug resistance gene expression, increasing sensitivity of breast cancer cells (MCF-7) to paclitaxel (11). However, the therapeutic application of curcumin is limited due to its poor water solubility and low bioavailability. Thus, some studies have investigated the use of nanoparticles (NPs) to deliver curcumin to breast cancer cells and enhance its bioavailability and efficacy (12).

Nanotechnology is a strong alternative tool to improve application of hydrophobic molecules. The use of NPs increases the stability and bioavailability of antitumor compounds, reduces therapeutic doses, and minimizes possible adverse effects (13). Several types of NPs can be used as drug delivery systems, such as polymer NPs, liposomes, nanoemulsions, metal NPs, micelles, solid lipid NPs, dendrimers, nanospheres, and nanocapsules (14). These NPs can also be associated with other molecules like aptamers, antibodies, or polymers as active targeting moieties. This surface modification can improve the specificity of NPs to tumor cells, facilitate their interaction, and, consequently, increase antitumor effects (13).

At present, there are several clinical trials in which curcumin has been evaluated, mainly after oral administration regimens, in breast cancer patients (*e.g.*, NCT03980509, NCT01042938, NCT03847623, NCT03865992, NCT01740323, NCT01975363, NCT02556632, NCT01246973, NCT03482401) (15). So far, only one clinical trial using intravenous administration of a curcumin water-soluble formulation (CUC-1®) in combination with paclitaxel in breast cancer patients has been registered (NCT03072992) (15).

A substantial number of studies have been published describing the activity of Cur-NPs in *in vivo* models of breast cancer. Nevertheless, to the best of our knowledge, a systematic review on this subject has not been published yet. Therefore, considering the importance of *in vivo* studies and their clinical translation, the aim of this systematic review was to summarize published data regarding evaluations about efficacy and toxicity of Cur-NPs in *in vivo* models of breast cancer, as well as showing evidence for the potential of this therapeutic approach for clinical trial investigations. Although several works describing interesting data regarding the combination of curcumin with chemotherapeutic drugs have been published (16, 17), the present systematic review was performed to cover studies evaluating curcumin as the active antitumor agent, associated with NPs, to understand better the effects on breast tumor progression of curcumin itself and the advantages/limitations of using NPs as its dug carrier.

# MATERIALS AND METHODS

## Protocol and Registration

The present study was conducted according to the Preferred Reporting Items for Systematic Reviews and Meta-Analyses (PRISMA) guidelines (18). The protocol for this systematic review was registered in the International Prospective Register of Systematic Reviews (PROSPERO) (19) with registration number: CRD42020209159.

### Eligibility Criteria

#### *Inclusion Criteria*

This systematic review based the inclusion criteria on the PICOS (Population, Intervention, Comparison, Outcome, and Study Design) approach (20). We considered studies which evaluated the efficacy and toxicity (O) of Cur-NPs (I) compared with free curcumin and/or negative control (C) on *in vivo* models of breast cancer in mice or rats (P).

#### *Exclusion Criteria*

Studies were excluded for the following reasons: i) reviews, letters, personal opinions, book chapters, and conference abstracts; ii) *in vitro* studies and clinical trials; iii) use of only free curcumin or curcumin derivatives; iv) other types of cancer; v) use of Cur-NPs associated with other antitumor compounds; vi) full paper copy not available; vii) low quality.

### Information Sources and Search Strategy

Individual search strategies were designed for each of the following bibliographic databases: CINAHL, Cochrane, LILACS, Embase, FSTA, MEDLINE, ProQuest, BSV regional portal, PubMed, ScienceDirect, Scopus, and Web of Science (**Table S1**). The search on databases was performed on August 10 and 11, 2020, with no time restriction. Duplicated references were removed by reference manager software (Mendeley®). There were no restrictions on language and period of publication.

### Study Selection

The articles were selected in two phases: screening of titles and abstracts (phase 1) and full text reading (phase 2). In phase 1, two authors (A.S.O. and V.R.P.S) reviewed titles and abstracts of all references identified in the electronic databases and selected articles that seemed to meet the inclusion criteria. In phase 2, six pairs of authors (A.S.O and V.R.P.S.; L.R.A and G.J.F; W.O.P and A.C.P; J.V.O and M.P.G; M.S and G.F.G; P.M.C. and G.A.J.) were formed to independently analyze the full text of articles selected in phase 1 and exclude studies that did not meet the inclusion criteria (**Table S2**). A third author was consulted if disagreements between the two initial evaluators were not solved by consensus. Extraction of relevant data was done in all included studies to identify animal model, intervention (treatment regimen, dose, route, and NP platform) and outcomes (antitumoral activity and toxicity analysis).

### Risks of Bias and Quality in Individual Studies

The quality of the articles included was estimated by applying the 10-question form from SYRCLE's RoB Toll (**Table S3**) (21), to

analyze the risk of selection, performance, detection, attrition, and other bias. The items were answered in each study by two reviewers individually and the disagreements were resolved by a third reviewer. YES answers indicated low risk of bias, NO indicated high risk of bias, and UNCLEAR indicated it was not possible to assign bias. As a secondary analysis, the quality of the studies was also assessed through 15 questions related to the methodology (**Table S4**) [based and adapted from the ARRIVE Guideline (22)], and measurement of the outcomes, which were raised by the reviewers and applied in order to classify the studies according to the percentage of YES responses to the criteria raised, being considered as high quality studies with > 70%, moderate quality with 50–69%, and low quality < 49%.

# RESULTS

## Study Selection

Research on breast cancer has significantly increased. This can be observed, for example, when using the search string "(TITLE-ABS-KEY ((“Breast Cancer” OR “Breast Neoplasm” OR “Mammary Cancer” OR “Malignant Neoplasm of Breast” OR (“Mammary Carcinoma” AND Human) OR “Breast Carcinoma” OR “Cancer of Breast”)))", on September 27, 2020, in the scientific database Scopus (23), for example, 530,186 document results were found. Of these, some of the regions/countries that published the most were: United States > China > United Kingdom > Germany > Italy > France > Japan > Canada > Australia > India, where the United States published 33.53% and China 8.32% of the studies.

When filtering these results with the search string "(TITLE-ABS-KEY ((“Breast Cancer” OR “Breast Neoplasm” OR “Mammary Cancer” OR “Malignant Neoplasm of Breast” OR (“Mammary Carcinoma” AND human) OR “Breast Carcinoma” OR “Cancer of Breast”) AND (curcumin OR “Turmeric Yellow” OR (yellow AND turmeric) OR diferuloylmethane)) AND TITLE-ABS KEY ((nanoparticles OR nanoparticle OR nanogels OR “Nanocomposite Gels” OR “Nanocomposite Gel” OR nanocapsule OR nanocapsules OR nanoemulsion OR micelle OR micelles OR liposome OR liposomal)))," in order to find studies that have specifically investigated curcumin associated with NPs, 402 documents were obtained (**Figure 1**). The countries/regions that most published on "breast cancer AND curcumin AND nanotechnology" were India, United States, China, Iran, Italy, among others, according to the Scopus database.

When conducting a bibliometric study of the results obtained in the last search in the Scopus database, using the VOSviewer 1.6.15 program (24), 159 terms were obtained, when establishing at least 10 co-occurrences and "binary count" (presence or absence in each study) configurations. **Figure 2** shows the interrelation of three clusters among the most recurrent terms used, where therapy, cytotoxicity, anticancer activity, and apoptosis were among the terms of greatest interest to the scientific community regarding the evaluated topic.

Data presented in **Figures 1** and **2** were obtained using only the Scopus database in order to give a general overview of the topics discussed herein. However, in the present systematic review, a total of 528 studies were identified from different databases (57 from ScienceDirect; 35 from LILACS; 113 from Embase; 52 from MEDLINE; 60 from Portal Regional da BSV; 55 from PubMed; 41 from Web of Science; 112 from Scopus; 1 from CINAHL, 1 from FSTA, and 1 from ProQuest) (**Table S1**). After duplicate removal, 320 studies remained and an evaluation of "title and abstract" resulted in the exclusion of 244 studies. The remaining 76 articles were analyzed by full-text review. This process led to exclusion of 50 articles according to exclusion criteria (**Table S2**). In the end, 26 articles were maintained and

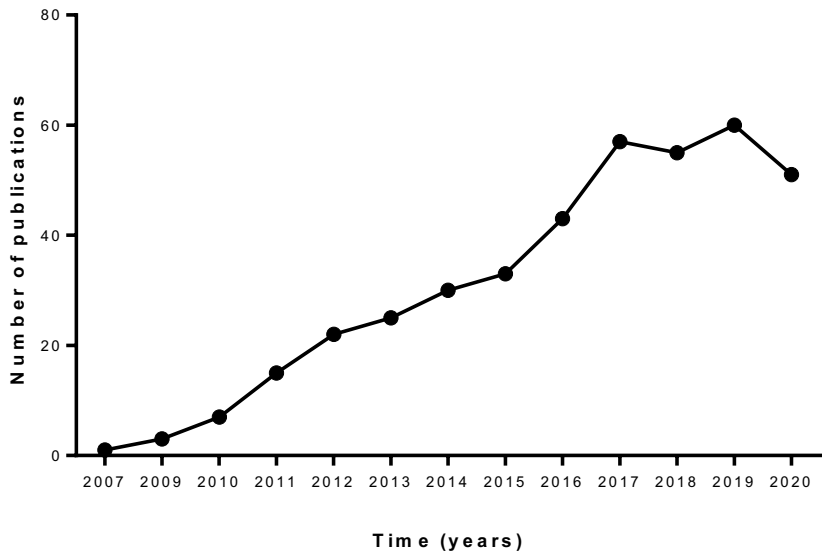


**FIGURE 1** | Number of publications listed in Scopus database with MeSH terms for curcumin nanoparticles and breast cancer. Data obtained on September 27, 2020.

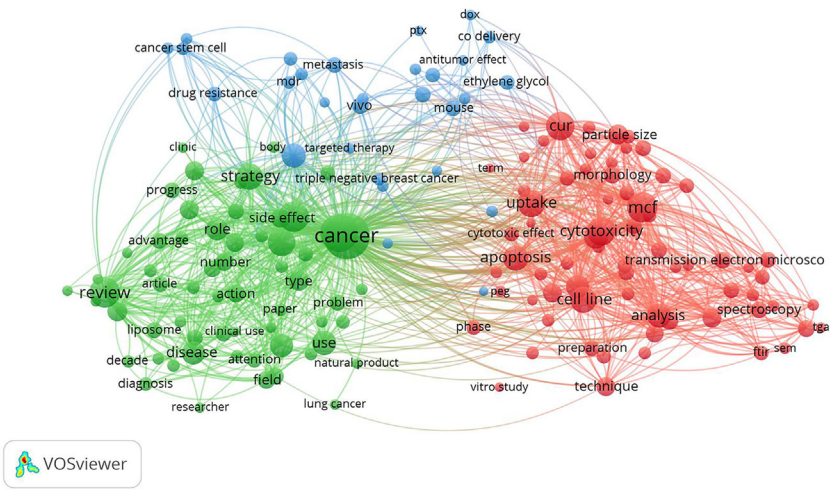


**FIGURE 2** | Bibliometric study of publications listed in Scopus database, with MeSH terms for curcumin nanoparticles and breast cancer, using the VOSviewer program (24), in "title and abstract", with at least 10 co-occurrences and binary count configurations. Data obtained on September 27, 2020.

included in this systematic review (**Table 1**) (25–29, 31–50). A flowchart detailing this process is shown in **Figure 3**.

## Characteristics of the Included Studies

All included studies are research articles that evaluated antitumoral activity of Cur-NPs in *in vivo* models of breast cancer. The main characteristics of the studies are summarized in **Table 1**.

The studies were conducted in several countries: China (n = 13); India (n = 6); Bahrain (n = 1); Iran (n = 4); Italy (n = 1); US (n = 1); Republic of Korea (n = 1), and all of them were published from 2014 to 2020 in the English language.

Cur-NPs used in the included studies were mainly described by hydrodynamic diameter (HD) (n=26), polydispersity index (PdI) (n=17), and zeta potential (n=21) through dynamic light scattering and electrophoretic mobility. Some studies assessed NPs' size and/or morphology by transmission electron microscopy (TEM) and/or scanning electron microscopy (SEM). Curcumin encapsulation efficiency (EE%) was evaluated mostly by high-performance liquid chromatography (HPLC) (n=18).

All *in vivo* studies followed the progression of tumor volume during the experimental period by measuring tumor small/large diameters or width/length and calculating the final volumes with mathematical formulas. Studies also assessed tumor weight (n=16); survival time (n=3); tumoral stem cells through flow cytometry (n=2); ratio of M1/M2 macrophages through RT-PCR (n=1); apoptosis (n=8), necrosis (n=5), proliferation (n=4), angiogenesis (n=5), cell density (n=4), inflammatory response in the tumor (n=1), and metastasis (n=1) through classical histology (HE) and immunohistochemistry. Regarding toxicity analysis, 21 studies used at least one parameter of evaluation. Studies assessed weight loss (n=15); damage of major organs through classical histology (HE) (n=9); food intake/behavior (n=1); inflammatory cytokine levels (n=1) through ELISA; hemolysis (n=2) through absorbance; and hematological (n=3) and biochemical parameters (n=6) through animal blood counter and commercial kits.

## Quality and Risk of Bias in Individual Studies

When analyzed by questions based on ARRIVE guidelines, as seen in **Table 2**, 23 studies were graded as of high quality and 3 as of moderate quality. Most studies clearly reported the encapsulation methods of curcumin (n=24) and investigated characteristics of NPs (n=23). Animal models were considered adequate in all studies and ethical committee approval was clearly reported in 18 studies. Six studies did not clearly report ethical approval and two other articles did not mention this criterion. Furthermore, animal conditions during the experiment were not clearly described in 13 studies. The study design of anticancer activity was well executed in most studies and some articles clearly mentioned time of treatment (n=25), route of administration (n=22), dose of curcumin (n=25), and presence of control groups (n=25). Nevertheless, only 15 studies investigated anticancer activity of free curcumin to compare with the Cur-NP effect. Additionally, a toxicity assay was performed in 21 studies. Lastly, statistical models were considered as unclear in all studies due to lack of information.

Risk of bias assessment based on SYRCLEs' RoB guidelines of all included studies is summarized in **Table 3**. Criteria were considered unclear when they were not clearly reported or gave incomplete information. Most studies did not clearly describe information on allocation, randomization, and blinding, which is required for quality assessment. Animals were not randomly housed during the experiment in two studies. Additionally, three studies did not adequately address incomplete outcome data. In parallel, the experimental groups were considered similar in 18

**TABLE 1** | Summary of descriptive characteristics of the included studies.

| Study | Population | Intervention | | | Outcomes | |
|---|---|---|---|---|---|---|
| **Authors, year (reference)/country** | **Animal model[a]** | **Treatment regimen[b]** | **Dose; route** | **Nanostructure platform** | **Antitumor activity** | **Toxicity analysis** |
| Shukla et al. (25)/India | Balb/c mice/n = 3/ | Ten days from tumor inoculation; | 100 mg/kg; | Lipid based CPC-SNEDDS NPs (Phospholipid, castor oil, Tween 80, PEG 400); | 1) Cur-NP ↓TV (58.9%); free Cur ↓TV (29.5%); p<0.001 | (ND) |
| | 4T1/mouse/ | Daily for 28 days | Oral | HD: 83.27 nm/PDI: 0.151; | | |
| | ($1 \times 10^6$ cells)/ | - Free Cur vehicle: | | ZP: −16 mV/EE: 29.1% | | |
| | subcutaneously on back skin | gum acacia (1%, w/v). | | | | |
| Chen et al. (26)/China | Balb/c nude mice/n = 5/ | TV of 200 $mm^3$ | 5 mg/kg; | Micelles NPs [POCA4C6 (phosphorylated calixarene) micelles—PM]; | 1) Cur-NP ↓TV (~60%) and ↓ TW (~80%); free Cur: ↓TV (~34%) and ↓ TW (~60%); p<0.05 | No damage in major organs; |
| | BT-549/human/ | Fourteen days at every 2 days | Intratumoral | HD: 3.86 nm/PDI: 0.125; | 2) Cur-NP ↑TNC and ↑TAP | No WL; hematological indices: ~ control |
| | ($2 \times 10^6$ cells)/ | - Free Cur vehicle: (NM) | | ZP: −25.18 mV/EE: 95.4% | 3) Cur-NP ↓CD44+ CD133+ cancer stem cells | |
| | Subcutaneously on the upper right thigh | | | | | p<0.05 |
| Mahalunkar et al. (27)/ India, Germany, and Norway | Balb/c mice/n = 6/ | First day of treatment: (NM) | 10 mg/kg; | Metal gold NPs (CurAu-PVP) with folic acid (FA) ($HAuCl_4$ and PVP polymer). | 1) Cur-NP-FA ↓TV (~51%); free Cur: no ↓TV; p<0.006 | (ND) |
| | 4T1/mouse/ | Twice a week for 2 weeks | Intratumoral | HD: 358.7 nm/PDI: 0.6 | 2) Cur-NP-FA ↓TW (~44%); free Cur: no TV↓; p<0.05 | |
| | ($1 \times 10^5$ cells)/ Mammary fat pad | - Free Cur vehicle: (NM) | | ZP: −12.5 mV/EE: (NM) | | |
| Alizadeh et al. (28)/Iran | Balb/c mice/n = 8/ | 14 days after tumor induction; | Dose: (NM); | Micelles/polymersomes NPs (PNP) [monomethoxy-PEG (mPEG 2000), oleic acid (OA)] | 1) Cur-NP ↓TV (~80%); p<0.05 | 31.25 mg/Kg of PNP-CUR: no damage in major organs; |
| | Transplantation of spontaneous mouse mammary tumor/ | Daily for 24 days | Intraperitoneal | HD: 99.44 nm/PDI: 0.182; | 2) Cur-NP ↑TAP; ↓ANG (CD31); ↓PROL (Ki-67); p<0.05 | Hematological and biochemical indices: ~ control |
| | Pieces < 0.3 $cm^3$/ Subcutaneous on the left flank | | | ZP: −29.3 mV mV/EE: 64% | | p<0.05 |
| Jung et al. (29)/ Republic of Korea | Balb/c nude mice/n = 4/ | TV of 50 $mm^3$; | 10 mg/kg; | Micelle NPs (DSPE-PEG micelle with or without EGFR specific targeting—EGF-Cur-NP) | 1) Cur-NP-EGFR ↓TV (~59.1%); Cur-NP no ↓TV; p<0.05 | No WL |
| | MDA-MB-468/human/ | Three times a week; total of eight injections | Intraperitoneal | Cur-NP and EGF-Cur-NP: HD: 248.9 and 229.3 nm/ PDI: 0.170 and 0.200, respectively | | p<0.05 |
| | ($5 \times 10^6$ cells)/ | | | Cur-NP and EGF-Cur-NP: ZP: −3.6 and −1.73 mV, respectively/EE: (NM) | | |
| | Right shoulder | | | | | |
| Wang et al. (30)/China | Nuke mice/n = (NM)/ | Two months after tumor induction; | $1 \times 10^{-3}$ M; | Polymeric NPs (MPEG-PCL); | 1) Cur-NP ↓TV (~82%); free Cur:↓TV (~49%); p<0.01 | (ND) |
| | MDA-MB-231/human/ ($1.5 \times 10^6$ cells)/ Subcutaneous | Daily for 2 weeks - Free Cur vehicle: (NM) | Intravenous | HD: 139 nm/PDI: (NM); ZP and EE: (NM) | 2) Cur-NP ↑TAP | |

*(Continued)*

**TABLE 1** | Continued

| Study | Population | Intervention | | | Outcomes | |
|---|---|---|---|---|---|---|
| **Authors, year (reference)/country** | **Animal model[a]** | **Treatment regimen[b]** | **Dose; route** | **Nanostructure platform** | **Antitumor activity** | **Toxicity analysis** |
| Laha et al. (31)/India and USA | Balb/c mice/n =6/ | Ten days after tumor induction; | 2 mg/kg (*unclear); | Metal organic frameworks NPs (IRMOF-3) with or without folic acid (FA) [(Zn $(NO_3)_2$; $NH_2$-$H_2$BDC] | 1) Cur-NP-FA ↓TV (~61%); Cur-NP↓TV (~44%); p<0.05 | Biochemical markers for liver and kidney: ~ control |
| | 4T1/mouse/ | Every 5 days for 4 times | Route of administration: (NM) | HD: 371,7 nm/PDI: 0.397 | 2) Cur-NP ↓TW (~74%); Cur-NP-FA ↓TW (~85%); p<0.05 | p<0.05 |
| | (NM)/ | | | ZP: −10.9 mV/EE: 98% | 3) Cur-NP and Cur-NP-FA ↓ tumor cell density | |
| | Mammary fat pad | | | | | |
| Vakilinezhad et al. (32)/ Iran | Sprague Dawley rats/n = 6/ | Four months after tumor induction; | 2.5 mg; | Polymeric NPs (PLGA-PVA) | 1) Cur-NP ↓TV (~20%); Free Cur: ↓TV (~16%); p<0.05 | (ND) |
| | Chemically induced mammary tumors (MNU) | Once a week for 4 weeks | Intravenous | HD: 92.4 nm/PDI: 0.150 | | |
| | | - Free Cur vehicle: aqueous suspension | | ZP: −5.12 mV/EE: 89.4% | | |
| Yuan et al. (33)/China | Balb/c nude mice/n = 6/ | TV of 100 $mm^3$; | 2.5 mg/kg; | Polymeric NPs (mPEG- PLGA-Pglu) | 1) Cur-NP ↓TV (~28.0%); p<0.05 | No damage in major organs; |
| | MCF-7/human/ | Every other day 4 times; total 18 d | Intravenous | HD: 228.5 nm/PDI: (NM) | 2) Cur-NP ↓TW (~22.5%); p<0.05 | No WL |
| | (3 x $10^6$ cells)/ | | | ZP: −23.8 mV/EE: 76.9% | 3) Cur-NP ↓breast cancer stem cells (~62%); p<0.05 | p<0.05 |
| | Right flank | | | | | |
| Sahne et al. (34)/Iran | Balb/c mice/n = 4/ | TV of 50–100 $mm^3$; | 4 mg/kg; | Graphene oxide NPs (GO NPs with CMC, PVP, PEG, FA); | 1) Cur-NP-FA↓TV (~86%); p<0.05 | No damage in major organs; |
| | 4T1/mouse/ (NM)/ | Daily for a total 3 weeks | Intravenous | HD: ~60 nm/PDI: (NM) ZP: −48 mV/EE: 94% | 2) Cur-NP-FA ↓TW (~76%); p<0.05 3) Cur-NP-FA ↑ ST and ↓ metastasis; p<0.05 | No WL p<0.05 |
| | Subcutaneous on the flank | | | | 4) Cur-NP-FA: ↑TNC; ↓ cell density; ↓ANG (CD31, CD34); ↑ pro-inflammatory response in the tumor microenvironment; p<0.05 | |
| Ji et al. (35)/China | Balb/c mice/n = 5/ | First day of treatment: (NM); | 5 mg/kg; | Nanocrystals NPs with or without HA | 1) Cur-NP-HA ↓TV (~86%); Cur-NP↓TV (~39%); free Cur: ↓TV (~21%); p<0.05 | No damage in major organs; no WL; |
| | 4T1/mouse/ | Every 2 days for a total 10 days | Intravenous | Cur-NP and HA-Cur-NP: HD: 101.4 and 161.9 nm/ PDI: ~0.330 and 0.250, respectively | 2) Cur-NP-HA ↓TW (~75%); Cur-NP↓TW (~37.5%); Free Cur: ↓TW (~25%); p<0.05 | No hemolysis (<5%); |
| | (1 x $10^6$ cells)/ | - Free Cur vehicle: (NM) | | HA-Cur-NP: ZP: −25.0 mV, respectively/EE: (NM) | 3) ↑ ST: Cur-NP-HA > Cur-NP > Free Cur; p<0.05 | Hematological and biochemical indices: ~ healthy control p<0.05 |
| | Subcutaneous on the right flank | | | | | |

*(Continued)*

**TABLE 1** | Continued

| Study | Population | Intervention | | | Outcomes | |
|---|---|---|---|---|---|---|
| **Authors, year (reference)/country** | **Animal model[a]** | **Treatment regimen[b]** | **Dose; route** | **Nanostructure platform** | **Antitumor activity** | **Toxicity analysis** |
| He et al. (36)/China | Balb/c mice/n = 6/ | TV of 100 $mm^3$ | 5mg/kg; | Polymeric micellar NPs [amphiphilic diblock copolymer— mPEG-b-PLG (Se)-TP]; | 1) Cur-NP ↓TV (~65%); Free Cur: ↓TV (~49%); p<0.05 | No damage in major organs; no WL |
| | 4T1/mouse/ | Every 4 days, for 4 times; total 21 days | Intravenous | HD: 136 nm/PDI: 0.071 | 2) Cur-NP ↓TW (~82%); free Cur: ↓TW (~62%); p<0.05 | p<0.05 |
| | (1 x $10^6$ cells)/ | - Free Cur vehicle: (NM) | | ZP: (NM)/EE: ~ 68% | 3) Cur-NP ↑TNC and ↑TAP; ↓ANG (CD31); ↓PROL (Ki-67); p<0.05 | |
| | Subcutaneous on the right back | | | | | |
| Jin et al. (37)/China and USA | Balb/c nude mice/n = 5/ | 7 days after tumor induction; | 5 mg/kg; | Polymeric NPs with or without EGFR-targeting peptides (GE11) (PLGA-PEG); | 1) Cur-NP-GE11 and Cur-NP ↓TV (~80%); free Cur: no TV↓; p<0.05 | Inflammatory cytokine levels: ~ healthy mice |
| | MCF-7/human/ | Every 24 h for 20 times | Intravenous | HD: 210 nm/PDI: 0.112; | 2) Cur-NP-GE11↓TW (~56%); Cur-NP ↓TW (~48%); free Cur: no TW↓; p<0.05 | p<0.05 |
| | (1 x $10^7$ cells)/ | | | ZP: –22 mV/EE: 92.3 | 3) Cur-NP-GE11and Cur-NP ↑TAP | |
| | Subcutaneous on the dorsal flank | - Free Cur vehicle: (NM) | | | | |
| Abd-Ellatef et al. (38)/ Italy and Egypt | Balb/c mice/n = 8/ | TV of 50 $mm^3$; | 5 mg/kg; | Solid lipid nanoparticles (SLN) with or without chitosan (CS) coating (cholesterol; trilaurin, butyl lactate, Epikuron®200, Cremophor®RH60, sodium taurocholate, Pluronic® F68); | 1) Cur-NP-CS and Cur-NP ↓TV (~35%); Free Cur: no TV↓; p<0.01 | Biochemical indices: ~ control |
| | JC/mouse/ | Thrice (on day $1^{st}$, $7^{th}$, $14^{th}$) | Intravenous | HD: < 200 nm/PDI: (NM) | | p<0.05 |
| | (1 x $10^7$ cells)/ | - Free Cur vehicle: 10% v/v DMSO suspension | | ZP: (NM)/EE: 70–75% | | |
| | Mammary fat pad | | | | | |
| Li et al. (39)/China | Balb/c mice/n = 4/ | Tumor diameter of 4 mm; | 8 mg/kg; | Mesoporous silica nanoparticles with hyaluronan (MSN-HA) or polyethyleneimine-folic acid (MSN-PEI-FA). | 1) Cur-NP-PEI-HA ↓TV (~50%); Free Cur: no TV↓; p<0.01 | No damage in major organs; no WL; |
| | MDA-MB-231/human/ | Every 3 days for a total of six times | Intravenous | HD: < 300 nm/PDI: (NM)/ | 2) Cur-NP-PEI-HA ↓TW (~70%); free Cur: no TW↓; p<0.01 | Hemolysis (<5%); |
| | (1 x $10^7$ cells)/ | - Free Cur vehicle: (NM) | | ZP: ~ –20 mV (MSN-HA); ~ +40 mV (MSN-PEI-FA) | | Biochemical indices: ~ healthy control |
| | Subcutaneous | | | | | p<0.05 |
| Kundu et al. (40)/India | Swiss albine mice/n = 6/ | Ten days after induction; | 10 mg/kg; | Metal NPs [Zinc oxide nanoparticles (ZnO) with PBA]; | 1) Cur-NP↓TV (~77%); free Cur: ↓TV (~66%); p<0.05 | No damage in the liver and kidney; |
| | Ehrlish ascites carcinoma cells/ | Alternate days for 14 days. | Intravenous | HD: 413.63 nm/PDI: (NM) | 2) Cur-NP ↓TW (~72%); free Cur: ↓TW (~50%); p<0.05 | Biochemical markers: ~control; ↓ tumor-induced splenomegaly |
| | (1.0 x $10^7$/ml) Left flank | - Free Cur vehicle: (NM) | | ZP: –16.4 mV/EE: 27% | 3) Cur-NP and free Cur: ↑TAP; p<0.05 | p<0.05 |

*(Continued)*

**TABLE 1** | Continued

| Study | Population | Intervention | | | Outcomes | |
|---|---|---|---|---|---|---|
| **Authors, year (reference)/country** | **Animal model[a]** | **Treatment regimen[b]** | **Dose; route** | **Nanostructure platform** | **Antitumor activity** | **Toxicity analysis** |
| Lv et al. (41)/China | Kunming (mice)/n = 6/ | TV of 300 $mm^3$; | 10 mg/kg; | Polymeric NPs (PEG-PCDA) with or without biotin; | 1) Cur-NP ↓TV (~69%); Cur-NP-biotin ↓TV (~79%); free Cur: ↓TV (~32%); p<0.05 | no WL |
| | EMT6/mouse/ | Daily for 9 days; total 14 days | Intravenous | PEG-PCDA and biotin-PEG-PCDA: HD: 94.2 and 125.1 nm/PDI: 0.170 and 0.08, respectively | 2) Cur-NP ↓TW (~70%); Cur-NP-biotin ↓TW (~85%); free Cur: ↓TW (~25%); p<0.05 | p<0.05 |
| | (1.0 x $10^7$/ml) | - Free Cur vehicle: cremophor EL: dehydrated alcohol (1:1, v/v) and diluted with physiological saline | | PEG-PCDA and biotin-PEG-PCDA: ZP: −9.56 and −12.86 mV/EE: (NM) | 3) Cur-NP and Cur-NP-biotin: ↑TNC and ↑TAP; ↓ANG (CD31; VEGF; COX-2); ↓PROL (Ki-67); p<0.05 | |
| | Subcutaneously | | | | | |
| Yang et al. (42)/China | Balb/c nude mice/n = 5 | TV of 200 $mm^3$ | 10 mg/kg; | Micelle NPs (triblock copolymer PPBV); | 1) Cur-NP ↓TV (~58.5%, day 12); ↓TV (~28.9%, day 20); p<0.05 | No WL |
| | MCF-7/human/ | Every other day for 5 times; total 20 days | Intravenous | HD: 6.7 nm/PDI: 0.117 | 2) Cur-NP ↓TW (~22%, day 20); p<0.05 | p<0.05 |
| | (1 x $10^7$ cells)/ | | | ZP: −1.42 mV/EE: 68.5% | | |
| | Subcutaneous on the flank | - Free Cur vehicle: (NM) | | | | |
| Yang et al. (43)/China | Balb/c nude mice/n = 5/ | TV of 200 $mm^3$ | 15 mg/kg; | Hybrid NPs [PLGA NPs coated with a modified hialuronic acid (HA-hybrid)] | 1) Cur-NP-HA ↓TV (~43.8%, day 12); ↓TV (~24%, day 20); p<0.05 | No WL |
| | MCF-7/human/ | Every other day for 5 times; total 20 days | Intravenous | HD: 350 nm/PDI: (NM) | 2) Cur-NP-HA ↓TW (~22%, day 20); p<0.05 | p<0.05 |
| | (1 x $10^7$ cells)/ | | | ZP: −22 mV/EE: 32% | 3) Cur-NP-HA ↓tumor cell density; p<0.05 | |
| | Subcutaneous on the flank | - Free Cur vehicle: (NM) | | | | |
| Greish et al. (44)/ Bahrain | Balb/c mice/n = 5/ | TV of 100 $mm^3$; | 10 and 20 mg/kg; | Micelles (curcumin–metal complex and SMA) | 1) Cur-NP-10mg/Kg ↓TV (~61%); Cur-NP-20mg/Kg ↓TV (~92%); p<0.05 | (ND) |
| | 4T1/mouse/ | frequency of treatment: unclear; total 10 days | Intravenous | HD: 248 nm/PDI: 0.274; | | |
| | (1 x $10^6$ cells)/ | | | ZP: −11 mV/EE: 80% | | |
| | Bilaterally on the flanks | | | | | |
| Mukerjee et al. (45)/ USA | Balb/c nude mice/n = 8/ | TV of 70 $mm^3$; | 20 mg/kg; | Polymeric NPs [PLGA/PVA with or without antibody targeting (AnxA2)] | 1) Cur-NP- AnxA2 ↓TV (~44.0%); Cur-NP ↓TV (~33.5%); p<0.05 | No WL |
| | MCF10CA1a/human/ | Thrice week for a total 30 days | Intravenous | Cur-NP and AnxA2-Cur-NP: HD: 150 and 157 nm/ PDI: ~0.240 and 0.200, respectively | 2) Cur-NP- AnxA2 ↓TW (~53.0%); Cur-NP ↓TW (~30%); p<0.05 | p<0.05 |
| | (3 x $10^6$ cells)/ | | | Cur-NP and AnxA2-Cur-NP: ZP: −27.5 and −28.5 mV, respectively/EE: 89.2% | 3) Cur-NP- AnxA2 and Cur-NP: ↓ANG; ↓ NFkβ; ↓PROL (Ki-67); p<0.05 | |
| | Flank | | | | | |
| Mukhopadhyay et al. (46)/India | Balb/c nude mice/n = 5/ | 8 days after induction; | 20 mg/kg | Polymeric NPs [PLGA/PVA with or without folate (F)] | 1) Cur-NP-F ↓TV (~90%); Cur-NP↓TV (~75%); p<0.05 | No damage in major organs |
| | MDA-MB-231/human/ | Thrice week for a total 21 days | Route of administration: unclear | HD: 170 nm/PDI: 0.186; | 2) Cur-NP-F ↓TW (~92%); Cur-NP↓TW (~61.5%); p<0.05 | p<0.05 |

*(Continued)*

**TABLE 1** | Continued

| Study | Population | Intervention | | | Outcomes | |
|---|---|---|---|---|---|---|
| **Authors, year (reference)/country** | **Animal model[a]** | **Treatment regimen[b]** | **Dose; route** | **Nanostructure platform** | **Antitumor activity** | **Toxicity analysis** |
| | (5 x $10^6$ cells)/ Right flank | | | ZP: –28.2 mV/EE: 68.6% | 3) Cur-NP-F and Cur-NP ↓ cell density | |
| Yu et al. (47)/China | Balb/c nude mice/n = 5/ | TV of 100–400 $mm^3$; | 40 mg/kg | Micelles NPs (MPEG-PLA with or without PAE) | 1) Cur-NP-PAE ↓TV (~65.6%); Cur-NP ↓TV (~47.1%); p<0.05 | no WL |
| | MCF-7/human/ (3 x $10^6$ cells)/ Subcutaneously right flank | Every other day for 5 times for a total 24 days | Intravenous | HD: 128.4 nm to 171.0 nm/ PDI: 0.118 to 0.134 ZP: –2.0 to +4.0 mV/ EE: 96.5 to 98.8% | 2) Cur-NP-PAE ↓TW (~76%); Cur-NP ↓TW (~53%); p<0.05 | p<0.05 |
| Huang et al. (48)/China | Balb/c mice/n = 5/ | TV of 40–50 $mm^3$/ | 50 mg/kg | Polymeric NPs (HA-CHEMS); pH-sensitive | 1) Cur-NP ↓TV (~38%); p<0.05 | ↓ Damage in major organs |
| | 4T1/mouse/ (NM)/ Flank | Every 2 days for a total of 5 times | Intravenous | HD: 144 nm/PDI: (NM); ZP: –21.25 mV/EE: (NM) | 2) Cur-NP ↑ ST; 3) Cur-NP ↑TNC and ↑TAP | no WL p<0.05 |
| Shiri et al. (49)/Iran | Balb/c mice/n = 9/ | Third day after tumor induction/ | 40 mg/kg or 80 mg/kg | Dendrosome NPs (DNC) [composition: not mentioned (patent number: 71753)] | 1) NP-40mg/Kg ↓TV (~72%); NP-80mg/Kg ↓TV (~76%); p<0.05 | no WL |
| | 4T1/mouse/ (1 x $10^6$ cells)/ left flank | daily for 35 consecutive days | Route of administration: (NM) | HD; PD; ZP; EEI: (NM) | 2) NP-40mg/Kg ↓TV (~61%); NP-80mg/Kg ↓TV (~64%); p<0.05 3) NP ↑ ratio of M1/M2 macrophages | No change in food intake and behavior p<0.05 |
| Lin et al. (50)/China | Balb/c nude mice/n = 6/ | First day of treatment: (NM)/ | Dose: (NM)/ | Lipid based NPs (NLC) with or without folate (FA) coating (PEG-DSPE, soya lecithin, castor oil, Tween 80, Precirol ATO-5); | 1) Cur-NP-FA ↓TV (~83%); Cur-NP ↓TV (~66%); free Cur: ↓TV (~31%); | No WL |
| | MCF-7/human/ (NM)/ Subcutaneous in the right armpit | once every 3 days for 15 days - Free Cur vehicle: (NM) | Intravenous | HD: 126.8 nm/PDI: 0.16 ZP: +12.6 mV/EE: 82.7% | | p<0.05 |

[a]*Animal type/replicates/cell type injected/source/cell concentration/local of cell insertion;*

[b]*First day of treatment (or tumor volume)/treatment frequence and total experiment time; ANG, angiogenesis; CHEMS, cholesteryl hemisuccinate; CMC, carboxymethyl cellulose; CPC-SNEDDS, curcumin-phospholipid complex self-nanoemulsifying drug delivery systems; Cur, curcumin; d, days; DSPE, distearoyl phosphatidyl- ethanolamine; EGFR, epidermal growth factor receptor; FA, folic acid; HA, hyaluronic acid; MNU, N-methyl nitroso urea; mPEG-b-PLG (Se)-TP, poly-(ethylene glycol)-b-poly(L-glutamic acid)-two-photon AIE fluorophores [mPEG-b-PLG (Se)-TP] amphiphilic copolymer with selenide group (Se) conjugated and a two-photon AIE fluorogen (TP) on the terminal group of PLG segments.; MPEG-PCL, methoxypoly(ethylene glycol)-polycaprolactone; NF-κB, nuclear factor kappa b; NH2-H2BDC, 2-amino terephthalic acid; (ND), not determined; (NM), not mentioned; NPs, nanoparticles; PAE, poly (b-aminoester; PBA, phenyl boronic acid; PCDA, pentacosadiynoic acid; PEG, poly(ethylene glycol); PGlu, poly L-glutamic acid; PLA, polylactic-co-glycolic acid; PPBV, mPEG-PBLA-PVlm triblock copolymer; PROL, tumor proliferation; PVA, polyvinyl alcohol; PVP, polyvinylpyrrolidone; SMA, poly(styrene)-co-maleic acid; ST, survival time; TAP, tumor apoptosis; TNC, tumor necrosis; TV, tumor volume; TW, tumor weight; WL, weight loss.*

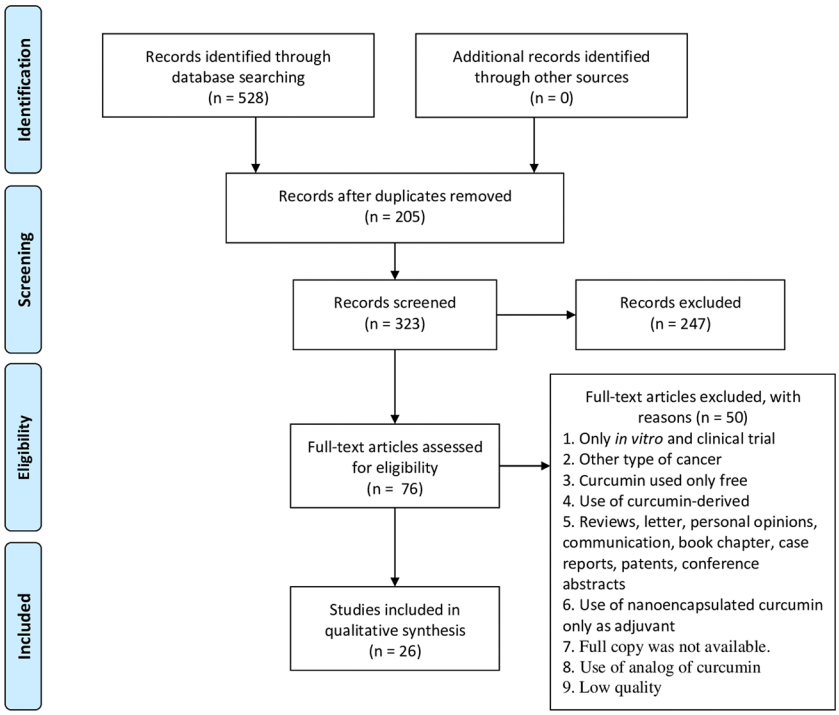


**FIGURE 3** | Flow diagram of literature search and selection criteria adapted from PRISMA (18).

studies, and 24 studies showed low risk of selection bias of reported outcomes.

## Synthesis of Results

A wide variety of NP types were used in the included studies. Polymer NPs were mostly used for curcumin delivery (n = 9), followed by micelles (n = 6), lipid-based NPs (n=3), metal NPs (n = 2), hybrid NPs (n=2), dendrosomal NP (n =1), nanocrystal (n=1), graphene oxide NP (n=1), and mesoporous silica NP (n=1). Poly (ethylene glycol) chains (PEG) were present in NP composition in 11 studies. Nine studies evaluated NPs associated with targeting moieties such as folic acid (n=5), hyaluronic acid (n=1), EGF peptides (n=2), and AnxA2 (n=1). With HD ranging from 101.4 to 371.7 nm, most Cur-NPs presented negative Zeta potential (−48 to +40 mV) (n=22) and EE% from 32 to 98% (**Table 1**).

Concerning experimental design, studies were heterogeneous regarding animal model, route of administration, duration of the experiment, and dose of treatment. Ten studies adopted nude mice as animal models when tumor was induced with human cells and another 16 used mice with a native immune system for tumor induction with murine cells. One study used rats with MNU-chemically induced mammary tumors (n=1). The main human cell lines used were MCF-7 (n=6), MDA-MB-231 (n=3), MDA-MD-468 (n=1), MCF10CA1a (n=1), and BT-549 (n=1). The murine cell lines used were 4T1 (n=9), EMT6 (n=1), JC (n=1), and Ehrlich ascites carcinoma cells (n=1). One study used the transplantation of spontaneous mouse mammary tumor pieces (n=1) as the breast cancer model. Implantation of tumor cells into the mammary fat comprised three studies, while the others adopted subcutaneous implantation into the flank (n=14) or armpit (n=1).

The first day of treatment was described according to days after induction (n=9), ranging from 3 days to 4 months, or tumor volume (n=13) in the range of 40 to 400 $mm^3$. The curcumin doses used in the treatments varied between 2 and 100 mg/Kg and were administered daily (n=8), every other day (every 2 days) (n=7), three times a week (n=6); twice a week or less (n=4). Intravenous administration was the main route of administration used in the included studies (n=18). Few studies used intraperitoneal (n=2), intratumoral (n=2), or oral administration route (n=1); and one did not clearly mention this information (n=1).

# DISCUSSION

## Summary of Evidence

The structure of curcumin has chemical groups that allow interactions of diverse chemical natures (*e.g.*, covalent, non-covalent, hydrophobic, and hydrogen bonds) with molecules involved in the different pathways of breast carcinogenesis (9, 16). It has been reported that curcumin inhibits cell proliferation, tumor invasion, and angiogenesis. As an anti-proliferative agent, curcumin induces cell cycle arrest and p53-dependent apoptosis. It also alters signaling protein expression, such as Ras, protein kinase B (Akt), and phosphatidylinositol-3-kinase (PI3K) (51).

**TABLE 2 |** Overall quality of the selected studies. Detailed description of the evaluated parameters is found in **Table S4**.

| Critical analysis of the articles included | | | | | | | | | | | | | | | | | | |
|---|---|---|---|---|---|---|---|---|---|---|---|---|---|---|---|---|---|---|
| **Author** | **Year** | **Methodology** | | | | | | | | | | | **Toxicity** | | **Outcomes** | | **Score** | **Classification** |
| | | **1** | **2** | **3** | **4** | **5** | **6** | **7** | **8** | **9** | **10** | **11** | **12** | **13** | **14** | **15** | **%** | |
| Abd-Ellatef et al. (38) | 2020 | | | | | | | | | | | | | | | | 93 | High quality |
| Alizadeh et al. (28) | 2015 | | | | | | | | | | | | | | | | 80 | High quality |
| Chen et al. (26) | 2017 | | | | | | | | | | | | | | | | 93 | High quality |
| Greish et al. (44) | 2018 | | | | | | | | | | | | | | | | 73 | High quality |
| He et al. (36) | 2019 | | | | | | | | | | | | | | | | 86 | High quality |
| Huang et al. (48) | 2020 | | | | | | | | | | | | | | | | 66 | Moderate quality |
| Ji et al. (35) | 2020 | | | | | | | | | | | | | | | | 86 | High quality |
| Jin et al. (37) | 2017 | | | | | | | | | | | | | | | | 86 | High quality |
| Jung et al. (29) | 2018 | | | | | | | | | | | | - | - | | | 86 | High quality |
| Kundu et al. (40) | 2019 | | | | | | | | | | | | | | | | 80 | High quality |
| Laha et al. (31) | 2019 | | | | | | | | | | | | | | | | 73 | High quality |
| Li et al. (39) | 2018 | | | | | | | | | | | | | | | | 86 | High quality |
| Lin et al. (50) | 2016 | | | | | | | | | | | | | | | | 80 | High quality |
| Lv et al. (41) | 2015 | | | | | | | | | | | | | | | | 60 | Moderate quality |
| Mahalunkar et al. (27) | 2019 | | | | | | | | | | | | - | - | | | 86 | High quality |
| Murkerjee et al. (45) | 2016 | | | | | | | | | | | | - | - | | | 73 | High quality |
| Mukhopadhyay et al. (46) | 2020 | | | | | | | | | | | | | | | | 80 | High quality |
| Sahne et al. (34) | 2019 | | | | | | | | | | | | | | | | 93 | High quality |
| Shiri et al. (49) | 2015 | | | | | | | | | | | | - | - | | | 53 | Moderate quality |
| Shukla et al. (25) | 2017 | | | | | | | | | | | | | | | | 86 | High quality |
| Vaklinezhad et al. (32) | 2019 | | | | | | | | | | | | - | - | | | 73 | High quality |
| Wang et al. (30) | 2018 | | | | | | | | | | | | - | - | | | 86 | High quality |
| Yang et al. (42) | 2017a | | | | | | | | | | | | | | | | 86 | High quality |
| Yang et al. (43) | 2017b | | | | | | | | | | | | | | | | 80 | High quality |
| Yu et al. (47) | 2014 | | | | | | | | | | | | | | | | 80 | High quality |
| Yuan et al. (33) | 2018 | | | | | | | | | | | | | | | | 86 | High quality |

*Yes* *No* *Unclear - Not evaluated.*

Additionally, the use of curcumin has been described as a potential strategy for inhibiting EZH2 (enhancer of zeste homolog-2), a histone modifier protein subunit involved in tumor growth, metastatic potential, and in the regulation of drug resistance. In breast cancer, it has been reported that curcumin is able to inhibit the proliferation of human breast cancer MDA-MB-435 cells in correlation with the downregulation of EZH2 expression (52, 53).

Curcumin has demonstrated anti-invasive effects through downregulation of matrix metalloproteinase (MMP-2) and upregulation of tissue inhibitor of metalloproteinase (TIMP-1) in MDA-MB-231 breast cancer cells (54). Interestingly, emerging evidence indicates that the chemopreventive and chemotherapeutic properties of curcumin are closely linked to the modulation of miRNAs involved in tumorigenesis and metastasis signaling pathways, *e.g.*, hedgehog, notch-1, PI3K/Akt/mTOR, Wnt/β-catenin, IGF, VEGF, and TGF-β/smad3 pathways (55, 56). Gallardo et al. (57) demonstrated that curcumin prevents the migration and invasion of breast cancer cells (MCF-10F and MDA-MB-231) by targeting miR-34a as a regulator of *Rho-A* and other genes involved in epithelial-mesenchymal transition, such as *Axl*, *Slug*, and *CD24* (57). Curcumin can also prevent angiogenesis by inhibiting vascular endothelial growth factor (VEGF) (58, 59) and suppressing angiogenic cytokine interleukin-6 (60). All of the mentioned mechanisms cited above along with anti-inflammatory action and inhibition of cell growth factors, support confirmation of the wide activity of curcumin in the regulation of tumor growth by acting in different cancer hallmarks (9).

However, the hydrophobic property of curcumin limits its applications and demonstrates less impressive success in clinical trials (14). Additionally, free curcumin can undergo biomodifications and may be mostly excreted in feces or in bile in animal models (61). Therefore, the use of drug delivery systems, such as NP platforms, is an alternative to improve drug bioavailability, administer lower doses, increase time of circulation, and enhance its biological activity. The natural product-based nanomedicine field for cancer treatment has increased and demonstrated great potential (6, 14). The present systematic review reports the effects of Cur-NPs on antitumoral activity and toxicity of in *in vivo* models of breast cancer.

Analysis of the included studies showed that curcumin evaluated in *in vivo* models of breast cancer has been loaded in a wide variety of NP platforms, including different compositions, sizes, and zeta potential. In fact, advantages were evidenced in all the included studies that compared tumor volume reduction

**TABLE 3 |** Risk of bias in individual studies (SYRCLE's Rob toll criteria). YES answers indicated low risk of bias, NO indicated high risk of bias, and UNCLEAR indicated it was not possible to assign bias. Detailed description of the evaluated parameters is found in **Table S3**.

| | | SYRCLE's Risk of Bias | | | | | | | | | |
|---|---|---|---|---|---|---|---|---|---|---|---|
| **Author** | **Year** | **Selection** | | | **Performance** | | **Detection** | | **Attrition** | **Reporting** | **Other** |
| | | **1** | **2** | **3** | **4** | **5** | **6** | **7** | **8** | **9** | **10** |
| Abd-Ellatef et al. (38) | 2020 | ● | ● | ● | ● | ● | ● | ● | ● | ● | ● |
| Alizadeh et al. (28) | 2015 | ● | ● | ● | ● | ● | ● | ● | ● | ● | ● |
| Chen et al. (26) | 2017 | ● | ● | ● | ● | ● | ● | ● | ● | ● | ● |
| Greish et al. (44) | 2018 | ● | ● | ● | ● | ● | ● | ● | ● | ● | ● |
| He et al. (36) | 2019 | ● | ● | ● | ● | ● | ● | ● | ● | ● | ● |
| Huang et al. (48) | 2020 | ● | ● | ● | ● | ● | ● | ● | ● | ● | ● |
| Ji et al. (35) | 2020 | ● | ● | ● | ● | ● | ● | ● | ● | ● | ● |
| Jin et al. (37) | 2017 | ● | ● | ● | ● | ● | ● | ● | ● | ● | ● |
| Jung et al. (29) | 2018 | ● | ● | ● | ● | ● | ● | ● | ● | ● | ● |
| Kundu et al. (40) | 2019 | ● | ● | ● | ● | ● | ● | ● | ● | ● | ● |
| Laha et al. (31) | 2019 | ● | ● | ● | ● | ● | ● | ● | ● | ● | ● |
| Li et al. (39) | 2018 | ● | ● | ● | ● | ● | ● | ● | ● | ● | ● |
| Lin et al. (50) | 2016 | ● | ● | ● | ● | ● | ● | ● | ● | ● | ● |
| Lv et al. (41) | 2015 | ● | ● | ● | ● | ● | ● | ● | ● | ● | ● |
| Mahalunkar et al. (27) | 2019 | ● | ● | ● | ● | ● | ● | ● | ● | ● | ● |
| Murkerjee et al. (45) | 2016 | ● | ● | ● | ● | ● | ● | ● | ● | ● | ● |
| Mukhopadhyay et al. (46) | 2020 | ● | ● | ● | ● | ● | ● | ● | ● | ● | ● |
| Sahne et al. (34) | 2019 | ● | ● | ● | ● | ● | ● | ● | ● | ● | ● |
| Shiri et al. (49) | 2015 | ● | ● | ● | ● | ● | ● | ● | ● | ● | ● |
| Shukla et al. (25) | 2017 | ● | ● | ● | ● | ● | ● | ● | ● | ● | ● |
| Vaklinezhad et al. (32) | 2019 | ● | ● | ● | ● | ● | ● | ● | ● | ● | ● |
| Wang et al. (30) | 2018 | ● | ● | ● | ● | ● | ● | ● | ● | ● | ● |
| Yang et al. (42) | 2017a | ● | ● | ● | ● | ● | ● | ● | ● | ● | ● |
| Yang et al. (43) | 2017b | ● | ● | ● | ● | ● | ● | ● | ● | ● | ● |
| Yu et al. (47) | 2014 | ● | ● | ● | ● | ● | ● | ● | ● | ● | ● |
| Yuan et al. (33) | 2018 | ● | ● | ● | ● | ● | ● | ● | ● | ● | ● |

● *Yes* ● *No* ● *Unclear - Not evaluated.*

after Cur-NP treatment with curcumin treatments in its free form and/or with negative controls (**Table 1**). For instance, a volume reduction of ~21% was observed in tumors of animals treated with free curcumin, while a significant reduction of ~86% was observed in animals treated with curcumin nanocrystals coated with hyaluronic acid (35).

NPs are able to accumulate into solid tumors (*e.g.*, breast cancer). The classical concept states that NPs extravasate the tumor's vascular barrier through gaps between endothelial cells (owing to irregular angiogenic growth) and are retained in the tumor mass due to poor local lymphatic drainage—a passive process known as the enhanced permeability and retention (EPR) effect (62, 63) Nevertheless, this pathway has been currently under debate, and updated data show evidence that it may not be the dominant mechanism of NPs' extravasation into solid tumors (64, 65). Other mechanisms of NPs' tumor accumulation have been investigated, such as the trans-endothelial pathway, which is a metabolically active process that requires endothelial cells to rearrange their structure to present vesicles that can uptake NPs and further deliver them to tumor cells nearby (64).

Improvements in tumor NP accumulation and favorable interaction between NPs and cancer cells can be obtained by tailoring the surface of the NP with moieties able to confer prolonged blood-circulation time (*e.g.*, PEG) and specific active targeting (*e.g.*, ligands with affinity to molecules overexpressed in tumor cells) (66). The main active targeting moieties found in the included studies were folic acid (FA) and hyaluronic acid (HA). FA shows affinity to folate receptors, which are tumor-associated proteins overexpressed in more than 40% of human tumors, including breast cancer (67). A metal organic framework of FA-Cur-NPs significantly improved curcumin antitumor efficacy (~61%), while non-modified NP accounted for ~44% for tumor volume reduction (31). Similarly, attachment of HA, a natural polysaccharide consisting of repeating disaccharide units, to the surface of NPs, has been investigated since it binds to the cell surface molecule CD44, a surface protein widely expressed in breast cancer (68). Curcumin associated with HA-mesoporous silica NPs showed a significant ~70% reduction in tumor weight, while no significant effect was observed for free curcumin (39). Other modifications of the curcumin-NP surface with ligands

specific to different tumor surface biomarkers for breast cancer have also been explored (29, 37, 45).

Once in the tumor site, NPs can be internalized by tumor cells and/or release their cargo in the tumor microenvironment. It is known that the tumor microenvironment is acidic (69), and this pathological characteristic of cancer can be used as a strategy for the controlled release of NPs responsive to acidic pH (40). This strategy prevents cargo release to non-target tissues and aids in the mitigation of possible adverse effects. Kundu and co-workers (40) designed their study based on this approach by using pH-sensitive NPs. They observed that the release of curcumin from the nanohybrid zinc oxide NPs was improved in decreased pH and resulted in an increased accumulation of curcumin in tumor tissue and a significative tumor volume reduction (~77%). In addition, no biochemical modifications or structural damage were observed in the liver and kidneys (40). Huang and co-workers (48) encapsulated curcumin in pH-sensitive polymeric NPs and showed a significant reduction in tumor volume followed by increased survival time (**Table 1**) (48). Internalization of NPs can be mediated or not by active targeting ligands (depending on the mechanism triggered), and it occurs mainly through endocytosis pathways where the main mechanisms comprise a) clathrin-mediated endocytosis; b) caveolae-mediated endocytosis, for NPs up to 200 nm; c) macropinocytosis; and d) other clathrin and caveola-independent endocytosis for NPs with sizes between 250 nm and 3 μm (70, 71). Once inside the cells, NPs can interact with specific organelles and/or release their cargo to reach potential targets, such as the ones involved in cell death/survival and cell proliferation pathways (66).

Curcumin can modulate multiple apoptosis signaling pathways. The predominant apoptotic mechanism—extrinsic (receptor-mediated) or intrinsic (mitochondrial) – differs between cell types, differentiation stages, or curcumin concentrations. Increase of Bax/Bcl-2 ratio, activation of caspase-3, inhibition of telomerase, DNA fragmentation, and induction of redox signaling are some of the apoptotic mechanisms activated by curcumin in distinct breast cancer cells (72–74). Cell cycle arrest by free curcumin has also been described and is potentially associated with its antiproliferative effects (74). Regarding the antitumor mechanisms reported in the included studies, Cur-NPs were shown to induce at least tumor apoptosis, necrosis, and/or cell proliferation blockage in *in vivo* breast cancer models (26, 28, 30, 34, 36, 37, 40, 41, 45, 48).

Angiogenesis involves the development of new blood vessels from pre-existing vessels and plays an important role in tumor growth, maintenance, and metastasis (26, 30). Free curcumin has been described presenting anti-angiogenesis effects by inhibiting or modulating many pro-angiogenesis factors such as vascular endothelial growth factor (VEGF), matrix metalloproteinases (MMPs), and basic fibroblast growth factor (bFGF) in *in vitro* and *in vivo* studies (26, 30, 58). Similar effects were reported in the included studies when curcumin was associated with micelles, graphene oxide, or polymeric NPs and administered in *in vivo* breast cancer models (28, 34, 36, 41, 45).

It is known that a population of cancer stem cells (CSCs) is present within the tumor microenvironment. These cells are able to activate self-sustaining and self-renewal mechanisms, giving rise to heterogeneous cancer cells that comprise the tumor (75). CSCs are also known to present a high expression of P-glycoprotein, a well-known protein involved in multidrug resistance (MDR), making them less susceptible to antitumor therapies (76). Interestingly, free curcumin has been described affecting CSCs with no toxicity to normal stem cells. The mechanisms involve modulation of P-glycoprotein (77); suppression of the release of cytokines such as interleukin (IL)-6, IL-8, and IL-1, which stimulate CSCs; among others (75). Cur-NPs of the studies evaluated herein seems to maintain this property since studies with curcumin associated with micelles and polymeric NPs have shown a significant reduction in the proportion of CSCs present in *in vivo* breast cancer models (26, 33) (**Table 1**).

Metastasis is the process where cells from the primary tumor spread to distant sites and give rise to a secondary tumor. Advanced breast cancer includes both stage (IV) of metastatic breast cancer and inoperable locally advanced breast cancer, which has not spread to distant organs. The most common site affected by breast cancer cells are the axillary lymph nodes, lungs, liver, and bones (1, 78). In the present review, Cur-NPs showed significant effects against tumor metastasis in *in vivo* breast cancer models. For instance, curcumin associated with graphene oxide NPs reduced the regions of metastasis in a triple negative breast cancer model (34).

Different routes of administration were adopted among the studies evaluated herein. The oral administration route is preferred over other routes for drugs and NPs due to advantages such as ease of ingestion, good patient compliance, and pain avoidance. The main limitation of this route is the knowledge of the real dose absorbed (79). Only one included study explored oral administration with curcumin entrapped in a lipid-based NP (25). Interestingly, a remarkable tumor volume reduction of ~60% was achieved; nevertheless, the dose of curcumin administered was the highest among all the other studies (100 mg/Kg), probably due to variations in NP absorption through this route.

Other routes of administration can be applied to avoid the gastrointestinal tract and potential degradation (80). Intratumoral administration is an interesting option for breast cancer therapy. NPs can be administered with a minimal invasive procedure with a regular biopsy needle, for example, right in the tumor site, increasing the lifetime of drugs in contact with malignant target cells, reducing adverse effects on healthy tissues, and bypassing liver metabolism (81). Two of the included studies used this route to administer micelle NPs to triple negative breast cancer models and showed similar outcomes in terms of tumor volume reduction (51–60%) (26, 27).

The intraperitoneal (IP) route is commonly used in rodents and consists of an injection of pharmacological drugs into the peritoneal cavity. Quick and minimally stressful for animals, the IP route permits safe administration of a large volume of drug and it is more appropriate when the intravenous route is challenging. The IP route is an entry portal for blood circulation through the capillary system (80). Two of the included studies reported the success of Cur-micelle NP

administration *via* IP route with a reduction of tumor volume of ~80 and ~59.1%, respectively (28, 29).

The intravenous (IV) route of administration enables the rapid circulation of an administered drug in the bloodstream. Although approximately 70% of the included studies adopted this route of administration, precise efficacy comparisons regarding composition and other characteristics (*e.g.*, HD, PDI, PZ) of NPs are limited due to variations in cell lines, number of cells used for induction, moment of the first treatment, and dose/treatment regimens. However, some comparisons involving dose concentrations and presence of active targeting were possible when analyzing studies that evaluated more than one experimental variable in the same experimental design. In general, it was observed that all the types of NPs used led to improved outcomes in terms of tumor volume reduction in models of estrogen receptor (ER) positive, chemically induced, and triple negative breast cancer (**Table 1**).

MCF-7 is one of the human cell lines most commonly used for breast cancer research, since it expresses substantial levels of estrogen receptor (ER) mimicking the majority of breast cancers diagnosed nowadays (82). Analyzing MCF-7 models of the included studies, it was observed that the influence of active targeting in improved efficacy outcomes depends on the moiety used. Lin and co-workers (50) reported significant improvements in tumor volume reduction when attaching FA, as the targeting moiety, to lipid-based NPs (~83%) when compared to non-targeted NPs (~66%) (50). Similar results were observed in MDA-MB-231 *in vivo* models (triple negative breast cancer), where the presence of folate, as an active targeting moiety, showed improved tumor volume reduction (~90%) when compared to non-targeted NPs (~75%) (46). On the other hand, no significant improvements were observed when peptide moieties with affinity to EGFR were used in polymeric NPs when compared with non-targeted NPs (37). Another interesting aspect that seems to improve efficacy outcomes in MCF-7 models is the design of pH-sensitive NPs. Yu and co-workers (47) reported improved reduction of tumor volume in animals treated with pH-sensitive micelles (mPEG-PLA with PAE) (~65.6%) when compared to the ones treated with non-pH-sensitive micelles (~47.1%) (47).

Both MCF-7 and MDA-MB-231 conventional *in vivo* models are induced in immunocompromised mice due to the human origin of these cell lines (83). These models, also known as xenograft, lack relevance when the study aims to evaluate/associate the outcomes with a functional immune system. In this case, syngeneic models, where cells of the same genetic background (murine) are implanted into a mouse with a native immune system, are recommended (83). Syngeneic breast cancer models usually use the 4T1 cell line as a representative model that mimics triple negative breast cancers (84). Analyzing 4T1 models used in the included studies, it was observed that the outcome of tumor volume reduction showed a tendency to respond in a dose-dependent manner. Greish and co-workers (44) showed that a 20mg/Kg dose led to improved tumor volume reduction (~92%) when compared to a 10 mg/ml dose (~61%) (44). Nevertheless, when comparing high doses, such as 40 and 80 mg/Kg, no significant improvements were observed between them (49). The presence of the active targeting moieties FA or HA in the NPs showed improved efficacy, as reported by Laha and co-workers (31) and Ji and co-workers (31, 35).

Analyzing only the studies of Sahne and co-workers (34), Ji and co-workers (35) and He and co-workers (36), all with breast cancer induction with 4T1 cells ($10^6$) in Balb/c mice, and with the treatments performed intravenously and in very similar doses, 4 or 5 mg/kg, but with a difference in the treatment schedule (**Table 1**), (in the work of Sahne and co-workers, the treatment was daily, for 21 days; in the work of Ji and co-workers, the treatment was every two days for 10 days; and in the work of He and co-workers, it was every four days in 21 total days), it can be observed that, interestingly, the treatments with the Cur-NPs, either by FA-GO-NP or HA-Cur-NP, promoted a similar percentage of reduction in tumor volume (approximately 86%, **Table 1**). Assessing NPs, HA-Cur-NP is a nanocrystal that has a 162 nm HD, while FA-GO-NP is a graphene oxide NP that has a 60 nm HD. In the treatment aspect, treatment every 2 days for only 10 days of HA-Cur-NP had the same antitumor efficiency as daily treatment for 21 days of FA-GO-NP. Therefore, it is a shorter and less aggressive therapeutic regimen, presenting similar efficiency (34–36).

The elimination of NPs occurs in organs and tissue systems after i.v. injection by two main clearance systems: reticuloendothelial system (RES) or mononuclear phagocyte system (MPS) and by renal and hepatic systems. Properties of NPs, including core type, surface chemistry, size, shape, degradability, and surface charge influence the process of clearance (85). The MPS is based on phagocytosis (mostly for NPs between 50 and 200 nm) or pinocytosis, and degraded NPs are excreted into the blood circulation, decreasing the injected dose (85, 86). Renal and hepatic systems are the main clearance organs of NPs less than 100 nm through glomerular filtration and tubular secretion in the kidney. NPs that are not cleared by the kidney can be processed in the liver due to the presence of a large number of Kupffer cells that can sequester foreign bodies, and the very permeable sinusoidal endothelial cells that enhance liver uptake and retention of NPs (85).

Among the included studies that evaluated toxicity effects, none of the Cur-NPs provoked toxicity, considering biochemical markers, hematological changes, damage to major organs, and weight loss (**Table 1**). It is worth pointing out that the majority of studies (~80%) analyzing the efficacy of Cur-NPs also evaluated at least one toxicity outcome, showing that research into NPs is not only interested in treatment efficacy but also considers safety issues. Nevertheless, ~33% of such studies used only body weight as a parameter for toxicity analysis. Thus, it is important to pursue deeper investigations beyond these parameters in order to understand better the safety of the treatment and enable its clinical translation.

## LIMITATIONS

Some limitations were encountered during the elaboration of this systematic review. First, there was high heterogeneity

regarding NP type, characteristics of NPs, animal models, period of administration, and intervention concentrations which made meta-analysis unfeasible. Furthermore, one study was excluded in phase 2 because its full copy could not be obtained. Moreover, most SYRCLE' RoB criteria were unclearly reported in most included studies therefore, limiting the evaluation of study quality.

## CONCLUSION

This systematic review evidences that the use of NPs as drug delivery systems for curcumin is a promising approach for the treatment of breast cancer. The results show significant tumor volume reduction in all breast cancer models, which could be attributed to increased apoptosis and necrosis rate, reduction of tumor cell proliferation and impairment of angiogenesis, and even reduction of the population of stem cancer cells, which might also be correlated with improved survival times. All of these improved outcomes are also related to no or low adverse effects in terms of body weight, histopathology of major organs (*e.g.*, liver, kidneys, lungs, spleen), or alterations in hematological/biochemical parameters.

Variations in NP structure should be considered according to the type of breast tumor as well as the route of administration and dose schedule. In addition, the cost-effective and large-scale manufacturing of the proposed NP platforms is also of considerable importance to enable a real translation of these remarkable technologies from the bench to the bedside.

Although Cur-NPs' association with other therapeutic approaches is not within the scope of the present work, it is recommended that systematic evaluations of outcomes regarding efficacy and toxicity of Cur-NPs when associated with other plant-derived molecules or currently prescribed therapies (*e.g.*, chemotherapy, radiotherapy) should be further considered. Altogether, this systematic review supports the proposal that Cur-NPs provide an effective and safe therapeutic approach in *in vivo* models of breast cancer, reinforcing the currently available evidence that their usage should be further analyzed in clinical trials for breast cancer treatments.

## DATA AVAILABILITY STATEMENT

The original contributions presented in the study are included in the article/**Supplementary Material**. Further inquiries can be directed to the corresponding author.

## AUTHOR CONTRIBUTIONS

AO, VS, GL, and GJ conceived the idea and prepared, edited, and finalized the manuscript. The articles were selected in two phases: screening of titles and abstracts (phase 1), and full-text reading (phase 2). In phase 1, two authors (AO and VS) reviewed titles and abstracts of all references identified in the electronic databases and selected articles that seemed to meet the inclusion criteria. In phase 2, six pairs of authors (AO and VS; LA and GF; WP and AP; JO and MG; MS and GG; PC and GJ) were formed to independently analyze the full text of articles selected in phase 1 and exclude studies that did not meet the inclusion criteria. LA and PC revised the manuscript. GG prepared the graphical abstract. All authors contributed to the article and approved the submitted version.

## FUNDING

This work was supported by Coordenação de Aperfeiçoamento de Pessoal de Nível Superior (CAPES—Finance Code 001), Conselho Nacional de Desenvolvimento Cientifico e Tecnológico (CNPq), Instituto Nacional de Ciência e Tecnologia em Nanobiotecnologia (INCT Nanobiotecnologia), and Fundação de Amparo à Pesquisa do Distrito Federal (FAP-DF). The funders had no role in study design, data collection and analysis, decision to publish, or preparation of the manuscript.

## SUPPLEMENTARY MATERIAL

The Supplementary Material for this article can be found online at: https://www.frontiersin.org/articles/10.3389/fonc.2021.612903/full#supplementary-material

## REFERENCES

1. Harbeck N, Penault-Llorca F, Cortes J, Gnant M, Houssami N, Poortmans P, et al. Breast cancer. *Nat Rev Dis Primers* (2019) 5:1–2. doi: 10.1038/s41572-019-0111-2
2. WHO. *Breast cancer*. (2020). Available at: https://www.who.int/cancer/prevention/diagnosis-screening/breast-cancer/en.
3. Waks AG, Winer EP. Breast Cancer Treatment: A Review. *JAMA - J Am Med Assoc* (2019) 321(3):288–300. doi: 10.1001/jama.2018.19323
4. Falagan-Lotsch P, Grzincic EM, Murphy CJ. New advances in nanotechnology-based diagnosis and therapeutics for breast cancer: An assessment of active-targeting inorganic nanoplatforms. *Bioconjug Chem* (2017) 28(1):135–52. doi: 10.1021/acs.bioconjchem.6b00591
5. Hu S, Xu Y, Meng L, Huang L, Sun H. Curcumin inhibits proliferation and promotes apoptosis of breast cancer cells. *Exp Ther Med* (2018) 16(2):1266–72. doi: 10.3892/etm.2018.6345
6. Kashyap D, Tuli HS, Yerer MB, Sharma A, Sak K, Srivastava S, et al. Natural product-based nanoformulations for cancer therapy: Opportunities and challenges. *Semin Cancer Biol* (2019). Academic Press. doi: 10.1016/j.semcancer.2019.08.014
7. Sharifi-Rad J, Rayess Y EL, Rizk AA, Sadaka C, Zgheib R, Zam W, et al. Turmeric and Its Major Compound Curcumin on Health: Bioactive Effects and Safety Profiles for Food, Pharmaceutical, Biotechnological and Medicinal Applications. *Front Pharmacol* (2020) 11:1021. doi: 10.3389/fphar.2020.01021
8. Kuttan R, Bhanumathy P, Nirmala K, George MC. Potential anticancer activity of turmeric (Curcuma longa). *Cancer Lett* (1985) 29(2):197–202. doi: 10.1016/0304-3835(85)90159-4
9. Banik U, Parasuraman S, Adhikary AK, Othman NH. Curcumin: The spicy modulator of breast carcinogenesis. *J Exp Clin Cancer Res* (2017) 36(1):1–16. doi: 10.1186/s13046-017-0566-5
10. Wen C, Fu L, Huang J, Dai Y, Wang B, Xu G, et al. Curcumin reverses doxorubicin resistance via inhibition the efflux function of ABCB4 in

doxorubicin–resistant breast cancer cells. *Mol Med Rep* (2019) 19(6):5162–8. doi: 10.3892/mmr.2019.10180
11. Attia YM, El-Kersh DM, Ammar RA, Adel A, Khalil A, Walid H, et al. Inhibition of aldehyde dehydrogenase-1 and p-glycoprotein-mediated multidrug resistance by curcumin and vitamin D3 increases sensitivity to paclitaxel in breast cancer. *Chem Biol Interact* (2020) 315:108865. doi: 10.1016/j.cbi.2019.108865
12. Javadi M, Khadem Haghighian H, Goodarzy S, Abbasi M, Nassiri-Asl M. Effect of curcumin nanomicelle on the clinical symptoms of patients with rheumatoid arthritis: A randomized, double-blind, controlled trial. *Int J Rheum Dis* (2019) 22(10):1857–62. doi: 10.1111/1756-185X.13688
13. Kalyane D, Raval N, Maheshwari R, Tambe V, Kalia K, Tekade RK. Employment of enhanced permeability and retention effect (EPR): Nanoparticle-based precision tools for targeting of therapeutic and diagnostic agent in cancer. *Mater Sci Eng C* (2019) 98::1252–76. doi: 10.1016/j.msec.2019.01.066
14. Watkins R, Wu L, Zhang C, Davis RM, Xu B. Natural product-based nanomedicine: Recent advances and issues. *Int J Nanomedicine* (2015) 10:6055–74. Dove Medical Press Ltd. doi: 10.2147/IJN.S92162
15. Home. *ClinicalTrials.gov*. (2020). Available at: https://www.clinicaltrials.gov.
16. Giordano A, Tommonaro G. Curcumin and cancer. *Nutrients* (2019) 11:2376. MDPI AG. doi: 10.3390/nu11102376
17. Momtazi-Borojeni AA, Ghasemi F, Hesari A, Majeed M, Caraglia M, Sahebkar A. Anti-Cancer and Radio-Sensitizing Effects of Curcumin in Nasopharyngeal Carcinoma. *Curr Pharm Des* (2018) 24(19):2121–8. doi: 10.2174/1381612824666180522105202
18. Moher D, Liberati A, Tetzlaff J, Altman DG. Preferred Reporting Items for Systematic Reviews and Meta-Analyses: The PRISMA Statement. *PloS Med* (2009) 6(7):e1000097. doi: 10.1371/journal.pmed.1000097
19. PROSPERO. (2020). https://www.crd.york.ac.uk/prospero/.
20. Methley AM, Campbell S, Chew-Graham C, McNally R, Cheraghi-Sohi S. PICO. PICOS and SPIDER: A comparison study of specificity and sensitivity in three search tools for qualitative systematic reviews. *BMC Health Serv Res* (2014) 14(1):2. doi: 10.1186/s12913-014-0579-0
21. Hooijmans CR, Rovers MM, De Vries RBM, Leenaars M, Ritskes-Hoitinga M, Langendam MW. SYRCLE's risk of bias tool for animal studies. *BMC Med Res Methodol* (2014) 14(1):1–9. doi: 10.1186/1471-2288-14-43
22. Percie du Sert N, Hurst V, Ahluwalia A, Alam S, Avey MT, Baker M, et al. The ARRIVE guidelines 2.0: Updated guidelines for reporting animal research. *PloS Biol* (2020) 18(7):e3000410. doi: 10.1371/journal.pbio.3000410
23. Scopus preview. *Scopus - Welcome to Scopus*. (2020). Available at: https://www.scopus.com/home.uri.
24. VOSviewer. *Features - Highlights*. (2020). Available at: https://www.vosviewer.com/features/highlights.
25. Shukla M, Jaiswal S, Sharma A, Srivastava PK, Arya A, Dwivedi AK, et al. A combination of complexation and self-nanoemulsifying drug delivery system for enhancing oral bioavailability and anticancer efficacy of curcumin. *Drug Dev Ind Pharm [Internet]* (2017) 43(5):847–61. doi: 10.1080/03639045.2016.1239732
26. Chen W, Li L, Zhang X, Liang Y, Pu Z, Wang L, et al. Curcumin: A calixarene derivative micelle potentiates anti-breast cancer stem cells effects in xenografted, triple-negative breast cancer mouse models. *Drug Deliv* (2017) 24(1):1470–81. doi: 10.1080/10717544.2017.1381198
27. Mahalunkar S, Yadav AS, Gorain M, Pawar V, Braathen R, Weiss S, et al. Functional design of pH-responsive folate-targeted polymer-coated gold nanoparticles for drug delivery and in vivo therapy in breast cancer. *Int J Nanomed* (2019) 14:8285–302. doi: 10.2147/IJN.S215142
28. Alizadeh AM, Sadeghizadeh M, Najafi F, Ardestani SK, Erfani-Moghadam V, Khaniki M, et al. Encapsulation of curcumin in diblock copolymer micelles for cancer therapy. *BioMed Res Int* (2015) 2015:2–7. doi: 10.1155/2015/824746
29. Jung K-HKH, Lee JHJH, Park JWJW, Kim DHDH, Moon SHS-H, Cho YSYS, et al. Targeted therapy of triple negative MDA-MB-468 breast cancer with curcumin delivered by epidermal growth factor-conjugated phospholipid nanoparticles. *Oncol Lett* (2018) 15(6):9093–100. doi: 10.3892/ol.2018.8471
30. Wang Y, Luo Z, Wang Z, You M, Xie S, Peng Y, et al. Effect of curcumin-loaded nanoparticles on mitochondrial dysfunctions of breast cancer cells. *J Nanopart Res* (2018) 20(10):2–6. doi: 10.1007/s11051-018-4382-4
31. Laha D, Pal K, Chowdhuri AR, Parida PK, Sahu SK, Jana K, et al. Fabrication of curcumin-loaded folic acid-tagged metal organic framework for triple negative breast cancer therapy in in vitro and in vivo systems. *New J Chem* (2019) 43(1):217–29. doi: 10.1039/C8NJ03350A
32. Vakilinezhad MA, Amini A, Dara T, Alipour S. Methotrexate and Curcumin co-encapsulated PLGA nanoparticles as a potential breast cancer therapeutic system: In vitro and in vivo evaluation. *Colloids Surf B Biointerfaces* (2019) 184:110515. doi: 10.1016/j.colsurfb.2019.110515
33. Yuan JD, ZhuGe DL, Tong MQ, Lin MT, Xu XF, Tang X, et al. pH-sensitive polymeric nanoparticles of mPEG-PLGA-PGlu with hybrid core for simultaneous encapsulation of curcumin and doxorubicin to kill the heterogeneous tumour cells in breast cancer. *Artif Cells Nanomed Biotechnol* (2018) 46(sup1):302–13. doi: 10.1080/21691401.2017.1423495
34. Sahne F, Mohammadi M, Najafpour GD. Single-Layer Assembly of Multifunctional Carboxymethylcellulose on Graphene Oxide Nanoparticles for Improving in Vivo Curcumin Delivery into Tumor Cells. *ACS Biomater Sci Eng* (2019) 5(5):2595–609. doi: 10.1021/acsbiomaterials.8b01628
35. Ji P, Wang L, Chen Y, Wang S, Wu Z, Qi X. Hyaluronic acid hydrophilic surface rehabilitating curcumin nanocrystals for targeted breast cancer treatment with prolonged biodistribution. *Biomater Sci* (2020) 8(1):462–72. doi: 10.1039/C9BM01605H
36. He H, Zhuang W, Ma B, Su X, Yu T, Hu J, et al. Oxidation-Responsive and Aggregation-Induced Emission Polymeric Micelles with Two-Photon Excitation for Cancer Therapy and Bioimaging. *ACS Biomater Sci Eng* (2019) 5(5):2577–86. doi: 10.1021/acsbiomaterials.9b00212
37. Jin H, Pi J, Zhao Y, Jiang J, Li T, Zeng X, et al. EGFR-targeting PLGA-PEG nanoparticles as a curcumin delivery system for breast cancer therapy. *Nanoscale* (2017) 9(42):16365–74. doi: 10.1039/C7NR06898K
38. Abd-Ellatef GEF, Gazzano E, Chirio D, Hamed AR, Belisario DC, Zuddas C, et al. Curcumin-loaded solid lipid nanoparticles bypass p-glycoprotein mediated doxorubicin resistance in triple negative breast cancer cells. *Pharmaceutics* (2020) 12(2):1–20. doi: 10.3390/pharmaceutics12020096
39. Li N, Wang Z, Zhang Y, Zhang K, Xie J, Liu Y, et al. Curcumin-loaded redox-responsive mesoporous silica nanoparticles for targeted breast cancer therapy. *Artif Cells Nanomed Biotechnol* (2018) 46(sup2):921–35. doi: 10.1080/21691401.2018.1473412
40. Kundu M, Sadhukhan P, Ghosh N, Chatterjee S, Manna P, Das J, et al. pH-responsive and targeted delivery of curcumin via phenylboronic acid-functionalized ZnO nanoparticles for breast cancer therapy. *J Adv Res* (2019) 18:161–72. doi: 10.1016/j.jare.2019.02.036
41. Lv L, Guo Y, Shen Y, Liu J, Zhang W, Zhou D, et al. Intracellularly Degradable, Self-Assembled Amphiphilic Block Copolycurcumin Nanoparticles for Efficient In Vivo Cancer Chemotherapy. *Adv Healthc Mater* (2015) 4 (10):1496–501. doi: 10.1002/adhm.201500075
42. Yang Z, Sun N, Cheng R, Zhao C, Liu J, Tian Z. Hybrid nanoparticles coated with hyaluronic acid lipoid for targeted co-delivery of paclitaxel and curcumin to synergistically eliminate breast cancer stem cells. *J Mater Chem B* (2017) 5 (33):6762–75. doi: 10.1039/C7TB01510K
43. Yang Z, Sun N, Cheng R, Zhao C, Liu Z, Li X, et al. pH multistage responsive micellar system with charge-switch and PEG layer detachment for co-delivery of paclitaxel and curcumin to synergistically eliminate breast cancer stem cells. *Biomaterials* (2017) 147:53–67. doi: 10.1016/j.biomaterials.2017.09.013
44. Greish K, Pittalà V, Taurin S, Taha S, Bahman F, Mathur A, et al. Curcumin–copper complex nanoparticles for the management of triple-negative breast cancer. *Nanomaterials* (2018) 8(11):2–8. doi: 10.3390/nano8110884
45. Mukerjee A, Ranjan AP, Vishwanatha JK. Targeted Nanocurcumin Therapy Using Annexin A2 Anitbody Improves Tumor Accumulation and Therapeutic Efficacy Against Highly Metastatic Breast Cancer. *J Biomed Nanotechnol* (2016) 12: (7):1374–92. doi: 10.1166/jbn.2016.2240
46. Mukhopadhyay R, Sen R, Paul B, Kazi J, Ganguly S, Debnath MC. Gemcitabine Co-Encapsulated with Curcumin in Folate Decorated PLGA Nanoparticles; a Novel Approach to Treat Breast Adenocarcinoma. *Pharm Res* (2020) 37(3):10–14. doi: 10.1007/s11095-020-2758-5
47. Yu Y, Zhang X, Qiu L. The anti-tumor efficacy of curcumin when delivered by size/charge-changing multistage polymeric micelles based on amphiphilic poly(β-amino ester) derivates. *Biomaterials* (2014) 35(10):3–10. doi: 10.1016/j.biomaterials.2013.12.096
48. Huang C, Chen F, Zhang L, Yang Y, Yang X, Pan W. 99mTc radiolabeled HA/TPGS-based curcumin-loaded nanoparticle for breast cancer synergistic

theranostics: Design, in vitro and in vivo evaluation. *Int J Nanomedicine* (2020) 15:2987–98. doi: 10.2147/IJN.S242490
49. Shiri S, Alizadeh AM, Baradaran B, Farhanghi B, Shanehbandi D, Khodayari S, et al. Dendrosomal curcumin suppresses metastatic breast cancer in mice by changing M1/M2 macrophage balance in the tumor microenvironment. *Asian Pac J Cancer Prev* (2015) 16(9):3917–22. doi: 10.7314/APJCP.2015.16.9.3917
50. Lin M, Teng L, Wang Y, Zhang J, Sun X. Curcumin-guided nanotherapy: a lipid-based nanomedicine for targeted drug delivery in breast cancer therapy. *Drug Deliv* (2016) 23(4):1420–5. doi: 10.3109/10717544.2015.1066902
51. Song X, Zhang M, Dai E, Luo Y. Molecular targets of curcumin in breast cancer (Review). *Mol Med Rep* (2019) 19(1):23–9. doi: 10.3892/mmr.2018.9665
52. Shahabipour F, Caraglia M, Majeed M, Derosa G, Maffioli P, Sahebkar A. Naturally occurring anti-cancer agents targeting EZH2. *Cancer Lett* (2017) 400:325–35. doi: 10.1016/j.canlet.2017.03.020
53. Hua WF, Fu YS, Liao YJ, Xia WJ, Chen YC, Zeng YX, et al. Curcumin induces down-regulation of EZH2 expression through the MAPK pathway in MDA-MB-435 human breast cancer cells. *Eur J Pharmacol* (2010) 637(1–3):16–21. doi: 10.1016/j.ejphar.2010.03.051
54. Shao ZM, Shen ZZ, Liu CH, Sartippour MR, Go VL, Heber D, et al. Curcumin exerts multiple suppressive effects on human breast carcinoma cells. *Int J Cancer* (2002) 98(2):234–40. doi: 10.1002/ijc.10183
55. Simental-Mendía LE, Caraglia M, Majeed M, Sahebkar A. Impact of curcumin on the regulation of microRNAs in colorectal cancer. *Expert Rev Gastroenterol Hepatol* (2017) 11:99–101. doi: 10.1080/17474124.2017.1268528
56. Li J, Wei H, Liu Y, Li Q, Guo H, Guo Y, et al. Curcumin Inhibits Hepatocellular Carcinoma via Regulating miR-21/TIMP3 Axis. *Evidence-Based Complement Altern Med* (2020) 2020:4–8. doi: 10.1155/2020/2892917
57. Gallardo M, Kemmerling U, Aguayo F, Bleak TC, Muñoz JP, Calaf GM. Curcumin rescues breast cells from epithelial–mesenchymal transition and invasion induced by anti–miR–34a. *Int J Oncol* (2020) 56(2):480–93. doi: 10.3892/ijo.2019.4939
58. Saberi-Karimian M, Katsiki N, Caraglia M, Boccellino M, Majeed M, Sahebkar A. Vascular endothelial growth factor: An important molecular target of curcumin. *Crit Rev Food Sci Nutr* (2019) 59:299–312. doi: 10.1080/10408398.2017.1366892
59. Ferreira L, Arbab A, Jardim-Perassi B, Borin T, Varma N, Iskander A, et al. Effect of Curcumin on Pro-angiogenic Factors in the Xenograft Model of Breast Cancer. *Anticancer Agents Med Chem* (2015) 15 (10):1285–96. doi: 10.2174/1871520615666150520093644
60. Ghandadi M, Sahebkar A. Curcumin: An Effective Inhibitor of Interleukin-6. *Curr Pharm Des* (2016) 23: (6):921–31. doi: 10.2174/1381612822666161006151605
61. Basnet P, Skalko-Basnet N. Curcumin: An anti-inflammatory molecule from a curry spice on the path to cancer treatment. *Molecules* (2011) 16(6):4567–98. doi: 10.3390/molecules16064567
62. Maeda H. Toward a full understanding of the EPR effect in primary and metastatic tumors as well as issues related to its heterogeneity. *Adv Drug Deliv Rev* (2015) 91:3–6. doi: 10.1016/j.addr.2015.01.002
63. Wilhelm S, Tavares AJ, Dai Q, Ohta S, Audet J, Dvorak HF, et al. Analysis of nanoparticle delivery to tumours. *Nat Rev Mater* (2016) 1:16014. doi: 10.1038/natrevmats.2016.14
64. Sindhwani S, Syed AM, Ngai J, Kingston BR, Maiorino L, Rothschild J, et al. The entry of nanoparticles into solid tumours. Nat Mater. *Nat Mater* (2020) 19(5):566–75. doi: 10.1038/s41563-019-0566-2
65. Shi Y, van der Meel R, Chen X, Lammers T. The EPR effect and beyond: Strategies to improve tumor targeting and cancer nanomedicine treatment efficacy. *Theranostics* (2020) 10:7921–4. doi: 10.7150/thno.49577
66. Gmeiner WH, Ghosh S. Nanotechnology for cancer. *Nanotechnol Rev* (2014) 3: (2):111–22. doi: 10.1515/ntrev-2013-0013
67. Jordan Price R, Lillycrop KA, Burdge GC. Folic acid induces cell type-specific changes in the transcriptome of breast cancer cell lines: A proof-of-concept study. *J Nutr Sci* (2016) 5:1–8. doi: 10.1017/jns.2016.8
68. Tan S, Yamashita A, Gao SJ, Kurisawa M. Hyaluronic acid hydrogels with defined crosslink density for the efficient enrichment of breast cancer stem cells. *Acta Biomater* (2019) 94:320–9. doi: 10.1016/j.actbio.2019.05.040
69. Anemone A, Consolino L, Arena F, Capozza M, Longo DL. Imaging tumor acidosis: a survey of the available techniques for mapping in vivo tumor pH. *Cancer Metastasis Rev* (2019) 38:25–49. doi: 10.1007/s10555-019-09782-9
70. Sahay G, Alakhova DY, Kabanov AV. Endocytosis of nanomedicines. *J Controlled Release* (2010) 145:182–95. doi: 10.1016/j.jconrel.2010.01.036
71. Manzanares D, Ceña V. Endocytosis: The nanoparticle and submicron nanocompounds gateway into the cellMDPI AG. *Pharmaceutics* (2020) 12:6. doi: 10.3390/pharmaceutics12040371
72. Karunagaran D, Rashmi R, Kumar T. Induction of Apoptosis by Curcumin and Its Implications for Cancer Therapy. *Curr Cancer Drug Targets* (2005) 5 (2):117–29. doi: 10.2174/1568009053202081
73. Reuter S, Eifes S, Dicato M, Aggarwal BB, Diederich M. Modulation of anti-apoptotic and survival pathways by curcumin as a strategy to induce apoptosis in cancer cells. *Biochem Pharmacol* (2008) 76:4. doi: 10.1016/j.bcp.2008.07.031
74. Liczbiński P, Michałowicz J, Bukowska B. Molecular mechanism of curcumin action in signaling pathways: Review of the latest research. *Phytother Res* (2020) 34:1992–2005. doi: 10.1002/ptr.6663
75. Sordillo PP, Helson L. Curcumin and cancer stem cells: Curcumin has asymmetrical effects on cancer and normal stem cells. *Anticancer Res* (2015) 35(2):599–614.
76. Cho Y, Kim YK. Cancer Stem Cells as a Potential Target to Overcome Multidrug Resistance. *Front Oncol* (2020) 10:764. doi: 10.3389/fonc.2020.00764
77. Lopes-Rodrigues V, Sousa E, Vasconcelos MH. Curcumin as a modulator of P-glycoprotein in cancer: Challenges and perspectives. *Pharmaceuticals* (2016) 9:4–5. doi: 10.3390/ph9040071
78. Cao H, Dan Z, He X, Zhang Z, Yu H, Yin Q, et al. Liposomes Coated with Isolated Macrophage Membrane Can Target Lung Metastasis of Breast Cancer. *ACS Nano* (2016) 10(8):7738–48. doi: 10.1021/acsnano.6b03148
79. Zhang J, Xie Z, Zhang N, Zhong J. Nanosuspension drug delivery system: preparation, characterization, postproduction processing, dosage form, and application. In: . *Nanostructures for Drug Delivery* (2017). p. 413–43.
80. Al Shoyaib A, Archie SR, Karamyan VT. Intraperitoneal Route of Drug Administration: Should it Be Used in Experimental Animal Studies? *Pharm Res* (2020) 37(1):1. doi: 10.1007/s11095-019-2745-x
81. Kollenda SA, Klose J, Knuschke T, Sokolova V, Schmitz J, Staniszewska M, et al. In vivo biodistribution of calcium phosphate nanoparticles after intravascular, intramuscular, intratumoral, and soft tissue administration in mice investigated by small animal PET/CT. *Acta Biomater* (2020) 109:244–53. doi: 10.1016/j.actbio.2020.03.031
82. Lee AV, Oesterreich S, Davidson NE. MCF-7 Cells - Changing the Course of Breast Cancer Research and Care for 45 Years. *J Natl Cancer Inst* (2015) 107:1–2. doi: 10.1093/jnci/djv073
83. Holen I, Speirs V, Morrissey B, Blyth K. In vivo models in breast cancer research: Progress, challenges and future directions. *Dis Model Mech* (2017) 10:359–71. doi: 10.1242/dmm.028274
84. Paschall AV, Liu K. An Orthotopic mouse model of spontaneous breast cancer metastasis. *J Vis Exp* (2016) 2016(114):2–5. doi: 10.3791/54040
85. Wei Y, Quan L, Zhou C, Zhan Q. Factors relating to the biodistribution & clearance of nanoparticles & their effects on in vivo application. *Nanomedicine* (2018) 13(12):1495–512. doi: 10.2217/nnm-2018-0040
86. Shreffler JW, Pullan JE, Dailey KM, Mallik S, Brooks AE. Overcoming hurdles in nanoparticle clinical translation: The influence of experimental design and surface modification. *Int J Mol Sci* (2019) 20(23):1–25. doi: 10.3390/ijms20236056

**Conflict of Interest:** The authors declare that the research was conducted in the absence of any commercial or financial relationships that could be construed as a potential conflict of interest.

frontiers in Oncology

REVIEW
published: 16 March 2021
doi: 10.3389/fonc.2021.623760

# Triggered Drug Release From Liposomes: Exploiting the Outer and Inner Tumor Environment

*Marina Santiago Franco*, Eliza Rocha Gomes, Marjorie Coimbra Roque and Mônica Cristina Oliveira**

*Department of Pharmaceutical Products, Faculty of Pharmacy, Universidade Federal de Minas Gerais, Belo Horizonte, Brazil*

Since more than 40 years liposomes have being extensively studied for their potential as carriers of anticancer drugs. The basic principle behind their use for cancer treatment consists on the idea that they can take advantage of the leaky vasculature and poor lymphatic drainage present at the tumor tissue, passively accumulating in this region. Aiming to further improve their efficacy, different strategies have been employed such as PEGlation, which enables longer circulation times, or the attachment of ligands to liposomal surface for active targeting of cancer cells. A great challenge for drug delivery to cancer treatment now, is the possibility to trigger release from nanosystems at the tumor site, providing efficacious levels of drug in the tumor. Different strategies have been proposed to exploit the outer and inner tumor environment for triggering drug release from liposomes and are the focus of this review.

**Keywords: cancer, chemotherapy, liposome, triggered release, tumor environment**

OPEN ACCESS

***Edited by:***
*Luis Alexandre Muehlmann, University of Brasilia, Brazil*

***Reviewed by:***
*Fong-Yu Cheng, Chinese Culture University, Taiwan*
*Alessio Giubellino, University of Minnesota Twin Cities, United States*

****Correspondence:***
*Marina Santiago Franco*
*franco.marinasantiago@gmail.com*
*Mônica Cristina Oliveira*
*itabra2001@yahoo.com.br*

***Specialty section:***
*This article was submitted to Cancer Molecular Targets and Therapeutics, a section of the journal Frontiers in Oncology*

***Received:*** *30 October 2020*
***Accepted:*** *02 February 2021*
***Published:*** *16 March 2021*

***Citation:***
*Franco MS, Gomes ER, Roque MC and Oliveira MC (2021) Triggered Drug Release From Liposomes: Exploiting the Outer and Inner Tumor Environment. Front. Oncol. 11:623760. doi: 10.3389/fonc.2021.623760*

## INTRODUCTION

A liposome is a spherical vesicle composed of a phospholipid bilayer formed into an enclosed aqueous pocket. They were first described by Alec Bangham in the mid-60s, who was interested in the system as an *in vitro* model of biological membranes (1). It was Gregory Gregoriadis in 1973, who first proposed their use as a drug delivery system (2). As drug carriers, liposomes are extremely versatile, as the phospholipid bilayer can accommodate hydrophobic drugs, while hydrophilic drugs can be entrapped on the aqueous inner compartment. In 1974, Gregoriadis et al. first suggested the potential of liposomes as carriers of anticancer drugs, based on the observation that they were able to accumulate in the tumors (3). This accumulation ability was later explained by the idea that liposomes take advantage of the leaky vasculature and poor lymphatic drainage present at tumor tissue to passively accumulate in this region, what is known as Enhanced Permeability Retention (EPR) effect (4–6). A major drawback of the first generation liposomes consisted on its rapid uptake by the mononuclear phagocyte system (MPS) after systemic administration, which limited their application. It was in 1990 that Klibanov et al. reported the first step on liposome's evolution: the possibility of enhancing circulation time by coating the liposomal surface with inert biocompatible polymers, such as polyethylene glycol (PEG). This coat prevents the recognition of liposomes by opsonins and thus reduces their clearance by the cells of the MPS (7). As the EPR effect is a progressive phenomenon, requiring many passages of the nanosystem through tumor vasculature, long circulating liposomes have a better chance to accumulate in tumors (5). The strategy of coating

liposomes with PEG allowed for the development of Doxil®, the first FDA-approved nano-drug (8, 9).

Aiming on further improving tumor target, research efforts have been made to develop liposomes able to actively target the tumor site. The strategy consists on attaching a ligand to the liposome surface, directed to a molecule or receptor over expressed on the tumor cell. This strategy is also complementary to EPR effect as actively-targeted liposomes require being in the vicinity of their target to recognize and interact with it. No actively targeted liposomal formulation is commercially available; however, some have made it to the clinical development stages (10).

For both targeted and non-targeted liposomes, drug release kinetics is critical to the anticancer effects, thus a great challenge now facing drug delivery for cancer treatment is liposomal trigger at tumor site. Liposomes designed upon this concept should be optimized to prevent drug release in the bloodstream and normal tissues and release their contents only when exposed to a trigger stimulus at tumor site, obtaining optimum anticancer effects (11, 12). This strategy aims on enhancing efficacy and reducing toxicity, is highly dependent on EPR effect, and can also benefit from active target. **Figure 1** exemplifies the idea of liposomes as carriers of anticancer drugs and its evolution.

Different strategies have been proposed to exploit the outer and inner tumor environment for triggering drug release from liposomes. Formulations designed to be triggered by extracorporeal physical stimuli include thermo-, magnetic-, ultrasound-, light-, chemically- and electric-triggered liposomes (13). Physiological signals present at the tumor microenvironment, such as the presence of acidic pH, redox potential (glutathione, GSH), enzymes, hypoxia, and adenosine-50- triphosphate (ATP) have been explored as endogenous trigger stimuli (14). Compared to endogenous triggers, exogenous triggers have the advantage of being much more controllable. It is not only possible to better control when the treatment occurs and its duration but additionally there are less inter-patient variations as for the endogenous signals (14). To date the only formulation planned according to this concept to reach clinical trials is Thermodox®, thermo-sensitive liposomes currently in phase III trial (15). The different liposomal trigger strategies will be further discussed herein. It is beyond the scope of this review to make an exhaustive list of the formulations developed to date. On the contrary, we aim to give key examples of formulations built upon each of these strategies, providing an overview of the state of the art on possible liposomal compositions and trigger mechanisms.

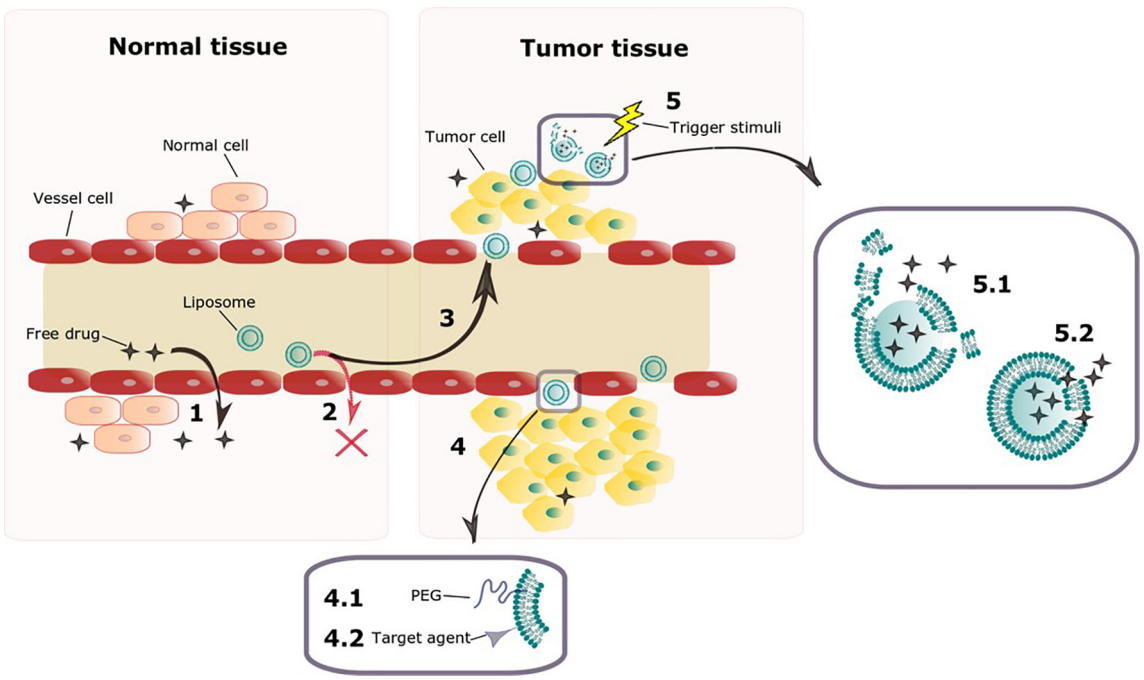


**FIGURE 1** | Schematic representation of key features of liposomes as carriers of anticancer drugs and its evolution. The tight endothelial junctions of cells on normal vessels allow free drug to overflow from blood vessel to normal tissue (1). Liposomes however are too big to penetrate through the tight junctions on vessels from normal tissues (2), accumulating preferably on tumor tissue, where vessels present a defective architecture (3) on a process known as EPR effect. Liposomal surface functionalization can be done aiming on improving its characteristics (4). Surface PEGylation enhances circulation time so that EPR effect is enhanced (4.1). Attaching targeting ligands allows liposomes to recognize tumor cells once they leak through the vasculature (4.2). Once on tumor tissue, different endogenous and exogenous trigger stimuli are being investigated as possibilities to improve drug release on this site (5). A trigger stimulus can either disrupt completely the liposomal membrane (5.1) or enhance its permeability (5.2) allowing the drug to escape.

# TRIGGERED DRUG RELEASE BY EXOGENOUS STIMULI

## Thermo-Triggered Liposomes

### Thermal Therapy and Thermo Sensitive Liposomes

The earliest historical evidence of the use of thermal therapy (or hyperthermia) as cancer treatment was recorded by the Egyptian Edwin Smith Surgical Papyrus in 3000 B.C (16). The role of thermal therapy on cancer management is based on the higher sensitivity of cancer cells to temperature oscillations when compared to normal cells (17–19). Different heating modalities such as radiofrequency (RF), ultrasound transducers, laser and microwave based methods have been exploited to deliver local hyperthermia treatment to deeply seated tumors (16). High temperatures not only cause direct injury to cancer cells but also sensitize them to other treatment modalities, such as chemotherapy and radiotherapy (18). Concerning the combination with chemotherapy, the strategy is further improved when the drugs are encapsulated in nanosystems, as mild hyperthermia (39–42°C for ~ 60 min) can induce several effects on tissues. These effects include increased blood flow, improved perfusion, enhanced oxygenation and increased permeability, which enhances EPR effect, favoring the extravasation of the nanosystems into the tumor. Additionally, mild hyperthermia can be the trigger for a site specific release of the drug from thermosensitive nanosystems (16, 20). Different nanosystems such as polymeric micelles, hydrogels and dendrimers have been described as thermosensitive, however, liposomes are the most successful example of this concept to date (21). A thermosensitive liposome (TSL) formulation, ThermoDox®, reached Phase III clinical trials (15). For TSL to be effective, two main requirements must be fulfilled: minimum leakage of the encapsulated drug under physiological temperature (37°C), and release of the encapsulated drug under mild hyperthermia (22). Knowing that drugs are released from TSL at the melting phase transition temperature (Tm) of the lipid bilayer, these requirements can be fulfilled by taking advantage of the physical properties of liposomal membranes. At Tm, the structure of the lipid bilayer changes, as a transfer from a solid gel phase (Lβ) to a liquid-crystalline phase occurs (Lα). This results in an increased permeability of the lipid bilayer to its aqueous contents *via* passive transfer through the disordered membrane phase boundaries. Thus, TSL have been designed with transition temperatures around 40–42°C, so that the leakage is minimized at body temperature but content is rapidly released when liposome passes through a tumor heated to a temperature around Tm (20, 23).

### The First Steps on Thermo Sensitive Liposomes Development

In 1978, Yatvin et al. described the first TSL, composed of dipalmitoyl phosphatidylcholine (DPPC, Tm= 41°C) and distearoyl phosphatidylcholine (DSPC, Tm = 54°C) at a 3:1 molar ratio. They demonstrated that the ratio of release of the contents from these liposomes at 44°C to that at 37°C could be made greater than 100:1 in the presence of fetal bovine serum. That drew attention for the possible applications of these systems for cancer treatment (24). On the next year, Weinstein et al. (25) published the results showing that a formulation composed of DPPC : DSPC (7:3 weight ratio) encapsulating methotrexate delivered more than four times as much the drug to murine tumors heated to 42°C compared to unheated control tumors. This formulation however, was largely cleared from circulation in 1 h (25). Since then, various modified compositions were proposed for TSL, aiming to increase stability at body temperature (reducing leakage) and enhancing the blood circulation time. Gaber et al. (26) evaluated a series of liposomes composed of DPPC, hydrogenated soybean phosphatidylcholine (HSPC, Tm=52°C), cholesterol (CHOL) and 1,2-distearoyl-sn-glycero-3-phosphoethanolamine-N-[methoxy(polyethylene glycol)-2000] (DSPE-PEG2000) aiming on optimizing the thermo-sensitivity and circulation time of TSL, as illustrated in **Figure 2**. They reported that the presence of CHOL is important to stabilize liposomes containing DSPE-

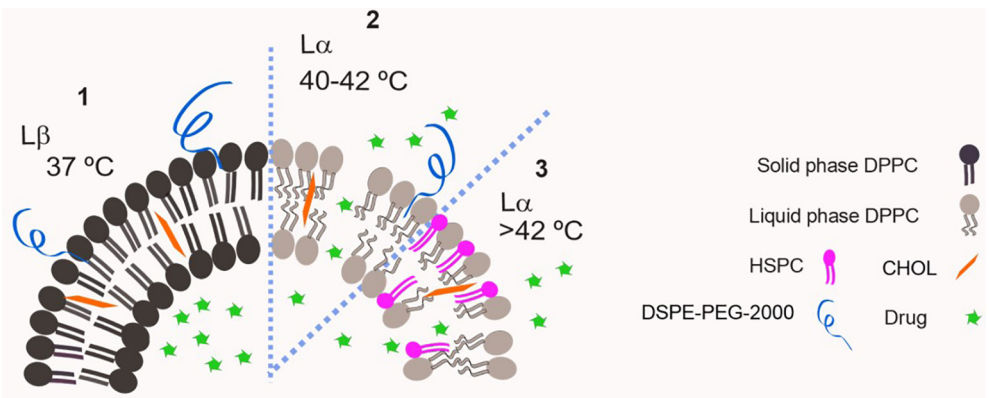


**FIGURE 2** | Schematic representation of a classic thermo-sensitive liposome. DPPC has a Tm= 41°C therefore it is in solid phase at 37°C and bilayer permeability is low (1). Increasing temperature above Tm leads to high bilayer permeability and drug leakage as DPPC is in liquid phase (2). The insertion of a lipid with higher Tm on the bilayer e.g. HSPC, Tm=52°C, allows the modulation of transition temperature of the membrane (3).

PEG2000 on human plasma, however if CHOL concentrations are above 30% the phase transition is avoided and thermo-sensitivity is lost (26). They defined the optimal formulation as DPPC : HSPC : CHOL : DSPE-PEG2000 (50:25:15:3 molar ratio), which was then used to encapsulate DXR and tested *in vivo* on a model of mammary adenocarcinoma in rat skin. At the skin temperature (34°C) a negligible release was observed, and it increased 38 and 76-fold when skin temperature was raised to 42 and 45°C, respectively, for 1 h (26).

### Lysolipid-Containing Thermo Sensitive Liposomes

In 2000, Needham et al. reported the results for a lysolipid-containing TSL, which is considered the major breakthrough on the field to date. The obtained liposomes were composed of DPPC:1-myristoyl-2-palmitoyl-sn-glycero-3-phosphocholine (MPPC):DSPE-PEG2000 (90:10:4 molar ratio) (11). The presence of a few mol% of the MPPC lysolipid in the bilayer leads to a dramatically enhanced grain boundary permeabilization, possibly due to the formation of nanopores in these regions, as illustrated in **Figure 3** (27). That allows for a rapid release of liposome contents in response to a heat stimulus within the mild, clinically-achievable hyperthermia range of 40–42°C. These liposomes were used to encapsulate DXR, and released 45% of its contents in 20 s when exposed to 42°C. As means of comparison, they prepared a formulation composed of DPPC : HSPC : CHOL : DSPE-PEG2000 (50:25:15:3 molar ratio) as described previously by Gaber et al. and as expected this formulation took 30 min to release 40% of its content at 42°C. They also prepared a non-thermo-sensitive liposomal formulation composed of HSPC : CHOL : DSPE-PEG2000 (75:50:3 molar ratio), which did not release any drug upon heating to 42°C. When tested for its antitumor efficacy in a human squamous cell (FaDu) carcinoma xenograft, the lysolipid-containing TSL (100% of animals presented tumor local control (LC) defined as no tumor present at 60 days after treatment). It was significantly more effective than non-thermo-sensitive liposomal formulation (0% LC) or the formulation described by Gaber et al. (10% LC), thus showing the importance of enhanced drug release for achieving the best antitumor efficacy (11). Other preclinical studies using different mice models and a Phase I trial with dogs presenting spontaneous tumors were performed confirming the potential of the formulation (28, 29). The encouraging tumor responses supported clinical evaluation of this formulation. For that, it was slightly modified to DPPC: 1-myristoyl-2-stearoyl-sn-glycero-3-phosphocholine (MSPC):DSPE-PEG2000 (86:10:4 molar ratio) and so called ThermoDox®.

To date, ThermoDox® has predominantly been used clinically in conjunction with radiofrequency ablation (RFA). The idea consists on achieving tumor core ablation with RFA as DXR is intended to improve therapy of the tumor borders (30). A phase I study revealed that ThermoDox® could be safely administered systemically at its maximum tolerated dose (MTD) (50 mg/m$^2$) in combination with RFA, with limited and manageable toxicity (31). The combination treatment moved directly into a Phase III evaluation (HEAT trial) which included 701 patients with hepatocellular carcinoma (HCC) in 79 clinical sites in 11 countries. In 2013 it was announced that this study did not meet its primary endpoint of a 33% improvement in progression-free survival (PFS) compared to RFA alone. A post-hoc subgroup analysis however, demonstrated a 53% risk improvement in overall survival (OS) in the subset of patients that received optimized RFA treatment for 45 min or more combined with ThermoDox®, compared to RFA alone (15, 30). Another phase III clinical study of ThermoDox®, so called "OPTIMA trial", was initiated standardizing the RFA to 45 min or more for patients with HCC. It was initiated in June 2014 and is estimated to enroll about 550 patients. The primary endpoint is OS with PFS as a secondary endpoint. The "TARDOX trial" is a phase I clinical trial aiming on evaluating the feasibility of the combination of ThermoDox® with focused ultrasound (FUS) for treatment of patients with liver tumors. Unlike RFA, FUS is a non-invasive clinical treatment modality. ThermoDox® is also been evaluated for the treatment of other solid tumors. In the "DIGNITY trial", ThermoDox® is being investigated for the treatment of chest wall cancer under superficial hyperthermia (30). There are also Phase I studies to evaluate its combination with local hyperthermia for

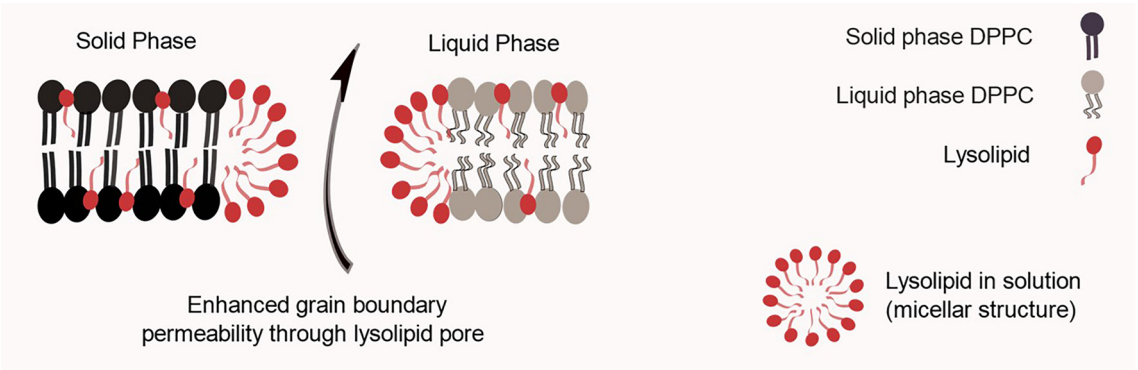


**FIGURE 3** | Schematic representation of a lysolipid containing thermo-sensitive liposomal bilayer. One hypothesis for lysolipid triggering mechanism is based on its tendency to form micelles, which leads to nanopores in grain boundary regions.

patients with breast cancer and with high-intensity focused ultrasound guided by magnetic resonance for pediatric refractory solid tumors (32, 33).

As promising components of TSL, other lysolipids continue to be investigated. Lyu et al. (35) described liposomes containing the lysolipid 1-stearoyl-2-hydroxy-sn-glycerol-3-phosphocholine (1-StePc) for delivering Marimastat (MATT), a matrix metalloproteinases (MMPs) inhibitor, to the tumor microenvironment. For evaluating the *in vitro* drug release abilities, liposomes composed of DPPC:1-StePc : DSPE-PEG2000 (86:10:4 weight ratio) encapsulating (6)-carboxyfluorescein (CF) were analyzed for its release profile. After 90 min, fluorescence intensity for liposomes kept at 43°C was around nine times higher when compared to that observed for liposomes kept at 39°C. When tested *in vivo* for its antitumor activity, animals receiving the MATT-TSL with applied hyperthermia showed 15-fold tumor growth, contrasting with the observed 35-fold growth for animals on control group receiving saline. Regarding the metastatic foci, animals receiving the MATT-TSL plus hyperthermia presented a 7-fold decrease in metastatic lung foci compared to animals on control group. Unfortunately authors did not include groups treated with MATT-TSL only, without hyperthermia, or a treatment with non-TSL liposomes encapsulating MATT for means of comparison (34).

### Other Strategies for Thermo Sensitive Liposomes Development

Other strategies for improving TSL have been described. One of these strategies is the use of 1,2-dipalmitoyl-sn-glycero-phosphodiglycerol (DPPG2, Tm = 39.7°C). This phospholipid allows for an increase in the circulation half-life of vesicles with the advantage that it can be used in concentrations up to 70% mol, against around 10% of PEGylated lipids, which act like surfactants in high concentrations (35). A simplified TSL was developed by Tagami et al. (36). This formulation is composed of DPPC : Brij78 (96:4 molar ratio). Brij78 is a non-ionic surfactant consisting of a PEGylated acylchain and was evaluated as a substitute for the MSPC lysolipid. They reported a 1.4-fold increase in drug delivery to the locally heated tumor (~43°C) and enhanced tumor regression for the new liposomes compared to ThermoDox® (36).

Another strategy is the conjugation of elastin-like polypeptides (ELPs; either in N-terminus or in lysine residues) to liposomes containing N- hydroxysuccinimide (NHS) groups in their bilayer. ELPs are thermo-responsive protein-based biopolymers based on the amino acid sequence of elastin. They are thermo sensitive going an inverse temperature transition (ITT) in response to temperature change, which means they are soluble in aqueous solution at temperatures below their ITT, but above their ITT they are insoluble and aggregate (37).

Choi et al. (38) obtained liposomes composed of HSPC : CHOL : DSPE-PEG-NHS (75: 50: 3 molar ratio) and conjugated different ELPs to the liposome surface. Single conjugated ELP liposomes were obtained by using ELPs with only one amino group at each N-terminus and multiple conjugated ELP liposomes were obtained when ELPs containing internal lysine residues were used. They could show that above the transition temperature of the ELPs, they aggregate and distort the liposome membrane resulting in a crack followed by drug release. The extension and speed of drug release was shown to be closely dependent on the conjugation manner and also on the length of the ELP (38).

## Magnetically Triggered Liposomes

The biomedical applications of magnetic fields involve both diagnostic and therapeutic applications. Magnetic resonance imaging (MRI) is widely used on cancer management, as it plays a pivotal role in diagnosis, staging and monitoring treatment efficacy for certain tumors (39). Paramagnetic and superparamagnetic nanoparticles enhance MRI specificity and can be obtained from different materials, such as metals (gold, silver, and cobalt) or metal oxides ($Fe_3O_4$, $TiO_2$, and $SiO_2$). By now, iron oxides have been the most widely used in the clinics (40). Magnetic nanosystems are also widely investigated for tumor targeting and hyperthermal therapy. The first consists on applying an external magnetic field to surface tumors, what should attract and maintain magnetic nanoparticles (MN) into this area. Hyperthermal therapy consists on the exposure of MN to an alternating magnetic field, allowing for a local temperature rise and tumor cell kill (41–44). The magnetic-trigger of nanosystems is another promising strategy. Among the different available options for external stimulus, magnetism is considered as one of the best, as almost no physical interaction with the body occurs when comparing to light irradiation, ultrasound or electrical fields as stimuli (45).

Different nanosystems having a magnetic material on their composition have shown to be triggered by applying an alternating magnetic field, such as polymeric nanosystems, nanoparticles, micelles and liposomes (46–57). Most of the times, the strategy consists on combining thermo to magnetically trigger. Once magnetic components are added to thermoresponsive carriers, they can generate heat in response to a high-frequency (in the range of hundreds of kilohertz or higher) alternating current magnetic field (ACMF). Once this generated heat raises the temperature of the liposome's membrane around the Tm, its permeability is greatly enhanced and the cargo can thus be release (54). This strategy is superior to those for thermo-trigger alone as ACMF penetrates deep into the tissue, so that it reaches the magnetic nanosystems to generate a localized heat without damaging normal hypodermal tissues (48, 50). Another possibility is still the mechanical deformation of a nanocarrier when submitted to a low-frequency ACMF. This acts as the immediate cause of drug release and is of practical importance for cases on which hyperthermia might be detrimental (13, 56).

Nanosystems containing iron oxides, particularly magnetite (Fe3O4), maghemite (γ-Fe2O3) and ferrites (mixed oxides of iron and other transition metals) are the most promising because of their low toxicity and easy clearance, heat generation ability and chemical stability (13, 50). Different coatings of iron oxides allow the MN to present different water solubilities. Liposomes herein presented were all obtained by thin-film hydration method. On different formulations, hydrophobic iron oxide

MN were added directly to the lipids during film formation (54, 57) and hydrophilic iron oxide MN were added during the film hydration (52, 53, 55, 56). Theoretical studies suggest a threshold maximum nanoparticle diameter of 6.5 nm for incorporation of neutral nanoparticles into lipid bilayer (54).The MN used on different formulations herein presented had mean diameter ranging from 3 to 10 nm.

### Magnetic Trigger Using Thermosensitive Liposomal Bilayers

Different *in vitro* release studies have demonstrated that the submission of liposomes encapsulating a MN to ACMF allows an augmented content release. Tai et al. (52) developed a formulation composed of DPPC : CHOL (5:1 weight ratio) encapsulating dextran-coated iron oxide nanoparticles (3–5 nm) and a fluorescent tracing molecule, CF. This formulation was able to release the whole CF content in around 3 min when exposed to ACMF, while liposomes without the MN led to no significant CF release under the same conditions (52). Amstad et al. (54) obtained liposomes composed of DSPC : DSPE-PEG2000 (10:0.5 molar ratio) encapsulating palmityl-nitro DOPA-stabilized iron oxide MN (5-10 nM) and the self-quenching dye calcein. An increase in fluorescence directly translates into release of calcein, and the fluorescence of liposomes lacking MN did not change upon ACMF treatment, while an increase of around 270% on the fluorescence of liposomes containing the MN in their membrane when submitted to an ACMF was observed. In this study, they evaluated the liposomes after exposure to ACMF, observing that it did not affect the hydrodynamic diameter of the vesicles loaded with MN. Also, no precipitation of MN was observed after ACMF treatment, demonstrating that the liposomes remained intact and at constant size during this treatment. It was possible to conclude that the calcein release was due to a change in membrane permeability and not their rupture or fusion, what allows for the content to be repeatedly and nondestructively released (54). Hardiansyah et al. (56) obtained liposomes composed of HSPC : DSPE : CHOL (12.5:1:8.25 mole ratios) encapsulating citric acid-coated iron oxide MN (10 nm) and doxorubicin (DXR). Liposomes encapsulating both MN and DXR presented 80% DXR release in the end of 10 min when exposed to ACMF against around 50% for non-magnetic liposomes (55). Hardiansyah et al. (57) obtained liposomes composed of DPPC : CHOL : DSPE-PEG2000 (80:20:5 molar ratio). Cumulative curcumin release during 30 min from liposomes submitted to ACMF treatment was 15 and 2.7-fold higher than that observed for liposomes incubated at 37 and 45°C, respectively, without ACMF treatment (57).

Pradhan et al. (53) designed liposomes that are both magneto-thermosensitive and actively targeted to folate receptors. These liposomes were composed of DPPC : CHOL : DSPE-PEG2000:DSPE-PEG2000-Folate (80:20:4.5:0.5 molar ratio) encapsulating DXR and MN (FluidMag-HS, 10 nM). The thermosensitivity on DXR release at 43°C was demonstrated as 53% of DXR content was released at this temperature against 17% at 37°C. When exposed to a permanent magnetic field *in vitro* aiming to physically target cell lines expressing folate receptor (KB and Hela cell lines), higher uptake was observed for the formulation compared to commercially available liposomal DXR, non-magnetic folate-targeted liposomes and free DXR, which resulted in superior cytotoxicity. Magnetic hyperthermia at 42.5°C and 43.5°C further increased the cytotoxicity of the obtained liposomes, which was attributed to the superior release of DXR triggered by heat generated by the MN (53).

### Magnetic Trigger Using Non-Thermosensitive Liposomal Bilayers

Avoiding hyperthermia generation has potential application for some cancers where temperature changes are detrimental, such as brain cancers. Based on this fact, Guo et al. (56) designed a magnetic formulation that is not thermosensitive, and that does not imply any increase of temperature. These liposomes were composed of phosphatidyl-choline (PC):CHOL:amphiphilic carboxymethyl dextran (CMD) (55:40:0.5 molar ratio) encapsulating iron oxide MN and DXR. Exposure of these liposomes to a low-frequency ACFM at pH 5.0 allowed for 74% of DXR release while in 24h incubation only 35% release was observed for liposomes that were not submitted to ACFM. When influence of ACFM on liposomal structure was investigated, it was observed that they became much larger after the exposure to ACFM. Thus, the initial drug release from the liposomes under ACFM was attributed to the drug leakage resulting from the liposomal structure deformation (56).

## Ultrasound-Triggered Liposomes

Ultrasounds (US) are mechanical longitudinal waves with a periodic vibration in frequencies superior to human audible range (20 kHz) that propagate due to pressure changes in the medium (58, 59). This technology is already widely used in the medical field for diagnosis and therapeutic purposes due to non-invasiveness, safety and cost effectiveness.

However, some disadvantages can be pointed out, such as cavitation skin burns due to the presence of air between the transducer and the body surface. This also limits the treatment of extensive superficial regions, such as breast cancer, and regions where air is inherently present, such as lungs and intestines. The presence of obstacles such as bones in the proximity of the organ under treatment also complicates access to the region. Yet another challenge is to focus on organs that have movement (59, 60).

US can be used to trigger liposomes. Different mechanisms might explain the trigger by US, such as cavitation, acoustic streaming and hyperthermia, and most probably they are not independent (61).

In acoustic cavitation, there is the interaction of acoustic waves with gas bubbles. On stable cavitation, bubbles oscillate around an equilibrium radius causing fluids to flow around the bubbles. As acoustic pressure increases, the process known as inertial cavitation takes place, in which the gas bubbles undergo rapid growth and violent collapse upon US exposure. This creates high pressures and increases the local temperature, inducing thermal dissociation of water and, therefore, the

formation of reactive oxygen species (ROS). Acoustic streaming such as microstreaming is another effect of cavitation that can induce shear stresses that can destabilize liposomes and permeabilize cell membranes (58, 60, 61).

The hyperthermia caused by US is associated to the absorption of the ultrasonic waves by the tissue, creating mechanical compression and decompression. Some of this mechanical energy is lost due to friction effects and converted into heat. The composition of the lipid bilayer of the liposomes is known to play a role on their US sensitivity, increasing their content release. Liposomes with thermo-sensitive composition, as previously described, facilitate the release of drugs by US induced hyperthermia. The presence of PEG also contributes to this function since it absorbs the energy of the ultrasound by concentrating it on the surface of the vesicle (60).

TSL composed of DPPC: MPPC: DSPE-PEG2000: DSPE-PEG2000-iRGD (86:10:2:2 molar ratio) encapsulating DXR (iRGD-LTSL-DXR) were obtained by Deng et al. (62). iRGD peptide, like conventional RGD peptides, target tumors by binding to αv integrins selectively overexpressed on the tumor angiogenic endothelial cells as well as tumor cells. When iRGD-LTSL-DXR was administered to mice bearing 4T1 breast cancer tumors, to explore the anti-tumor effects in combination with high intensity focused ultrasound (HIFU) they observed delayed tumor growth after a single-dose treatment (at a DXR equivalent of 5 mg/kg). The inhibition of iRGD-LTSL-DXR + HIFU were 65.2 ± 6.1% ($p < 0.001$), while without HIFU, the tumor inhibition rate of iRGD-LTSL-DXR was only 33.1 ± 7.6% (62).

Vanosdol et al. (63) prepared TSL composed of DPPC: MSPC : DSPE-mPEG2000 (85.3: 9.7: 5.0 molar ratio) encapsulating DXR. In order to take advantage of cavitation, they also prepared this formulation with incorporated perfluoropentane gas (PFP5). *In vivo* biodistribution studies showed that when tumors were submitted to high intensity focused ultrasound (HIFU) reaching 42°C, DXR accumulation was higher compared to that observed for tumors at body temperature (37°C). For the non-PFP5 formulation, ~0.9 μg DXR/gram of tissue was observed for non-HIFU treated tumors while ~3.8 μg DXR/gram of tissue was observed for HIFU treated tumors. For the formulation encapsulating PFP, ~2.1 μg DXR/gram of tissue was observed for non-HIFU treated tumors while ~5.1 μg DXR/gram of tissue was observed for HIFU treated tumors. This approximate 1.4-fold greater drug delivery observed for the PFP5 containing formulation at 42°C indicated that the additive response of cavitation to HIFU treatment (63).

For mitochondria targeted sonodynamic therapy (SDT), using ultrasound and a sonosensitizing chemical substance, Chen et al. (64) developed a liposomal formulation composed of soy lecithin:CHOL : CHOL-anchored 3-carboxypropyl triphenylphosphine bromide (3:0.7:0.3 weight ratio). This formulation was used to encapsulate the sonosensitizer hematoporphyrin monomethyl ether (HMME) (64). The presence of CHOL-anchored 3-carboxypropyl triphenylphosphine bromide (CHOL-TPP) allows for mitochondria targeting. Because of their role in regulating key cellular functions, mitochondrial targeting compounds represent a promising approach to eradicate cancer cells that are refractory to chemotherapy. The release of HMME from liposomes could be triggered by ultrasound due to the oxidation of the lipid in liposomes. After incubation with cancer cells, the TPP modified liposomes (Lipo-TPP) could accumulate in the mitochondria and assist the HMME to achieve greater cancer cell inhibition effect in SDT. *In vitro* cytotoxicity studies of liposomes containing the sonosensitizer HMME and the mitochondrial target TPP followed by ultrasound for 3 min (HMME-Lipo-TPP + SDT) against MCF-7 cells was evaluated. This study indicated that the cell viability for the HMME-Lipo-TPP + SDT treatment was approximately 35%. On the other hand, cell viability around 75% was observed for cells treated with liposomes containing only TPP (Lipo-TPP + SDT), showing that there was a significant increase in cytotoxicity when using the sonosensitizer associated with ultrasound (64).

In 2016, Ninomiya et al. obtained liposomes composed of 1,2-dimyristoyl-sn-glycero-3-phosphatidic acid (DMPA), DPPC and CHOL (1:4:5 molar ratio). These liposomes were modified with avidin, which has an affinity for cancer cells and the envelope of the hemagglutinating virus of Japan (HVJ), which promotes the fusion of liposomes to cells and then used to encapsulate perfluoropentane nanoemulsion PFC5. The PFC5 liquid has a low boiling, and the nanoemulsion droplets are converted into much larger gas bubbles by ultrasonic induced droplet aporization (ADV). These bubbles elongate and disrupture the liposome membrane, allowing for the encapsulated drug to be released. The increased US-mediated disruption of liposomes encapsulating PFC5 was confirmed on an assay evaluating the optical density at a wavelength of 600 nm ($OD_{600}$). After US irradiation, liposomes without PFC5 presented a relative $OD_{600}$ value of 92.7% of that without US irradiation, indicating no significant disruption of the liposomes by US. On the other hand, for PFC5-loaded liposomes, the turbidity of the suspension decreased after US irradiation with a relative $OD_{600}$ of only 9.5% of that without US irradiation. To investigate cancer cell injuries mediated by this formulation, MCF-7 cells (human breast cancer) were treated and either submitted to US irradiation or not. Cell viability was then determined. Cells receiving the formulation followed by US irradiation had their viability reduced to 43%, whereas cells receiving treatment with the formulation in the absence of US showed cell viability equal to 80%. Cell viability of those which received US-irradiation alone was about 80%, confirming that the US potentializes the formulation (65).

## Light-Triggered Liposomes

The use of light stimuli to trigger the controlled release of drugs from liposomes has been studied as the wavelength, energy intensity and time of exposure and beam diameter are adjustable with high precision, which may aid in individual pharmacotherapy (64, 66, 67). Photodynamic therapy is based on the local or systemic application of a photosensitive compound - the photosensitizer, which is accumulated in pathological tissues. Photosensitizing molecules absorb light from the appropriate wavelength, initiating activation processes

leading to the selective destruction of inappropriate cells. Photo cytotoxic reactions occur only within the pathological tissues, in the area of distribution of the photosensitizer, allowing the selective destruction (68) Photosensitizing agents, when added to liposomes, can generate ROS, like singlet oxygen, upon excitation by light at specific wavelengths. This singlet oxygen consequently induces oxidative stress, rupture of the membranes and formation of pores allowing the contents of the vesicle to escape (69–71)

Based on photodynamic therapy Luo et al. (72) developed liposomes composed of DSPC: Dioleoylphosphatidylcholine (DOPC): CHOL: Porphyrin-phospholipid (PoP) containing encapsulated DXR. The presence of the unsaturated lipid DOPC accelerates the DXR release by oxidation mechanisms of this lipid. The inclusion of the photosensitizer POP would enhance this release. Thus, the team evaluated different concentrations of DOPC, between 0 and 10 moles, and also POP. It has been proven by mass spectrometry that DOPC accelerates the release of DXR and that in the presence of an oxygen scavenger or an antioxidant, the release of the drug is inhibited, suggesting the mechanism of release by oxidation. The inclusion of increasing amounts of DOPC accelerated and increased DXR release. At 5 mole% DOPC and 0.3 mole% POP, a 50% DXR release was observed in 43 s. Higher amounts of DOPC led to destabilization of the vesicles in the absence of light. Therefore, the final formulation of work developed was composed of DSPC: DOPC: CHOL: PoP, in the 54.7: 5: 40: 0.3 molar ratios respectively (72).

In another moment, Luo et al. (73), encapsulated DXR in a similar liposomal formulation composed of DSPC: CHOL: DSPE -PEG: PoP, (53:40:5:2 molar ratio). This time, DSPE-PEG was used to obtain stealth liposomes to treat human pancreatic adenocarcinoma. *In vivo* drug release was triggered by the oxidation of DOPC and CHOL after exposure to 665 nm NIR. Tumor uptake of DXR was assessed and shown to be 7-fold higher for tumors of animals receiving PoP-DXR followed by laser exposure when compared to treated animals without laser exposure. An inhibition of tumor growth *in vivo* demonstrated excellent chemotherapy efficacy. Treatment with PoP-DXR (DXR=7mg/Kg) led to regression of tumor volume to values below 20 $mm^3$ after 2 weeks of treatment. In animals treated with liposomes without PoP, therefore not light triggered, tumors evolved up to 500 $mm^3$. Animals treated with PoP-DXR survived until the end of the study, 60 days, while animals receiving the same treatment but without laser stimulation died after 40 days of treatment due to disease progression (73).

Following the same principle, in a study by Fuse et al. (74) liposomes co-encapsulating the photosensitizer talaporfin sodium (TPS) and the drug gemcitabine (GEM) were evaluated for their cytotoxic activity against EMT6/P breast cancer cells. Liposomes were composed of DSPC: DOPE: CHOL: DSPE-PEG2000 (85:10:5:5 molar ratio). Cells receiving NIR laser irradiation after incubation with the formulation had cell viability lower than 5%, In contrast, around 90% cell viability was observed for cells exposed to the formulation only, without NIR laser irradiation (74).

Also based on photodynamic therapy, Li et al. (75) developed NIR sensitive liposomes for breast cancer treatment. A phospholipid material of special structure 1-(1z-octadecenyl) -2-oleoyl-sn-glycero-3-phosphocholine (PLsPC) and a hydrophobically modified fotosensibilizer Indocyanine green and octadecylamine (ICG-ODA) were employed for liposome light-sensitivity (LSL). The other used lipids were CHOL and DSPE-PEG2000. DXR was encapsulated in the liposome which surface was subsequently conjugated with Her2 antibodies and obtained the unique nanosystem Her2-I &D-LSL. The encapsulation efficiency and stability were closely related to the ratio of S100 and PLsPC and the proportion of ICG-ODA. The formulation S100: CHOL = 5:1, S100 : PLsPC = 4:1 or 2:1 and ICG-ODA: total lipid = 1:10, with a high EE % and low DXR leakage was chose to proceed the study. *In vitro* cytotoxicity of this formulation followed by NIR laser irradiation was evaluated against MCF-7 (human breast cancer) cell line. After treatment with Her2-I & D-LSL combined to laser, there was almost 100% cell death, against over 60% of death for cells treated with Her2-I &D-LSL without laser irradiation. The same was evaluated for a non- HER2 targeted formulation. Cytotoxicity was approximately 65% for cells that received this treatment followed by laser versus only 40% for cells that received the treatment in the absence of the NIR (75).

*In vivo* antitumor was evaluated in mice bearing MCF-7 tumors. A significant difference in the volume and weight of tumors of animals exposed to both Her2-I &D-LSL and laser compared to those treated with the formulation only was observed. After 30 days of Her2-I & D-LSL plus laser treatment, tumors had a weight of approximately 25 mg while tumors of animals treated in the absence of the NIR had an approximate weight of 150 mg. For animals with SKOV-3 cell tumors a similar pattern was observed. After treatment with Her2-I & D-LSL plus laser, the tumor showed almost total regression whereas the treatment without NIR allowed the tumor to reach a weight close to 0.4 g (75).

Making use of photosensitizers to generate ROS under irradiation, Zhang et al. (76) developed a formulation for the treatment of cancer of breast. In liposomes composed of Lecithin, CHOL, DSPE-PEG2000 and PEG-NI (ethyl 6- (2-nitroimidazolyl) hexanoate coupled to PEG and chlorine e6 (Ce6) photostabilizer (6:4:0.5:0.5:0.5 molar ratio). The prodrug Tirapazamine (TPZ) and the miRNA-155 gene probe were incorporated into the liposomes. After irradiation with 670 nm laser on Ce6, the oxygen consumption for ROS generation occurs. Oxygen consumption leads to local hypoxia resulting in the reduction of prodrug TPZ to the active drug. ROS can lead cancer cells to death as well as local hypoxia, which act synergistically with TPZ chemotherapy. Finally, the miRNA-155 sonnet co-delivered with the drug could detect an oncogenic intracellular marker for diagnosis. Ce6 is added to the lipid bilayer, the incidence of the laser on it leads to destabilization of the vesicles and release of its components. This formulation was named Lip-Ce6-TPZ. The release study of TPZ was performed for the Lip-Ce6-TPZ formulation. The formulation received laser irradiation for 10 min. After 6 h, a release of 82.3% of the drug

was observed. In contrast, only 29.7% of TPZ was released from the non-irradiated formulation, confirming that the laser leads to the destruction of the vesicle and therefore greater release of the drug. *In vitro*, the formation of ROS and hypoxia areas in MCF-7 cells, was 3-fold higher for treatment with Lip-Ce6-TPZ + laser compared to treatment without irradiation. *In vivo*, the relative tumor volume (RTV) in MCF-7 cell tumor bearing mice treated with Lip-Ce6-TPZ + laser was close to zero, a value seven times lower than that found for Lip-Ce6-TPZ treatment in absence of the laser (76).

In a study by Yang et al. (68) a liposome composed of PC and CHOL (4:1 weight ratio), encapsulating TPZ and the IR780 photosensitizer was developed (Lip(IR780&TPZ)). When liposomes are exposed to 808 nm irradiation the liposomal membranes rupture releasing the drug. For all concentrations of drug tested against 4T1 cells *in vitro*, irradiated liposomes lead to significantly higher cell death compared to non-irradiated liposomes. Apoptosis differed between these treatments being 36.2% and 12%, respectively. On an *in vivo* study, after 15 days of treatment mice that received the formulation followed by laser irradiation had an extremely significant reduction of tumor weight (~1g) when compared to the group that did not receive laser (~4,5g) (68).

## Photocrosslinking, Photoisomerization, Photocleavage, and Photothermal Release

On a smaller scale, other strategies too have been reported to promote the release of liposome contents by light among them photocrosslinking, photoisomerization, photocleavage, and photothermal release (70, 77, 78). These approaches will be discussed below. The photocrosslinking is established by the polymerization of the unsaturated bonds present in the hydrophobic region of the bilayer. At the time such polymerized domains are irradiated with light at specific wavelengths, a crosslinking reaction occurs between them. From this, the lipid bilayer of the liposomes shrinks the domain where the sensitizers are present leading to a conformational change. This change in the structure leads to the formation of pores promoting a greater membrane permeability and release of the contents (79).

Yavlovich et al. (80) showed that liposomes encapsulating DXR which have the **photopolymerizable** lipid 1,2-bis (tricosa-10,12-diynoyl) sn-glycer-3-phosphocholine (DC 8.9 PC) allow superior cell death in MCF-7 breast cancer cells when exposed to light treatment (514 nm laser), compared to the same treatment without exposure to light. Formulations composed of DPPC: DC 8.9 PC: DSPE-PEG2000 (86:10:04 molar ratio) encapsulating DXR had its membranes destabilized after laser irradiation. This destabilization was accompanied by the release of DXR and cytotoxicity-enhancement cell culture, leading to 90% cell inhibition, compared to only 40% found in the absence of the laser irradiation (80).

The **photoisomerization** process is based on the conformational change (for example trans to cis) in molecules having rotating constraints, such as double bonds. This modification leads to the rupture of the lipid bilayers and expulsion of their contents (81, 82). Liu et al. (83), synthesized CHOL derivatives containing portions of azobenzenes of different polarities. These modified molecules were combined to egg PC (EPC) in the preparation of light-triggered liposomes. These liposomes were irradiated with 360 nm UV light. The conversion of the modified lipid from trans to cis was around 90% in the liposomes composed of the derivative AB lipid 3 (**Figure 4**) (EPC : AB3, 1:1 molar ratio). The release behavior of these liposomes was investigated in a calcein release study. It has been known that azobenzene derivatives in CHCl3 solution undergo trans-to-cis isomerization by UV light irradiation and cis-to-trans isomerization by visible light irradiation. Periodical UV and visible light irradiation (UV, 10 min; Visible, 15 min; both every 4 h) was carried out. at 37° C. At the end of 40 h, 55% of the calcein was released, compared to only 25% released from the liposomes not exposed to light. In this experiment, it was also verified that UV light increases the release in greater proportion compared to visible light (83).

In **photocleavage**, the mechanism involves a photolabile group, for example 2-nitrobenzyl, which is inserted into the lipid bilayer. This group is cleaved after irradiation of visible/UV light. Such cleavage leads to destabilization of the vesicle membrane and release of the encapsulated contents. Amichal et al. (84) reported the synthesis of a new photocleavable phospholipid derived from phosphatidylcholine (PC), called NB-PC as shown in **Figure 5** (84).

For this, they modified the PC including a 2-nitrobenzyl group on the acyl chain at the sn-2 position. Liposomes with varying concentrations of NB-PC, phosphatidylethanolamine (PE), PEG-PE and CHOL were prepared. After irradiation of 350 nm, the release of Nile red was increased, proportionally to the increase of the modified lipid concentration. Inclusion of 10, 25, and 50% of NB-PC resulted in a gradual increase of 36, 48, and 62% in the emission of Nile red. These rates were all lower

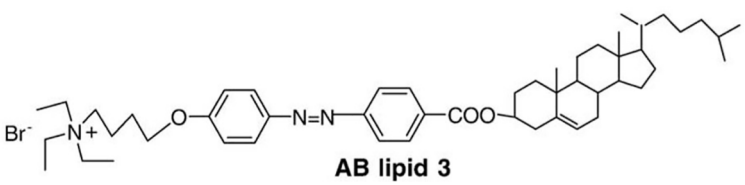


**FIGURE 4** | A cholesterol derivative containing portions of azobenzene Synthesized by Liu et al. (83), this derivative was called AB lipid 3.

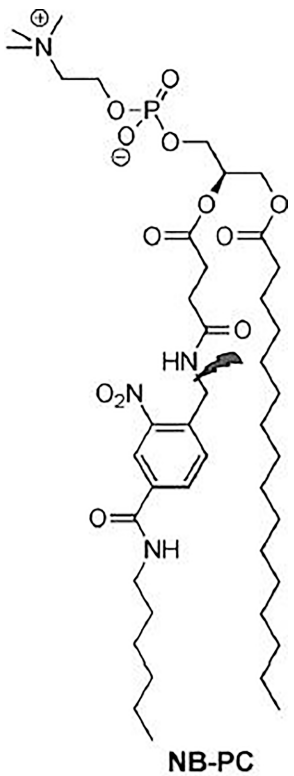


**FIGURE 5** | A photocleavable phospholipid derived from phosphatidylcholine Synthesized by Amichal et al. (84), this derivative was called NB-PC.

than liposomes composed exclusively of NB-PC (80%). Controls that did not receive irradiation had a minimal release. These data show that the release can be performed using a wide range of percentages of NB-PC in liposomes, and that the percentage can be used to adjust the release properties of the vesicles. It should also be noted that variations in the percentage of NB-PC had no effect on the release of non-irradiated liposomes. These liposomes ranged from 12 to 19% in, emission rate reduction, indicating that NB-PC incorporation does not destabilize the membrane peak, even for vesicles composed exclusively of the modified lipid, due to the similarity of NB-PC to natural PC (85).

Finally, the **photothermic** release consists on the conversion of light into heat in order to induce membrane permeability or rupture. The photothermal effect induces a phase transition in the bilayer, which makes it permeable increasing the release of loaded drugs. Some materials have been described for the purpose of triggering photothermal transduction, for example gold nanoparticles, carbon nanotubes and graphene-based nanosheets. After specific light irradiation, photothermal electron-rich agents can convert photon energy into vibrational energy, inducing the excitation of electrons followed by energy oscillation. Photothermal agents can transduce NIR light (wavelength between 700 and 1100 nm) to heat, triggering a local hyperthermia that can disrupt a carrier containing thermosensitive components (70, 71, 77).

Kautzka et al. (86), generated ROS in the tumor region, especially singlet oxygen using photosensitizers such as rose bengal (RB) in liposomes. For this purpose, they prepared liposomes encapsulating DXR composed of HSPC: phosphoethanolamine-N-hexanoylamine (PE-NH 2): gold nanoparticles (AuNPs) (57:5:17 molar ratio). The gold nanoparticles were added to explore the thermal property of light, due to their suitability for photothermal conversion (86). AuNPs absorb visible light and NIR and released energy as heat. The high temperatures reached by the AuNPs can induce a permeability of the lipid bilayer or its rupture, followed by the release of the charge (70). The formulation was tested *in vitro* against HCT116 human colorectal cancer cells, followed by light irradiation at 532 nm wavelength. With this study they concluded that the treatment with liposomes containing AuNPs+RB+DXR was more effective (40% cell death), than chemotherapy using the liposomes with RB+DXR (20% cell death) showing the contribution of the thermal property of light when used with photosensitizers (86).

Selection of adequate light sources determines the efficacy of light-stimulated therapies. Usually the preference is given to light with wavelengths near the infrared (NIR) range (700 nm to 2,500 nm), as they do not penetrate so deeply into the tissues (less than 1 cm) thus avoiding damage to DNA and cell proteins (87, 88). Therefore, NIR to induce drug release can be performed on diseases affecting surface tissues (88). However, the inability of light to penetrate biological tissues *in vivo* or the difficulty in matching the energy of photons from the light source is a barrier to the success of light-triggered liposomes (89). Another difficulty encountered in the pharmacotechnical development of these liposomes relates to the normally hydrophobic properties of the photosensitizers, which induces the formation of aggregates in water (87).

## Electrically-Triggered Liposomes

Electricity has several advantages as trigger mechanism for drug release compared to other types of stimuli due to the precise control of drug release as the magnitude of current and duration of electric pulse can be adjusted. Additionally, no complex instrumentation is required (90, 91).

When exposed to an external electrical field, membrane permeability of lipidic vesicles such as cells and liposomes increases because of the formation of hydrophilic pores in the lipid bilayer, on a phenomenon called electroporation (EP). Nowadays, EP is used in many fields of biology, biotechnology, and medicine (92). EP can be a permanent or transient effect. If exposure is not too long and the electric field not too strong, the pores might reseal in seconds to minutes after exposure (92–94). Reversible EP can facilitate liposome accumulation on tumor site by affecting the vascular permeability, potentially enhancing EPR effect as recently demonstrated by Srimathveeravalli et al. (2018) (95). In the same way as it is possible to get molecules into cells, it is proposed that molecules should be able to be released from liposomes (93). Irreversible EP for example, is a strategy that consists on a form of non-thermal ablation on which very high electric fields are employed to permanently compromise cell

membranes (96, 97). Reversible EP is already widely used in cell culture to control diffusion of external compounds into a cell.

A great challenge behind this strategy, however, is to obtain EP conditions that will be able to trigger release from the liposomes, without damaging permanently normal cells. Different theoretical works using molecular dynamics simulations demonstrated that both the size and composition of liposomes have a great impact on EP. The amplitude needed for liposome EP strongly depends on their size, presenting a proportional inverse relationship. It has also been demonstrated that liposomes with a higher internal conductivity and lower membrane permittivity compared to other similar-sized organelles could be favorably electroporated when the pulses are few nanoseconds long. Therefore, evaluating appropriate pulse parameters and rationally designing the liposomal formulations increases the possibility of selective EP of liposomes with respect to the cell itself or its organelles (92, 94).

Yi et al. (93) designed a study to test the hypothesis that doping liposomes with amphiphilic proteins, such as nisin, could reduce the electric field required to electroporate liposomes. They prepared liposomes composed of DOPC : CHOL (10:4 weight ratio) encapsulating nisin and a fluorescent dye, CF. When exposed to 3000 V the mean release percentage of CF from the liposomes without nisin was around 12%. Liposomes containing nisin however, released approximately 14% of its content when exposed to only 200V. This significant reduction of the electric field required to release the contents of liposomes highlights the feasibility of the strategy for drug release *in vivo* (93).

## Chemically Triggered Liposomes

Chemical trigger is based on the idea of delivering an exogenous chemical to trigger a previous administered nanosystem. There are some advantages of this strategy in detriment of other external triggering methods: 1) chemical triggers are able to reach the nanosystem on any part of the body, dismissing the need of knowing the exact location of the tumor; 2) they are able to efficiently reach deep tissues and 3) no technological and expensive equipment are necessary. Many chemicals are known to disrupt the membrane bilayer; however, this strategy is still poor developed. That is probably due to the great challenge of finding a liposomal composition that is selectively destroyed by an exogenous chemical trigger which on the other hand has little affinity to the host cell membranes (98, 99).

Xiong et al. (12) demonstrated that chloroquine (CQ) triggers the release of daunorubicin (DAU) from liposomes composed of HSPC : CHOL:mPEG2000-DSPE:folate–PEG–CHEMS (55:40:4.5:0.5, molar ratio). As CQ was added to the formulation, it quickly loaded into liposomes expelling the DAU, possibly through a mechanism involving intraliposomal pH rising. An enhancement in cytotoxicity against L1210JF (murine lymphocytic leukemia) cell line was observed when CQ was added to DAU liposomes. The observed IC50 were 20.0 ± 1.8 μM without CQ and 11.2 ± 1.2 μM in the presence of 10 μM of CQ, a concentration supposed to be non-toxic. However, the *in vitro* gains did not translate to *in vivo* using a DBA/2 mice carrying L1210JF tumors (12).

Plaunt et al. (98) reported that a zinc(II)-dipicolylamine (ZnDPA) complex, shown in **Figure 6** can act as a chemical trigger by associating selectively with anionic bilayer membranes (such as from liposomes containing phosphatidylserine, PS), inducing the leakage of water-soluble contents. Healthy mammalian cells present zwitterionic membranes, which are not targeted, insuring the selectivity of the trigger agent. They prepared liposomes composed of DPPC : CHOL : POPS (67:28:5 molar ratio) and showed that, in a CF leakage assay, it released 55% of its content in 120 s, when exposed to 10 μM of the ZnDPA complex. A negligible CF leakage (3%) was observed for zwitterionic liposomes mimicking healthy cells, composed DPPC: CHOL (67:28 molar ratio), under the same conditions. Knowing that PS-rich liposomes need an extensive steric protection to prevent its capture by the MPS, they also tested a formulation containing PEG. This formulation, composed of DPPC : CHOL : POPS : DPPE-PEG2000 (67:28:5:8 molar ratio), released 84% of its CF content in 120 s when exposed to the ZnDPA complex. This higher trigger for a sterically protected liposome could be explained by the fact that the DPPE-PEG2000 is also anionic, and could associate with the ZnDPA complex. Liposomes exposed to the ZnDPA complex showed no significant change in the hydrodynamic diameter, which was evidence against liposome fusion and against a lysis process. They proposed that association of cationic ZnDPA complex with the anionic POPS head group induces domain formation and perhaps phase separation. This creates line tension and

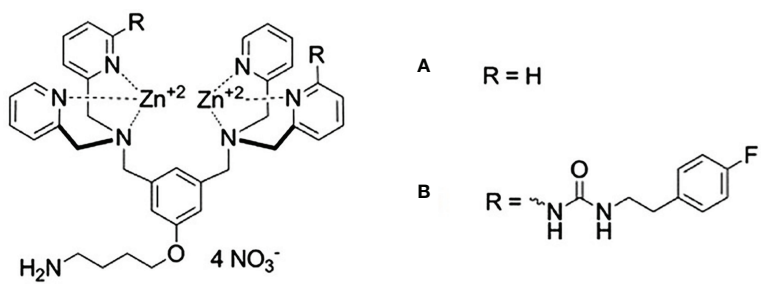


**FIGURE 6** | Zinc(II)-dipicolylamine (ZnDPA) complexes of first **(A)** and second generation **(B)**. Designed by Plaunt et al. (98), these complexes were used as triggering agents for anionic liposomes.

mismatched membrane thickness at the domain interfaces, promoting drug leakage (98).

This initial release studies were performed in TES (N-Tris (Hydroxymethyl)Methyl-2-aminoethane sulfonic acid) buffer. When release was later evaluated by Plaunt et al. (99) in phosphate buffered saline, which is closer to a physiologically relevant media, the DPPE-PEG2000 containing formulation released only 34% of its content. That motivated the search for a next-generation chemical trigger that operates more effectively than the old one. They obtained the modified ZnDPA complex, shown in **Figure 6B**, and showed that DPPC : CHOL : POPS : DPPE-PEG2000 (67:28:5:8 molar ratio), released 71% of its CF content in 120 s when exposed to the modified ZnDPA complex in PBS. Formulation was used to encapsulate 5-Aminolevulinic acid (5-ALA) and evaluated for its release. In the absence of chemical trigger the liposomes remained intact, releasing <10% of the encapsulated 5-ALA and upon exposure to the chemical trigger, 80% release of the encapsulated 5-ALA was observed after 24 h (99).

On **Table 1**, we summarize the most important aspects of important liposomal formulations triggered by different exogenous stimuli developed to date.

# TRIGGERED DRUG RELEASE BY ENDOGENOUS STIMULI

## PH-Triggered Systems

The pH of normal tissue and blood under physiologic conditions is around 7.4. However, the extracellular pH of malignant tumors is lower than normal tissue, with average pH values of 6.8. Intracellular compartments such as endosomes and lysosomes are the most acidic with pH values between 4.5–6.5. pH-sensitive liposomes have been developed as anticancer agent's delivery systems mainly due to their ability to fuse with the endosomal membrane, releasing their content into the cytoplasm. This allows the accumulation of anticancer drugs in tumors as a specific release of the drug controlled by the tumor environment occurs. Besides that, the intracellular delivery of anticancer agents by pH-sensitive liposomes presents an efficient mean to overcome the multidrug resistance, one of the main causes of tumor recurrence (100–103).

The polymorphic lipid PE or its derivatives, such as dioleoylphosphatidylethanolamine (DOPE), are the most common used molecules to obtain pH-sensitive liposomes (101). At neutral or physiological pH, these molecules are not able to organize themselves in bilayers, inducing the inverted hexagonal phase ($H_{II}$) organization, due to the small volume of the polar head compared to the hydrocarbon chain, favoring strong intermolecular interactions between amine and phosphate groups (101, 104). The insertion of an amphiphilic acid, such as cholesteryl hemisuccinate (CHEMS), at neutral pH, causes an electrostatic repulsion between phosphate and carboxylate groups, favoring the formation of lamellar phases (105). When exposed to the acid environment, such as endosomes, the carboxyl group of CHEMS is protonated causing an electrostatic repulsion which results in a transition from lamellar phase to $H_{II}$ and consequent release of the encapsulated drug, as represented in **Figure 7** (101, 105).

pH-sensitive liposomes incorporating estrone derivative conjugated to DSPE-PEG (ES-PEG-DSPE), were developed by Paliwal et al. (106) to targetly deliver DXR to estrogen receptors (ER)-bearing tumor cells. This liposome was composed of DOPE : HSPC : CHEMS : CHOL : ES-PEG-DSPE (ES-pH-SL). As control, a non-pH sensitive liposomes (ES-SL) was prepared with HSPC : CHOL : ES-PEG-DSPE. ES-pH-SL and ES-SL were prepared at various molar ratios with ES-PEG-DSPE at 5 mol % to phospholipids. The DXR encapsulation efficiency was similar for liposomes with different compositions (approximately 90%). To evaluate pH-sensibility, the release profile of DXR from liposomes was investigated at different pH values. The DXR release from ES-pH-SL within 2 h at pH 5.5 was 90%, compared to only 40% after 24 h at pH 7.4. However, the release of DXR from ES-SL was approximately same, at both pH, about 30% after 24 h. The ES-pH-SL at pH 5.5 exhibited a 6-fold increase in mean diameter, indicating vesicle aggregation and/or membrane fusion, but ES-SL did not show any difference in vesicle size at the same pH. *In vivo* biodistribution and antitumor efficacy were evaluated in female Balb/C mice with 7,12-dimethylbenz[a]anthracene (DMBA) induced breast tumor. After DXR administration at a dose of 5 mg/kg, the DXR concentration in tumor tissue was about 1.4-fold higher for ES-pH-SL compared to ES-SL. In addition, the DXR concentration of the ES-pH-SL in the heart was significantly lower than ES-SL or free DXR, an important result facing DXR cardiotoxicity. The tumor volume in the control group increased rapidly over 30 days (increase of 40%). The treatment of mice with ES-pH-SL significantly reduced the tumor volume (reduction of 80%) compared to those animals treated with ES-SL or free DXR (reductions of 60% and 20%, respectively), in relation to the tumor volume of the control group at the start of drug treatment (day 0) (106).

Silva et al. (107) prepared long-circulating pH-sensitive liposomes encapsulating DXR (SpHL-DXR) composed of DOPE : CHEMS : DSPE-PEG2000 (5.7:3.8:0.5 molar ratio). As control, non-pH-sensitive liposomes were prepared, composed of HSPC : CHOL : DSPE-PEG2000 (5.7:3.8:0.5 molar ratio) (nSpHL-DXR). In order to confirm the pH sensibility of the formulation and track liposome´s fate *in vivo*, blank liposomes were incubated with the radiolabeled complex [$^{99m}$Tc]-DXR as an imaging probe. The pH sensitivity for SpHL-[$^{99m}$Tc]-DXR was confirmed in a study of [$^{99m}$Tc]-DXR leakage at different pH, showing a higher release in acidic conditions (51.3%, pH=6.0) compared to neutral condition (13.5%, pH=7.4). This enhanced release at pH=6.0 was significantly higher compared to the release from nSpHL-[$^{99m}$Tc]-DXR in the same pH (30.8%). The biodistribution profile of SpHL-[$^{99m}$Tc]-DXR and nSpHL-[$^{99m}$Tc]-DXR were evaluated after intravenous injection in Balb/C female mice bearing 4T1 breast tumor. A higher uptake of SpHL-[$^{99m}$Tc]-DXR and nSpHL-[$^{99m}$Tc]-DXR by the tumor site

**TABLE 1** | Summary of important liposomal formulations triggered by different exogenous stimuli.

| Trigger stimulus | Lipid composition | Encapsulated agent(s) | Encapsulated percentage | Mean diameter | Reference |
|---|---|---|---|---|---|
| **Thermo** | DPPC : DSPC (7:3 weight ratio) | Methotrexate | N.A. | N.A. | (25) |
| **Thermo** | DPPC : HSPC : CHOL : DPPE-PEG (50:25:15:3 molar ratio) | DXR | N.A. | 127 nm | (26) |
| **Thermo** | DPPC : MPPC : DSPE-PEG2000 (90:10:4 molar ratio) | DXR | N.A. | ~ 140 nm | (11) |
| **Thermo** | DPPC: MSPC: DSPE-PEG2000 (86:10:4 molar ratio) | DXR | N.A. | N.A. | (27) |
| **Thermo** | DPPC/DSPC/DPPG2 (50:20:30 molar ratio) | – | N.A. | 175 nm | (35) |
| **Thermo** | DPPC : Brij78 (96:4 molar ratio) | DXR | N.A. | N.A. | (36) |
| **Thermo** | DPPC: 1-StePc: DSPE-PEG2000 (86:10:4 weight ratio) | MATT | 56% | 100 nm | (34) |
| **Thermo** | HSPC : CHOL : DSPE-PEG-NHS (75: 50: 3 molar ratio) with elastin-like polypeptides modified surface | DXR | N.A. | 151 nm | (38) |
| **Magnetic (HF)** | DPPC : CHOL (5:1 weight ratio) | dextran-coated iron oxide MN (3–5 nm); carboxylfluorescein (CF) | N.A. | 150–230 nm | (52) |
| **Magnetic (HF)** | DPPC : CHOL : DSPE-PEG2000:DSPE-PEG-2000-Folate (80:20:4.5:0.5 molar ratio) | Iron oxide MN (10 nm); DXR | about 24% and 85%, respectively | 360 nm | (53) |
| **Magnetic (HF)** | DSPC: MPEG-2000-DSPE (10:0.5 molar ratio) | palmityl-nitroDOPA-stabilized iron oxide MN (5–10 nM); calcein. | N.A. | N.A. | (54) |
| **Magnetic (HF)** | HSPC/DSPE/CHOL (12.5:1:8.25 molar ratio) | citric acid-coated iron oxide MN (10 nm); DXR | 15.5% for DXR | 130 nm | (55) |
| **Magnetic (HF)** | DPPC : CHOL : MPEG-2000-DSPE (80:20:5 molar ratio) | Oleic acid coated iron oxide MN (10 nM); curcumin | 76.15% for curcumin | 120 nm | (57) |
| **Magnetic (LF)** | PC : CHOL:amphiphilic carboxymethyl dextran (CMD) (55:40:0.5 molar ratio) | citric acid-coated Iron oxide MN (3–5nm); DXR | 96.9% for DXR | 220 nm | (56) |
| **Ultrasound** | DPPC: MPPC: DSPE-PEG2000: DSPE-PEG-2000-iRGD (86: 10: 2: 2 molar ratio) | DXR | >95% | 94.2 ± 2.0 nm | (62) |
| **Ultrasound** | DPPC: MSPC: DSPE-mPEG2000 (85.3: 9.7: 5.0 molar ratio) | DXR + PFP gas | ≅ 67% DXR | 171.6 ± 0.5 nm | (63) |
| **Ultrasound** | soy lecithin and CHOL/CHOL-TPP (0.7/0.3 weight ratio) | hematoporphyrin monomethyl ether | 74,6% | 110 nm | (64) |
| **Ultrasound** | DMPA: DPPC: CHOL (1:4:5 molar ratio) avidin/HVJ | perfluoropentane | N.A. | N.A. | (65) |
| **Light** | DSPC: DOPC: CHOL: Porphyrin-phospholipid (54.7: 5: 40: 0.3 molar ratio) | DXR | ≅ 95% | ~ 120 nm | (72) |
| **Light** | DSPC : CHOL : DSPE-PEG2000 : PoP (53:40:5:2 molar ratio) | DXR | ≅ 95% | ~ 100 nm | (73) |
| **Light** | DSPC: DOPE: CHOL: DSPE-PEG2000 (85: 10: 5: 5 molar ratio) | talaporfin sodium (TPS)+ gemcitabine (GEM) | TPS 11.6 ± 3.0% and GEM 2.3 ± 0.5%, respectively | 115.8 ± 3.8 nm | (74) |
| **Light** | 1- (1z-octadecenyl) -2-oleoyl-sn-glycero-3-phosphocholine (PLsPC): CHOL : DSPE-PEG-2000: soya bean lecithin (S100) [S100:CHOL (5:1); S100:PLsPC (4:1 or 2:1)] (molar ratio) | DXR | N.A. | 128.1 ± 1.8 nm | (75) |
| **Light** | Lecithin: CHOL: DSPE-PEG2000: PEG-NI (ethyl 6- (2-nitroimidazolyl) hexanoate coupled to polyethylene glycol): chlorine e6 (6: 4: 0.5: 0.5: 0.5 molar ratio) | Tirapazamin | N.A. | 162 ± 4 nm | (76) |
| **Light** | PC : CHOL (4 :1 weight ratio) | Tirapazamin | 51,84% | 130 nm | (68) |
| **Light** | DPPC: DC 8.9 PC: DSPE-PEG2000 (86:10:04 molar ratio) | DXR | 1335 ng per nmol Pi | 159.9 ± 6 nm (25°C) | (80) |
| **Light** | EPC: AB3 (1: 1 molar ratio) | Calcein | N.A | N.A | (83) |
| **Light** | NB-PC : PE: PEG-PE : CHOL (various concentrations) | Nile red | N.A | N.A | (85) |
| **Light** | HSPC: phosphoethanolamine-N-hexanoylamine (PE-NH 2): gold nanoparticles (AuNPs) (57: 5: 17 molar ratio) | DXR + rose Bengal (RB) | 23.4% e 88% respectively. N° of gold nanoparticles in each liposme ~ 109. | 124.6 ± 2.3 nm | (86) |
| **Electrically** | DOPC : CHOL 10mg:4mg | Carboxyfluorescein and nisin 2.5 mg/L | N.A. | N.A. | (93) |
| **Chemical (**chloroquine) | HSPC : CHOL:mPEG2000-DSPE:folate–PEG–CHEMS (55:40:4.5:0.5, molar ratio) | daunorubicin | 95% | N.A. | (12) |
| **Chemical (**ZnDPA complex) | DPPC : CHOL : POPS : DPPE-PEG-2000 (67:28: 5:8 molar ratio) | 5-ALA | 2% | 200 nm | (98, 99) |

was observed when compared to the contralateral muscle. Additionally, the tumor-to-muscle ratio observed for SpHL-[$^{99m}$Tc]-DXR was significantly higher (approximately 2-fold) than the observed for nSpHL-[$^{99m}$Tc]-DXR at 4 and 24 h, suggesting that the pH sensitivity contributed to higher uptakes of [$^{99m}$Tc]-DXR by the tumor (107).

In order to improve liposomal endocytosis, Silva et al. (108) modified the surface of the SpHL-DXR with folic acid, aiming on

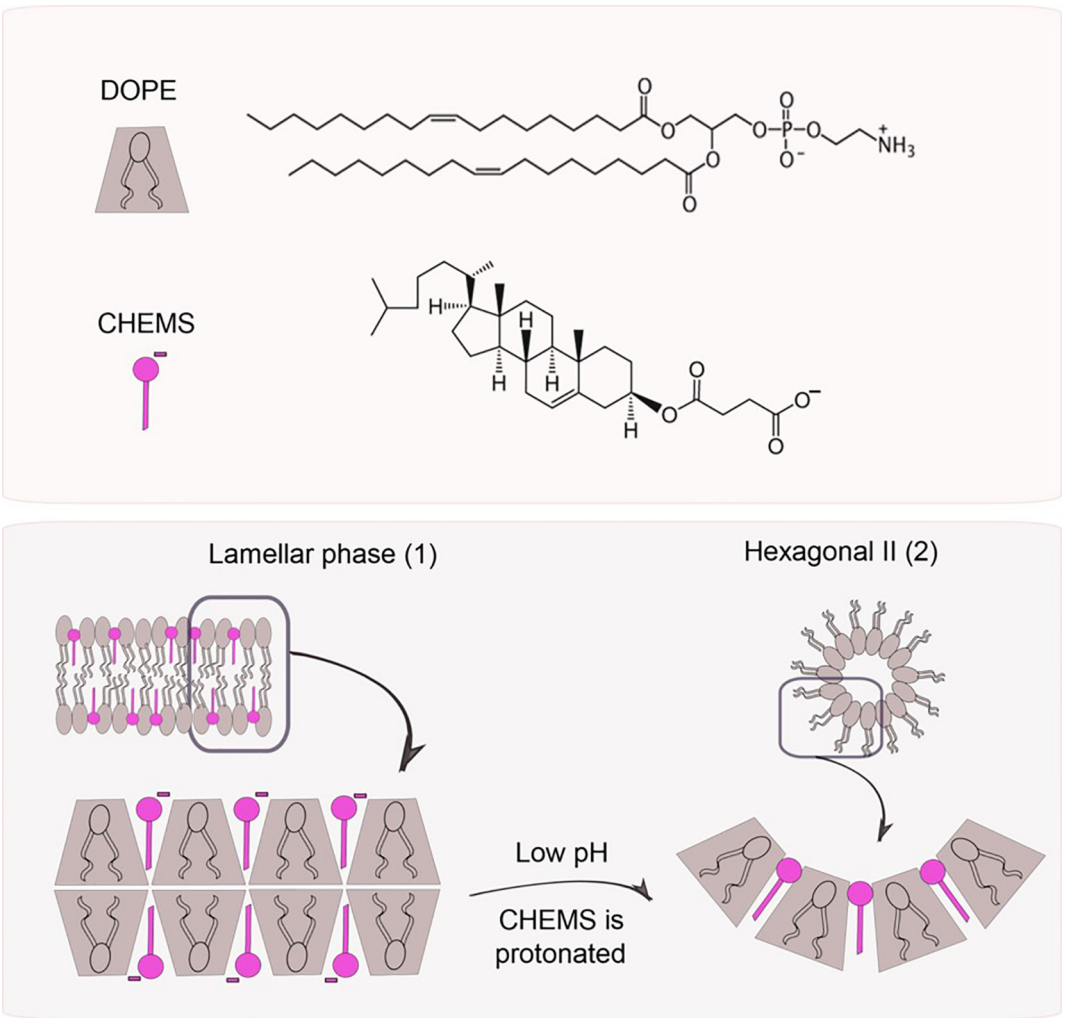


**FIGURE 7** | pH triggers phase changes in liposomes composed of dioleoylphosphatidylethanol-amine (DOPE) and cholesteryl hemisuccinate (CHEMS). When alone, DOPE molecules organize themselves in an inverted hexagonal phase due to their conic geometry. When combined with CHEMS at physiological pH, it is possible to obtain a bilayer (lamellar phase, 1). Once exposed to acidic pH, the protonation of carboxylate groups takes place leading to liposome destabilization (hexagonal phase II, 2), followed by the release of the encapsulated agents.

the overexpressed folate receptors (FR) on the surface of breast cancer cells. These folate-coated, long-circulating and DXR-loaded pH-sensitive liposomes (SpHL-DXR-Fol) were composed of DOPE, CHEMS, DSPE-PEG2000, and DSPE-PEG2000-Fol (5.8:3.7:0.45:0.05 molar ratio). The non-folate-coated SpHL-DXR were used as control. The pH-sensitivity of SpHL-DXR-Fol was determined by dialysis in HEPES-saline buffer. After 24 h incubation at pH 5.0, DXR leakage of 53.6% was observed for the SpHL-DXR-Fol, compared to only 21.5% leakage at pH 7.4. The antitumor activity was evaluated *in vivo* using a 4T1 breast cancer model. The results showed that SpHL-DXR-Fol treatment was the most effective, presenting a higher inhibition ratio (IR) of the RTV compared to SpHL-DXR and free DXR (68%, 56% and 37%, respectively) (108).

Another way to develop pH-sensitive liposomes is by insertion of a pH-responsive peptide that change their conformation in acid ambient, causing destabilization of the liposomes. Also, responsive polymers can be used to produce these pH sensitive systems (101, 109). Some polymers used in pH-sensitive liposomes destabilize the phospholipid bilayer, while others cause the fusion of the liposome with endosome/lysosome membranes (103).

Chiang et al. (110) developed liposomes composed of DPPC and a pH responsive polymer methoxy-poly(ethyleneglycol)-b-poly(N-2-hydroxypropyl methacrylamide-co-histidine)-cholesterol (mPEG-P(HPMA-g-His)-CHOL) linked by biotin-PEG-biotin (biotin2-PEG) (34:1:12,5 molar ratio). These liposomes were used to encapsulate DXR, and evaluated in

colon rectal cancer. When exposed to acidic environment the imidazole ring of histidine in the polymer is protonated generating a repulsive force that destabilizes the liposome lipidic bilayer releasing the DXR. When tested *in vitro*, the DXR release from sensitive liposomes was 90% in pH 5.0 and 30% in pH 7.4. On the other hand, the conventional liposomes, composed by DPPC without polymer, released only 30% of DXR content in both pH. The IC50 values of polymer-biotin-sensitive liposome for HCT116 colon rectal cancer cells at pH 7.4 was 19.3 μg/ml, which was similar to free DXR and non-sensitive liposome. When evaluated for the antitumor efficacy in mice bearing HCT116 the inhibition of tumor growth in mice receiving pH sensitive liposomes was near to 90%, while that for non-responsive formulation was only near to 70% (110).

In a study by Zhao et al. (111) DXR was encapsulated in liposomes composed of DOPE: CHEMS: DSPE-PEG: DSPE-PEG-$H_7K(R_2)_2$ (65:30:4:1 molar ratio). The tumor-specific pH-responsive peptide $H_7K(R_2)_2$ (the sequence is RRK (HHHHHHH)RR) contains the cell-penetrating oligoarginine $(R_2)_2$ and the pH trigger oligohistidine $H_7$. As control liposomes DXR-PSL and DXR-SSL were prepared with DOPE : CHEMS : DSPE-PEG and EPC : CHOL : DSPE-PEG (65:30:5 molar ratio), respectively. The release of DXR from DXR-SSL, DXR-PSL and DXR-PSL- $H_7K(R_2)_2$ were evaluated in pH 5.5, 6.0, 6.5, and 7.4 for 24 h. To SSL after 24 h the content of DXR released was near to 20% in the four different pH evaluated. The release profiles of DXR-PSL and DXR-PSL- $H_7K(R_2)_2$ were similar, near to 20% in pH 7.4 and near to 80% in pH 5.5, 6.0, and 6.5. The coumarin-6 uptake by C6 and U87 cells from coumarin-6-SSL, coumarin-6-PSL and coumarin-6-PSL- $H_7K(R_2)_2$ were analyzed by flow cytometry. The fluorescence intensity of coumarin-6 in pH 7.4 were almost identical to the three formulations. However, in pH 6.8 the fluorescence intensity of coumarin-6 from coumarin-6-PSL and coumarin-6-PSL- $H_7K(R_2)_2$ were higher than coumarin-6-SSL about 1.2 and 1.7-fold, respectively. The C6 cell line was used to investigate the *in vitro* cytotoxicity of liposomes. At pH 7.4, the $IC_{50}$ values determined for DXR-SSL (14.9 ± 2.4 μg/ml), DXR-PSL (12.4 ± 1.7 μg/ml) and DXR- PSL-$H_7K(R_2)_2$ (12.6 ± 0.7 μg/ml) were similar. At pH 6.8, the $IC_{50}$ values determined for DXR-SSL (12.2 ± 0.3 μg/ml), DXR-PSL (3.7 ± 0.5 μg/ml) and DXR- PSL- $H_7K(R_2)_2$ (3.2 ± 0.4 μg/ml), unlike DXR-SSL group, were significantly reduced compared with that at pH 7.4. The antitumor efficacy was evaluated in human C6 xenograft model and after 21 days the mean tumor sizes determined for DXR-SSL, DXR-PSL and DXR-PSL-$H_7K(R_2)_2$ groups were 4369 ± 793, 1989 ± 205 and 1148 ± 285 $mm^3$, respectively, confirming that the pH-sensibility by polymorphic lipid and peptide can be a good strategy to produce an efficient responsive system to anticancer drug delivery (111).

## GSH-Triggered Liposomes

Aerobic life demands oxygen, and the respiration process leads to the formation of ROS that leads to oxidative stress. Glutathione (L-γ -glutamyl-L-cysteinylglycine, GSH), is one of the most important cellular antioxidant systems (112). GSH protects the biological system from oxidizing factors, such as ROS, by terminating them. In this process, GSH itself is oxidized to glutathione disulfide (GSSG), which is reduced back to GSH by glutathione reductase (GR), as shown in **Figure 8** (113).

GSH concentrations vary both from extracellular to intracellular environment and from normal to tumor cells. GSH concentrations in blood and extracellular matrix have been reported to be up to 1000-fold lower than that observed in the intracellular environment. In tumor cells, GSH levels have been reported to be up to 100-fold higher than that of normal cells. This high redox potential difference allows for the design of nanosystems that are selectively triggered in the tumor tissue (114).

Different nanocarriers have been designed upon this concept such as micelles (115), nanoparticles based on hydroxyethyl starch (116), gold-nanoparticle (117) and liposomes (118–120). Most of the materials used to obtain these nanosystems contain characteristic disulfide (S-S) bonds. These bonds are highly stable when exposed to low levels of GSH, like that on extracellular environments, but tend to be rapidly cleaved in the intracellular highly reducing environments, by GSH mediated thiol-disulfide exchange reaction. **Figure 9** represents this reaction, which starts with the nucleofilic attack of a disulfide bond by a deprotonated thiol resulting on the S-S bond cleavage producing a new disulfide and a new thiol (121).

Fu et al. (118) prepared redox-sensitive liposomes modified with TAT, a cell-penetrating peptide. The formulation was composed of CHOL, SPC, DSPE-S-S-PEG5000, and DSPE-PEG2000-TAT (10:69.5:10:0.5 molar ratio) and used to encapsulate PTX. When evaluated against murine melanoma B16F1 tumor xenograft model, in the end of 14 days the RTV for animals treated with the redox-sensitive TAT modified liposomes (~250%) was significantly lower compared to animals treated with non-redox sensitive and non TAT modified liposomes (CHOL : SPC:DSPE-PEG2000, 10:75:5 molar ratio; RTV ~700%) and compared to non-redox sensitive TAT modified liposomes (CHOL : SPC:DSPE-PEG5000: DSPE-PEG2000-TAT, 10:69.5:10:0.5 molar ratio; RTV ~400%). These results showed that both the S-S binder and TAT modification had an important role in enhancing the antitumor efficacy (118).

Chi et al. (122) prepared redox-sensitive liposomes composed of SPC, CHOL, DOTAP, DOPE, and PEG2000 conjugated with CHOL through a bio-reducible disulfide linker (CHOL-SS-mPEG) at a 4:1:2:2:1 molar ratio. Non redox-sensitive liposomes were prepared using CHOL-mPEG instead of CHOL-SS-mPEG. These liposomes were coated with hyaluronic acid, a ligand to CD44, and used to encapsulate DXR. An *in vitro* burst release was observed for this formulation in the presence of 10 mM GSH with >60% of DXR released in the first 4 h. In contrast, the non-redox sensitive liposomes released only approximately 30% of DXR after 72 h, independent of the GSH concentration. When tested for antitumor activity against xenograft osteosarcoma (MG63) mouse model, the redox-sensitive liposomes showed the best efficacy (tumor volume ~0.5$cm^3$) compared to non-redox-sensitive liposomes (tumor volume ~1.25$cm^3$) and free DXR (tumor volume ~1.75$cm^3$) in the end of 24 experimental days (122).


**FIGURE 8** | Glutathione (GSH) is oxidized to glutathione disulfide (GSSG) in the presence of reactive oxygen species (ROS). GSSG is reduced back to GSH by glutathione reductase (GR).

**FIGURE 9** | The thiol disulfide exchange reaction.

Chen et al. (120), prepared redox-sensitive oligopeptide liposomes composed of the redox-sensitive cationic lipid (LHSSG2C14), natural soybean phosphatidylcholine (SPC) and CHOL (5:5:1 weight ratio) encapsulating PTX and anti-survinin siRNA. The formulation was evaluated for PTX and siRNA release *in vitro* in GSH concentrations of 10 μM, which simulated the extracellular environment, and 10 mM, which simulates the intracellular environment. When exposed to 10 μM of GSH, less than 30% of PTX was released in 36 h. When the GSH concentration was 10 mM, the accumulated release of PTX was more than 80% in 36 h. In comparison, a non-redox sensitive formulation (prepared with LHG2C14 instead of LHSSG2C14) released less than 25% of PTX in 36h when GSH concentration was 10 mM. The bands of siRNA in agarose electrophoresis experiment could be detected after 2 h of incubation with 10 mM GSH but were not detected after incubation with 10 μM of GSH even after 8 experimental h. These results implied a relative stability of the formulation under the physiological conditions with targeted release in the presence of high GSH concentrations. When evaluated for its cytotoxicity, the redox-sensitive liposomes presented an IC50 value of 0.35 μg/ml against 4T1 breast cancer cells, while the non-redox sensitive liposomes and Taxol® presented IC50 values of 0.82 μg/ml and 0.85 μg/ml, respectively (120).

## Enzyme-Triggered Liposomes

Enzymes are proteins with extreme biorecognition ability and catalytic function in chemical reactions. They can be used as diagnostic markers for pathologies or target-therapeutics, since some diseases present differences in their expression compared to healthy tissues (123, 124). The over expression of proteases and phospholipases in tumor tissue, when compared to the normal tissue, has been explored to develop enzyme-triggered liposomes (125, 126). Enzyme-responsive liposomes release their content in response to pathologically increased enzyme levels at the target site (127).

## Protease Triggered Liposomes

Proteases are responsible for breaking peptide bonds between the amino acids of proteins. Metalloproteases (MMP) are proteases that attack collagen, elastin, fibronectin and proteoglycan, which causes the degradation of extracellular matrices. MMP-2 e MMP-9 are overexpressed in almost all cancers, being an attractive target to develop enzyme-triggered delivery systems (126).

Sarkar et al. (128) explored the MMP-9 to trigger liposomes composed of DSPC and a lipopeptide (LP1; $[CH_3(CH_2)_{16}COHNGPQGIAGQR(GPO)_4GG\text{-}COOH]$). The MMP-9 recognizes and unwinds the triple helical structure of LP1 on the liposomal surface, resulting in their destabilization and release of the encapsulated material. For release studies, liposomes composed of DSPC : LP1 (90:10 molar ratio) or 100% DSPC (control) were loaded with CF dye. When exposed to MMP-9 for 5 h, the responsive liposomes released around 55% of CF, while no CF release was observed for control liposomes. In contrast, without MMP-9, the responsive liposomes released only 10% of the dye, confirming the triggering potential of the enzyme (128).

In a study by Kulkarni et al. (129), gemcitabine was encapsulated in liposomes composed of 1-palmitoyl-2-oleoyl-sn-glycero-3-phosphocholine (POPC): LP1: PEGylated 1-palmitoyl-2-oleoyl-sn-glycero-3-phosphoethanolamine (POPE-

S-S-PEG5000): CHEMS: lissamine rhodamine lipid (59:30:5:5:1 molar ratio). These liposomes were designed to be sequentially GSH and enzyme (MMP-9) triggered. The disulfide bonds of POPE-S-S-PEG5000 are cleaved by GSH mediated reaction, resulting in the exposure of LP1 that is hydrolyzed by MMP-9. Free and liposome-encapsulated gemcitabine showed similar cytotoxicity for the PANC-1 cells (viability around 30-35%) and MIAPaCa-2 cells (viability around 45-50%). The higher cytotoxicity in PANC-1 cells was suggested to be due to the higher concentration of MMP-9 measured on the conditioned media of PANC-1 (126 ± 23 pg/ml) compared to that of MIAPaCa-2 cells (8 ± 4 pg/ml). The antitumor efficacy was evaluated in nude-Foxn1 mice with PANC-1 xenograft tumor. Animals treated with gemcitabine (10 mg/kg/week) encapsulated in MMP-9 responsive liposomes presented lower increase in tumor volume (increase of 125%) when compared to gemcitabine encapsulated in liposomes without LP1 (increase of 175%) in the end of 4 weeks (129).

## Phospholipase Triggered Liposomes

Phospholipase A2 (PLA2) degrades phospholipids and is over expressed in a variety of cancer types, namely prostate, lung, breast and pancreatic (126, 127). This catalytic activity is enhanced when phospholipids are organized, such as in liposomes, compared to lipid monomers; and is dependent on the lipid composition and membrane charge. The negative charge of phospholipids has also an important role in activity of the PLA2 (130). PLA2 acts at the lipid–water interface. Initially, interacts with the membrane by its interfacial binding surface and later the lipid is hydrolyzed in the active site of the enzyme (127).

Mock et al. (133) prepared two different PLA2 responsive liposomes composed of DSPC : DSPE-PEG : CHOL : DSPG (SPRL-G) (8:1:5:1 molar ratio) and of DSPC : DSPE-PEG : CHOL : DSPE (SPRL-E) (8:1:5:1 molar ratio) and a control liposome, without negative charge, composed of DSPC : DSPE-PEG : CHOL (9:1:5 molar ratio). CF was added to the formulations on the lipidic film hydration and DXR was encapsulated by remote loading. Release studies showed that CF released from the different liposomal formulations was negligible in the end of 108 h when PLA2 was absent. In contrast, in the presence of PLA2 there was an increased CF release from control liposomes (11%) SPRL-E (11%) and SPRL-G (14%) in the end of 108 h. A significant CF release from SPRL-E and SPRL-G started at 24–36 h, but for control liposomes it started only after 48 h. The antitumor efficacy of SPRL-E and the control liposomes was evaluated in human PC-3 xenograft model, that received the treatments containing 5mg/Kg of DXR on a weekly basis for four weeks. After 35 days, the tumor volume in the SPRL-E and control groups were $300mm^3$ and $500mm^3$, respectively, suggesting that SPRL-E are more effective for tumor growth inhibition (131).

## Hypoxia-Triggered Liposomes

The rapid growth of tumor cells demands a large amount of oxygen. As the tumor vasculature is irregular and abnormal, the oxygen supply is deficient, thus resulting in hypoxic regions. The hypoxia is a pathological phenomenon that consists in an important hallmark of tumor microenvironment. The oxygen partial pressure on some tumor tissues can be as low as 5–10 mm Hg, compared to the healthy tissue where it is near 30–50 mm Hg (132, 133). Due to this significant difference in the amount of oxygen, hypoxia is a promising target for cancer therapy (124). It is reported that the pathological phenomenon of hypoxia causes an increase in reductive stress, resulting in overexpression of nitroreductase, azoreductase, and quinone reductase (134).That in mind, pro-drugs that are activated to form the cytotoxic agent in hypoxia regions were designed (132), as well as hypoxia-triggered drug delivery systems to release drugs to hypoxic sites (133).

Liu et al. (135) obtained a new lipid called MDH. For that, first the hypoxic radiosensitizer 2-Methyl-5-nitroimidazole-1-ethanol (metronidazole) was conjugated to hexadecanedioic acid (HA) with a hydrolysable ester bond, in order to form (16-(2-(2-methyl-5-nitro-1H-imidazol-1-yl) ethoxy)-16-oxohexadecanoic acid (MHA). The MHA was then coupled with 3-dimethylaminopropane-1, 2-diol (DA) to form ester linked MDH. The tertiary amine group on the MDH becomes protonated when exposed to the acidic ambient of tumor, enhancing the cellular uptake of liposomes. The nitro group on the MDH can be converted to a hydrophilic amino group by nitroreductases in hypoxic conditions, leading to the destabilization of the liposomes and the release of its content. The MDH lipid was used for obtaining hypoxia-responsive liposomes composed of DSPE-PEG2000: MDH: CHOL (1:6:3 molar ratio) encapsulating DXR. These liposomes were evaluated for DXR release and in 5 h under hypoxic conditions 65.78% of the drug was released, versus approximately 25% in normoxic conditions. As a control, non-hypoxia-responsive liposomes composed of *1,2-Bis(palmitoyloxy)-3-(dimethylamino) propane (*PD): DSPE-PEG2000: CHOL (1:6:3 molar ratio) encapsulating DXR were prepared. These liposomes have the tertiary amine as well as the MDH-liposomes, but it does not present the hypoxia-responsive nitro group.

The hypoxic-responsive DXR release from hypoxia-responsive liposomes was investigated. Under hypoxic conditions, the liposomes released 65.8% of its DXR content within 5h while no significant DXR release was observed under normoxic conditions. The rapid DXR release of the hypoxia-responsive liposomes was examined in U87 cells. These cells were exposed to either hypoxia-responsive or non-hypoxia-responsive liposomes under hypoxic (2% oxygen concentration) or normoxic (21% oxygen concentration) conditions for 2 h. Cells were then collected and DXR fluorescence analyzed by flow cytometry. Hypoxia-responsive liposomes presented a higher DXR fluorescence under hypoxic conditions compared to that under normoxic conditions. On the other hand, for non-hypoxia-responsive liposomes, the DXR fluorescence intensity was nearly the same for both conditions, demonstrating that presence of MDH is necessary for liposome destabilization under hypoxia.

To evaluate the biodistribution and the antitumoral efficacy of the formulation, a xenograft glioma model was obtained by

intracranial injection of human glioblastoma U87 cells in Balb/c nude mice. The hypoxia-responsive liposomes encapsulating DXR and free DXR were injected intravenously and after 4 h animals were examined by an *in vivo* fluorescence microscopy imaging system. For animals treated with free DXR almost no DXR fluorescence was observed in the glioma, while a strong DXR fluorescence in the glioma of the animals treated with the hypoxia-responsive liposomes was observed. That demonstrated that the formulation could penetrate the blood-brain barrier delivering DXR to the tumor. The bioluminescence imaging was used to measure tumor growth. At day 30, the tumor growth rates in mice treated with non-hypoxia-responsive and hypoxia responsive liposomes were 2.72 fold and 0.79 fold, respectively, compared to day 10, and the median survival time were 55.5 and 65.5 days, respectively, demonstrating that the hypoxia-responsive liposomes exhibited higher antitumor efficacy in xenograft glioma model (135).

In another study, Liu et al. (136) used hypoxia responsive and non-hypoxia responsive liposomes as carriers of PLK1 siRNA for the treatment of glioma. The hypoxia responsive liposomes were composed of DSPE-PEG2000: CHOL: MDH (7,5:35:57,5 molar ratio) and non-hypoxia-responsive liposomes were composed of DSPE-PEG2000: CHOL: PD (7,5:35:57,5 molar ratio). The cellular uptake and intracellular distribution of these formulations were evaluated in hypoxic and normoxic conditions by fluorescence microscopy and flow cytometry in rat glial tumor C6 cells. The non-hypoxia-responsive liposomes showed slight and similar intracellular fluorescence intensity in C6 cells under hypoxic and normoxic conditions. Differently, the hypoxia-responsive liposomes showed higher intracellular fluorescence intensity compared to the non-hypoxia-responsive liposomes, especially under hypoxic conditions. The apoptosis-inducing effect was detected using the Annexin-V-FITC/PI in C6 cells. The hypoxia-responsive liposomes carrying siRNA showed 16.9% and 9% apoptotic ratio under hypoxic and normoxic conditions, respectively. The non-hypoxia-responsive liposomes carrying siRNA showed 5.5% apoptotic ratio under both oxygen conditions. The proliferation inhibition was evaluated by MTT assay. Hypoxia-responsive liposomes carrying siRNA inhibited the cell proliferation in 72.2% and 38.4% under hypoxic and normoxic conditions, respectively. The non-hypoxia-responsive liposomes carrying siRNA had only slight cell proliferation inhibition under both oxygen conditions. To evaluate the antitumoral efficacy of these formulations by bioluminescence imaging, a xenograft glioma model was obtained by intracranial injection of C6 cells to mice. Twenty-seven days after the different treatments, the tumor burden on animals treated with non-hypoxia-responsive liposomes was equal to 64.6% of that of the control (PBS) group. For animals treated with hypoxia responsive liposomes, tumor burden was 41.1% of the control group, suggesting this formulation is significantly superior on inhibiting the growth of glioma (136).

## ATP-Triggered Liposomes

In recent years, studies exploit the potential of ATP as a possible endogenous liposome trigger. This molecule is of extreme importance in cell signaling and metabolism and its concentration differs in extra and intracellular environments, allowing for the development of ATP-triggered drug delivery systems. In the extracellular fluid the ATP concentration is lower than 5 μM and double that amount is found inside the cells (14). Additionally, intratumoral interstitial ATP levels are between $10^3$-$10^4$ fold higher when compared to levels found in normal tissues (137).

For the nanosystem to be sensitive to this ATP gradient, different strategies are possible. For example, the incorporation of single chain DNA aptamers, which are specifically recognized and activated by ATP. Another possibility is to use enzymes that use ATP as an energy source. The nanocarriers are than able to selectively release their drug content through a conformational switch under an ATP rich environment (138, 139). Although these concepts are already solid and elucidated, systems that use ATP as a stimulus for drug delivery are still under test of concept and need further studies to become a clinical reality. These studies include the investigation of ATP concentrations in the different organelles, the regulation of the glucose-dependent ATP response, and the discovery of aptamers capable of differentiating ATP from the adenosine diphosphate (ADP) molecule. In addition, it is necessary to evaluate the immunogenicity potentials of the bio-macromolecules used as ATP probes, since aptamers and enzymes are always made of DNA and proteins. However, like other endogenous triggers, the release of drugs into the ATP-stimulated tumor region has the advantage of not requiring any special equipment (139).

In order to exploit antitumor release using ATP-triggered liposomes, Mo et al. (140), have developed a fusogenic liposome composed of EPC : DOPE : CHOL (2.5:2.5:1 weight ratio) encapsulating DXR and a ATP-responsive aptamer (DXR-FL). This aptamer with high binding affinity to ADP/ATP was selected *in vitro* from a large set of random ssDNA sequences. A second liposome composed of EPC : DOTAP : CHOL (5:1:0.1 weight ratio) encapsulating ATP (ATP-L) was obtained and co-administered. The idea consisted on the co-internalization of these formulations in endosomes, followed by their pH-responsive membrane fusion and ATP-triggered DXR release and accumulation in the cell nucleus. When evaluated for its cytotoxicity against the human breast cancer cell line MCF-7, the IC50 of DXR-FL alone was 2.6 μg/ml while the IC50 of DXR-FL co-incubated with ATP-L was 1.5 μg/ml. When evaluated *in vivo* in a mouse model with MCF-7 tumor, DXR-FL co-delivered with ATP-L led to a higher tumor growth suppression compared to DXR-FL alone (tumor volumes around 0.25 $cm^3$ and 0.35 $cm^3$, respectively), confirming the effective role of extrinsic ATP in DXR release (140). In this study, extrinsic ATP is provided therefore it is a chemical exogenous trigger stimulus. Unfortunately, authors did not compare the DXR-FL to a non-ATP-sensitive formulation in order to compare to the potential of the endogenous ATP alone.

On **Table 2**, we summarize the most important aspects of important liposomal formulations triggered by different endogenous stimuli developed to date.

**TABLE 2 |** Summary of important liposomal formulations triggered by different endogenous stimuli.

| Trigger stimulus | Lipid composition | Encapsulated agent(s) | Encapsulated percentage | Mean diameter | Reference |
|---|---|---|---|---|---|
| **pH** | DOPE : HSPC : CHOL : CHEMS : ES-PEG-DSPE (at various molar ratio) | DXR | 90% | 151 nm | (106) |
| **pH** | DOPE : CHEMS : DSPE-PEG2000 (5,7:3,8:0,5) 40mM | DXR | 25.5% | 114.8 nm | (107) |
| **pH** | DOPE : CHEMS : DSPE-PEG2000: DSPEPEG2000-Fol (5,7:3,8:0,45:0,05) 20mM | DXR | 97.6% | 129 nm | (108) |
| **pH** | DPPC:mPEG-P(HPMA-g-His)-CHOL: biotin2-PEG (34:1:12,5 molar ratio) | DXR | 84.7% | 90 nm | (110) |
| **pH** | DOPE : CHEMS : DSPE-PEG : DSPE-PEG-$H_7K(R_2)_2$. (65:30:4:1 molar ratio) | DXR | 91% | 92 nm | (111) |
| **GSH** | CHOL, SPC, DSPE-S-S-PEG5000 and DSPE-PEG2000-TAT (10:69.5:10:0.5 molar ratio) | PTX | 84.30 ± 3.51% | 102.70 ± 4.42 nm | (118) |
| **GSH** | SPC, CHOL, DOTAP, DOPE and CHOL-SS-mPEG at a 4:1:2:2:1 molar ratio, and hyaluronic acid 45mg | DXR | 91.3 ± 3.2% | 165.3 ± 0.2 nm | (122) |
| **GSH** | LHSSG2C14:SPC : CHOL 5:5:1 | PTX) and anti-survinin siRNA | 95.8 ± 2.8% | 92.3 ± 1.6 nm | (120) |
| **Enzyme (**MMP-9**)** | LP1:DSPC (10:90 molar ratio) | 5-carboxy fluorescein | N.A. | N.A. | (128) |
| **Enzyme (**MMP-9**)** | POPC: lipopeptide LP1: POPE-S-S-PEG5000: CHEMS: lissamine rhodamine lipid (59:30:5:5:1 molar ratio). | Gemcitabine | 50% | 86 nm | (129) |
| **Enzyme (**PLA2**)** | DSPC : DSPE-PEG : CHOL : DSPG (8:1:5:1 molar ratio) and DSPC : DSPE-PEG : CHOL : DSPE (8:1:5:1 molar ratio) | DXR | N.A. | 100 nm | (131) |
| **Hypoxia** | DSPE-PEG2000: MDH: CHOL (MLP-DXR) (1:6:3 molar ratio). | DXR | 8.7% | 169.4 nm | (135) |
| **Hypoxia** | DSPE-PEG2000: CHOL: MDH (MLP-siRNA) (7,5:35:57,5 molar ratio) | SiRNA | N.A. | 114 nm | (136) |
| **ATP** | DOPE : EPC:CHOL + ssDNA (2.5:2.5:1 weight ratio) | DXR | N.A | 195 nm | (140) |
| | DOTAP : EPC:CHOL (5:1:0.1 weight ratio) | ATP | 16.7% | 100 nm | |

## CONCLUDING REMARKS

The strategy of liposomal triggered release at the tumor site is part of liposomal evolution together with other strategies (e.g., long-circulating liposomes or active targeting) that aim on obtaining efficacious levels of drug in the tumor. Both the outer and inner tumor environment are being explored as means for liposomal triggered release. Herein, key studies concerning this topic were reviewed. As a relatively new strategy, its applications have not yet been fully developed, with a thermo-sensitive liposome being the only to make it to clinical studies so far. A special focus should be on liposomal formulations that are simple in composition, and that demand inexpensive trigger devices, thence enhancing the chances of clinical translation.

## AUTHOR CONTRIBUTIONS

Conception or design of the work and figures: MF. Drafting the paper: MF, EG, MR, and MO. Revising it critically for important intellectual content: MF and MO. All authors contributed to the article and approved the submitted version.

## FUNDING

The authors would like to thank Conselho Nacional de Desenvolvimento Científico e Tecnológico – CNPq for supporting Mônica Cristina Oliveira with research grant (307098/2018-4).

## REFERENCES

1. Bangham AD, Standish MM, Watkins JC. Diffusion of univalent ions across the lamellae of swollen phospholipids. *J Mol Biol* (1965) 13(1):238–IN27. doi: 10.1016/S0022-2836(65)80093-6
2. Gregoriadis G. Drug entrapment in liposomes. *FEBS Lett [Internet]* (1973) Nov 136(3):292–6. doi: 10.1016/0014-5793(73)80394-1
3. Gregoriadis G, Swain CP, Wills EJ, Tavill AS. Drug-Carrier Potential of Liposomes in Cancer Chemotherapy. *Lancet* (1974) 303(7870):1313–6. doi: 10.1016/S0140-6736(74)90682-5
4. Danhier F, Feron O, Préat V. To exploit the tumor microenvironment: Passive and active tumor targeting of nanocarriers for anti-cancer drug delivery. *J Control Release* (2010) 148(2):135–46. doi: 10.1016/j.jconrel.2010.08.027
5. Kaasgaard T, Andresen TL. Liposomal cancer therapy: exploiting tumor characteristics. *Expert Opin Drug Deliv* (2010) 7(2):225–43. doi: 10.1517/17425240903427940
6. Narang AS, Varia S. Role of tumor vascular architecture in drug delivery. *Adv Drug Delivery Rev* (2011) 63(8):640–58. doi: 10.1016/j.addr.2011.04.002
7. Klibanov AL, Maruyama K, Torchilin VP, Huang L. Amphipathic polyethyleneglycols effectively prolong the circulation time of liposomes. *FEBS Lett* (1990) 268(1):235–7. doi: 10.1016/0014-5793(90)81016-H
8. Gabizon A, Catane R, Uziely B, Kaufman B, Safra T, Cohen R, et al. Prolonged Circulation Time and Enhanced Accumulation in Malignant Exudates of Doxorubicin Encapsulated in Polyethylene-glycol Coated Liposomes. *Cancer Res* (1994) 54(4):987–92.
9. Barenholz Y. Doxil® - The first FDA-approved nano-drug: Lessons learned. *J Control Release [Internet]* (2012) 160(2):117–34. doi: 10.1016/j.jconrel.2012.03.020

10. Bertrand N, Wu J, Xu X, Kamaly N, Farokhzad OC. Cancer nanotechnology: The impact of passive and active targeting in the era of modern cancer biology. *Adv Drug Delivery Rev* (2014) 66:2–25. doi: 10.1016/j.addr.2013.11.009
11. Needham D, Anyarambhatla G, Kong G, Dewhirst MW. A new temperature-sensitive liposome for use with mild hyperthermia: Characterization and testing in a human tumor xenograft model. *Cancer Res* (2000) 60(5):1197–201.
12. Xiong S, Li H, Yu B, Wu J, Lee RJ. Triggering Liposomal Drug Release With a Lysosomotropic Agent. *J Pharm Sci* (2010) 99:5011–8. doi: 10.1002/jps.22210
13. Wang Y, Kohane DS. External triggering and triggered targeting strategies for drug delivery. *Nat Rev Mater [Internet]* (2017) 2(6):17020. doi: 10.1038/natrevmats.2017.20
14. Mo R, Gu Z. Tumor microenvironment and intracellular signal-activated nanomaterials for anticancer drug delivery. *Mater Today* (2016) 19(5):274–83. doi: 10.1016/j.mattod.2015.11.025
15. Tak WY, Lin SM, Wang Y, Zheng J, Vecchione A, Park SY, et al. Phase III HEAT study adding lyso-thermosensitive liposomal doxorubicin to radiofrequency ablation in patients with unresectable hepatocellular carcinoma lesions. *Clin Cancer Res* (2018) 24(1):73–83. doi: 10.1158/1078-0432.CCR-16-2433
16. Dou Y, Hynynen K, Allen C. To heat or not to heat: Challenges with clinical translation of thermosensitive liposomes. *J Control Release* (2017) 249:63–73. doi: 10.1016/j.jconrel.2017.01.025
17. Soares P IP, Ferreira I MM, Igreja R AGBN, Novo C MM, P.M.R. Borges J. Application of Hyperthermia for Cancer Treatment: Recent Patents Review. *Recent Pat Anticancer Drug Discovery* (2012) 7(1):64–73. doi: 10.2174/157489212798358038
18. Behrouzkia Z, Joveini Z, Keshavarzi B, Eyvazzadeh N, Aghdam RZ. Hyperthermia: How can it be used? *Oman Med J* (2016) 31(2):89–97. doi: 10.5001/omj.2016.19
19. Jha S, Sharma PK, Malviya R. Hyperthermia: Role and Risk Factor for Cancer Treatment. *Achiev Life Sci* (2016) 10(2):161–7. doi: 10.1016/j.als.2016.11.004
20. May JP, Li S. Hyperthermia-induced drug targeting. *Expert Opin Drug Delivery* (2013) 10(4):511–27. doi: 10.1517/17425247.2013.758631
21. Shao P, Wang B, Wang Y, Li J, Zhang Y. The Application of Thermosensitive Nanocarriers in Controlled Drug Delivery. *J Nanomater [Internet]* (2011) 2011:1–12. doi: 10.1155/2011/389640
22. Motamarry A, Asemani D, Haemmerich D. Thermosensitive Liposomes. In: *Liposomes*. London, UK: InTech (2017). p. 13. Available at: http://www.intechopen.com/books/liposomes/thermosensitive-liposomes. doi: 10.5772/intechopen.68159
23. Kneidl B, Peller M, Winter G, Lindner L, Hossann M. Thermosensitive liposomal drug delivery systems: state of the art review. *Int J Nanomed* (2014) 9:4387. doi: 10.2147/IJN.S49297
24. Yatvin MB, Weinstein JN, Dennis WH, Blumenthal R. Design of Liposomes for Enhanced Local Release of Drugs by hyperthermia. *Source Sci New Ser* (1978) 202(4374):1290–3. doi: 10.1126/science.364652
25. Weinstein J, Magin R, Yatvin M, Zaharko D. Liposomes and local hyperthermia: selective delivery of methotrexate to heated tumors. *Sci (80)* (1979) 204(4389):188–91. doi: 10.1126/science.432641
26. Gaber MH, Wu NZ, Hong K, Huang SK, Dewhirst MW, Papahadjopoulos D. Thermosensitive liposomes: Extravasation and release of contents in tumor microvascular networks. *Int J Radiat Oncol* (1996) 36(5):1177–87. doi: 10.1016/S0360-3016(96)00389-6
27. Landon CD. Nanoscale Drug Delivery and Hyperthermia: The Materials Design and Preclinical and Clinical Testing of Low Temperature-Sensitive Liposomes Used in Combination with Mild Hyperthermia in the Treatment of Local Cancer. *Open Nanomed J* (2011) 3(1):24–37. doi: 10.2174/1875933501103010038
28. Hauck ML. Phase I Trial of Doxorubicin-Containing Low Temperature Sensitive Liposomes in Spontaneous Canine Tumors. *Clin Cancer Res* (2006) 12(13):4004–10. doi: 10.1158/1078-0432.CCR-06-0226
29. Yarmolenko PS, Zhao Y, Landon C, Spasojevic I, Yuan F, Needham D, et al. Comparative effects of thermosensitive doxorubicin-containing liposomes and hyperthermia in human and murine tumours. *Int J Hyperth* (2010) 26(5):485–98. doi: 10.3109/02656731003789284
30. Lyon PC, Griffiths LF, Lee J, Chung D, Carlisle R, Wu F, et al. Clinical trial protocol for TARDOX: A phase I study to investigate the feasibility of targeted release of lyso-thermosensitive liposomal doxorubicin (ThermoDox®) using focused ultrasound in patients with liver tumours. *J Ther Ultrasound* (2017) 5(1):1–8. doi: 10.1186/s40349-017-0104-0
31. Wood BJ, Poon RT, Locklin JK, Dreher MR, Ng KK, Eugeni M, et al. Phase I Study of Heat-Deployed Liposomal Doxorubicin during Radiofrequency Ablation for Hepatic Malignancies. *J Vasc Interv Radiol* (2012) 23(2):248–255.e7. doi: 10.1016/j.jvir.2011.10.018
32. Zagar TM, Vujaskovic Z, Formenti S, Rugo H, Muggia F, O'Connor B, et al. Two phase I dose-escalation/pharmacokinetics studies of low temperature liposomal doxorubicin (LTLD) and mild local hyperthermia in heavily pretreated patients with local regionally recurrent breast cancer. *Int J Hyperth* (2014) 30(5):285–94. doi: 10.3109/02656736.2014.936049
33. Kim A, Sharma K, Yarmolenko P, Celik H, Kaplan RN, Dome J, et al. Phase 1 trial of lyso-thermosensitive liposomal doxorubicin (LTLD) and magnetic resonance guided high intensity focused ultrasound (MR-HIFU) for pediatric refractory solid tumors. *J Clin Oncol* (2017) 35(15_suppl): TPS10579–TPS10579. doi: 10.1200/JCO.2017.35.15_suppl.TPS10579
34. Lyu Y, Xiao Q, Yin L, Yang L, He W. Potent delivery of an MMP inhibitor to the tumor microenvironment with thermosensitive liposomes for the suppression of metastasis and angiogenesis. *Signal Transd Target Ther* (2019) 4(1):1–9. doi: 10.1038/s41392-019-0054-9
35. Lindner LH, Eichhorn ME, Eibl H, Teichert N, Schmitt-Sody M, Issels RD, et al. Novel Temperature-Sensitive Liposomes with Prolonged Circulation Time. *Clin Cancer Res* (2004) 10(6):2168–78. doi: 10.1158/1078-0432.CCR-03-0035
36. Tagami T, Ernsting MJ, Li SD. Efficient tumor regression by a single and low dose treatment with a novel and enhanced formulation of thermosensitive liposomal doxorubicin. *J Control Release* (2011) 152(2):303–9. doi: 10.1016/j.jconrel.2011.02.009
37. Saxena R, Nanjan MJ. Elastin-like polypeptides and their applications in anticancer drug delivery systems: A review. *Drug Deliv* (2015) 22(2):156–67. doi: 10.3109/10717544.2013.853210
38. Choi H, Won J-I. Characterization of Thermo-sensitive ELP-liposome Complexes According to the Conjugation Manner. *Biotechnol Bioprocess Eng* (2019) 24(4):680–6. doi: 10.1007/s12257-019-0117-3
39. Lu J, Feng F, Jin Z. Cancer Diagnosis and Treatment Guidance: Role of MRI and MRI Probes in the Era of Molecular Imaging. *Curr Pharm Biotechnol* (2014) 14(8):714–22. doi: 10.2174/1389201014666131226105916
40. Blasiak B, van Veggel FCJM, Tomanek B. Applications of Nanoparticles for MRI Cancer Diagnosis and Therapy. *J Nanomater* (2013) 2013:1–12. doi: 10.1155/2013/148578
41. Giustini AJ, Petryk AA, Cassim SA, Tate JA, Baker I, Hoopes PJ. Magnetic Nanoparticle Hyperthermia in Cancer Treatment. *Nano Life* (2013) 1:1–23. doi: 10.1142/S1793984410000067
42. Bañobre-López M, Teijeiro A, Rivas J. Magnetic nanoparticle-based hyperthermia for cancer treatment. *Rep Pract Oncol Radiother* (2013) 18(6):397–400. doi: 10.1016/j.rpor.2013.09.011
43. Gobbo OL, Sjaastad K, Radomski MW, Volkov Y, Prina-Mello A. Magnetic Nanoparticles in Cancer Theranostics. *Theranostics* (2015) 5(11):1249–63. doi: 10.7150/thno.11544
44. Williams HM. The application of magnetic nanoparticles in the treatment and monitoring of cancer and infectious diseases. *Biosci Horizons Int J Student Res* (2017) 10:1–10. doi: 10.1093/biohorizons/hzx009/4079886
45. Karimi M, Ghasemi A, Sahandi Zangabad P, Rahighi R, Moosavi Basri SM, Mirshekari H, et al. Smart micro/nanoparticles in stimulus-responsive drug/gene delivery systems. *Chem Soc Rev* (2016) 45(5):1457–501. doi: 10.1039/C5CS00798D
46. Oliveira H, Pérez-Andrés E, Thevenot J, Sandre O, Berra E, Lecommandoux S. Magnetic field triggered drug release from polymersomes for cancer therapeutics. *J Control Release [Internet]* (2013) Aug169(3):165–70. doi: 10.1016/j.jconrel.2013.01.013
47. Jaiswal MK, Pradhan A, Banerjee R, Bahadur D. Dual pH and Temperature Stimuli-Responsive Magnetic Nanohydrogels for Thermo-Chemotherapy. *J Nanosci Nanotechnol* (2014) 14(6):4082–9. doi: 10.1166/jnn.2014.8662
48. Hayashi K, Nakamura M, Miki H, Ozaki S, Abe M, Matsumoto T, et al. Magnetically Responsive Smart Nanoparticles for Cancer Treatment with a

Combination of Magnetic Hyperthermia and Remote-Control Drug Release. *Theranostics* (2014) 4(8):834–44. doi: 10.7150/thno.9199
49. Hua X, Yang Q, Dong Z, Zhang J, Zhang W, Wang Q, et al. Magnetically triggered drug release from nanoparticles and its applications in anti-tumor treatment. *Drug Delivery* (2017) 24(1):511–8. doi: 10.1080/10717544.2016.1256001
50. Yao A, Chen Q, Ai F, Wang D, Huang W. Preparation and characterization of temperature-responsive magnetic composite particles for multi-modal cancer therapy. *J Mater Sci Mater Med* (2011) 22(10):2239–47. doi: 10.1007/s10856-011-4413-5
51. Kim D-H, Vitol EA, Liu J, Balasubramanian S, Gosztola DJ, Cohen EE, et al. Stimuli-Responsive Magnetic Nanomicelles as Multifunctional Heat and Cargo Delivery Vehicles. *Langmuir* (2013) 29(24):7425–32. doi: 10.1021/la3044158
52. Tai L-A, Tsai P-J, Wang Y-C, Wang Y-J, Lo L-W, Yang C-S. Thermosensitive liposomes entrapping iron oxide nanoparticles for controllable drug release. *Nanotechnology* (2009) 20(13):135101. doi: 10.1088/0957-4484/20/13/135101
53. Pradhan P, Giri J, Rieken F, Koch C, Mykhaylyk O, Döblinger M, et al. Targeted temperature sensitive magnetic liposomes for thermo-chemotherapy. *J Control Release* (2010) 142(1):108–21. doi: 10.1016/j.jconrel.2009.10.002
54. Amstad E, Kohlbrecher J, Müller E, Schweizer T, Textor M, Reimhult E. Triggered Release from Liposomes through Magnetic Actuation of Iron Oxide Nanoparticle Containing Membranes. *Nano Lett* (2011) 11(4):1664–70. doi: 10.1021/nl2001499
55. Hardiansyah A, Huang LY, Yang MC, Liu TY, Tsai SC, Yang CY, et al. Magnetic liposomes for colorectal cancer cells therapy by high-frequency magnetic field treatment. *Nanoscale Res Lett* (2014) 9(1):1–13. doi: 10.1186/1556-276X-9-497
56. Guo H, Chen W, Sun X, Liu Y-N, Li J, Wang J. Theranostic magnetoliposomes coated by carboxymethyl dextran with controlled release by low-frequency alternating magnetic field. *Carbohydr Polym* (2015) 118:209–17. doi: 10.1016/j.carbpol.2014.10.076
57. Hardiansyah A, Yang M-C, Liu T-Y, Kuo C-Y, Huang L-Y, Chan T-Y. Hydrophobic Drug-Loaded PEGylated Magnetic Liposomes for Drug-Controlled Release. *Nanoscale Res Lett* (2017) 12(1):355. doi: 10.1186/s11671-017-2119-4
58. Canavese G, Ancona A, Racca L, Canta M, Dumontel B, Barbaresco F, et al. Nanoparticle-assisted ultrasound: A special focus on sonodynamic therapy against cancer. *Chem Eng J* (2018) 340(January):155–72. doi: 10.1016/j.cej.2018.01.060
59. Boissenot T, Bordat A, Fattal E, Tsapis N. Ultrasound-triggered drug delivery for cancer treatment using drug delivery systems: From theoretical considerations to practical applications. *J Control Release* (2016) 241:144–63. doi: 10.1016/j.jconrel.2016.09.026
60. Schroeder A, Kost J, Barenholz Y. Ultrasound, liposomes, and drug delivery: principles for using ultrasound to control the release of drugs from liposomes. *Chem Phys Lipids* (2009) 162(1–2):1–16. doi: 10.1016/j.chemphyslip.2009.08.003
61. Sirsi SR, Borden MA. State-of-the-art materials for ultrasound-triggered drug delivery. *Adv Drug Delivery Rev* (2014) 72:3–14. doi: 10.1016/j.addr.2013.12.010
62. Deng Z, Xiao Y, Pan M, Li F, Duan W, Meng L, et al. Hyperthermia-triggered drug delivery from iRGD-modified temperature-sensitive liposomes enhances the anti-tumor efficacy using high intensity focused ultrasound. *J Control Release* (2016) 243:333–41. doi: 10.1016/j.jconrel.2016.10.030
63. VanOsdol J, Ektate K, Ramasami S, Maples D, Collins W, Malayer J, et al. Sequential HIFU heating and nanobubble encapsulation provide efficient drug penetration from stealth and temperature sensitive liposomes in colon cancer. *J Control Release* (2017) 10: (247):55–63. doi: 10.1016/j.jconrel.2016.12.033
64. Chen MJ, Xu A, He W, Ma W, Shen S. Ultrasound triggered drug delivery for mitochondria targeted sonodynamic therapy. *J Drug Delivery Sci Technol* (2017) 39:501–7. doi: 10.1016/j.jddst.2017.05.009
65. Ninomiya K, Yamashita T, Tanabe Y, Imai M, Takahashi K, Shimizu N. Targeted and ultrasound-triggered cancer cell injury using perfluorocarbon emulsion-loaded liposomes endowed with cancer cell-targeting and fusogenic capabilities. *Ultrason Sonochem* (2016) 28:54–61. doi: 10.1016/j.ultsonch.2015.06.032
66. Paasonen L, Sipilä T, Subrizi A, Laurinmäki P, Butcher SJ, Rappolt M, et al. Gold-embedded photosensitive liposomes for drug delivery: Triggering mechanism and intracellular release. *J Control Release* (2010) 147(1):136–43. doi: 10.1016/j.jconrel.2010.07.095
67. Saneja A, Kumar R, Arora D, Kumar S, Panda AK, Jaglan S. Recent advances in near-infrared light-responsive nanocarriers for cancer therapy. *Drug Discovery Today* (2018) 23(5):1115–25. doi: 10.1016/j.drudis.2018.02.005
68. Yang Y, Yang X, Li H, Li C, Ding H, Zhang M, et al. Near-infrared light triggered liposomes combining photodynamic and chemotherapy for synergistic breast tumor therapy. *Colloids Surfaces B Biointerfaces* (2019) 173(October 2018):564–70. doi: 10.1016/j.colsurfb.2018.10.019
69. Kwiatkowski S, Knap B, Przystupski D, Saczko J, Kędzierska E, Knap-Czop K, et al. Photodynamic therapy – mechanisms, photosensitizers and combinations. *BioMed Pharmacother* (2018) 106(July):1098–107. doi: 10.1016/j.biopha.2018.07.049
70. Miranda D, Lovell JF. Mechanisms of light-induced liposome permeabilization. *Bioeng Transl Med* (2016) 1(3):267–76. doi: 10.1002/btm2.10032
71. Shim G, Ko S, Kim D, Le QV, Park GT, Lee J, et al. Light-switchable systems for remotely controlled drug delivery. *J Control Release* (2017) 267 (August):67–79. doi: 10.1016/j.jconrel.2017.09.009
72. Luo D, Li N, Carter KA, LIn C, Geng J, Shao S, et al. Rapid Light-triggered Drug Release in Liposomes Containing Small Amounts of Unsaturated and Porphyrin Phospholipids. *Small* (2017) 12(22):3039–47. doi: 10.1002/smll.201503966
73. Luo D, Carter KA, Razi A, Geng J, Shao S, Giraldo D, et al. Doxorubicin encapsulated in stealth liposomes conferred with light-triggered drug release. *Biomaterials* (2016) 75:193–202. doi: 10.1016/j.biomaterials.2015.10.027
74. Fuse T, Tagami T, Tane M, Ozeki T. Effective light-triggered contents release from helper lipid-incorporated liposomes co-encapsulating gemcitabine and a water-soluble photosensitizer. *Int J Pharm* (2018) 540(1–2):50–6. doi: 10.1016/j.ijpharm.2018.01.040
75. Li Q, Li W, Di H, Luo L, Zhu C, Yang J, et al. A photosensitive liposome with NIR light triggered doxorubicin release as a combined photodynamic-chemo therapy system. *J Control Release* (2018) 277(January):114–25. doi: 10.1016/j.jconrel.2018.02.001
76. Zhang K, Zhang Y, Meng X, Lu H, Chang H, Dong H, et al. Light-triggered theranostic liposomes for tumor diagnosis and combined photodynamic and hypoxia-activated prodrug therapy. *Biomaterials* (2018) 185(July):301–9. doi: 10.1016/j.biomaterials.2018.09.033
77. Mathiyazhakan M, Wiraja C, Xu C. A Concise Review of Gold Nanoparticles-Based Photo-Responsive Liposomes for Controlled Drug Delivery. *Nano-Micro Lett* (2018) 10(1):1–10. doi: 10.1007/s40820-017-0166-0
78. Lino MM, Ferreira L. Light-triggerable formulations for the intracellular controlled release of biomolecules. *Drug Discovery Today* (2018) 23(5):1062–70. doi: 10.1016/j.drudis.2018.01.019
79. Fomina N, Sankaranarayanan AA. Photochemical mechanisms of light-triggered release from nanocarrie. *Adv Drug Delivery Rev* (2013) 64 (11):1005–20. doi: 10.1016/j.addr.2012.02.006
80. Yavlovich A, Singh A, Blumenthal RPA. A Novel class of Photo-triggerable liposomes containing DPPC:DC8,9 PC as Vehicles for Delivery of Doxorubcin to Cells. *Biochim Biophys Acta* (2011) 1808(1):117–26. doi: 10.1016/j.bbamem.2010.07.030
81. Leung SJ, Romanowski M. Light-activated content release from liposomes. *Theranostics* (2012) 2(10):1020–36. doi: 10.7150/thno.4847
82. Hester TJ, Dennison SR, Baker MJ, Snape TJ. Functionalising the azobenzene motif delivers a light-responsive membrane-interactive compound with the potential for photodynamic therapy applications. *Org Biomol Chem* (2015) 13(29):8067–70. doi: 10.1039/C5OB00465A
83. Liu XM, Yang B, Wang YL, Wang JY. Photoisomerisable cholesterol derivatives as photo-trigger of liposomes: Effect of lipid polarity, temperature, incorporation ratio, and cholesterol. *Biochim Biophys Acta - Biomembr* (2005) 1720(1–2):28–34. doi: 10.1016/j.bbamem.2005.10.016

84. Amichal Y, Brandon S, Kshitij G, Robert B, Anu P. Light-sensitive Lipid-based Nanoparticles for Drug Delivery. *Mol Membr Biol* (2010) 27(7):364–81. doi: 10.3109/09687688.2010.507788
85. Bayer AM, Alam S, Mattern-Schain SI, Best MD. Triggered liposomal release through a synthetic phosphatidylcholine analogue bearing a photocleavable moiety embedded within the sn-2 acyl chain. *Chem - A Eur J* (2014) 20 (12):3350–7. doi: 10.1002/chem.201304094
86. Kautzka Z, Clement S, Goldys EM, Deng W. light-triggered liposomal cargo delivery platform incorporating photosensitizers and gold nanoparticles for enhanced singlet oxygen generation and increased cytotoxicity. *Int J Nanomedicine* (2017) 12:969–77. doi: 10.2147/IJN.S126553
87. Puri A. Phototriggerable liposomes: Current research and future perspectives. *Pharmaceutics* (2014) 6(1):1–25. doi: 10.3390/pharmaceutics6010001
88. Lajunen T, Nurmi R, Kontturi L, Viitala L, Yliperttula M, Murtomäki L, et al. Light activated liposomes: Functionality and prospects in ocular drug delivery. *J Control Release* (2016) 244:157–66. doi: 10.1016/j.jconrel.2016.08.024
89. Sine J, Urban C, Thayer D, Charron H, Valim N, Tata DB, et al. Photo activation of HPPH encapsulated in "Pocket" liposomes triggers multiple drug release and tumor cell killing in mouse breast cancer xenografts. *Int J Nanomed* (2014) 10:125–45. doi: 10.2147/IJN.S72143
90. Samanta D, Mehrotra R, Margulis K, Zare RN. On-demand electrically controlled drug release from resorbable nanocomposite films. *Nanoscale* (2017) 9(42):16429–36. doi: 10.1039/C7NR06443H
91. Murdan S. E lectro-responsive drug delivery from hydrogels. *J Control Release* (2003) 92:1–17. doi: 10.1016/S0168-3659(03)00303-1
92. Retelj L, Pucihar G, Miklavcic D. Electroporation of intracellular liposomes using nanosecond electric pulses-a theoretical study. *IEEE Trans BioMed Eng* (2013) 60(9):2624–35. doi: 10.1109/TBME.2013.2262177
93. Yi J, Barrow AJ, Yu N, O'Neill BE. Efficient electroporation of liposomes doped with pore stabilizing nisin. *J Liposome Res* (2013) 23(3):197–202. doi: 10.3109/08982104.2013.788024
94. Polak A, Tarek M, Tomšič M, Valant J, Ulrih NP, Jamnik A, et al. Electroporation of archaeal lipid membranes using MD simulations. *Bioelectrochemistry* (2014) 100:18–26. doi: 10.1016/j.bioelechem.2013.12.006
95. Srimathveeravalli G, Abdel-Atti D, Pérez-Medina C, Takaki H, Solomon SB, Mulder WJM, et al. Reversible Electroporation–Mediated Liposomal Doxorubicin Delivery to Tumors Can Be Monitored With 89 Zr-Labeled Reporter Nanoparticles. *Mol Imaging* (2018) 17:1–9. doi: 10.1177/1536012117749726
96. Jourabchi N, Beroukhim K, Tafti BA, Kee ST, Lee EW. Irreversible electroporation (NanoKnife) in cancer treatment. *Gastrointest Interv* (2014) 3(1):8–18. doi: 10.1016/j.gii.2014.02.002
97. Silk M, Tahour D, Srimathveeravalli G, Solomon SB, Thornton RH. The state of irreversible electroporation in interventional oncology. *Semin Intervent Radiol* (2014) 31(2):111–7. doi: 10.1055/s-0034-1373785
98. Plaunt AJ, Courbanou MB, Cuison KD, Harmatys KM, Smith BD. Selective non-covalent triggered release from liposomes. *Chem Commun* (2012) 48 (65):8123. doi: 10.1039/c2cc32962j
99. Plaunt AJ, Harmatys KM, Hendrie KA, Musso AJ, Smith BD. Chemically triggered release of 5-aminolevulinic acid from liposomes. Bönig H, editor. *RSC Adv* (2014) 4(101):57983–90. doi: 10.1039/C4RA10340H
100. Manchun S, Dass CR, Sriamornsak P. Targeted therapy for cancer using pH-responsive nanocarrier systems. *Life Sci* (2012) 90:381–7. doi: 10.1016/j.lfs.2012.01.008
101. Ferreira D dos S, Lopes SC de A, Franco MS, Oliveira MC. pH-sensitive liposomes for drug delivery in cancer treatment. *Ther Deliv* (2013) 4(9):1–24. doi: 10.4155/tde.13.80
102. Paliwal SR, Paliwal R, Vyas SP. A review of mechanistic insight and application of pH-sensitive liposomes in drug delivery. *Drug Delivery* (2015) 22(3):231–42. doi: 10.3109/10717544.2014.882469
103. Aghdam MA, Bagheri R, Mosafer J, Hashemzaei M, Baghbanzadeh A, De M. Recent advances on thermosensitive and pH-sensitive liposomes employed in controlled release. *J Control Release* (2019) 315:1–22. doi: 10.1016/j.jconrel.2019.09.018
104. Monteiro LOF, Lopes SCA, Barros ALB, Magalhães-Paniago R, Malachias Â, Oliveira MC, et al. Phase behavior of dioleyphosphatidylethanolamine molecules in the presence of components of pH-sensitive liposomes and paclitaxel. *Colloids Surfaces B Biointerfaces* (2016) 144:276–83. doi: 10.1016/j.colsurfb.2016.04.011
105. Monteiro LOF, Malachias Â, Pound-Lana G, Magalhães-Paniago R, Mosqueira VCF, Oliveira MC, et al. Paclitaxel-Loaded pH-Sensitive Liposome: New Insights on Structural and Physicochemical Characterization. *Langmuir* (2018) 34(20):5728–37. doi: 10.1021/acs.langmuir.8b00411
106. Paliwal SR, Paliwal R, Pal HC, Saxena AK, Sharma PR, Gupta PN, et al. Estrogen-anchored pH-sensitive liposomes as nanomodule designed for site-specific delivery of doxorubicin in breast cancer therapy. *Mol Pharm* (2012) 9:176–86. doi: 10.1021/mp200439z
107. Silva JO, Fernandes RS, Lopes SCA, Cardoso VN, Leite EA, Cassali GD, et al. pH-Sensitive, Long-Circulating Liposomes as an Alternative Tool to Deliver Doxorubicin into Tumors: a Feasibility Animal Study. *Mol Imaging Biol* (2016) 18(6):898–904. doi: 10.1007/s11307-016-0964-7
108. de Oliveira Silva J, Fernandes RS, Ramos Oda CM, Ferreira TH, Machado Botelho AF, Martins Melo M, et al. Folate-coated, long-circulating and pH-sensitive liposomes enhance doxorubicin antitumor effect in a breast cancer animal model. *BioMed Pharmacother* (2019) 118(June):109323. doi: 10.1016/j.biopha.2019.109323
109. Liu X, Huang G. Formation strategies, mechanism of intracellular delivery and potential clinical applications of pH-sensitive liposomes. *Asian J Pharm Sci* (2013) 8:319–28. doi: 10.1016/j.ajps.2013.11.002
110. Chiang YT, Lo CL. PH-Responsive polymer-liposomes for intracellular drug delivery and tumor extracellular matrix switched-on targeted cancer therapy. *Biomaterials* (2014) 35(20):5414–24. doi: 10.1016/j.biomaterials.2014.03.046
111. Zhao Y, Ren W, Zhong T, Zhang S, Huang D, Guo Y, et al. Tumor-specific pH-responsive peptide-modified pH-sensitive liposomes containing doxorubicin for enhancing glioma targeting and anti-tumor activity. *J Control Release* (2016) 222:56–66. doi: 10.1016/j.jconrel.2015.12.006
112. Couto N, Wood J, Barber J. The role of glutathione reductase and related enzymes on cellular redox homoeostasis network. *Free Radic Biol Med* (2016) 95:27–42. doi: 10.1016/j.freeradbiomed.2016.02.028
113. Sadhu SS, Xie J, Zhang H, Perumal O, Guan X. Glutathione disulfide liposomes - A research tool for the study of glutathione disulfide associated functions and dysfunctions. *Biochem Biophys Rep* (2016) 7:225–9. doi: 10.1016/j.bbrep.2016.06.017
114. Zhu L, Torchilin VP. Stimulus-responsive nanopreparations for tumor targeting. *Integr Biol (United Kingdom)* (2013) 5(1):96–107. doi: 10.1039/c2ib20135f
115. Lv S, Tang Z, Zhang D, Song W, Li M, Lin J, et al. Well-defined polymer-drug conjugate engineered with redox and pH-sensitive release mechanism for efficient delivery of paclitaxel. *J Control Release* (2014) 194:220–7. doi: 10.1016/j.jconrel.2014.09.009
116. Li Y, Hu H, Zhou Q, Ao Y, Xiao C. Alpha-amylase and redox- responsive nanoparticles for tumor targeted drug delivery. *ACS Appl Mater Interf* (2017) 9(22):19215–30. doi: 10.1021/acsami.7b04066
117. Ghosh PS, Kim C, Han G, Forbes NS, Rotello VM. Efficient Gene Delivery Vectors by Tuning the Surface Charge Density of amino acid-functionalized gold nanoparticles. *J Am Chem Soc* (2008) 2(11):2213–8. doi: 10.1021/nn800507t
118. Fu H, Shi K, Hu G, Yang Y, Kuang Q, Lu L, et al. Tumor-targeted paclitaxel delivery and enhanced penetration using TAT-decorated liposomes comprising redox-responsive poly(ethylene glycol). *J Pharm Sci* (2015) 103:1160–73. doi: 10.1002/jps.24291
119. Zhou G, Li L, Xing J, Jalde S, Li Y, Cai J, et al. Redox responsive liposomal nanohybrid cerasomes for intracellular drug delivery. *Colloids Surfaces B Biointerfaces* (2016) 148:518–25. doi: 10.1016/j.colsurfb.2016.09.033
120. Chen X, Zhang Y, Tang C, Tian C, Sun Q, Su Z, et al. Co-delivery of paclitaxel and anti-survivin siRNA via redox-sensitive oligopeptide liposomes for the synergistic treatment of breast cancer and metastasis. *Int J Pharm* (2017) 529(1–2):102–15. doi: 10.1016/j.ijpharm.2017.06.071
121. Brülisauer L, Gauthier MA, Leroux JC. Disulfide-containing parenteral delivery systems and their redox-biological fate. *J Control Release* (2014) 195:147–54. doi: 10.1016/j.jconrel.2014.06.012
122. Chi Y, Yin X, Sun K, Feng S, Liu J, Chen D, et al. Redox-sensitive and hyaluronic acid functionalized liposomes for cytoplasmic drug delivery to

osteosarcoma in animal models. *J Control Release* (2017) 261:113–25. doi: 10.1016/j.jconrel.2017.06.027
123. He H, Sun L, Ye J, Liu E, Chen S, Liang Q, et al. Enzyme-triggered, cell penetrating peptide-mediated delivery of anti-tumor agents. *J Control Release* (2016) 240:67–76. doi: 10.1016/j.jconrel.2015.10.040
124. Mo L, Song JG, Lee H, Zhao M, Kim HY, Lee YJ, et al. PEGylated hyaluronic acid-coated liposome for enhanced in vivo efficacy of sorafenib via active tumor cell targeting and prolonged systemic exposure. *Nanomed Nanotechnol Biol Med* (2018) 14(2):557–67. doi: 10.1016/j.nano.2017.12.003
125. Hu Q, Katti PS, Gu Z. Enzyme-responsive nanomaterials for controlled drug delivery. *Nanoscale* (2014) 6(21):12273–86. doi: 10.1039/C4NR04249B
126. Hayashi JY, Tamanoi F. Exploiting Enzyme Alterations in Cancer for Drug Activation, Drug Delivery, and Nanotherapy. In: *The Enzymes*, *1st ed*, vol. 42. Amsterdam, Netherlands: Elsevier Inc (2017). p. 153–72. doi: 10.1016/bs.enz.2017.08.005
127. Shchegravina ES, Tretiakova DS, Alekseeva AS, Galimzyanov TR, Utkin YN, Ermakov YA, et al. Phospholipidic Colchicinoids as Promising Prodrugs Incorporated into Enzyme-Responsive Liposomes: Chemical, Biophysical, and Enzymological Aspects. *Bioconjug Chem* (2019) 30(4):1098–113. doi: 10.1021/acs.bioconjchem.9b00051
128. Sarkar NR, Rosendahl T, Krueger AB, Banerjee AL, Benton K, Mallik S, et al. "Uncorking" of liposomes by matrix metalloproteinase-9. *Chem Commun* (2005) 8):999–1001. doi: 10.1039/B416827E
129. Kulkarni PS, Haldar MK, Nahire RR, Katti P, Ambre AH, Muhonen WW, et al. MMP-9 responsive PEG cleavable nanovesicles for efficient delivery of chemotherapeutics to pancreatic cancer. *Mol Pharm* (2014) 11(7):2390–9. doi: 10.1021/mp500108p
130. Andresen TL, Thompson DH, Kaasgaard T. Enzyme-triggered nanomedicine: Drug release strategies in cancer therapy (Invited Review). *Mol Membr Biol* (2010) 27(7):353–63. doi: 10.3109/09687688.2010.515950
131. Mock JN, Costyn LJ, Wilding SL, Arnold RD, Cummings BS. Evidence for distinct mechanisms of uptake and antitumor activity of secretory phospholipase A2 responsive liposome in prostate cancer. *Integr Biol (United Kingdom)* (2013) 5:172–82. doi: 10.1039/c2ib20108a
132. Coates JT, Skwarski M, Higgins GS. Targeting tumor hypoxia: shifting focus from oxygen supply to demand. *Br J Radiol* (2019) 92(1093):1–3. doi: 10.1259/bjr.20170843
133. He H, Zhu R, Sun W, Cai K, Chen Y, Yin L. Selective cancer treatment: Via photodynamic sensitization of hypoxia-responsive drug delivery. *Nanoscale* (2018) 10(6):2856–65. doi: 10.1039/C7NR07677K
134. Li Y, Lu A, Long M, Cui L, Chen Z, Zhu L. Nitroimidazole derivative incorporated liposomes for hypoxia-triggered drug delivery and enhanced therapeutic efficacy in patient-derived tumor xenografts. *Acta Biomater* (2019) 83:334–48. doi: 10.1016/j.actbio.2018.10.029
135. Liu H, Xie Y, Zhang Y, Cai Y, Li B, Mao H, et al. Development of a hypoxia-triggered and hypoxic radiosensitized liposome as a doxorubicin carrier to promote synergetic chemo-/radio-therapy for glioma. *Biomaterials* (2017) 121:130–43. doi: 10.1016/j.biomaterials.2017.01.001
136. Liu HM, Zhang YF, Xie YD, Cai YF, Li BY, Li W, et al. Hypoxia-responsive ionizable liposome delivery siRNA for glioma therapy. *Int J Nanomed* (2017) 12:1065–83. doi: 10.2147/IJN.S125286
137. Qian Y, Wang X, Liu Y, Li Y, Colvin RA, Tong L, et al. Extracellular ATP is internalized by macropinocytosis and induces intracellular ATP increase and drug resistance in cancer cells. *Cancer Lett* (2014) 351(2):242–51. doi: 10.1016/j.canlet.2014.06.008
138. Mo R, Jiang T, Disanto R, Tai W, Gu Z. ATP-triggered anticancer drug delivery. *Nat Commun* (2014) 5:1–10. doi: 10.1038/ncomms4364
139. Sun Wujin GZ. ATP-Responsive Drug Delivery Systems. *Expert Opin Drug Delivery* (2016) 13(3):311–4. doi: 10.1517/17425247.2016.1140147
140. Mo R, Jiang T, Gu Z. Enhanced anticancer efficacy by ATP-mediated liposomal drug delivery. *Angew Chem - Int Ed* (2014) 53(23):5815–20. doi: 10.1002/anie.201400268

**Conflict of Interest:** The authors declare that the research was conducted in the absence of any commercial or financial relationships that could be construed as a potential conflict of interest.

frontiers in Oncology

REVIEW
published: 20 July 2021
doi: 10.3389/fonc.2021.594917

# Can Nimesulide Nanoparticles Be a Therapeutic Strategy for the Inhibition of the KRAS/PTEN Signaling Pathway in Pancreatic Cancer?

*Roseane Guimarães Ferreira*[1], *Luis Eduardo Mosquera Narvaez*[2], *Kaio Murilo Monteiro Espíndola*[2], *Amanda Caroline R. S. Rosario*[2], *Wenddy Graziela N. Lima*[2] *and Marta Chagas Monteiro*[1,2*]

[1] Neuroscience and Cell Biology Post-Graduation Program, Laboratory of In Vitro Tests, Immunology and Microbiology-LABEIM, Biological Sciences Institute, Federal University of Pará/UFPA, Belém, Brazil, [2] Pharmaceutical Science Post-Graduation Program, Laboratory of In Vitro Tests, Immunology and Microbiology-LABEIM, Health Science Institute, Federal University of Pará/UFPA, Belém, Brazil

OPEN ACCESS

**Edited by:**
Ricardo Bentes Azevedo, University of Brasilia, Brazil

**Reviewed by:**
Michele Caraglia, University of Campania Luigi Vanvitelli, Italy
Ho Sup Yoon, Nanyang Technological University, Singapore

***Correspondence:**
Marta Chagas Monteiro
martachagas2@yahoo.com.br

**Specialty section:**
This article was submitted to Cancer Molecular Targets and Therapeutics, a section of the journal Frontiers in Oncology

**Received:** 14 August 2020
**Accepted:** 22 June 2021
**Published:** 20 July 2021

**Citation:**
Ferreira RG, Narvaez LEM, Espíndola KMM, Rosario ACRS, Lima WGN and Monteiro MC (2021) Can Nimesulide Nanoparticles Be a Therapeutic Strategy for the Inhibition of the KRAS/PTEN Signaling Pathway in Pancreatic Cancer? Front. Oncol. 11:594917. doi: 10.3389/fonc.2021.594917

Pancreatic cancer is an aggressive, devastating disease due to its invasiveness, rapid progression, and resistance to surgical, pharmacological, chemotherapy, and radiotherapy treatments. The disease develops from PanINs lesions that progress through different stages. KRAS mutations are frequently observed in these lesions, accompanied by inactivation of PTEN, hyperactivation of the PI3K/AKT pathway, and chronic inflammation with overexpression of COX-2. Nimesulide is a selective COX-2 inhibitor that has shown anticancer effects in neoplastic pancreatic cells. This drug works by increasing the levels of PTEN expression and inhibiting proliferation and apoptosis. However, there is a need to improve nimesulide through its encapsulation by solid lipid nanoparticles to overcome problems related to the hepatotoxicity and bioavailability of the drug.

**Keywords: pancreatic cancer, KRAS, PTEN, nimesulide, solid lipid nanoparticles**

## INTRODUCTION

The pancreas is a retroperitoneal organ formed by a connective tissue capsule, with the parenchyma and lobes separated by thin dividing walls containing nerves, excretory ducts, and lymphatic and blood vessels (1–3). Containing exocrine epitheliums (ducts and acini, comprising 90% of the gland mass) and endocrine epitheliums (Islets of Langerhans, comprising approximately 2% of the glandular mass) and carrying out functions of synthesis, secretion, regulation, and storage of digestive enzymes (exocrine part) and hormones (endocrine part), the organ is essential for the digestion of carbohydrates, proteins, and fats in food (1–3).

Pancreatic cancer is the fourth leading cause of cancer death and the most frequent gastrointestinal neoplasia, characterized by its lethality with an average survival of 3–6 months and a 5-year survival rate of less than 5% (4–6). The increase in life expectancy (pancreatic cancer

mainly affects the older population), obesity, and diabetes mellitus are the main risk factors for the development of the disease (4–6). Surgery is the most recommended procedure in the treatment of pancreatic cancer; however, it must be accompanied by adjuvant therapy, which nonetheless guarantees only a 5-year survival rate for patients. Therefore, there is a need to develop more efficient therapeutic approaches for the treatment of this neoplasm (6–9).

Pancreatic cancer develops from PanINs lesions (pancreatic intraepithelial neoplasms) that progress through different stages (low, medium, and high grade) (6–9). All stages harbor the accumulation of genetic mutations in several genes, where the KRAS mutation (Kirsten rat viral sarcoma oncogene homolog) is the first change observed in all grades of PanINs (approximately 99%) (10–12), followed by loss of CDKN2A function, and genetic inactivation of TP53 and SMAD4 (10, 12, 13). The KRAS mutation follows the loss of PTEN (phosphatase and tensin homolog), a tumor suppressor that inhibits the activation of the PI3K/Akt pathway, which is hyperactivated in 60% of pancreatic cancer cases (10, 12–14). The disease is also associated with chronic inflammation, with overexpression of COX-2 (15, 16).

Drug repositioning is a promising strategy that offers many opportunities for drugs already known to show their functionality in other diseases such as cancer (17, 18). Nimesulide is a selective COX-2 inhibitor that has demonstrated multiple anticancer effects, including reduced cell proliferation and induction of apoptosis in different types of PanIN lesions in pancreatic cancer (15, 16). However, there are problems related to its hepatotoxicity and bioavailability and, consequently, there is a need to improve this medication, potentially through the application of nanotechnology (19). Thus, the objective of this review is to show the action of nimesulide in the PTEN/PI3K/AKT/COX2 pathway, as well as to suggest an alternative for the improvement of this drug *via* its encapsulation within solid lipid nanoparticles.

## PANCREATIC CANCER

Pancreatic cancer is the term used to describe the formation of a tumor in the cellular epithelium of the glandular structures of the pancreas (3, 8, 9). It is characterized by being a highly aggressive and devastating disease due to its invasiveness (with perineural and vascular growth), rapid progression (distant and early metastases), and profound resistance to pharmacological therapies, chemotherapy, radiotherapy, and targeted molecular therapy (8, 9). This type of cancer is one of the most prevalent worldwide, being the fourth leading cause of death in the USA (United States of America) and eighth in Europe, second only to lung, prostate, or breast and colon cancer (6, 7, 20).

Among solid tumors, pancreatic cancer has the worst survival (less than 6 months) with a mortality reaching 90% of cases (6, 7, 21). The prediction of experts is that by 2030 this disease will be the second leading cause of cancer-related death, due to the ever increasing rise in its incidence (about 43,000 to 53,070 new cases are diagnosed annually) (6, 7).

The main factor contributing to this high mortality rate is the occurrence of non-specific symptoms in the early stages of the disease, which include asthenia (loss or decrease in physical strength), loss of weight, anorexia, abdominal pain, dark urine, jaundice, nausea, back pain, diarrhea, vomiting, steatorrhea (fatty stools), dyspepsia (abdominal discomfort), lethargy, and diabetes of recent onset; this makes it difficult to start early diagnosis and, consequently, leads to the worsening of the neoplasm (5, 8).

The risk factors that contribute to the appearance of pancreatic cancer are still uncertain, but it is strongly related to the aging of the population (90% of the diagnosed population is over 55 years old) (5, 22) and is seen more frequently in developed countries than in developing countries, where people tend to live longer (5, 22). Other factors include smoking, alcohol, obesity, diet, physical inactivity, chronic diseases (gastric diseases, diabetes, pancreatitis, hepatitis virus), and genetic mutations [amplification or overexpression of oncogenes (KRAS) and alterations in tumor suppressor genes (T53)] (5, 8, 22, 23).

Pancreatic cancer can be classified according to its appearance (solid or cystic), mucin production, and cell differentiation [exocrine (ductal or acinar) or endocrine] (5, 8). Solid types are the most aggressive including, for example, pancreatic ductal adenocarcinoma (the most common type, occurring in 85% of cases), neuroendocrine neoplasms, acinar cell carcinomas, and pancreatoblastomas. Cystic types include mucinous cystic neoplasms, intraductal papillary mucinous neoplasms, and solid pseudopapillary neoplasms (5, 8).

## PHYSIOPATHOLOGY OF PANCREATIC CANCER

The development of pancreatic cancer is a slow and gradual process, occurring in several stages through the formation of precursor lesions, inactivation of tumor suppressor genes, activation of oncogenes, and deregulation of the cell cycle (8, 24–26). The precursor lesions may be of the intraductal papillary mucinous neoplasia type (IPMN, mucin producing neoplastic cells located in the duct), mucinous cystic neoplasia type (MCN, mucin producing neoplastic cells that do not connect to the duct), and pancreatic intraepithelial neoplasia type (PanIN, cells with non-invasive microscopic epithelial neoplasm), with the latter being the most common precursor in humans (8, 24, 25, 27).

Thus, pancreatic cancer appears through PanIN proliferative lesions (located in the pancreatic ducts) evolving to PanIN-1 (low grade lesions with infiltration of the carcinoma and accumulation of genetic alterations and infiltration), PanIN-2 (intermediate lesions with histological progression, hyperplasia, and primary carcinoma), PanIN3 (high grade lesions, with metastasis called "carcinoma *in situ*"), and finally pancreatic ductal adenocarcinoma (the most prevalent and lethal form of this type of neoplasia) (10, 12, 24–26, 28) (**Figure 1**). The gradual progression of PanIN lesions to the formation of pancreatic

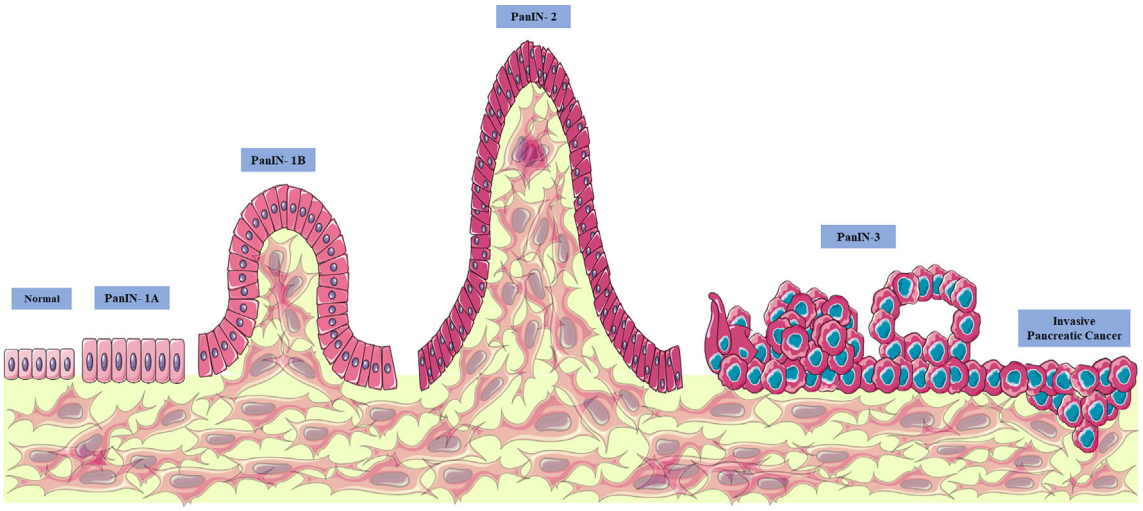


**FIGURE 1** | Evolution of pancreatic cancer. Pancreatic cancer appears through proliferative lesions PanINs (located in the pancreatic ducts), evolving to PanIN-1 (low grade lesions with infiltration of the carcinoma and accumulation of genetic alterations and infiltration), intermediate lesions with progression histological, hyperplasia, and primary carcinoma) and PanIN3 (high grade lesions with metastasis, called "carcinoma in *situ*") and finally pancreatic ductal adenocarcinoma (the most prevalent and lethal form of this type of neoplasia). From: Author. This figure used elements from Servier Medical Art.

ductal adenocarcinoma involves the accumulation of several important genetic mutations that contribute to the worsening of the pathology. The four most frequently mutated genetic factors are three tumor suppressor genes, CDKN2A, TP53, and SMAD4 (**Figure 2**), and the KRAS oncogene (8, 10, 12, 24).

## INACTIVATION OF TUMOR SUPPRESSOR GENES

### CDKN2A

CDKN2A (cyclin-dependent 2K kinase inhibitor) is a tumor suppressor gene that is found to be mutated in 95% of cases of pancreatic adenocarcinoma, usually from PanIN-2 lesions (8, 10, 14). This gene encodes the p16 protein that binds to cyclin dependent kinase 4/6 (Cdk4/6), interrupting the cell cycle in the G1 phase (8, 10, 14). The inactivation of CDKN2A by homozygous deletions, loss of single allele combined with intragenic mutation in the second allele, or hypermethylation of the promoter, causes the functional deactivation of the p16 protein and, consequently, increased cell proliferation, contributing to tumor formation and growth (8, 14).

### SMAD4

The mutation in this gene (a member of the large SMAD4 family) occurs in 55% of cases of pancreatic adenocarcinoma PanIN-3 lesions (8, 10, 14). SMAD4 is located on chromosome 18q and encodes the beta transcription factor (TGF-b) involved in the regulation of important cellular functions, such as tissue differentiation, cell proliferation, migration, and apoptosis (8, 10, 14). Inactivation of SMAD4 by homozygous exclusion of both alleles or in the intragenic form of an allele, results in the interruption of the normal cell cycle, contributing to tumor metastasis (8, 10, 14).

### TP53

TP53 (tumor protein p53) is the tumor suppressor gene that mutates in 70% of pancreatic cancer PanIN-3 lesions (8, 10, 14). TP53 activates target genes (p21, Bax, Apaf-1) in response to cell oxidative stress and DNA damage, participating in the control of cell growth and apoptosis through gene transcription (8, 10, 14). The inactivation of this gene causes dysregulation of the cell cycle and worsening of neoplastic lesions (8, 10, 14).

### KRAS

The KRAS oncogene (viral oncogene homologous to Kirsten rat sarcoma) is considered the most frequent mutation in pancreatic adenocarcinoma (in 95% of cases), and this is one of the first changes that occurs in the pancreatic tumorigenesis process (PanIN-1), being observed in all degrees of PanINs (8, 14, 29). This oncogene is involved in the signal transduction of an important cell signaling pathway, the P13K/PTEN/AKT pathway (8, 14, 29). A point mutation of KRAS at codon 12 induces permanent activation of the RAs protein, causing progressive dysregulation in the process of differentiation, cell growth, and apoptosis. This leads to the formation of pre-neoplastic cells, foci of hyperplasia, and metastasis in the pancreatic duct (8, 14, 29).

### Via KRAS/P13K/PTEN/AKT

KRAS encodes the Ras protein through a small GTPase-binding protein, which alternates between the active (GTP) and inactive (GDP) states of Ras (3, 10, 30). The active state of the protein is promoted by guanine nucleotide exchange factors (GEFs), which help to shift from GDP to GTP in response to stimulation of a

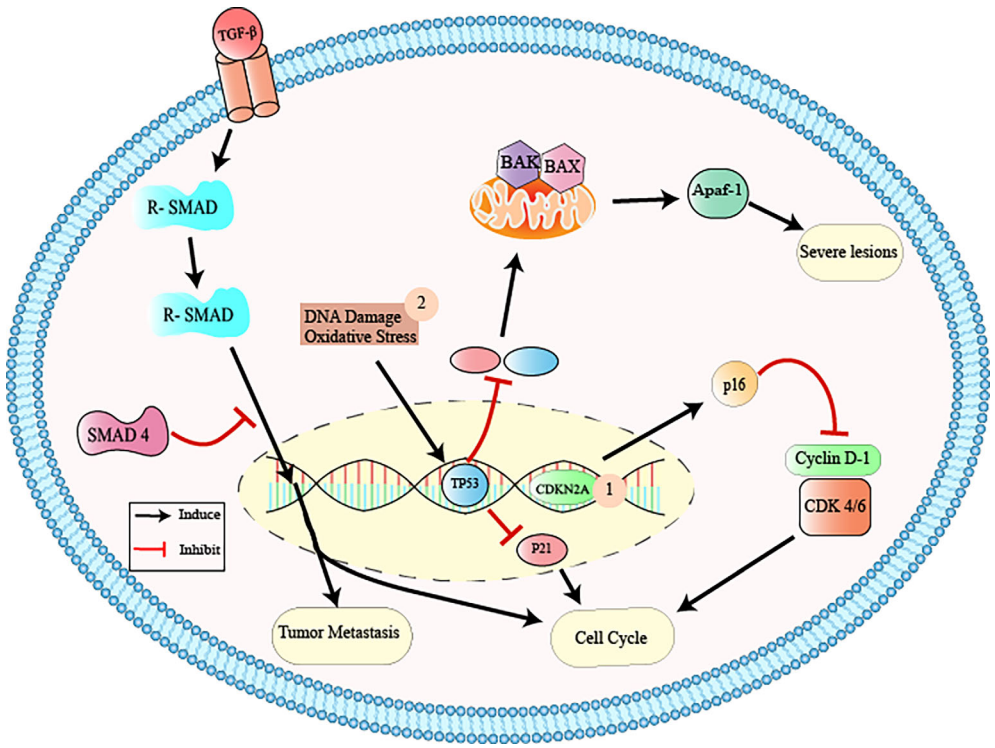


**FIGURE 2** | Inactivation of tumor suppressor genes *via* CDKN2A, TP53, and SMAD4. 1: CDKN2A (cyclin-dependent 2K kinase inhibitor) is a tumor suppressor gene that is found to be mutated usually in PanIN-2 lesions. This gene encodes the p16 protein that binds to cyclin dependent kinase 4/6 (Cdk4/6), interrupting the cell cycle in the G1 phase. The inactivation of CDKN2A causes the functional deactivation of the p16 protein and, consequently, increased cell proliferation, contributing to tumor formation and growth; 2: TP53 (tumor protein p53) is the tumor suppressor gene that activates target genes (p21, Bax, Apaf-1) in response to cell oxidative stress and DNA damage, participating in the control of cell growth and apoptosis through gene transcription. The inactivation of this gene causes dysregulation of the cell cycle and worsening of neoplastic lesions; 3: The SMAD4 (mothers against decapentaplegic homolog 4) is located on chromosome 18q and encodes the beta transcription factor (TGF-b) involved in the regulation of important cellular functions, such as tissue differentiation, cell proliferation, migration, and apoptosis. Inactivation of SMAD4 results in the interruption of the normal cell cycle, contributing to tumor metastasis. From: Author.

cell surface receptor, epidermal growth factor receptor (EGFR, a member of the human tyrosine kinase epidermal receptor family) (3, 10, 30). The activation of Ras results in the recruitment of PI3K (phosphatidylinositol-3-kinase), a heterodimeric protein formed by two subunits: a regulatory and a catalytic one (3, 10, 30).

The activation of PI3Ks occurs through the catalytic subunit SH2 (Src-homology domain 2), where it transfers an ATP-derived phosphate to the D-3 position of the inositol ring of the phosphoinositide membrane, forming PIP2 (phosphatidylinositol 4,5-bisphosphate) and then PIP3 (phosphatidylinositol 4,5-triphosphate) (3, 10, 30). The second messenger PIP3 recruits the membrane AKT (serine/threonine kinase) and PDK1 (phosphoinositide-dependent kinase 1) (3, 10, 30).

AKT affects various signaling pathways, such as the mTOR pathway (mammalian target of rapamycin), which regulates the nutrient, oxygen, and energy levels in cells (3, 10, 30) and also the NF-κB (nuclear factor kappa B) pathway, with pro and anti-inflammatory functions (31–33). The activation of PI3K is negatively controlled by a protein called PTEN, which regulates the intensity of the production of this protein and consequently its effects on the intracellular signal transduction cascade (3, 10, 30).

## PTEN

PTEN (phosphatase and tensin homolog) is a member of the tyrosine phosphatase type I family and is located on chromosome 10q23, with nine exons and 1,209 nucleotides that are encoded to form a single 403 amino acid protein (34–38). This protein is composed of five domains: an N-terminal phosphatase that facilitates phospholipid hydrolysis, a short N-terminal binding domain (PIP2), a C2 domain (responsible for mediating protein binding with the cell plasma membrane), a C-terminal tail enriched with amino acids (proline, glutamic acid, serine, and threonine, and various phosphorylation sites), and a PDZ protein interaction domain that can bind to the lipid (34–38).

This protein is an important tumor suppressor that controls cell proliferation, growth, survival, and metabolism at all stages (G1, S, G2, and M) (36, 39–42). PTEN is the only lipid phosphatase that can inhibit the PI3K signaling pathway, preventing the hydrolysis of PIP2 to PIP3 (34–38). In its active state, this phosphatase homolog is recruited from the cytosol to the membrane, where its C-terminal portion is dephosphorylated, leading to the opening of its

phosphatase domain (34–38). This allows binding to the cell membrane through the PDZ protein domain (34–38). Thus, PTEN acts on PI3K by preventing PIP2 from being hydrolyzed to PIP3 (located inside the membrane) and, consequently, the events related to this pathway (AKT/mTOR) (34–38). PTEN deficiency or absence causes hyperactivity of the PI3K pathway due to the accumulation of PIP3, leading to the appearance of high degrees of neoplastic transformations (34–38) (**Figure 3**).

PTEN can lose its function through genetic mutations, such as point mutations, large chromosomal deletions (homozygous/heterozygous exclusion), microRNA regulation, post-translational modifications, and epigenetic mechanisms (hypermethylation of the promoter region) (35, 43). PTEN mutations are seen in some syndromes, such as PTEN hereditary tumor syndromes (PHTS), Cowden syndrome, Bannayan–Riley–Ruvalcaba syndrome, and Proteus syndrome; patients with these syndromes develop benign tumors in various organs and are prone to the development of cancers of the thyroid, prostate, or breast (34, 36–38).

PTEN is frequently found mutated in the final stages of pancreatic cancer (PanIN-3), contributing to the onset of the most severe disease (ductal pancreatic adenocarcinoma) (34, 36–38). For this reason, PTEN becomes an interesting pharmacological target, since drugs that act to reactivate its tumor suppressor function can contribute to the prevention of progression in pancreatic cancer (35).

## PANCREATIC CANCER TREATMENT

Pancreatic cancer therapy has long been a challenge for the scientific community, which seeks to overcome resistance to different treatment modalities, such as radiotherapy, chemotherapy, and targeted therapies (44–46). Surgery remains the best option to cure patients with this neoplasia. However, this procedure alone is not enough, since the majority (90%) of patients relapse and die if additional therapy is not administered (28, 45, 47). Many adjuvant therapies have been evaluated over the years; one of the first used was based on fluoropyrimidines, 5-fluorouracil (5-FU), or capecitabine combined with radiation. Next, gemcitabine or fluoropyrimidines were tested, followed by chemoradiation (28, 45, 47).

At the moment, the most frequently used therapy is the combination of FOLFIRINOX (folinic acid, 5-fluoracil, irinotecan, and oxaliplatin) or gemcitabine plus nab-paclitaxel, with or without chemoradiation (28, 45, 47). Despite representing one of the best therapeutic options against pancreatic cancer, the combination of gemcitabine plus nab-paclitaxel has undesirable side effects associated with peripheral neuropathy and myelosuppression (28, 45, 47). Likewise, FOLFIRINOX is associated with an increased risk of febrile neutropenia, sensory neuropathy, gastrointestinal toxicity and alopecia (28, 45, 47). Even with the help of adjuvant therapy, patient survival is short of 5 years (28, 45, 47).

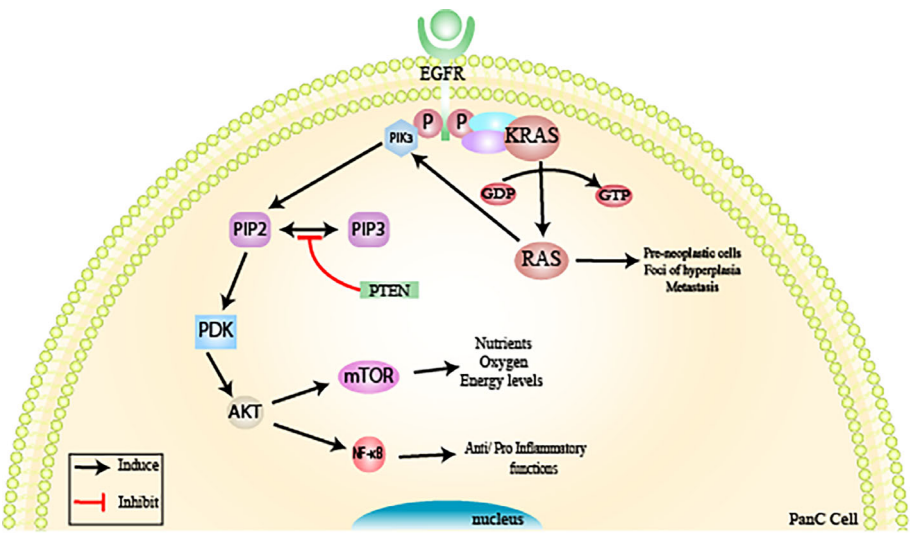


**FIGURE 3** | Inactivation of tumor suppressor genes *via* KRAS/PI3K/PTEN/AKT. The KRAS oncogene is considered the most frequent mutation in the pancreatic tumorigenesis process observed in pancreatic adenocarcinoma (PanIN-1) and is involved in signal transduction of an important cell signaling pathway, the PI3K/PTEN/AKT pathway. KRAS encodes the Ras protein through a small GTPase-binding protein. Active RAS is promoted by guanine nucleotide exchange factors (GEFs) in response to stimulation of a cell surface receptor, epidermal growth factor receptor (EGFR, a member of the human tyrosine kinase epidermal receptor family), resulting in the recruitment of PI3K. PI3K will form PIP2 (phosphatidylinositol 4,5-bisphosphate) and then PIP3 (phosphatidylinositol 4,5-triphosphate. The second messenger PIP3 recruits AKT (serine/threonine kinase) and PDK1 (phosphoinositide-dependent kinase 1 to the membrane). AKT affects various signaling pathways, such as the mTOR pathway, which regulates nutrient, oxygen, and energy levels in cells and the NF-κB pathway (nuclear factor kappa B). PTEN is responsible for regulating the intensity of PI3K and, consequently, its effects on the intracellular signal transduction cascade. PTEN deficiency or absence causes hyperactivity of the PI3K pathway, due to the accumulation of PIP3, leading to the appearance of high degrees of neoplastic transformations. From: Author.

## DRUG REPOSITIONING AND THE USE OF NSAIDS IN CANCER TREATMENT

In recent years, the reuse or repositioning of drugs already known and approved for other therapeutic purposes has intensified (17, 18, 48). Previous knowledge about the pharmacological characteristics of these drugs (efficacy, interactions, safety, and toxicity) allows a reduction in cost and time, accelerating their entry into experimental clinical trials on pancreatic cancer (17, 18, 48). A promising example of repositioning comes from non-steroidal anti-inflammatory drugs (NSAIDs), given that the development of pancreatic cancer is associated with chronic inflammatory processes, as observed in patients with pancreatitis who are 10 to 20 times more likely to experience this neoplasm (49–51).

NSAIDs are a class of commonly prescribed heterogeneous drugs with analgesic, antipyretic, and anti-inflammatory actions, which act by inhibiting cyclooxygenase (COX), and consequently the transformation of arachidonic acid into prostaglandins (responsible for the events causing pain, fever, and inflammation) (49–51). There are two isoforms of COX: COX-1 and COX-2. COX-1, also called a constitutive enzyme, is present in almost all tissues (blood vessels, stomach, kidneys) and is involved in the production of prostaglandin and the maintenance of homeostasis in the tissues in which it is located (49–51). COX-2, known as an inductive enzyme, is also present in almost all tissues; however its synthesis is stimulated in inflammatory processes, mediating pain, fever, and inflammation. COX-2 levels are overexpressed in pancreatic cancer cases, and several COX-2 inhibitors are used to treat this condition (49–51).

## NIMESULIDE

Nimesulide [N-(4-nitro-2-phenoxyphenyl)methanesulfonamide] (**Figure 4**) is an NSAID belonging to the class of selective COX-2 inhibitors and the acid sulfonamide subgroup, which contains a methylsulfonamide portion in its structure (52–54). The large volume of the methylsulfonamide portion increases the bond strength between nimesulide and COX-2, explaining the high selectivity of this isoform (54, 55). The drug is a potent analgesic, anti-inflammatory, and antipyretic used orally (tablet) in doses of 100 mg twice daily; it is also used in the pharmaceutical form of drops (for children from 5 to 12 years old), a suppository (200 mg twice a day) and a gel (52–54, 56, 57). However, the limit for treatment duration is only 15 consecutive days (58). This limit was determined by the European Medicines Agency (EMA) to minimize the risks of hepatotoxicity associated with the use of this drug (53).

Nimesulide is a weak acid, with an acidity constant ranging from 6.4 to 6.8 and a melting point between 147 and 148°C (59). It has good solubility in acetone, chloroform, and ethyl acetate, with relative solubility in ethanol and little solubility in water (59). The drug has a multifactorial mechanism of action, acting by blocking the superoxide anion released by leukocytes, inhibiting phosphodiesterase type IV, increasing levels of glutathione (tGSH) in stomach tissue, blocking histamine, attenuating hydrochloric acid, and inhibiting metalloprotease and platelet activation (PAF) (55, 56, 60, 61).

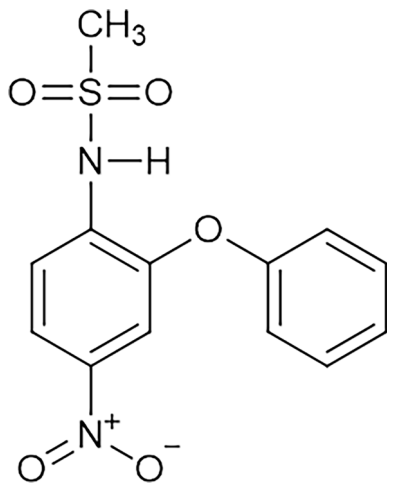


**FIGURE 4** | Molecular structure of nimesulide. Nimesulide (N-(4-nitro-2-phenoxyphenyl)-methanesulfonamide) is a non-steroidal anti-inflammatory (NSAID), which contains a methylsulfonamide portion in its structure and is a weak acid. It has an acidity constant ranging from 6.4 to 6.8, and the melting point occurs between 147°C and 148°C. In addition, it has good solubility in acetone, chloroform, and ethyl acetate, with relative solubility in ethanol, and low solubility in water. This figure is from: https://pubchem.ncbi.nlm.nih.gov/compound/Nimesulide (accessed on Mar. 14, 2020).

Nimesulide has suppressive effects on cancer cells and an antiproliferative action (54, 62, 63). The drug is able to inhibit lung cancer cell proliferation (55), stimulate apoptosis in breast cancer cells (64), and suppress gastric carcinogenesis associated with *Helicobacter pylori* (65). In addition, this NSAID can slow the progression of pancreatic cancer precursor lesions, inhibit proliferation, and induce apoptosis (16).

## MECHANISM OF ACTION OF NIMESULIDE IN PANCREATIC CANCER

Studies carried out by Chu et al. (16) demonstrated that nimesulide inhibits proliferation and promotes apoptosis of PANC-1 cells (cell line isolated from a ductal pancreatic adenocarcinoma) *via* increased expression of PTEN (16). PTEN mutation and inactivation in pancreatic adenocarcinoma lead to hyperactivation of the PI3K/AKT pathway. AKT regulates a series of important effector proteins such as NF-kB (nuclear factor Kappa B), COX-2, VEGF, Bcl-2, and Bax which, when deregulated, lead to uncontrolled proliferation, survival, growth, and other cellular events such as inflammation, causing metastasis (16, 66).

Nimesulide inhibits angiogenesis by inducing an increase in PTEN levels (16). PTEN suppresses AKT by decreasing VEGF levels in PANC-1 cells (16). VEGF (vascular endothelial growth factor) is responsible for supplying blood cells with oxygen and

nutrients, contributing to the formation of new blood vessels (angiogenesis) (16, 67). This growth factor is overexpressed in pancreatic cancer (16). PTEN reactivation appears to be related to decreased expression of COX-2, since overexpression of this isoform causes PTEN inactivation (15, 16, 66). In turn, PTEN also acts by suppressing AKT and consequently inhibiting NF-kB, which decreases the expression of COX-2 (15, 68, 69). In any case, the action of nimesulide is related to the interaction between PTEN and COX-2 (16).

NF-kB is a protein complex that performs functions as a transcription factor and plays an important role in inflammation, suppression of apoptosis, and cell proliferation (68, 69). One study has also shown that nimesulide induces apoptosis by decreasing Bcl-2 expression levels and increasing Bax levels in PANC-1 (16) (**Figure 5**). Despite the beneficial effects of nimesulide on cancer, in recent years, reports also show that long-term oral use of nimesulide can lead to severe hepatotoxicity, leading to cases of fulminant liver failure requiring liver transplantation (68, 69). This hepatotoxicity has been associated with the effects of uncoupling in the mitochondria of nimesulide, which shows that it is a potent protonophoretic uncoupling and oxidizer of NAD (P) H (68, 69).

## HEPATOTOXICITY

Hepatotoxicity associated with nimesulide has been reported in recent years, involving significant biochemical changes in the levels of ALT/AST (liver transaminases), with histological lesions suggestive of fulminant liver failure (61, 70). The first report about the hepatotoxicity of this drug occurred in 1997, with severe and even fatal cases of liver damage. This led to the restriction or withdrawal of nimesulide from the market in Spain and Finland in 2002 (61, 70). In 2004, the European Medicines

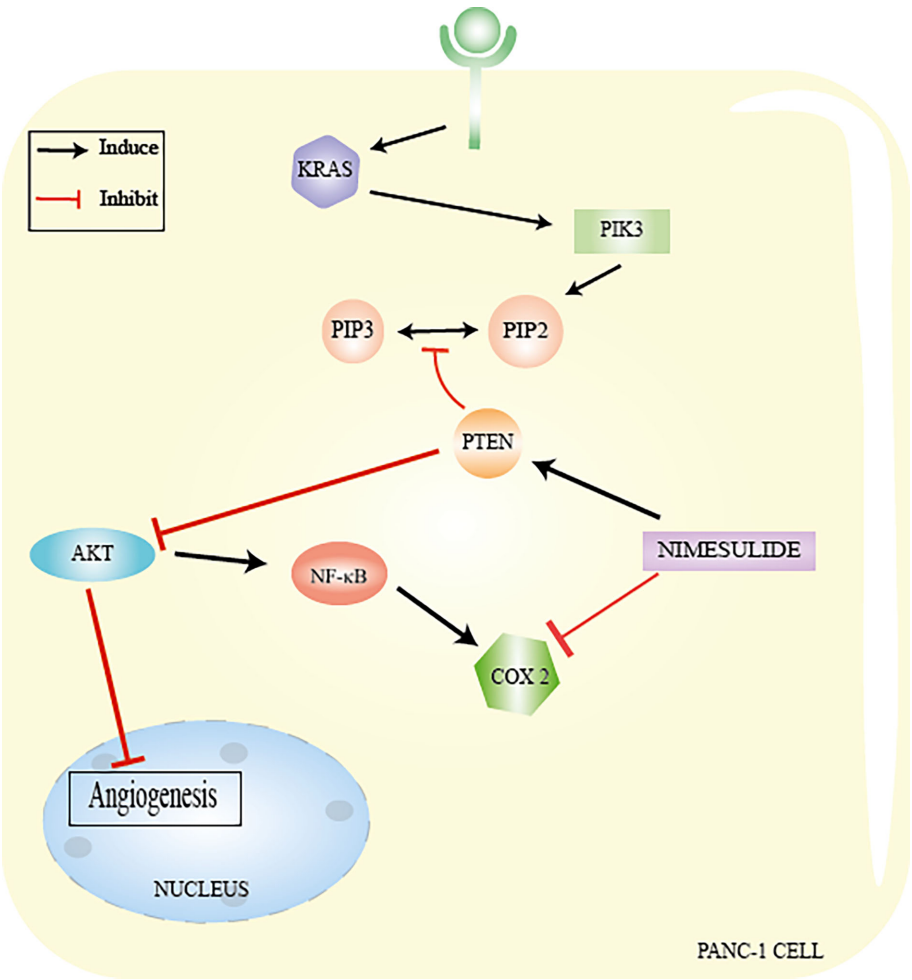


**FIGURE 5** | Nimesulide in PANC–1 cells. Nimesulide inhibits proliferation and promotes apoptosis of PANC-1 cells (cell line isolated from a ductal pancreatic adenocarcinoma) *via* increased expression of PTEN. AKT regulates a series of important effector proteins, such as NFkB, COX-2, VEGF, Bcl-2, and Bax. Nimesulide inhibits angiogenesis by inducing an increase in PTEN levels and leading to suppression of AKT by decreasing VEGF levels. PTEN reactivation appears to be related to a decreased expression of COX-2 and also acts by suppressing AKT and consequently inhibiting NF-kB, which decreases the expression of COX-2. From: Author.

Agency (EMA) restricted the indications for this NSAID and recommended a maximum daily dose of 200 mg (61, 70). New reports of fulminant liver failure cases requiring liver transplantation resulted in nimesulide commercialization being suspended in 2007 and led to a new safety review of the drug (61, 70). The review of the safety standards of the drug was completed in 2012, and found that the benefits of nimesulide outweigh the risks of potential liver toxicity (61, 70).

Liver damage associated with nimesulide is mainly caused by metabolites formed from its biotransformation in the liver. This process generates nitrous or hydroxylamine derivatives (19, 71), the most important being M1 [2-(4′-hydroxyphenoxy)-4-nitro-methanesulfonanilide:4-hydroxinumesulide], which can be easily traced and found in the plasma (71, 72). An isoenzyme of the cytochrome P450 family, CYP1A2 may be responsible for the hydroxylation of nimesulide (71, 73, 74). However, CYP2C9 and CYP2C19 may also be involved (71, 73) together with nitroreductases, which are flavoproteins responsible for the reduction of nitroarenes to aminoarenes (71, 75).

The mechanism involved in hepatotoxicity has not yet been fully elucidated; however, both mitochondrial dysfunction and oxidative stress have been implicated in the contribution to liver injury (19, 71). Mitochondria are the main sources of energy, also acting as the signaling center responsible for the beginning of cell death (apoptosis or necrosis), regardless of the route (19, 71).

In this organelle, the biotransformation of nimesulide generates reactive metabolites derived from nitrous or hydroxylamine (19, 76). The nitro group (O=N=O) has the ability to interfere with energy production and intracellular calcium hemostasis (77). Nimesulide transfers protons to the mitochondrial matrix, decreasing the membrane potential and increasing respiration (19). The increase in mitochondrial respiration leads to a progressive depletion of the enzyme nicotinamide adenine nucleotide phosphate (NADP), the oxidation and depletion of glutathione, and an intracellular increase in reactive oxygen species (ROS) (76).

The physical, chemical, and pharmacological limitations of nimesulide include low solubility and availability and proven hepatotoxicity, which compromises its efficacy and safety of use (53, 77–79). It is therefore necessary to use new transport systems as a strategy to improve the medication, seeking to meet requirements for optimal distribution and, consequently, reduce adverse effects (78, 79). Nanoparticles are particles ranging in size from 10 to 1,000 nm in diameter, which function as drug transport and distribution systems and whose main advantages are increased bioavailability, solubility, and the specificity of the action of the drug (78, 79). These benefits favor a reduction in the amount of drug needed to produce the ideal therapeutic effect, leading to a decrease in its toxicity and side effects for non-target tissues and cells (78, 79).

## NANOPARTICLES IN CANCER TREATMENT

Nanotechnology is emerging in cancer therapy as a promising field of interdisciplinary research (80, 81). The versatility, flexibility, and adaptability of nanoparticulate delivery systems have shown potential for providing the necessary health care for patients, improving their adherence to treatment (80, 81). Nanoparticles are formed by groups of particles of different sizes, shapes, materials, and chemical and surface properties (80, 81). These systems can be divided into two main groups: organic and inorganic carriers. Organic nanoparticles can be subdivided into polymers (homopolymers and copolymers) and lipids (80, 81). Homopolymers include nanospheres, nanocapsules, hydrogel, and dendrimers, and copolymers are micelles and polymersomes. The lipid category comprises solid lipids, liposomes, and micelles, while inorganic nanoparticles are metallic nanoparticles, fullerenes, carbon nanotubes, and ceramic nanoparticles (80, 81) (**Figure 6**). Solid lipid nanoparticles stand out from the others for the following advantages: the use of biodegradable physiological lipids that reduce acute and chronic toxicity and avoid the use of organic solvents in production methods, improving the solubility of hydrophilic and lipophilic drugs; specificity in medication administration; skin penetration by dermal application; large scale production using a high pressure homogenization technique; the control and release of modified drugs; the protection of labile chemical agents against chemical, photochemical, and oxidative degradation; better stability (for up to three years); increased drug bioavailability; a high concentration of the functional compound; and controlled drug release over several weeks (79, 81, 82).

## ORGANIC NANOPARTICLES

### Homopolymers

#### Nanocapsules

Nanocapsules are nano-vesicular systems (smaller than 200 nm) with a hollow spherical core–shell structure, surrounded by a membrane or polymer coating (83–85). The internal cavity can be filled with lipophilic or hydrophilic substances, in liquid form (polar or non-polar), solid form, or as a dispersion of molecules (83–85). These systems can be prepared by the interfacial deposition of preformed polymers and also by the solvent displacement technique, in which an oil is added to the organic stage of the process (83–85). Nanocapsules are used as intelligent drug carriers with specific chemical receptors that bind only to specific cellular receptors; other advantages in their use include the rapid absorption of active substances, greater bioavailability of the drug, greater safety and therapeutic efficacy, and improved patient adhesion to treatment (83–85).

#### Experimental Study

Huerta et al. (53) used nanoparticles loaded with nimesulide prepared from polylactide-co-glycolide (PLGA) (NPNS) and eventually coated then with chitosan (NPNSCS) (using the emulsion-solvent evaporation technique). Characterization of the nanoparticles showed an ideal size of 379.59 nm for NPNS and 393.66 nm for NPNSCS and zeta potentials of 15.3 mV for NPNS at 10.4 mV for NPNSCS, suggesting an efficient coating. The drug encapsulation rate was 30 and 70%, with NPNSCS and

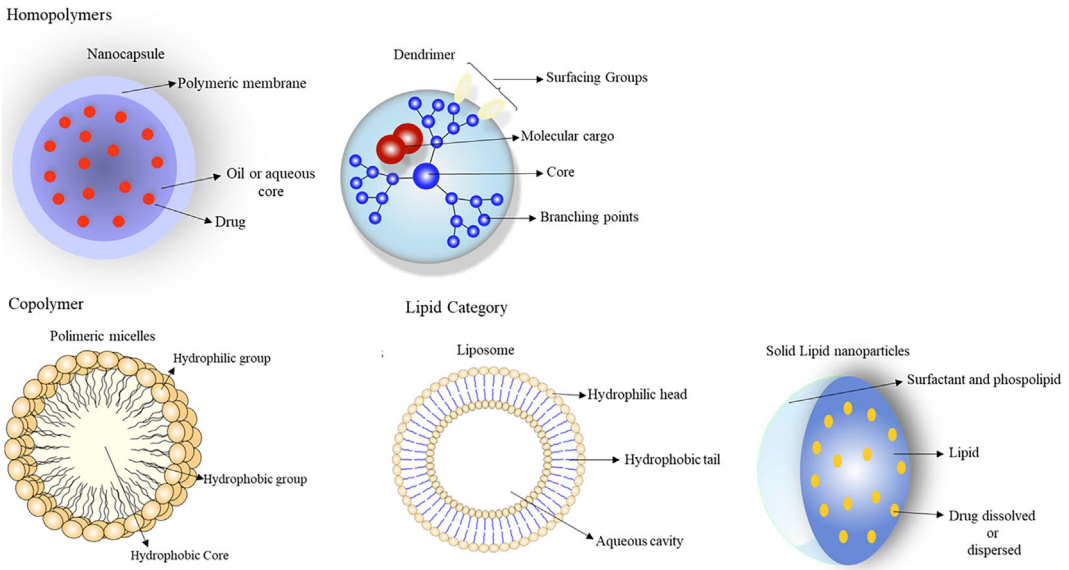


**FIGURE 6** | These systems can be divided into two main groups: organic and inorganic carriers. Organic nanoparticles can be subdivided into: polymeric (homopolymers and copolymers) and lipids. Homopolymers include: nanospheres, nanocapsules, hydrogel, and dendrimers; copolymers are micelles and polymersomes. The lipid category comprises solid lipids, liposomes, and micelles, since metallic nanoparticles, fullerenes, carbon nanotubes, and ceramic nanoparticles are inorganic nanoparticles. From: Author.

NPNS diluted 1/100 in PBS, respectively. An *in vitro* permeability assay of the nanocarriers demonstrated the permeability of free nimesulide as 1–1.5 105 cm/s when compared with NPNS 6.4–8.1 106 cm/s, and NPNSCS = 5.5–7.0 106 cm/s using the PAMPA (parallel artificial membrane) assay. *In vitro* cytotoxicity was tested in prostate cancer cells PC-3 and DU-145, showing a dose-dependent effect on the proliferation of PC-3 and DU-145 cells, the latter being more sensitive (IC50 139 and 90 mM, respectively). NPNS incubated with PC-3 cells showed a less inhibitory effect than the free drug (IC50 242 mM), and NPNSCS had the same inhibitory effect as the free drug (IC50 89 mM).

Senguel-Turk et al. (64) developed a poly (ethylene glycol)-block-poly ($\epsilon$-caprolactone) nanocapsule (PEG-b-PCL) with nimesulide to assess its anticancer activity against MCF-7 breast cancer cells. PEG-b-PCL was encapsulated with nimesulide using three different production techniques: emulsion solvent evaporation using a high-shear homogenizer (method H), evaporation of emulsion-solvent using an ultrasonicator (method U), and nanoprecipitation (method N). The nanoparticles were evaluated for particle size, drug release rates, *in vitro* cell viability assays (MTT) and apoptosis (cytofluorometric analyses). All nanoparticle formulations in the cumulative dissolution profiles *in vitro* exhibited a biphasic release pattern that demonstrated a greater burst of drug release with the sustained release of nimesulide. The amount of drug released from the nanoparticles was approximately 63% for Method H, 54% for Method U, and 68% for Method N in the first 24 h. A particle size below 200 nm caused an increase in the rate of drug release (Method N). At a particle size of 200–250 nm, however, the drug release rate decreased by the U method and increased by the H method. Cell viability was shown to be reduced in both free and conjugated forms with nimesulide nanoparticles, with doses ranging from 10 to 500 µM. At doses of 10 and 100 µM, the free nimesulide caused 92.29 ± 2.05% and 88.51 ± 7.52% of cell viability, respectively. Both the U method (57.31 ± 10.39% at 10 µM and 45.04 ± 6.94% at 100 µM) and the N method showed more cytotoxicity in the profile (47.96 ± 5.22% at 10 µM and 46.83 ± 5.81% at 100 µM) of cell viability. Cytofluorimetric analysis of apoptotic events was performed through exposure to annexin V in MCF-7 cells, showing that 48 h of treatment with 250 and 500 µM free and a nanoparticle form prepared using the U method (the only method tested) induced more than 50% of MCF-7 cells to undergo apoptosis compared to control.

## Dendrimers

Dendrimers are branched macromolecules (2–10 nm in diameter) with a three-dimensional tree-like structure, with a specific shape (globular, spherical), specific size and with a great deal of functionality and versatility (86–89). These nanoparticles are monodispersed, composed of an atom or a group of atoms (central symmetrical nucleus), and internal layers (generations) composed of repeated units, where branches of carbon and other elements are added by chemical reactions or physical interventions, conferring the unique properties of this nanocarrier (terminal functionality) (86–89).

Dendrimers have multiple applications, such as electron catalysis, drug release, gene therapy, and chemotherapy, and are synthesized using different techniques: divergent growth, convergent growth, double and mixed exponential growth, hypercores and branched monomer growth, Lego chemistry,

and click chemistry (86–89). Types include polypropylene imine dendrimers (PPIs), polyamidoamine dendrimers (PAMAMs), Frechet type dendrimers, core–shell dendrimers, chiral dendrimers, liquid-crystalline dendrimers, peptide dendrimers, peptide dendrimers, dendrimer peptides glycodendrimers, hybrid dendrimers, and polyester dendrimers (86–89).

There are many advantages to using this polymeric system, including varied sizes of scale, providing dimensions of biological building blocks for proteins and DNA; the aggregation of specific functional groups on the terminal surface; an adequate number of functional groups for drug bio-conjugation; signaling groups; targeting portions or biocompatibility groups; and an empty interior space that can be used to encapsulate small molecule drugs (reduces drug toxicity and facilitates controlled release) (86–89).

### Experimental Study

Murugan et al. (90) used the generation 3 quaternized poly (propylene imine) dendrimer (QPPI G3) as a carrier of the poorly soluble nimesulide drug. The transport potential of this dendrimer for the drug was evaluated through studies of solubility (phase solubility analysis method), *in vitro* release (dialysis method) and *in vitro* cytotoxicity (MTT diphenyltetrazolium bromide colorimetric assay). The results showed that the solubility of nimesulide increased in the presence of QPPI G3 (0.05 to 0.35 mM), just as this dendrimer allowed the sustained release of the drug (35.69% after 5 h). Cytotoxicity studies (cell line Vero and HBL-100) showed that QPPI G3 increases the biocompatibility and the tolerated concentration of nimesulide in dendrimer formulations (IC50 of 0.56 mM Vero and 0.42 mM in HBL-100).

Uram et al. (63) carried out studies with the third-generation poly (amidoamine) dendrimer (PAMAM) biotinylated conjugates with covalently linked 18 (G3B18N) and 31 (G3B31N), both linked to nimesulide. This nanoparticle was evaluated for its biological properties, including *in vitro* cytotoxicity (MTT method), proliferation and caspase 3/7 activities in relation to COX-2/PGE2 (prostaglandin) signaling in normal human fibroblasts (BJ) and carcinoma of squamous cells (SCC-15). The G3B18N conjugate was significantly cytotoxic against SCC-15 cells at a concentration of 5 μM and against BJ cells at a concentration of 10 μM (about 70 and 55% of cell viability, respectively). For the G3B31N conjugate, the viability value of SCC-15 cells was 1.25 μM and that of BJ cells was 2.5 μM. In the proliferation assay, G3B18N exercised high selectivity against cancer cells. The inhibition of SCC-15 cell proliferation was observed at a concentration of 2.5 μM, with a decrease in the number of cells to about 30%, with no significant changes observed in normal fibroblasts. G3B31N inhibited proliferation at a concentration of 1.25 μM for both SCC-15 and BJ cells. Dendrimer conjugates have a pro-apoptotic effect, with greater caspase 3/7 activity observed in fibroblasts. The most significant stimulatory effect of G3B18N was observed at concentrations of 5–10 μM. Caspase activity was doubled in BJ at the 10 μM concentration and increased by 60% in SCC-15 cells. The effect of the G3B31N conjugate was much more pronounced, particularly for fibroblasts. In BJ cells, an increase in caspase activity was observed by 2.5 μM. A minor but significant effect was seen in SCC-15 cells. At the 2.5 μM concentration, the increase in caspase activity was 150%. Caspase 3/7 activity was dependent on the increase in PGE2 production by COX-1/COX-2 (63).

## Copolymers

### Polymeric Micelles

Polymeric micelles are nanometric, spherical, and colloidal particles (diameter less than 100 nm) that can be produced by copolymer self-assemblies (89, 91–94). This nanoparticle has a shell-like inner core that serves as the storage of hydrophobic (lipophilic) molecules and is surrounded by a hydrophilic polymeric outer shell (89, 91–94). In an aqueous system, the hydrophobic portion of amphiphilic molecules form the nucleus of the micelle, while the hydrophilic portion forms the crown (89, 91–94). This is due to the formation of a Van der Waals bond resulting from free energy in the system (89, 91–94). In a polymeric micellar system, pharmaceutical products of a non-polar character are bound within the nucleus, while polar substances are retained on the surface of the micelle, and the intermediate polarity molecules are distributed along the intermediate polarity molecules (91, 92, 94).

Micellar nanoparticles follow specific criteria for their best functioning, involving: critical micellar concentration (balance between the concentrations of hydrophilic and hydrophobic molecules)—the lower the critical micellar concentration, the greater the solubility for the drug carried and the greater the micellar stability; a critical micellization temperature; and the size and shape of the final structure (89, 92, 94). These criteria are dependent on the conformation of the polymer chains in copolymer blocks; for example, lengths of a remarkably high hydrophilic block prevent the formation of copolymers in water, and on the other hand, exceptionally long hydrophobic molecules form blocks of non-micellar structure such as rods and lamellae (92, 94).

The micellar nucleus must have a high load capacity, controlled drug release profile, and compatibility between the nucleus-forming polymers and the drug (91, 92). The micellar crown must determine the hydrophilicity of the micelle, the charge, the length, and the surface density of the hydrophilic blocks, as well as the presence of reactive groups suitable for other micelles (91, 92). These characteristics of the crown control the important pharmacokinetic and pharmacodynamic parameters of a micellar transporter, such as its biodistribution, biocompatibility, longevity, surface adsorption of biomacromolecules, adhesion to biosurfaces, and targeting capacity (91, 92).

The hydrophilic micellar crown can be composed of copolymers of blocks of polyethylene glycol (PEG) with a molecular weight of 1 to 15 kDa (92), or a poly(N-vinyl-2-pyrrolidone) (PVP) or poly(alcohol vinyl), poly(vinyl alcohol-covinyloleate) copolymer, oligomeric hydrophilic polyethyleneimine block (92). The hydrophobic micellar nucleus can be made up of propylene oxide monomers, L-lysine, aspartic acid, b-benzoyl-L-aspartate, g-benzyl-L-glutamate, caprolactone, D, L-lactic acid, and spermine (95–99).

The main advantages of polymeric micellar nanoparticles as drug carriers are: increased water solubility of moderately insoluble drugs, increased bioavailability, capability to load micelles with 5 to 25% of the drug, reduced toxicity and adverse effects, the capability of small size micelles to facilitate drug accumulation in areas of the body with compromised vasculature, increased half-life in the blood after intravenous administration, and protection against the inactivation of biological medication agents (91, 92, 100).

### Experimental Study

Parmar et al. (101) characterized micellar nanoparticles of nimesulide *in vitro*, solubilized in three block copolymers; PEO (polyethylene oxide), PPO (polypropylene oxide), and PEO. The micellar parameters of such copolymers were characterized using dynamic light scattering (to evaluate hydrodynamic diameter) and UV-VIS spectrophotometry (evaluating the critical micellar concentration and critical micellar temperature). The data showed that when nimesulide was used at a concentration of 0.045 mmol $L^{-1}$ and 3,250 g $mol^{-1}$ with different% TPEO = 30, 40, and 50%, respectively, in aqueous solutions, these copolymers showed a decrease in aggregates in a temperature of up to 30°C, maintaining a particle size of 15 nm. These data are in accordance with the ideal characteristics for its use as a nano-container of hydrophobic drugs.

Wang et al. (102), evaluated the anti-inflammatory profile of a delivery system of polymeric micelles modified by peptides loaded with low doses of methotrexate and nimesulide in a fixed dose combination. The micellar nanoparticulate system (5.6 µl/mg of both drugs) inhibited angiogenesis in SD rats (intravenously), and also reduced joint swelling, bone erosion, and serum levels of inflammatory cytokines (nanoparticle containing 0.6 mg/kg of methotrexate and 3.0 mg/kg of nimesulide). The polymeric micelles (25 and 65 nm) were prepared using the filming-rehydration method, with a combination of RGD-PEG3400-PLA2000 peptide preformed with copolymer (40 mg).

## Lipid Nanoparticles

### Liposomes

Liposomes are spherical vesicles of 0.05–5.0 µm in diameter formed by two layers, where the aqueous volume is surrounded by a membranous lipid bilayer composed of natural or synthetic phospholipids, such as cholesterols, non-toxic surfactants, sphingolipids, glycolipids, chain long fatty acids, and even membrane proteins (103–105). These liposomal systems can be encapsulated with lipophilic drugs and can be used in diseases such as cancer (103–105). They can also transport water and non-ionic substances, thus offering protection against oxidative wear, improving the stability of linked drugs and controlling the hydration of the molecule (103–105). Liposomes release the drug in a sustained way so as to improve its pharmacokinetics, reducing the dose necessary for a therapeutic effect and causing a decrease in toxicity. These formulations are also capable of directing the drug to specific sites of action, such as cancer cells, thus preserving healthy cells and optimizing therapy. However, this system has some limitations regarding its use, such as a short half-life, the oxidation of phospholipids, high production cost, and allergic reactions to constituents of the liposome (103–105).

Liposomal vesicles carry drugs using passive and active carrier techniques (103–105). Passive transport can be by three methods: mechanical dispersion (lipid hydration by manual agitation or freeze drying, micro emulsification, sonication, French pressure cell, membrane extrusions, dry reconstituted vesicle, freeze–thawed liposome), solvent dispersion (ethanol injection, ether injection, double emulsion vesicle, reverse phase evaporation vesicle, stable plurilamellar vesicle), and detergent removal (detergent removed from mixed micelles, column chromatography dialysis) (103–105).On the other hand, active loading can be done by mechanical dispersion, solvent dispersion, and detergent solubilization (103–105).

Liposomes can also be classified according to the structure (small unilamellar vesicle, large unilamellar, giant unilamellar, multilamellar, oligolamellar, multivesicular), preparation method (passive or active), composition (conventional liposome, fusogenic liposome, liposomes pH sensitive, cationic liposomes, long-circulating liposome, immunoliposome), and as conventional liposomes (stabilizing mixtures of natural lecithin, synthetic identical chain phospholipids, glycolipids containing liposomes) and specific liposomes (bipolar fatty acid, antibody-directed liposome, liposome linked to 3-methyl/methylene, liposome coated with carbohydrate, multiple encapsulated liposomes) (103–105).

### Experimental Study

Ferreira et al. (106) quantified the extent of the interaction between liposomal nimesulide (50 µmol $L^{-1}$ prepared by dry evaporation) and membrane phospholipids using parameters such as the partition coefficient (Kp) and egg phosphatidylcholine (EPC) as cell membrane models. The liposome/aqueous phase partition coefficients were determined under physiological conditions by derived spectrophotometry and fluorescence extinction. The two techniques produce similar results, in which the membrane surface is not altered, indicating that the liposomal nimesulide binds to the lipid bilayer mainly through hydrophobic interactions.

Studies carried out by Kumar et al. (107) characterized the liposomal drug release system for nimesulide (drug, 10 mg; lipid, 40–60 mg; cholesterol, 40–50 mg; and stearic acid, 10 mg) prepared using two methods: ethanol injection and technique rotary evaporator. Preparation using the injection method showed an average particle size between 270 and 703 nm, with the drug entrapment percentage varying between 49 and 58%, drug release between 65 and 71% and the zeta potential −21.23 mV. Using the rotary evaporation technique, the average particle size was 1–12 µm, drug entrapment percentage 69–86%, drug release 76.97%, and the zeta potential −26.78 mV. The rotary evaporator technique thus proved to be the best method for preparing liposomal nimesulide.

## SOLID LIPID NANOPARTICLES

Polymeric nanoparticle systems are produced from synthetic or natural polymers and initially emerged as an alternative for drug

delivery; however, the shortage of safe polymers, the lack of regulatory approval, and the high cost of production limited the use of these nanoparticles in the pharmaceutical field (78, 81, 108). In order to overcome these limitations, solid lipid nanoparticles that were colloidal dispersions of submicron size (less than 1,000 nm) were launched on the market, where the liquid lipid matrix (oil) was replaced by a physiological solid lipid (waxes) (79, 81, 108, 109).

Solid liquid nanoparticles are formed by a mixture of solid lipids, emulsifiers, and solvent (78, 79, 110). The lipids used in these formulations are biocompatible, fully tolerated by the body, and can be triglycerides (tri-stearin, corn, olives, peanuts, soy oils, vegetable oils), fatty acids (stearic acid, palmitic acid), steroids (cholesterol), and waxes (cetyl palmitate) (78, 79, 110). Various emulsifiers and their combinations (poloxamer, polysorbates, lecithin, and bile acids) are used to stabilize dispersed lipids, preventing lipid clumping more efficiently (78, 79, 110). These nanoparticulate conveyors can be manufactured using various methods, such as the high hot and cold pressure homogenization technique (allows for large scale production), high speed ultrasound or homogenization, solvent emulsification/evaporation, microemulsion, spray drying, and double emulsion (78, 79, 110).

After preparing these nanoparticles, it is necessary to make the appropriate characterization for their quality control (82, 108, 110). The most important parameters to evaluate include particle size, size distribution kinetics (zeta potential), degree of crystallinity, and lipid modification (polymorphism), the coexistence of additional colloidal structures (micelles, liposomes, supercooled, melts, drug nanoparticles), process distribution time scale, drug content, *in vitro* drug release and surface morphology (82, 108, 110). Nanoparticulate carriers generally deliver the drug using two processes: active or passive delivery (111, 112).

## ACTIVE DELIVERY MECHANISMS

A tumor has a high rate of cell proliferation and a high demand for nutrients, causing an overexpression of transporters in order to nourish the tumor cells (111–113). Active delivery by nanoparticles is based on the recognition of target molecules on the surface of tumor cells as overexpressed receptors or transporters, redirecting the supply of drugs selectively to neoplastic cells, decreasing both damage to normal cells and side effects (111–113). In this mechanism, nanoparticles are designed to adhere to specific biological structures in tumors through the recognition of ligands attached to the surface (111–113).

## PASSIVE DELIVERY MECHANISM

Passive delivery is based on the accumulation of the drug or the transport system with the drug at a target location (111–113). This process is possible due to the physicochemical characteristics inherent in the size of the nanoparticle and pharmacological factors related to cancer, such as tumor vasculature, the permeability and retention effect, and tumor microenvironment (111–113). Angiogenesis in the tumor environment favors the development of irregular blood vessels with discontinuous epithelium. This epithelial irregularity between cells (size between 100 and 800 nm), allows the displacement of nanoparticles through the interstitial space (111–113).

Tumor tissues are characterized by lymphatic dysfunction with insufficient drainage, enabling the accumulation of nanoparticles in the tumor cell (111–113). The transport of nanoparticles benefited by the permeability and retention process does not work for all types of tumors, because it depends on many factors, such as the type and size of the stomach tumor (111–113). Drug accumulation was greater in pancreatic, breast, colon and stomach tumors (111–113).

## EXPERIMENTAL STUDY

Bondi et al. (111) described the preparation, physicochemical characterization, and *in vitro* antitumor activity of nimesulide solid lipid nanoparticles administered parenterally in human colorectal cancer HT-29 and SW-480 cells present in solid tumors. Four samples of nanoparticles loaded with the drug were prepared using palmitic acid (Sample A), stearic acid (Sample B), Compritol 888 ATO (sample C), and a mixture of Compritol 888 ATO and 20% Miglyol as the lipid matrix total lipid weight (Sample D).

Nimesulide nanoparticles were prepared using the precipitation technique, with Epikuron 200 and taurocholate sodium salt as surfactant and co-surfactant, respectively, because they are acceptable components through parenteral administration. All samples were characterized in terms of particle size, PDI (polydispersity index), and zeta potential. The results showed that all nanoparticles with the drug had an ideal size (colloidal size ranging from 93 to 170 nm) and were homogeneous, with very small PDI values and negative surface load values (111).

The load capacity (LC%) of nanoparticles, evaluated by dissolving the batch in chloroform and subsequent HPLC analysis of the solution, was 9.3, 8.7, 17.8, and 15.8% by weight, respectively. The results also showed that the survival of HT-29 and SW480 cells decreased in a dose-dependent manner in the presence of free nimesulide or nanoparticles loaded with the drug, demonstrating that nimesulide activity is not reduced in the presence of the nanoparticle carrier (111).

Pushpendra et al. (114) developed, characterized, and tested the solid lipid nanoparticles of nimesulide for their controlled release *in vitro*. The preparation of the nanoparticle was based on emulsification and the low temperature solidification method. Various formulations were prepared based on individual factors, such as agitation speed (500, 1,000, 2,000, and 3,000 rpm), agitation time (15, 30, 45, and 60 min), and formulation parameters (concentration of lecithin surfactant,

concentration drug concentration and surfactant concentration) in trapping efficiency.

Ab agitation speed of 3,000 rpm resulted in nanodispersion, characterized by a spherical shape under photon correlation spectroscopy, with an average diameter of 187 ± 1.23 nm, and a trapping efficiency of approximately 60%. The concentrations of lecithin, drug, and sodium taurocholate (solid lipid) were optimized with respect to trapping efficiency, and optimum concentrations were 10, 10, and 0.8% respectively (114).

Drug release from the solid lipid nanoparticle appears to consist of two phases: an initial rapid release followed by a slower exponential stage. The results obtained in up to 2 h of study of the drug release *in vitro* were not considered, since the effect of the explosion does not correspond to the real drug release mechanism in solid nanoparticles (114).

Campos et al. (115) produced a formulation of solid lipid nanoparticles for carrying nimesulide using the high pressure hot homogenization (HPH) method. The optimized formulation was composed of 10% by weight of glyceryl behenate and 2.5% by weight of poloxamer 188, solid lipid and surfactant respectively. Immediately after production, the Z-ave of the nanoparticle carried with the drug (mean particle size) was 166.1 ± 0.114 nm, with a PI index of 0.171 ± 0.051, and an almost neutral zeta potential of −3.10 ± 0.166 mV.

The release profile of the particle with nimesulide followed a sustained pattern, with 30% of the drug released within 24 h. The cytotoxicity of both the free drug and the nanoparticle carrying nimesulide was tested in Caco-2 cells of human colon adenocarcinoma and demonstrated activity in the concentration of 100 µg/ml up to 48 h with a cell viability of 80%. Long-term stability studies have shown that both the free drug and the nanoparticle carrying nimesulide were physically stable, attributed to changes below 10% in TurbiscanLab® (instrument used to measure quality control parameters) (115).

## CONCLUSION

Solid lipid nanoparticles have potential alternative for the treatment of pancreatic cancer, as they have the ability to interfere in the permeability of nimesulide at extra and intracellular levels. This improves the action of nimesulide in increasing the levels of PTEN expression and, consequently, inhibiting the processes of proliferation and apoptosis in PanIN lesions in the cells of the pancreas. Solid lipid nanoparticles are biocompatible lipids with low toxicity, which, in addition to maintaining the pharmacological activity of nimesulide, allow its administration through various routes, such as oral, intratumor, intravenous, and intradermal injection. They are also synthesized at low cost, and are a viable and commercially important alternative in the treatment of cancer.

To date, no experimental study has been carried out to evaluate the activity of these nimesulide nanopaths in regulating PTEN expression levels and inhibiting pancreatic cancer lesions. Preclinical studies such as *in vitro* and *in vivo* tests are therefore needed to clarify important aspects such as the effectiveness and toxicity of this nanoparticulate system. We thus conclude that these results are limited by the lack of experimental information about nimesulide in solid lipid nanoparticles allowing an effective and tolerated dose to be predicted and the most appropriate route of administration in pancreatic cancer therapy.

## AUTHOR CONTRIBUTIONS

All authors contributed to the article and approved the submitted version. MM participated in the study coordination and helped to draft the manuscript. RF, LN, KE, AR, and WL have designed and prepared the manuscript figures.

## FUNDING

The authors were supported by the Brazilian's agencies: Conselho Nacional de Desenvolvimento Científico e Tecnológico (CNPq), Coordenação de Aperfeiçoamento de Pessoal de Nível Superior (CAPES), Fundação Amazônia Paraense de Amparo à Pesquisa (FAPESPA), Federal University of Pará, and MM thanks for the fellowship from CNPq.

## REFERENCES

1. Rovasio RA. Development and Structure of the Pancreas. In: *Pancreatic Cancer* (2010). New York, NY: Springer New York. p. 27–38. doi: 10.1007/978-0-387-77498-5_2
2. Murtaugh LC, Cleaver O, MacDonald RJ. *Developmental Molecular Biology of the Pancreas*. Springer New York (2018) . doi: 10.1007/978-1-4939-7193-0_4
3. Aier I, Semwal R, Sharma A, Varadwaj PK. A Systematic Assessment of Statistics, Risk Factors, and Underlying Features Involved in Pancreatic Cancer. *Cancer Epidemiol* (2019) 58:104–10. doi: 10.1016/j.canep.2018.12.001
4. Li S, Gu Z, Xiao Z, Zhou T, Li J, Sun K. Anti-Tumor Effect and Mechanism of Cyclooxygenase-2 Inhibitor Through Matrix Metalloproteinase 14 Pathway in PANC-1 Cells. *Int J Clin Exp Pathol* (2015) 8:1737–42.
5. Gupta R, Amanam I, Chung V. Current and Future Therapies for Advanced Pancreatic Cancer. *J Surg Oncol* (2017) 116:25–34. doi: 10.1002/jso.24623
6. Jiang J, Zhou H, Ni C, Hu X, Mou Y, Huang D, et al. Immunotherapy in Pancreatic Cancer: New Hope or Mission Impossible? *Cancer Lett* (2019) 445:57–64. doi: 10.1016/j.canlet.2018.10.045
7. Morrison AH, Byrne KT, Vonderheide RH. Immunotherapy and Prevention of Pancreatic Cancer. *Trends Cancer* (2018) 4:418–428. doi: 10.1016/j.trecan.2018.04.001
8. Kamisawa T, Wood LD, Itoi T, Takaori K. Pancreatic Cancer. *Lancet* (2016) 388:73–85. doi: 10.1016/S0140-6736(16)00141-0
9. Jelski W, Mroczko B. Biochemical Diagnostics of Pancreatic Cancer - Present and Future. *Clin Chim Acta* (2019) 498:47–51. doi: 10.1016/j.cca.2019.08.013
10. Tanaka S. Molecular Pathogenesis and Targeted Therapy of Pancreatic Cancer. *Ann Surg Oncol* (2016) 23:197–205. doi: 10.1245/s10434-015-4463-x
11. Benzel J, Fendrich V. Familial Pancreatic Cancer. *Oncol Res Treat* (2018) 41:611–8. doi: 10.1159/000493473

12. Wood LD, Yurgelun MB, Goggins MG. Genetics of Familial and Sporadic Pancreatic Cancer. *Gastroenterology* (2019) 156:2041–55. doi: 10.1053/j.gastro.2018.12.039
13. Ying H, Dey P, Yao W, Kimmelman AC, Draetta GF, Maitra A, et al. Genetics and Biology of Pancreatic Ductal Adenocarcinoma. *Genes Dev* (2016) 30:355–85. doi: 10.1101/gad.275776.115
14. Maitra A, Kern SE, Hruban RH. Molecular Pathogenesis of Pancreatic Cancer. *Best Pract Res Clin Gastroenterol* (2006) (2):211–26. doi: 10.1016/j.bpg.2005.10.002
15. Roseweir AK, Powell AGMT, Bennett L, Van Wyk HC, Park J, McMillan DC, et al. Relationship Between Tumour PTEN/Akt/COX-2 Expression, Inflammatory Response and Survival in Patients With Colorectal Cancer. *Oncotarget* (2016) 7:70601–12. doi: 10.18632/oncotarget.12134
16. Chu M, Wang T, Sun A, Chen Y. Nimesulide Inhibits Proliferation and Induces Apoptosis of Pancreatic Cancer Cells by Enhancing Expression of PTEN. *Exp Ther Med* (2018) 16:370–6. doi: 10.3892/etm.2018.6191
17. Turanli B, Altay O, Borén J, Turkez H, Nielsen J, Uhlen M, et al. Systems Biology Based Drug Repositioning for Development of Cancer Therapy. *Semin Cancer Biol* (2019) 47–58. doi: 10.1016/j.semcancer.2019.09.020
18. Nowak-Sliwinska P, Scapozza L, Ruiz i Altaba A. Drug Repurposing in Oncology: Compounds, Pathways, Phenotypes and Computational Approaches for Colorectal Cancer. *Biochim Biophys Acta - Rev Cancer* (2019) 1871:434–54. doi: 10.1016/j.bbcan.2019.04.005
19. Berson A, Cazanave S, Descatoire V. The Anti-Inflammatory Drug, Nimesulide (4-Nitro-2-Phenoxymethane-Sulfoanilide), Uncouples Mitochondria and Induces Mitochondrial Permeability Transition in Human. *J Pharmacol Exp Ther* (2006) 318:444–54. doi: 10.1124/jpet.106.104125
20. Cappellani A, Cavallaro A, Di Vita M, Zanghi A, Piccolo G, Lo Menzo E, et al. Diet and Pancreatic Cancer: Many Questions With Few Certainties. *Eur Rev Med Pharmacol Sci* (2012) 16:192–206.
21. Lin QJ, Yang F, Jin C, Fu DL. Current Status and Progress of Pancreatic Cancer in China. *World J Gastroenterol* (2015) (26):7988–8003. doi: 10.3748/wjg.v21.i26.7988
22. Tamm EP, Silverman PM, Charnsangavej C, Evans DB. Diagnosis, Staging, and Surveillance of Pancreatic Cancer. *Am J Roentgenol* (2003) 180:1311–23. doi: 10.2214/ajr.180.5.1801311
23. Ilic M, Ilic I. Epidemiology of Pancreatic Cancer. *World J Gastroenterol* (2016) 22:9694. doi: 10.3748/wjg.v22.i44.9694
24. He XY, Yuan YZ. Advances in Pancreatic Cancer Research: Moving Towards Early Detection. *World J Gastroenterol* (2014) 20:11241–8. doi: 10.3748/wjg.v20.i32.11241
25. Goral V. Pancreatic Cancer: Pathogenesis and Diagnosis. *Asian Pacific J Cancer Prev* (2015) 16:5619–24. doi: 10.7314/APJCP.2015.16.14.5619
26. Zhang Q, Zeng L, Chen Y, Lian G, Qian C, Chen S, et al. Pancreatic Cancer Epidemiology, Detection, and Management. *Gastroenterol Res Pract* (2016) 2016:1–10. doi: 10.1155/2016/8962321
27. Neureiter D, Jäger T, Ocker M, Kiesslich T. Epigenetics and Pancreatic Cancer: Pathophysiology and Novel Treatment Aspects. *World J Gastroenterol* (2014) 20:7830–48. doi: 10.3748/wjg.v20.i24.7830
28. McGuigan A, Kelly P, Turkington RC, Jones C, Coleman HG, McCain RS. Pancreatic Cancer: A Review of Clinical Diagnosis, Epidemiology, Treatment and Outcomes. *World J Gastroenterol* (2018) 24(43):4846–4861. doi: 10.3748/wjg.v24.i43.4846
29. Magee CJ, Greenhalf W, Howes N, Ghaneh P, Neoptolemos JP. Molecular Pathogenesis of Pancreatic Ductal Adenocarcinoma and Clinical Implications. *Surg Oncol* (2001) 10:1–23. doi: 10.1016/S0960-7404(01)00016-0
30. Grant TJ, Hua K, Singh A. Molecular Pathogenesis of Pancreatic Cancer. In: *Progress in Molecular Biology and Translational Science.* (2016) 144:241–75. doi: 10.1016/bs.pmbts.2016.09.008
31. Lawrence T. The Nuclear Factor NF-kappaB Pathway in Inflammation. *Cold Spring Harb Perspect Biol* (2009) 24(43):4846–61. doi: 10.1101/cshperspect.a001651
32. Biswas R, Bagchi A. NFkB Pathway and Inhibition: An Overview. *Comput Mol Biol* (2016) 6:1–20. doi: 10.5376/cmb.2016.06.0001
33. Dorrington MG, Fraser IDC. NF-κb Signaling in Macrophages: Dynamics, Crosstalk, and Signal Integration. *Front Immunol* (2019) 10:705. doi: 10.3389/fimmu.2019.00705
34. Yin Y, Shen WH. PTEN: A New Guardian of the Genome. *Oncogene* (2008) 27:5443–53. doi: 10.1038/onc.2008.241
35. Zhang S, Yu D. PI(3)king Apart PTEN's Role in Cancer. *Clin Cancer Res* (2010) 16:4325–30. doi: 10.1158/1078-0432.CCR-09-2990
36. Hopkins BD, Hodakoski C, Barrows D, Mense SM, Parsons RE. PTEN Function: The Long and the Short of It. *Trends Biochem Sci* (2014) 39:183–90. doi: 10.1016/j.tibs.2014.02.006
37. Roberta A, Elisa G, Mara B, Andrea C. New Treatment Opportunities in Phosphatase and Tensin Homolo(PTen)-Deficient Tumors: Focus on PTen/focal Adhesion Kinase Pathway. *Front Oncol* (2017) 7:170. doi: 10.3389/fonc.2017.00170
38. Chen CY, Chen J, He L, Stiles BL. PTEN: Tumor Suppressor and Metabolic Regulator. *Front Endocrinol (Lausanne)* (2018) 9:338. doi: 10.3389/fendo.2018.00338
39. Furnari FB, Su Huang HJ, Cavenee WK. The Phosphoinositol Phosphatase Activity of PTEN Mediates a Serum- Sensitive G1 Growth Arrest in Glioma Cells. *Cancer Res* (1998) 58:5002–8.
40. Seminario MC, Precht P, Wersto RP, Gorospe M, Wange RL. PTEN Expression in PTEN-Null Leukaemic T Cell Lines Leads to Reduced Proliferation *via* Slowed Cell Cycle Progression. *Oncogene* (2003) 22:8195–204. doi: 10.1038/sj.onc.1206872
41. Puc J, Keniry M, Li HS, Pandita TK, Choudhury AD, Memeo L, et al. Lack of PTEN Sequesters CHK1 and Initiates Genetic Instability. *Cancer Cell* (2005) 7:193–204. doi: 10.1016/j.ccr.2005.01.009
42. Brandmaier A, Hou S-Q, Shen WH. Cell Cycle Control by PTEN. *J Mol Biol* (2017) 429:2265–77. doi: 10.1016/j.jmb.2017.06.004
43. Xu W, Yang Z, Zhou SF, Lu N. Posttranslational Regulation of Phosphatase and Tensin Homolog (PTEN) and Its Functional Impact on Cancer Behaviors. *Drug Des Devel Ther* (2014) 8:1745–51. doi: 10.2147/DDDT.S71061
44. Ferlay J, Soerjomataram I, Dikshit R, Eser S, Mathers C, Rebelo M, et al. Cancer Incidence and Mortality Worldwide: Sources, Methods and Major Patterns in GLOBOCAN 2012. *Int J Cancer* (2015) 136:E359–86. doi: 10.1002/ijc.29210
45. Spadi R, Brusa F, Ponzetti A, Chiappino I, Birocco N, Ciuffreda L, et al. Current Therapeutic Strategies for Advanced Pancreatic Cancer: A Review for Clinicians. *World J Clin Oncol* (2016) 7:27–43. doi: 10.5306/wjco.v7.i1.27
46. Neoptolemos JP, Kleeff J, Michl P, Costello E, Greenhalf W, Palmer DH. Therapeutic Developments in Pancreatic Cancer: Current and Future Perspectives. *Nat Rev Gastroenterol Hepatol* (2018) 15:333–48. doi: 10.1038/s41575-018-0005-x
47. Fong CYK, Burke E, Cunningham D, Starling N. Up-To-Date Tailored Systemic Treatment in Pancreatic Ductal Adenocarcinoma. *Gastroenterol Res Pract* (2019). doi: 10.1155/2019/7135437
48. Abdelaleem M, Ezzat H, Osama M, Megahed A, Alaa W, Gaber A, et al. Prospects for Repurposing CNS Drugs for Cancer Treatment. *Oncol Rev* (2019) 13:37–42. doi: 10.4081/oncol.2019.411
49. Okami J, Nakamori S, Hiraoka N, Tsujie M, Hayashi N, Yamamoto H, et al. Suppression of Pancreatic Cancer Cell Invasion by a Cyclooxygenase-2-Specific Inhibitor. *Clin Exp Metastasis* (2003) 20:577–84. doi: 10.1023/a:1027319903359
50. Rayburn E. Anti-Inflammatory Agents for Cancer Therapy. *Mol Cell Pharmacol* (2009) 1:29–43. doi: 10.4255/mcpharmacol.09.05
51. Hiľovská L, Jendželovský R, Fedoročko P. Potency of Non-Steroidal Anti-Inflammatory Drugs in Chemotherapy. *Mol Clin Oncol* (2015) 3:3–12. doi: 10.3892/mco.2014.446
52. Tripathi M, Singh BK, Raisuddin S, Kakkar P. Abrogation of Nimesulide Induced Oxidative Stress and Mitochondria Mediated Apoptosis by Fumaria Parviflora Lam. Extract. *J Ethnopharmacol* (2011) 136:94–102. doi: 10.1016/j.jep.2011.04.014
53. Huerta C, Aberturas M del R, Molpeceres J. Nimesulide-Loaded Nanoparticles for the Potential Coadjuvant Treatment of Prostate Cancer. *Int J Pharm* (2015) 493:152–60. doi: 10.1016/j.ijpharm.2015.07.027
54. Catarro M, Serrano JL, Ramos SS, Silvestre S, Almeida P. Nimesulide Analogues: From Anti-Inflammatory to Antitumor Agents. *Bioorg Chem* (2019) 88:102966. doi: 10.1016/j.bioorg.2019.102966
55. Suleyman H, Cadirci E, Albayrak A, Halici Z. Nimesulide is a Selective COX-2 Inhibitory, Atypical Non-Steroidal Anti-Inflammatory Drug. *Curr Med Chem* (2008) 15:278–83. doi: 10.2174/092986708783497247

56. Bernareggi A. Clinical Pharmacokinetics of Nimesulide. *Clin Pharmacokinet* (1998) 35:247–74. doi: 10.2165/00003088-199835040-00001
57. Bernareggi A. Clinical Pharmacokinetics and Metabolism of Nimesulide. *Inflammopharmacology* (2001) 9:81–9. doi: 10.1163/156856001300248353
58. Kress HG, Baltov A, Basiński A, Berghea F, Castellsague J, Codreanu C, et al. Acute Pain: A Multifaceted Challenge - The Role of Nimesulide. *Curr Med Res Opin* (2016) 32:23–36. doi: 10.1185/03007995.2015.1100986
59. Singla AK, Chawla M, Singh A. Review Nimesulide: Some Pharmaceutical and Pharmacological Aspects—An Update. *J Pharm Pharmacol* (2000) 52:467–86. doi: 10.1211/0022357001774255
60. Rainsford KD. Current Status of the Therapeutic Uses and Actions of the Preferential Cyclo-Oxygenase-2 NSAID, Nimesulide. *Inflammopharmacology* (2006) 14:120–37. doi: 10.1007/s10787-006-1505-9
61. Bessone F, Colombato L, Fassio E, Virginia Reggiardo M, Vorobioff J, Tanno H. The Spectrum of Nimesulide-Induced-Hepatotoxicity. An Overview. *Antiinflamm Antiallergy Agents Med Chem* (2010) 9:355–65. doi: 10.2174/1871523011009040355
62. Caiazzo E, Ialenti A, Cicala C. The Relatively Selective Cyclooxygenase-2 Inhibitor Nimesulide: What's Going on? *Eur J Pharmacol* (2019) 848:105–11. doi: 10.1016/j.ejphar.2019.01.044
63. Uram Ł, Filipowicz-Rachwał A, Misiorek M, Winiarz A, Wałajtys-Rode E, Wołowiec S. Synthesis and Different Effects of Biotinylated PAMAM G3 Dendrimer Substituted With Nimesulide in Human Normal Fibroblasts and Squamous Carcinoma Cells. *Biomolecules* (2019) 9(9):437. doi: 10.3390/biom9090437
64. Sengel-Turk CT, Hascicek C, Bakar F, Simsek E. Comparative Evaluation of Nimesulide-Loaded Nanoparticles for Anticancer Activity Against Breast Cancer Cells. *AAPS PharmSciTech* (2017) 18:393–403. doi: 10.1208/s12249-016-0514-2
65. Nam KT, Hahm KB, Oh SY, Yeo M, Han SU, Ahn B, et al. The Selective Cyclooxygenase-2 Inhibitor Nimesulide Prevents Helicobacter Pylori-Associated Gastric Cancer Development in a Mouse Model. *Clin Cancer Res* (2004) 10:8105–13. doi: 10.1158/1078-0432.CCR-04-0896
66. Wu JC, Tsai HE, Hsiao YH, Wu JS, Wu CS, Tai MH. Topical MTII Therapy Suppresses Melanoma Through PTEN Upregulation and Cyclooxygenase II Inhibition. *Int J Mol Sci* (2020) 21(2):681. doi: 10.3390/ijms21020681
67. Yoo SY, Kwon SM. Angiogenesis and its Therapeutic Opportunities. *Mediators Inflammation* (2013). doi: 10.1155/2013/127170
68. Li B, Lu Y, Yu L, Han X, Wang H, Mao J, et al. miR-221/222 Promote Cancer Stem-Like Cell Properties and Tumor Growth of Breast Cancer *via* Targeting PTEN and Sustained Akt/NF-κb/COX-2 Activation. *Chem Biol Interact* (2017) 277:33–42. doi: 10.1016/j.cbi.2017.08.014
69. Jin Y, Liu L, Chen B, Bai Y, Zhang F, Li Q, et al. Involvement of the PI3K/Akt/NF- B Signaling Pathway in the Attenuation of Severe Acute Pancreatitis-Associated Acute Lung Injury by Sedum Sarmentosum Bunge Extract. *BioMed Res Int* (2017) 2017:16–9. doi: 10.1155/2017/9698410
70. Donati M, Conforti A, Lenti MC, Capuano A, Bortolami O, Motola D, et al. Risk of Acute and Serious Liver Injury Associated to Nimesulide and Other NSAIDs: Data From Drug-Induced Liver Injury Case-Control Study in Italy. *Br J Clin Pharmacol* (2016) 82:238–48. doi: 10.1111/bcp.12938
71. Sun X, Xue KL, Jiao XY, Chen Q, Xu L, Zheng H, et al. Simultaneous Determination of Nimesulide and Its Four Possible Metabolites in Human Plasma by LC-MS/MS and Its Application in a Study of Pharmacokinetics. *J Chromatogr B Anal Technol BioMed Life Sci* (2016) 1027:139–48. doi: 10.1016/j.jchromb.2016.05.008
72. Carini M, Aldini G, Stefani R, Marinello C, Maffei Facino R. Mass Spectrometric Characterization and HPLC Determination of the Main Urinary Metabolites of Nimesulide in Man. *J Pharm BioMed Anal* (1998) 18:201–11. doi: 10.1016/S0731-7085(98)00172-1
73. Rainsford KD. Pharmacology and Toxicology of COX-2 Inhibitors. In: *COX-2 Inhibitors*. (2006) Basel: Birkhäuser Basel. p. 67–131. doi: 10.1007/978-3-0348-7879-1_4
74. Macpherson D. The Biotransformation and Pharmacokinetics of 14C-Nimesulide in Humans Following a Single Dose Oral Administration. *J Drug Metab Toxicol* (2012) 04:1–13. doi: 10.4172/2157-7609.1000140
75. Dupont L, Pirotte B, Masereel B, Delarge J, Geczy J. Nimesulide. *Acta Crystallogr Sect C Cryst Struct Commun* (1995) 51:507–9. doi: 10.1107/S0108270194010334
76. Boelsterli UA. Mechanisms of NSAID-Induced Hepatotoxicity. *Drug Saf* (2002) 25(9):633–48. doi: 10.2165/00002018-200225090-00003
77. Mingatto FE, Rodrigues T, Pigoso AA, Uyemura SA, Curti C, Santos AC. The Critical Role of Mitochondrial Energetic Impairment in the Toxicity of Nimesulide to Hepatocytes. *J Pharmacol Exp Ther* (2002) 303(2):601–7. doi: 10.1124/jpet.102.038620
78. Mukherjee S, Ray S, Thakur RS. Solid Lipid Nanoparticles: A Modern Formulation Approach in Drug Delivery System. *Indian J Pharm Sci* (2009) 71:349–58. doi: 10.4103/0250-474X.57282
79. García-Pinel B, Porras-Alcalá C, Ortega-Rodríguez A, Sarabia F, Prados J, Melguizo C, et al. Lipid-Based Nanoparticles: Application and Recent Advances in Cancer Treatment. *Nanomaterials* (2019) 9:1–23. doi: 10.3390/nano9040638
80. Misra R, Acharya S, Sahoo SK. Cancer Nanotechnology: Application of Nanotechnology in Cancer Therapy. *Drug Discov Today* (2010) 15:842–50. doi: 10.1016/j.drudis.2010.08.006
81. Yadav N, Khatak S, Singh Sara UV. Solid Lipid Nanoparticles- A Review. *Int J Appl Pharm* (2013) 5:8–18. doi: 10.9790/3013-26103444
82. Garud A, Singh D, Garud N. Solid Lipid Nanoparticles (SLN): Method, Characterization and Applications. *Int Curr Pharm J* (2012) 1:384–93. doi: 10.3329/icpj.v1i11.12065
83. Letchford K, Burt H. A Review of the Formation and Classification of Amphiphilic Block Copolymer Nanoparticulate Structures: Micelles, Nanospheres, Nanocapsules and Polymersomes. *Eur J Pharm Biopharm* (2007) 65:259–69. doi: 10.1016/j.ejpb.2006.11.009
84. Mora-Huertas CE, Fessi H, Elaissari A. Polymer-Based Nanocapsules for Drug Delivery. *Int J Pharm* (2010) 385:113–42. doi: 10.1016/j.ijpharm.2009.10.018
85. Radhika PR, Sasikanth ST. Nanocapsules: A New Approach in Drug Delivery. *Int J Pharm Sci Res* (2011) 2:1426–9. http://www.embase.com/search/results?subaction=viewrecord&from=export&id=L368483562%5Cnhttp://www.ijpsr.com/V2I6/11. doi: 10.13040/IJPSR.0975-8232.2(6).1426-29
86. Mathur V, Satrawala Y, Rajput MS. Dendrimers: A Review Dendrimers : A Review. (2015) 1.
87. Baig T, Nayak J, Dwivedi V, Singh A. Tripathi PK. A Review About Dendrimers: Synthesis, Types, Characterization and Applications. *Int J Adv Pharmacy Biol Chem* (2015) 4:44–59.
88. Ebada SS, El-Neketi M, Ebrahim W, Mándi A, Kurtán T, Kalscheuer R, et al. Cytotoxic Secondary Metabolites From the Endophytic Fungus Aspergillus Versicolor KU258497. *Phytochem Lett* (2018) 24:88–93. doi: 10.1016/j.phytol.2018.01.010
89. Aghebati-Maleki A, Dolati S, Ahmadi M, Baghbanzhadeh A, Asadi M, Fotouhi A, et al. Nanoparticles and Cancer Therapy: Perspectives for Application of Nanoparticles in the Treatment of Cancers. *J Cell Physiol* (2020) 235:1962–72. doi: 10.1002/jcp.29126
90. Murugan E, Geetha Rani DP, Yogaraj V. Drug Delivery Investigations of Quaternised Poly(Propylene Imine) Dendrimer Using Nimesulide as a Model Drug. *Colloids Surf B Biointerf* (2014) 114:121–9. doi: 10.1016/j.colsurfb.2013.10.002
91. Torchilin V. Lipid-Core Micelles for Targeted Drug Delivery. *Curr Drug Delivery* (2005) 2:319–27. doi: 10.2174/156720105774370221
92. Torchilin VP. Micellar Nanocarriers: Pharmaceutical Perspectives. *Pharm Res* (2007) 24:1–16. doi: 10.1007/s11095-006-9132-0
93. Haley B, Frenkel E. Nanoparticles for Drug Delivery in Cancer Treatment. *Urol Oncol Semin Orig Investig* (2008) 26(1):57–64. doi: 10.1016/j.urolonc.2007.03.015
94. Swain S, Sahu P, Beg S, Babu S. Nanoparticles for Cancer Targeting: Current and Future Directions. *Curr Drug Deliv* (2016) 13:1290–302. doi: 10.2174/1567201813666160713121122
95. Masayuki Y, Mizue M, Noriko Y, Teruo O, Yasuhisa S, Kazunori K, et al. Polymer Micelles as Novel Drug Carrier: Adriamycin-Conjugated Poly (Ethylene Glycol)-Poly(Aspartic Acid) Block Copolymer. *J Control Release* (1990) 11:269–78. doi: 10.1016/0168-3659(90)90139-K
96. Almgren M, Brown W, Hvidt S. Self-Aggregation and Phase Behavior of Poly(Ethylene Oxide)-Poly(Propylene Oxide)-Poly(Ethylene Oxide) Block Copolymers in Aqueous Solution. *Colloid Polym Sci* (1995) 273:2–15. doi: 10.1007/BF00655668
97. Jeong JH, Park TG. Poly(L-Lysine)-G-Poly(D,L-Lactic-Co-Glycolic Acid) Micelles for Low Cytotoxic Biodegradable Gene Delivery Carriers. *J Control Release* (2002) 82:159–66. doi: 10.1016/S0168-3659(02)00131-1

98. Itaka K, Yamauchi K, Harada A, Nakamura K, Kawaguchi H, Kataoka K. Polyion Complex Micelles From Plasmid DNA and Poly(Ethylene Glycol)-Poly(L-Lysine) Block Copolymer as Serum-Tolerable Polyplex System: Physicochemical Properties of Micelles Relevant to Gene Transfection Efficiency. *Biomaterials* (2003) 24:4495–506. doi: 10.1016/S0142-9612(03)00347-8
99. Torchilin V. Polymeric Micelles as Pharmaceutical Carriers. In: *Polymers in Drug Delivery*. (2006) 1(6):111–130.
100. Lukyanov AN, Torchilin VP. Micelles From Lipid Derivatives of Water-Soluble Polymers as Delivery Systems for Poorly Soluble Drugs. *Adv Drug Deliv Rev* (2004) 56:1273–89. doi: 10.1016/j.addr.2003.12.004
101. Parmar A, Parekh P, Bahadur P. Solubilization and Release of a Model Drug Nimesulide From PEO-PPO-PEO Block Copolymer Core-Shell Micelles: Effect of Size of PEO Blocks. *J Solution Chem* (2013) 42:80–101. doi: 10.1007/s10953-012-9949-6
102. Wang Y, Liu Z, Li T, Chen L, Lyu J, Li C, et al. Enhanced Therapeutic Effect of RGD-Modified Polymeric Micelles Loaded With Low-Dose Methotrexate and Nimesulide on Rheumatoid Arthritis. *Theranostics* (2019) 9:708–20. doi: 10.7150/thno.30418
103. Samad A, Sultana Y, Aqil M. Liposomal Drug Delivery Systems: An Update Review. *Curr Drug Deliv* (2007) 4:297–305. doi: 10.2174/156720107782151269
104. Maheswaran A, Brindha P, Mullaicharam AR, Masilamani K. Liposomal Drug Delivery Systems - A Review. *Int J Pharm Sci Rev Res* (2013) 23:295–301. doi: 10.31069/japsr.v3i3.2
105. Banerjee S, Mandal M. Stimuli-Responsive Nanostructured Silica Matrix Targeting Drug Delivery Applications. *Biol Pharm Appl Nanomater* (2015) 22–57. doi: 10.1201/b18654-5
106. Ferreira H, Lúcio M, De Castro B, Gameiro P, Lima JLFC, Reis S. Partition and Location of Nimesulide in EPC Liposomes: A Spectrophotometric and Fluorescence Study. *Anal Bioanal Chem* (2003) 377:293–8. doi: 10.1007/s00216-003-2089-5
107. Kumar A, Badde S, Kamble R, Pokharkar VB. Development and Characterization of Liposomal Drug Delivery System for Nimesulide. *Int J Pharm Pharm Sci* (2010) 2:87–9.
108. Ghasemiyeh P, Mohammadi-Samani S. Solid Lipid Nanoparticles and Nanostructured Lipid Carriers as Novel Drug Delivery Systems: Applications, Advantages and Disadvantages. *Res Pharm Sci* (2018) 13:288–303. doi: 10.4103/1735-5362.235156
109. Mathur V, Satrawala Y, Rajput MS, Kumar P, Shrivastava P, Vishvkarma A. Solid Lipid Nanoparticles in Cancer Therapy. *Int J Drug Delivery* (2010) 2:192–9. doi: 10.5138/ijdd.2010.0975.0215.02029
110. Naseri N, Valizadeh H, Zakeri-Milani P. Solid Lipid Nanoparticles and Nanostructured Lipid Carriers: Structure Preparation and Application. *Adv Pharm Bull* (2015) 5:305–13. doi: 10.15171/apb.2015.043
111. Bondi M, Azzolina A, Craparo E, Capuano G, Lampiasi N, Giammona G, et al. Solid Lipid Nanoparticles Containing Nimesulide: Preparation, Characterization and Cytotoxicity Studies. *Curr Nanosci* (2009) 40 (spc):63–73. doi: 10.2174/157341309787314575
112. Bayón-Cordero L, Alkorta I, Arana L. Application of Solid Lipid Nanoparticles to Improve the Efficiency of Anticancer Drugs. *Nanomaterials* (2019) 9(3):474. doi: 10.3390/nano9030474
113. Pauwels E, Kairemo K, Erba P, Bergstrom K. Nanoparticles in Cancer. *Curr Radiopharm* (2010) 1:30–6. doi: 10.2174/1874471010801010030
114. Pushpendra J, Amit M KY, Patil K, Baghel S. Formulation Development and Characterization of Solid Lipid Nanoparticles Containing Nimesulide. *Int J Drug Deliv Technol* (2009) 1:24–7. doi: 10.25258/ijddt.v1i1.8835
115. Campos JR, Fernandes AR, Sousa R, Fangueiro JF, Boonme P, Garcia ML, et al. Optimization of Nimesulide-Loaded Solid Lipid Nanoparticles (SLN) by Factorial Design, Release Profile and Cytotoxicity in Human Colon Adenocarcinoma Cell Line. *Pharm Dev Technol* (2019) 24(5):616–22. doi: 10.1080/10837450.2018.1549075

**Conflict of Interest:** The authors declare that the research was conducted in the absence of any commercial or financial relationships that could be construed as a potential conflict of interest.

# Advantages of publishing in Frontiers

**OPEN ACCESS**
Articles are free to read for greatest visibility and readership

**FAST PUBLICATION**
Around 90 days from submission to decision

**HIGH QUALITY PEER-REVIEW**
Rigorous, collaborative, and constructive peer-review

**TRANSPARENT PEER-REVIEW**
Editors and reviewers acknowledged by name on published articles

**Frontiers**
Avenue du Tribunal-Fédéral 34
1005 Lausanne | Switzerland

**Visit us:** www.frontiersin.org
**Contact us:** frontiersin.org/about/contact

**REPRODUCIBILITY OF RESEARCH**
Support open data and methods to enhance research reproducibility

**DIGITAL PUBLISHING**
Articles designed for optimal readership across devices

**FOLLOW US**
@frontiersin

**IMPACT METRICS**
Advanced article metrics track visibility across digital media

**EXTENSIVE PROMOTION**
Marketing and promotion of impactful research

**LOOP RESEARCH NETWORK**
Our network increases your article's readership